I have forgotten much that I thought I knew, and learned again much that I had forgotten.

Gandalf the White

GHENT UNIVERSITY

FACULTY OF BIOSCIENCE ENGINEERING

Development of porous organic polymers as heterogeneous photocatalysts

ir. Maarten Debruyne

Thesis submitted in fulfillment of the requirements for the degree of doctor (PhD) of Bioscience Engineering: Chemistry and Bioprocess Technology

Members of the Jury

Prof. dr. ir. Frank Devlieghere (Chairman)

Prof. dr. ing. Timothy Noël

Prof. dr. Tatjana Parac-Vogt

Prof. dr. Annemieke Madder

Dr. Karen Leus

Prof. dr. ir. Thomas Heugebaert

Prof. dr. ir. Matthias D'hooghe

Promotors	Prof. dr. ir. Christian Stevens
	Department of Green Chemistry and Technology
	Faculty of Bioscience Engineering, Ghent University
	Prof. dr. ir. Veronique Van Speybroeck,
	Department of Applied physics
	Faculty of Engineering and Architecture, Ghent University
	Department of Physics and astronomy
	Faculty of Sciences, Ghent University
Dean	Prof. dr. Els Van Damme
Rector	Prof. dr. ir. Rik Van de Walle

Dutch translation of the title

Ontwikkeling van poreuze organische polymeren als heterogene fotokatalysatoren

To be cited as

Debruyne M., 'Development of porous organic polymers as heterogeneous photocatalysts', PhD dissertation, Ghent University, 2023

Cover illustration

Created with starryai

Funding

The research was funded by the Research Board of Ghent University (BOF GOA2017000303)

ISBN: 9789463576000

Ghent, February 2023

The author,

Ir. Maarten Debruyne

The promoters,

Prof. dr. ir. Christian Stevens

Prof. dr. ir. Veronique Van Speybroeck

Woord vooraf

Bij deze komt er een einde aan vier mooie jaren. Ik had nooit gedacht dat ik ooit een doctoraat zou behalen. Soms heb ik het vervloekt, maar nu ben ik toch wel blij dat het eindelijk is gelukt. Dit zou niet mogelijk zijn geweest zonder de steun van iedereen die me tijdens dit proces heeft bijgestaan, daarom wil ik jullie nu toch even bedanken.

Allereerst wil ik mijn promotors, Chris en Veronique, van harte bedanken voor hun begeleiding gedurende dit doctoraat. Veronique, bedankt om dit onderzoek mee mogelijk te maken. Chris, ik kon altijd bij je terecht, ondanks je drukke agenda. Bedankt dat je in mij geloofde en mij zoveel vrijheid gaf. Uiteindelijk zijn we kilometers ver beland van het eerste stukje waarop ik werkte, maar dat behoort tot de reis. Niet veel proffen wagen zich aan crowdsurfen op een congres, en ik ben heel trots dat de mijne daar niet voor terugdeinst!

Furthermore, I would like to thank the members of the examination committee: Prof. Frank Devlieghere, Prof. Timothy Noël, Prof. Tatjana Parac-Vogt, Prof. Annemieke Madder, Dr. Karen Leus, Prof. Thomas Heugebaert, and Prof. Matthias D'hooghe for your time and effort in making this a better PhD.

Vervolgens wil ik ook de mensen bedanken die deze laatste vier jaar zoveel aangenamer hebben gemaakt: mijn allerbeste collega's. Ik wil jullie allemaal bedanken om onze groep zo leuk te maken; er is een reden dat ik nog wat blijf plakken! De lunchpauzes, congressen, activiteiten (behalve bowlen dan) en de sfeer in het algemeen waren allemaal fantastisch. Zwemmen in de Noordzee, leuke dilemma's verzinnen, roddelen over de BDC, rennen naar de nooddouche; ik ben blij dat jullie in mijn team zaten. Bij deze bedank ik jullie allemaal voor de mooie jaren.

Mijn reis begon op het nulde met Arno, Benz, Tim, Jonas, Flore en Silke als bureaugenoten. Bedankt dat jullie me meteen in de groep hebben opgenomen. Bedankt om er zo op te staan dat we elke dag samen lunchten, voor de pauzes, office drinks en naschoolse activiteiten. Ik heb het altijd jammer gevonden dat ons grote plan om allemaal op het vijfde of zesde te geraken niet is kunnen doorgaan. Tim, ik ben blij dat we uiteindelijk vrienden zijn geworden! Ik vind het ook nog steeds spijtig dat ik onze 'cola Burj Khalifa' moest afbreken vanwege protesten van andere bureaugenoten. Silke, bedankt voor alle gesprekken, je steun en luisterend oor voor mijn geklaag. Sari, ook al zat je niet op het nulde, Tnulde + Sari is toch wel echt een ding geworden. Het is volledig aan jou te danken dat de lay-out van dit boekje er goed uitziet. Bedankt om altijd zo grondig je tijd te nemen om mij (en anderen) te helpen. Ik hoop dat we nog veel naar NMRs gaan kunnen staren.

Bij mijn grote migratie naar het vijfde verdiep heb ik natuurlijk ook weer wat leuke collega's beter leren kennen: Stein, Pieter, Eli, Melike, en recenter Jonas, Kato en Mehrsa: bedankt om ook hier voor zo een leuke sfeer te zorgen. Ik kijk er al naar uit om deze zomer weer een airco die niets doet te proberen, ventilators te zetten en veel te puffen en te zweten. Voor Jonas en Kato: misschien moet je mijn advies toch maar blijven negeren?

Hier schieten me nog een paar dingen te binnen. Andreas, bedankt voor de voortdurende ego-boosts (knapperd, spetter) en ons romantische avontuur in Namen. Pierre, bedankt om je *work wife* voor een week uit te lenen (met mijn kledingstijl weet je natuurlijk dat ik geen echte concurrentie ben). Katarina, bedankt voor de late night snacks! Baafje, bedankt om mij zo vaak aan het lachen te brengen. Lena, bedankt om mij op te leiden als onderzoeker. Nathan, bedankt voor je hulp met de Hantzsch esters. Een welgemeende dank aan het ATP team: Ans, Els, Pieter en Maarten, om het labo draaiende

te houden en om altijd zo behulpzaam te zijn. Een speciale bedanking voor Ans, voor uw organisatorisch vermogen, boze brief naar de rector en de fijne gesprekken. Isabelle en Jolien, bedankt om zo'n enthousiaste matrozen (thesisstudenten) te zijn! Mijn dank gaat ook uit naar de andere kapteins van het COFschip: Hadi, Jonas en Flore. Hadi, I'm really glad I got to know you. Jonas, we zaten wat in hetzelfde schuitje en ik ben blij dat we samen deze moeilijke wateren hebben getrotseerd. Flore, bedankt om altijd het moreel zo hoog te houden.

Ik ben op heel wat excursies naar de Sterre geweest, vaak met wat gezucht wegens de (in mijn ogen) verre fietstocht. Op deze uitstapjes ben ik steeds enorm goed geholpen geweest door leden van COMOC, LumiLab en de EMR group, waarvoor een hartelijke dank.

Als voorlaatste wil ik mijn familie en vrienden bedanken: jullie snapten niet heel veel van wat ik aan het doen was, buiten dat het wat lastig was, maar zijn mij altijd blijven steunen, bedankt! Mama en Anne, bedankt om er altijd voor mij te zijn.

En dan, last but not least, wil ik Paas (Hilke) en de tsjoerels bedanken. Bedankt voor alle mooie momenten, de steun, om mee te gaan (met mate) in al mijn gekheid, bedankt om ons huis zo warm te maken.

Maarten Debruyne

Maart 2023

Table of Contents

List of abbreviations

Ac	Acetyl
acac	Acetyl acetonate
AcOH	Acetic acid
AI	*Ab initio*
AIBN	Azobis(isobutyronitrile)
4-AP	4-Aminophenol
Aq.	Aqueous
Ar	Aryl
Arom	Aromatic
ATR	Attenuated total reflectance
a.u.	Arbitrary units
Ben	Benzene
BET	Brunauer-Emmett-Teller
BINOL	1,1'-Bi-2-naphthol
[bmpy]	1-Butyl-3-methylpyridinium
Bn	Benzyl
Boc	*Tert*-butoxycarbonyl
Bpy	2,2'-Bipyridine *or* 2,2'-bipyridine-5,5'-diamine
br.	Broad
BTD	Benzothiadiazole
[C12MIM]	1-Dodecyl-3-methylimidazolium
CAN	Cerium ammonium nitrate
Calcd.	Calculated
Cat.	Catalytic amount
CB	Conduction band
CCS	Carbon capture and sequestration
CDC	Cross-dehydrogenative coupling
CFL	Compact fluorescent lamp
CMP	Conjugated microporous polymer
COF	Covalent organic framework
Conc.	Concentrated
CTF	Covalent triazine framework
Cy	Cyclohexyl
Cz	Carbazole
d	Doublet *or* days
δ	Chemical shift
DABCO	1,4-diazabicyclo[2.2.2]octane
DBAD	Di-*tert*-butyl azodicarboxylate
DBU	1,8-diazabicyclo[5.4.0]undec-7-ene
DCC	Dynamic covalent chemistry
DCE	Dichloroethane
DDQ	2,3-Dichloro-5,6-dicyano-1,4-benzoquinone

DEB	1,4-Diethynylbenzene
DFT	Density functional theory
DIPEA	*N*,*N*-diisopropylethylamine
DIBAL	Diisobutylaluminium hydride
DMAc	*N*,*N*-dimethylacetamide
DMAP	4-Dimethylaminopyridine
DMC	Dimethyl carbonate
DMF	*N*,*N*-dimethylformamide
DMFDMA	*N*,*N*-dimethylformamide dimethyl acetal
DMOB	Dimethoxybenzene
DMPO	5,5-Dimethyl-1-pyrroline-*N*-oxide
DMS	Dimethyl sulfate
DMSO	Dimethyl sulfoxide
dppf	1,1'-Bis(diphenylphosphino)ferrocene
dr	Diastereomeric ratio
DVB	Divinylbenzene
EA	Elemental analysis
ECH	Epichlorohydrin
ee	Enantiomeric excess
E_g	Bandgap energy
E_{ox}	Oxidation potential
EPR	Electron paramagnetic resonance
E_{red}	Reduction potential
Eq.	Equivalent(s)
eV	Electron volt
EWG	Electron withdrawing group
FDMA	Formaldehyde dimethyl acetal
FF	Force field
Fl	Fluorene
FTIR	Fourier transform infrared
FTO	Fluorine doped tin oxide
GMP	Good manufacturing practice
g-C_3N_4	Graphitic carbon nitride
H2P	5,10,15,20-Tetrakis(4'-tetraphenylamino) porphyrin
HAT	Hydrogen atom transfer
HATU	Hexafluorophosphate azobenzotriazole tetramethyl uronium
HBTU	Hexafluorophosphate benzotriazole tetramethyl uronium
hcb	Honeycomb
HCP	Hypercrosslinked polymer
HFIP	Hexafluoroisopropanol
HMF	5-(hydroxymethyl)furfural
HMTA	Hexamethylenetetramine
HMTrux	Hexamethyltruxene
HOMO	Highest occupied molecular orbital
HPLC	High-performance liquid chromatography
HRMS	High-resolution mass spectrometry
Hz	Hertz

IBX	2-Iodoxybenzoic acid
ICP-OES	Inductively coupled plasma optical emission spectroscopy
*i*Pr	Isopropyl
*i*Bu	Isobutyl
IUPAC	International Union of Pure and Applied Chemistry
J	Coupling constant
KHMDS	Potassium bis(trimethylsilyl)amide
kt.	Kamertemperatuur
LC-MS	Liquid chromatography-mass spectrometry
LED	Light-emitting diode
LUMO	Lowest unoccupied molecular orbital
m	Multiplet
m	*Meta*
M	Mother ion
MCR	Multicomponent reaction
MD	Molecular dynamics
MOF	Metal organic framework
MOMCl	Chloromethyl methyl ether
MS	Molecular sieves *or* mass spectrometry
MW	Microwave
m/z	Mass number over charge number
n	*Normal*
NADH	Nicotinamide adenine dinucleotide
nbd	Norbornadiene
NBS	*N*-bromosuccinimide
NBT	Nitro blue tetrazolium chloride
NCS	*N*-Chlorosuccinimide
NHC	*N*-Heterocyclic carbene
NHE	Neutral hydrogen electrode
NHPI	*N*-Hydroxyphthalimide
NMR	Nuclear magnetic resonance
NMM	*N*-Methylmorpholine
NPs	Nanoparticles
4-NP	4-Nitrophenol
n.r.	No reaction
o	*Ortho*
$O_2^{-\bullet}$	Superoxide radical anion
$^1O_2$	Singlet oxygen
*o*DCB	*Ortho*-dichlorobenzene
OTf	Triflate
p	*Para*
PAF	Porous aromatic framework
PAW	Projector augmented wave
PCC	Pyridinium chlorochromate
PDVB	Polydivinylbenzene
PE	Petroleum ether
PEG	Polyethylene glycol

PES	Potential energy surface
PGE	Phenyl glycidyl ether
PIM	Polymer of intrinsic microporosity
pin	Pinacol group
PG	Protecting group
PMP	*Para*-methoxyphenyl
PMO	Periodic mesoporous organosilica
PO	Propylene oxide
POP	Porous organic polymer
pPy	6-(4-aminophenyl)pyridin-3-amine
PXRD	Powder X-ray diffraction
Py	Pyridine
Pyr	Pyrene
q	Quadruplet
QSDFT	Quenched solid density functional theory
r.t.	Room temperature
s	Singlet
Sat.	Saturated
SAR	Structure activity relationship
S_{BET}	BET surface area
SEM	Scanning electron microscopy
SET	Single electron transfer
SO	Styrene oxide
STY	Space time yield
SXRD	Single Crystal X-Ray Diffraction
RED	Rotation Electron Diffraction
RMSD	Root mean square deviation
ROS	Reactive oxygen species
t	Triplet *or* time
T	Temperature
TAPT	1,3,5-Tris-(4-aminophenyl)triazine
TBAB	Tetrabutyl ammonium bromide
$TBAPF_6$	Tetra-*n*-butylammonium hexafluorophosphate
TBDMS	*Tert*-Butyldimethylsilyl
TEB	1,3,5-Triethynylbenzene
TEM	Transmission electron microscopy
TEMP	2,2,6,6-Tetramethylpiperidine
TEMPO	2,2,6,6-Tetramethylpiperidine-1-oxyl
TEOA	Tris(2-hydroxyethyl)amine
TEPM	Tetrakis(4-ethynylphenyl)methane
TFA	Trifluoracetic acid
TfOH	Triflic acid
THF	Tetrahydrofuran
TLC	Thin layer chromatography
TMS	Tetramethylsilane *or* trimethylsilyl
TOF	Turnover frequency
TON	Turnover number

TPAP	Tetrapropyl ammonium bromide
Tp	1,3,5-Triformylphloroglucinol
TPB	1,3,5-Tris(4-aminophenyl)benzene
TpOMe	2,4,6-Trimethoxybenzene-1,3,5-tricarbaldehyde
TRPL	Time-resolved photoluminescence
Trux	Truxene
TTT	2,4,6-Tri(thiophen-2-yl)-1,3,5-triazine
UV-Vis	Ultraviolet-visible
vim	1-Vinylimidazolate
vpr	1-Vinyl-2-pyrrolidone
vpy	4-Vinylpyridine
VB	Valence band
VASP	Vienna ab initio simulation package
wt%	Weight percent
XPS	X-ray photoelectron spectroscopy
XRF	X-ray fluorescence
2D/3D	Two-/three-dimensional

Bookmarked POPs

Chapter 1

Chapter 2

Chapter 3

Chapter 4

Outline

Catalysis is essential for the chemical industry, and therefore the world. Without efficient catalysis society as we know it would not be possible, as the chemical reactions that drive industry would not be occurring. Especially considering the current environmental crisis, having a chemical industry that is as efficient as possible is of paramount importance. The search for new and more advanced catalysts is therefore ever ongoing. Heterogeneous, solid catalysts are essential in this regard, as these catalysts do not dissolve and can therefore easily be recovered by filtration, or better yet, be used in continuous flow.

The focal point of this work was the development of porous organic polymers (POPs), and covalent organic frameworks (COFs) in particular, as a new class of heterogeneous catalysts. These new, advanced, porous polymers are at the forefront of material science. They are synthesized completely from organic building blocks and are therefore lightweight and possess good stabilities through the strong covalent bonds holding the structures together. The main applications of these materials are in gas storage and separation, energy storage, optoelectronics, sensing and, importantly, heterogeneous catalysis. As the development of these materials is still in its infancy, much more research is still needed on their design, structure, properties and applications. In this light two main avenues were developed in this work. In the first part the effect of small variations in building blocks on the photocatalytic properties of COFs was studied. These COFs were then used for aerobic oxidation/cyclization reactions. The other avenue focused on the use of easily synthesized POPs as photocatalysts for the aromatization of *N*-heterocycles.

In **Chapter 1**, the reader is introduced to porous organic materials and a detailed literature review is given on the application of POPs as (metal-free) heterogeneous catalysts. Organocatalytic reactions (acid, base, combined acid-base and hydrogen bonding catalysis) are addressed. Alongside this, the application of POPs as photocatalysts is described. After this literature study, the objectives of the thesis are outlined.

In **chapter 2**, the work performed during this PhD on the application of COFs as photocatalysts is described. A brief introduction on COFs is given, to shine more light on these extraordinary materials. Both the synthesis of the used linkers is detailed, as the synthesis and characterization of the COFs themselves. The application of these materials as photocatalysts for the oxidation of boronic acids and benzylamines is discussed. Next to this the COF catalyzed aerobic oxidation/Povarov cyclization and α-oxidation of a range of glycine derivatives is described.

In **chapter 3** the focus was the development of amorphous POPs as photocatalysts. A range of POPs were synthesized from simple, unfunctionalized aromatic building blocks using Friedel-Crafts alkylation. These easily synthesized materials were applied as photocatalysts for the aromatization of *N*-heterocycles, a new application for POPs. Using the most effective POP a wide range of pyridines, dihydroquinoline-5-ones, tetrahydroacridine-1,8-diones and pyrazoles could be obtained in generally excellent yields and under very mild conditions.

In **chapter 4** the attempted development of NHC-containing COFs is described, followed by conclusions, perspectives and a summary of the work done in this thesis.

Chapter 1: Introduction, literature review and goals

This chapter is based on a published literature review that was extended to include photocatalysis.

Porous organic polymers as metal free heterogeneous organocatalysts. M. Debruyne, V. Van Speybroeck, P. Van Der Voort, C. V. Stevens. *Green Chem.*, **2021**, *23*(19), 7361–7434.

Abstract: Efficient catalysis is essential from a green chemistry perspective. Porous organic polymers (POPs) have recently emerged as highly effective materials for catalytic applications. POPs possess controllable compositions and functionalities, high surface areas and can be very stable. In this review we focus on the application of POPs as metal-free heterogeneous organocatalysts, a booming field in green chemistry. Acid, base, combined acid-base and hydrogen bonding catalysis are addressed. In addition, chiral catalysis and CO_2 utilization with POPs are discussed. The aim is to provide a comprehensive overview of the field, exploring all different types of POPs as metal-free catalysts. Special attention is given to the synthesis conditions to provide the reader more insight in the construction of these types of materials.

Graphical abstract:

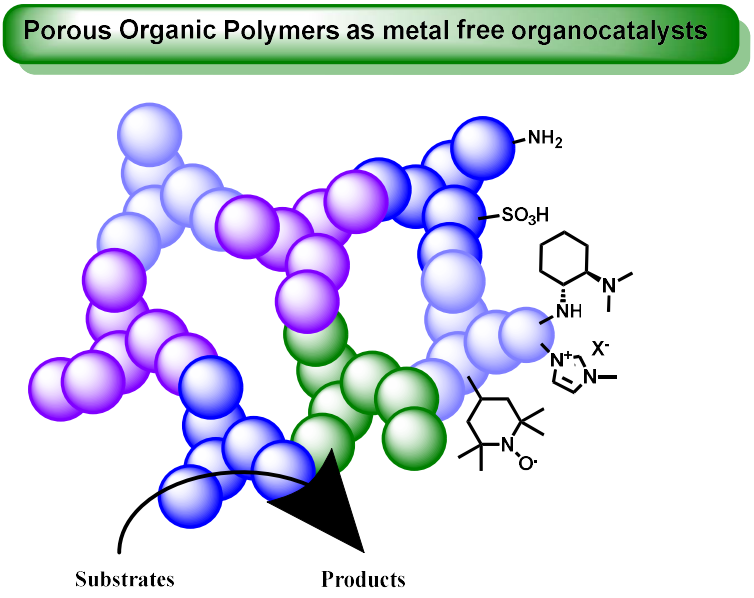

1.1 Introduction

Modern life is impossible without catalysis. It is central to the products we use, the air we breathe, the food we eat… Catalysis stands at the core of the chemical industry and forms a central field of current science with enormous importance and challenges.[1] Due to the booming economy and the rising world population, producing in the most environmentally friendly way possible is of critical importance and here catalysis plays a central role. The 9th principle of green chemistry highlights this: 'Catalytic reagents, as selective as possible, are superior to stoichiometric reagents'.[2] Of the processes that take place in the chemical industry 85% are catalytic and in 80% of those processes heterogeneous catalysts are used.[3,4]

The importance of catalysis doesn't have to surprise. Without a catalyst driving the transformation many reactions either do not work at all, or give mixtures of products. Selective catalysts on the other hand can reduce by-products or waste and lead to milder process conditions.[5] For example, catalysts allow replacing stoichiometric oxidizing agents (*e.g.* PCC, $K_2Cr_2O_7$, $KMnO_4$…) with catalytic oxidations using O_2 or H_2O_2 or allow catalytic carbonylation utilizing CO instead of toxic and corrosive phosgene.[6,7] Heterogeneous catalysts are generally preferred over homogeneous catalysts. These catalysts are recyclable, provide easier separation and work up of reaction mixtures, lower leaching of metals and they lend themselves exceptionally well to continuous production.[5,8,9]

Porous materials are often used as heterogeneous catalysts due to their high internal surface where reactions can occur. These porous solids contain voids and thus the material will have an internal surface area and pores. IUPAC classifies the pores into three types: microporous ($d < 2$ nm), mesoporous (2 nm $< d <$ 50 nm) and macroporous ($d >$ 50 nm).[10] Many naturally occurring porous materials exist: rocks, soils, zeolites, biological tissues (*e.g.* bones, wood), and many more have been made by man: bricks, textiles, sponges, etc. Porosity is typically measured by argon or nitrogen physisorption and is characterized by a large (BET) surface area and pore volume.[11,12]

Zeolites are microporous, aluminosilicate minerals with widespread applications as adsorbents and catalysts and serve as the workhorse heterogeneous catalysts in the chemical industry. They are naturally occurring, but are also produced industrially.[13] However, many other porous materials can be utilized and are currently being developed for catalytic applications, for example, mesoporous silicas, polystyrene resins and metal organic frameworks (MOFs). The mesoporous silicas are normally alkaline sensitive and polystyrene resins often have low surface areas. MOFs are extended crystalline frameworks consisting of metal ions or clusters as the nodes, providing direction to the charged organic linkers.[14–16] Examples of stable MOFs are known, however for widespread catalytic applications they are still hampered by their generally low stability.[17] Therefore, research into stable, lightweight, highly porous and purely organic materials is gaining a lot of traction. This field of porous organic polymers (POPs) has exploded in the last years. POPs all share the following defining characteristics: high porosity, being composed of lightweight elements and strong covalent bonds holding their 2/3D structures together.[18] In what follows, a short historical overview is given and a typical example of each class of POPs is shown (Scheme 1). POPs are classified depending on their degree of long range order (amorphous or crystalline) and the type of linkages used in their synthesis.

The oldest POPs are the hypercrosslinked polymers (HCPs). Crosslinked polystyrene networks were already reported in the 1930's.[19] Development of a truly porous crosslinked polymer took place by Davankov *et al*. in the 1970's, by crosslinking linear polystyrene **1** with crosslinkers such as α,α'-dichloro-*p*-xylene **2** or chloromethyl methyl ether. The high level of crosslinks led to porous structures, with the rigid backbones preventing the structure from collapse and providing BET surface areas up

to 1106 m^2/g.[20,21] HCPs can also be formed by Friedel-Crafts type crosslinking of monomers, typically using Lewis acids such as $FeCl_3$ or $AlCl_3$.[22]

Polymers of intrinsic microporosity (PIMs), reported for the first time in 2004, are one-dimensional polymers containing twisted polymer backbones which result in inefficient packing and porosity. Unlike typical POPs, these polymers are able to dissolve in solvents, making them solution processable.[23,24]

Covalent organic frameworks (COFs), first reported in 2005 by Yaghi *et al*., are crystalline extended 2D or 3D organic solids formed by reversible condensation reactions.[25] The first COF was formed by condensation of 1,4-phenylenediboronic acid **5** in sealed ampoules at 120 degrees for three days. In the years after the discovery of the first crystalline 2D (2005)[25] and 3D COFs (2007),[26] research in this area has boomed. A lot of this effort has gone into identifying new suitable reactions for the synthesis of COFs. For every new reaction appropriate conditions have to be found, ensuring the formation of crystalline materials. The reactions need to be sufficiently reversible, so that self-correction of defects is possible. One class of COFs are the covalent triazine frameworks (CTFs). These materials are typically formed by trimerization of aromatic nitriles in zinc chloride at elevated temperatures (400-500 °C) to ensure reversibility, however these harsh conditions lead to partial carbonization and loss of crystallinity. CTFs are therefore typically amorphous with only some CTFs being crystalline.[27–29]

Conjugated microporous polymers (CMPs) are porous polymers with fully conjugated skeletons, they can be viewed as amorphous analogues of COFs. These are typically synthesized via palladium catalyzed coupling reactions (Sonogashira-Hagihara, Suzuki-Miyaura, Heck) or nickel catalyzed Yamamoto couplings, but many more reaction types are known such as oxidative coupling, Schiff base formation, phenazine ring fusion, cyclotrimerization of alkynes or nitriles, etc.[18,30] A first example in 2007 consisted of the synthesis of **CMP-1**, formed by Sonogashira cross-coupling between 1,4-diiodobenzene **6** and 1,3,5-triethynylbenzene **7**.[31] Analogous to CMPs are porous aromatic frameworks (PAFs), which are formed using similar reactions. PAFs however do not possess extended π-conjugation because of the inclusion of tetrahedral, sp^3 hybridized tetraphenylmethane nodes.[18,32] **PAF-1** was synthesized in 2009, by nickel(0)-catalyzed Yamamoto coupling of tetrakis(4-bromophenyl)methane **8** as the tetrahedral building block, leading to a porous material with extremely high surface areas (5600 m^2/g).[33] The silane, bismuth, tin and antimony analogues of PAFs are called element organic frameworks (EOFs).[34,35]

POPs, together with the other porous materials, have widespread uses in adsorption, catalysis, separation, purification and energy storage or production.[36] Catalytically POPs can be useful as a support for metal complexes or nanoparticles,[37] but also as metal-free catalysts. In this literature review the focus will lie on the application of metal-free POPs as heterogeneous catalysts. A comprehensive overview is offered on the complete field of POPs as organocatalysts, covering acid, base, hydrogen bonding, combined acid-base, nucleophilic and chiral catalysis. Catalytical applications where a metal is used in combination with an organocatalytical POP will also be reviewed. Next to this, the use of POPs as photocatalysts for organic transformations is also covered extensively. Lastly, we also take a critical look at the green character of these materials after which the goals of this thesis are outlined.

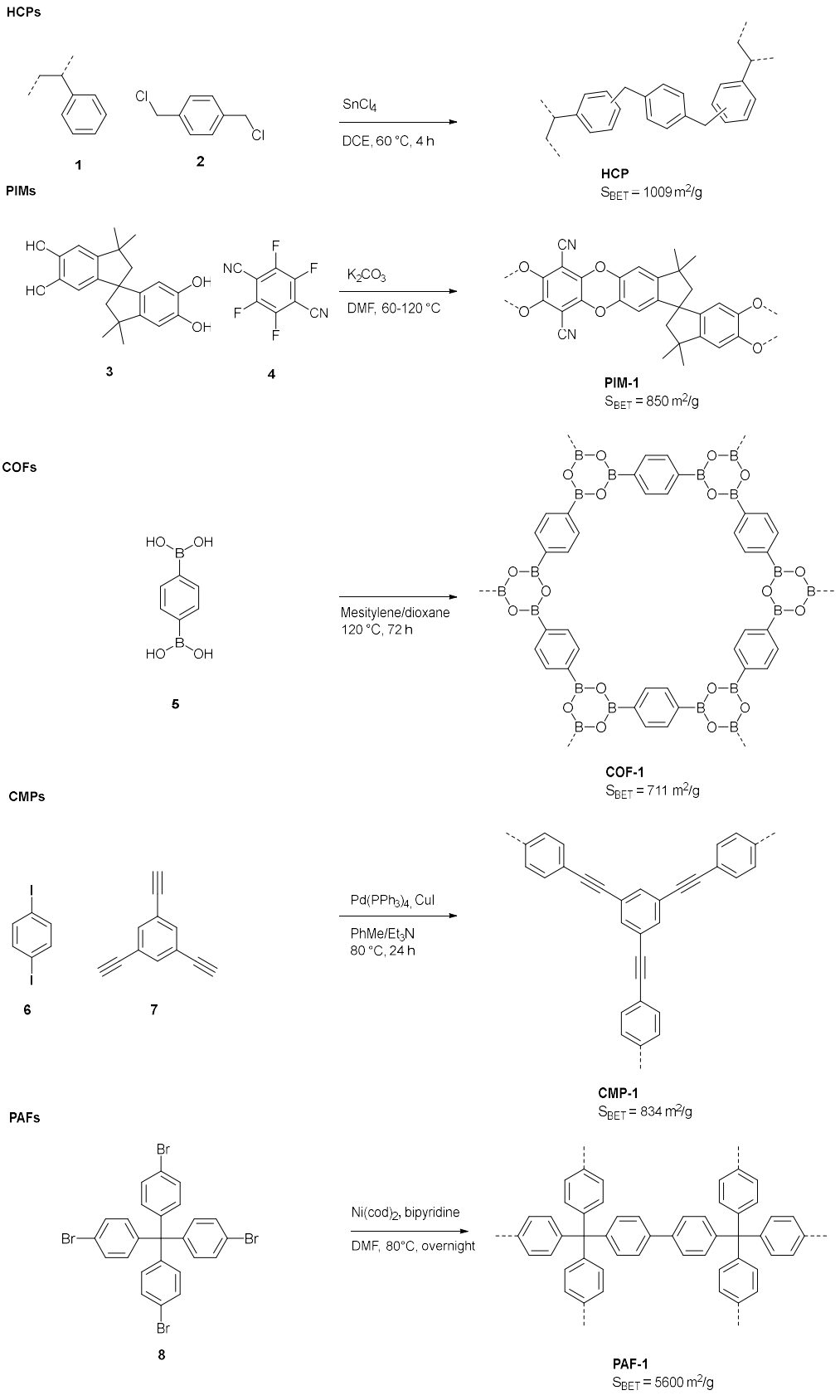

Scheme 1: Examples of the different classes of POPs.[20,23,25,31,33]

1.2 Acid catalysis

The catalysts now generally used for acid catalyzed reactions in industry are homogeneous, liquid acids (H_2SO_4, HF, H_3PO_4…). Replacing these mineral liquid acids with porous acidic materials has many advantages, such as easy separation of the catalyst, recyclability, reduction of corrosion… all leading to greener chemical synthesis.[38,39] Heterogeneous solid acids can be created by incorporating acidic groups in solid materials, either through direct synthesis or postfunctionalization. Many types of heterogeneous acids such as resins, zeolites and mesoporous silicas (MCM-41,[40,41] SBA-15[42]) have been developed. In general, silicas possess a lower catalytic activity than concentrated sulfuric acid or zeolites due to the presence of hydrophilic silanol groups on the surface of these materials. In many acid catalyzed reactions (*e.g.* esterification) water is a byproduct and adsorption of this byproduct near the acidic catalytic centers will compete with the reagents (*e.g.* an alcohol) resulting in reduced catalytic activity.[43,44] Zeolites generally possess pores that are quite small resulting in slow conversion of bulky substrates.[45] Sulfonated resins such as Amberlyst 15 can be effective acidic catalysts, but are challenged by their low surface areas and stabilities as the BET surface area of Amberlyst 15 amounts to only about 50 m^2/g.[46,47] Therefore, a lot of research has been performed to develop new, porous, fully organic acidic catalysts. This part will cover heterogeneous achiral acids, heterogeneous chiral phosphoric acids will be addressed in the part on chiral catalysts.

1.2.1 Sulfonic acids

In 2007, the Wu group introduced sulfonic acid moieties into purely organic mesoporous materials for the first time. To this end Fudan University (FDU)-type mesoporous polymers with cubic and hexagonal mesostructures **FDU-14** and **FDU-15** were prepared and sulfonated (Table 1, entry 1). FDU-type polymers are hydrothermally synthesized by a soft templating method were phenol **9** and formaldehyde **10** are polymerized around a templating agent, a triblock copolymer such as pluronic P123. The template is then removed, by thermal decomposition under vacuum at 350 °C, obtaining porous (463-545 m^2/g) and well-ordered polymeric materials.[48] Sulfonation was carried out by contacting the polymer powders with vapors from fuming sulfuric acid, to not destroy the ordered structures by direct contact with the acid. Following this, the porosity was well retained (447-539 m^2/g). The catalytic activity was evaluated for the liquid-phase Beckmann rearrangement of cyclohexanone oxime and the acetalization of hindered aldehydes. The sulfonated polymers performed much better than conventional acid resins (Dowex) or microporous zeolites (Beta, ZSM-5 or USY), especially when moving from benzaldehyde to the much more bulky 1-pyrenecarboxyaldehyde (Figure 1). Microporous materials pose much more stringent size limitations, and thus for bulky substrates only the external surface and the area nearby the pore entrances are accessible. However FDU type polymers possess much larger pore dimensions (>2 nm), and therefore can accept bulkier substrates.[43]

The first acid functionalized HCP was prepared by Xiao and coworkers in 2010 by sulfonation of superhydrophobic mesoporous polydivinylbenzenes (PDVB). These materials were prepared by hydrothermal polymerization of divinylbenzene (DVB) **11** in a sealed reaction medium at high temperatures and pressures (Table 1, entry 2). The solvent acts as a template and the polymer network is formed around it. Depending on the water/THF ratio different porosities were obtained. Functionalization by sulfonation was carried out by treatment with chlorosulfonic acid in dichloromethane or with sulfuric acid leading to **PDVB-x-SO_3H** possessing large surface areas (280-380

m^2/g), mesoporosity and a high density of sulfonic acid groups (3.9-4.1 mmol/g). The catalytic activity was evaluated by esterification of acetic, hexanoic and lauric acid with ethanol or cyclohexanol and by acylation of anisole with acetyl chloride. Higher activities than solid catalysts such as Amberlyst 15 or silicas (SBA-15-Pr-SO_3H, SBA-15-Ar-SO_3H) were obtained.[49]

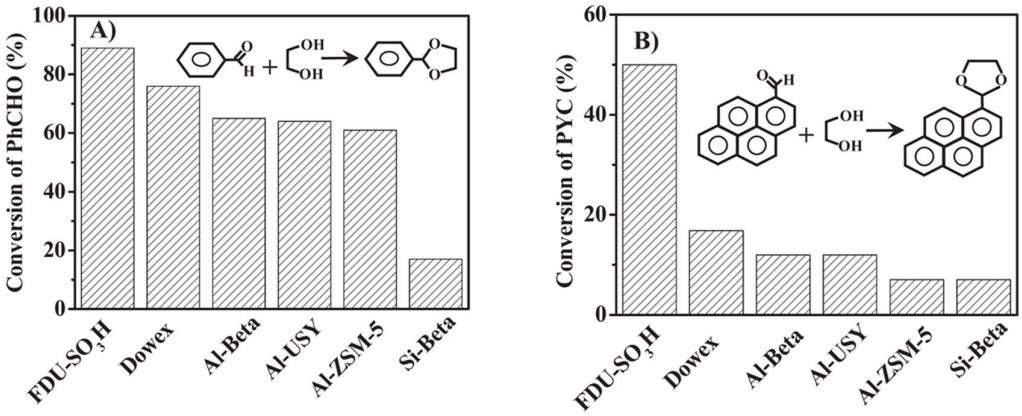

Figure 1: **FDU14-SO_3H** is a more active catalyst than other acidic heterogeneous catalysts for acetalization reactions, especially for bulky substrates. Reproduced from ref. [49].

Liu *et al*. prepared HCPs by copolymerization of a sulfonated monomer, sodium *p*-styrene sulfonate **12**, with DVB **11** resulting in very hydrophobic acid catalysts **H-PDVB-x-SO_3H's** where x is the molar ratio sulfonate to DVB ranging from 0.05 to 1.5 (Table 1, entry 3). Polymerization took place under solvothermal conditions, and after ion-exchange by washing with sulfuric acid highly porous networks (143-535 m^2/g) with abundant acidic sites (0.26-1.86 mol/g) were formed. The hydrophobicity of the polymers was studied by measurement of the contact angle of a water droplet in contact with the material. This angle ranged from 118° to 148° pointing to the high hydrophobicity of **H-PDVB-X-SO_3H's**. **PDVB-SO_3H** and Amberlyst 15 possess much lower contact angles of, respectively, 38° and 8°. These polymers are much more hydrophilic which correlates well with their higher acid loading of 4 and 4.7 mmol acid sites/g. The catalytic activity was evaluated for the esterification of acetic acid with cyclohexanol or 1-butanol, with conversion depending on the acid loading reaching, respectively, 55-78% and 70-90%. The acetalization of benzaldehyde with ethylene glycol could also be efficiently catalyzed, reaching 77-91% conversion. **H-PDVB-X-SO_3H's** performed ~20-30% better than **PDVB-SO_3H** or Amberlyst 15 and comparable to sulfuric acid, the homogeneous analogue. Importantly, the most hydrophobic POP, **H-PDVB-0.05-SO_3H**, showed the highest turnover frequency (TOF). This proves that the isolation of water from the catalytic sites leads to a significant enhancing of the reaction rate.[50]

The same group then used these superhydrophobic acid catalysts for hydroxymethylfurfural (HMF) **15** production by acid catalyzed dehydration of fructose **14**. Fructose, a simple carbohydrate that can be obtained from glucose **13** and thus also from cellulose, can in this way be transformed to a potential platform chemical. However this reaction typically is accompanied by yield reduction by hydration of HMF **15** to levulinic acid **16** and formic acid **17** (Scheme 2).[51,52,53] Using a superhydrophobic **H-PDVB-0.05-SO_3H** based catalyst the hydration can be prevented by isolating the acidic sites from water. In this way high yields (>99%) with HMF as a sole product were reached. Using H_2SO_4 or Amberlyst 15 the formation of side products by hydration was observed, leading to much lower yields of 54-62% and 46-66%, respectively. Furthermore, the authors developed a one-pot procedure directly converting glucose **13** *via* fructose **14** into HMF **15** by combining this acid catalyst with a hydrophilic

solid base synthesized by copolymerization of divinylbenzene, 1-vinylimidazole, and *N*,*N*-methylenediacrylamide and this combined system could reach high yields of up to 95%.[54]

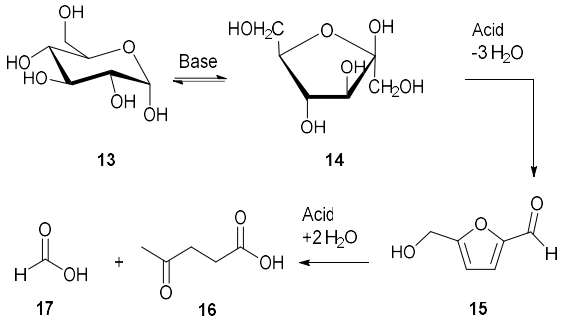

Scheme 2: HMF production by isomerization and dehydration of glucose **13**.

Noncovalent interactions around catalytic centers have an enormous influence on the selectivity and activity of catalysts. In enzymes, multiple non-covalent substrate-catalyst interactions, individually weak but collectively strong, stabilize transition states.[55] Synthetically precise control over the environment of a catalytical site, particularly in heterogeneous catalysts, remains a big challenge. In this light, Sun *et al*. encapsulated a polymeric solvent analogue in a COF functionalized with acidic sites to modulate the reaction environment (Scheme 3). These authors synthesized intermediate COFs via a three component condensation reaction with 1,3,5-tris(4-aminophenyl)benzene **18**, 2,5-dihydroxyterephthtalaldehyde **19** and 2,5-dimethoxyterephthtalaldehyde **20**. The phenolic groups of these COFs were then functionalized by reaction with 1,2,2-trifluoro-2-hydroxy-1-trifluoromethylethane-sulfonic acid sultone **21**. Polyvinylpyrrolidone (PVP) could subsequently be encapsulated by *in situ* polymerization of 1-vinyl-2-pyrrolidone **22** in the presence of the COF. PVP **23** is a polymeric analogue of *N*-methyl-pyrrolidinone (NMP), a high boiling and difficult to remove solvent known to suppress the formation of side products in fructose dehydration to HMF.[56,57] Using **PVP@[SO_3H]$_{0.17}$-COF** 100% conversion of fructose with 99% HMF yield was possible using THF as an easily removable solvent. This compared favorably to sulfonated resins such as Nafion™ NR50, Amberlyst 15 or homogeneous *p*-toluenesulfonic acid which only reached 9-29% fructose conversion and 5-21% HMF yield.[58]

Staying in the field of the renewable resources, Kundu *et al*. synthesized pyrene-based pops **PPOP-1,2,3** through Friedel-Crafts alkylation between pyrene **24** and 1,4-bis-(bromomethyl)benzene **25** at different molar ratio's in the presence of $FeCl_3$ as a catalyst. These materials were functionalized with sulfonic acid groups (2.15-3.22 mmol/g) by treatment with chlorosulfonic acid (Table 1, entry 4). These sulfonated polymers **SPPOP-1,2,3** were efficient catalysts for the synthesis of biodiesels at room temperature via (trans)esterification.[59] The same group prepared another sulfonated POP by postfunctionalization of **PDVTA-1**, a porous co-polymer prepared from divinylbenzene **11** and triallylamine **25** (Table 1, entry 5). Similar to the pyrene based materials these were highly active esterification catalysts for biodiesel production at room temperature.[60]

Another sulfonated POP for biodiesel production was prepared by Maiti *et al*. by Sonogashira coupling of triethynylbenzene **7** with brominated benzoselenadiazole **26** leading to **COP-1**. This material was then sulfonated furnishing **COP-2** (Table 1, entry 6) and used as an effective catalyst for the transesterification of free fatty acids at room temperature with yields reaching up to 100%.[61]

Yadav *et al*. prepared a sulfonated HCP **MeBP@H** through postmodification of a HCP consisting of tetramethylbiphenyl **27** crosslinked with 1,4-bis(chloromethyl)benzene **2** (Table 1, entry 7). **MeBP@H** was used as an acid catalyst for the synthesis of photochromic diphenylbenzo/naphthopyrans **30** from

phenols or naphthol's **29** and propargyl alcohols **28** (Scheme 4).[62] A wide range of substrates could be prepared in generally very good yields (54-95%). Triazole synthesis by cycloaddition of sodium azide to β-nitrostyrenes **31** could also be efficiently catalyzed, with a wide range of substituted β-nitrostyrenes **31** showing good conversion (86-95%). The authors reported that **MeBP@H** could be recycled at least ten times with no loss of activity.[63]

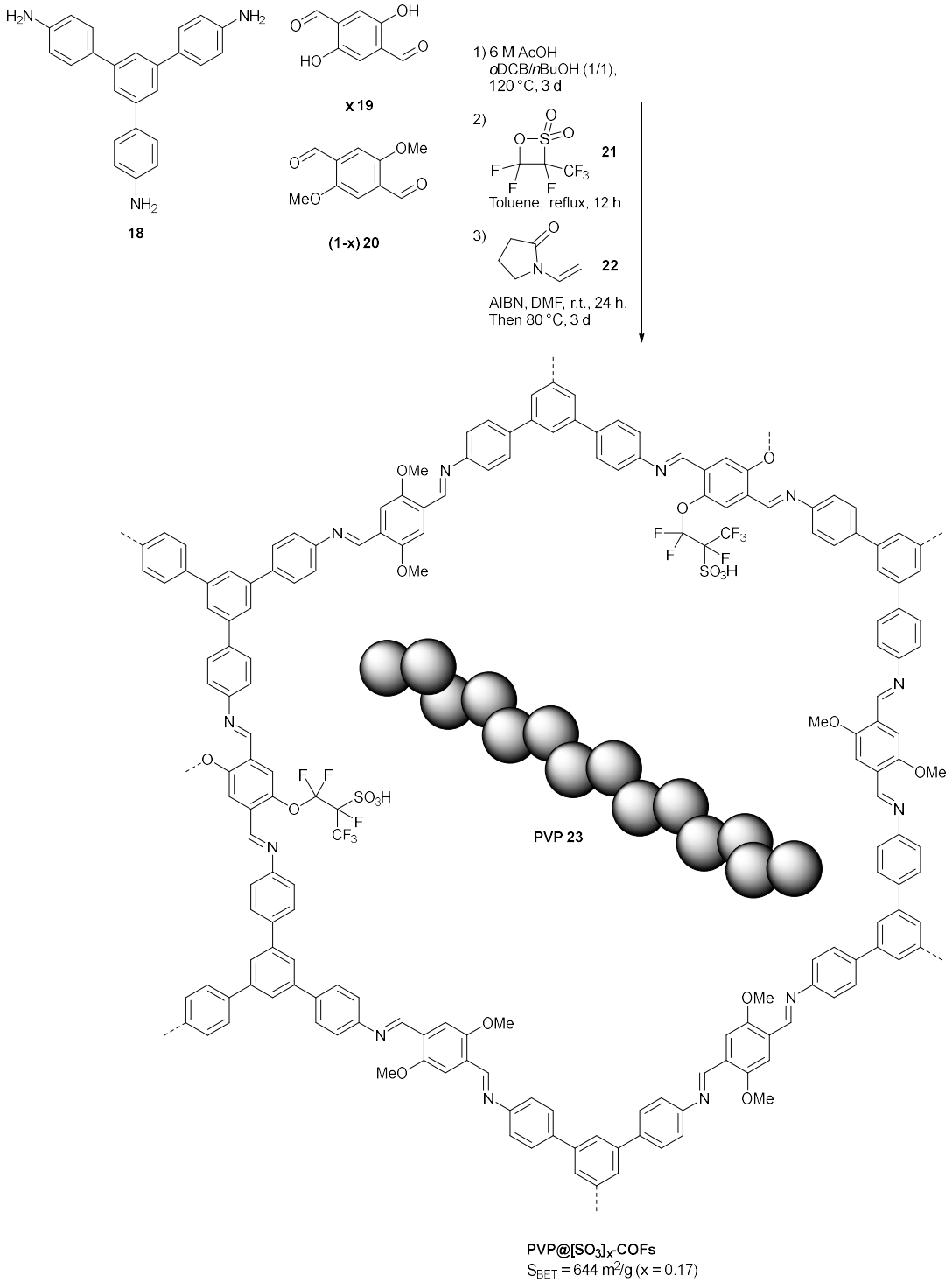

Scheme 3: Synthesis and postfunctionalization of a COF for HMF production.[58]

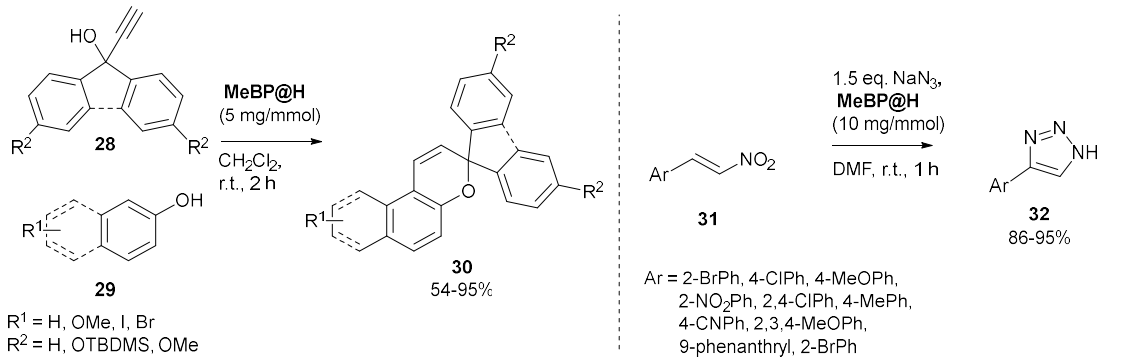

Scheme 4: Pyran and triazole synthesis catalyzed by **MeBP@H**.[63]

1.2.2 Carbon based acids

Weaker, carbon based acids can also be immobilized on porous polymers. In 2014, the Bhaumik group prepared POPs with free carboxylic acids by post-synthetic benzylic oxidation. A porous polymer was synthesized through Friedel-Crafts based $FeCl_3$ catalyzed crosslinking between 2,4,6-tris(bromomethyl)mesitylene **33** and 4,4'-bis(bromomethyl)-1,1'-biphenyl **34**. Treatment of this material with alkaline $KMnO_4$ oxidized the benzylic carbons furnishing **COP-A** with a high surface area of 1020 m^2/g (Table 1, entry 8). **COP-A** possessed abundant acidic sites (4.4 mmol/g) and could be used as an effective heterogeneous catalyst for indole C3 functionalization using benzhydrols **36** or aldehydes **39** as electrophiles (Scheme 5). For benzhydrols high catalyst loadings (44 mol%) and rather long reaction times were used and only moderate yields (55-65%) were attained. The aromatic aldehydes gave better results reaching high yields with lower catalyst loading and reaction times for a wide range of aldehydes. **COP-A** could be recycled at least five times, however yield reduction and reduction of the surface area to 740 m^2/g was observed.[64]

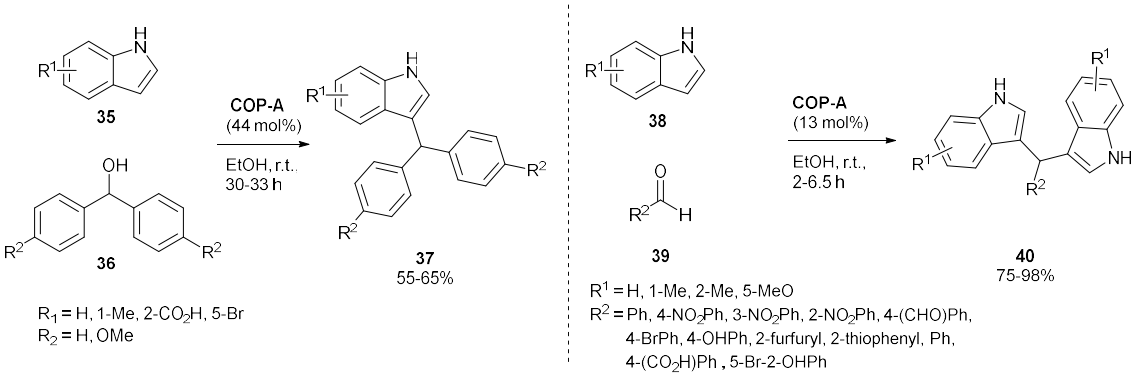

Scheme 5: Indole C3 functionalization with benzhydrols **37** or aldehydes **40** using **COP-A** as a catalyst.[64]

Even weaker acidic groups, such as terminal ethynyl hydrogens, can serve as acid catalysts. Sekerová *et al*. prepared HCPs by rhodium catalyzed crosslinking of monomers with two, three or four terminal ethynyl groups: 1,4-diethynylbenzene (DEB) **41**, 1,3,5-triethynylbenzene (TEB) **7**, tetrakis(4-ethynylphenyl)methane (TEPM) **42** (Table 1, entry 9). The resulting polymers were highly porous (711-1007 m^2/g) and possessed residual, unreacted acidic ethynyl groups (0.58-0.8 mmol/g). The acetalization of methanol with aldehydes gave moderate to high yields (50-98%) for the best performing network **P(TEB)**. Ketones, however, reacted much more sluggishly (13-36%) and

esterification of acetic, propionic and *cis*-hex-3-enoic acid gave only low yields (30-39%). The heterogeneous catalysts however were more active than their homogeneous counterpart phenylacetylene. The higher reactivity was explained by the increased acidity of the terminal hydrogen in the porous network due to the larger conjugated system formed by polymerization.[65]

1.2.3 Hydrogen bond catalysis

Hydrogen bonding organocatalysis forms an attractive alternative to Lewis acids.[66] The difference between polymers that catalyze reactions via hydrogen bonds and polymers containing basic nitrogens is not always very pronounced. Hydrogen bond forming polymers that act as catalysts in typically acidic transformations (*e.g.* acetalization) or hydrogen bond catalyzed transformations (*e.g.* Michael addition) will be discussed here. *N*-based polymers for other reactions will be discussed with the basic catalysts.

Zhang and coworkers prepared an aminal-linked POP **mPMF** by polymerization of melamine **43** with formaldehyde **10** in DMSO (Table 1, entry 10). This material possessed high porosity and served as an efficient hydrogen-bonding catalyst for the chemoselective acetalization of aldehydes, converting aldehydes, but not the less reactive ketones or esters. The catalytic activity is explained by dual activation: hydrogen bonding of the melamine nitrogens activating the alcohol **44** and hydrogen bonding of the aminal moieties activating the aldehyde **45** (Scheme 6).[67] Analogously, **MPOP** was synthesized by condensation of melamine **43** with terephthalaldehyde **46** in DMSO under microwave irradiation (Table 1, entry 11). This material possessed a high surface area (811 m^2/g) and was an effective catalyst for the acetalization of three different aldehydes with methanol or ethylene glycol in high yields (68-95%).[68] The same POP has also been reported as a catalyst for the Knoevenagel condensation and styrene oxidation (*vide infra*).[69,70]

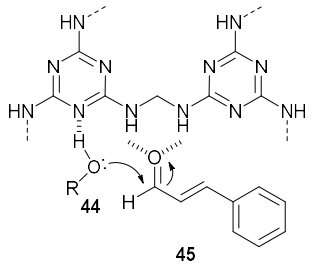

Scheme 6: Catalytic activity of **mPMF** by alcohol and carbonyl activation.[67]

Squaramide moieties can be excellent hydrogen bond catalysts, possessing hydrogen bond donating and accepting functionalities owing to their carbonyl and N-H groups. Self-aggregation can pose availability problems, but this can be solved conveniently by incorporating the catalytic moieties in heterogeneous frameworks, such as in MOFs constructed with squaramide based linkers.[71–73] A squaramide decorated framework **COF-SQ** was synthesized by Li *et al*. through condensation of squaramide amine linker **47** and tritopic aldehyde **48** (Table 1, entry 12). In this work, the term 'topicity' is used to describe the number of connecting points present on a building block. **COF-SQ** was reported as a good catalyst for the Michael addition of dicarbonyl compounds **50** with nitrostyrenes **49** (Scheme 7, A). A wide range of electrophiles and nucleophiles could be converted in high yields (63-98%). **COF-SQ** was stable, could be reused at least four times. **COF-SQ** showed much higher activity than the homogeneous monomer **47** and a model compound consisting of the monomer condensed

with benzaldehyde, due to the inability of the squaramide moieties in the framework to self-aggregate.[74]

Recently, Wu *et al*. synthesized novel POPs based on the condensation of amine **52** with isothiocyanate **53** (Table 1, entry 13). These materials **POP-TUs** possessed rather low porosities, which seems to be a general issue with urea or thiourea based POPs. This is postulated to be caused by hydrogen bonding interactions between reactant and solvent molecules during framework synthesis. The formed thiourea networks were active catalysts in the Michael reaction of nitrostyrenes **49** with diethylmalonate **50** (Scheme 7, B). A very wide range of substrates could be converted in high yields (56-89%) using low catalyst loadings.[75]

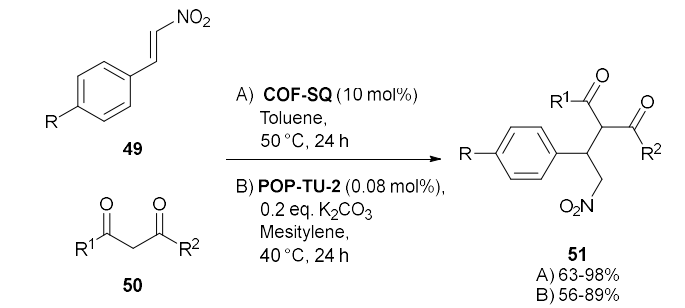

A) R = Ph, 4-MePh, 4-MeOPh, 4-ClPh, 4-BrPh
R^1, R^2 = H, H; H, OEt; H, OMe; Me, OMe

B) R = Ph, 2-ClPh, 3-ClPh, 4-ClPh, 4-BrPh, 4-FPh, 4-MePh, 4-EtPh, 4-MeOPh, 3-MeOPh, 2-CF_3Ph, 2-NO_2Ph. 3-Br-4-FPh, 2-Furyl, 2-Naphthyl
$R^1 = R^2$ = OEt

Scheme 7: Michael addition catalyzed by **COF-SQ** or **POP-TU-2**. [74,75]

1.2.4 Outlook on POPs as acid catalysts

To conclude, sulfonated POPs reach efficiencies comparable to or higher than homogeneous sulfuric acid, and typically higher than sulfonated resins such as Amberlyst-15. This resin is a commonly available solid acid for which many applications as a green catalyst have been described: etherification, olefin hydration, esterification, etc.[76–78] The higher efficiency of the POPs is caused by: their generally higher porosity, in some cases a more pronounced mesoporosity (*e.g.* the FDU type polymers) and in other cases the highly hydrophobic character of the used POPs.

A plethora of catalytic systems have already been described for the production of HMF, however, unless when using harsh conditions (such as heating at 160 °C under microwave irradiation) quite low yields are reached.[79,80] A state of the art heterogeneous (metal-free) catalyst would be an Amberlyst resin used in DMSO at 120 °C.[80,81] The performance of the two catalytic systems described, which worked well at 100 °C in THF, giving no side reactions, can thus be considered as state of the art. Catalytic biodiesel production has been extensively reviewed and typical catalysts are acids, bases or enzymes (lipases).[82,83,84] Homogeneous cheap bases, such as KOH or NaOH, are preferred in industry. However, they pose environmental concerns and no regeneration of these catalysts is possible. Moreover, alkali catalysts, while more active than acidic catalysts[83,84] are incompatible with the presence of water and free fatty acids (FFAs) due to saponification reducing the yield and quality of the resulting biodiesel.[85,86] Acids, whilst less active than bases for this transformation tolerate FFAs because they also catalyze esterification, allowing the use of lower quality waste oil.[84] Generally, in

literature very harsh conditions are reported for acceptable conversions under acidic catalysis. Sulfated metal oxides, metal oxide mixtures and supported heteropolyacids are reported, however, they suffer from high required temperatures, leaching or deactivation in the presence of water.[84] The organic solid acids consist mainly of resins such as Amberlyst-15 and these are less effective than the POPs we discussed, providing lower conversions or requiring higher temperatures.[87]

The POPs discussed here as hydrogen bond catalysts, whilst interesting materials, are lagging behind the state of the art for homogeneous hydrogen bond mediated catalysis, which is already applied in the catalysis of enantioselective transformations.

The synthesis of the polymers, in the case of the HCPs synthesized by radical crosslinking, **PDVB-x-SO_3H**, **H-PDVB-X-SO_3H**, **PDVTA-SO_3H** (Table 1, entry 2, 3 and 5), was comparable to the synthesis of Amberlyst-15, *i.e.* crosslinking by co-polymerization with divinylbenzene followed by sulfonation. In the case of the amidine-linked polymers **mPMF** and **M-POP** (Table 1, entry 10 and 11) no catalysts or dangerous solvents were needed, however, in many cases the synthesis is more problematic. The HCPs synthesized by Friedel-Crafts crosslinking **SPPOP-1,2,3, MeBP@H** and **COP-A** (Table 1, entry 4, 7 and 8) typically use very large excesses of corrosive Lewis Acids ($FeCl_3$, $AlCl_3$) and toxic and carcinogenic DCE as a solvent. The CMPs **COP-2** and **P(DEB)**, **P(TEB)** and **P(TEPM)** (Table 1, entry 6 and 9) use precious metal based catalysts and non-recommended solvents (DCE, CH_2Cl_2, Et_3N).[88] The ethynyl functionalized building blocks **7**, **41** and **42** also pose problems, being very expensive or even commercially unavailable. The COF **PVP@$[SO_3H]_{0.17}$-COF** (Scheme 3) while being very performant, has a problematic synthesis, which extends into COF synthesis in general. All three building blocks **18**, **19** and **20** are barely commercially available and require multiple step synthesis, using hazardous reagents. Triflic acid and hydrazine were used in the synthesis of the amine **18**. A blanc chloromethylation, known to produce highly carcinogenic bis (chloromethyl)ether as a side product[89] is one of the steps to synthetize the aldehydes **19** and **20**. Moreover, the polymerization itself is only reported (as is typical for COFs) on a small scale (0.5 mmol, ~200 mg), required heating at 120 °C for three days and three more postfunctionalization steps. **COF-SQ** (Table 1, entry 12) is similarly hampered by difficult to synthesize building blocks. Aldehyde **48** is typically produced by a very inefficient synthesis starting from 1,3,5-benzenetricarboxylic acid requiring esterification to the triester, reduction to the triol with hazardous $LiAlH_4$ and oxidation with carcinogenic hexavalent chromium based PCC.[90] The polymerization into the COF itself used non-recommended solvents, required heating at 120 °C for three days and at was again performed at a very small scale (0.15 mmol, ~50 mg).

Table 1: POPs as acidic or hydrogen bonding catalysts.

Entry: Name	Monomers	Linkage	Conditions	Surface area (m^2/g)	Ref.
1: **FDU14-SO_3H**, **FDU15-SO_3H**	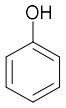 **9**  **10**	C-C	1) 0.1 M NaOH, H_2O, 72 °C, 1.5 h 2) Pluronic P123, H_2O, 72 °C, 120 h, Then 80°C, 48 h 3) 350 °C, 6 h 4) 50% SO_3/H_2SO_4 vapors, 60 °C, 24 h	447-539	[43]
2: **PDVB-x-SO_3H**	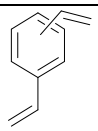 **11**	C-C	1) AIBN, THF/H_2O (x), r.t, 3 h, Then 100 °C, 48 h 2) $ClSO_3H$, CH_2Cl_2, 0 °C, 12 h	280-380	[49]
3: **H-PDVB-X-SO_3H**	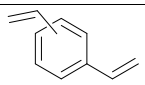 **11** 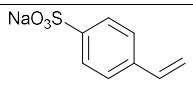 **12**	C-C	1) AIBN, THF/H_2O, r.t., 3 h Then 100 °C, 24 h 2) 1 M H_2SO_4, r.t., 24 h	143-535	[50]
4: **SPPOP-1,2,3**	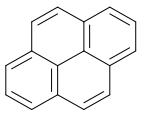 **24** 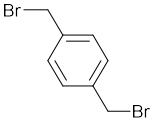 **25**	C-C	1) $FeCl_3$, DCE, 80 °C, 20 h 2) $ClSO_3H$, CH_2Cl_2, r.t., 48 h	205-280	[59]
5: **PDVTA-SO_3H**	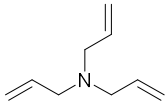 **26** 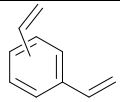 **11**	C-C	1) AIBN, Acetone, 120 °C, 24 h 2) $ClSO_3H$, CH_2Cl_2, r.t., 4 h	406	[60]
6: **COP-2**	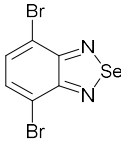 **26** 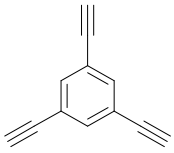 **7**	C-C	1) $Pd(PPh_3)_2Cl_2$, CuI Et_3N, 72 h 2) $ClSO_3H$, CH_2Cl_2, 0 °C, 48 h	159	[61]
7: **MeBP@H**	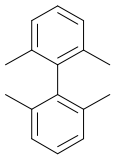 **27** 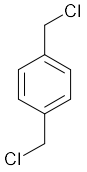 **2**	C-C	1) $FeCl_3$, DCE, 80°C, 48 h 2) $ClSO_3H$, CH_2Cl_2, 0 °C to r.t., 72 h	766	[63]
8: **COP-A**	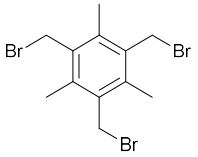 **33** 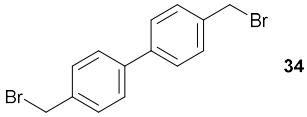 **34**	C-C	1) FDMA, $FeCl_3$, DCE, reflux, 20 h 2) $KMnO_4$, NaOH, H_2O/EtOH, 30-32 h, 80 °C	1020	[64]

9: **P(DEB), P(TEB), P(TEPM)**	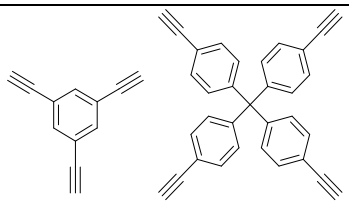 7 42 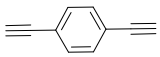 41	C-C	Rh(nbd)(acac), CH_2Cl_2, 70 °C, 72 h	711-1007	[65]
10: **mPMF**	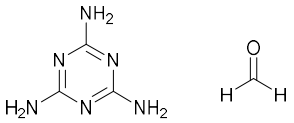 43 10	Amidine	Paraformaldehyde, DMSO, 120 °C, 1 h, Then 170 °C, 72 h	930	[67]
11: **M-POP**	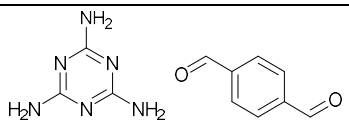 43 46	Amidine	MW, DMSO, 160 °C, 2 h	811	[68]
12: **COF-SQ**	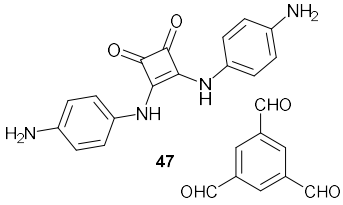 47 48	Imine	6 M AcOH, Mesitylene/dioxane (1/1) 120 °C, 72 h	1195	[74]
13: **POP-TUs**	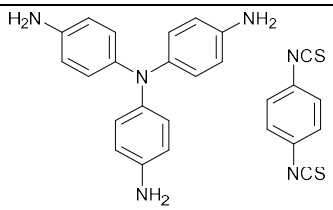 52 53	Thiourea	DMF, Dioxane, EtOH or EtOH/Dioxane, 60 °C, 72 h	23-49	[75]

1.3 Basic and nucleophilic catalysts

1.3.1 The Knoevenagel condensation

The condensation between a carbonyl group **55** and active methylene compounds **54**, or the Knoevenagel condensation, is a powerful and frequently used reaction for the formation of C–C bonds and is applied in industry (Scheme 8).[91,92] Typically homogeneous catalysts[93–96] are used, but many heterogeneous catalysts such as MOFs,[97,98] periodic mesoporous organosilicas (PMOs),[99] zeolites[100] and graphene-based materials[101,102] have been developed. The Knoevenagel condensation serves as a reference reaction of sorts for heterogeneous basic catalysts. In general these materials contain high amounts of nitrogen and have high CO_2 adsorption and selectivity.

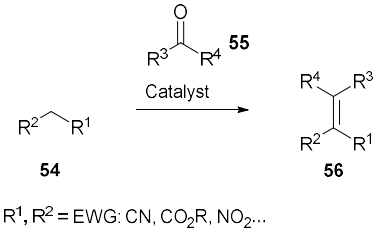

Scheme 8: The Knoevenagel condensation.[92]

In one of the earliest reports on porous polymers applied in the field of heterogeneous organocatalysis, Makowski *et al*. utilized a mesoporous polybenzimidazole network **mp-PDI** as a catalyst for the Knoevenagel condensation. **mp-PDI** was synthesized by LUDOX templated polybenzimidazole synthesis of monomers **57**, **58** and **59** (Table 2, entry 1).[103] LUDOX HS-40 is a commercially available 40 wt% dispersion of silica nanoparticles, with a diameter of about 13 nm, which act as a hard template in the polymerization reaction. By heating of the monomer mixture up to 400 °C, complete ring closure could be achieved. The template was then removed by etching with ammonium hydrogen difluoride (NH_4HF_2), followed by washing with dilute sodium hydroxide to deprotonate the imidazolium moieties. High yields of up to 100% were reported for the reaction of ethyl cyanoacetate or malononitrile with a range of aldehydes at room temperature or at 100 °C.[104]

Liu *et al.* synthesized another porous polymer **JUC-Z12** by benzimidazole formation between tetra(4-formylphenyl)methane **61** and 3,3'-diaminobenzidine **60** (Table 2, entry 2). **JUC-Z12** possessed a large surface area of 750 m^2/g and by virtue of its basic benzimidazole moieties could serve as an efficient catalyst for the Knoevenagel reaction.[105]

Another benzimidazole containing polymer was synthesized by Wang and coworkers through Sonogashira coupling of brominated benzimidazole **64** with tritopic building block **62** or tetratopic building block **63** furnishing **BPOP-1** and **BPOP-2** (Table 2, entry 3). The latter possessed good porosity (668 m^2/g), however the former was non-porous for nitrogen. Both POPs were capable of CO_2 adsorption with **BPOP-1** and **BPOP-2** absorbing, respectively, 50 mg/g and 103 mg/g CO_2 (273 K, 1 bar). Predictably due to its higher porosity **BPOP-2** was able to catalyze the Knoevenagel condensation better.[106]

Dang *et al.* synthesized heptazine based polymer networks **Cy-pip** via coupling of cyameluric chloride **66** and piperazine **65** (Table 2, entry 4). Heptazines, with their large conjugated systems consisting of three condensed triazine rings have already found widespread application in heptazine based carbon nitrides. The resulting framework had a relatively low BET surface area of 116 m^2/g. The high nitrogen

content furnished **Cy-pip** with a good CO_2 uptake capacity (103 mg/g, 1 bar, 273 K) and catalytic activity for the Knoevenagel reaction, converting a range of aldehydes in generally excellent yields (up to 97%).[107]

Carta *et al.* applied a polymerization reaction based on the formation of Tröger's base on triamino-triptycene monomers **67** (Scheme 9 and Table 2, entry 5). Tröger's base is a bridged bicyclic amine, formed by condensation of *p*-toluidine and formaldehyde dimethyl acetal (FDMA) **68**. The basicity of its nitrogen is enhanced due to the constraints in the rigid bicyclic system reducing the conjugation of the free nitrogen electrons into the aromatic rings.[108] After polymerization of monomers **67** in trifluoroacetic acid, polymers **PIM-Tb-Trip1,2** with a high density of basic amine sites of up to 8.5 mmol/g and high surface areas of up to 1035 m^2/g, were obtained. Copolymerization with a flexible, bis-amine co-monomer **69** led to **PIM-Tb-Trip1**. The co-monomer allows formation of a more flexible network that is able to fill space more efficiently, and thus the resulting material possessed no surface area. All three materials were able to catalyze the Knoevenagel condensation. **PIM-Tb-Trip3** was as active as homogeneous Tröger's base, while for **PIM-Tb-Trip1,2** the turnover number and frequency (TON and TOF) indicate that the catalytic units embedded in the polymer are more than twice as active than when freely soluble as a homogeneous catalyst.[109]

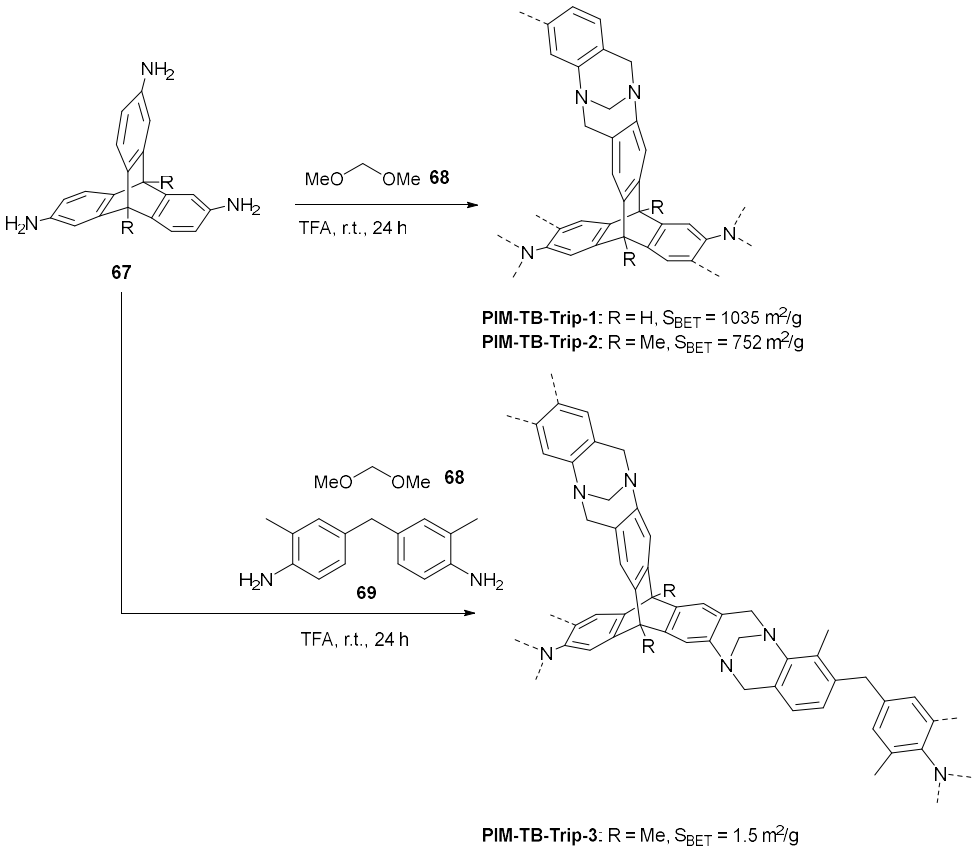

Scheme 9: Synthesis of **PIM-TB-Trip-1-3** by Tröger's base formation.[109]

The first application of a 3D COF as a heterogeneous catalyst was reported by Fang *et al*. in 2014. These authors utilized adamantylamine based COFs as amine base catalysts for the Knoevenagel condensation. Two 3D COFs were formed by condensation of tetrahedral alkyl amine 1,3,5,7-tetraaminoadamantane **70** with 1,3,5-triformylbenzene **48** or triformylphloroglucinol **71** (Table 2, entry 6). Due to the alkylamine building block being endowed with higher basicity than aromatic

amines, the formed imines were more basic than in the typically fully aromatic imine-linked COFs. **BF-COF-1** and **BF-COF-2** were active in the Knoevenagel condensation and importantly showed very high size selectivity. The reaction of benzaldehyde with malononitrile gave almost full conversion of 96% or 98% for **BF-COF-1** and **BF-COF-2**, respectively, however larger substrates such as 4-methylbenzaldehyde, 4-phenylbenzaldehyde, 4-(4-methylphenyl)benzaldehyde showed almost no conversion (2-4%). The product of the reaction with benzaldehyde has a size of 7.6*10.4 $Å^2$ and is small enough to fit inside the pores, which have a size of 7.8 x 11.3 $Å^2$ and 7.7 x 10.5 $Å^2$ for **BF-COF-1** and **BF-COF-2**, respectively. However for the larger substrates, the products no longer fit inside the pores, thus the reaction is only possible at the outer surface of the materials and is therefore much slower.[110]

The aminal-linked POP formed by condensation of melamine **43** with terephthalaldehyde **46** in DMSO (Table 2, entry 11) could also efficiently catalyze the Knoevenagel condensation of aromatic aldehydes with ethyl cyanoacetate in a green solvent, water, at 120 °C under microwave heating showing good conversions and selectivities of 44-99% and 65-99%, respectively, within ten minutes.[69]

Zhang *et al*. synthesized a carbazole based polymer **MFCMP-1** by oxidative polymerization of easily synthesized 2,4,6-tris-(carbazolo)-1,3,5-triazine **72** (Table 2, entry 7). The resulting highly porous (843 m^2/g) material was multifunctional, showing high CO_2 adsorption capacity of 16.2 wt% or 3.69 mmol/g (273 K, 1 bar) and great catalytic activity for a range of aldehydes in the Knoevenagel condensation. Next to this, it demonstrated selective fluorescence quenching in presence of nitroaromatic compounds, a useful luminescent property for the detection of explosive compounds.[111]

A hypercrosslinked porous polyporphyrin was prepared by Feng *et al.* by crosslinking of tetracarbazole substituted porphyrin **73** with FDMA **68** (Table 2, entry 8). The resulting material **HCP-TCPP** possessed a high surface area of 1050 m^2/g and was an effective catalyst for the Knoevenagel condensation between various aldehydes and malononitrile with yields ranging from 85 to 95%.[112] Liu *et al*. synthesized a metal-free porphyrin-linked polymer **HP_E-CMP** by alkyne-alkyne homocoupling of building block **74** furnishing a highly porous (662 m^2/g) material with a high carbon dioxide uptake of 3.58 mmol/g (273K, 1 bar) and good activity in the Knoevenagel reaction (Table 2, entry 9). The material could be recycled at least ten times and in a large-scale experiment with one gram of benzaldehyde, only a milligram of catalyst resulted in a high yield of 92% after ten hours.[113] Another porphyrin POP **Fe-PoP-1** was synthesized by Bhaumik and coworkers through $FeCl_3$ catalyzed aromatic substitution of pyrrole **75** and terephthalaldehyde **46** (Table 2, entry 10).[114] It should be mentioned that this polymerization reaction resulted in very low yields (21-44%). Nevertheless, the resulting bifunctional material possessed basic sites able to catalyze Knoevenagel condensations of malononitrile with a range of aldehydes. Furthermore, the Fe^{III} sites were able to catalyze selective oxidation reactions of a wide range of alcohols to aldehydes or ketones using *tert*-butyl-hydroperoxide as oxidant.[115]

Most existing POPs possess monomodal porosity. Constructing materials with well controlled hierarchical porosity can lead to higher surface areas and better mass transfer. Ideally continuous macroporous channels are combined with micro- and mesopores. Zhang *et al*. developed a promising methodology to synthetize hierarchical porous materials by templating of core-shell bottlebrushes. Bottlebrush copolymers are highly branched macromolecules, possessing comb like architectures with steric repulsions of the side chains constraining the backbone of the polymer in an extended chain conformation.[116] Hypercrosslinking of the styrene shell of bottlebrush **76**, followed by etching of the PLA core and Boc-deprotection led to formation of amino functionalized microporous organic nanotube networks **NH_2-MONNs** with a BET surface area of 936 m^2/g (Scheme 10 and Table 2, entry 11). This material could serve as a highly efficient catalyst in the Knoevenagel condensation between

benzaldehyde and ethyl cyanoacetate with the conversion reaching 97% after only fifteen minutes. A nonporous polymer analogue and the homogeneous NH_2-bottlebrush reacted much slower with conversions of only 14% and 81%, respectively, after 45 minutes. The **NH_2-MONNs** could be recycled more than ten times with no significant decrease in catalytic activity and a range of aldehydes were reacted in high yields (85-99%). Moreover, **NH_2-MONNs** could also catalyze the Henry reaction between *p*-nitrobenzaldehyde and nitromethane in 99% yield after seventeen hours. Analogous polymers have also been used to perform one-pot deacetalization-Knoevenagel reactions (Section 1.4.1).[117]

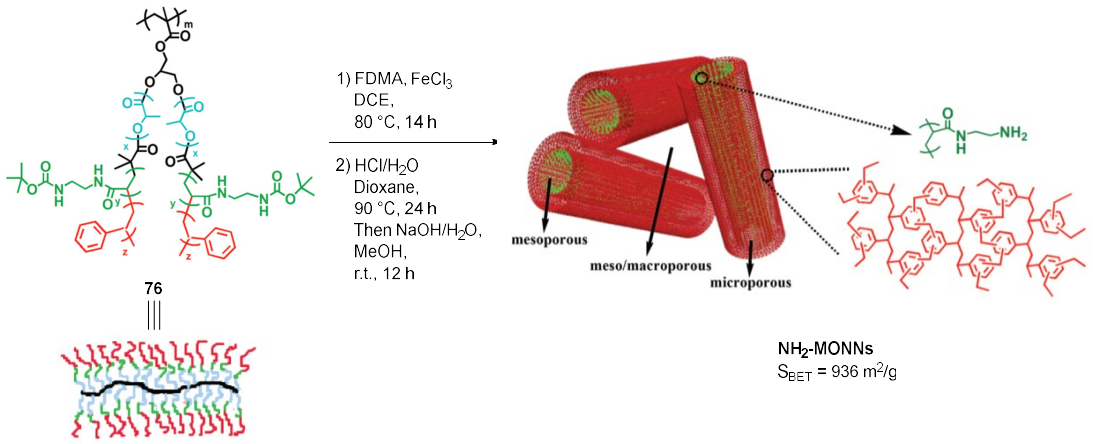

Scheme 10: Synthesis of NH_2-MONNs by crosslinking, etching and deprotection of bottlebrush polymer **76**. Adapted from ref. [117].

Similarly, Zhu *et al*. prepared urea functionalized mesoporous polymers **urea-MPs** through polymerization of phenol **9**, formaldehyde **10** and urea **77** around a block copolymer (F127), followed by calcination at 350 °C to remove the template. Depending on the urea content, surface areas of 258 to 403 m^2/g were reached (Table 2, entry 12). **Urea-MPs** were good catalysts for the Knoevenagel condensation in water, reaching high yields (up to 94%) for both aryl aldehydes substituted with electron donating (*e.g.* methoxy) and electron withdrawing (*e.g.* nitro) substituents and different active methylene compounds (1,3-diketone, β-keto-ester and 1,3-diester).[118] Dey *et al*. synthesized a microporous polyurethane **MPU** by reaction between di-isocyanate **78** and triol **79** in DMSO (Table 2, entry 13). Interestingly, as was the case with **BF-COF-1 and BF-COF-2**, size selectivity was observed. **MPU** was able to catalyze the Knoevenagel condensation (95-99%) for a wide range of substituted benzaldehydes. However 9-anthracenecarboxaldehyde and biphenyl-4-carboxaldehyde did not react at all, suggesting that the reaction occurs in the pores of the materials.[119]

An amide-linked polymer **Am-POP** was synthesized by reaction of *p*-phenylenediamine **81** with trimesoyl chloride **80** (Table 2, entry 14). **Am-POP** possessed no surface or uptake for N_2 or other gases such H_2 or Ar, however it did show CO_2 affinity (36 mg/g, 273 K, 1 bar). This was calculated to occur mainly through Lewis acid-base interaction of CO_2 with the amide oxygen, weak hydrogen bonding with the phenyl C-H and π-π stacking. Furthermore, **Am-POP** demonstrated good activity in the Knoevenagel reaction. This contrasts with its homogeneous analogue triphenylbenzamide, which showed no appreciable conversion.[120]

Base functionalized ionic liquids are known alternatives for traditional bases.[121] Therefore, Wang *et al*. prepared basic mesoporous poly(ionic liquid)s **PAMBn** by radical copolymerization of 1-aminoethyl-3-vinylimidazolium bromide **82** with divinylbenzene **11** followed by ion exchange of the bromide with sodium hydroxide (Table 2, entry 15). The resulting materials possessed surface areas of 123 to 429

m^2/g, depending on the ratio of imidazolium monomer to crosslinker. These polymers were good catalysts in the Knoevenagel and aldol condensations. A range of aldehydes were converted with ethyl cyanoacetate or malononitrile in short reaction times and good yields (93-99%). Very high TOFs of up to 572/h were reported, about five times more than the homogeneous monomer. The reaction is enhanced by the combination of nucleophilic (NH_2) and basic (OH^-) moieties. Like the already discussed sulfonated HCPs these polymers are superhydrophobic. This property prevents poisoning by moisture if stored in air, and allows for the quick release of the formed water during the reaction. Moreover, the material was able to catalyze the aldol condensation between benzaldehyde and acetophenone, under solvent free conditions at 120 °C, furnishing 85% conversion to chalcone.[122]

1.3.1.1 Outlook on POPs catalyzing the Knoevenagel reaction

Enormous amounts of (heterogeneous) catalysts have been reported to catalyze the Knoevenagel condensation: zeolites, MOFs, mesoporous silicas, metal oxides, carbon nitrides, etc.[123,124] However, homogeneous simple bases such as piperidine, β-alanine, pyridine or even NaOH are still used most often for this transformation. For example, β-alanine is used in the synthesis of atorvastatin (Lipitor), Pfizer's blockbuster, cholesterol lowering drug. Piperidine is applied in the synthesis of pioglitazone, an anti-diabetic medication.[125] NaOH is being used in the commercial production of lumefantrine, an antimalarial drug.[126] These homogeneous catalysts are commonly available, cheap and perform well, making it harder for more complex, heterogeneous catalysts to find widespread adaptation. The POPs described in this review generally showed very good activity. However, often there was no comparison with other catalysts, and it is difficult to compare the results because barely any (initial) TOFs or TONs are reported. Similarly to many basic MOFs, the reaction was frequently only performed as a proof of concept and not studied in detail.[123]

Regarding the synthesis of the materials many of the same remarks as before can be made. In a lot of cases very harsh conditions and hazardous reagents were being used. For example, the HCP **MFCMP-1** (Table 2, entry 7) required a very large excess (>15 equivalents) of hazardous $FeCl_3$, which is typical for HCPs produced by Friedel-Crafts crosslinking. The CMPs (Table 2, entry 3 and 9) required precious metal based couplings. Moreover, many difficult to access monomers were being used such as the borylated compounds **62** and **63**, amine **70**, aldehydes **48** and **71**, porphyrins **73** and **74** and bottlebrush copolymer **76**.

Table 2: POPs for the Knoevenagel condensation.

Entry: Name	Monomers	Linkage	Conditions	Surface area (m^2/g)	Ref.
1: **Mp-PDI**	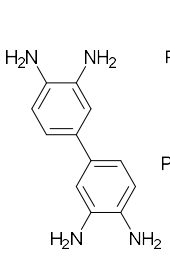 57 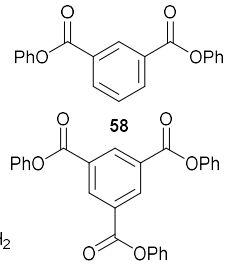 58 59	Benz-imidazole	1) LUDOX-HS-40, 200 °C, 1.5 h Then 400 °C, 0.5 h 2) 4 M NH_4HF_2, r.t., 72 h 3) 0.1 M NaOH	180	[103], [104]
2: **JUC-Z12**	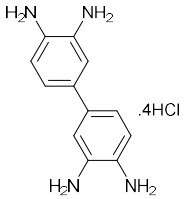 60 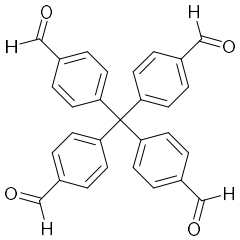 61	Benz-imidazole	DMF, -40 °C to r.t., 130 °C, 3 d	750	[105]
3: **BPOP-1/2**	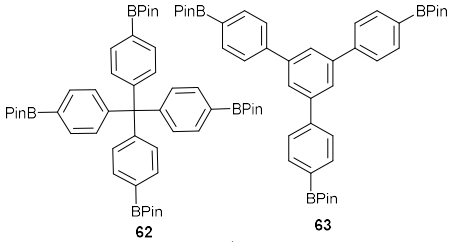 62 63 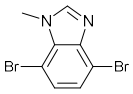 64	C-C	$Pd(PPh_3)_4$, K_2CO_3, Dioxane, 110 °C, 24 h	0-668	[106]
4: **Cy-pip**	 65 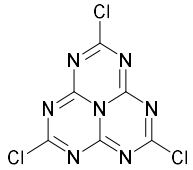 66	N-C	DIPEA, THF, 0 °C, 4 h Then r.t., 4 h Then reflux, overnight	116	[107]
5: **PIM-Tb-Trip1/2/3**	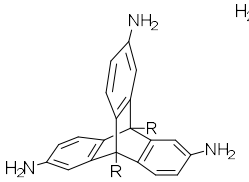 67 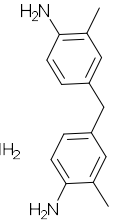 69	N-C	FDMA, TFA, r.t., 24 h	1.5-1035	[109]
6: **BF- COF-1/2**	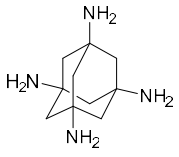 70 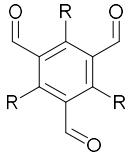 **48**: R = H **71**: R = OH	**51**: imine **52**: β-keto enamine	3 M AcOH, mesitylene, 120 °C, 5 d	**51** (BF-COF-1): 730 **52** (BF-COF-2): 680	[110]

7: **MFCMP-1**	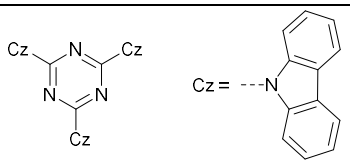 **72**	C-C	$FeCl_3$, $CHCl_3$, reflux, 72 h	843	[111]
8: **HCP-TCPP**	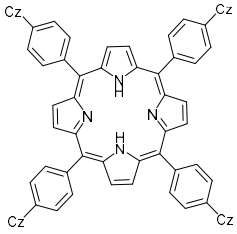 **73**	C-C	FDMA, TfOH, *o*DCB, 100°C, 12 h	1050	[112]
9: **HPE-CMP**	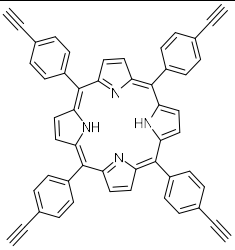 **74**	C-C	$Pd(PPh_3)_2Cl_2$, CuI, THF/Et_3N, 80 °C, 72 h	662	[113]
10: **Fe-PoP-1**	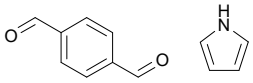 **46** **75**	Porphyrin	$FeCl_3$, AcOH, r.t., 3 h, Then 180 °C, 72 h	875	[114], [115]
11: **NH2-MONNs**	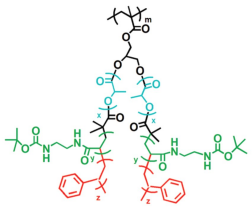 **76**	C-C	1) FDMA, $FeCl_3$, DCE, 80 °C, 14 h 2) Aq. HCl, dioxane, 90 °C, 24 h, Then NaOH/H_2O, MeOH, r.t., 12 h	936	[117]
12: **Urea-MPs**	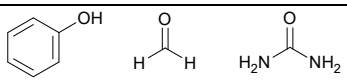 **9** **10** **77**	N-C, C-C	1) NaOH, 70 °C, 2 h 2) F127, EtOH, 120 °C, 24 h 3) 350 °C, 4 h	258-403	[118]
13: **MPU**	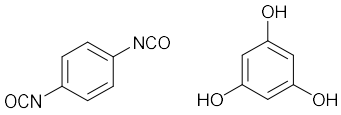 **78** **79**	Urethane	DMSO, 150 °C, 72 h	312	[119]
14: **Am-POP**	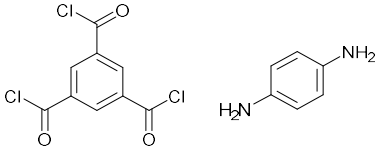 **80** **81**	Amide	Et_3N, THF, 0 °C to r.t., 18 h	/	[120]
15: **PAMBn** (n = **82**/**11**, 0.5-5)	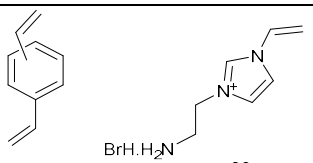 **11** **82**	C-C	1) AIBN, EtOH/H_2O (3/1), 80 °C, 24 h 2) 1 M NaOH, H_2O, r.t., 72 h	123-429	[122]

1.3.2 Transesterification

As stated before, a problem with base catalyzed transesterification of oils is the incompatibility of the basic catalysts with water and FFAs, common contaminants in waste oil.[85,86] To obtain a water-tolerant basic catalyst Liu *et al*. prepared **PDVB-VI-n** by hydrothermal co-polymerization of divinylbenzene **11** and 1-vinylimidazole (vim) **83** in different molar ratios. These materials possessed high surface areas (513-680 m^2/g) and very high contact angles (152° for **PDB-VI-0.5**) with a water droplet, indicating their superhydrophobicity. Transesterification of tripalmitin as well as virgin plant oil with methanol was efficiently carried out by the imidazole sites. Under very mild conditions, at 65 °C and atmospheric pressure, 97% yield after three hours was obtained for the transesterification of tripalmitin. Importantly, cheap vegetable oil, containing water and FFAs, could be used without side reactions such as saponification or slower reaction speeds.[127]

Analogously, the same authors prepared mesoporous polymers by hydrothermal polymerization of divinylbenzene **11** with 1-vinylimidazolate (vim) **83**, 4-vinylpyridine (vpy) **84** or 1-vinyl-2-pyrrolidone (vpr) **22**. These were further quaternized with methyl iodide, butyl bromide or 1,3-propanesultone **85** and anion exchanged furnishing ionic liquids immobilized on superhydrophobic polymers **PDVB-[$C_x$vim/vpy/vpr][SO_3CF_3]** (Scheme 11). Though not basic catalysts, they catalyze similar transformations and therefore are mentioned here. These materials were highly active catalysts, reaching up to 99.9% yield after sixteen hours for the transesterification of tripalmitin with methanol at 65 °C. The activity was even higher than the analogous homogeneous catalyst. In general, heterogeneous catalysts have a lower accessibility of the catalytic sites and thus often exhibit lower activities than their homogeneous counterparts. However, these polymers concentrate the reactants close to the catalytic sites and thus provide higher catalytic efficiencies. Furthermore these materials were also able to catalyze the Peckmann reaction between ethyl acetoacetate and resorcinol, the Kharasch addition between styrene and tetrachloromethane, the esterification of cyclohexanol with acetic acid and the hydration of propylene oxide.[128]

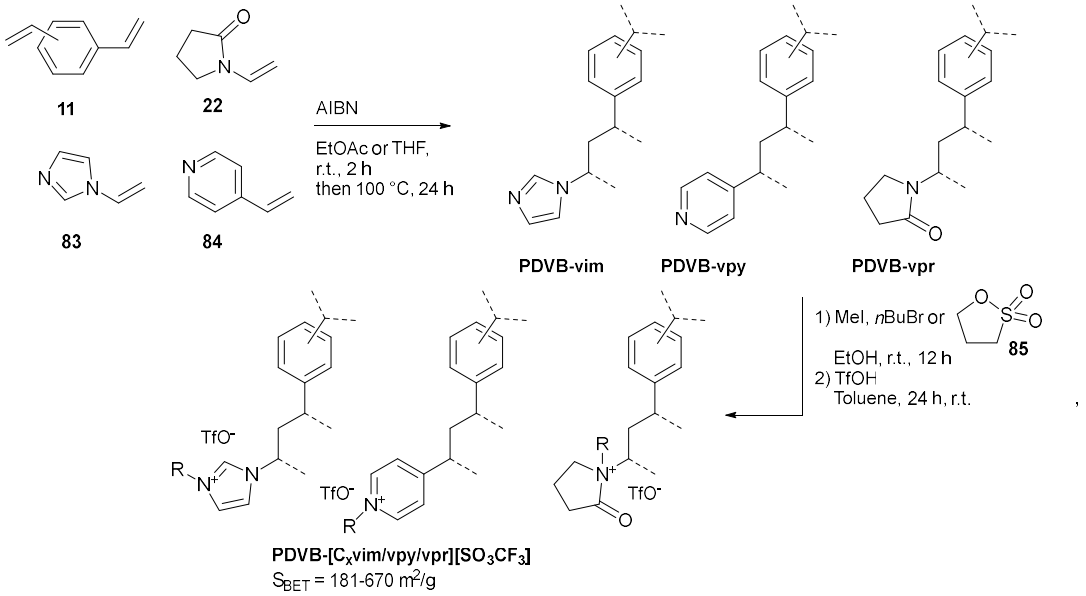

Scheme 11: Synthesis of ionic liquid functionalized HCPs by postsynthetic quaternization and ion exchange.[128]

1.3.3 Reactions catalyzed by heterogeneous 4-dimethylaminopyridine

4-Dimethylaminopyridine (DMAP) is an important nucleophilic catalyst for a variety of reactions such as acylation, silylation, tritylation…[129] A DMAP containing HCP was obtained by polymerization of divinylbenzene **11** with 4-(chloromethyl)styrene **86** by emulsion templating, followed by $FeCl_3$ catalyzed partial hypercrosslinking of the chloromethyl groups. This gave rise to a highly micro- and macroporous polymer **HXLPP**, with a BET area of 990 m^2/g and residual chloromethyl groups. These groups were then post-synthetically functionalized by nucleophilic substitution with 4-methylaminopyridine **87** (Scheme 12). The resulting polymer **NXLPP-MAP** was a highly active catalyst for the acylation of sterically hindered 1-methylcyclohexanol with acetic anhydride, reaching 100% conversion after three hours with a low catalyst loading of 1 mol%. This material clearly outperformed its nonporous analogues, unfortunately a comparison with homogeneous DMAP was not made.[130]

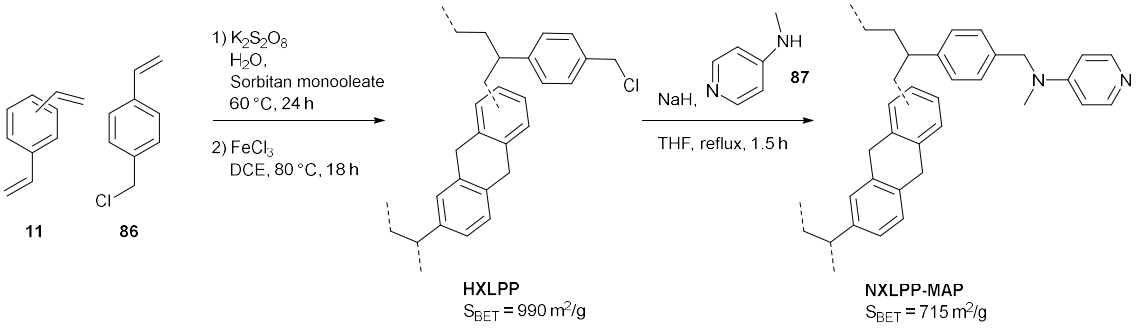

Scheme 12: DMAP immobilized by postsynthetic functionalization of a HCP.[130]

DMAP was also immobilized in CMPs by palladium catalyzed Sonogashira cross-coupling between 1,3,5-triethynylbenzene **7** and dibrominated DMAP **88**, thus incorporating a high loading of catalyst (2.02 mmol/g) into the porous framework **DMAP-NCP** (Scheme 13). The polymer showed good catalytic activity for the acylation of a wide range of alcohols obtaining high yields of 92 to 99% using 20 mol% loading and could be reused for at least fourteen times without loss of activity. Interestingly, the transformation could also be performed in continuous flow, with the catalyst staying fully active after more than 22 days of operation. **DMAP-NCP** was also a good catalyst for the silylation of alcohols and possessed a desirable selectivity for primary alcohols.[131]

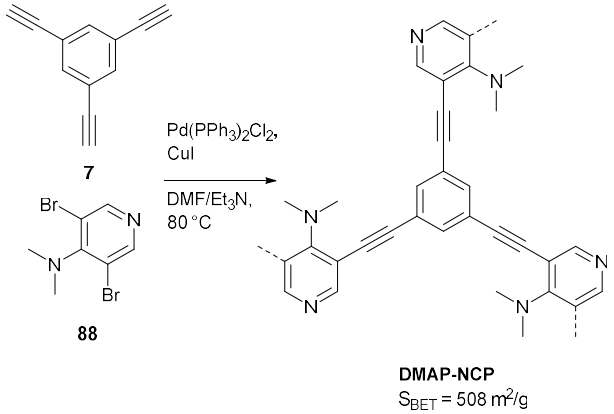

Scheme 13: Synthesis of a DMAP containing CMP by Sonogashira coupling.[131]

Lastly, Xu *et al*. synthesized polymers via Heck coupling between divinyl substituted DMAP **91** and 1,3,5-tris(4-iodophenyl)benzene **89** or 1,2,3,5-tetrakis(4-iodophenyl)adamantane **90** (Scheme 14). These networks possessed very low surface areas, however, they showed excellent catalytic activity for acylation reactions due to good solvent swelling properties.[132]

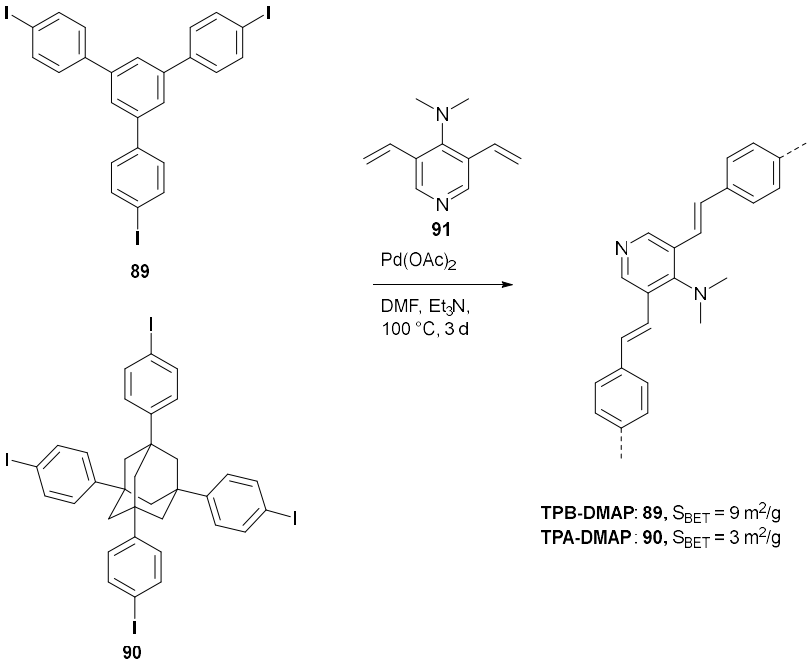

Scheme 14: Synthesis of DMAP containing polymers by Heck coupling.[132]

Many non-porous polymers or resins containing immobilized DMAP have been reported in the literature. However, whilst these possess good recoverability and reusability, in general these exhibit lower activities than homogeneous DMAP.[133–135] For example, D'Elia *et al*. resorted to immobilizing much more nucleophilic derivatives of DMAP on resins to obtain a heterogeneous catalyst with comparable activity to homogeneous DMAP. This lowered activity is caused by changing of the catalytic micro environment and due to mass transfer limitations: the increased difficulty of the reactants to diffuse to the catalytic center.[135] Permanently porous materials, such as POPs, possess intrinsic porosity, making them less dependent on swelling properties in organic solvents and increasing mass transfer. They can thus be used in a variety of solvents without changing their mass transfer properties much.[136,137] POPs, and especially COFs also can provide more precise control over the catalytic micro environment. Unfortunately, in the examples we discussed, no clear comparison to homogeneous DMAP was made. Furthermore, while the synthesis of **NXLPP-MAP** is comparable to that of DMAP containing polystyrene resins, the building blocks for **DMAP-NCP**, **TPB-DMAP** and **TPA-DMAP** are not commonly available. The structural building blocks **7**, **89** and **90** are available commercially, but are very expensive and the functional building blocks **88** and **91** require extra steps starting from DMAP, bromination to synthetize compound **88** and further Heck coupling to synthetize compound **91**.

1.3.4 Multicomponent reactions

Multicomponent reactions (MCRs) are an exciting field in organic chemistry. In MCRs, simple reaction procedures allow the formation of many bonds and complex structures in one-pot. MCRs are powerful tools in drug development, allowing the rapid generation of libraries of compounds.[138,139] In 2015, Bhaumik and coworkers developed a new triazine polymer **TPOP-2,** based on the condensation of *tris*(2-aminoethyl)amine **92** with cyanuric chloride **93** (Scheme 15). **TPOP-2** features a high density of amine and triazine nitrogens and a corresponding high surface basicity, allowing its use as a catalyst for the one-pot three component condensation reaction between aromatic aldehydes **96**, activated phenols (resorcinol **94** or 2-naphthol **95**) and malononitrile **97** leading to 2-amino-chromenes **98-99** (Scheme 16). These compounds are typically prepared with homogeneous organic bases such as piperidine.[140] **TPOP-2** proved to be a highly effective catalyst, obtaining high (82-88%) yields. With conventional basic catalysts, such as piperidine, pyridine, imidazole and *tris*(2-aminoethyl)amine), much lower yields of 35 to 46% were reported. A wide range of aromatic aldehydes with various electron withdrawing and donating groups were able to react and the catalyst could be recycled for at least five times without affecting the yield.[141]

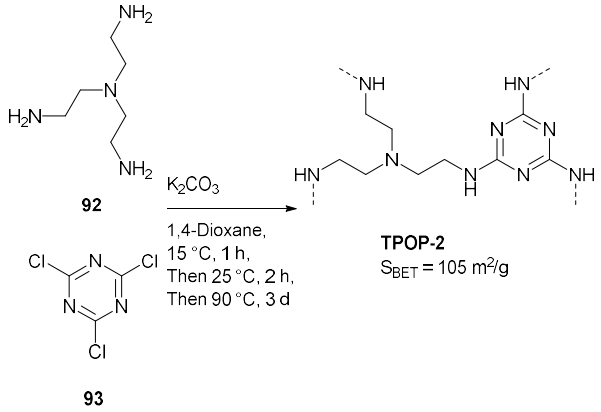

Scheme 15: Synthesis of **TPOP-2** by nucleophilic substitution of amine **92** with cyanuric chloride **93**.[141]

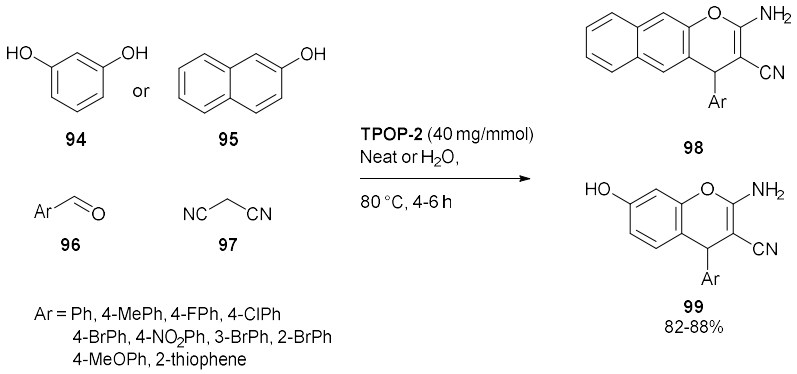

Scheme 16: 2-Amino-chromene synthesis catalyzed by **TPOP-2**.[141]

In 2016, the same group developed a porous organic polymer **PDVBTT-1** (poly-divinylbenzene-co-triallyloxytriazine) through radical co-polymerization of 2,4,6-triallyloxy-1,3,5-triazine **100** and divinylbenzene **11** (Scheme 17). The obtained surface areas were dependent on monomer ratios. Using only triazine **100**, the surface area obtained amounted to just 18 m^2/g, whilst using four equivalents of DVB **11** a surface area of 644 m^2/g was reached. This catalyst was also active in forming

2-amino-chromenes **98-99**, obtaining high yields (82-86%) for a range of aldehydes.[142] Interestingly, this same polymer has also been synthesized with surfactant P123 as a templating agent. In this way ordered 2D hexagonal mesopores along with micropores were obtained after template removal by refluxing in EtOH. This material possessed a higher surface area of 1016 m^2/g and was a good catalyst for the Knoevenagel condensation under microwave radiation.[143]

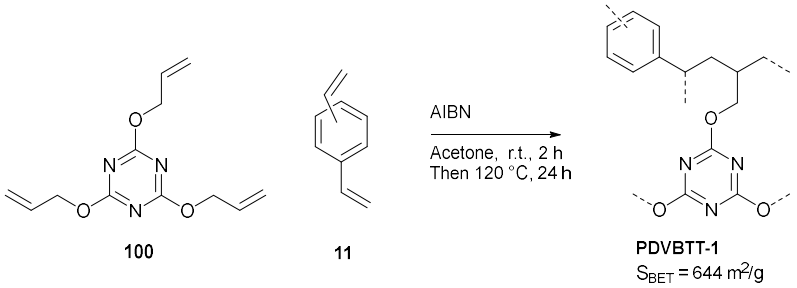

Scheme 17: HCP synthesis by radical polymerization of DVB **11** with allyl substituted triazine **100**.[142]

In further research from the Bhaumik group, the synthesis of a porous base **TrzMOP** was reported by reaction between tetratopic amine **101** and 2,5-thiophenedicarboxaldehyde **103**, creating aminal linkages (Scheme 18). This catalyst was used in another MCR, the polyhydroquinoline synthesis through four component one-pot Hantzsch condensation. A series of aldehydes could be converted with good to excellent yields (72-98%), comparable to morpholine, a homogeneous counterpart (Scheme 19). The catalyst was highly reusable and after the 7th run only a minor yield loss of 3% was observed.[144] The same group prepared another aminal-linked material **TrzPyPOP** by condensation of tetraamine **101** and pyrene-1-carboxyaldehyde **102** (Scheme 18). This material was used in a three component Biginelli condensation furnishing a range of dihydropyrimidones **109** (Scheme 20).[145] Lastly, Zaharani *et al.* utilized mesoporous poly melamine formaldehyde **mPMF** (*vide supra*) as a catalyst for the mechanochemical synthesis of 2-amino-4*H*-benzo[*b*]pyrans **112** (Scheme 21). These authors reported the conversion of a wide range of substrates in good yields (62-92%).[146]

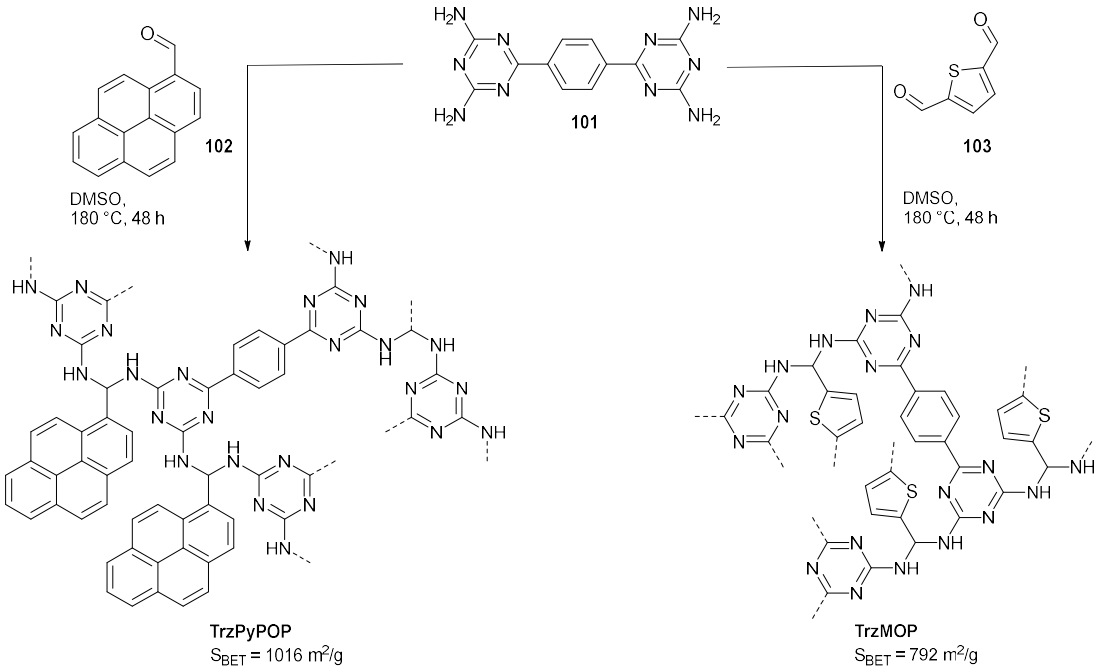

Scheme 18: Synthesis of **TrzMOP** and **TrzPyPOP** by aminal formation between amine **101** and aldehydes **102** and **103**.[144,145]

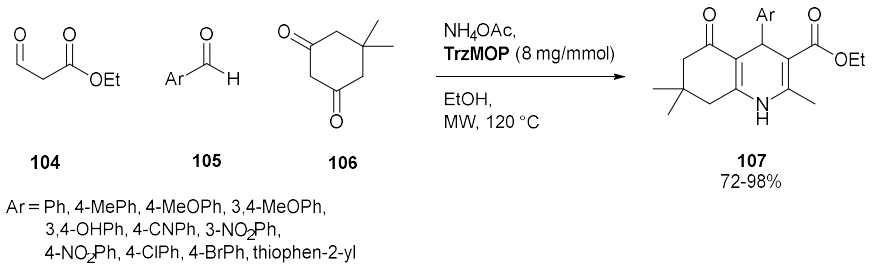

Scheme 19: Polyhydroquinoline synthesis mediated by **TrzMOP**.[144]

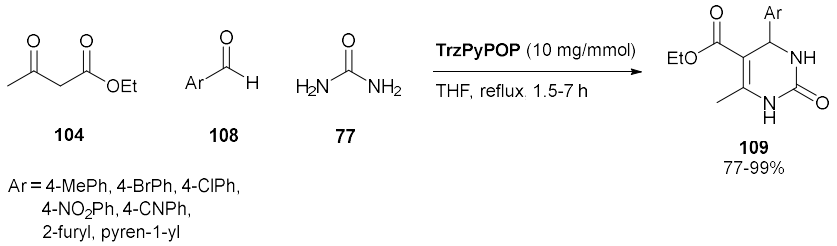

Scheme 20: Three component Biginelli condensation catalyzed by **TrzPyPOP**.[145]

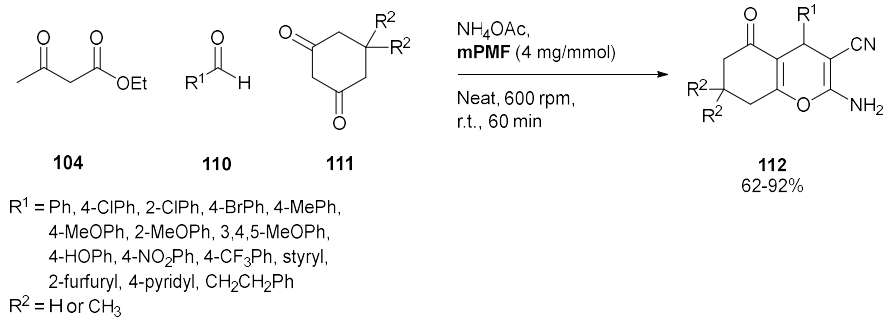

Scheme 21: **mPMF** catalyzed synthesis of 2-amino-4*H*-benzo[*b*]pyrans 112.[146]

In general the polymers catalyzing these multicomponent reactions possess interesting reactivities and work well. Regarding the **TPOP-2** catalyzed synthesis of 2-amino-chromenes: typically homogeneous bases are used in literature.[147] However, some other (green) catalysts are also available such as expanded perlite, a cheap green heterogeneous catalyst, that does not require any chemical synthesis, but does require regeneration by calcination at 800 °C.[148]

In the polyhydroquinoline synthesis through Hantzsch condensation **TrzMOP** performed comparable to a homogeneous base. Other (heterogeneous) catalysts have also been described for this transformation such as $HClO_4$-SiO_2, PW/SiO_2, barium nitrate, $CeCl_3.7H_2O$, etc.[149] Moreover, a very green protocol requiring only ammonium carbonate in water with mild heating to 55-60 °C has been reported, which of course makes a more difficult to synthetize heterogeneous catalyst less attractive.[150] Similarly, for the three component Biginelli condensation several other (green) methodologies exist using many possible catalyst and solvent combinations, ionic liquids, microwave technology…[151,152]

The described polymers were made using rather easily accessible reagents, especially for **PDVBTT1** and **TPOP-2** and under relatively mild conditions. In the case of the amidine-linked polymers **TrzMOP** and **TrzPyPOP** no catalysts are needed to prepare them, only intense heating.

1.3.5 NHC catalysis

N-heterocyclic carbenes (NHCs) are tunable and strong ligands for transition metal complexes, but can also be nucleophilic or basic organocatalysts by themselves.[153–155] Rose *et al*. synthesized *N*-heterocyclic carbene containing element organic frameworks **EOF-15** and **EOF-16** by Suzuki coupling of a bifunctional imidazolium linker **113** with tetrafunctional boronic acids **114** and **115** (Scheme 22). The EOFs were used as nucleophilic catalysts in the conjugated *umpolung* of cinnamaldehyde **116** and coupling with trifluoroacetophenone **117** (Scheme 23). The heterogeneous catalytic NHC species was generated *in situ* by deprotonation of the imidazolium salt with diazabicycloundecene (DBU). Moderate (46-84%) yields were obtained, comparable or slightly lower than homogeneous counterparts (83-85%).[156]

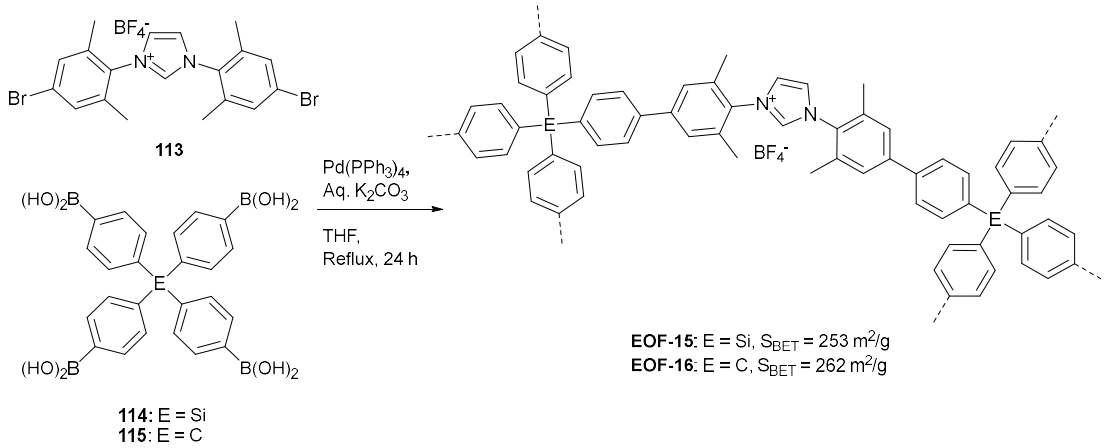

Scheme 22: Synthesis of imidazolium containing EOFs by Suzuki coupling.[156]

CTFs with embedded cationic imidazolium species have also been reported, yet these were always synthesized at the high (> 400 °C) temperatures required for the ionothermal trimerization of nitriles utilized in typical CTF synthesis.[157–160] However, Troschke *et al*. showed via thermogravimetric analysis of imidazolium precursors that substantial decomposition of these monomers already begins to occur at 300 °C, which raises doubts on the structural integrity of these CTFs. Therefore, these authors devised a finely adjusted synthetic protocol utilizing long reaction times but relatively low temperatures to preserve the imidazolium functionality of building block **120** in the resulting **imid-CTF** (Scheme 24). This CTF was non-porous for nitrogen and thus is not permanently porous. However, a significant uptake of CO_2 was measured (2.05 mmol, 1 bar, 273K). The authors performed vapor sorption experiments to evaluate catalytic applications in the liquid phase. Significant swelling of the CTF and adsorption of organic solvents such as EtOH or CH_3CN was found over the whole pressure range at 298K. These very polar and small solvents were well absorbed, due to interaction of the nitrogen-rich polymer with polar solvents, analogous to the quadrupole interactions of CO_2 with the framework. Apolar solvents, such as toluene, showed a negligible uptake. This was reflected in the catalytic activity for the *umpolung* reaction being solvent dependent, with the reaction working well in CH_3CN and EtOH, but *t*BuOH (too bulky) or apolar solvents resulting in very low yields. High yields (81%) were reached for the conjugated *umpolung* catalyzed by **imid-CTF** in CH_3CN (Scheme 23). However, when the CTF was fabricated at higher temperatures no significant product formation was observed. CTFs produced at slightly higher temperatures of 320 °C or 330 °C, respectively, already resulted in 8% or 1% yield only.[161] This refutes recent findings in literature[157–160] proposing intact imidazolium moieties in CTFs produced at high temperatures.

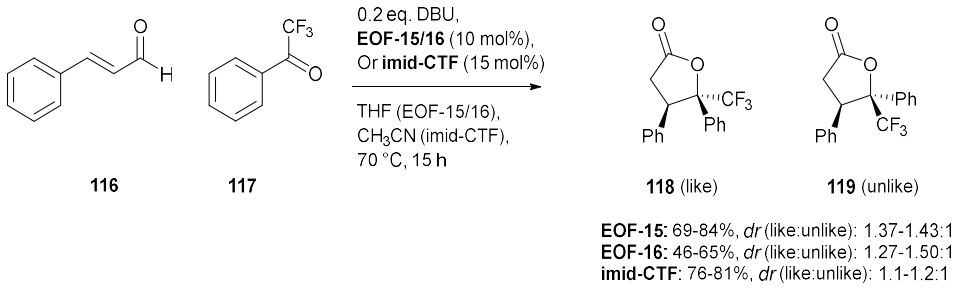

Scheme 23: Heterogeneous NHC catalyzed *umpolung* reaction.[156,161]

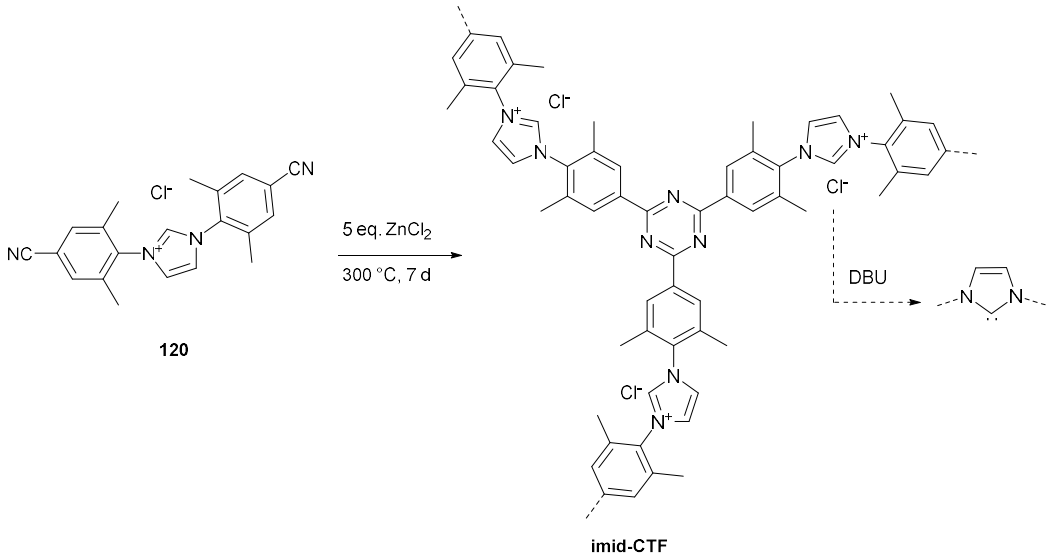

Scheme 24: Synthesis of **imid-CTF** by ionothermal polymerization at lower temperatures, preserving the structure.[161]

1.4 Cascade reactions

1.4.1 Simultaneous acid and base catalysis

Cascade reactions, incorporating several reactions to give the final product in one operation, are a promising approach towards more sustainable chemistry since they reduce both waste and time.[162] Generally, several active components (catalysts, acids, bases, ligands…) are involved in such a multistep process.[163] Integrating multiple catalytic sites into a single recyclable material is of course of great interest.

Nature regularly employs multistep cascade reactions in enzymes. These often employ multiple acid-base sites in one catalyst, for example, catalytic triads in serine proteases.[164] Simultaneous acid and base catalysis is impossible with homogeneous catalysts, as they will neutralize each other. Heterogeneous systems however can overcome this limitation. Quite some bifunctional acid-base POPs have been reported and often a one-pot deacetalization-Knoevenagel of dimethyl acetal protected benzaldehyde **121** is carried out as a reference reaction for these materials (Scheme 25 and Table 3).

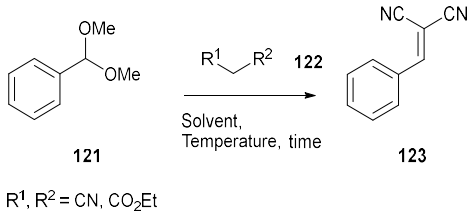

Scheme 25 and **Table 3**: The one-pot deacetalization-Knoevenagel reaction.

Entry	Conditions	Yield (%)	Ref
1	2-(2-bromophenyl)-1,3-dioxolane instead of **121**, **HCP-A-B** (133 mg/ mmol), H_2O, r.t., 8 h	95	[165]
2	1.2 eq. malononitrile, 250 mol% **P(DVB-0.2-VBS)**, 500 mol% **P(DVB-0.2-VBA)**, toluene, 80 °C, 30 min	99	[166]
3	1.2 eq. malononitrile, 10 mol% **PPAF-SO_3H-NH_2**, Toluene, water, 90 °C, 1 h	100	[167]
4	2 eq. malononitrile, **PAF-1-$NHCH_2CH_2NH_2$-SO_3H** (50 mg/mmol), Toluene, 90 °C, 3 h	99	[168]
5	1.2 eq. malononitrile, **TxPPs-SO_3H-NH_2** (130 mg/mmol), Toluene, water, 90 °C, 1 h	75	[169]
6	1.1 eq. malononitrile, 2 mol% **PP-x** (8 mg/mmol), Toluene, water, 90 °C, 1 h	>95	[170]
7	4 eq. malononitrile, 10 mol% **MONNs-SO_3H-NH_2**, Toluene, 80 °C, 2 h	>99	[171]
8	4 eq. ethyl cyanoacetate, 10 mol% **SO_3-MONNs and NH_2-MONNs**, Toluene, 80 °C, 2 h	>99	[172]
9	4 eq. ethyl cyanoacetate, 10 mol% **NH_2-SO_3-H-ONTFs**, Toluene, 80 °C, 2 h	>99	[173]
10	10 eq. ethyl cyanoacetate, **Acid base nanotubes** (231 mg/mmol), water, r.t., 24 h	100	[174]
11	1.1 eq. malononitrile, **COF-OH** (10 mg/mmol), Toluene/water (1.5/5), 80 °C, 85 min	96	[175]
12	1.1 eq. malononitrile, **COF-OMe** (10 mg/mmol), Toluene/water (1.5/5), 80 °C, 90 min	52	[175]
13	2-(2-bromophenyl)-1,3-dioxolane instead of **121**, 1.2 eq. malononitrile, **HCPs–SO_3H–50** (33 mg/mmol) and **HCPs–CH_2NH_2–50** (133 mg/mmol), toluene, H_2O	96	[176]

Jia *et al*. synthesized hypercrosslinked hollow spheres with acidic and basic sites **HCP-A-B** (Scheme 26). Firstly, a microporous hollow nanosphere **HCP** was synthesized using silica polystyrene composite particles, SiO_2@PS, as a precursor. The polystyrene was alkylated using methoxymethyl chloride, followed by hypercrosslinking of the chloromethyl moieties and etching of the silica template. Sulfonic acid groups were introduced in this **HCP** using acetyl sulfate **124**. Reaction with *N*-(hydroxymethyl)phthalimide **125** followed by deprotection with hydrazine led to the incorporation of amine functionalities. **HCP–A–B** displayed high catalytic efficiency in both a deacetalization/Henry and a deacetalization/Knoevenagel reaction of 2-(2-bromophenyl)-1,3-dioxolane. The Knoevenagel reaction took place under very mild conditions, in water at room temperature (Table 3, entry 1). Moreover, these authors developed a new reaction, the synthesis of 2-cyclohexen-1-ones **127** from 2-alkoxy-3,4 dihydropyran derivatives **126** by a ring opening-aldol condensation-dehydration sequence (Scheme 27, A).[165]

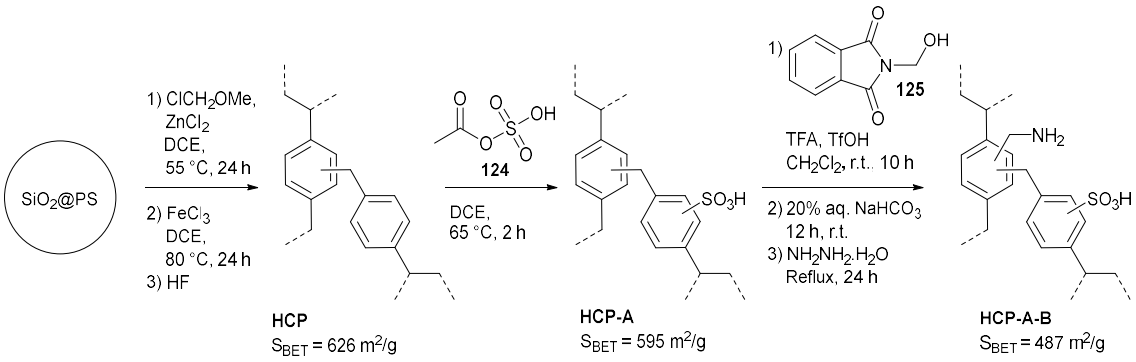

Scheme 26: Synthesis of hypercrosslinked nanospheres by crosslinking, etching, sulfonation and amination.[165]

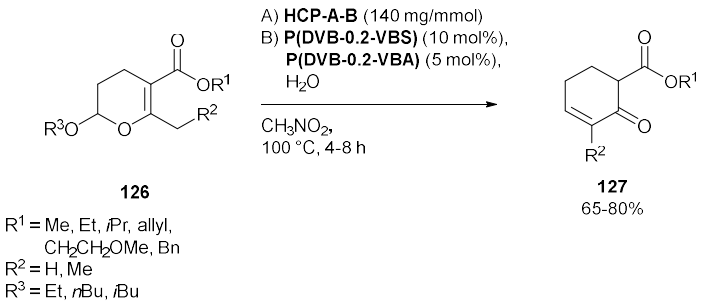

Scheme 27: Acid-base mediated rearrangement of 3,4-dihydropyrans **126** to α-ester cyclohexenones **127**.[165,166]

Physical combinations of solid acids and bases can also be applied. Sun *et al*. synthesized amino or sulfonic acid functionalized POPs through radical polymerization of protected sulfonic acid functionalized building block **128** or amino containing compound **129** with divinylbenzene **11** (Scheme 28). The physical combination of these two materials was used as a simultaneous acid base catalyst for one-pot deacetalization-Henry condensation reactions with yields reaching up to 100%. These materials were also able to catalyze the deacetalization-Knoevenagel condensation (Table 3, entry 2) and transformation of 3,4-dihydropyran derivatives **126** to α-ester cyclohexenones **127** (Scheme 27, B).[166]

In 2013, Félix Sánchez *et al*. reported the functionalization of a spirobisfluorene PAF with both acidic and basic sites and its utilization as a catalyst. To this end 2,2',7,7'-tetraiodo/bromo-9,9'-spirobisfluorene **130-131** was polymerized with benzene-1,4-diboronic acid **5** through a Suzuki coupling (Scheme 29). The more reactive iodo-substituted building block **131** resulted in slightly higher

surface areas. Subsequent sulfonation, nitration and reduction of the nitro groups gave rise to **PPAF-SO_3-NH_2** with a BET surface area of 310 m^2/g. This acid and base functionalized porous catalyst was used in the one-pot deacetalization-Knoevenagel reaching 100% yield after one hour using 10 mol% catalyst (Table 3, entry 3).[167]

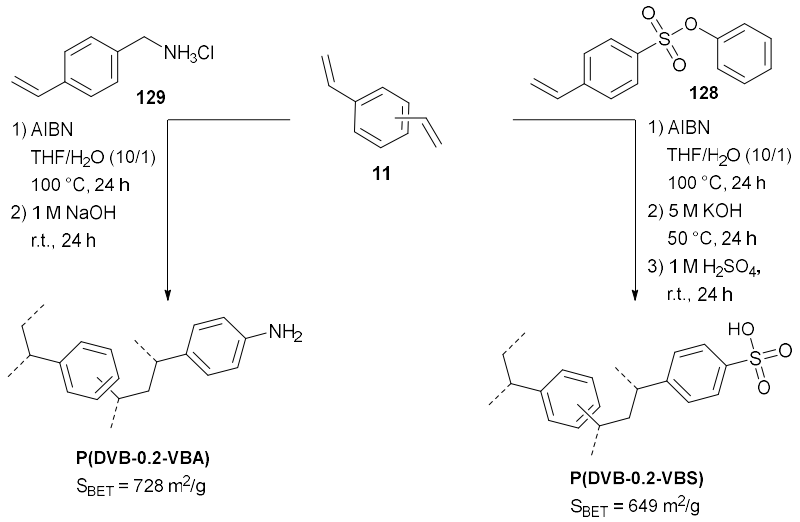

Scheme 28: Synthesis of amino or sulfonic acid functionalized HCPs.[166]

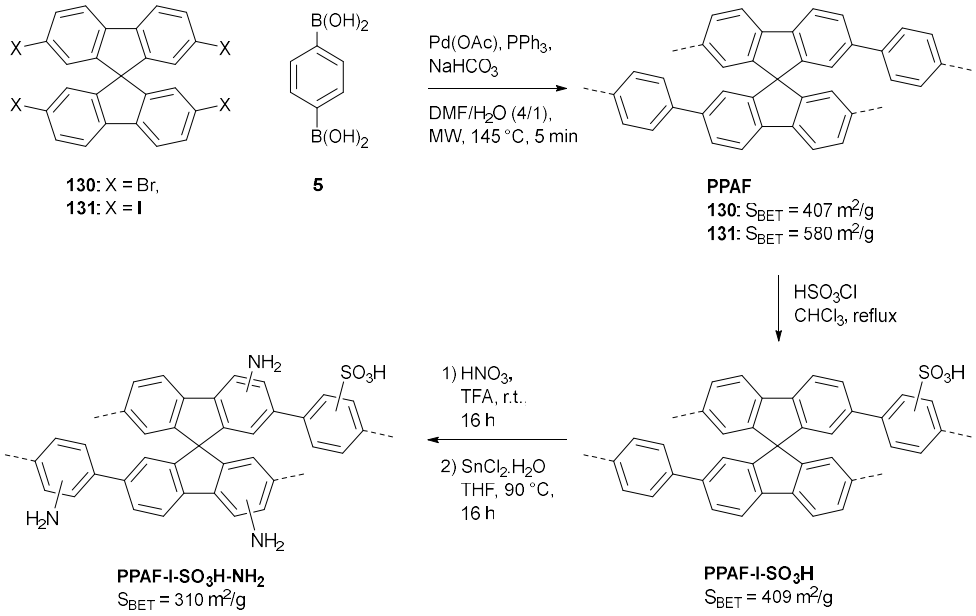

Scheme 29: Synthesis of bifunctional spirobisfluorene based POPs by Suzuki coupling and postfunctionalization by sulfonation, nitration and reduction.[167]

Similarly, Zhang *et al*. prepared another acid and base functionalized PAF starting from **PAF-1**. First, an amine functionalized **PAF-1-NH_2** was synthesized by nitration and reduction. The amino groups of this material were then reacted with Boc protected compound **132**, followed by sulfonation and deprotection furnishing **PAF-1-$NHCH_2CH_2NH_2$-SO_3H** (Scheme 30). The functionalized material still possessed a BET Surface area of 1672 m^2/g, which is higher than other bifunctional POPs. In deacetalization-Henry reactions up to 97% yield was reported, and for the deacetalization-Knoevenagel condensation a 99% yield was obtained (Table 3, entry 4).[168]

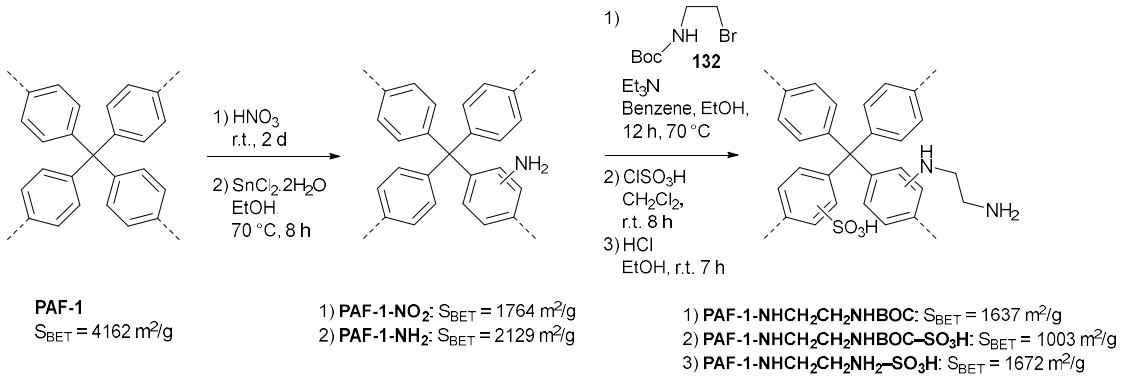

Scheme 30: Synthesis of amino and sulfonic acid functionalized PAFs by postfunctionalization.[168]

Guadalupe *et al*. prepared acid-base functionalized truxene based POPs via $AlCl_3$ catalyzed crosslinking followed by functionalization. As a crosslinker for the hexamethyltruxene monomer **133** the solvent dichloromethane, or an extra crosslinker 1,4-bis(bromomethyl)benzene **25** could be used, resulting in polymers **TxPP** and **TxBnPP** (Scheme 31). When more sterically hindered truxene monomers (*e.g.* hexabutyltruxene) were reacted, no polymeric materials were obtained, and starting material was recovered almost quantitively. Truxene possesses intrinsic photoactivity, therefore **TxPP** itself could be used as a heterogeneous photocatalyst for the oxidative dimerization of benzylamine. High conversion (91%) was attained after 24 hours and the catalyst was recyclable up to five times with no loss of yield. Furthermore, **TxPP** was postfunctionalized with amines, sulfonic acids or both resulting in **TxPPs-SO_3H**, **TxPPs-NH_2** or **TxPPs-SO_3H-NH_2**, respectively. **TxPPs-SO_3H** was applied as a catalyst for esterification and transesterification reactions. A range of long chain fatty acids could be converted into their corresponding methyl esters in generally high to quantitative yields (91-99%) in methanol at room temperature in three hours. Ethyl cyanoacetate could be transesterified with methanol to its corresponding methyl ester in 88% yield under the same conditions. For the deacetalization-Knoevenagel reaction, after optimization of the ratio of acid and base catalysts, 75% yield could be reached after one hour (Table 3, entry 5). Interestingly, a physical mixture of acid and base functionalized catalysts performed better than the bifunctional catalyst, due to a more optimal ratio of acid to base being used.[169]

Bhaumik and coworkers polymerized 4-tritylaniline **134** under Lewis acidic conditions with dimethoxymethane obtaining porous polymers **PP-1,2,3** whose morphology depended on the amount of crosslinker used (Scheme 32). **PP1** was obtained as hollow tubes, whereas **PP-2** formed microflowers and **PP-3** formed larger interconnected hollow tubes. The authors proposed that the residual alkoxy groups from the crosslinker interacted with the amino groups and thus influenced the morphology, as these hollow structures are generally only formed when a template is used. **PP-1,2,3** were grafted with sulfonic acid groups forming **PP-1,2,3S** and used in the one-pot acetalization-Knoevenagel reaction giving high yield (>95%, Table 3, entry 6).[170]

Wang *et al*. prepared acid or base functionalized microporous polymers **HCP-NH_2-x** and **HCP-SO_3-x** from simple prefunctionalized aromatic building blocks **136** or **137** and benzene **135** through $FeCl_3$ catalyzed crosslinking with dimethoxymethane (Scheme 33). As the amount of benzene decreases the surface areas decrease dramatically. These materials were able to catalyze one-pot deacetalization-Knoevenagel (Table 3, entry 13) and Henry reactions. Predictably, combining heterogeneous acid with homogeneous base or *vice versa* resulted in very low yields. This is caused by neutralization when one of the catalysts is in the homogeneous phase, resulting in cascade failure.[176]

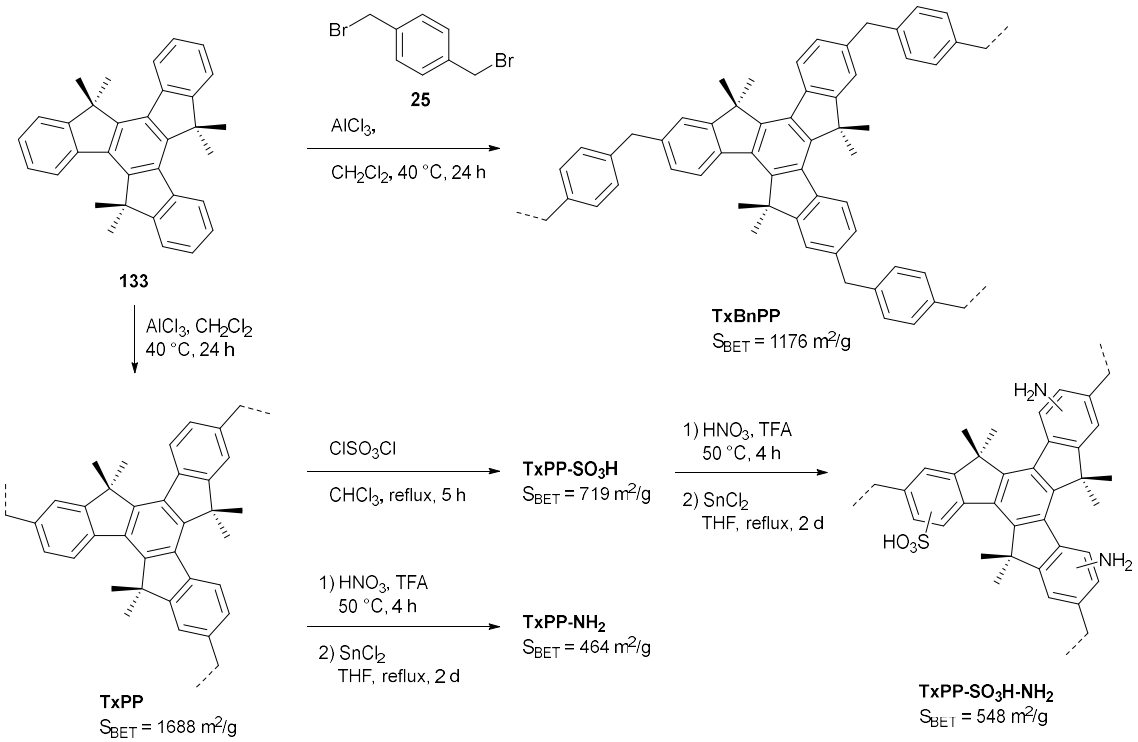

Scheme 31: Synthesis and functionalization of truxene based POPs.[169]

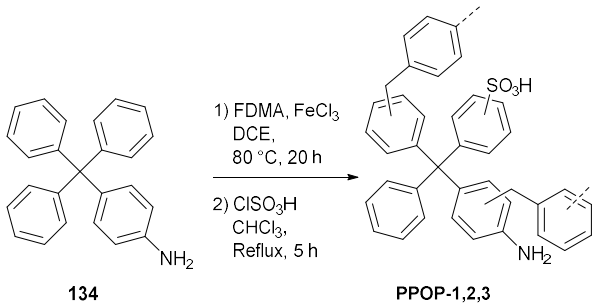

Scheme 32: Preparation of sulfonic acid and amino functionalized HCPs by polymerization of 4-trityl aniline **134**.[170]

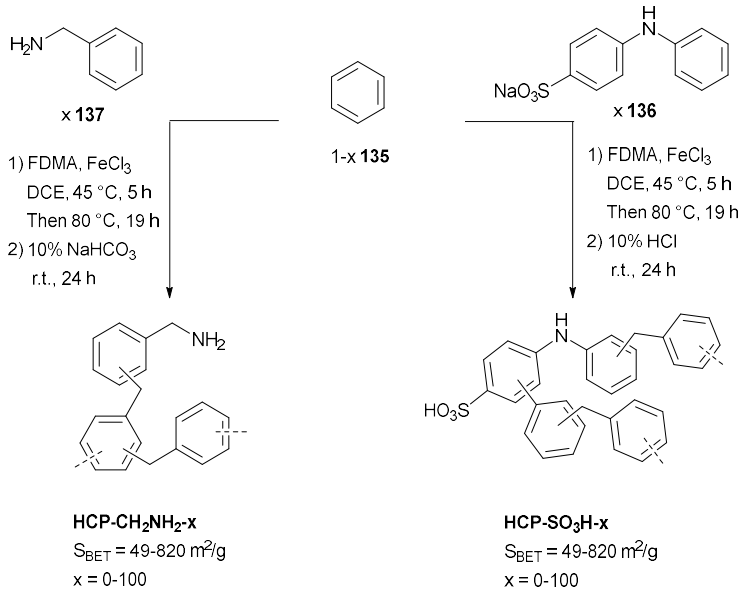

Scheme 33: Synthesis of acid or base functionalized HCPs by Friedel-Crafts crosslinking.[176]

The Huang group, who prepared the amino functionalized microporous organic nanotube networks **NH_2-MONNs** (Scheme 10), used very similar materials as catalysts for the one-pot deacetalization-Knoevenagel reaction. Hypercrosslinking bottlebrush polymer **138** (Figure 2), containing phenoxy protected sulfonic acid or Boc protected amines, followed by etching of the PLA core and deprotection produced **SO_3-MONNs** and **NH_2-MONNs**. A physical mixture of those two catalysts was then successfully applied in de deacetalization Knoevenagel reaction (Table 3, entry 8).[172] In further research, the same group reported on the synthesis of a truly bifunctional nanotube network. This network **NH_2-SO_3-H-ONTFs** with a surface area of 845 m^2/g was synthesized starting from bottlebrush copolymer **139** (Figure 2) by crosslinking and etching of the PLA core followed by Boc and phenoxy deprotection. A wide range of acetals could be reacted with active methylene compounds in one-pot deacetalization-Knoevenagel reactions in very high yields (Table 3, entry 9).[173]

A nanotube network with imidazole basic sites was synthesized by the same group starting from bottlebrush copolymer **140**. The terminal double bonds of **140** were polymerized via Grubbs metathesis catalysis. Azide groups were then introduced via nucleophilic substitution of the chloromethyl group. Imidazoles were formed from these azides, by alkyne-azide click reaction (Scheme 34). The resulting **acid-base nanotubes** could catalyze the hydrolysis-Knoevenagel reaction in water at ambient conditions, however it required very high catalyst loadings (Table 3, entry 10).[174] Lastly, these same authors prepared bifunctional acid base nanotubes by a postfunctionalization strategy. To this end bottlebrush polymer **142** was hypercrosslinked with FDMA, followed by etching of the PLA core, sulfonation, nitration and reduction of the nitro groups (Scheme 35). Similar to the aforementioned materials, **MONNs-SO_3H-NH_2** was an effective catalyst for the tandem reaction (Table 3, entry 7).[171]

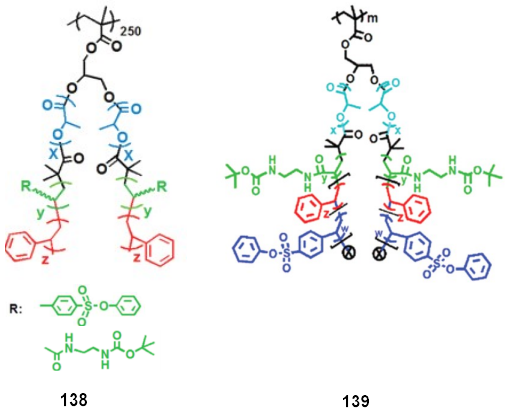

138 139

Figure 2: Bottlebrush copolymers used in the synthesis of nanotube networks.[172,173]

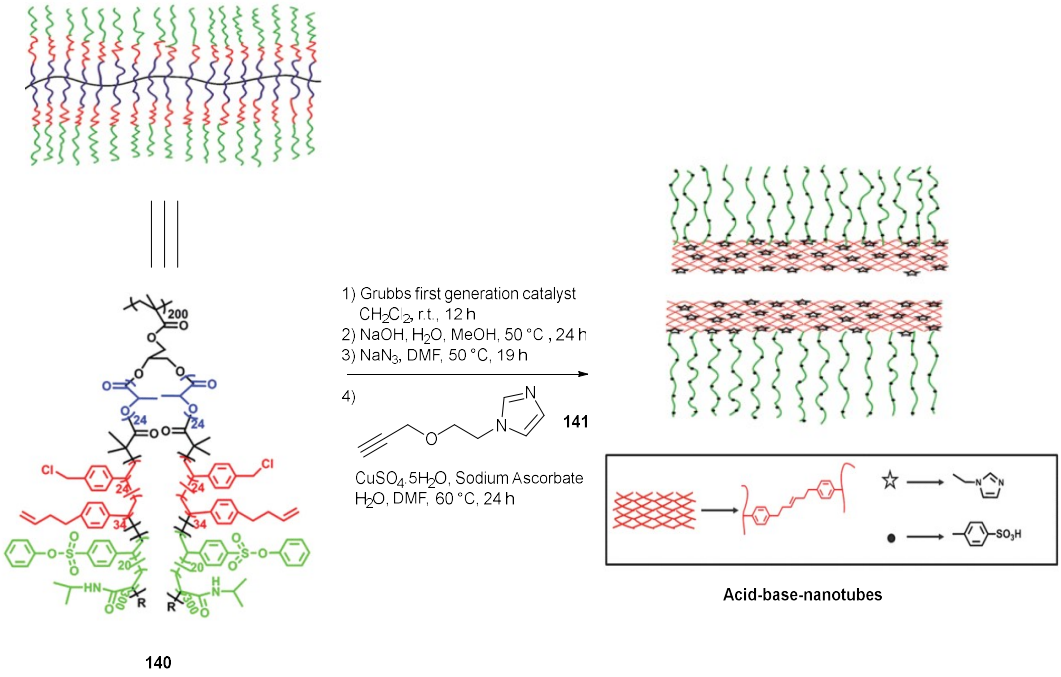

Scheme 34: Synthesis of **Acid base nanotubes** by double bond metathesis – sulfonic acid deprotection – nucleophilic substitution and click reaction.[174]

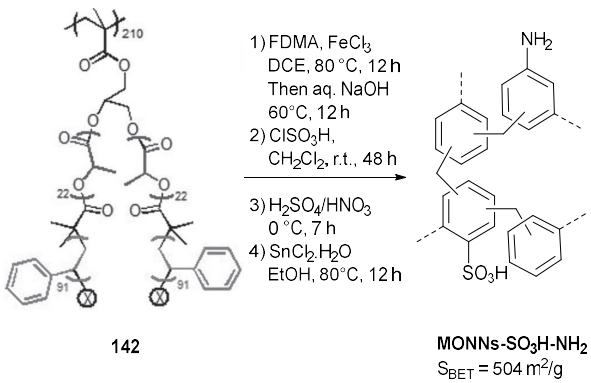

Scheme 35: Synthesis of **MONNs-SO_3H-NH_2** postfunctionalization.[171]

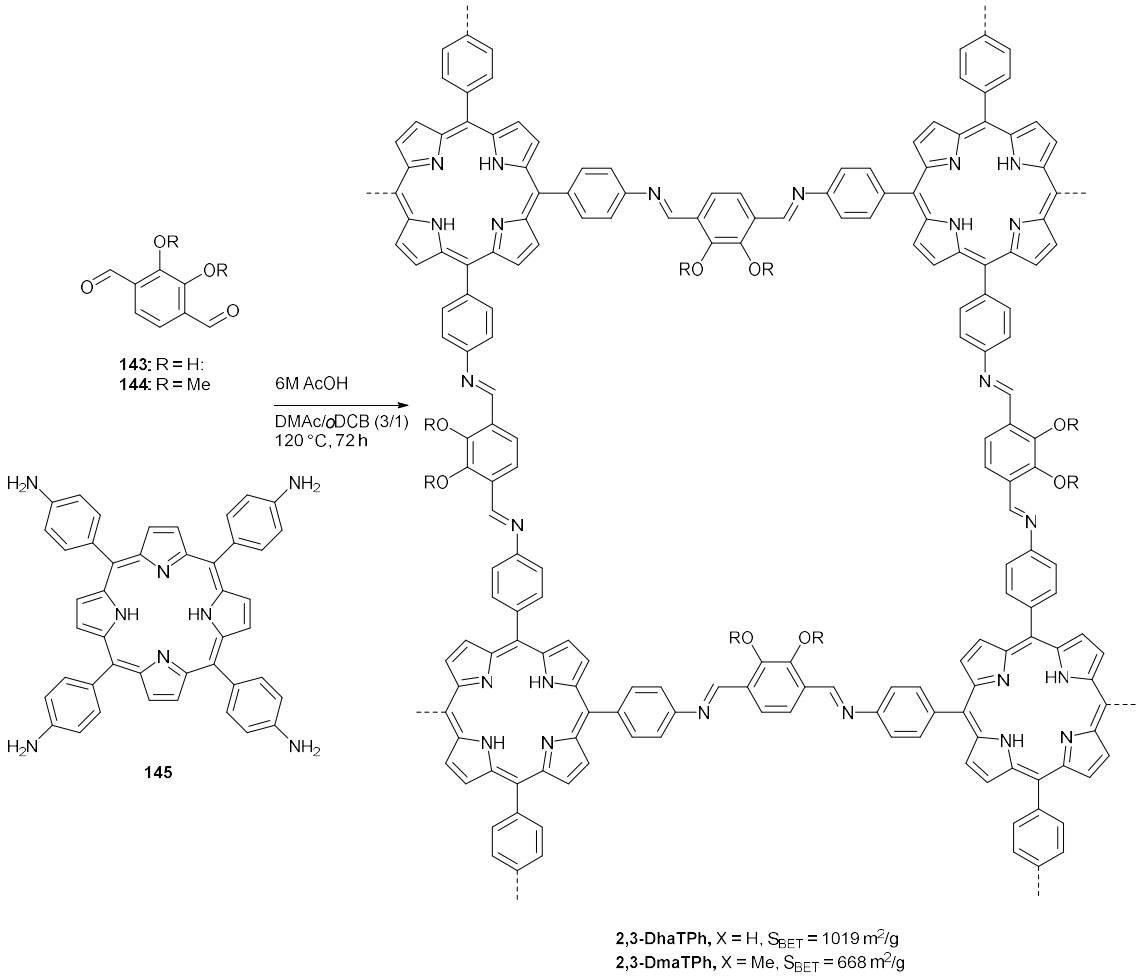

Scheme 36: Synthesis of a bifunctional acid-base COF.[175]

In 2015, the Banerjee group synthesized a COF able to perform simultaneous acid and base catalysis due to the incorporation of acidic (catechol) and basic (porphyrin and imine) sites. Two highly crystalline and acid and base stable COFs **2,3-DhaTph** and **2,3-DmaTph** were synthesized by Schiff-base reaction between 2,3-dihydroxyterephthalaldehyde **143** or 2,3-dimethoxyterephthaldehyde **144** and 5,10,15,20-tetrakis(4-aminophenyl)-21*H*-23*H*-porphine **145** under solvothermal conditions (Scheme 36). The model reaction between benzaldehyde dimethyl acetal and malononitrile worked very well with the bifunctional COF **2,3-DhaTph** (Table 3, entry 11). **2,3-DmaTph** lacking the acidic functionalities showed much lower activity (Table 3, entry 12), proving the necessity of both functionalities. **2,3-DhaTph** could be recycled at least five times, however the yield dropped by 10-15%.[175]

1.4.2 Other cascade reactions

In 2016, Sanchez and coworkers developed a multifunctional catalyst based on simultaneous organo- and metal catalysis on a PAF. Polymers **PAF_{AD}** and **PAF_{C}** were prepared by Suzuki coupling of tetraphenyladamantane or tetraphenylmethane based iodinated monomers **146** and **147** with benzene-1,4-diboronic acid **5** (Scheme 37). Porous materials were obtained quantitatively after only

five minutes of microwave heating. These polymers were then postsynthetically modified by nitration, reduction, amide coupling, Boc-deprotection and metalation. The resulting polymers **PAF$_C$-NProRh** and **PAF$_{AD}$-NProRh** were bifunctional catalysts. The basic proline moieties were able to catalyze the Knoevenagel condensation of benzaldehyde **148** with malononitrile **149** to intermediate benzylidinemalononitrile **151**. The rhodium metal catalyzed the hydrogenation reaction into product **150**. Several aldehydes and malononitrile or ethyl cyanoacetate were able to react. Interestingly for 4-nitrobenzaldehyde, reduction of the nitro group but not of the double bond took place (Scheme 38). **PAF$_C$** could be recycled ten times with essentially unchanged conversions and no significant rhodium leaching. Furthermore, this system was combined with a sulfonated PAF to perform simultaneous deacetalization-Knoevenagel-hydrogenation one-pot cascade reactions.[177]

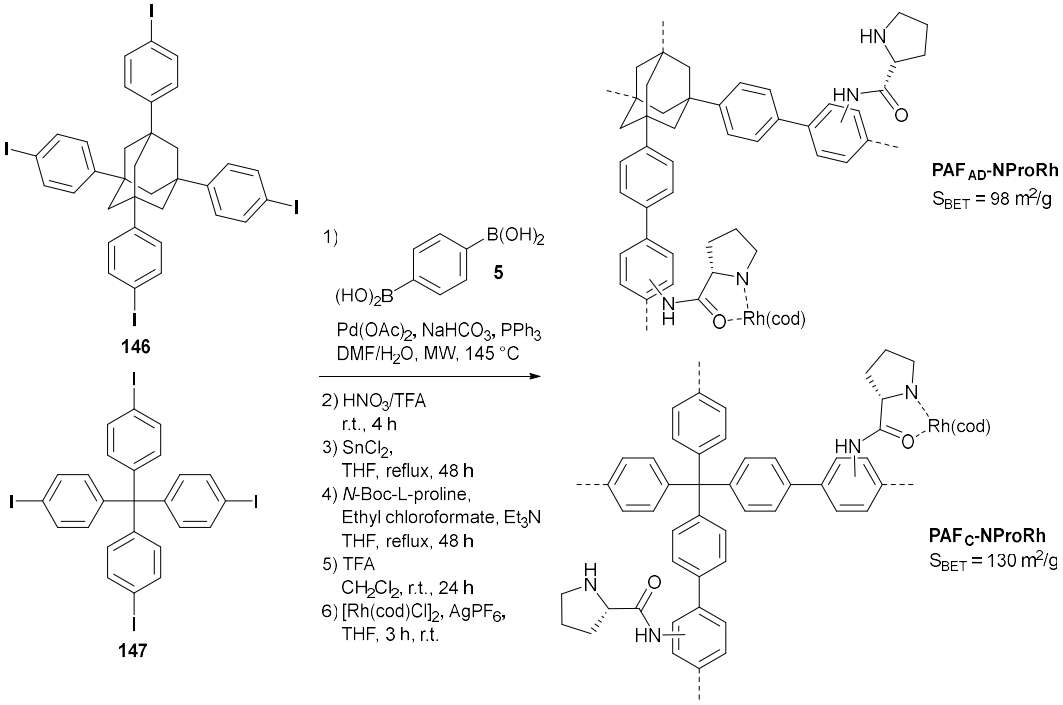

Scheme 37: Synthesis of bifunctional PAFs.[177]

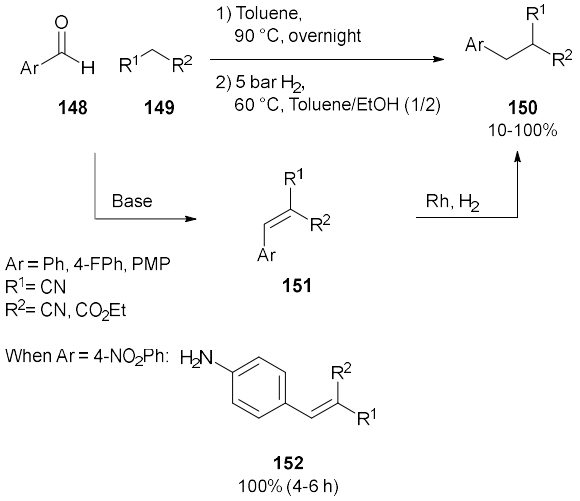

Scheme 38: One-pot Knoevenagel-reduction reaction catalyzed by Rhodium and proline containing PAFs.[177]

A bifunctional COF was synthesized by metalation of a β-ketoenamine-linked **COF-TpPa-Py** with $Pd(OAc)_2$ (Scheme 39). By virtue of the metal loading and the basic pyridine units this **COF-TpPa-Py** could oxidize a range of alcohols to their corresponding aldehydes which were then reacted with malononitrile in one-pot to form the Knoevenagel products in high yields (91-99%).[178]

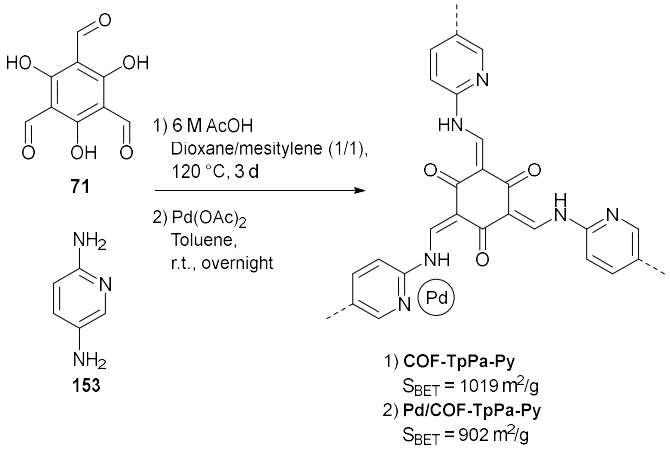

Scheme 39: Synthesis of bifunctional **COF-TpPa-Py**.[178]

1.4.3 Outlook on POPs as bifunctional catalysts

The combination of a strong acid with a base is of course only possible in heterogeneous systems, where there is spatial separation of the catalytic sites. Similar materials to these POPs also exist based on silicas or PMOs[179,180] and bifunctional MOFs[181,182] containing both acidic and basic sites. These are used in analogous transformations with similar performances, however, POPs possess the advantages of being metal-free and highly stable.

The synthesis of bi- or multifunctional POPs, combining different catalytic sites on a single material functioning in tandem, is still in its infancy. It can be considered an ideal avenue for further POP research, as it leverages many of the advantages of POPs such as good mass transfer, excellent stability and designability.

Even so, the synthesis of these bifunctional materials is plagued by long postmodification-sequences utilizing quite hazardous chemicals. For example, in the synthesis of **HCP-A-B** (Scheme 26) four separate postmodification steps are needed using hazardous chemicals such as TFA, TfOH, hydrazine, etc. Moreover, the synthesis of the polymer itself requires highly dangerous MOMCl and HF. To produce acid-base functionalized materials by postfunctionalization generally three separate steps are needed: sulfonation, nitration and reduction. However, bottom-up synthesis can alleviate this problem (Scheme 28, 33 and 36). Lastly, the nanotube networks (Figure 2, Scheme 34 and 35) not only require complex postmodification, but also a core removal step and a lengthy synthesis of the bottlebrush polymers themselves. For example, starting from poly(glycidyl methacrylate) six steps are needed to synthesize compound **140**.[183]

1.5 Chiral catalysts

For many applications in pharmaceuticals, agriculture and other chemical industries it is essential to obtain optically pure compounds.[184] Enantiomerically pure products are typically produced via multistep syntheses, on a relatively small scale (~ 1-10000 ton/year for pharmaceuticals, 500-100000 ton/year for agrochemicals) and in batch. These products have high purity requirements and high added values, thus tolerating higher process costs.[136]

Asymmetric catalysis forms a convenient way to synthetize chiral molecules from achiral building blocks. This alleviates the need for costly resolution techniques or a chiral pool synthesis which can be long and convoluted. A good chiral catalyst should provide *ee*'s in the range of 99% in the case of pharmaceuticals, if further enrichment is impossible. For agrochemicals lower *ee*'s might be acceptable. TONs should range from 1000 to 50000, depending on the scale and value of the products, but for a recyclable catalyst much lower limits are possible. The catalyst should of course be stable, both mechanically and chemically (*i.e.* no leaching of the active component). Few homogeneous catalysts and ligands are commercially available in the needed, technical quantities and their synthesis is therefore often also a part of the process development. Heterogeneous catalysts are generally unavailable and their synthesis and characterization requires knowledge and machinery typically unavailable in a standard process lab, especially for newer types of catalysts.[136] However, heterogeneous catalysts can be a convenient alternative to expensive, non-recyclable and difficult to synthetize homogeneous chiral catalysts and can even confer higher selectivity.[8] The general advantages of a heterogeneous catalyst, such as easy work up and recycling of the catalyst, allow straightforward recovering and reuse of the chiral component, typically the most expensive part of the system.[185]

Two main strategies exist for obtaining catalytic chiral POPs: postsynthetic modification or a bottom-up approach. The first strategy entails the addition or immobilization of chiral catalytic moieties to the porous material, whereas in the second strategy the synthesis of the POPs starts from chiral monomers, thus incorporating their chirality in the porous material and reducing the step count. The postsynthetic modification or immobilization of homogeneous (chiral) catalysts on supports can be done by covalent binding, adsorption, ion pair formation or entrapment.[186] The examples of POPs in the literature thus far only used covalent binding.

As supports other than POPs linear, non-crosslinked polymers or dendrimers can be used. These require solvents that they are soluble in, but give catalysts with good mass transfer properties. Separation of the catalyst, however, requires precipitation or ultrafiltration and is therefore difficult or costly.[187] Swellable, slightly crosslinked polymers are easily separated, but these need to be used in solvents in which they swell well.[136] The most widely used support of this type, and by far the most common support for immobilized chiral catalysts in general, are the Merrifield type resins (polystyrene and styrene/divinylbenzene copolymers).[185] Heterogeneous catalysts based on these swellable polymers generally possess a lower activity compared to the non-supported homogeneous counterpart, as we have seen earlier in the section discussing DMAP. This can, at least partially, be alleviated through the use of spacers.[134] Lastly, permanently porous materials (MOFs, metal oxides, POPs) barely swell and thus can be used regardless of solvent choice.[136]

1.5.1 Heterogeneous chiral BINOL-derived phosphonic acids

Chiral 1,1'-bi-2-naphthol (BINOL) derived phosphonic acids are important homogeneous catalysts and form an active area of research.[188] These chiral acids have been used as highly enantioselective catalysts in diverse reactions such as hydrogenations,[189] aza-Henry reactions,[190] Friedel-Crafts alkylations,[191] etc. However, these BINOL-based homogeneous catalysts are expensive, suffer from tedious synthesis sequences and have a very high molecular weight. Heterogenizing these catalysts on porous supports could help alleviate these drawbacks.[192] In 2010, Rueping *et al*. reported the first immobilized chiral Brönsted acids, by AIBN catalyzed radical crosslinking of catalysts **154-156** with styrene and divinylbenzene **11** resulting in polymers **P154-156** (Figure 3). The bulkier monomers **155** and **156** were synthesized to increase the enantioselectivity. The activity of the polymers was evaluated in the transfer hydrogenation of quinolines and benzoxazines. Yields and *ee*'s of up to 96% were reported (Scheme 40 and Table 4, entry 1) and the catalysts did not lose enantioselectivity or activity upon reuse.[193]

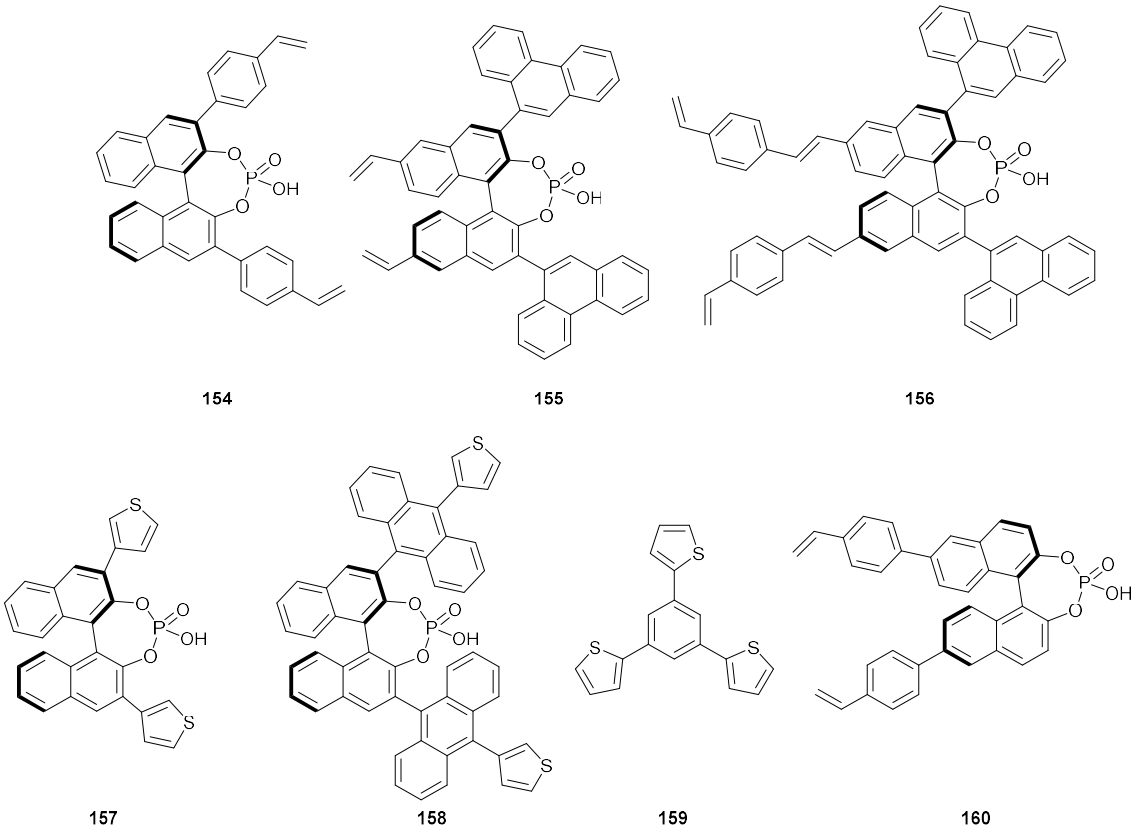

Figure 3: Monomers used to synthetize heterogeneous chiral Brönsted acids.[193,194,195,196,197]

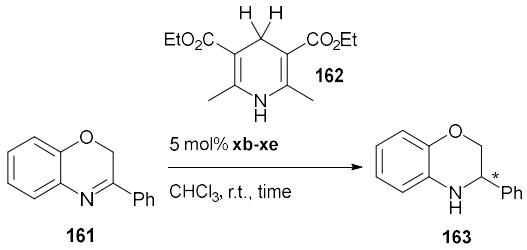

Entry	Catalyst, time	Yield (%)	*Ee* (%)	Ref.
1	P155, 20 h	92	64	[193]
2	P156, 20 h	96	96	[193]
3	157, 24 h	99	34	[194]
4	P157, 24 h	99	47	[194]
5	158, 2 h	99	99	[195]
6	P158, 2 h	99	98	[195]

Scheme 40 and Table 4: Catalytic asymmetric reduction of dihydro-2*H*-benzoxazine **161**.

In 2011, the group of Arne Thomas prepared a microporous polymer by oxidative $FeCl_3$ catalyzed polymerization of thiophene containing monomer **157** (Figure 3). This polymerization increased the steric hindrance of the side chains and thus positively influenced the selectivity of the catalyst. Due to solubility reasons, the acid chloride was polymerized, which after aqueous wash of the polymer yielded the phosphoric acid containing polymer with a BET surface of 88 m^2/g. These authors investigated the transfer hydrogenation of dihydro-2*H*-benzoxazine **161** (Scheme 40 and Table 4, entry 3 and 4). As predicted, the selectivity of the polymer **P157** (47%) was higher than that of the monomer **157** (34%), due to the crosslinking increasing the steric bulk close to the catalytic center. Interestingly, the enantioselectivity was also inversed. The reaction could be repeated three more times without loss in activity and with a slight increase in enantiomeric excess. This increase was hypothesized to be caused by the washing of residual acid from the pores that was catalyzing the racemic background reaction.[194]

In further research, the same group extended the linker with a phenanthrene moiety, obtaining building block **158**, which after oxidative polymerization resulted in a porous polymer with a BET surface of 386 m^2/g. This polymer was highly active and selective, obtaining 99% yield and 98% *ee* for the benzoxazine reduction (Scheme 40 and Table 4, entry 6), comparable to the homogeneous version (Table 4, entry 5) and retains its full activity and enantioselectivity after ten runs. Furthermore, these authors studied the reduction of 2-arylquinolines **164**, for which also high conversions (99%) and *ee*'s (87-97%) were reached (Scheme 41). The catalyst was also active in C-C bond formation by asymmetric Friedel-Crafts alkylation of pyrrole **167**, with nitrostyrene **166** and in an aza-ene reaction between substrates **169** and **170** (Scheme 42).[195] The same group copolymerized building block **158** with 1,3,5-tris(2-thienyl)benzene **159** to obtain increased surface areas. For 1:1 and 1:5 ratios of **158** to **159** networks with surface areas of, respectively, 577 and 668 m^2/g were reached. These increased surface areas translate into increased conversions compared to the polymer made from only monomer **158** for the reduction of 2-phenylquinoline.[196] Lastly, Huangfu *et al*. synthesized a porous chiral binaphthyl phosphoric acid based material **PPO-BNPA** by polymerization of **160**. This material catalyzed the asymmetric reduction of phenyl methyl ketone with borane, with conversion reaching 99%, however only an *ee* of 70% was reported.[197]

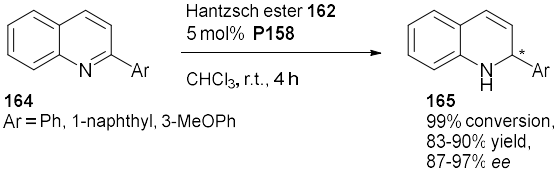

Scheme 41: Asymmetric reduction of 2-arylquinolines.[195]

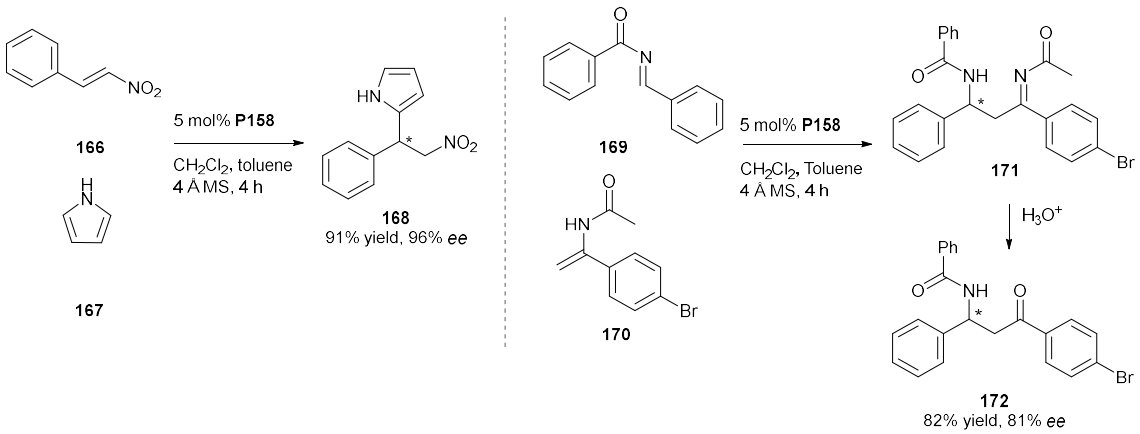

Scheme 42: Friedel-Crafts alkylation and aza-ene reaction catalyzed by **P158**.[195]

1.5.2 Chiral amine organocatalysis

Asymmetric catalysis using chiral amines is a very useful way to generate chirality, and has gained tremendous attention since seminal works of List *et al*. and MacMillan *et al*. in 2000.[198–200] However, applications on larger or industrial scales are limited by the amines low efficiency, the high catalyst loading of typically 10-30 mol% needed and the difficulty separating these high amounts of catalyst from the products. Therefore, the development of heterogeneous, recyclable chiral amine catalysts is a very hot topic.

1.5.2.1 Postsynthetic modification

Jiang *et al*. reported the first example of chiral organocatalytic COFs in 2013. These authors synthesized mesoporous imine-linked porphyrin COFs **[HC≡C]$_X$-H2P-COFs** by condensation of 5,10,15,20-tetrakis(4'-tetraphenylamino) porphyrin (H2P) **174** with varying amounts of 2,5-dihydroxyterephthalaldehyde **19** and 2,5-bis(2-propynyloxy)terephthalaldehyde **173** (Scheme 43). A click reaction of chiral azide **175** with the ethynyl groups of the COF anchored the chiral catalytic moieties to the pore walls leading to **[Pyr]$_X$-H2P-COFs**. The disappearance of the typical alkyne vibration bands was observed in the infrared spectrum, proving that all the ethynyl groups had reacted. The COFs with increased ethynyl content possessed a decreased crystallinity due to the larger number of amorphous units on the walls, and a decreased surface area, which declined further after the click reaction. **[Pyr]$_X$-H2P-COFs** were highly active catalysts for the Michael addition reaction between nitrostyrenes **177** and propion- or butyraldehyde **176** with the least substituted COF, **[Pyr]$_{25}$-H2P-COF**, being the most active (Scheme 44). The organocatalytic COF showed a much higher activity than a monomeric control. The authors hypothesize that the reagents, which are poorly soluble in the reaction mixture, accumulate on the walls of the COF, hereby increasing the activity. A variety of substrates were reacted and all reached full conversion in less than one hour with moderate *ee*'s and *dr*'s. The catalyst could be used at least four times, however the reaction time needed to be increased drastically. Upon the fourth time the required time had increased almost fivefold and the BET surface area also showed a massive decrease with only 104 m^2/g remaining. This could indicate that pore channels became blocked during the reaction. The authors also applied their catalyst in a continuous flow setup, and could maintain 100% conversion with 44% *ee* and 65/35 *dr* for more than two days.[201]

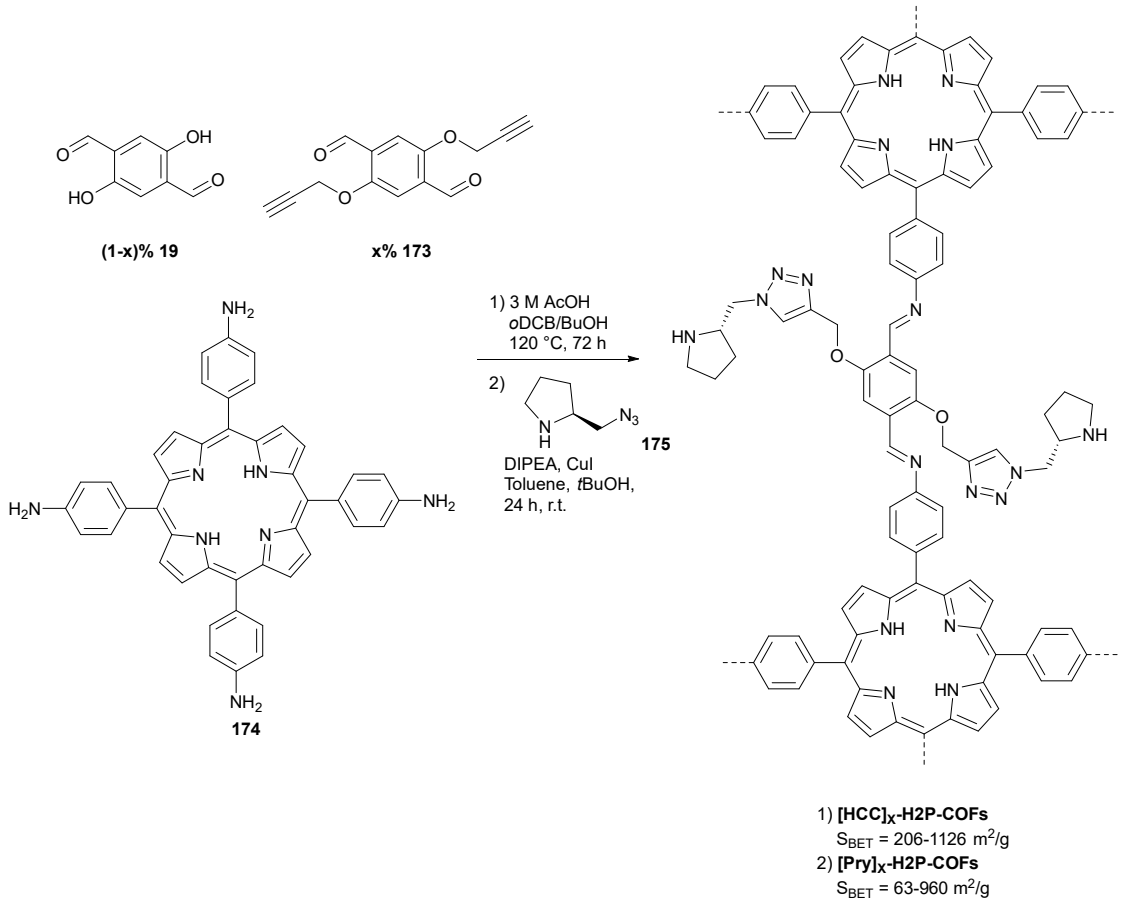

Scheme 43: Synthesis of chiral **[Pyr]$_X$-H2P-COFs** by click reaction with a chiral azide.[201]

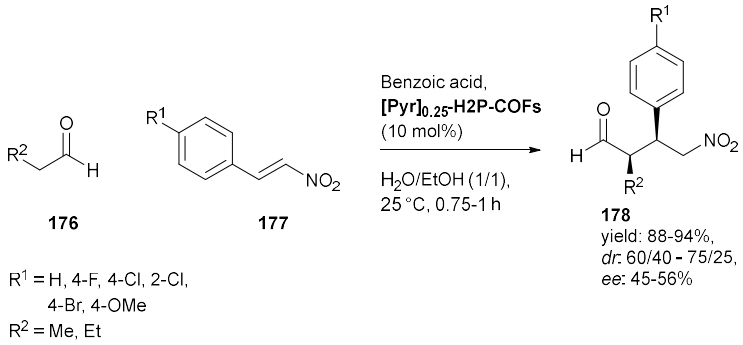

Scheme 44: Asymmetric reaction between nitrostyrenes **177** and aldehydes **176**.[201]

In 2015, Jiang *et al*. reported the design of chiral COF based on analogous principles. Triphenylbenzene knots **179** were used with 2,5-dimethoxyterephthtalaldehyde **20** and 2,5-bis(2-propynyloxy)terephthalaldehyde **173** linkers (Scheme 45). Interestingly, this resulted in extremely stable COFs originating from the methoxy substituted linkers. In imine COFs significant polarization of the C=N bond exists, due to the electronegativity difference between nitrogen and carbon. This polarization disrupts the interlayer force, responsible for keeping the structure together, and destabilizes the layered structures. The electron donating methoxy groups delocalize their oxygen lone pairs into the phenyl rings, hereby strengthening interlayer interactions, stabilizing the COF and aiding in crystallization.[202] The **[HC≡C]$_X$-TPB-DMTB-COFs** were highly porous (1297-1973 m^2/g), with large

pore diameters, and were stable in boiling water, strong acid and base. After the synthesis these materials were subjected to a click reaction with azide **180** furnishing **[(*S*)-Py]$_x$COFs** without affecting the porosity much. The chiral COFs could act as catalysts for Michael additions of cyclohexanone **181** with nitrostyrenes **182** in water with high activity and selectivity (Scheme 46). The least substituted (x = 0.17) COF showed the highest activity, obtaining 100% conversion after six hours, performing better than the homogeneous control, and was further used to transform a range of nitrostyrenes. When COFs with a higher loading of reactive sites were used, the reaction times needed were much longer. The high density of sites leads to overlap and reduces the accessibility of the active sites. Recycling was possible and the selectivity was unchanged, however as in the previous example reaching full conversions required much longer reaction times.[203]

1.5.2.2 Bottom-up approach

Building chiral polymers starting from chiral building blocks can have some advantages. The attachment of bulky amorphous groups onto the pore walls generally lowers the chemical stability, crystallinity and surface areas of the material. Starting from chiral building blocks also removes one extra step from the procedure, saving time, money and reducing possible complications. In 2016, Xu *et al*. constructed the first example of a chiral COF constructed by direct synthesis. Condensation followed by Boc-deprotection of chiral benzimidazolium monomer **184** with 1,3,5-triformylbenzene **48** or 2,4,6-triformylphloroglucinol **71** led to highly crystalline imine-linked **LZU-72** and β-ketoenamine-linked **LZU-76**, with BET surface areas of respectively 1114 m^2/g and 758 m^2/g (Scheme 47). Due to its higher acid stability **LZU-76** was evaluated in the asymmetric aldol reaction of arylaldehydes **185** with acetone yielding β-hydroxyketones **186** in moderate to good yields and with high *e.r.* compared to an homogeneous catalyst analogue (Scheme 48). **LZU-76** could be recycled up to five times, however the yield dropped drastically.[204]

The same group then developed a general strategy based on this benzimidazole scaffold to divergently synthetize a range of chiral COFs. Eight chiral aldehyde building blocks **188-195** were synthesized through nucleophilic substitution followed by Suzuki coupling of key building block **187**. Different chiral COFs with identical framework structures were prepared from these monomers through Schiff base condensation (Scheme 49). **MH-CCOF1-4** possess multiple hydrogen bonding sites, **TAH-CCOF1-2** possess both tertiary amine and hydrogen bonding sites. **SAH-CCOF-1-Boc** features secondary amine and hydrogen bonding sites and lastly **G-CCOF-1** has guanidine moieties. The authors studied the asymmetric amination reaction of ethyl 2-oxocyclopentane-1-carboxylate **196** with di-*tert*-butyl azodicarboxylate (DBAD) **197** to compare the performance of the different organocatalysts. **TAH-CCOF1** and **TAH-CCOF2** displayed the best activity, **TAH-CCOF2** was then used to convert a range of β-keto-esters in high yields and with high enantioselectivity of up to 98% and 91%, respectively (Scheme 50).[205]

Zhang *et al*. reported the synthesis of another range of chiral COFs. Four L-proline and L-imidazoline based 1,3,5-tris(4-aminophenyl)benzene (TPB) **199** building blocks were condensed with 2,5-dimethoxyterephthtalaldehyde **20**. Utilizing amine **TPB5**, no crystalline material could be obtained. The other, fully substituted COFs **DMTA-TPB1-4** were crystalline. However, after Boc and methyl ester deprotection only amorphous powders were formed. The high number of organocatalytic sites, containing bulky groups, probably interrupts the interlayer π-π interactions which stabilize the COFs. Especially after Boc-deprotection, the free amines can interact strongly with the methoxy and/or imine groups of the framework.[206] Co-synthesis with a substituent free building block **TPB-1** decreased the steric hindrance and weakened the interlayer repulsion, hereby increasing the crystallinity. When

utilizing a 1/1 ratio of building blocks **TPB2-5** with **TPB1** highly crystalline COFs **DMTA-TPB1/2-5** were formed. Deprotection furnished crystalline **DMTA-TPB1/2'-5'** containing free amine and carboxylic acid groups (Scheme 51). The organocatalytic COFs were applied in asymmetric α-amino-oxylation, aldol and Diels-Alder reactions with good yields, selectivity and recyclability (Scheme 52). Amorphous analogues were much less active and needed extended reaction times, due to the non-uniform distribution and limited accessibility of their catalytic moieties.[207]

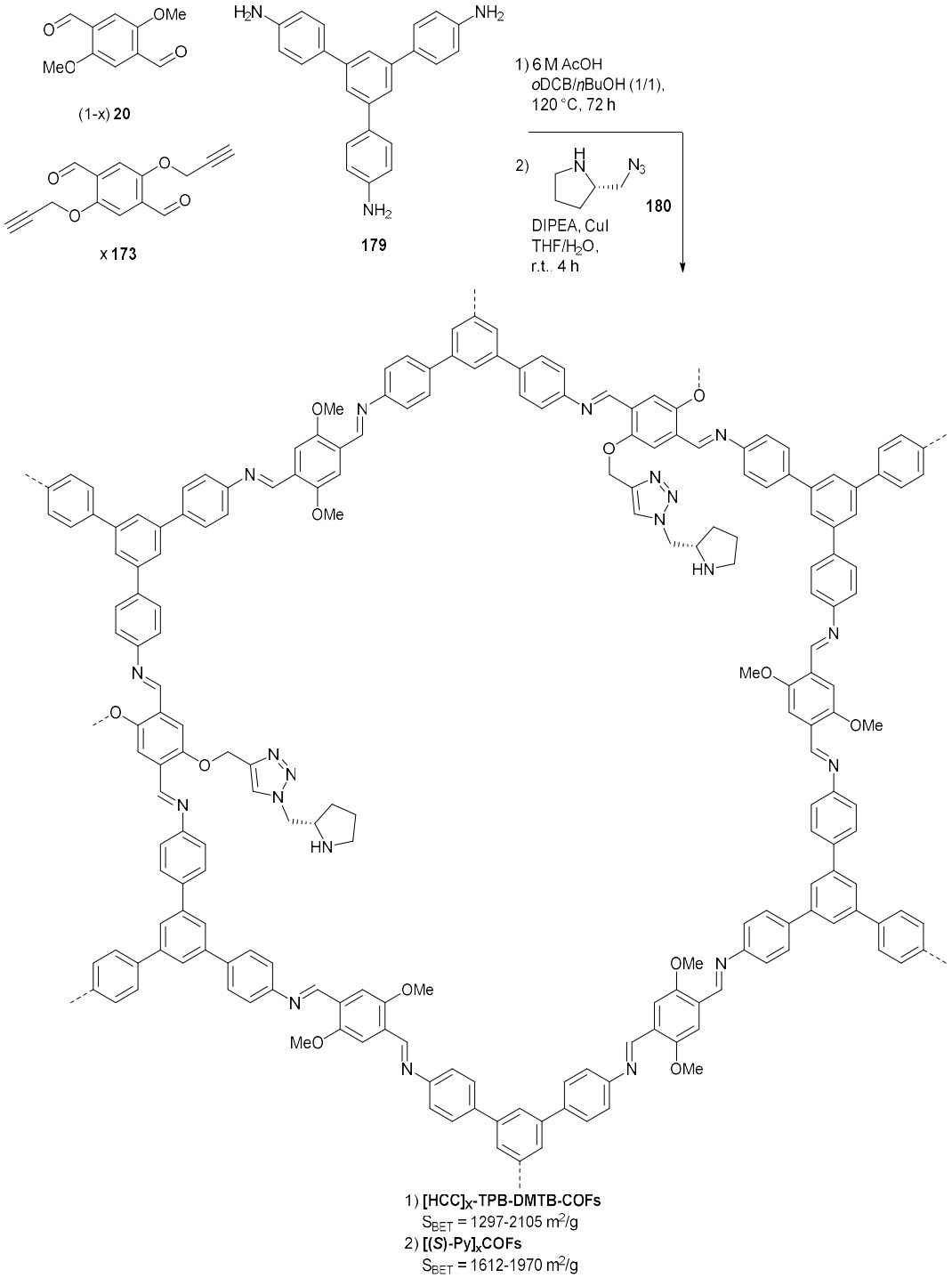

Scheme 45: Synthesis of chiral COFs by imine formation and click reaction.[203]

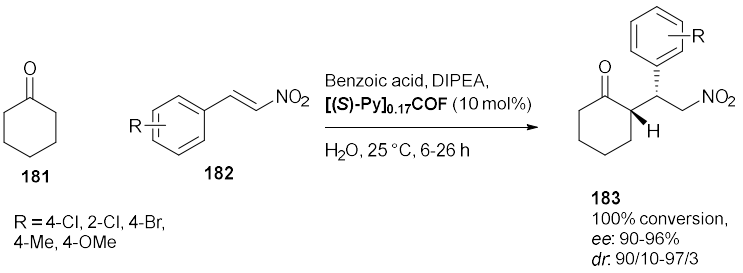

Scheme 46: Asymmetric Michael additions of cyclohexanone **181** with nitrostyrenes **182**.[203]

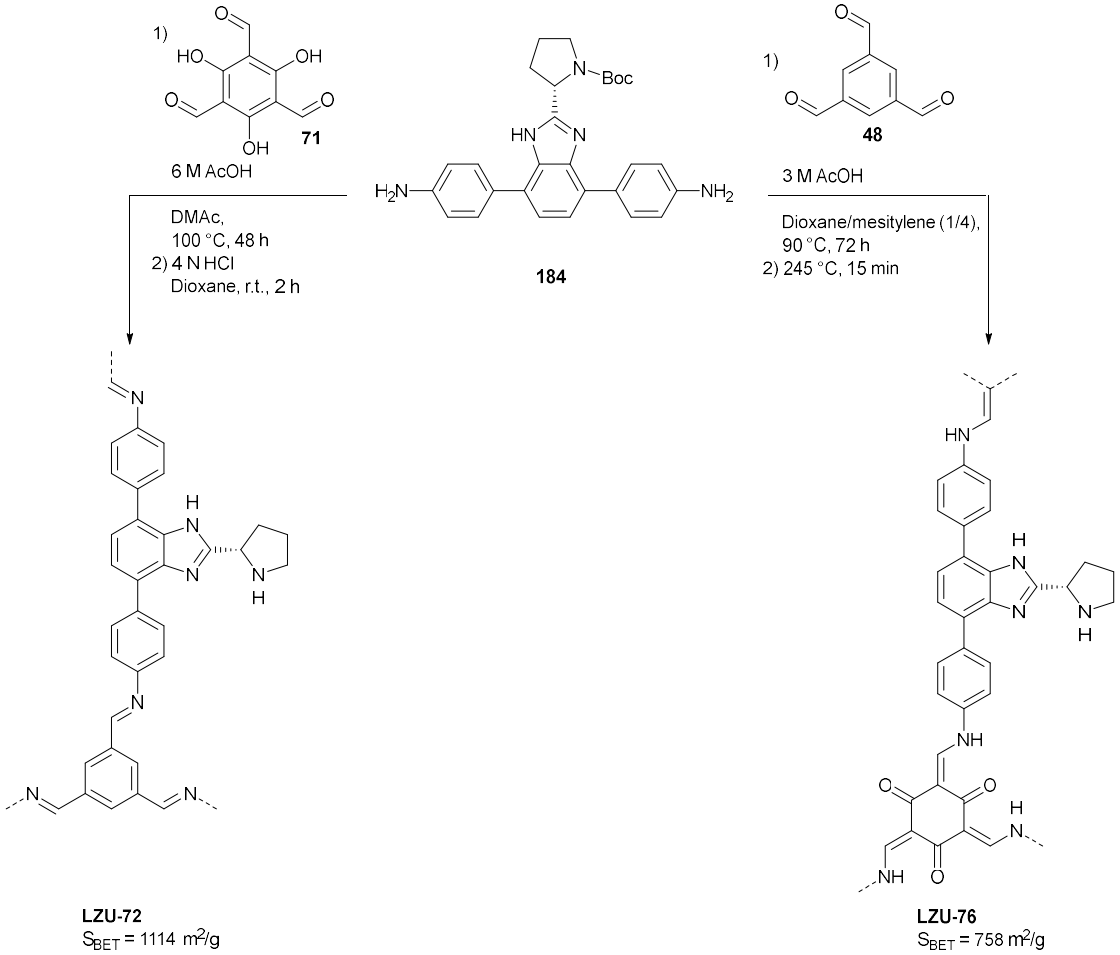

Scheme 47: Synthesis of chiral imine or β-ketoenamine-linked COFs **LZU-72** and **LZU-76** starting from chiral amine **184**.[204]

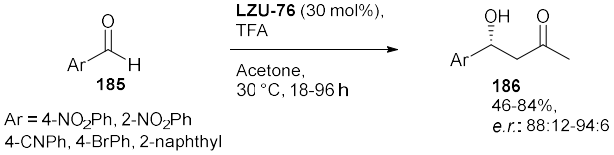

Scheme 48: **LZU-76** catalyzed asymmetric aldol reaction of arylaldehydes **185** with acetone.[204]

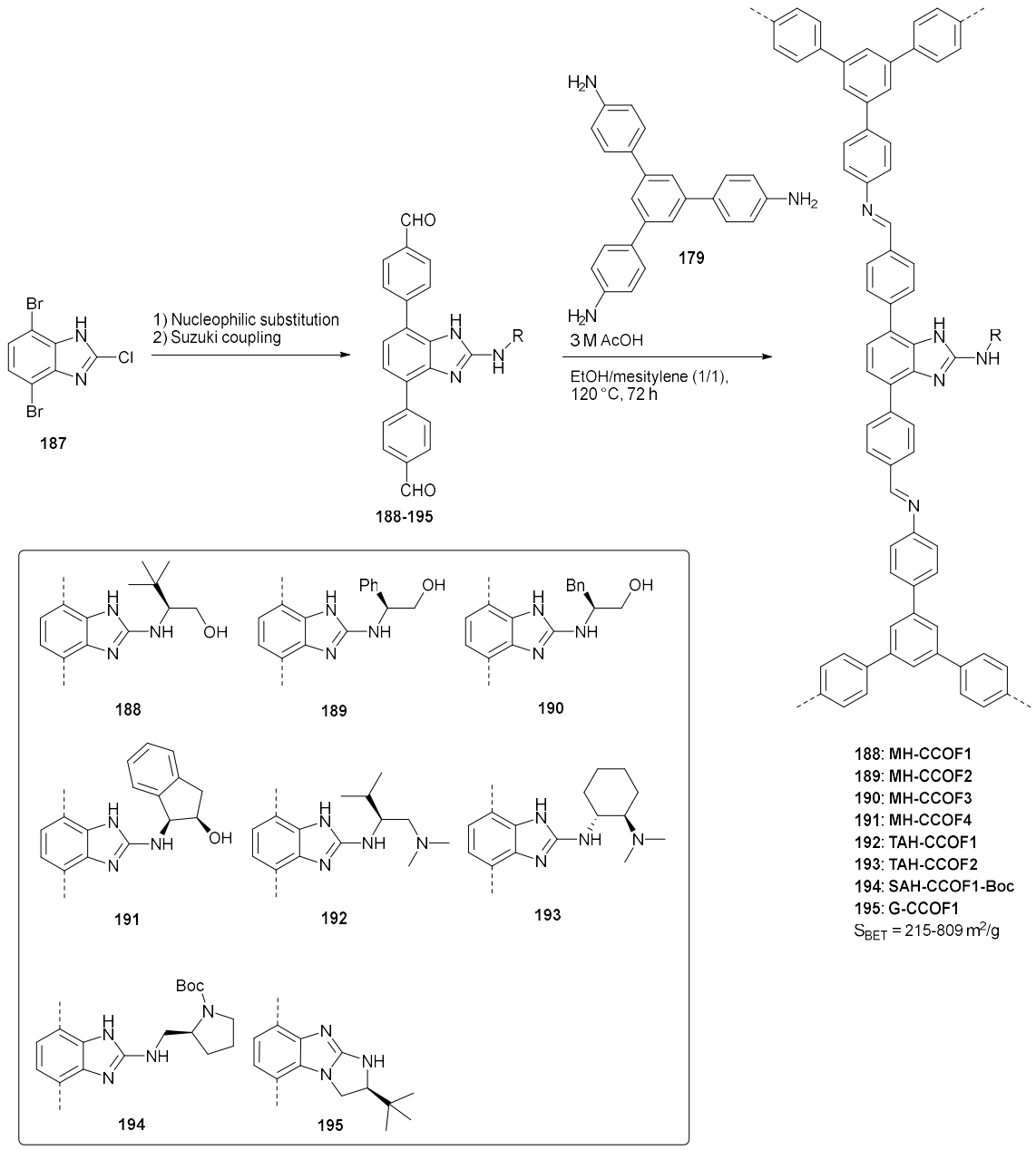

Scheme 49: Synthesis of a family of chiral COFs containing different types of organocatalytic moieties.[205]

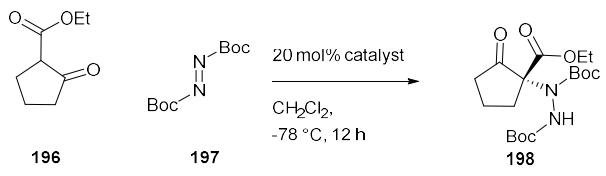

Catalyst	Yield (%)	*ee* (%)
MH-CCOF1	81	12
MH-CCOF2	72	8
MH-CCOF3	70	9
MH-CCOF4	65	5
TAH-CCOF1	94	89
TAH-CCOF2	96	99
SAH-CCOF1-Boc	67	27
G-CCOF1	61	3
Homogeneous control	78	92

Scheme 50: Asymmetric amination reaction of ethyl 2-oxocyclopentante-1-carboxylate **196** with DBAD **197**.[205]

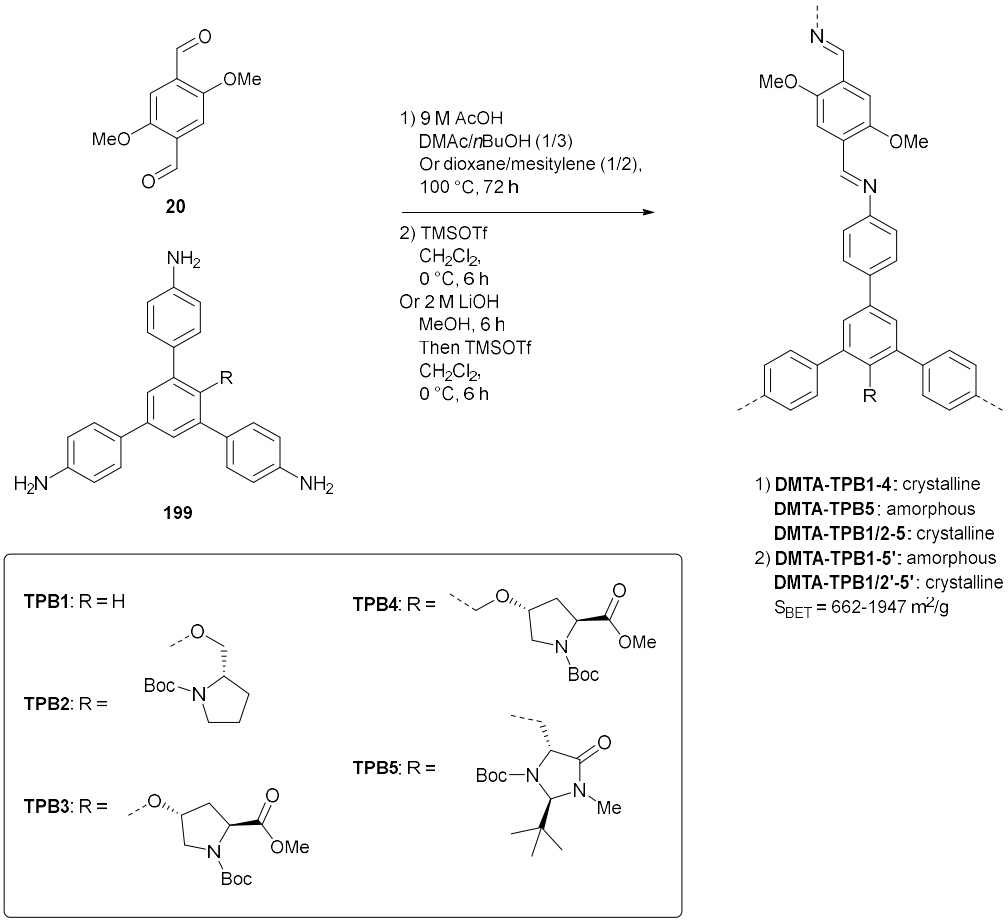

Scheme 51: Synthesis and deprotection of a range of chiral COFs based on 1,3,5-tris(4-aminophenyl)benzene **199**.[207]

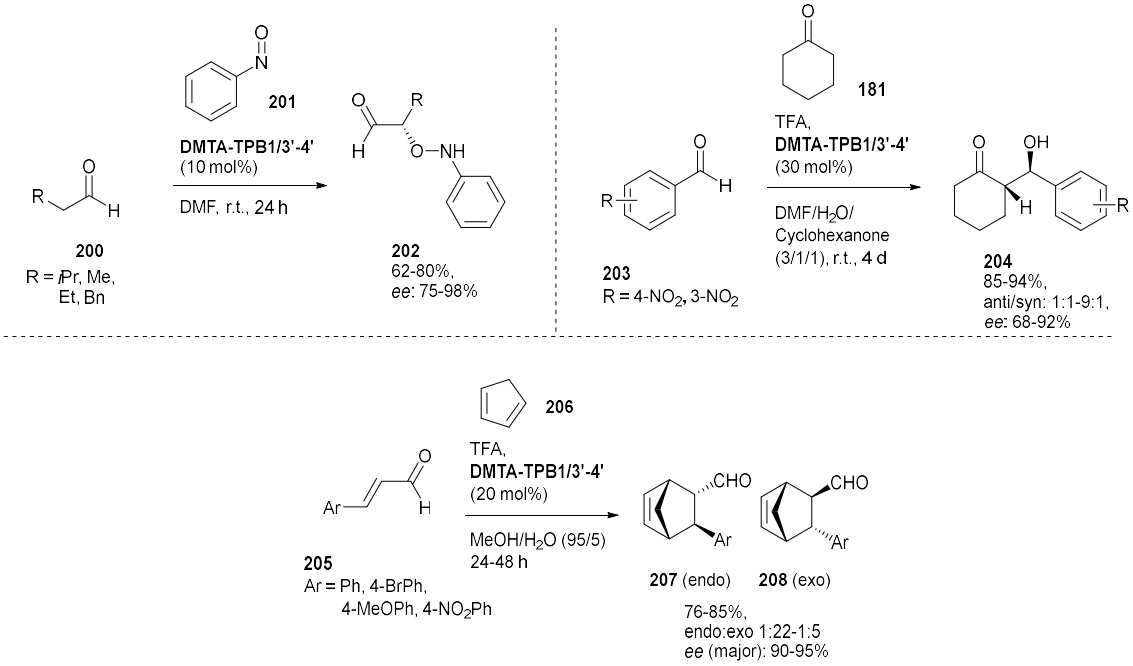

Scheme 52: Asymmetric α-amino-oxylation, aldol and Diels-Alder reactions catalyzed by **DMTA-TPB1/3'-4'**.[207]

In 2019, Cui and coworkers reported the synthesis of two chiral COFs by condensation of chiral building blocks **210** and **211** containing 6,7-dihydro-5*H*-pyrrolo[1,2-*a*]imidazole or pyrrolidine moieties resulting in **TPB2-COF** and **Tfp2-COF**, respectively (Scheme 53). **TBP2-COF** was able to reach high conversions and good *ee*'s, comparable to a homogeneous counterpart, in the Steglich rearrangement of oxazoles **212**, a convenient way to generate quaternary stereocenters (Scheme 54).[208] **Tfp2-COF** demonstrated good conversion and selectivity in the Michael reactions of nitrostyrenes **214** with cyclohexanone **181** (Scheme 54). Both COFs could be recycled at least five times and retained their porosity and crystallinity.[209]

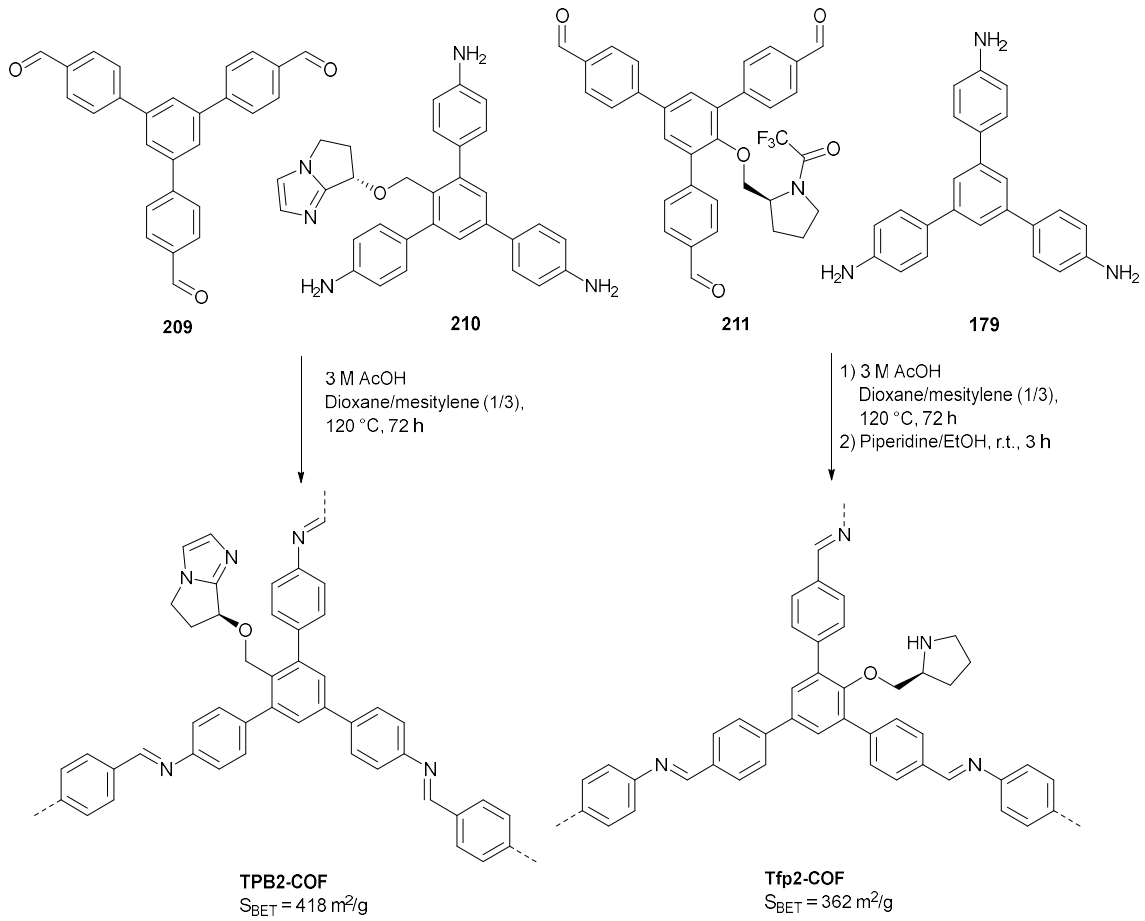

Scheme 53: Bottom-up synthesis of chiral COFs with pyrrolidine and 6,7-dihydro-5*H*-pyrrolo[1,2-*a*]imidazole moieties.[209]

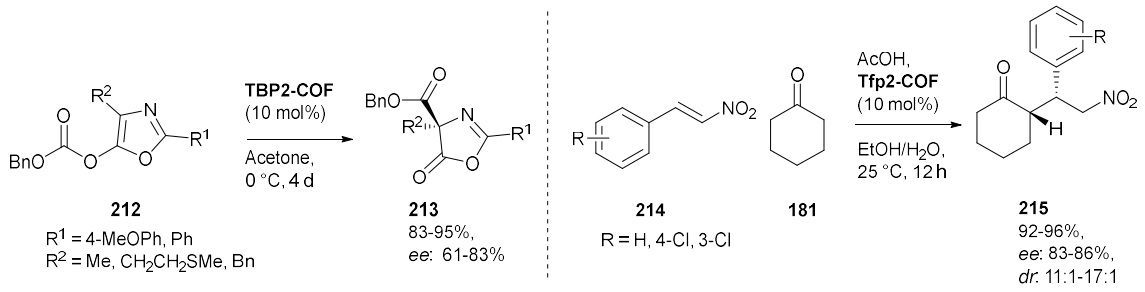

Scheme 54: Asymmetric Steglich rearrangement and Michael addition.[209]

Next to these aforementioned COFs many amorphous porous polymers with chiral moieties have been applied as catalysts. In 2012, Wang *et al*. reported a chiral POP containing Jørgensen-Hayashi catalysts (diarylprolinol silyl ethers).[210,211] This porous polymer **JH-CPP** was synthesized by alkyne trimerization mediated by dicobalt octacarbonyl of a chiral functional building block **216** and structural building block (tetra(4-ethynylphenyl)methane **42** (Scheme 55). The catalytic activity was tested by an asymmetric Michael addition between nitrostyrenes **218** and aldehydes **217** (Scheme 56). High yields and good enantio- and diastereoselectivities were reported for a wide variety of substrates. In recycling experiments the authors observed a lowering of the yield to 51% in the third run and a lowered surface area of 578 m^2/g after the fourth run. Structural analysis via solid state ^{13}C-NMR showed that the structure of the material was retained, however new signals appeared. The authors state that a part of the substrates stays bound to **JH-CPP** in the form of the catalyst resting state **220**, the bulky cyclobutane intermediate.[212] The inclusion of these bulky intermediates in the small pores slows down the reaction. This lowering of activity was also observed in similar proline containing polymers.[213]

In 2017, the same group reported new chiral POPs based on a MacMillan catalyst containing building block. **Mac-CPOP-1** and **Mac-CPOP-2** were obtained by palladium catalyzed Sonogashira coupling of chiral building block **222** with tritopic linkers **7** or **221** (Scheme 57). **Mac-CPOP-2** possessed a surface area of 468 m^2/g. However, **Mac-CPOP-1** showed no permanent porosity due to congestion of the imidazolidinone moieties inside the free volumes. These POPs showed good activity (64-95%) as enantioselective Diels-Alder catalysts for a wide range of β-unsaturated aldehydes **223** with cyclopentadiene **206** (Scheme 58).[214]

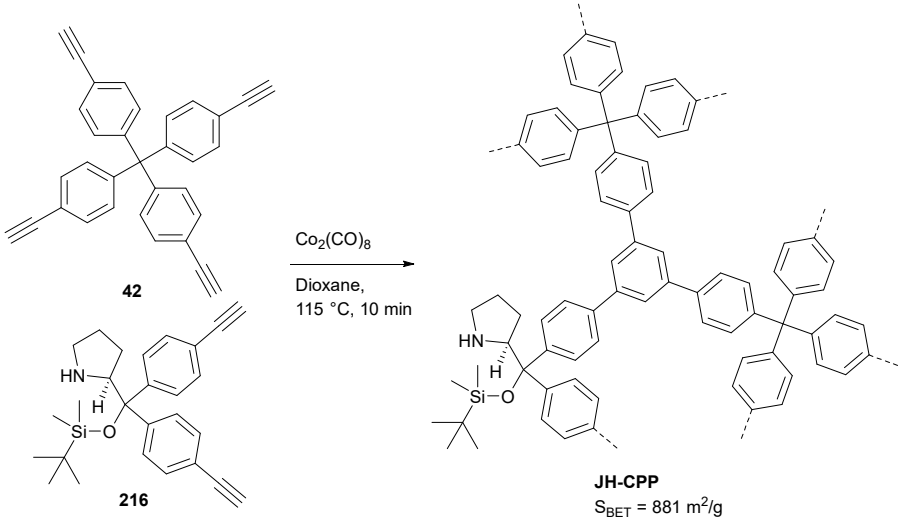

Scheme 55: Synthesis of **JH-CPP** by cobalt catalyzed alkyne trimerization.[213]

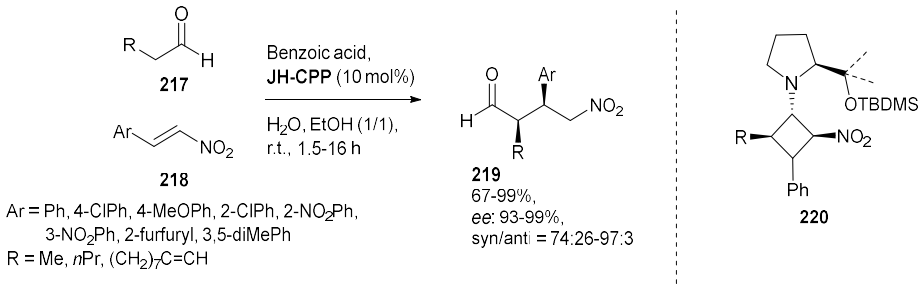

Scheme 56: Michael addition catalyzed by **JH-CPP** and proposed catalytic resting state intermediate **220**. [213]

In 2019, Lan *et al*. reported another direct synthesis of a chiral pyrrolidine based POP via a bottom-up strategy to perform Michael additions in water. From a green chemistry perspective, water is an extremely attractive solvent and therefore the development of effective organocatalytic Michael additions in water has attracted great interest. The followed strategy typically entails linking the polar organocatalytic moiety with large hydrophobic groups. These groups are capable of aggregating the hydrophobic reactants and intermediates in water and hereby increase the reaction rate. Via Sonogashira coupling of tetratopic building block **42** with functional building block **226** a chiral CMP **Py-CPP** with a modest surface area of 228 m^2/g was obtained (Scheme 59). A wide range of Michael products could be formed with high yield and selectivity at room temperature in water (Scheme 60). The authors state that the incorporation of the triazole moiety led to high stereoselectivities due to it shielding the *si* face of the enamine double bond.[215] This material also possessed size selectivity: a naphthyl substituted nitroolefin already showed a greatly decreased yield, and with a pyrene substituted substrate only trace amounts of product were observed.[216] Cao *et al*. prepared chiral PAFs by Yamamoto cross-coupling between brominated tetraphenylmethane compound **229** and mono or ditopic functional building blocks **230** and **231** furnishing dPOFs1-4 (Scheme 61). **dPOF4** formed from the 'low-connected', monotopic functional monomer **231**. 'Low-connected' building blocks are much more readily available or prepared. This greatly extends the type of POPs that can be easily prepared. These dPOFs catalyzed the aldol condensation between carbonyl compounds **233** and 2-,3- or 4-nitrobenzaldehyde **232** with moderate yields and ee's (Scheme 62).[217]

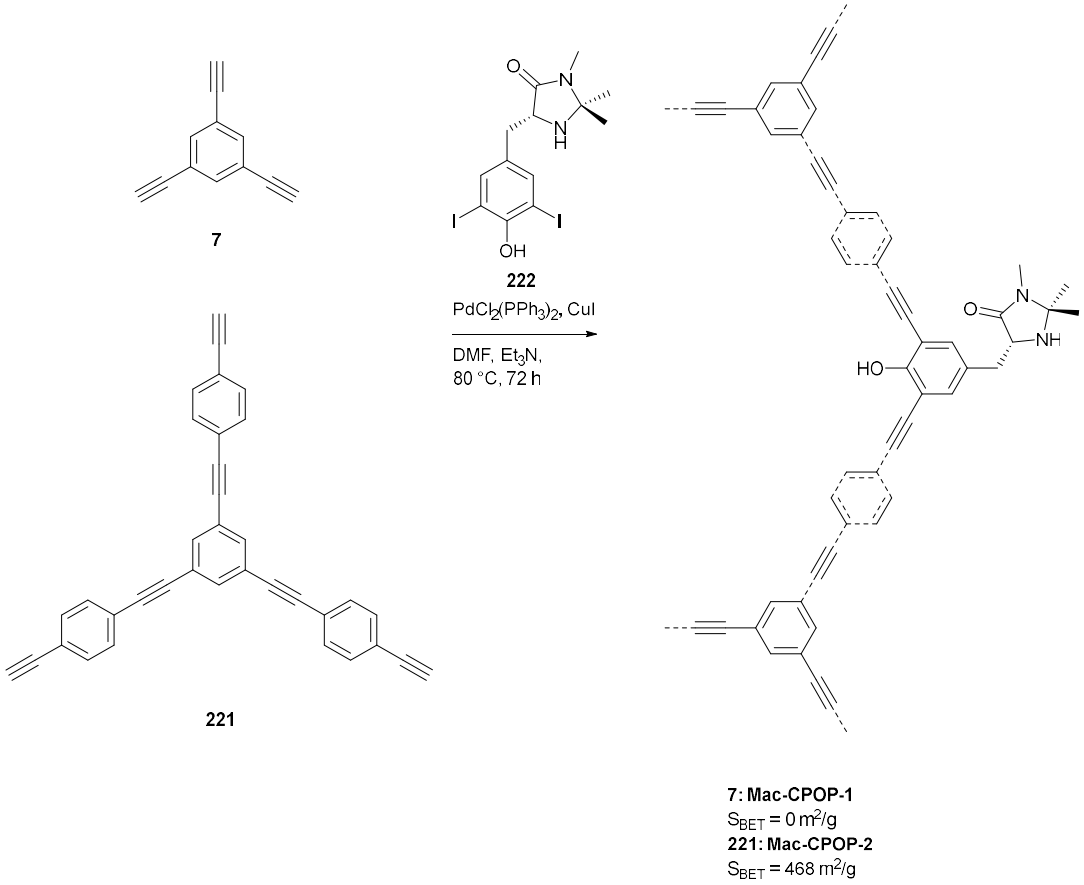

Scheme 57: Synthesis of Macmillan catalyst containing chiral POPs **Mac-CPOP-1** and **Mac-CPOP-2**.[214]

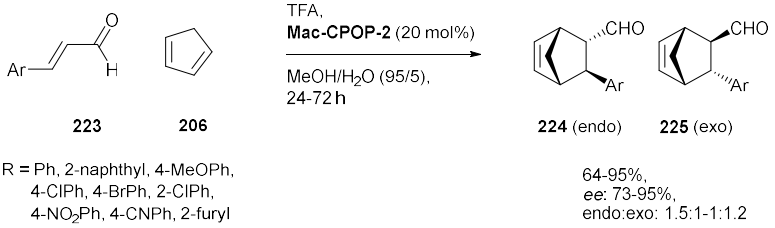

Scheme 58: Asymmetric Diels Alder reaction catalyzed by **Mac-CPOP-2**.[214]

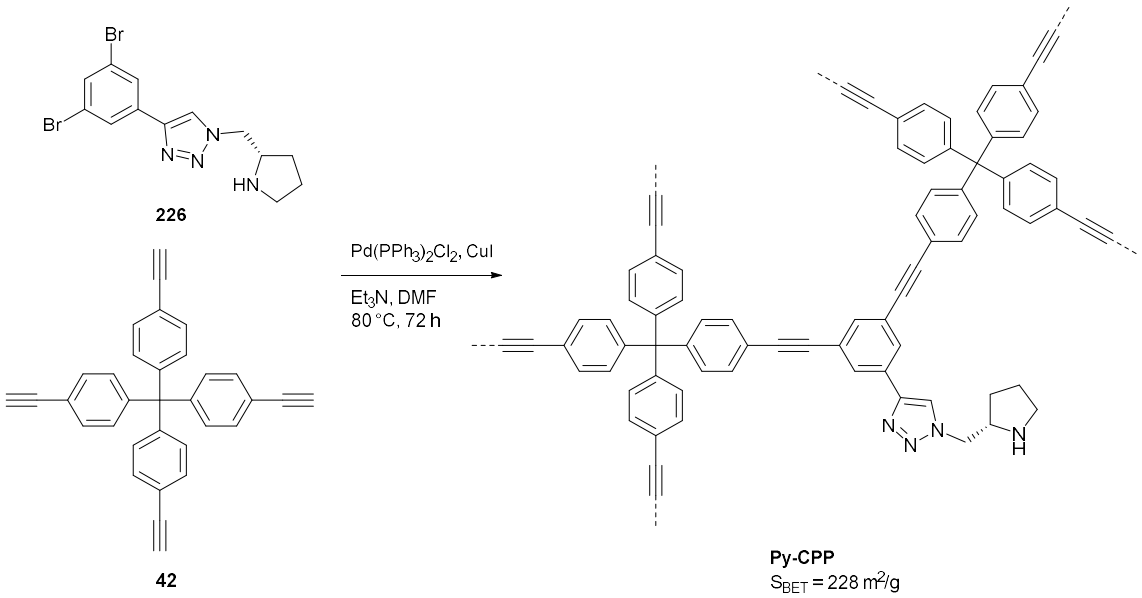

Scheme 59: POP containing chiral pyrrolidine moieties synthesized by Sonogashira coupling.[216]

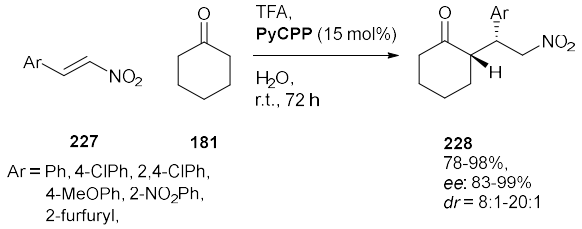

Scheme 60: Asymmetric Michael addition catalyzed by **PyCPP**.[216]

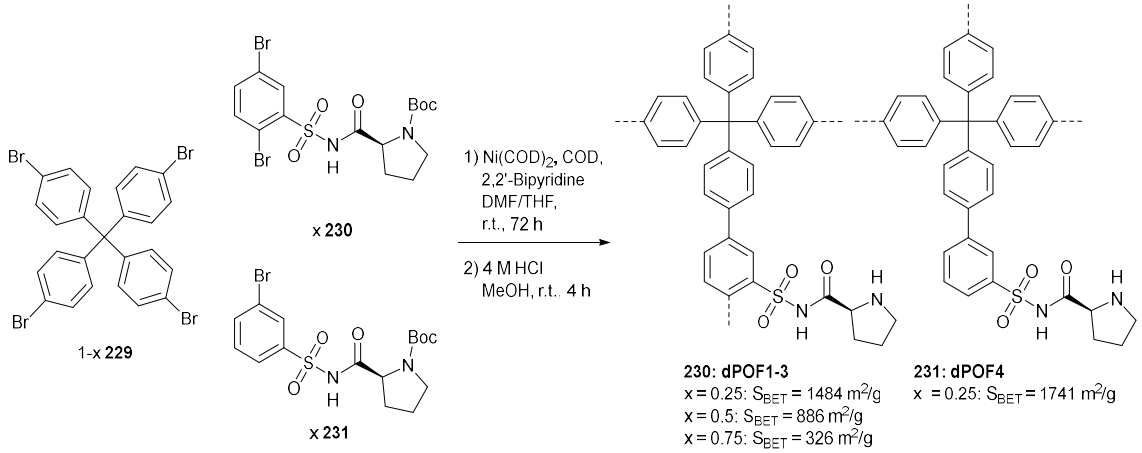

Scheme 61: Synthesis of chiral POPs by reactions with 'low-connected' building blocks.[217]

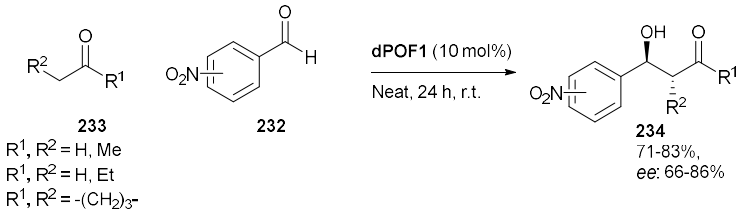

Scheme 62: **dPOF1** catalyzed aldol condensation.[217]

1.5.2.3 Asymmetric synthesis

Next to their direct synthesis and postsynthetic modification, chiral COFs can be synthesized by chiral induction or asymmetric catalysis.[218,219] Recently, Wang *et al*. synthesized chiral COFs, **(*R*)-** or **(*S*)-DTP-COF** via a multicomponent one-pot polymerization of dialdehyde **20**, amine **18** and phenylacetylene **235** catalyzed by chiral pyridine-2,6-bis(oxazolines)-Cu(I) complexes (Scheme 63). Circular dichroism spectra were taken to prove the chiral nature of these COFs. **(*S*)-DTP-COF** catalyzed the Michael addition between cyclohexanone and a wide range of nitrostyrenes with high yields (83-97%) and good selectivity (*ee*: 90-99% and *dr*: 68:32-88:12).[219]

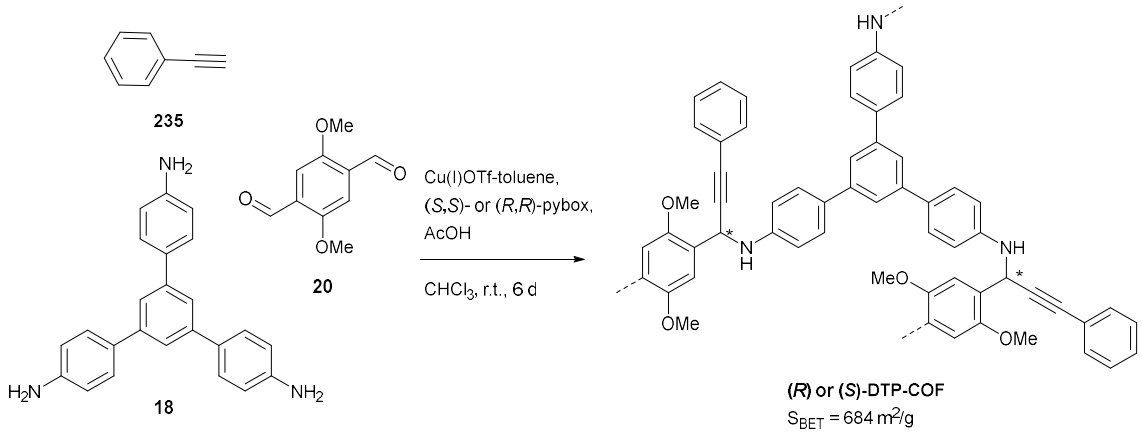

Scheme 63: A chiral COF synthesized by asymmetric synthesis.[232]

1.5.3 Other chiral catalysts

In a very early report in 2009 by Du *et al*. on metal-free POP catalysts, diiodo functionalized Tröger's base **236** was polymerized through Sonogashira coupling with triethynylbenzene **7** (Scheme 64). The resulting POP had a relatively high surface area (750 m^2/g) and showed reasonable activity (74% yield) for the addition of diethylzinc to 4-chlorobenzaldehyde. However, the polymer itself was racemic and thus the reaction was not enantioselective.[220]

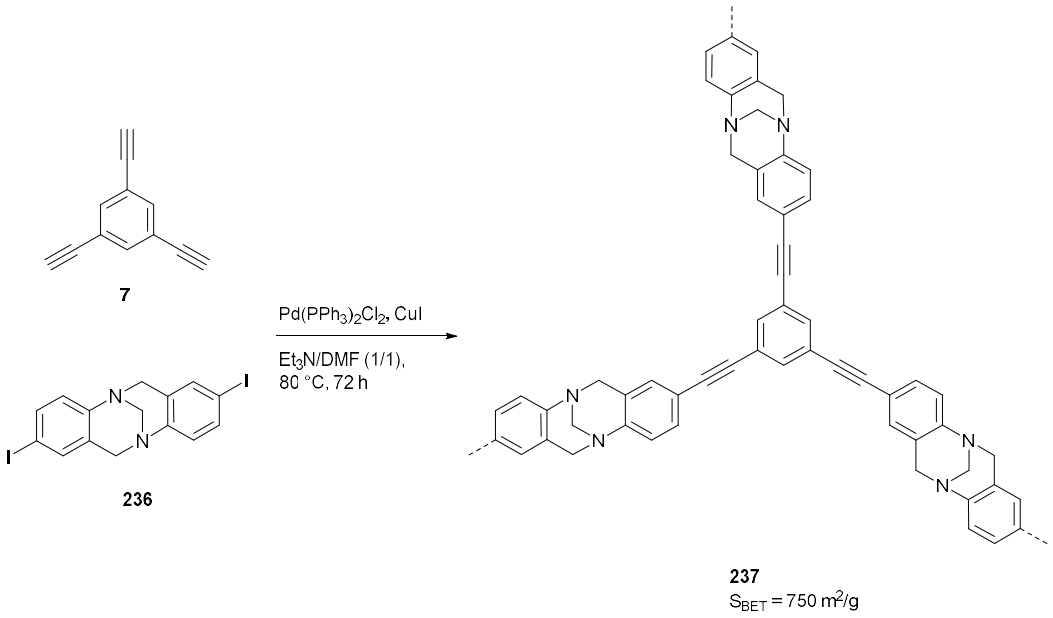

Scheme 64: Synthesis of a Tröger's base containing POP by Sonogashira coupling.[220]

The same reaction has been asymmetrically catalyzed by porous polymers synthesized by the trimerization of alkyne groups of BINOL derived building blocks. After treatment with titanium isopropoxide (Ti(O*i*Pr)$_4$), these polymers were converted into chiral heterogeneous Lewis acid catalysts, however only moderate *ee's* (up to 81%) were reached in the addition reaction.[221] Analogously, α,α,α',α'-tetraaryl-2,2-disubstituted 1,3-dioxolane-4,5-dimethanol (TADDOL) building blocks functionalized with alkynes were coupled via Sonogashira coupling with tetrakis(4-bromophenyl)methane. These materials were treated with Ti(O*i*Pr)$_4$ or reacted in the presence of Ti(O*i*Pr)$_4$ which gave higher *ee*'s (up to 91%).[222] Two-dimensional COFs with embedded chiral functionalities were synthesized by imine condensations of TADDOL-derived tetra-aldehydes with 4,4′-diaminodiphenylmethane. After postsynthetic modification of the chiral dihydroxy groups with Ti(O*i*Pr)$_4$ these COFs were efficient and recyclable heterogeneous catalysts for asymmetric addition of diethylzinc to aldehydes with high enantioselectivity (up to 94%).[223]

Recently, Ma *et al*. developed a chiral COF **(*R*)-CuTAPBN-COF** for the catalytic asymmetric synthesis of a key intermediate, (*S*)-CIK **242**, in the synthesis of (*S*)-clopidogrel **243**, an antiplatelet medication used as a heart disease and stroke risk reducer. The chiral COF was synthesized by imine formation between chiral BINOL derived dialdehyde **239** and cupper containing porphyrin based amine **238** (Scheme 65). (*S*)-CIK was obtained via an asymmetric **(*R*)-CuTAPBN-COF** catalyzed Strecker reaction between aldehyde **241** and amine **240** in 98% yield with 94% *ee* (Scheme 66). The BINOL derived moieties acted as chiral Lewis acids, whereas the porphyrin units acted as photothermal conversion units, converting light into heat, increasing the temperature in the reaction vessel from room temperature to 50 °C. In

the dark, at this temperature, a similarly high yield was obtained. However, in the dark, at room temperature no product could be detected. Moreover, these authors designed a model continuous flow-through setup for the gram scale preparation of (*S*)-CIK which proceeded smoothly, producing 1.29 grams in eight hours with a yield of 90% and 93% *ee*. Furthermore, a range of different aldehydes and secondary amines could be converted with excellent yield and *ee*'s, except for larger substrates such as fluorene-2-carboxaldehyde or 9-anthracenecarboxaldehyde.[224]

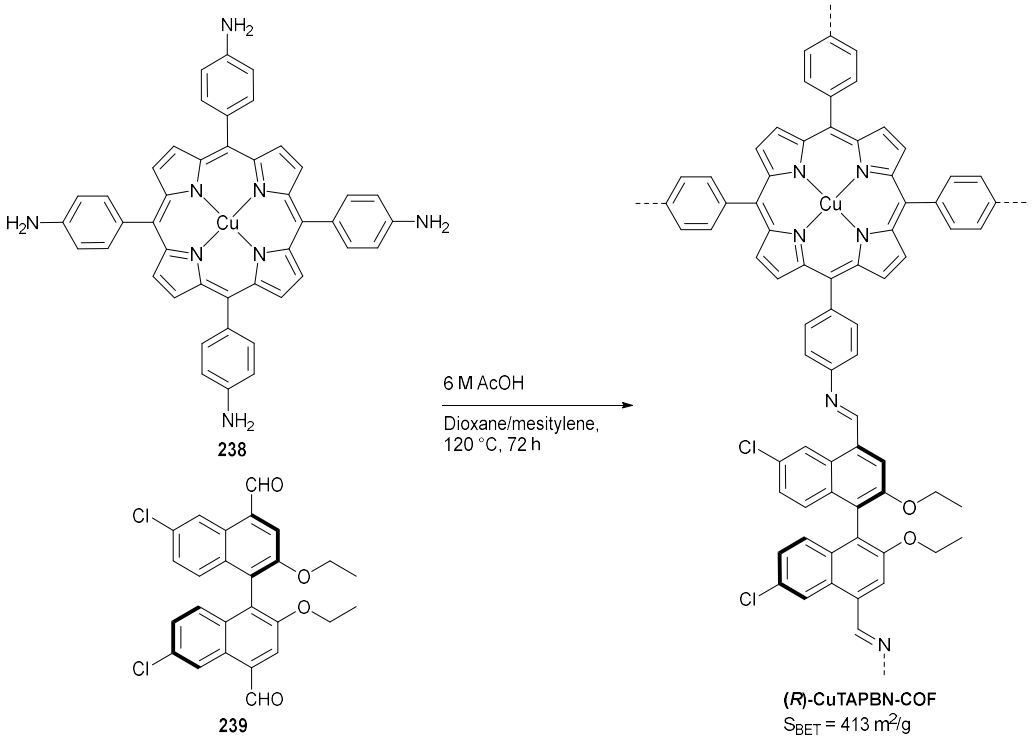

Scheme 65: Synthesis of a chiral COF by condensation between porphyrin **237** and BINOL based aldehyde **238**.[224]

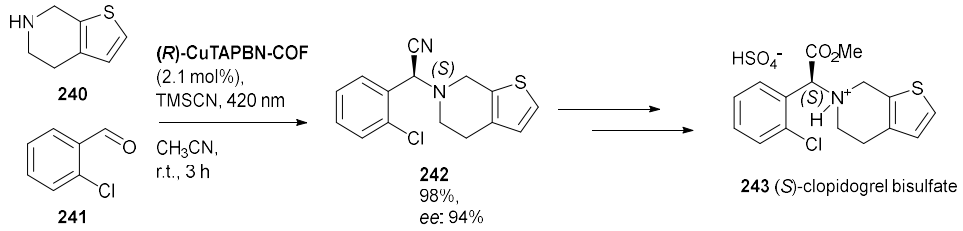

Scheme 66: COF mediated asymmetric Strecker reaction towards (*S*)-clopidogrel bisulfate **242**.[224]

1.5.4 Outlook on POPs as chiral catalysts

The aforementioned examples prove that POPs show great promise as chiral catalysts, with activities and selectivities often equal or greater than the homogeneous analogues. By varying the connectivity, size and geometry of the POP building blocks, theoretically, the catalytic environment can be very precisely controlled.[185] However, the full potential of these materials is yet to be realized. In most cases the POPs are used as a type of inert carrier material. Especially for COFs, the molecular structure is so well defined and allows precise manipulation that much more intricate and advanced designs should be possible. In enzymes multiple secondary interactions are responsible for stabilizing transition states and helping with substrate binding and such a tailored design of the catalytic sites would also be possible with COFs.[225] Moreover, the scope of the reactions covered still mainly focusses on enamine/iminium organocatalysis with other modes being underdeveloped.

The synthesis of the materials also deserves comment. In the case of the chiral phosphoric acids the used building blocks require very long and hazardous synthesis sequences. Compounds **155** and **156** require a ten step complex synthesis starting from BINOL, including hazardous chemicals such as MOMCl, BuLi, DIBAL, $POCl_3$, Br_2, etc. Similarly, compounds **157** and **158** required a five step synthesis from BINOL. The other synthesized chiral COFs have the typical synthetic shortcomings of COFs. Namely, difficult to access monomers and synthesis in unattractive conditions on small scales. The other, amorphous chiral POPs can typically be produced on bigger scales, however their synthesis conditions are still rather unattractive: precious metal based cross-couplings at high temperatures for long times, and the monomers can be rather exotic as well.

1.6 POPs as catalysts for CO_2 fixation

The accumulation of CO_2 in the atmosphere is the main cause of global warming. The reduction of CO_2 emissions is therefore a big challenge with many facets and possible solutions. Carbon capture and sequestration (CCS) forms one possible part of a solution, capturing and storing CO_2 as waste, or even better: turning this waste into high value chemicals.[226] One promising strategy is the cycloaddition of CO_2 with an epoxide forming cyclic carbonates, a very atom efficient transformation (Scheme 67). The carbonate products have applications as degreasers, monomers, green aprotic solvents, electrolytes in lithium ion batteries…[227–231]

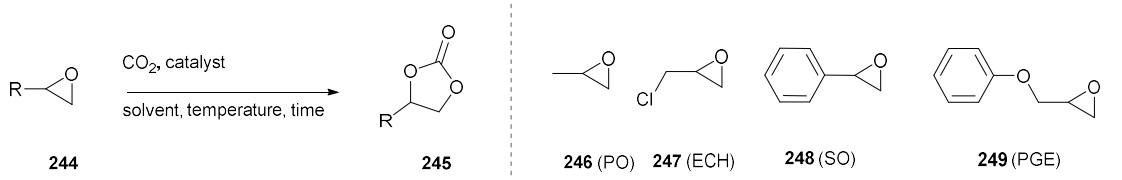

244 **245** **246** (PO) **247** (ECH) **248** (SO) **249** (PGE)

Scheme 67: The cycloaddition of CO_2 with epoxides and the most common substrates: propylene oxide (PO) **246**, epichlorohydrin (ECH) **247**, styrene oxide (SO) **248** and phenyl glycidyl ether (PGE) **249**.

The cycloaddition reaction is generally catalyzed by nucleophilic catalysts, to open the epoxide ring, and/or (Lewis) acid catalysts, to activate the epoxide towards nucleophilic attack. Industrially sodium iodide or tetra-*n*-butylammonium bromide (TBAB) are used as a catalysts, but new, greener catalysts are being developed. Homogeneously, efforts have been focused on ionic liquids,[232] transition-metal complexes[233] and organocatalysts.[234] Heterogeneously, the main challenge consists in constructing a (metal-free) recyclable catalyst capable of performing under ambient conditions. This implies a good CO_2 enrichment capability, for which ionic sites providing strong interactions, and micropores providing large surface areas are important. Most of the used POPs possess charged moieties, which can undergo dipole-quadrupole interactions with CO_2, thus giving these POPs intrinsic affinity for CO_2. First, imidazolium containing POPs and the related carbenes will be discussed, then phosphonium based POPs followed by COFs, CTFs and other polymers are reviewed.

1.6.1 Imidazolium based POPs

In 2007, Xie *et al*. immobilized ionic liquids through radical copolymerization of 3-butyl-1-vinylimidazolium chloride **250** with cross linker divinylbenzene **11**. In this way highly crosslinked polymer supported ionic liquids **PSIL**, with an ionic site loading of about 1 mmol/g, were prepared, a surface area was not reported (Scheme 68). **PSIL** was able to promote the cycloaddition of CO_2 with PO, reaching 97% yield after seven hours under high (6 MPa) CO_2 pressure (Table 5, entry 1), and could be recycled five times with no considerable reduction in yield. Furthermore, a wide range of epoxides could be converted with good yields (79-96%). **PSIL** performed better than homogeneous counterparts, which formed a separate phase in the reaction medium. The heterogeneous catalyst formed a dispersion leading to much better mass transfer and thus higher yields.[235]

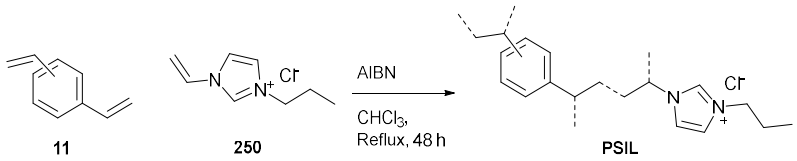

Scheme 68: Synthesis of **PSIL** by radical copolymerization.[235]

Polymerization of *e.g.* divinylimidazolium or similar building blocks without external crosslinkers, such as divinylbenzene, does not generate sufficient porosity. However, some methods exist to increase the surface area. Hard templating consists of the polymerization around additive inorganic components (generally silica), which are then etched away with acid or base.[236–238] Soft templating involves polymerization around an organic tri-block polymer template, which is afterwards removed via extraction.[239] Another option is electrostatic, template free crosslinking by complexation between polymerized (linear) ionic liquids with polyanions, thus forming a three dimensional net by polyelectrolyte complexation.[240–243]

In 2015, Wang *et al*. prepared ionic POPs by free radical polymerization of bis-vinyl imidazolium salts ([C_nDVIM]Br) **251**, without adding external templates or crosslinkers, by means of ionothermal polymerization in a mixture of ionic liquid **253** with water (Figure 4). The spacer length n between the imidazolium moieties was critical in achieving porous structures. For n = 1 a porous polymer **PDMBr** was obtained with a surface area of 205 m^2/g. With more flexible monomers (n = 2 or 4) low porosities were obtained. The influence of the alkyl length of the polymerization solvent **253** was also pronounced, with porosity increasing as alkyl length went up. But when n = 8 no porosity was obtained, pointing to pore collapse. Other ionic solvents such as [C_4Py]Br **254** and [P_{4444}]Br **255** produced nonporous polymers. However, tetrabutyl/propyl ammonium bromide (TBAB or TPAB) were successful in generating porous structures, for TPAB an even higher porosity of 260 m^2/g was reported. The used co-solvent was also essential, when water was replaced with other solvents (EtOH, AcOH, DMF, DMSO) poor porosities were obtained. The water containing IL contains both polar (imidazolium) and apolar (alkyl) moieties. The polar domain is where polymerization takes place and the apolar domains act as a template for pore formation. Larger alkyl chains thus lead to an expansion of the pore volumes due to the polymer being formed around a larger template. For **PDMBr** a high CO_2 adsorption of 1.02 mmol/g (25 °C, 1 atm) was measured and it proved to be highly active at catalyzing the cycloaddition reaction. The conversion of allyl glycidyl ether, for example, reached 99% after three hours under 1 MPa CO_2 pressure. Interestingly, **PDMBr** was also active under lower pressures and temperatures, only requiring extended reaction times and catalyst loading (Table 5, entry 2).[244]

In 2017, Qin *et al*. developed a novel strategy to increase the surface area of ionic polymers prepared through radical crosslinking, by utilizing monomers with bulky salicylate counterions followed by ion exchange with smaller ions (Scheme 69). Polymers prepared through direct synthesis with bromide/chloride/acetate counterions had much lower surface areas (18-26 m^2/g) than the ones prepared through anion exchange **AE-PIL-Cl/Br/I** (129-228 m^2/g). These higher surface area materials were more active in the cycloaddition reaction and **AE-PIL-Cl** was the most active (Table 5, entry 3). A range of substrates with increasing chain length were tested and activity generally decreased, but the decline was more pronounced for less porous polymers. Furthermore, these POPs catalyzed *N*-heterocyclic carbomethoxylation reactions of heterocycles **258** with dimethyl carbonate (Scheme 70).[245]

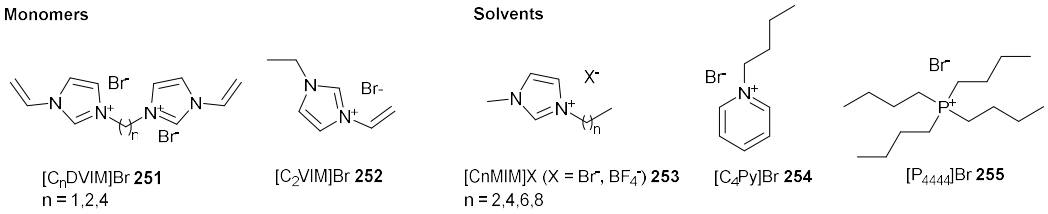

Figure 4: Monomers and solvents used in the synthesis of porous ionic liquids.[244]

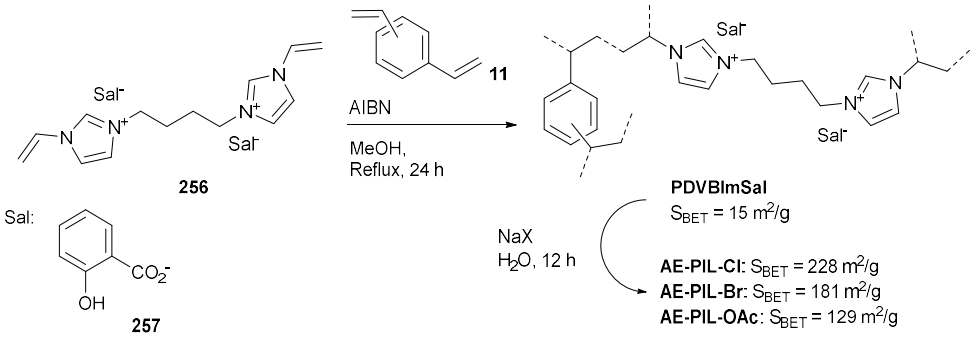

Scheme 69: Synthesis of porous ionic liquids by postsynthetic exchange of bulky anions.[245]

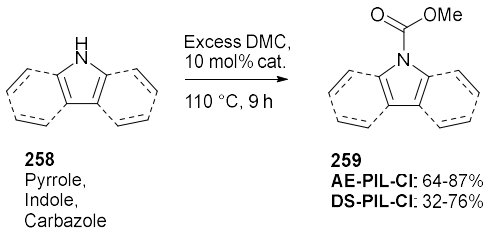

Scheme 70: Carbomethoxylation of *N*-heterocyles.[245]

The Wang group reported ionic HCPs **HIP-Cl/Br-1/2** by one-pot quaternization-Friedel-Crafts-alkylation reactions between 2-phenylimidazoline **260** and crosslinkers dichloro/bromoxylylene **2/25**. Nonionic HCPs **HCP-Cl/Br** were synthesized using only the crosslinker and the residual chloro- or bromomethyl groups were then reacted with 2-phenylimidazoline **260** forming ionic liquid grafted polymers **GHIP-Cl/Br** (Scheme 71). Of these catalysts **HIP-Br-2** was the most active (99%, Table 5, entry 4) for the conversion of styrene oxide, more active than the grafted polymers **GHIP-Cl** or **GHIP-Br** (75-86%), a polystyrene resin supported imidazolium salt (59%) or a homogeneous analogue (69%). Utilizing $ZnBr_2$ as Lewis acid co-catalyst (Table 5, entry 5) high yields could be obtained at room temperature using a flue gas analogue consisting of 15% CO_2 and 85% N_2. Direct capture of CO_2 from flue gas is highly advantageous due to the avoidance of energy intensive gas separation.[246]

The same group prepared a range of analogous imidazolium-functionalized ionic HCPs with diverse substituents by hypercrosslinking of substituted imidazolium salts **261** with crosslinker **2** (Scheme 72). Surface areas of 360-722 m^2/g were reported and the ethyl substituted polymer, **I_{C2}HCP**, was further optimized. By varying the monomer composition and the amount of $FeCl_3$ surface areas of up to 1017 m^2/g were reached. This optimized **I_{C2}HCP-5b** also possessed the highest CO_2 uptake of 3.05 mmol/g (1 bar, 0 °C) and was also the best performing catalyst. Using 3 MPa pressure of simulated flue gas 81% yield was reached using low catalyst loadings (Table 5**,** entry 6).[247]

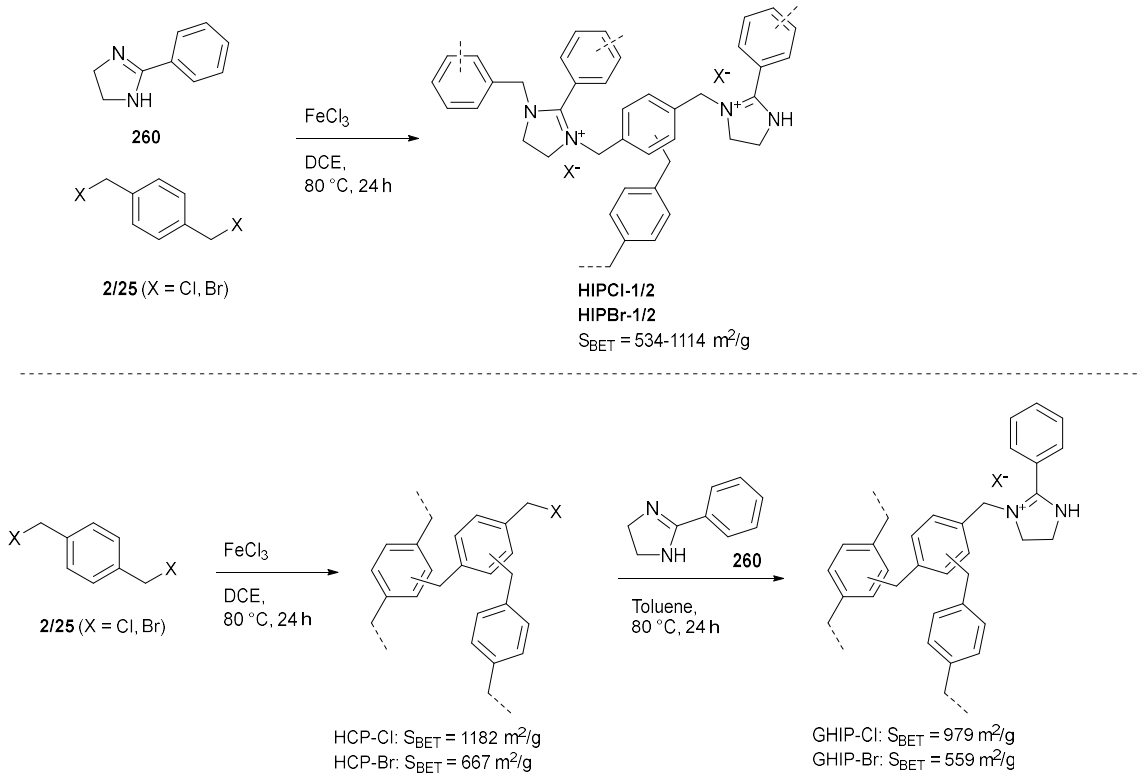

Scheme 71: Synthesis of porous ionic liquids by quaternization-Friedel-Crafts crosslinking (above) or grafting (below).[246]

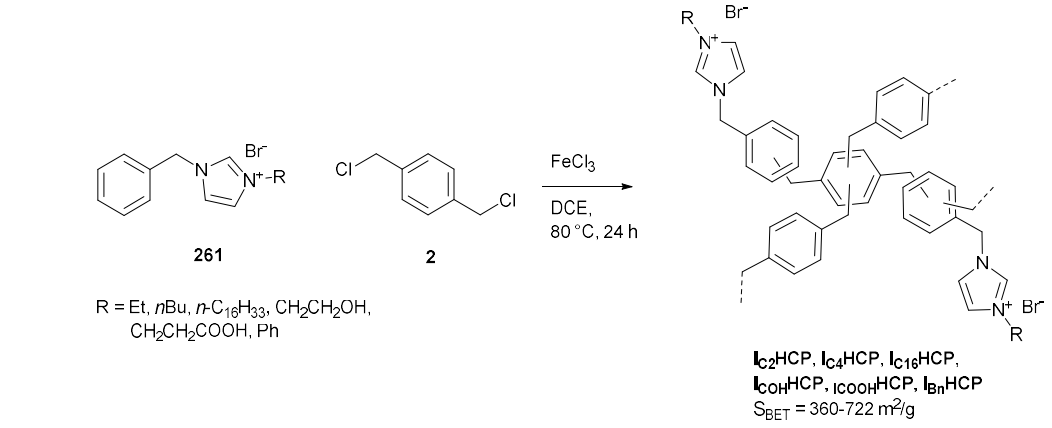

Scheme 72: Synthesis of a range of imidazolium HCPs by Friedel-Crafts crosslinking.[247]

Imidazolium grafted HCPs were reported by crosslinking of benzylhalides **2,25,262-265** and subsequent reaction of *N*-methylimidazole **266** with the residual bromo- or chloromethyl groups, leading to **POM1-6-Im** (Scheme 73). Of these catalysts **POM3IM** was the most effective in the conversion of a range of epoxides, reaching 92% conversion of PO (Table 5, entry 7).[248]

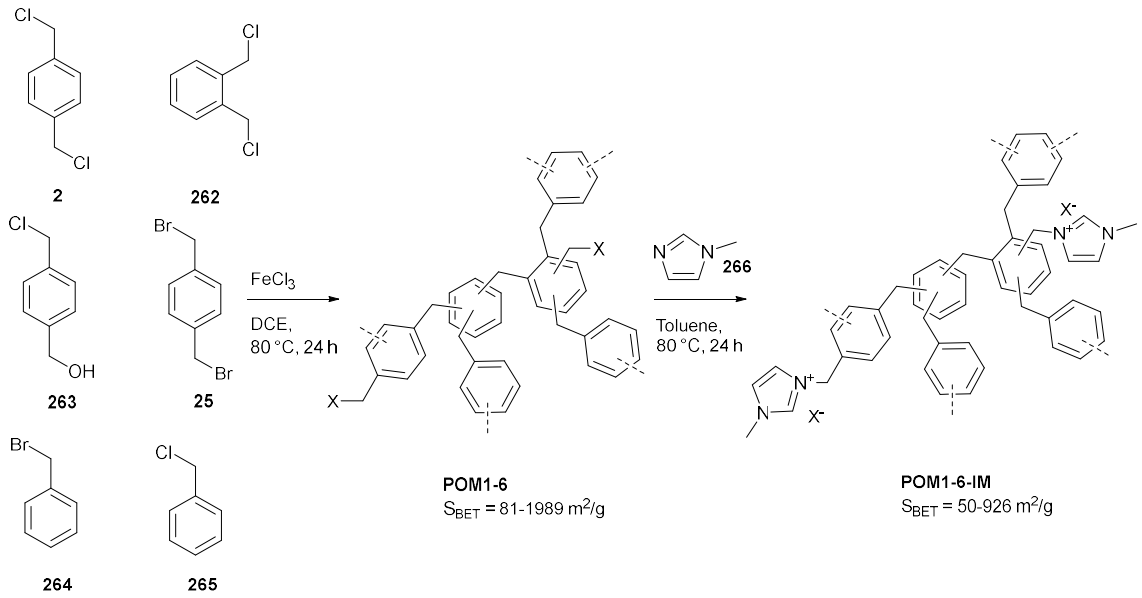

Scheme 73: Synthesis of ionic HCPs by postsynthetic functionalization of residual chloro/bromomethyl groups.[248]

In 2010, Cho *et al*. prepared tubular, ionic CMPs through Sonogashira coupling of tetrakis(4-ethynylphenyl)methane **42** and functional imidazolium building block **267** (Scheme 74). The morphology and growth process of the obtained material, **T-Im**, was studied through transmission and scanning electron microscopy (TEM and SEM). All materials had a hollow inner space and formed tubes. The formation of hollow spheres happened through Ostwald ripening. In the beginning of the reaction rods with a thin average diameter and a dense inner structure were observed and the diameter gradually increased as a hollow inner sphere was formed. **T-Im** was an active catalyst for a range of epoxides, for example, ECH could be converted in 85% yield utilizing 1 MPa CO_2 at 150 °C (Table 5, entry 8).[249]

Other ionic CMPs were reported by Sonogashira coupling of triazine based building block **268** with tetratopic **42**, thus incorporating two functionalities, triazines and imidazoliums, with high affinity for CO_2 in the resulting material (Scheme 75). This **IT-POP-1** was ion exchanged, replacing the small chloride anions with larger iodide or hexafluorophosphate anions forming **IT-POP-2/3**. The surface areas are hereby drastically lowered and pore size distribution analysis showed that the micropores are blocked. **IT-POP-1** was the most active catalyst by far, reaching 99% yield at 120 °C and 1 MPa CO_2 for the conversion of ECH (Table 5, entry 9). Due to their lower surface area **IT-POP-2** (89%) and **IT-POP-3** (33%) were much less active. For **IT-POP-3** the much lower nucleophilicity of the hexafluorophosphate anion reduced the activity drastically.[250]

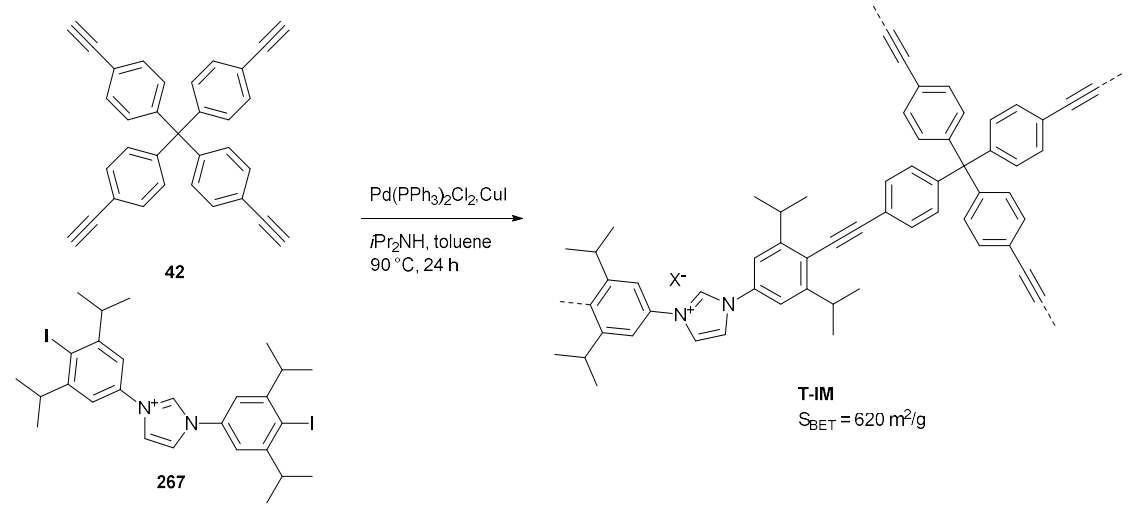

Scheme 74: Synthesis of an imidazolium containing CMP **T-IM** via Sonogashira coupling.[249]

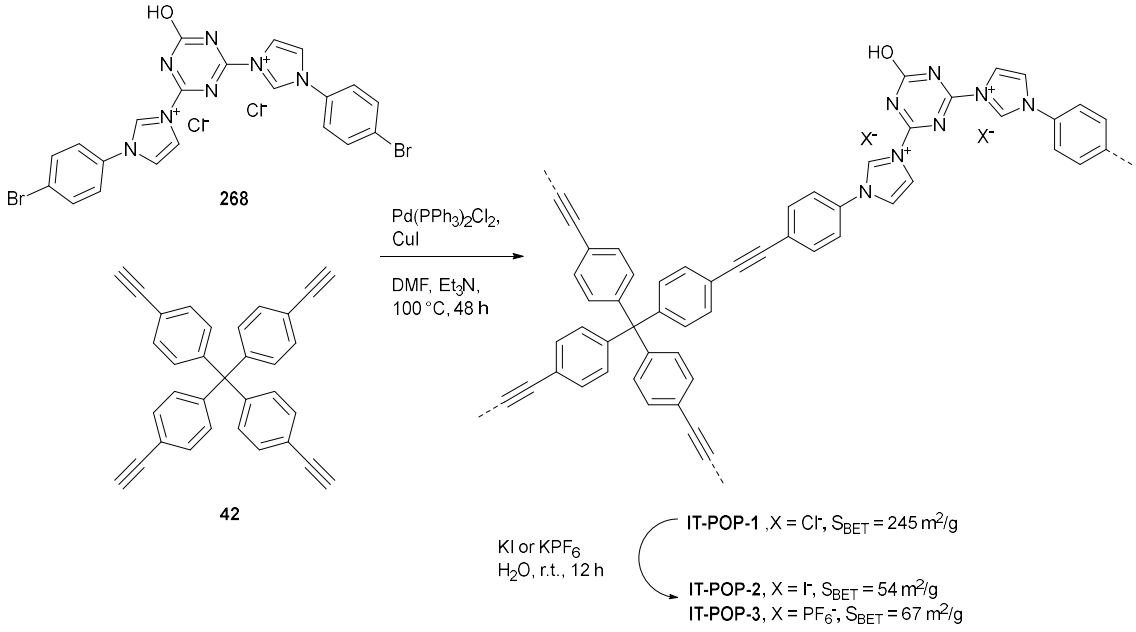

Scheme 75: Synthesis of an imidazolium and triazine containing CMP through Sonogashira coupling.[250]

Imidazolium moieties can also be generated post synthetically. In 2012 the Thomas group generated a POP with *N*-heterocyclic carbenes (NHCs) in the backbone using a stepwise approach (Scheme 76). Polymerization of tetrakis(4-aminophenyl)methane **269** with glyoxal **270** generated an imine network **PImin**, which was converted with chloromethyl ethyl ether **271** to the imidazolium polymer **PImCl**, which after deprotonation generated **PNHC**. Furthermore, copper could be immobilized and this polymer **PCuNHC** could serve as a catalyst for the deoxygenation of organic sulfoxides. Both **PNHC** and **PImCl** showed activity for the cycloaddition reaction with **PNHC** resulting in a slightly higher yield (Table 5, entry 11 and 12).[251]

Similarly, Talapaneni *et al*. generated imidazolium and NHC moieties post synthetically in a three step approach using a much more sterically hindered building block **272** (Scheme 77). In this way the NHC moieties were stabilized by sterical confinement, inhibiting dimerization and other side reactions. The authors proved the existence of the free carbenes by observing the formation of imidazolium carboxylates in solid state ^{13}C-NMR. Unlike in most postmodification sequences, here the surface areas increased due to the steric size of the imidazolium rings and the increasing rigidity of the framework. **NP-NHC** could catalyze the conversion of PO at atmospheric pressures of CO_2 in high yield (98%, Table 5, entry 13).[252]

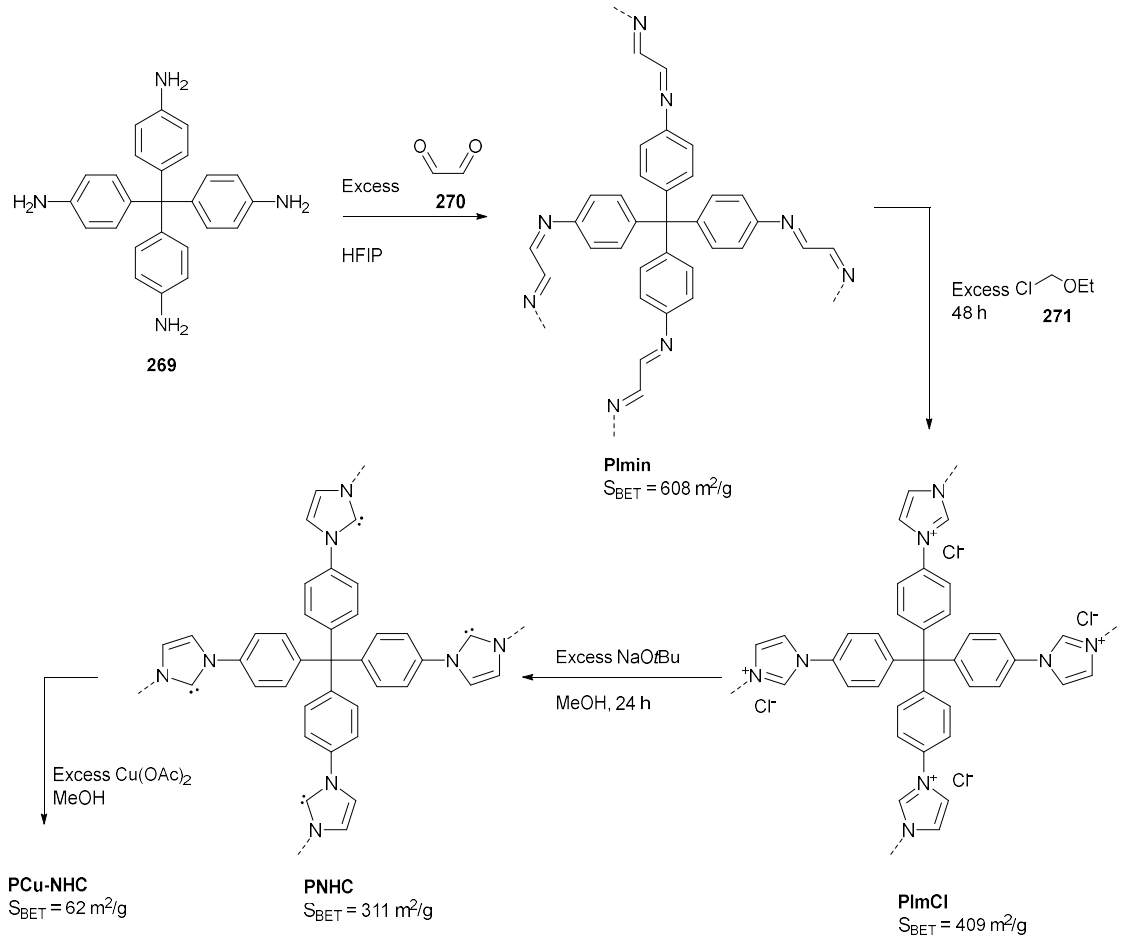

Scheme 76: Synthesis of NHC-containing POPs by Schiff base reaction, ring closure and deprotonation.[251]

Wang *et al*. synthesized a series of POPs incorporating NHC-CO_2 adducts via copolymerization of N-vinylimidazolate **83** with ethyleneglycol dimethacrylate **273**, followed by postsynthetic modification with dimethyl carbonate (Scheme 78). Under high pressure and temperature a good conversion of ECH was reached after only two hours, under ambient pressure longer reaction times were needed (Table 5, entry 14).[253] Lastly, in 2016 Wang *et al*. prepared a series of imidazolium, zinc halide and triphenylphosphine integrated POPs through radical polymerization of vinyl functionalized triphenylphosphine **274** and divinylimidazolium **275**, followed by zinc halide immobilization. These materials were effective cooperative catalysts, with **PPh_3-ILBr-$ZnBr_2$** being the most effective, reaching a very high TON of 2120 h^{-1} at 40 °C and an extremely high initial TOF of 5200 h^{-1} at 120 °C (Table 5, entry 15), which were at that time the highest reported for a heterogeneous catalyst.[254]

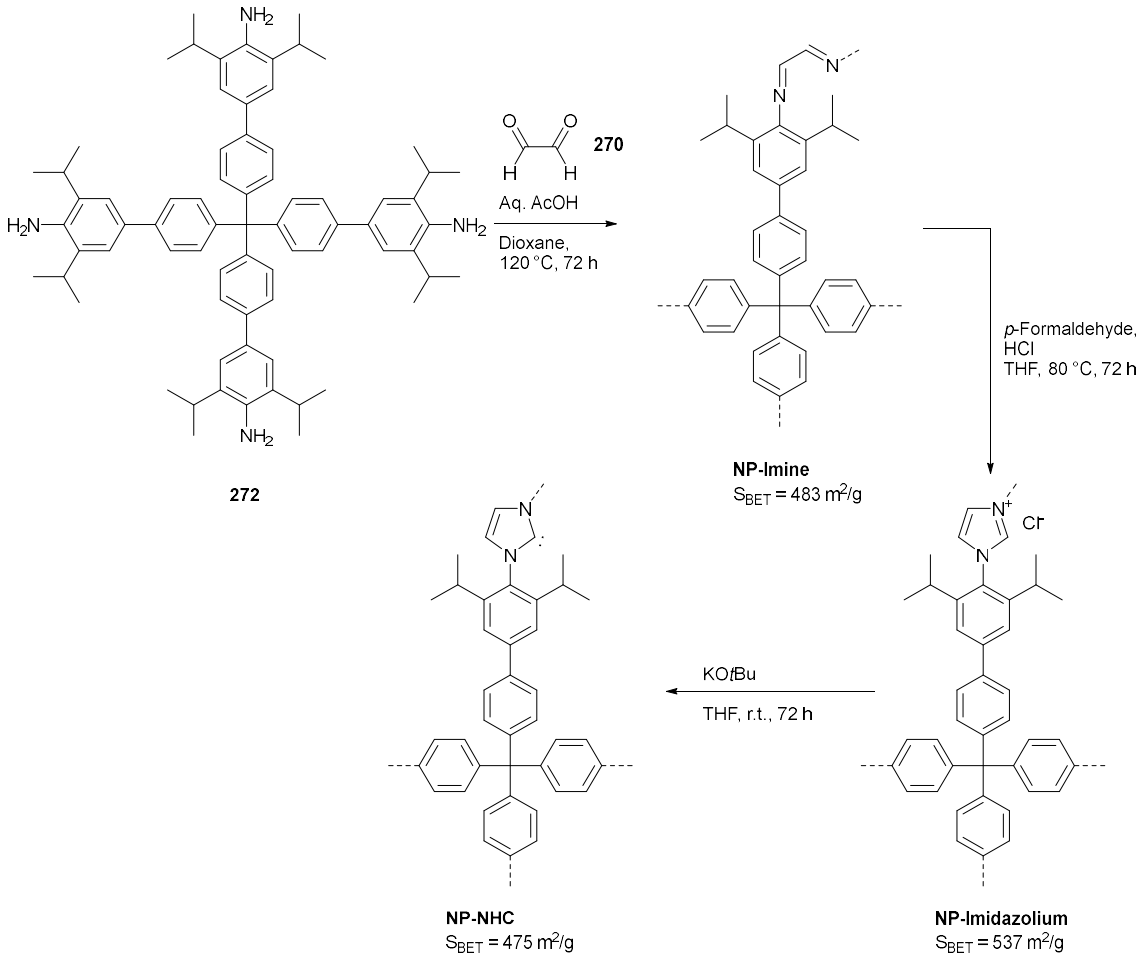

Scheme 77: Generation of a polymer network containing sterically confined NHCs.[252]

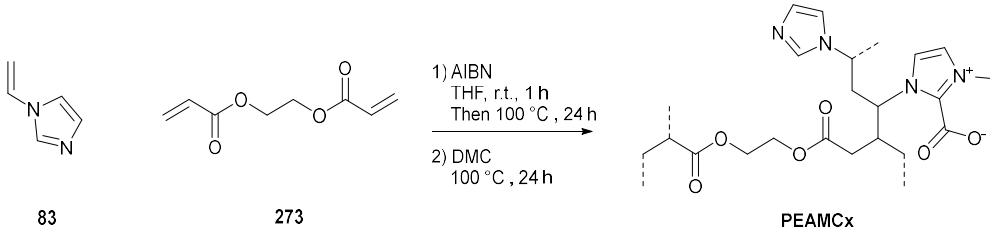

Scheme 78: Synthesis of polymers containing NHC-CO_2 adducts.[253]

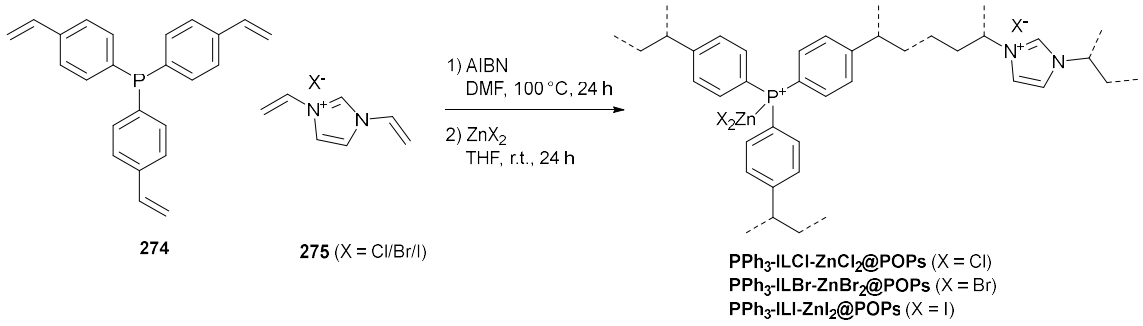

Scheme 79: Synthesis of imidazolium-triphenylphosphine polymers by radical copolymerization.[254]

1.6.2 Phosphonium based POPs

Phosphonium salt based CO_2 conversions are already applied in the OMEGA process by Shell and Mitsubishi chemicals. In this process ethylene glycol is produced from ethylene oxide, by reaction with CO_2, followed by hydrolysis of the formed ethylene carbonate.[255] In 2012, Zhang *et al*. prepared the first phosphonium containing POP, by nickel catalyzed Yamamoto coupling of monomer **276**. The resulting porous polymer, **PP-Br**, had a surface area of 650 m^2/g that could be tuned further via anion exchange (Scheme 80). This material was an effective catalyst for the cycloaddition reaction under atmospheric pressure, with a reported yield of 98% for phenyl glycidyl ether (Table 5, entry 16).[256]

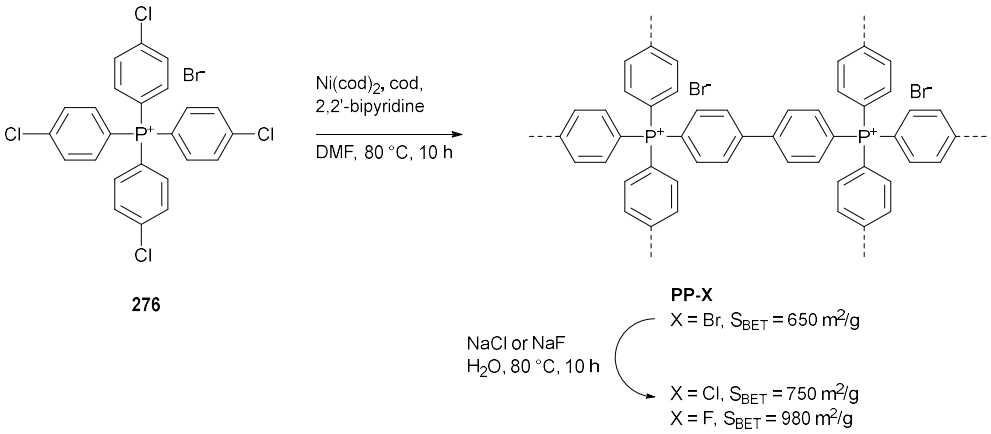

Scheme 80: Synthesis of phosphonium salt containing polymers by Yamamoto coupling.[256]

In 2015, Wang *et al*. prepared HCPs with phosphonium moieties through Friedel-Crafts polymerization of phosphonium salt monomers **277** with benzene and FDMA as a crosslinker. The co-monomer benzene is necessary due to the limited reactivity of the phosphonium benzene rings. Highly porous HCPs (770 – 1168 m^2/g) were reported and their surface areas decreased as the counterions and substituents got bigger (Scheme 81). Polymers with bromide as the anion and a small methyl substituents gave the best results, reaching 94% conversion of PO after nine hours (Table 5, entry 17). Co-polymerization of triphenylphosphine **277-6** with phosphonium salt **277-2** resulted in triphenylphosphine containing polymer **2+6**, onto which Lewis acid $ZnBr_2$ was immobilized and this proved to be a very effective combination, reaching 90% yield after only four hours (Table 5, entry 18).[257]

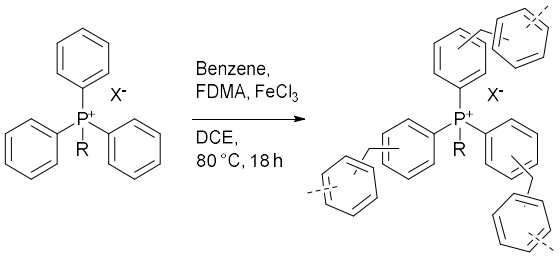

Scheme 81: Synthesis of phosphonium HCPs by Friedel-Crafts crosslinking.[257]

Sun *et al*. prepared ionic polymers by radical polymerization of vinyl functionalized quaternary phosphonium salt monomers **278**, leading to POPs with high surface areas (402-758 m^2/g). Polymers with different substituents and counterions were tested, and of these the highest catalytic activity was found for **PIP-Bn-Cl**, containing the more hindered benzyl substituent and chloride anion (Scheme 82). A more sterically hindered substituent can lead to looser ion binding and thus higher catalytic activity. This material could catalyze the cycloaddition of CO_2 with ECH in high yield (95%) under extremely mild conditions at room temperature under atmospheric CO_2 pressure and very low catalyst loadings, however requiring long reaction times. Heating at 100 °C shortened the reaction time to only three hours with >99% yield (Table 5, entry 19). Furthermore, the catalyst could be recycled at least ten times without any noticeable reduction of the yield.[258]

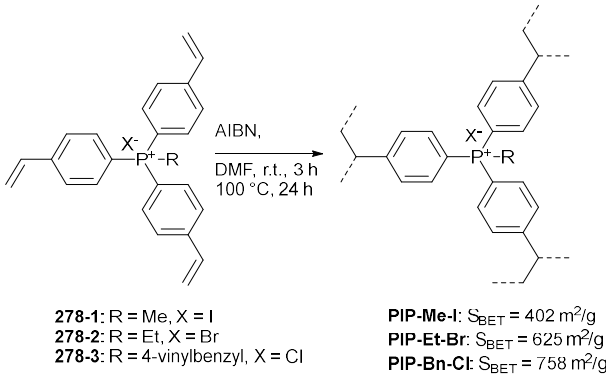

Scheme 82: Synthesis of phosphonium containing HCPs by radical polymerization.[258]

1.6.3 COFs

The **2,3-DhaTph** and **2,3-DmaTph** COFs (Scheme 36) reported by the Banjeree group were not only simultaneous acid base catalysts for the deacetalization-Knoevenagel reaction, but were also active for CO_2 conversion. **2,3-DhaTph** is a stable, highly porous COF and possesses both acidic (catechol) and basic (porphyrin) active sites. The catechol moieties activate the epoxide through hydrogen bonding and stabilize the oxyanion. Furthermore, the porphyrins have good affinity for CO_2. **2,3-DhaTph** performed well in the cycloaddition of epoxides at atmospheric CO_2 pressure when TBAI was used as a co-catalyst, and as expected **DmaTph** was less effective (Table 5, entry 20). **2,3-DhaTph** also catalyzed the conversion of a wide range of substituted aziridines **279** to oxazolidinones **280** and **281** in high yield and with good regioselectivity (Scheme 83).[259]

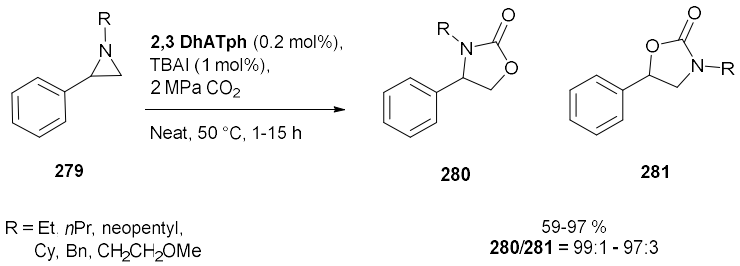

Scheme 83: COF mediated synthesis of oxazolidinones **280** and **281** by CO_2 cycloaddition to aziridines **279**.[271]

Two or more catalytic centers working together to perform a single transformation can be considered the state of the art in modern catalysis. However, for heterogeneous catalysts such as POPs the spatial separation in rigid frameworks makes this cooperation difficult. Sun *et al*. devised an elegant solution to this problem by encapsulating flexible ionic polymers with halide catalytic sites in a Lewis acid functionalized COF. These authors synthesized **COF-TpBpy** by Schiff base condensation between 5,5'diamino-2,2'-bipyridine (Bpy) **282** and 1,3,5-triformylphloroglucinol (Tp) **71**. Following this, *in situ* radical polymerization of phosphonium salt **283** encapsulated linear polystyrene chains in the COF channels. Copper was then immobilized on the bipyridines sites forming **PPS⊂COF-TpBpy-Cu**. The ionic polystyrene chains retained their flexibility, as signified by their sharp ^{31}P-NMR signals when contacted with solvent, and could be viewed as quasi homogeneous catalysts. The catalytic activity was tested for the conversion of ECH under atmospheric CO_2 pressure which reached a high yield (95%, Table 5, entry 21). Isolating the Br^- and Cu^{2+} active species, by using a physical mixture of **COF-TpBpy-Cu** and the phosphonium polymer, was much less effective (16%). A soluble ionic co-catalyst (PPh_3EtBr) only reached 73% conversion of ECH. A molecular catalyst is homogeneously distributed in solution, whereas the ionic catalytic component of the polystyrene chains are only present in the COF channels, increasing the chance of concerted catalysis. When divinylbenzene was copolymerized with the phosphonium salt **283** much more rigid chains were obtained, drastically lowering the yield (49%). The catalyst could be recycled at least ten times with negligible loss of activity. In a large-scale experiment extremely high TONs (>28000) were obtained, indicating possible practical applications.[260]

Recently, a fully metal-free variant of this concept was reported by Zhong *et al*. who synthesized a nitrogen-rich COF integrated with an imidazolium-based ionic polymer **ImIP@TT-COF**. The COF was produced by layering of an aqueous solution of 1*H*-1,2,4-triazole-3,5-diamine (TDA) **284** and *p*-toluenesulfonic acid on top of a dichloromethane solution of the aldehyde **71**. Free-radical polymerization of imidazolium **252** in presence of the COF gave rise to **ImIP@TT-COF** (Scheme 85). The COF served as a catalyst by virtue of its hydrogen bonding donor capabilities and CO_2 concentrating properties. The anions of the imidazolium polymers served as nucleophilic catalysts. Quantitative conversion of ECH was reported under atmospheric or even lower CO_2 pressures (Table 5, entry 22) with negligible loss of activity after six runs. Just as reported in similar examples the activity of this system is greater than the sum of its parts.[261]

Zhi *et al.* reported two triazine based covalent organic frameworks (**COF-JLU6** and **COF-JLU7**) that were synthesized by Schiff base condensation between aldehyde **19** and tritopic amines **285** and **286** (Scheme 86). The high nitrogen content of the pore walls increased the affinity for CO_2 and a high density of hydroxyl groups as Brønsted acids served to activate epoxides. Therefore, both COFs were effective at mild conditions (Table 5, entry 23) in the presence of co-catalyst TBAB.[262]

Yang *et al.* prepared three isostructural COFs based on the rigid 3,3',5,5'-tetrakisphenylbiphenyl (TPBP) aromatic core with either hydroxyl (**OH-TFBP-COF**), methoxy (**OMe-TFBP-COF**) or both (**OMe-OH-TFBP-COF**) groups (Scheme 87). **OMe-OH-TFBP-COF** performed best in the cycloaddition of ECH with CO_2 under very mild conditions, with TBAB as co-catalyst reaching 91% yield (Table 5, entry 24), slightly higher than **OH-TPBP-COF** (89%) and much higher than **OMe-TFBP-COF** which showed negligible activity.[263]

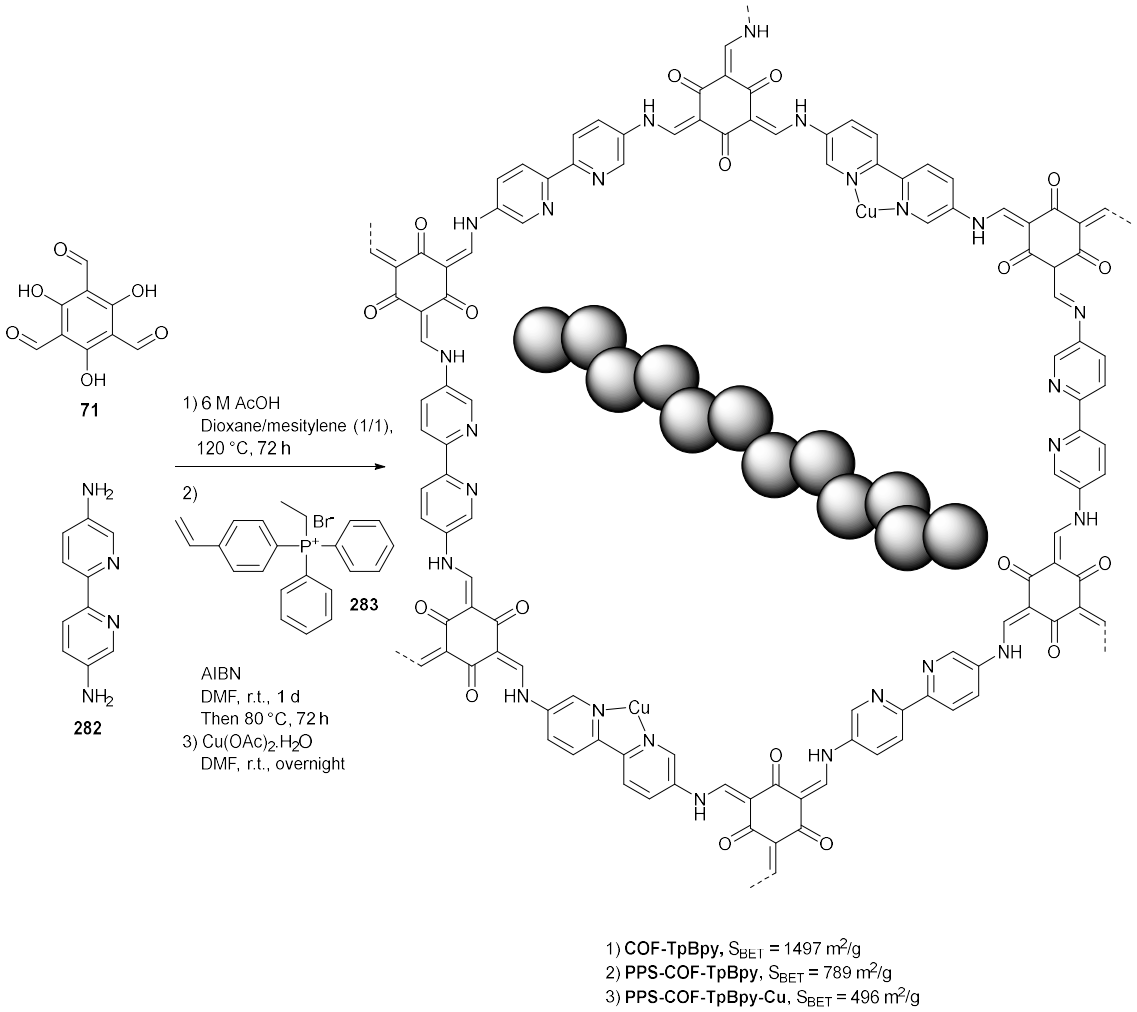

Scheme 84: Synthesis of a functionalized COF for CO_2 conversion by postfunctionalization with an ionic polymer and metalation with copper.[260]

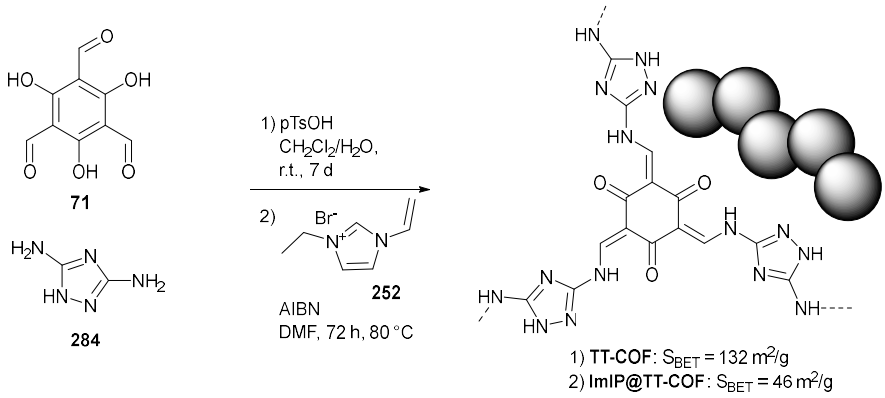

Scheme 85: Synthesis of a COF with integrated imidazolium polymers for CO_2 conversion.[261]

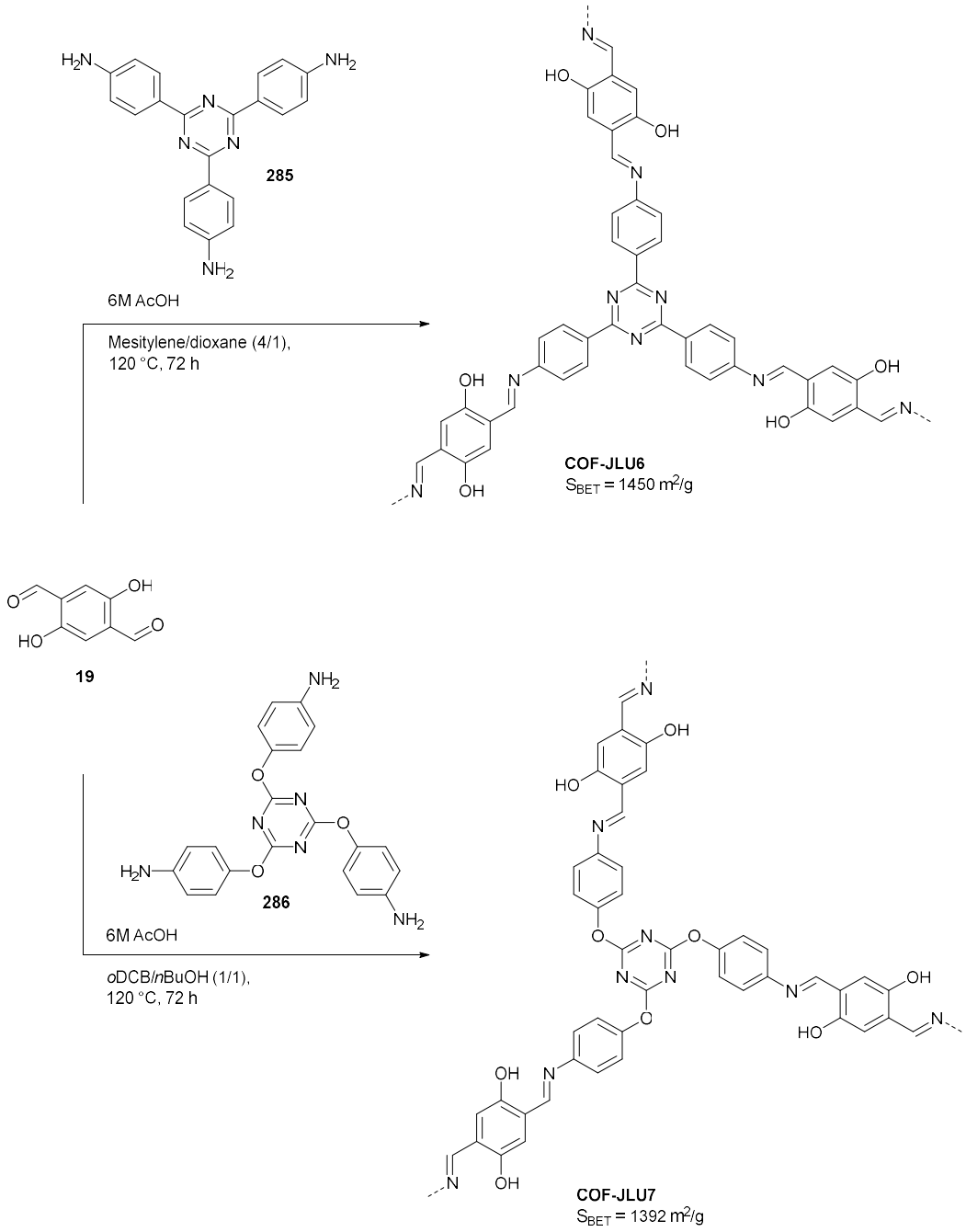

Scheme 86: Synthesis of triazine based COFs for CO_2 conversion.[262]

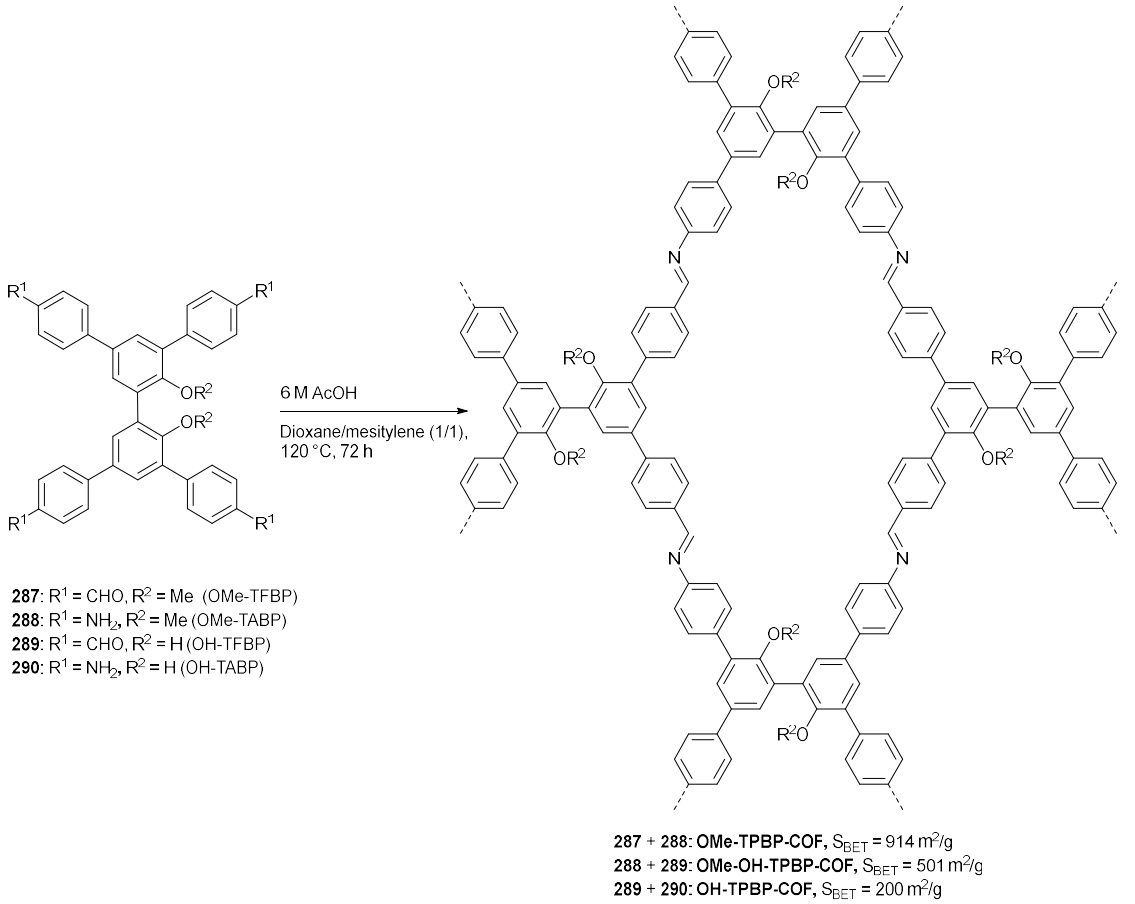

Scheme 87: Synthesis of three isostructural COFs for CO_2 conversion.[263]

Recently the zwitterion glycine betaine proved to be an efficient organocatalyst for the reduction of CO_2.[264] Mu *et al.* synthesized zwitterionic COFs as catalysts for the controllable reduction of CO_2 with hydrosilane, selectively forming different products depending on the reaction conditions. Through Schiff base condensation of tritopic amine **179** with aldehydes **19** and **20** **[OH]$_{x\%}$-TD-COFs** with variable amounts of hydroxyl groups were synthesized. These were then postfunctionalized through Williamson ether synthesis with brominated compound **291** forming **[BE]$_{x\%}$-TD-COFS** with good preservation of crystallinity and porosity (Scheme 88). Using these COFs, and by carefully choosing the equivalents of hydrosilane as reducing agent and CO_2 as carbon donor, amines **292** could be selectively transformed into formamides **293**, methylamines **294** or aminals **295** (Scheme 89). The carboxylate group of betaine activates CO_2 and enhances the reducing power of hydrosilane by forming hypervalent silicon species.[264] **[BE]$_{50\%}$-TD-COF** possessed the highest activity, as it probably has the ideal balance of sufficient functionalization without hindering mass transport by blocking of the pores.[265]

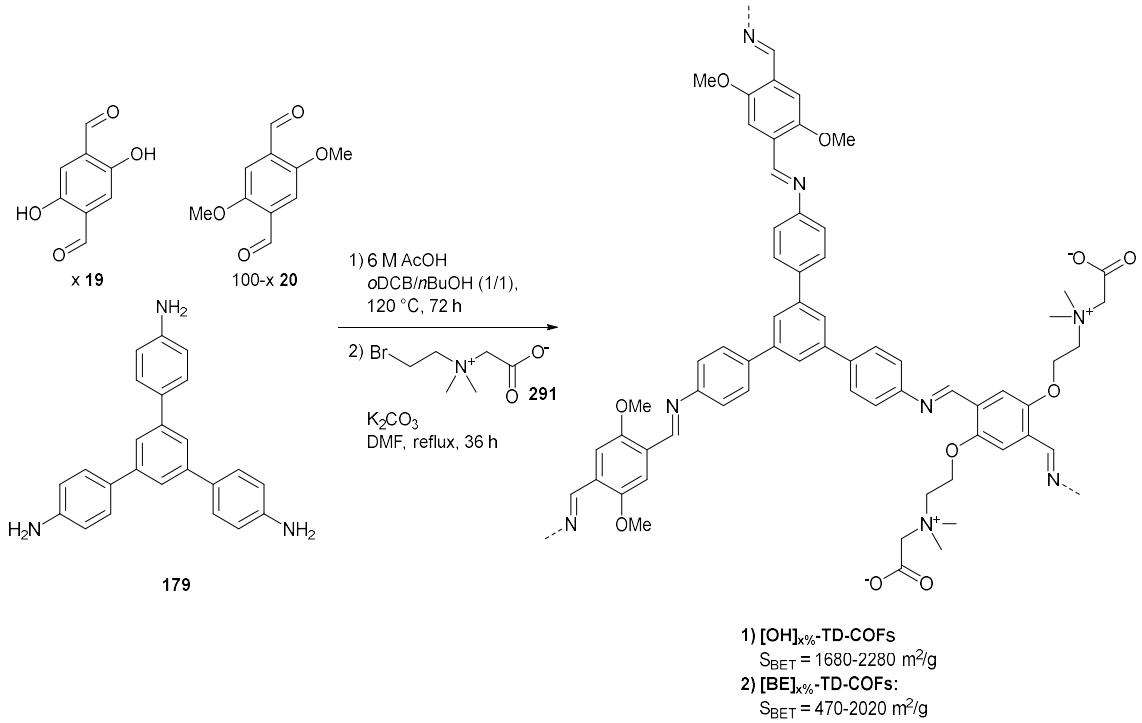

Scheme 88: Synthesis of betaine containing COFs for amine functionalization through CO_2 reduction.[265]

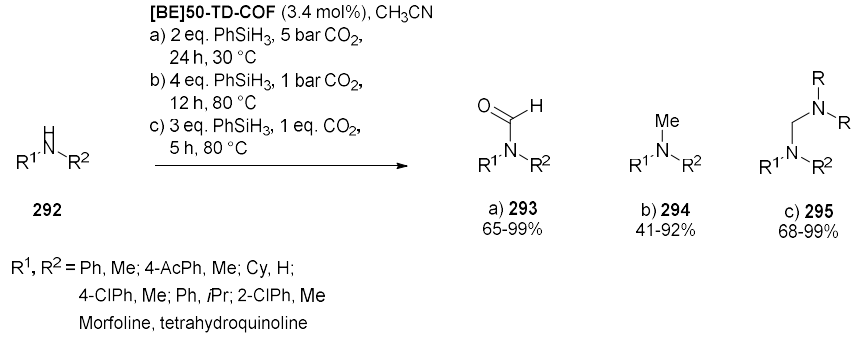

Scheme 89: Betaine containing COFs catalyze the functionalization of amines **292** with CO_2, selectively synthetizing formamides **293**, methylamines **294** or aminals **295**.[265]

1.6.4 CTFs

The unique properties of CTFs for CO_2 conversion were recognized in 2012 by the Thomas group. CTFs are typically synthesized through reversible ionothermal trimerization of aromatic polynitriles. These materials possess several interesting characteristics for catalytic applications, such as high thermal and chemical stability and tunable properties by the choice of the monomer and the synthetic procedure. These polymers can be used as support for catalytically active metal complexes or nanoparticles, however the materials themselves are also efficient basic catalysts by virtue of their basic nitrogen sites. Ionothermal synthesis typically takes place in a molten salt, $ZnCl_2$, at high temperatures (≥400 °C), with the salt acting as a solvent, catalyst and template. The products are typically amorphous, especially at higher temperatures (>400 °C) and when utilizing more equivalents of $ZnCl_2$. Heating at higher temperatures, *e.g.* 600 °C, leads to higher surface areas and mesoporosity, however increased carbonization also takes place, hereby lowering the nitrogen content of the material.[266] It is worth nothing that CTFs can also be synthesized by solvothermal reaction between amidines and aldehydes,[267] Friedel-Crafts reactions of aromatics with cyanuric chloride[268] and nucleophilic substitutions of amines or alcohols with cyanuric chloride.[269]

Thomas and co-workers synthesized three CTFs to compare the influence of porosity and chemical composition on the CO_2 cycloaddition. **CTF-1** and **CTF-1-HAS** were prepared by trimerization of 1,4-dicyanobenzene **296** at 400 °C or 600 °C and **CTF-P-HAS** by trimerization of 2,6-dicyanopyridine **297** at 600 °C (Scheme 90). The higher synthesis temperature of **CTF-1-HAS** compared with **CTF-1** led to a higher surface area, but a much lower nitrogen content due to carbonization. **CTF-P-HSA** possessed both a high surface area and nitrogen content, due to the nitrogen containing pyridinic monomer. The differences in structure can be attributed to incomplete condensation at lower temperatures and partial carbonization and removal of triazine at higher temperatures. The complete removal of potentially catalytically active $ZnCl_2$ was achieved by washing under concentrated acidic conditions. The structural differences had a major influence on the catalytic efficiency for the conversion of CO_2 to cyclic carbonates. Both high nitrogen amounts and high porosity are desired to obtain a high density of catalytic sites and good mass transfer. For the reaction of epichlorohydrin with CO_2 both **CTF-1-HAS** and **CTF-P-HAS** reached 100% conversion, whereas **CTF-1** could only manage 81% (Table 5, entry 25). However, for styrene carbonate and cyclohexene carbonate a very low selectivity was reported of only 14% and 48% respectively, with both epoxide hydrolysis and carbonate dimerization as side reactions. A two-step conversion of epoxides into cyclic carbonates, followed by transesterification with methanol furnishing dimethyl carbonate and vicinal diols, was also reported. The CTFs could reach high conversions, however with low selectivities (2-18%) for dimethylcarbonate.[270]

The Thomas group also prepared CTFs through trimerization of 1,3,5-tricyanobenzene **298** leading to **CTF-0** (Scheme 91). Crystalline frameworks with surface areas of around 500 m^2/g could be formed after careful optimization of the monomer/$ZnCl_2$ ratio, the reaction time and temperature. Increasing the reaction temperature to 600 °C furnished materials with a higher surface area (>500 m^2/g). Interestingly, the ideal structure was simulated to possess pores so small that they are inaccessible to N_2 and should therefore have zero surface area for nitrogen. This 'ideal' material could be synthesized by extending the reaction time to 80 hours after which a crystalline material with no porosity for N_2 was formed, however, this material could still absorb CO_2. **CTF-0** possessed an exceptionally high thermal stability, up to 600 °C in air. The high surface area variant of **CTF-0** showed good activity for CO_2 cycloaddition of ECH reaching 100% conversion with 93% selectivity (Table 5, entry 26).[271]

Another CTF was synthesized from 2,5-dicyanopyridine **299** at 400-600 °C with 10-12 equivalents of $ZnCl_2$ (Scheme 91). The **2,5-DCP-CTF** with the lowest porosity but highest nitrogen content was the most active and reached 95% yield for ECH (Table 5, entry 27), contrasting with other CTFs were in general the ones with the highest surface area were the most active.[272]

A charged, ionic CTF was synthesized by trimerization of dicationic viologen derivative **300** (Scheme 91). The surface areas and pore volumes were controlled by varying the temperature and $ZnCl_2$ content. The resulting CTF **cCTF-400/450/500** had high surface areas, up to 1247 m^2/g, and high stability, whilst the incorporation of the ionic moieties furnished a good CO_2 uptake (133 mg/g, 1 bar, 0 °C) and catalytic activity. Higher yields in the cycloaddition reaction than previously reported CTFs could be obtained, for example, for PO 99% yield was obtained (Table 5, entry 28).[273]

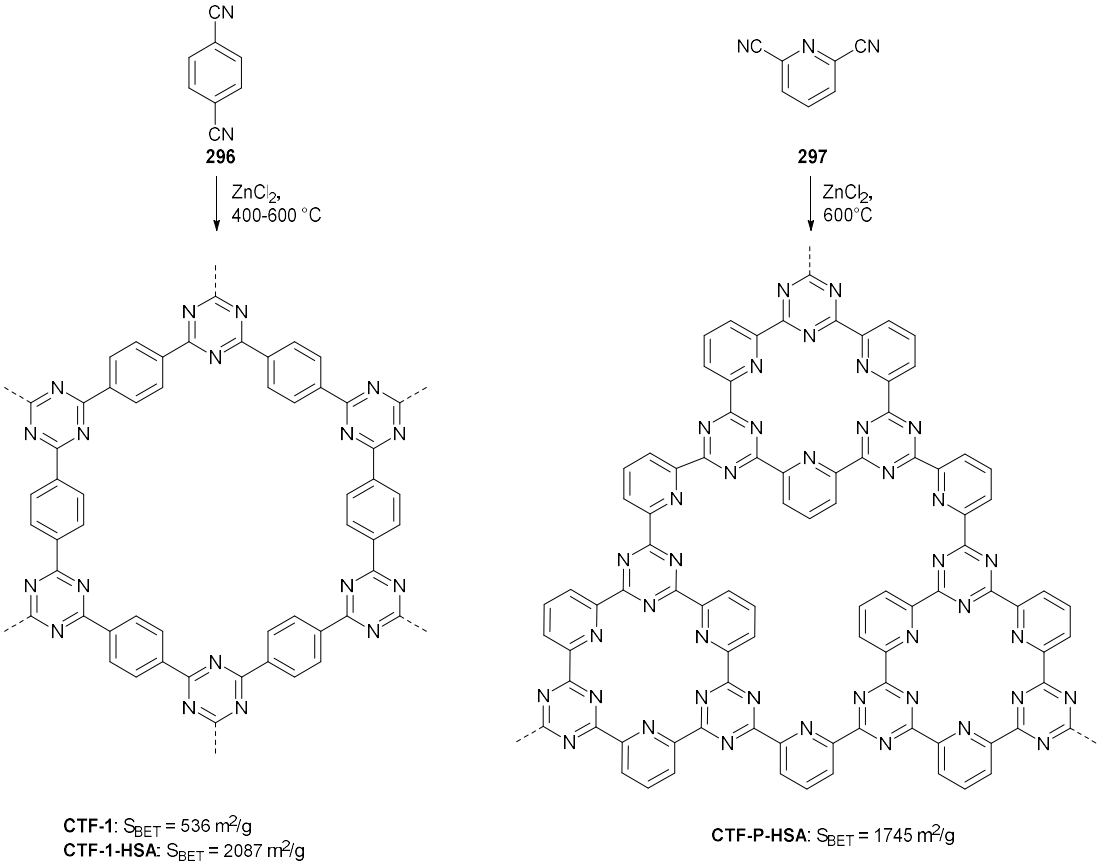

Scheme 90: CTF synthesis by ionothermal trimerization.[270]

Yu *et al*. synthesized porous ionic CTFs **IPF-CSU-1** by condensation of 2,2'-bipyridine **302** with cyanuric chloride **93**, without using any templates, metals, acids or bases (Scheme 92). The resulting polymer possessed an abundance of ionic sites and a high nitrogen content of 20.3 wt%. This polymer was an active catalyst at atmospheric pressure and ambient temperature, however a very large amount of TBAB as a co-catalyst was used to reach high conversions (99%, Table 5, entry 29).[274] Liu *et al.* prepared a hydrazine bridged CTF by reaction of cyanuric chloride **93** with 2,4,6-trihydrazinyl-1,3,5-triazine **301** resulting in **HB-CTP** (Scheme 92). This CTF possessed a rather low surface area (51 m^2/g) postulated to be caused by interlayer hydrogen bonding. However, this CTF exhibited good CO_2 capture capacity (8.2 wt%, 0°C, 0.1 MPa) and catalytic activity for the cyclo-addition of CO_2 with various epoxides in good to excellent yields (67-99%), although high temperatures, CO_2 pressures and a TBAB as co-catalyst were used (Table 5, entry 30).[275] Similarly, Biswas *et al.* prepared a CTF, **CYA-ANIS,** from

cyanuric chloride **93** and *o*-dianisidine **303** (Scheme 92). This material possessed a very low surface area of only 3 m^2/g. However, it catalyzed the cycloaddition well, reaching full conversions with co-catalyst TBAI under atmospheric pressures (Table 5, entry 31).[276]

While the building blocks of CTFs, typically aromatic polynitriles, are often quite accessible, the synthesis conditions themselves are harsh and not suited to larger scales. The typical ionothermal synthesis requires very high temperatures, large amounts of zinc chloride and takes place in vacuum sealed glass ampoules. The CTFs synthesized through nucleophilic addition of cyanuric chloride (Scheme 92) can be synthesized under milder conditions, but possess much lower surface areas and use a TBAX co-catalyst for the CO_2 cycloaddition.

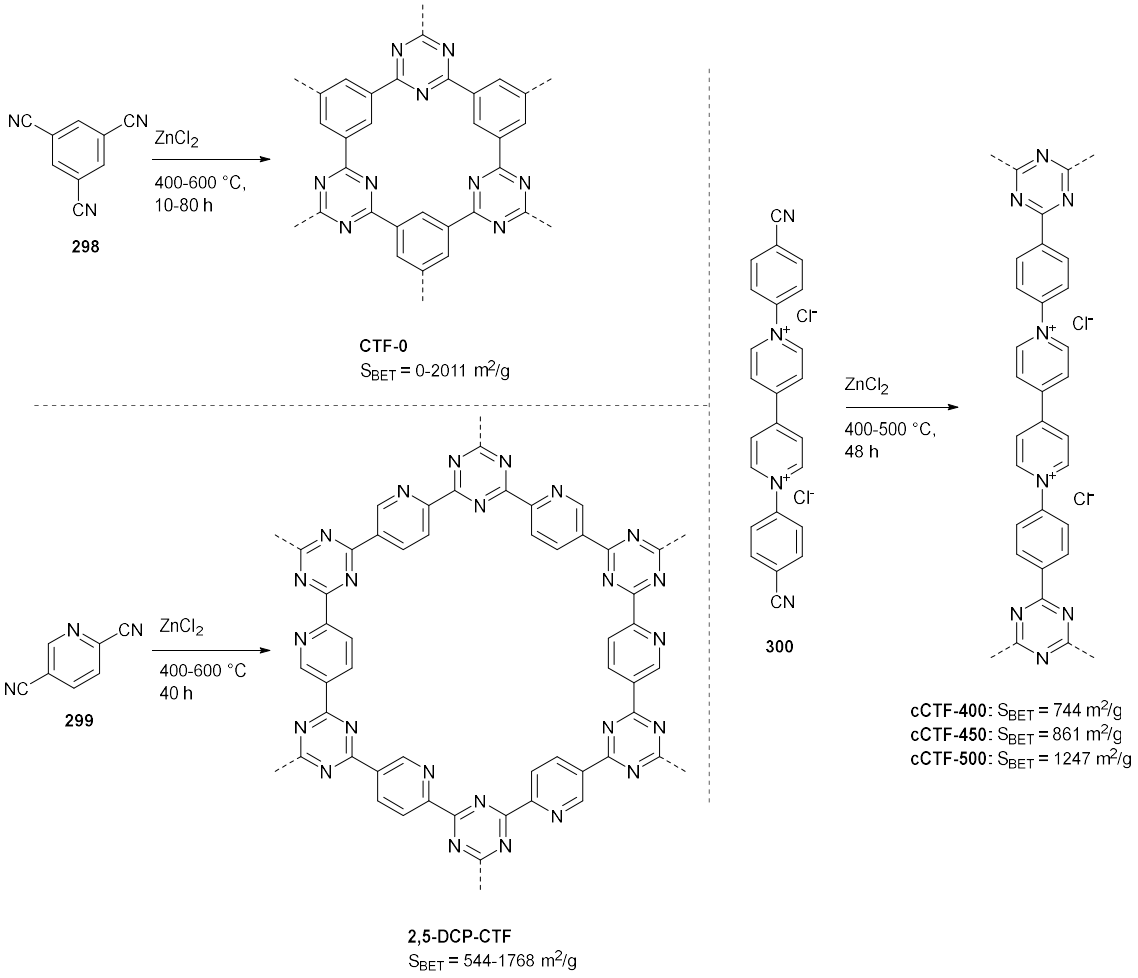

Scheme 91: Synthesis of **CTF-0**, **cCTFs** and **2,5-DCP-CTF** by ionothermal trimerization.[271, 272, 273]

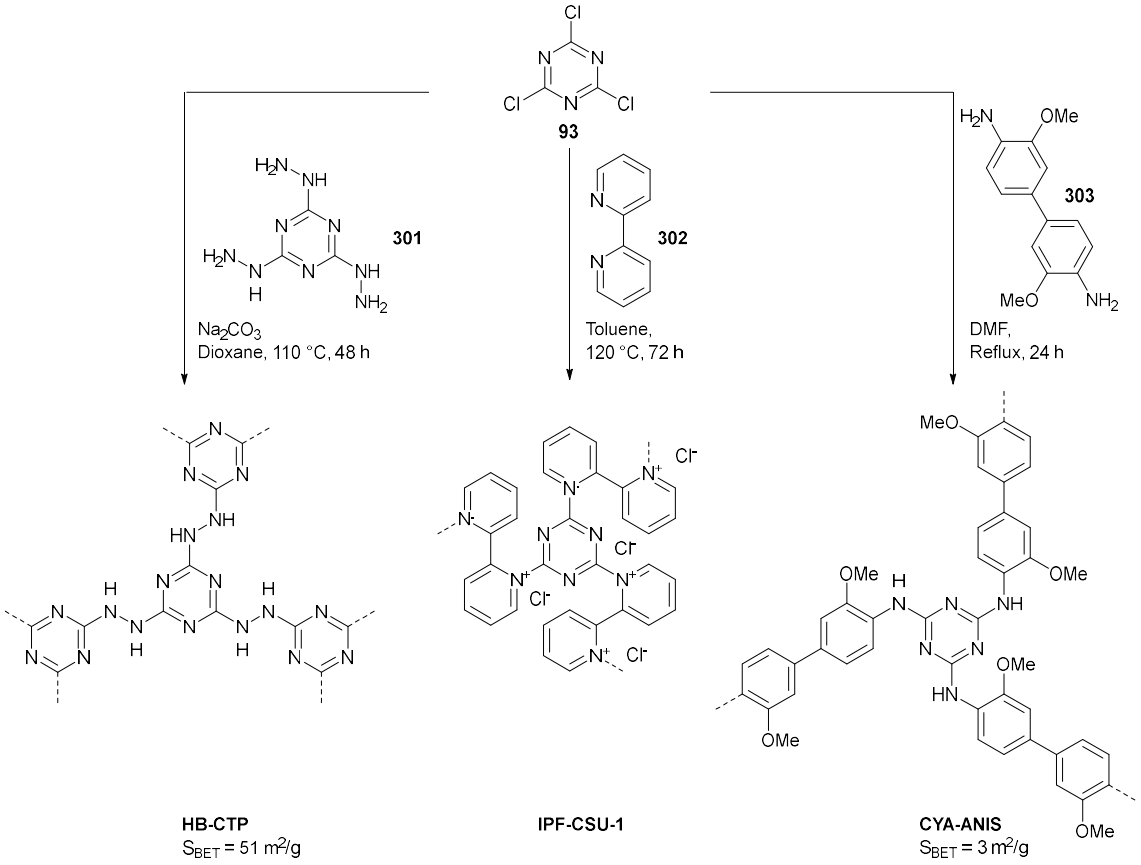

Scheme 92: Synthesis of CTFs by nucleophilic substitutions with cyanuric chloride **93**.[274,275,276]

1.6.5 Other POPs

Ma *et al*. prepared a bifunctional polymer **POF-PNA-Br**$^-$ by Sonogashira coupling between monomers **42** and **304**, followed by quaternization with bromoacetic acid **305** (Scheme 93). This led to a highly effective catalyst due to the synergy of the Brønsted acidic site of the carboxylic acid and the Br^- anion of the ionic moiety as a nucleophilic site. **POF-PNA-Br**$^-$ was able to effectively catalyze the conversion of epoxides at atmospheric CO_2 pressure and 40 °C with yields up to 94% (Table 5, entry 32). Both Cl^- and I^- containing **POF-PNA-Cl**$^-$ and **POF-PNA-I**$^-$ were less effective. The chloride anion possesses a much lower nucleophilicity, whilst the iodide anion has a very large radius, blocking pores and reducing mass transfer.[277]

Buyukcakir *et al*. prepared **PCP-Cl/BF_4/PF_6** with a viologen backbone through Sonogashira coupling between tetratopic building block **42** and the dichloride (Cl^-), ditetrafluoroborate (BF_4^-) and dihexafluorophosphate (PF_6^-) viologen salts **306** (Scheme 93). The surface area decreased as the radius of the anions increased. **PCP-Cl** possessed both the highest surface area, CO_2 adsorption capacity and catalytic activity. Good yields were obtained for the cycloaddition reaction when using high temperatures and CO_2 pressures (Table 5, entry 33). Moreover, due to the pronounced microporosity of the material bigger substrates such as styrene oxide (SO) could not react efficiently.[278]

Kim *et al*. prepared quaternary ammonium salt grafted HCPs via a two-step postfunctionalization sequence. The starting polymer, **COP-114** was prepared via a Friedel-Crafts reaction. Chloromethyl

groups were then introduced by reaction with chloromethyl methyl ether (MOMCl) and these were further functionalized by reaction with tertiary amines (Scheme 94). The material with the least sterically hindered trimethylammonium groups **COP-(114-$CH_2NMe_3^+$)Cl^-** was tested for the cycloaddition of CO_2 to epoxides. High conversions and yields were reported under atmospheric pressure, but a high temperature of 100 °C was required (Table 5, entry 34).[279]

Recently, Maya *et al*. prepared tetramethylguanidine functionalized polyphenylene POPs (Scheme 95). Amino groups were either directly incorporated in the monomers or introduced by postfunctionalization. These amine groups were then reacted with tetramethylurea in the presence of oxalyl chloride, furnishing tetramethylguanidine substituted polymers: **5PhTMG**, **2PhTMG** and **2PhCH$_2$TMG**. Only the polymer with the methylene spacer, **PhCH$_2$TMG**, possessed sufficient activity in the cycloaddition reaction. For SO 90% conversion was reported, however quite harsh conditions were applied (Table 5, entry 35).[280]

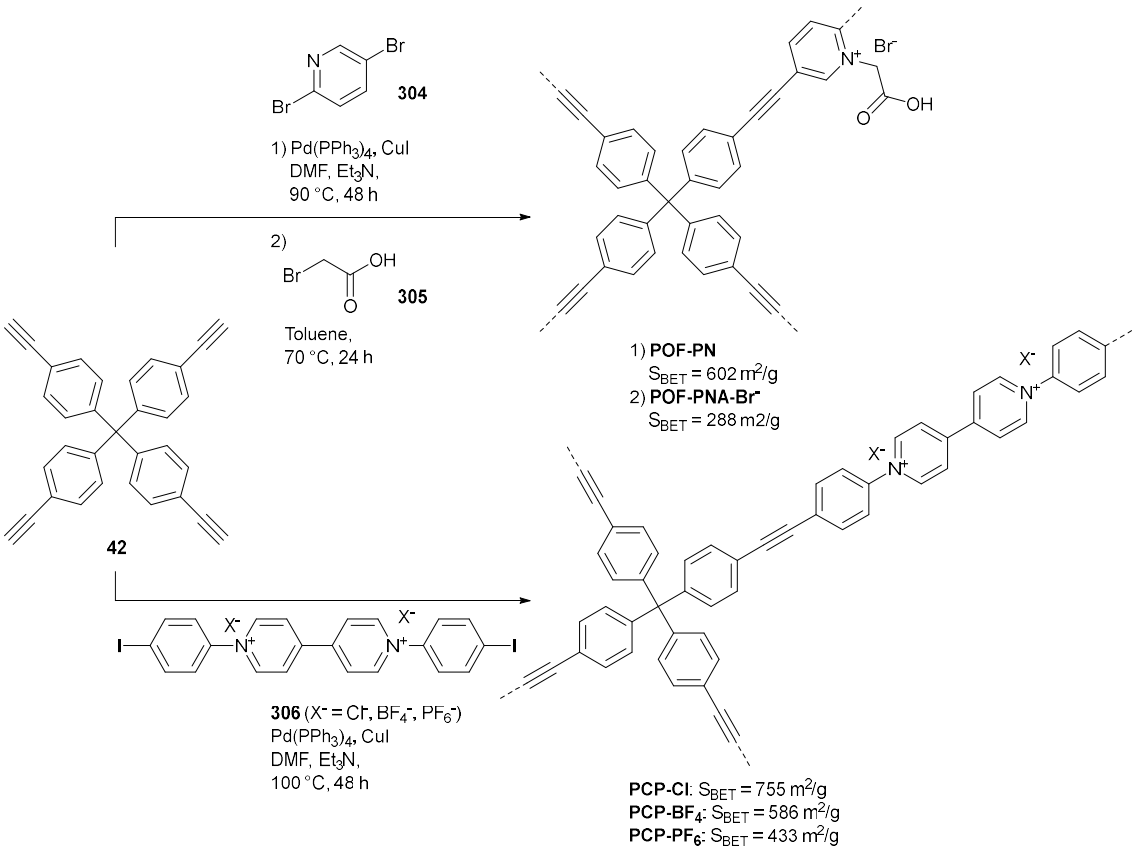

Scheme 93: Synthesis of ionic CMPs by Sonogashira coupling.[277,278]

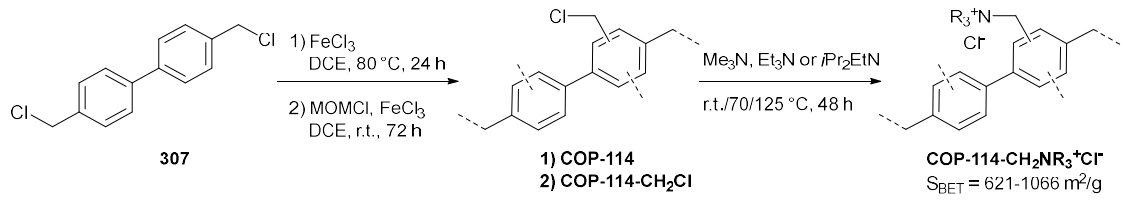

Scheme 94: Synthesis of ammonium grafted HCPs by polymerization, chloromethylation and substitution with amines.[279]

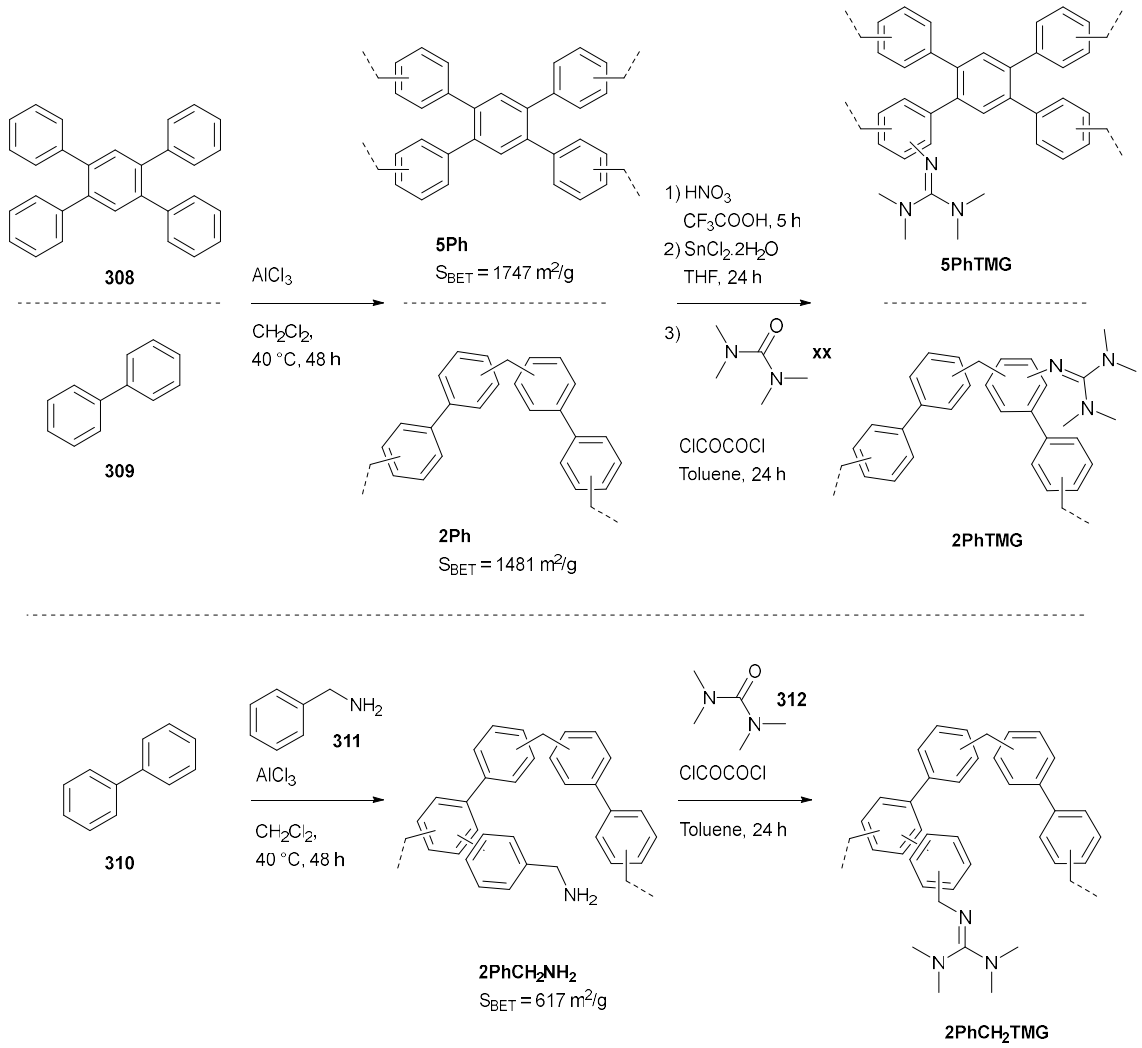

Scheme 95: Synthesis of tetramethyl urea functionalized HCPs by Friedel-Crafts polymerization of polyphenyl building blocks and reaction with tetramethylurea.[280]

A carbonyl containing aromatic polymer **CBAP-1** was synthesized by Ravi *et al*. via a Friedel-Crafts acylation reaction (Scheme 96). Post synthetically functionalization by reductive amination led to **CBAP-1(EDA)**. Zn^{2+} and Co^{2+} were also immobilized to enhance the catalytic activity by introduction of Lewis acidic sites. **CBAP-1(EDA)** reached high conversions for ECH (99%), however it required harsh conditions (Table 5, entry 36). Using TBAB as a co-catalyst reduced temperatures were possible.[281]

Zhang *et al*. synthesized a series of mesoporous POPs, **MOP-0-4**, by polycondensation of melamine **43** and aryl aldehydes **316**, forming amidine linkages (Scheme 97). By increasing the hydroxyl substitution of the aldehyde the CO_2 adsorption capacity increased, but the surface areas and catalytic activity decreased. **MOP-0** was the most active and reached 89% ECH conversion under high temperature and pressure (Table 5, entry 37).[282]

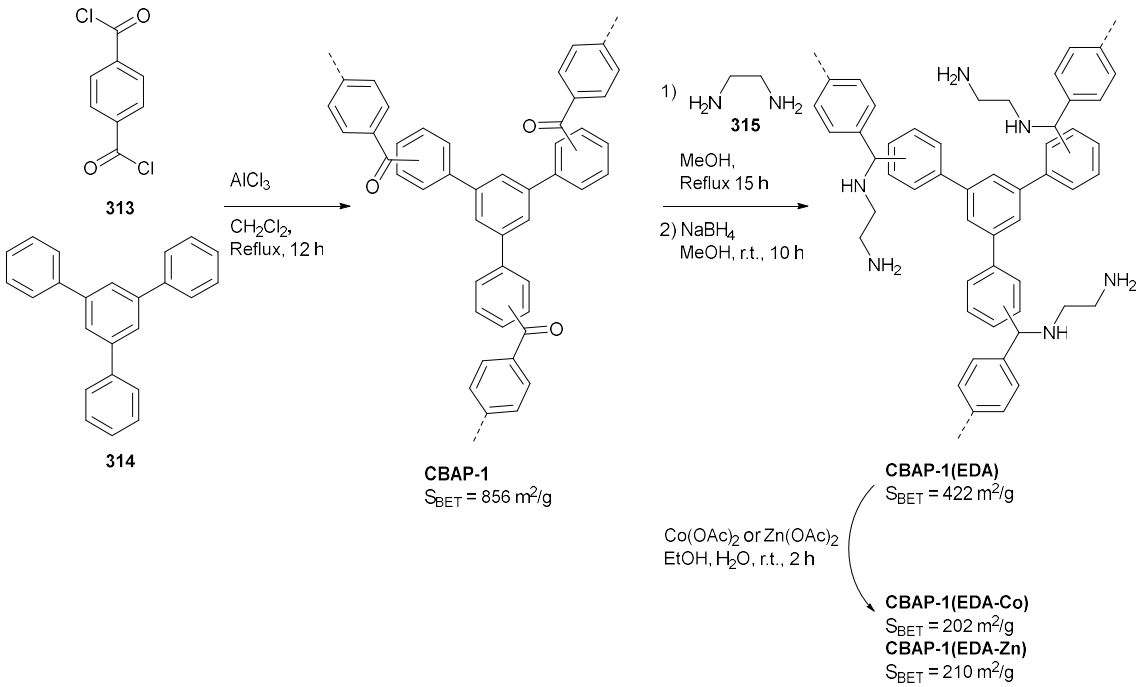

Scheme 96: Synthesis of a carbonyl containing polymer **CBAP-1** by Friedel-Crafts acylation, followed by reductive amination and metalation.[292,346]

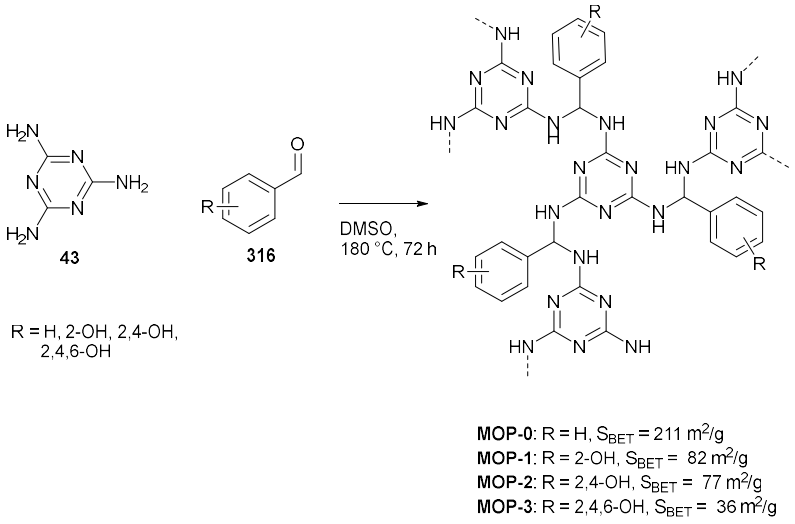

Scheme 97: Synthesis of a series of POPs by amidine formation.[282]

1.6.6 Outlook on POPs catalyzing CO_2 fixation

As stated in the introduction to this part, homogeneous catalysts used for the cycloaddition of CO_2 to epoxides are typically organic halides such as quaternary ammonium, phosphonium and imidazolium salts (ionic liquids). Next to these, strong organic bases are used. These catalysts generally need high temperatures (>80 °C) to achieve good yields, which is energy intensive and can lead to de-quaternization, sometimes thwarting their reuse.[283–285] To enable more effective catalysts the nucleophilic Lewis bases can be combined with Lewis acids, typically metal cations with ligands. Some of the most well studied examples of this class consist of metal-porphyrins, zinc β-diiminates and salen/salphen based complexes and the best of this class work well at mild conditions (≤ 60 °C, ≤ 10 bar).[286,287] However, such metal complexes are hampered by instability and long and costly synthesis routes.[288] Organocatalysts can be more economical, generally less toxic and minimize metal residues in products.[234] Therefore, homogeneous organocatalysts combining Lewis acids with Lewis bases are being developed, for example, ionic liquids with hydroxyl, carboxylic acid or amino groups that act as Lewis acids.[288,289]

Lewis basic heterogeneous catalysts for this transformation mainly consist of immobilized ionic liquids, onium salts and organic bases using polymers and silica based carrier materials,[290–294] including ordered mesoporous silicas such as MCM-41[295] and SBA-15.[288,291] Polystyrene resins have been used to immobilize 3,4-diaminopyridine analogues.[296] These purely Lewis basic heterogeneous catalysts also typically require high temperatures and pressures. Combinations of these types of catalysts with extra Lewis acidic metals exist, such as Zn/SBA-15 supported ammonium salt[297] or bifunctional ammonium-aluminum salen complexes supported on polystyrene or silica. These can work at milder conditions, up to ambient pressure and room temperature, however, in some cases lowered activity upon recycling was detected.[298,299]

Another class of materials that has been studied intensely for this transformation are the MOFs. Their metal nodes, when coordinatively unsaturated, can act as Lewis acidic sites or their organic linkers can coordinate Lewis acidic metals.[300] Harsh conditions and large amounts of an organic halide (TBAX) co-catalyst are often needed and the frameworks can be unstable under the required temperature or pressure.[301–305] A state of the art MOF, such as MIL-101-IP consisting of a chromium terephthalate MOF with an incorporated ionic polymer, was able to catalyze this transformation under atmospheric CO_2 pressure at room temperature, but still required a long time (48 hours) to achieve full conversion.[306]

Next to this, and most importantly in the context of this overview are the heterogeneous, fully metal-free organocatalysts that combine Lewis acidic and basic modes of activation. An early example of this were the silica supported phosphonium salts whose free silanol groups can act as Lewis acids. However, these catalysts required harsh conditions (100 °C, 10 MPa).[307] Ionic liquids containing hydroxyl or carboxylic acid moieties have also been immobilized on silica. For example, hydroxy containing triazolium compounds on SBA-15[308] or carboxyl-functionalized imidazolium-based ionic liquids grafted on silica,[309] but both still required high pressures and temperatures (110°C, >1.6 MPa). A similar catalyst has been reported in flow, using supercritical CO_2 at high temperatures and this material was unstable in the presence of even traces of water due to hydrolysis.[310] Polystyrene supported imidazolium based ionic liquids with incorporated hydroxy or vicinal diol groups have also been reported, but also required harsh conditions (≥120 °C, ≥ 2 MPa).[311,312] Resorcinarene containing quaternary ammonium groups with halide counterions have been immobilized on polystyrene resins, and likewise required quite harsh conditions (80 °C, 0.5 MPa).[296] A triazolium ionic liquid combined

with Lewis acidic pyrogallol moieties has been immobilized on a polystyrene resin and, interestingly, achieved full conversion at low temperature but high pressure (45 °C, 1 MPa).[313]

Lastly, cellulose and chitosan have been used as green materials to immobilize ionic moieties for this transformation. These catalysts again required high temperatures and pressures (≥120 °C, ≥ 1.2 MPa).[314–316]

To conclude, while this transformation has received widespread attention, not only in the POP field but in many other fields, the 'holy grail' of metal-free, efficient cycloaddition of CO_2 to epoxides at ambient temperature and pressure is still not achieved. The best in class fully metal-free POPs could achieve good conversion at atmospheric pressures and temperatures as low as 25 °C, but then required long reaction times (Table 5, entry 2, 19 and 32). This does compare favorably to other materials such as polystyrene resins and silicas where typically higher temperatures and pressures were used. Another fully metal-free catalytic system that worked at low pressure and temperature (Table 5, entry 29) required a very high amount of organic halide, diminishing its green potential.

It does seem that organocatalysis, is this case, is (still) not able to achieve the epoxide activating power of Lewis acidic metals. When combined with metals such as in **PPS⊂COF-TpBpy-Cu** (Table 5, entry 21) POPs can achieve extremely promising results, similar to or better than other state of the art catalysts such as MOFs.

Table 5: Cycloaddition of CO_2 with epoxides.

Entry: Name	Active site	Substrate	Reaction conditions	Yield (%)	Ref.
Imidazolium					
1: **PSIL**	Cl^-	PO	0.68 mol% **PSIL**, 6 MPa CO_2, 110 °C, 7 h	97	235
2: **PDMBr**	Br^-	Allyl glycidyl ether	1.3 mol% **PDMBr**, 1 MPa CO_2, 110 °C, 3 h	99	244
			2.6 mol% **PDMBr** 0.1 MPa, 120 °C, 12 h	99	
			2.6 mol% **PDMBr** 0.1 MPa, 70 °C, 48 h,	95	
3: **AE-PIL-Cl**	Cl^-	PO	1 mol% **AE-PIL-Cl**, 1 MPa CO_2, 140 °C, 6 h	100	245
		ECH		93	
4: **HIP-Br-2** **GHIP-Br**	Br^-	SO	0.2 mol% **HCP-Br-2/GHIP-Br**, 10 bar CO_2, 120 °C, 6 h	99	246
				86	
5: **HIP-Br-2/ZnBr$_2$**	Br^-, Zn^{2+}	SO	4 mol% **HIP-Br-2**, 4 mol% $ZnBr_2$, 1 bar CO_2, DMF, 25 °C, 120 h	93	246
6: **I$_{C2}$HCP-5b**	Br-	ECH	0.05 mol% **I$_{C2}$HCP-5b**, 3 MPa (15% CO_2), 120 °C, 4 h	81	247
7: **POM3IM**	Cl^-	PO	0.005 mol% **POM3IM**, 1 MPa CO_2, EtOH, 120 °C, 8 h	92	248
		ECH		90	
8: **T-Im**	I^-	ECH	0.065 mol% **T-Im**, 1 MPa CO_2, 150 °C	85	249
9: **IT-POP-1**	Cl^-	PO	mol% **IT-POP-1**, 1 MPa CO_2, 130 °C, 10 h	96	250
11: **PImCl**	Cl^-	ECH	5.6 mg **PImCl** or **PNHC**/mmol, 6.9 bar CO_2, 130 °C, 4 h	86	251
12: **PNHC**	Carbene	ECH		94	
13: **NP-NHC**	Carbene	ECH	5 w/w% **NP-NHC**, 1 bar CO_2, 120 °C, 24 h	98	252
14: **PEAMC1**	Carbene	ECH	10 mg **PEAMC1**/mmol, 10 bar CO_2, 120 °C, 2 h	99	253
		ECH	10 mg **PEAMC1**/mmol, 1 bar CO_2, 120 °C, 8 h	93	
15: **PPh$_3$-ILBr-ZnBr$_2$@POPs**	Br^-, Zn^{2+}	PO	0.0125 mol% **PPh$_3$-ILBr-ZnBr$_2$@POPs**, 3 MPa CO_2, 120 °C, 1 h	44	254
Phosphonium					
16: **PP-Br**	Br^-	PGE	1 mol% **PP-Br**,	99	256

			1 atm CO_2, DMF, 140 °C, 20 h		
17: **2**	Br^-	PO	0.0005 mol% **2**, 1 MPa CO_2, DMF, 100 °C, 9 h	94	[257]
18: **2+6**	Br^- + $ZnBr_2$	PO	0.0005 mol% **2+6**, 1 MPa CO_2, DMF, 100 °C, 4 h	90	[257]
19: **PIP-Bn-Cl**	Cl^-	ECH	0.46 mol% **PIP-Bn-Cl**, 0.1 MPa CO_2, 25 °C, 80 h	95	[258]
			0.46 mol% **PIP-Bn-Cl**, 0.1 MPa CO_2, 100 °C, 3 h	>99	
COFs					
20: **2,3-DhaTph COF**	Catechol	SO	0.2 mol% **2,3-DhaTph COF**, 0.5 mol% TBAI, 1 atm CO_2, 110 °C, 12 h	94	[259]
		PO		78	
		ECH		88	
21: **PPS⊂COF-TpBpy-Cu.**	Cu^{2+}, Br^-	ECH	0.17[a]/0.14[b] mol% **PPS⊂COF-TpBpy-Cu**, 1 atm CO_2, 40 °C, 24 h	95	[260]
22: **ImIP@TT-COF**	N-H, Br^-	ECH	3 mg **ImIP@TT-COF**/mmol, 0.15 atm CO_2, 24 h, 120°C	99	[261]
23: **COF-JLU6,** **COF-JLU7**	OH, Br^-	ECH	0.5 mol% **COF-JLU6/7**, 0.5 mol% TBAB, 0.1 MPa CO_2, 40 °C, 48 h	86 92	[262]
24: **OMe-OH-TPBP-COF,** **OH-TPBP-COF,** **OMe-TPBP-CF**	OH, Br^-	ECH	1 mol% **OMe/OH-TPBP-COF**, 5 mol% TBAB, 0.1 MPa CO_2, 40 °C, 24 h	91 89 41	[263]
CTFs					
25: **CTF1,** **CTF1-HAS,** **CTFP-HAS**	Basic *N*	ECH	5.6 mg **CTF**/mmol, 6.9 bar CO_2, 130 °C, 4 h	76 96 95	[270]
26: **CTF0-400/600-20/20-5**	Basic *N*	ECH	5.6 mg **CTF0-400/600-20/20-5**/ mmol, 6.9 bar CO_2, 130 °C, 4 h	93[c]	[271]
27: **2,5-DCP-CTF-0**	Basic *N*	ECH	5.6 mg **2,5-DCP-CTF-0**/mmol, 6.9 bar CO_2, 130 °C, 4 h	95	[272]
28: **cCTF-500**	Basic *N*, Cl^-	PO	4 wt% **cCTF-500**, 1 MPa CO_2, 90 °C, 12 h	99	[273]
		ECH		95	
		SO		36	
29: **IPF-CSU-1**	Cl^-, Br^-	PO	1 mol% **IPF-CSU-1**, 11.5 mol% TBAB, 0.1 MPa CO_2, 25 °C, 48 h	99	[274]
30: **HB-CTP**	Basic *N*, Br^-	PO	5 mg **HB-CTP**/mmol, 5 mol% TBAB, 2 MPa CO_2, 80 °C, 12 h	97	[275]
		ECH		99	
		SO		88	
		PGE		91	
31: **CYA-ANIS**	Basic *N*, I^-	ECH	6.7 mg **CYA-ANIS**/mmol, 1.67 mol% TBAI, 1.02 atm CO_2, 105 °C, 20 h	100	[276]
		SO		100	
		PGE		100	
Other					
32: **POF-PNA-Br**$^-$	Br^-, COOH	PO	1.7 mg **POF-PNA-Br**$^-$/mmol, 0.1 MPa CO_2, 40 °C, 48 h	92	[277]
33: **PCP-Cl**	Cl^-	PO	5 wt% **PCP-Cl**, 3 MPa CO_2, 100 °C, 12 h	99	[278]
		SO		16	
34: **COP-(114-$CH_2NMe_3^+$)Cl^-**	Cl^-	ECH	4 mg **COP-(114-$CH_2NMe_3^+$)Cl^-**/mmol, 1 bar CO_2, 100 °C, 24 h	>99	[279]
		SO		90	
35: **PhCH$_2$TMG**	Basic *N*	SO	0.1 mol% **PhCH$_2$TMG**, 7 bar CO_2, 100 °C, 4-20 h	90 100	[280]
36: **CBAP-1(EDA)**	Basic *N*	ECH	2 mg **CBAP-1(EDA)**/mmol (2 mol%), 1 MPa CO_2, 130 °C, 4 h	98	[281]
37: **MOP-0**	Basic *N*	ECH	5 mg **MOP-0**/mmol, 1 MPa CO_2, 100 °C, 24 h	89	[282]

[a] mmol of Cu^{2+}

[b] mmol of Br^-

1.7 Other reactions

1.7.1 Oxidation reactions

The reports on POPs as organocatalysts for oxidation reactions are rather limited. Huangfu *et al*. reported the synthesis of a (2,2,6,6-tetramethylpiperidin-1-yl)oxyl (TEMPO) containing porous organocatalyst **PPO-TEMPO**. This material was synthesized by polymerization and oxidation of vinyl functionalized monomer **317** (Scheme 98), and catalyzed the oxidation of alcohols to aldehydes or ketones. A range of alcohols, both benzylic and aliphatic, could be reacted with conversions and selectivities of up to 99%, using hypochlorite as an oxidant in dichloromethane. Due to the enrichment of reagents in the pores of the material its activity was much higher than the homogeneous equivalent.[197] Another TEMPO containing polymer was synthesized by $FeCl_3$ catalyzed oxidative polymerization of carbazolic building blocks **318,** with different linkages between the structural and functional (TEMPO) component (Scheme 99). Allylic, benzylic and aliphatic primary alcohols were able to react in acetic acid at room temperature under oxygen or air. $NaNO_2$ and 1,3-dibromo-5,5-dimethylhydantoin were used as a co-catalyst and auxiliary, respectively. The most active polymer, **TEMPO-CMP-4**, with the amide linker possessed a higher activity than the homogeneous monomer and could be recycled at least twenty times with retention of the activity.[317]

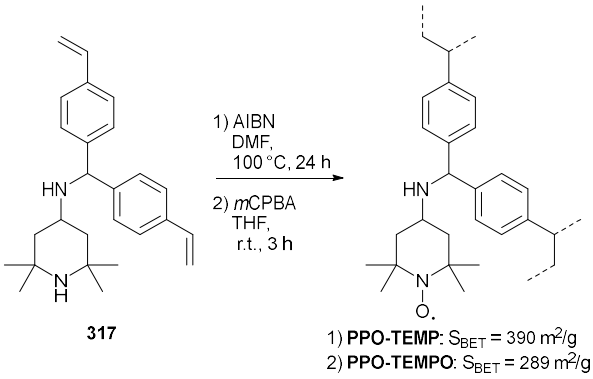

Scheme 98: Synthesis of a TEMPO based heterogeneous catalyst by crosslinking and postsynthetic oxidation.[197]

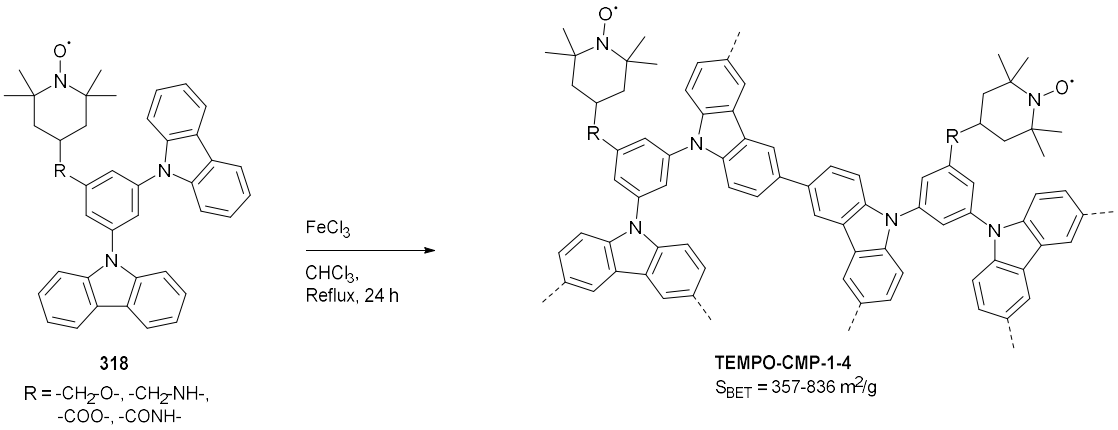

Scheme 99: Synthesis of TEMPO containing polymers by oxidative polymerization of carbazoles.[317]

Abednatanzi *et al*. synthesized a bipyridine CTF **bipy-CTF** as a support for an Ir^{III} complex for the aerobic oxidation of alcohols (Scheme 100). Interestingly the activity of the metal catalyst was hugely increased by the solid CTF support, by virtue of its nitrogen-rich sites activating oxygen and the alcohol substrates. A wide range of benzylic alcohols could be converted into the corresponding aldehydes in generally high yields, using only the catalyst and the most environmentally friendly oxidant: molecular oxygen, aliphatic alcohols however gave much lower conversions.[318]

In further research by the same group metal-free CTFs were used for the oxidation of benzylic alcohols and amines. Using easily prepared **CTF-1** (Scheme 90) and under similar conditions as the aforementioned iridium catalyzed reactions, a wide range of alcohols were converted in generally good yields. Furthermore, this material catalyzed the oxidative coupling of amines to imines for a wide range of substrates with high conversion (99%) and selectivity (>85%). The nitrogen composition of a range of CTFs was determined by XPS analysis and the conversion corresponded with the amount of quaternary nitrogens in the materials.[319] The mechanism of the oxygen activation is proposed to proceed by adsorption of oxygen on a carbon atom neighboring the quaternary *N*, resulting in formation of oxygen radicals as hypothesized by Arai and co-workers who studied a similar reaction using nitrogen doped carbon as a catalyst.[320] These oxidation reactions have also been reported photocatalytically, by CTFs synthesized from thiophene containing building blocks (Section 1.7.2.6).[321]

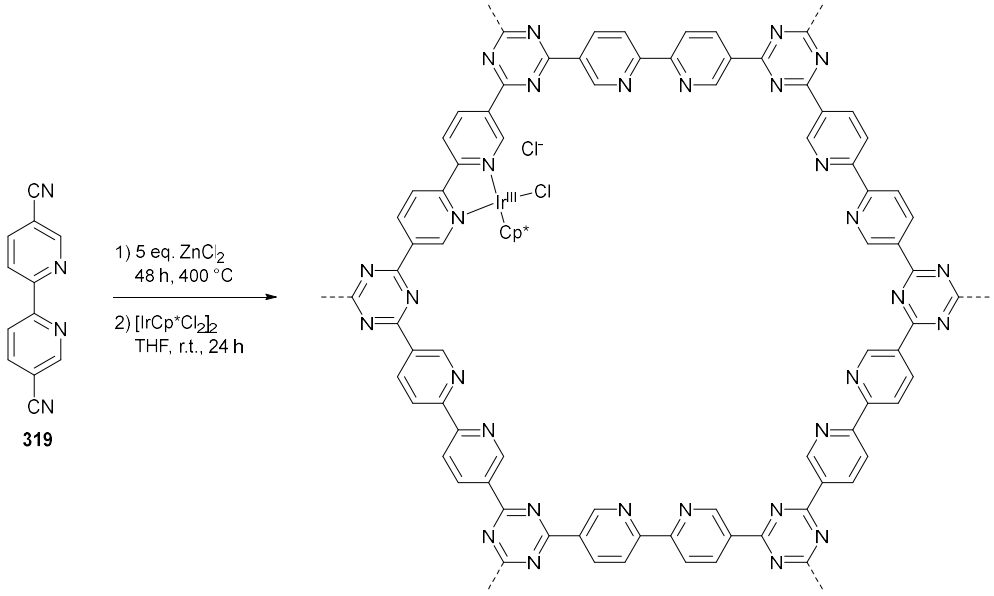

Scheme 100: Synthesis and postsynthetic metalation of a bipyridine based CTF.[318]

CTFs have also been applied for the oxidative depolymerization of lignin, a main constituent of biomass. Lignin is made up of methoxylated phenylpropane monomers and is a potential renewable source of aromatic building blocks for the chemical industry. However, its depolymerization is not a trivial process. To study the oxidative cleavage of a lignin model compound **320** several CTFs based on 1,4-dicyanobenzene, 1,3-dicyanobenzene and 4,4'-dicyanobiphenyl were synthesized. Phenoxyacetophenone **320** was converted into the cleavage products: phenol **9**, benzoic acid **321**, methyl benzoate **322**, methyl benzoylformate **323** and the ketal **324** (Scheme 101). The conversion stayed under 20% when no catalyst was used, applying CTFs the conversion could reach up to 99%. Furthermore, a range of different β-*O*-4 ketone compounds could be converted by the CTFs. The mechanism is proposed to proceed through the generation of a peroxide from the β-H, followed by decomposition with C-C or C-O bond cleavage and further reaction to the products.[322]

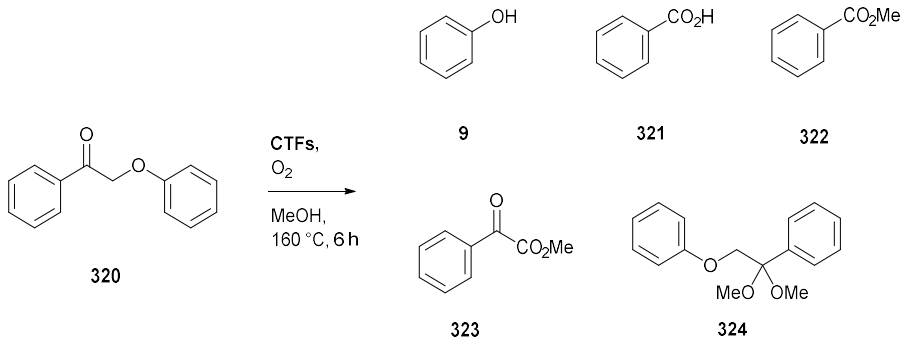

Scheme 101: CTF catalyzed decomposition of lignin model compound **320**.[322]

Lastly, Ansari *et al*. used the earlier mentioned polymer formed by condensation of formaldehyde with melamine (Table 1, entry 10) as a catalyst for the epoxidation of styrene to styrene oxide (SO). Using hydrogen peroxide in presence of $NaHCO_3$ 90% conversion and 98% selectivity for SO was obtained.[70]

1.7.2 Miscellaneous

Wu *et al.* synthesized **Py-An COF** by solvothermal condensation of 1,3,6,8-tetrakis(*p*-formylphenyl)pyrene **326** with 2,6-diaminoanthracene **325**. This COF with open one-dimensional channels and columnar π-walls promoted Diels Alder reactions of 9-hydroxymethyanthracene **327** and *N*-substituted maleimide derivatives **328** under ambient conditions. The authors suggest the COF increases both the effective concentration of the reactants within their pores and activates the substrates through C-H π-interactions, reducing the entropy loss and activation energy of the reaction.[323]

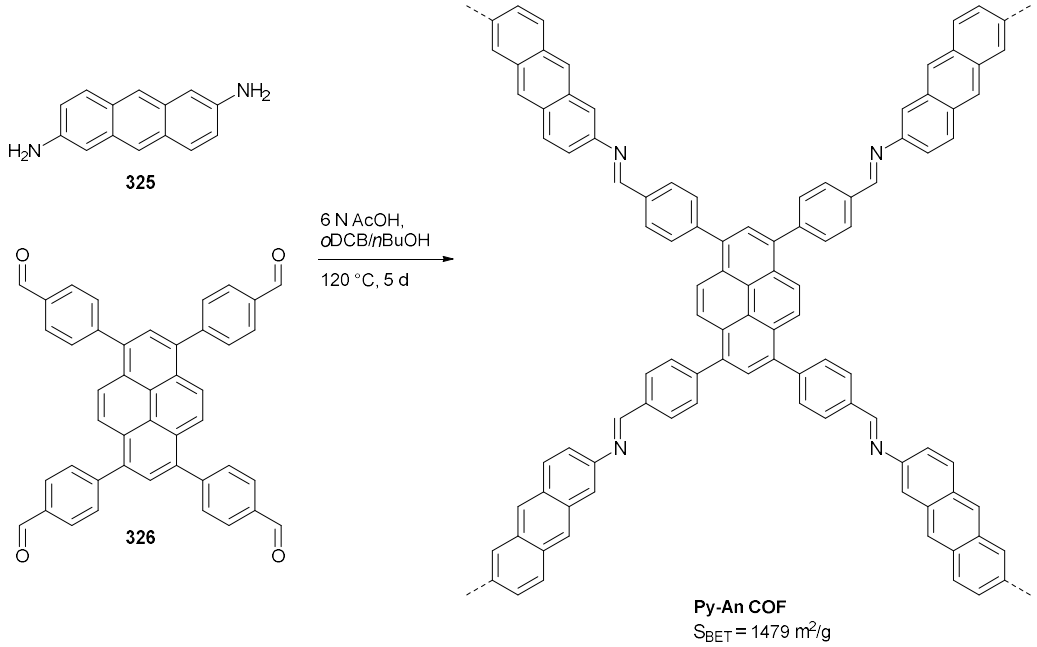

Scheme 102: Synthesis of **Py-An COF**.[323]

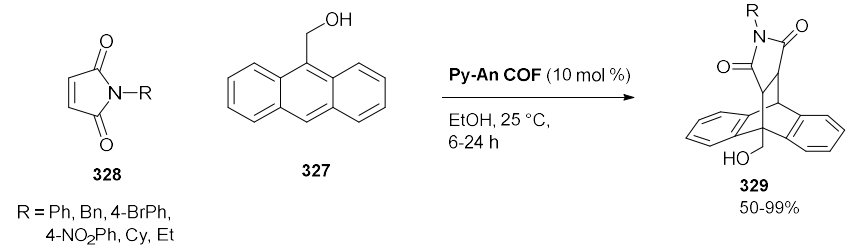

Scheme 103: Diels Alder reactions catalyzed by **Py-An COF**.[323]

1.8 Photocatalysis

1.8.1 Introduction

POPs have been applied as (metal-free) photocatalysts in organic synthesis, for hydrogen generation, the reduction of carbon dioxide and the degradation of pollutants in air or waste streams. In this part of the literature review the focus will be on the applications of POPs in organic synthesis, as this was the main aim of the research conducted during this PhD.

The general mechanism of photocatalysis by POPs follows similar pathways as with other semiconductors. Under light irradiation the POP can absorb photons with energy equal or greater than the band gap, which leads to electrons jumping from the valence to the conducting band (VB to CB), leaving behind 'holes' in the conducting band. After migration of these charge carriers to the surface of the material they can participate in redox reactions.[324–326] Next to this general mechanism, another possibility consists of direct energy transfer, without electron transfer, from the excited material to a suitable substrate (*e.g.* an alkene, oxygen). This produces the activated substrate, which can then undergo further reactions (Figure 4).

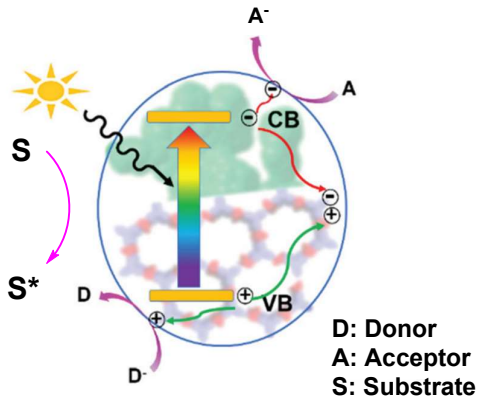

Figure 4: The general mechanism by which POPs act as photoredox catalysts. Adapted from reference [327].

For a certain reaction to be thermodynamically possible, the position of the valance and conducting bands of the catalyst and substrates need to match, *i.e.* the material needs to be sufficiently oxidizing and/or reducing. Furthermore, to obtain materials capable of utilizing visible light, the band gap between these energy levels needs to be sufficiently small, so that relatively low energy photons can be used. Additionally, to obtain a good catalyst the photogenerated electrons and holes need to separate and migrate to the surface efficiently. Lastly, the stability of the material in the reaction conditions needs to be high, to obtain a recyclable, heterogeneous catalyst.

An important design strategy to obtain photocatalysts which have these desirable characteristics, consists of the selection of suitable building blocks and linkages. A recurring theme in the synthesis of visible light active POPs is the combination of electron poor and electron rich building blocks, thus forming donor-acceptor polymers. This combination leads to smaller band gaps, better transport and separation of electron-hole pairs, and lower recombination of these photogenerated carriers.[328,329] Some typical donor and acceptor motifs are shown in Figure 5. It is also possible to immobilize organic dyes and metal complexes on POPs, as building blocks in a bottom-up approach or postsynthetically, to increase the photocatalytic activity.

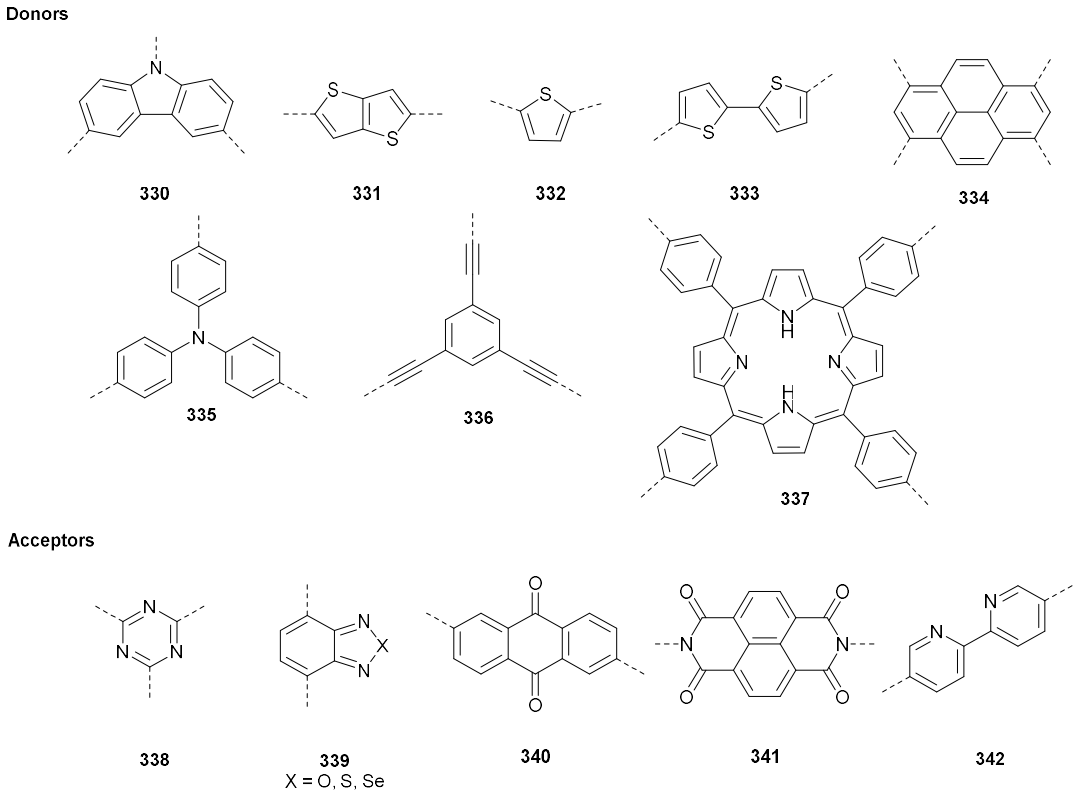

Figure 5: Typical donor and acceptor motifs found in photocatalytically active POPs.

Besides the choice in building blocks, the type of linkage is important as well. Imine linkages are widely used in COF synthesis, even though these linkages are relatively polarized and thus do not allow for extensive conjugation. The unpolarized C=C bond allows for more extensive π-conjugation. Therefore, recently attention has gone to the synthesis of C=C linked COFs by Horner-Wadsworth-Emmons reactions or Knoevenagel and aldol condensations.[330] It is also possible to postsynthetically convert a certain linkage into a more suitable linkage. For example, Wang *et al*. converted an imine-linked COF with thiophene units on the backbone to thieno[3,2-*c*]pyridine-linked COFs using a Pictet−Spengler reaction and applied these materials as photocatalysts for the regeneration of NADH (Section 1.8.3.1).[331] Similarly Zhao *et al*. converted imine-linked COFs into quinoline-linked COFs by rhodium-catalyzed dehydrogenative annulation. The resulting materials were more active as photocatalysts for the synthesis of 2,4,6-tris(aryl)pyridines (Section 1.8.2.3.2). [332] Non crystalline POPs, such as CMPs, are often synthesized by Pd-catalyzed couplings and are thus often linked by aryl-aryl bonds, which allow for good conjugation. However, non-crystalline materials generally perform worse as photocatalysts, as the defects in the material interrupt the conjugation and prevent efficient charge separation and migration.

Another important factor, which mainly concerns COFs, is the interlayer stacking behavior. While COFs are often displayed as an ordered sequence of eclipsed planar layers, in reality a range of stacking sequences are possible, and difficult to distinguish on the basis of experimental data. However, different stacking modes have a large influence on the electronic structure and therefore the photochemical properties, by changing the interlayer π-orbital overlap.[333] Whilst considerable attention has gone to the effects of building blocks and linkers on the bandgaps and positions, these stacking effects are still an underexplored topic and deserve further investigation.

A wide variety of reactions have been described in the literature as being catalyzed by POPs. For the purpose of this literature overview, a representative material for every reaction will be discussed. The reactions can be divided in oxidation reactions, reduction reactions and others. It should be noted that in some cases the classification can seem rather arbitrary. Some reactions are classified as oxidation reactions (*e.g.* cross-dehydrogenative couplings, cycloadditions of styrenes, etc.) due to the first step being the oxidation of the starting material, even if the final product is not necessarily oxidized compared to the substrate. Whilst in other reactions (*e.g.* alkylation of vinylarenes, photocatalytic Stille couplings…) one of the substrates is oxidized and the other reduced. In those cases, the most similar transformations were grouped together, to make this overview as clear as possible.

1.8.2 Oxidation reactions

The typical mechanism of a photocatalyzed oxidation reaction using oxygen goes through the photogeneration of reactive oxygen species (ROS). The superoxide radical anion ($O_2^{-\bullet}$) is produced by reduction of oxygen with photogenerated electrons. Furthermore, singlet oxygen ($^1O_2$) can be formed, either by one-electron oxidation of $O_2^{-\bullet}$, or directly, by energy transfer to oxygen from the excited POP. Both the photogenerated holes and the reactive oxygen species can accept electrons from the substrate, thus oxidizing it. Next to this, the ROS can also abstract protons and hydrogen atoms from the substrates.

1.8.2.1 Oxidation of sulfides

A typical reaction to probe the activity of photocatalysts is the selective oxidation of sulfides to sulfoxides. Zhang *et al*. recently constructed olefin-linked COFs to use as photocatalysts for this reaction. Two vinylene-linked COFs were synthesized by aldol-like condensation between 2,4,6-trimethyl-1,3,5-triazine **343** and 2,4,6-tris(4-formyl-phenyl)-1,3,5-triazine **344** or 1,3,5-tris(4-formylphenyl)-benzene **209** resulting in **TTO-COF** and **TBO-COF**, respectively (Scheme 104). As stated in the introduction of this chapter, the olefin linkage has the advantage of being unpolarized, unlike imines, and thus should offer higher activity. However, the construction of these COFs is also much more challenging due to the lower reversibility of the C=C bond forming reactions, compared with Schiff base formation. Interestingly, **TTO-COF**, which was based on the triazine containing aldehyde, possessed better photocatalytic performance and stability than **TBO-COF** during the photocatalytic oxidation of sulfides, possibly due to its higher crystallinity and tighter stacking. By using this material, a wide range of sulfides **345** were selectively oxidized (96-99%) in generally very high conversions (up to 99%). Quenching experiments pointed to the importance of both $O_2^{-\bullet}$ and $^1O_2$. Both ROS led to the formation of an intermediary persulfoxide **348**, either by direct oxidation with $^1O_2$, or by oxidation of the sulfide with a photogenerated hole, followed by reaction with $O_2^{-\bullet}$. Finally, the removal of water from the persulfoxide **348** leads to the product **349** (Scheme 105).[334]

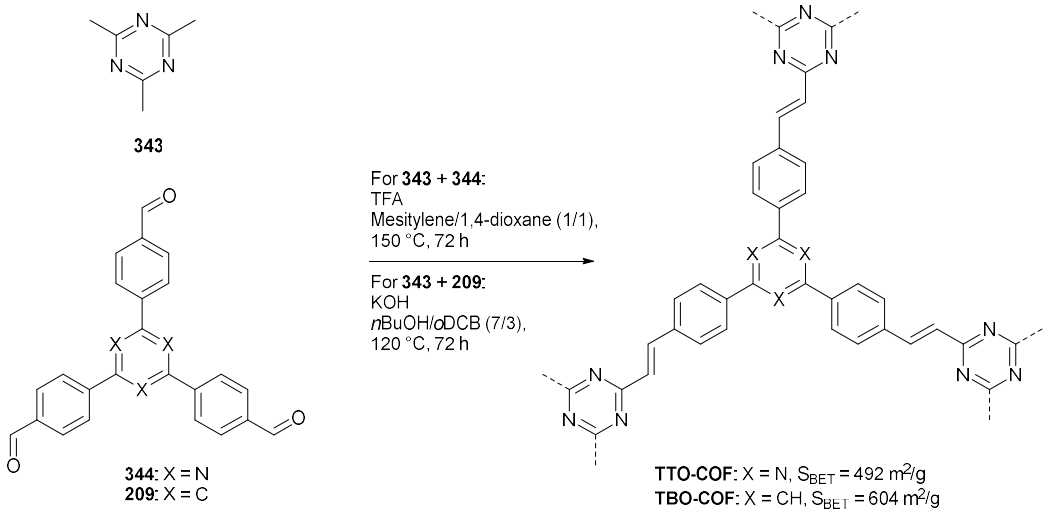

Scheme 104: Synthesis of vinylene-linked COFs **TTO-COF** and **TBO-COF.**[334]

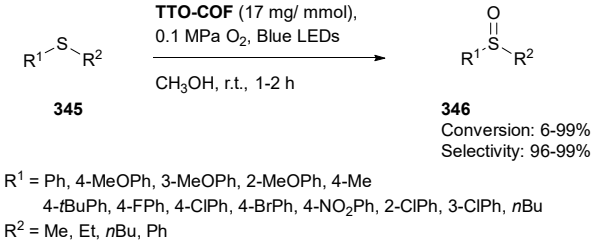

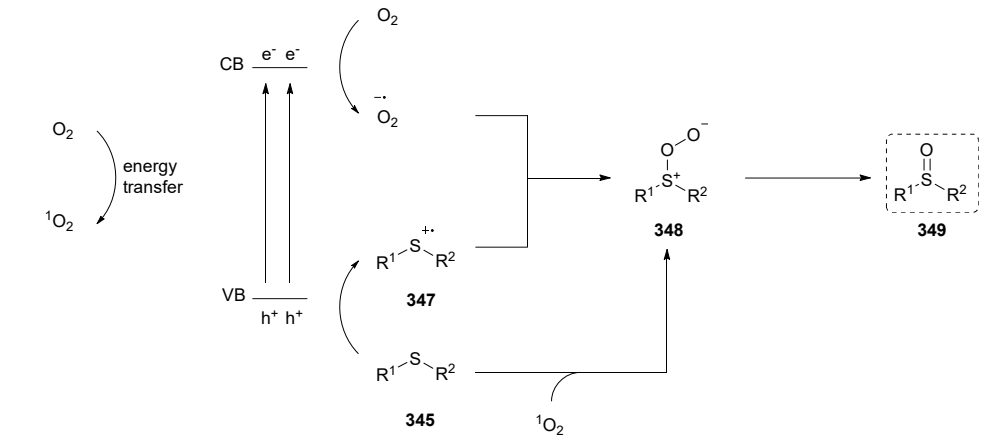

Scheme 105: Selective oxidation of sulfides catalyzed **by TTO-COF**.[334]

1.8.2.2 Oxidation of arylboronic acids

Another reaction that is reported often in the literature as an application of photo-active materials is the oxidation of arylboronic acids to the corresponding phenols. In 2018 Wei *et al*. synthesized benzoxazole-linked COFs for this reaction. This new type of linkage led to materials that are not only much more stable than conventional imine COFs, but also allow for more extensive conjugation. By condensation of aromatic aldehydes **48**, **344** and **326** with HCl salt of 2,5-diaminobenzene-1,4-diol **350** three benzoxazole-linked COFs **LZU-190**, **LZU-191** and **LZU-192** were formed (Scheme 106). The stability of these benzoxazole-linked materials was very high, as they retained their crystalline structure in harsh conditions such as TFA, 9M HCl and 9M NaOH. Using **LZU-190** as a photocatalyst and DIPEA as a sacrificial electron donor, a wide range of arylboronic acids **351** could be transformed into the corresponding phenols **352** in generally very high yields (Scheme 107). The mechanism consists of SET of the photogenerated electrons to oxygen forming $O_2^{-\bullet}$. This superoxide anion then performs nucleophilic attack on the empty p-orbital of the boronic acid to generate intermediate **353**. This intermediate will abstract a hydrogen atom from the ammonium radical cation **354** to form intermediate **356**. Rearrangement to compound **357** and subsequent hydrolysis results in the hydroxylated product **352**.[335]

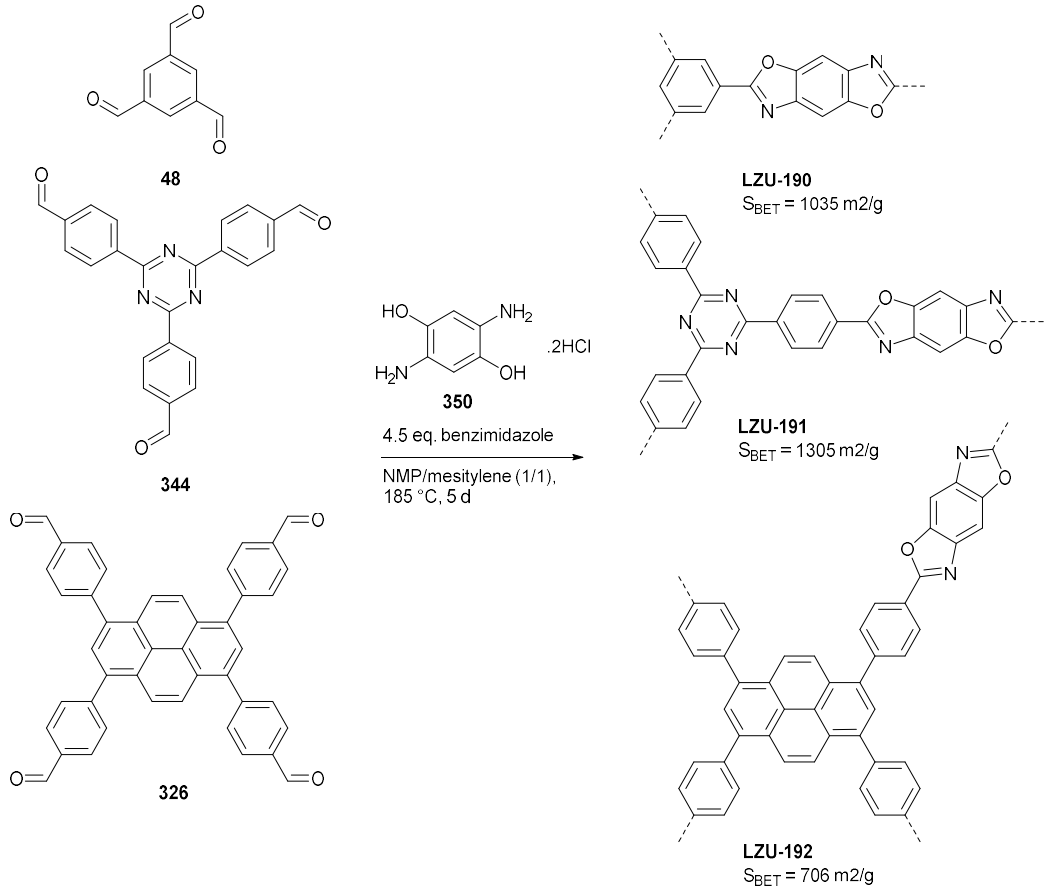

Scheme 106: Synthesis of benzoxazole-linked COFs.[335]

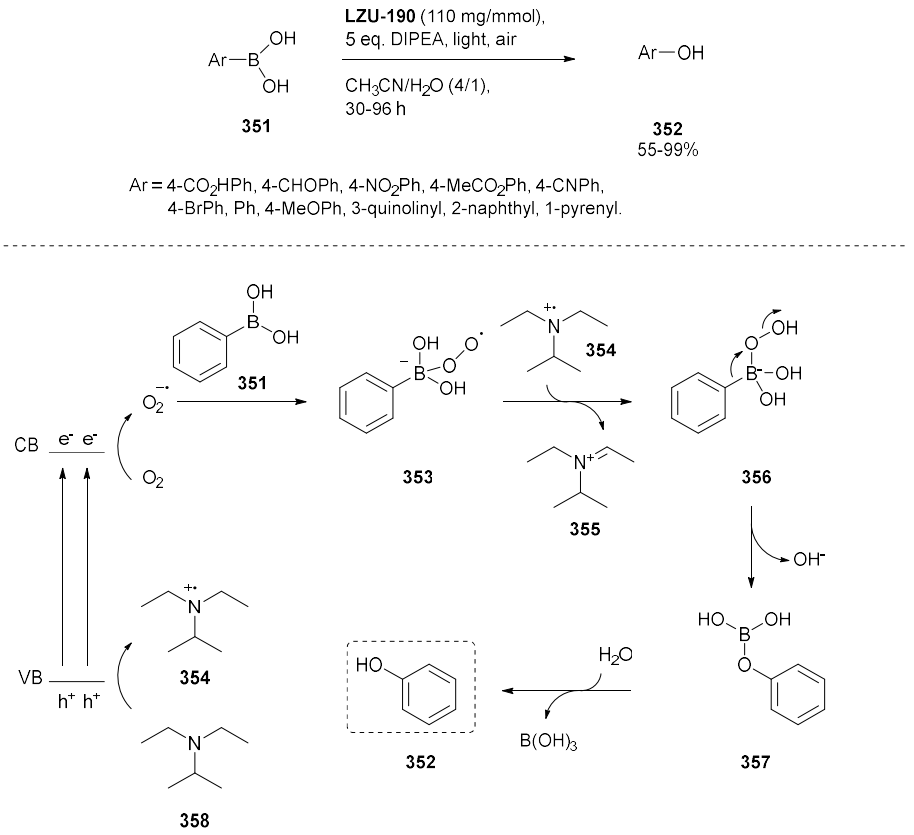

Scheme 107: Photocatalytic oxidation of arylboronic acids **351** to phenols **352** catalyzed by **LZU-190**. [335]

1.8.2.3 Oxidation of nitrogen containing compounds

1.8.2.3.1 Oxidation of amines into imines

Yet another reaction that is often studied is the oxidation of benzylic amines to imines, for which a plethora of POPs have been reported as photocatalysts.[336–340] An interesting example was reported in 2020, of a C=C linked COF which was able to utilize red light. **Por-sp^{2}c-COF** was synthesized by Knoevenagel condensation of porphyrin **362** with 1,4-phenylenediacetonitirle **363** (Scheme 108). This material was applied towards the oxidative coupling of benzylic amines to imines and the addition of TEMPO to this reaction doubled the yield. Interestingly, the addition of TEMPO did not improve the reaction when using an organic dye such as eosin Y, erythrosine Y, rose Bengal or sp^{2}c-CMP, an amorphous counterpart of the COF. The crystallinity of the COF is thus important to achieve the desired cooperative effect. Moreover, when the authors used an imine-linked analog of this material, it degraded during the reaction, due to the nucleophilic benzylic amines breaking down the imine linkages. Under optimized conditions a wide range of amines **364** could be oxidatively coupled with high conversion and selectivity. The more difficult to oxidize secondary amines **366** also reacted very efficiently in short reactions times (Scheme 109). The proposed mechanism goes via the oxidation of benzylamine **364** to the imine **371** via transfer of an electron and hydrogen atom to TEMPO$^+$ **369**, generating imine **371** and TEMPOH **370**. After loss of a proton the imine **372** can then react with another equivalent of benzylamine **364**, which after loss of ammonia forms the product **365**. TEMPOH **370** is oxidized by $O_2^{-\bullet}$, generating H_2O_2 and TEMPO **368**, which then is further oxidized by the holes of the COF, regenerating TEMPO$^+$ **369**.[341]

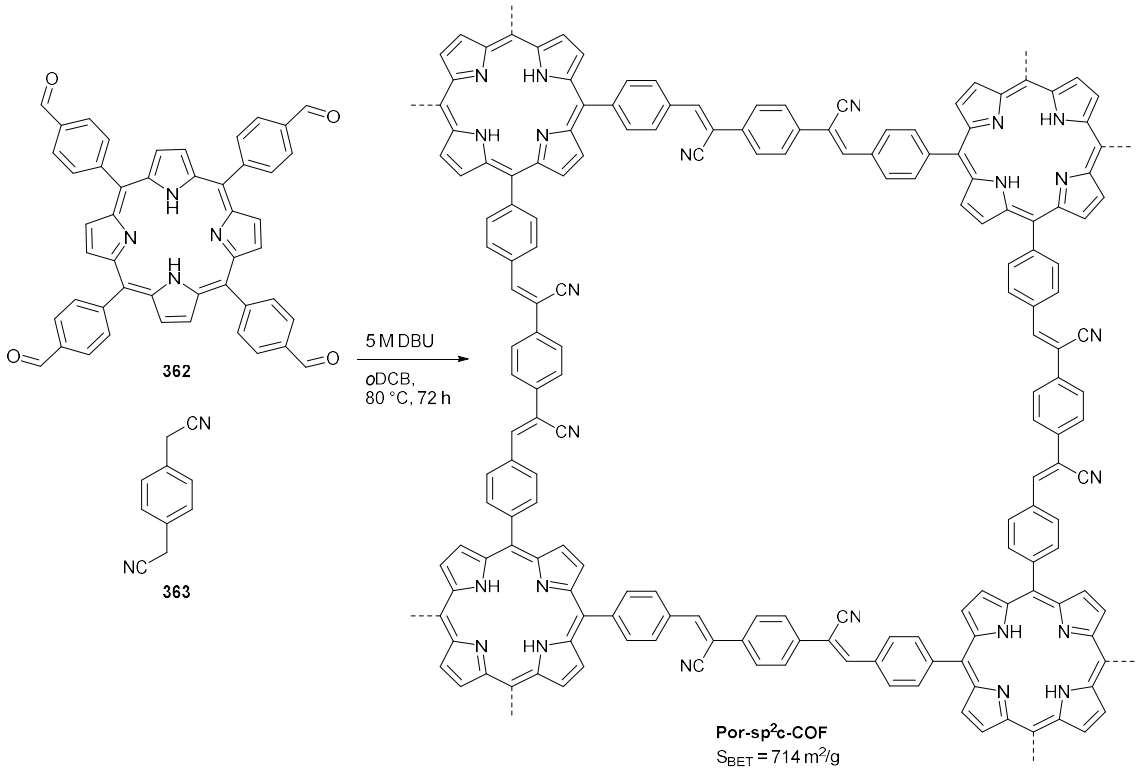

Scheme 108: Synthesis of vinylene-linked **Por-sp²c-COF**.[341]

1.8.2.3.2 Synthesis of 2,4,6-tris(aryl)pyridines

As discussed previously, the imine linkage, while often used in COF synthesis due to its reversible nature, is not ideal for (photo)catalysis. On the one hand, the linkage is relatively unstable, and on the other hand the polarized C=N bonds stand in the way of efficient conjugation throughout the network. A possible solution for this is the postsynthetic modification (PSM) of imine linkages to more stable linkages, which also allows for better conjugation. Very recently, a strategy was reported to 'lock' the imine as an unsubstituted quinoline by rhodium-catalyzed [4+2] annulation. First **COF$_{TFppyPh}$** was synthesized by Schiff base formation between pyrene-based aldehyde **326** and 1,4-diaminobenzene **81**. This was then postsynthetically modified into a quinoline-linked COF, **NQ-COF$_{TFppyPh}$**, by annulation with vinylene carbonate (Scheme 110). Interestingly, by doing this the surface area dropped from 2144 m^2/g to 1145 m^2/g, which is much more than was indicated by theoretical calculations. This was attributed to the decrease of crystallinity and generation of some amorphous oligomers in the pores of the COF during the PSM reaction. However, the material was still crystalline and possessed smaller band gaps: 1.83 eV for **NQ-COF$_{TFppyPh}$** versus 2.39 eV for **COF$_{TFppyPh}$**, and greater separation efficiency of photogenerated carriers. Next to this, it possessed exceptional chemical stability, both to strong acids (12 M HCl), superacids (TfOH), bases (14 M NaOH), reducing agents ($NaBH_4$), and nucleophiles (*n*-hexylamine). This material was used for the oxidative synthesis of 2,4,6-tris(aryl)pyridines **375** from aryl ketones **373** and benzylamines **374** (Scheme 111). The reaction occurs by the oxidation of benzylamine **374** to the imine **378**, with release of ammonia. The enol **380** adds to this imine to form intermediary **381** which also undergoes oxidation to produce another imine **382**. A second equivalent of enol **380** adds to this intermediate, followed by cyclization with ammonia to produce the tetrahydropyridine **384**. Finally, by loss of benzylamine **374** the pyridine **375** is formed.[332]

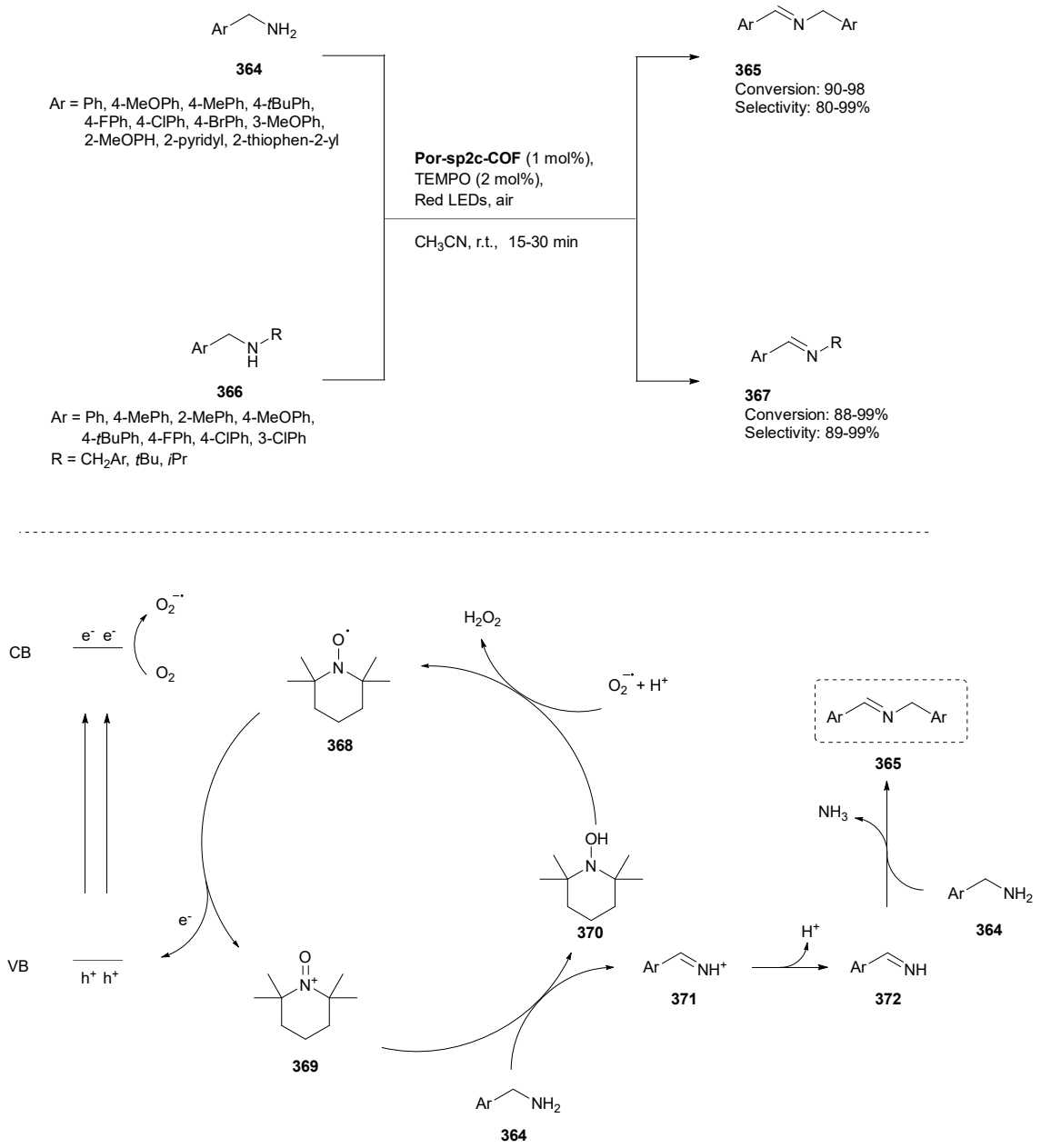

Scheme 109: Oxidation of benzylic amines to imines catalyzed by **Por-sp2c-COF**.[341]

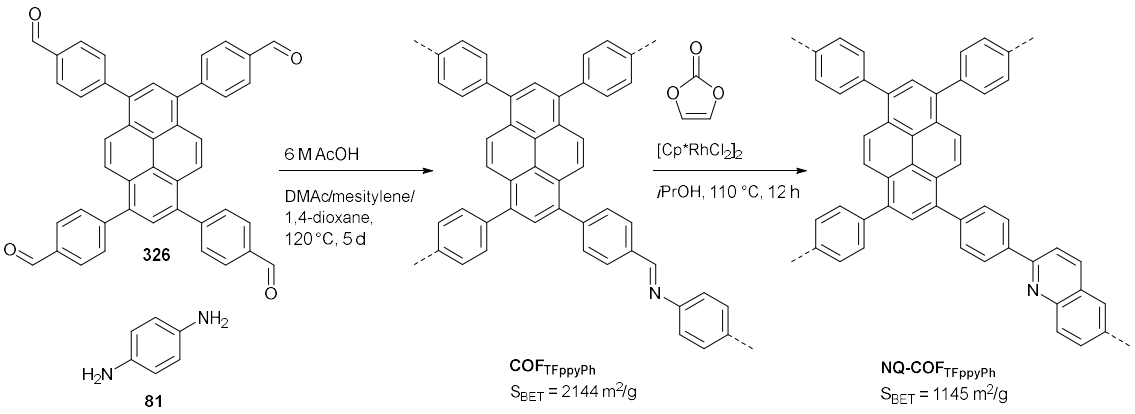

Scheme 110: Synthesis of quinoline-linked COFs by rhodium catalyzed annulation of imines with vinylene carbonate.[332]

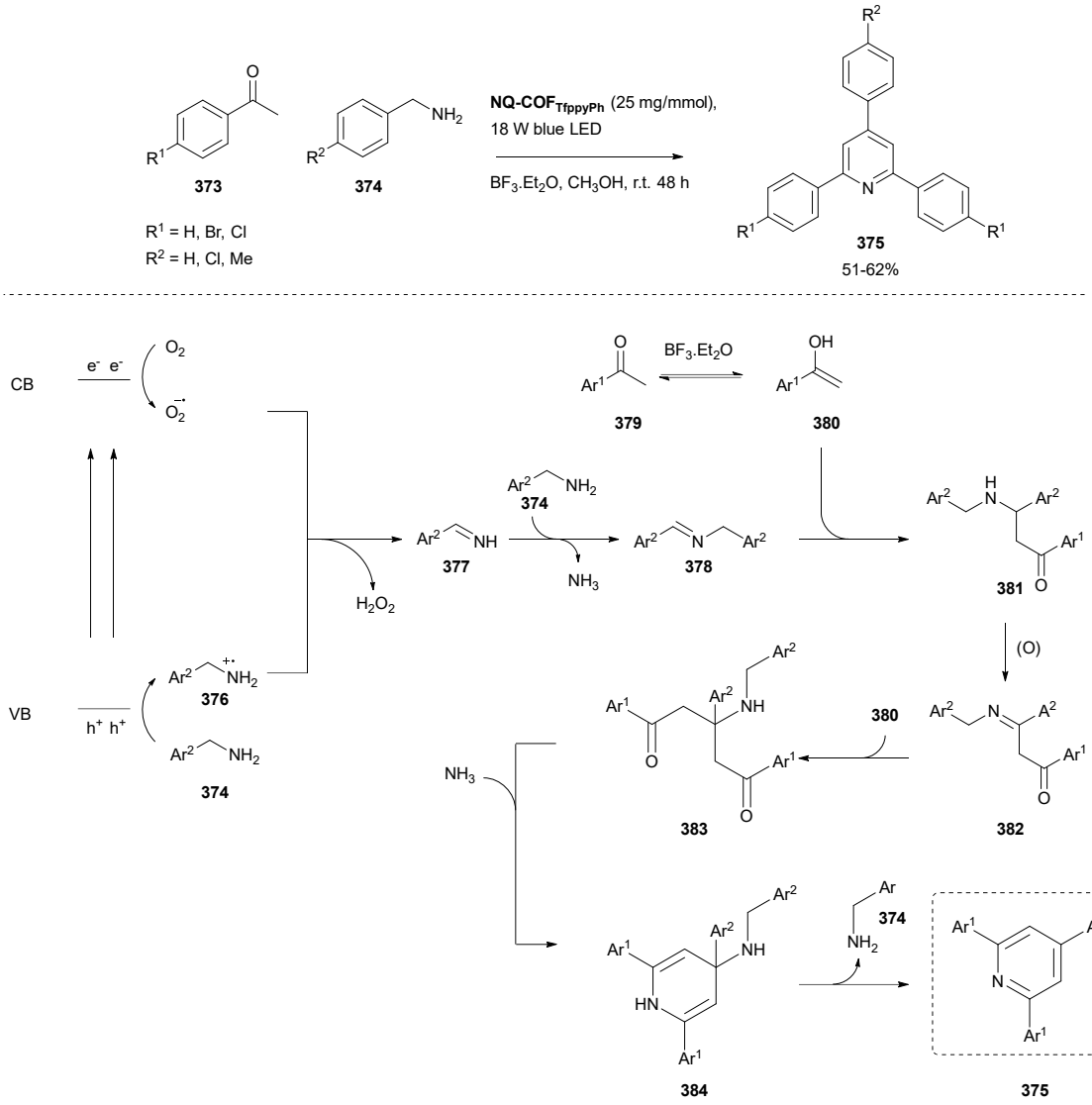

Scheme 111: Synthesis of 2,4,6-tris(aryl)pyridines **375** by oxidation of benzylamines **374**, enol addition of aryl ketones **373** and cyclization.[332]

1.8.2.3.3 Cross-dehydrogenative coupling of tetrahydroisoquinolines with nitromethane

Cross-dehydrogenative couplings (CDCs) consist of the construction of C-C bonds by oxidatively coupling two C-H bonds.[342] The CDC of tetrahydroisoquinolines with a variety of nucleophiles is a typical test reaction for photocatalysts. Kang *et al*. undertook the synthesis of a pair of twofold interpenetrated 3D COFs with a rare (3,4) connected ffc topology **COF-1** and **COF-2** by Schiff base formation between aldehydes **386** and **387** and amines **385** and **52** (Scheme 112). The triphenylamine moiety is the source of the 3D topology, due to its non-planar character and serves as an electron rich, hole-conducting moiety. A series of different tetrahydroisoquinoline derivatives **388** could react with nitromethane to give the coupled products **389** in 53-85% and 50-83% yield for **COF-1** and **COF-2**, respectively (Scheme 113). This happens through a similar mechanism as in the benzylamine oxidation, except in this case, due to the tetrahydroquinoline **388** being a tertiary amine an iminium ion **381** is formed. This can then react with the nitromethyl anion **392** to give the product **389**. Next to this reaction the authors studied the enantioselective α-alkylation of aldehydes with these COFs using the Macmillan imidazolidinone organocatalysts **546** as the co-catalyst (Section 1.8.3.2.1).[343]

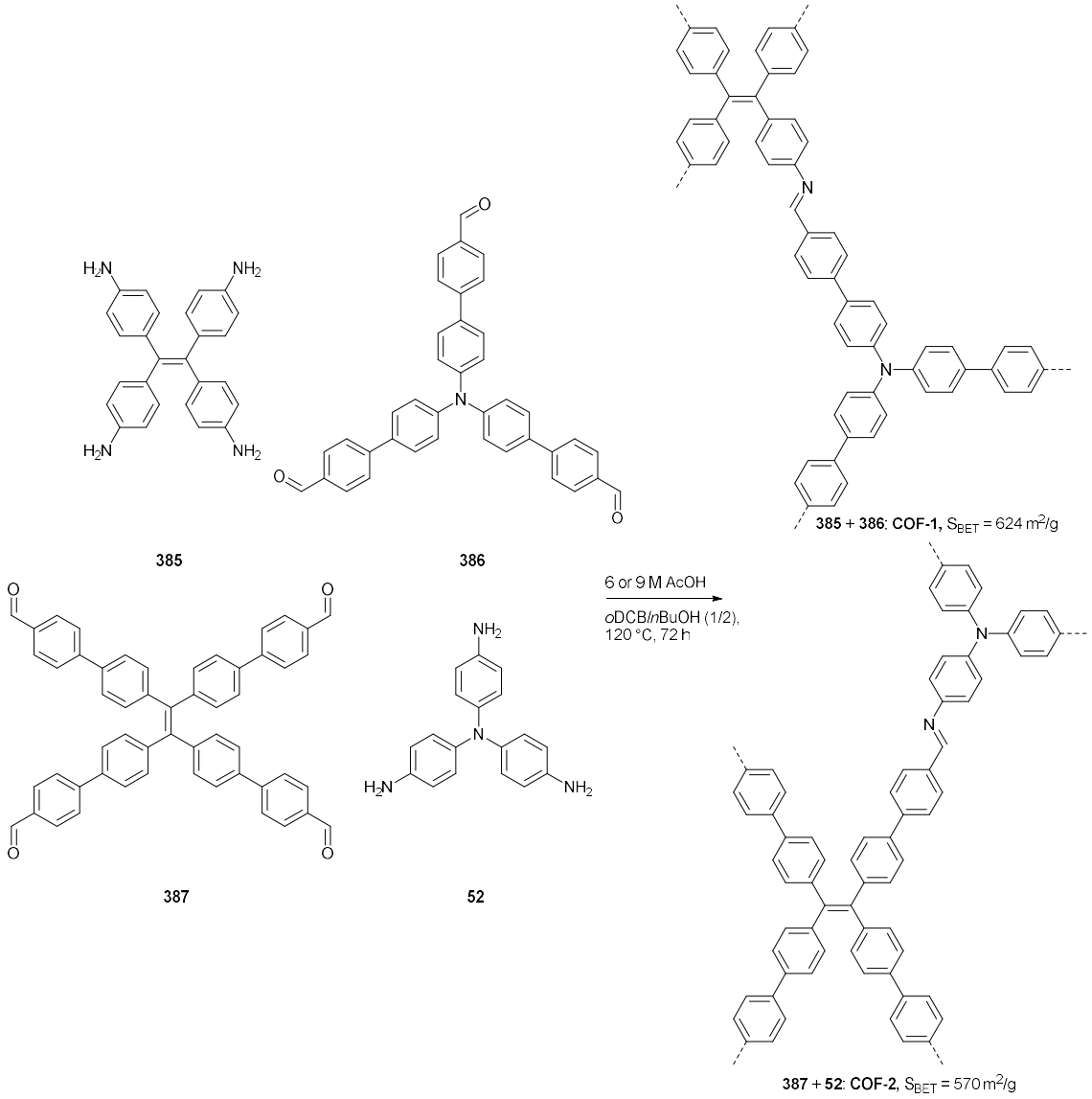

Scheme 112: Synthesis of 3D COFs by condensation of 1,1,2,2-tetraarylethene and triarylamine based building blocks.[343]

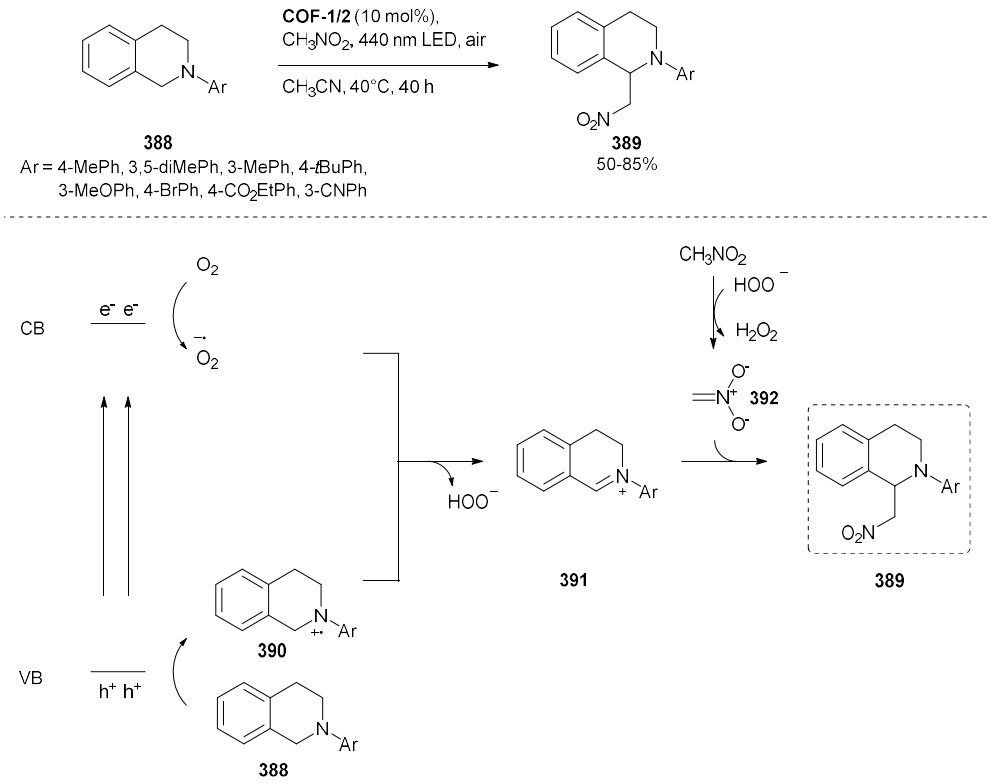

Scheme 113: Photocatalytic cross-dehydrogenative coupling between tetrahydroisoquinolines **388** and nitromethane.[343]

1.8.2.3.4 Benzimidazole formation

The oxidative formation of benzimidazoles from aromatic diamines and aldehydes forms a convenient route towards these important moieties. An *et al.* synthesized CMPs by Suzuki coupling between pinacol ester **393** and thiophene containing bromides **394** and **395** to produce **BTP-CMP** and **TPTP-CMP** (Scheme 114). These materials could catalyze the photocatalytic synthesis of 2-arylbenzimidazoles **398** in very high yields (91-98%). Mechanistically, the first step in this transformation is the Schiff base formation between the aldehyde **397** and the diamine **396** to form the intermediary imine **399**. This is then oxidized to the radical cation **400** by the photogenerated holes in the material. Hydrogen abstraction of this intermediate by photogenerated $O_2^{-\bullet}$ leads to intermediate **401**, which finally loses a hydrogen atom to form hydrogen peroxide and the benzimidazole product **398** (Scheme 115).[344]

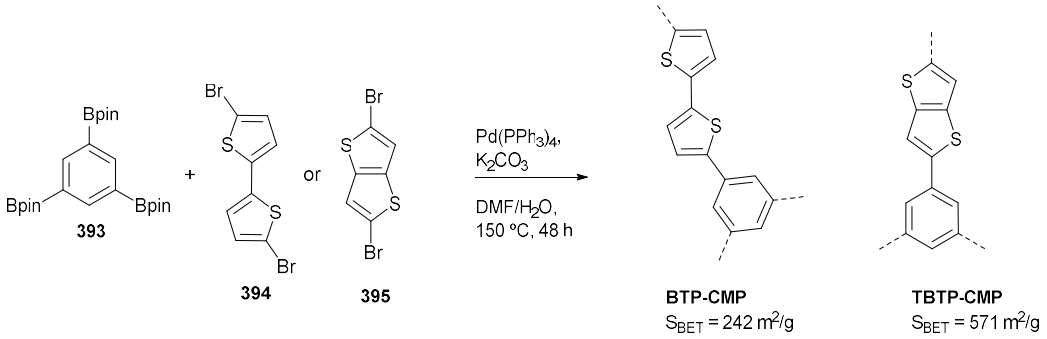

Scheme 114: Synthesis of thiophene containing CMPs **BTP-CMP** and **TBTP-CMP** by Suzuki coupling.[344]

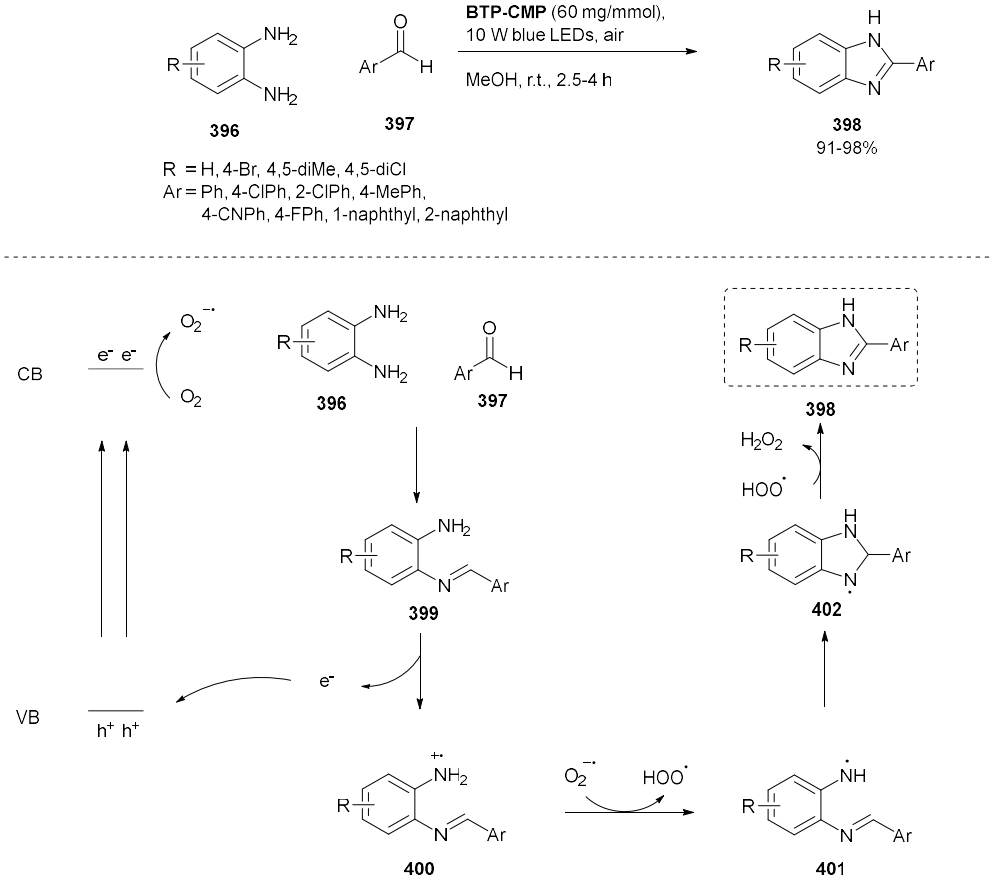

Scheme 115: Photocatalytic benzimidazole synthesis catalyzed by **BTP-CMP**.[344]

1.8.2.3.5 Thioamide cyclization

Another oxidative cyclization reaction has been reported by Li *et al.*, who used a C=C linked COF for the oxidative dimerization of thioamides to thiadiazoles. This fully conjugated, donor (pyrene) - acceptor (thiadiazole) polymer **CPy-BSZ-COF** was synthesized by Knoevenagel condensation between building blocks **326** and **403** (Scheme 116). The COF was a good catalyst for the photocatalytic oxidative coupling of benzylamines (*vide supra*), possessing a wide substrate selectivity and providing high conversion and selectivities (up to 99%). Moreover, a range of thioamides **404** could be cyclized to the corresponding 1,2,4-thiadiazoles **405** (Scheme 117). Mechanistically, this reaction happens via the oxidation of the thioamides **404** by photogenerated holes. This radical cation **406** then loses a proton to form radicals **407**-**408**. These intermediates then undergo dimerization to compound **409** which after ring closure form compound **410**. Aromatization of this intermediate is aided by the photogenerated $O_2^{-\bullet}$ to finally give the thiadiazoles **405**.[345]

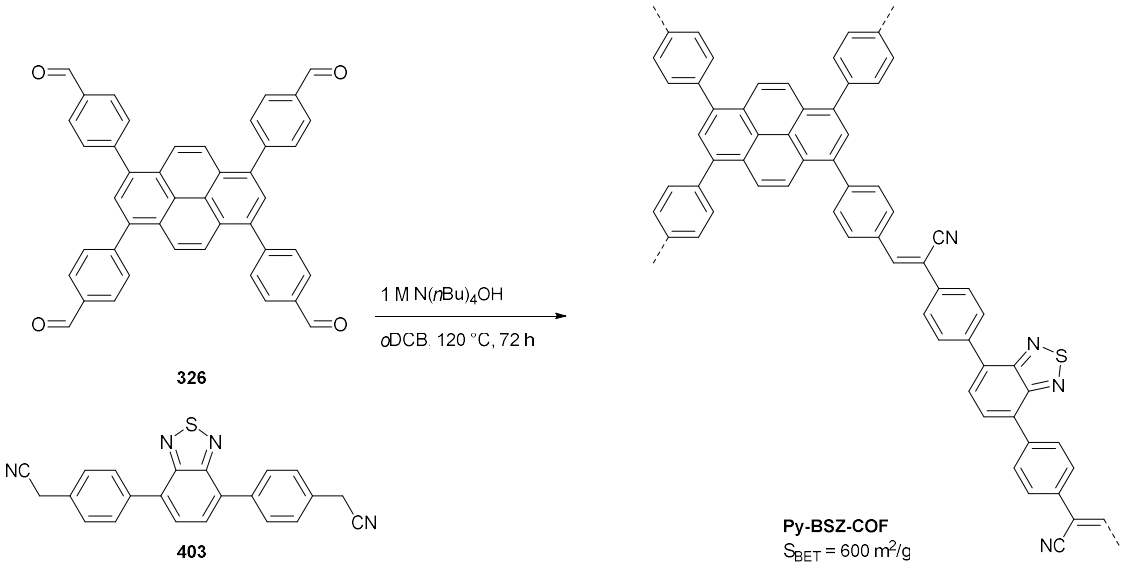

Scheme 116: Synthesis of the vinylene-linked **Py-BSZ-COF** by Knoevenagel condensation.[345]

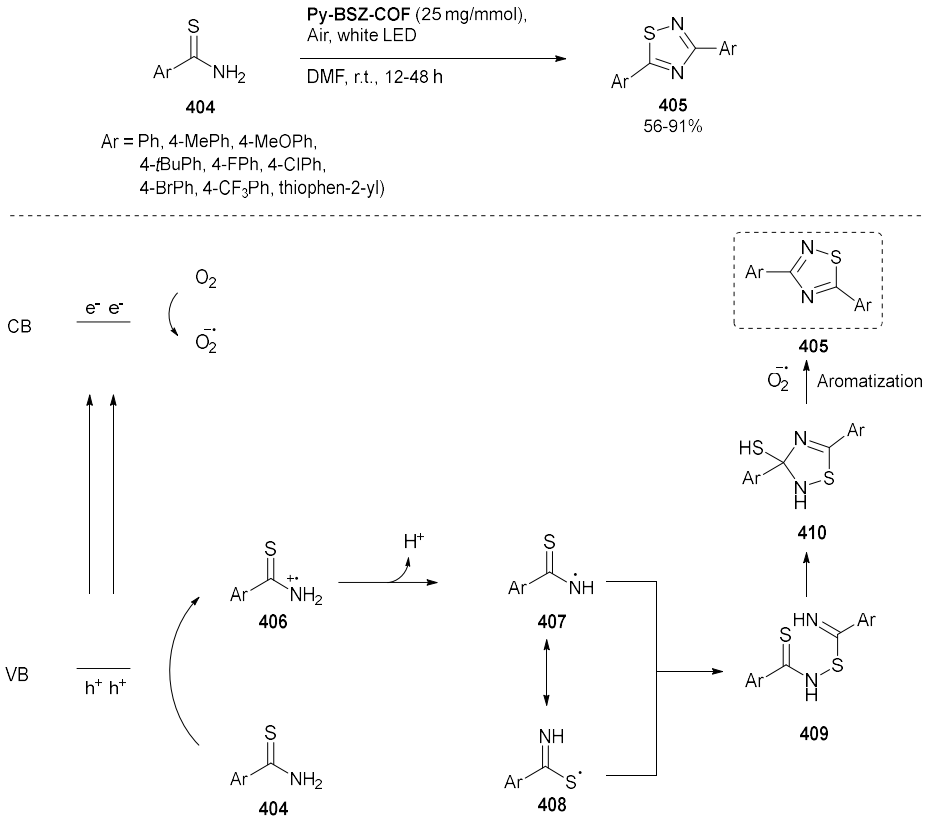

Scheme 117: Oxidative cyclization of thioamides **404** to 1,2,4-thiadiazoles **405** catalyzed by **Py-BSZ-COF**.[345]

1.8.2.3.6 Oxidation of anilines

The amine nitrogen of an aniline is relatively easily oxidized, which produces the aniline radical cation. This has a very diverse reactivity; if there is an alkyl chain on the aniline it can be deprotonated to form an α-aminoalkyl radical, a hydrogen atom can be abstracted to form an iminium ion, and lastly, direct reactions with other radicals are also possible.

1.8.2.3.6.1 Povarov reaction between N-phenylmaleimides and N,N-dimethylanilines

Liu *et al.* reported the synthesis of two imine COFs that were able to oxidize anilines. These materials, **QA-TAPT-COF** and **QA-TPB-COF** were based on the 'zigzag' quinacridone containing monomer **411** (Scheme 118). Interestingly, the aldehyde groups of this building block were protected as acetals, which is known to slow down the COF formation reaction and thus lead to materials with a higher crystallinity.[346] These materials were applied as catalysts for the oxidative Povarov reaction between *N*-phenylmaleimides **412** and *N*,*N*-dimethylanilines **413**, in which tetrahydroquinolines **414** were afforded in high yields (Scheme 119). As seen previously (Section 1.8.2.1), **QA-TAPT-COF** containing the triazine core performed better than **QA-TPB-COF** with a phenyl core. Mechanistically, this transformation is thought to occur via the oxidation of the aniline **413** by the holes of the COF, while the photogenerated electrons reduce oxygen to $O_2^{-\bullet}$. Deprotonation of intermediate **415** by $O_2^{-\bullet}$ leads to the α-aminoalkylradical **416**, which then undergoes a stepwise cyclization with the maleimide **412**. Hydrogen atom transfer from intermediate **418** to HOO$^\bullet$ generates the desired tetrahydroquinolines **414** and H_2O_2 as a side product.[347]

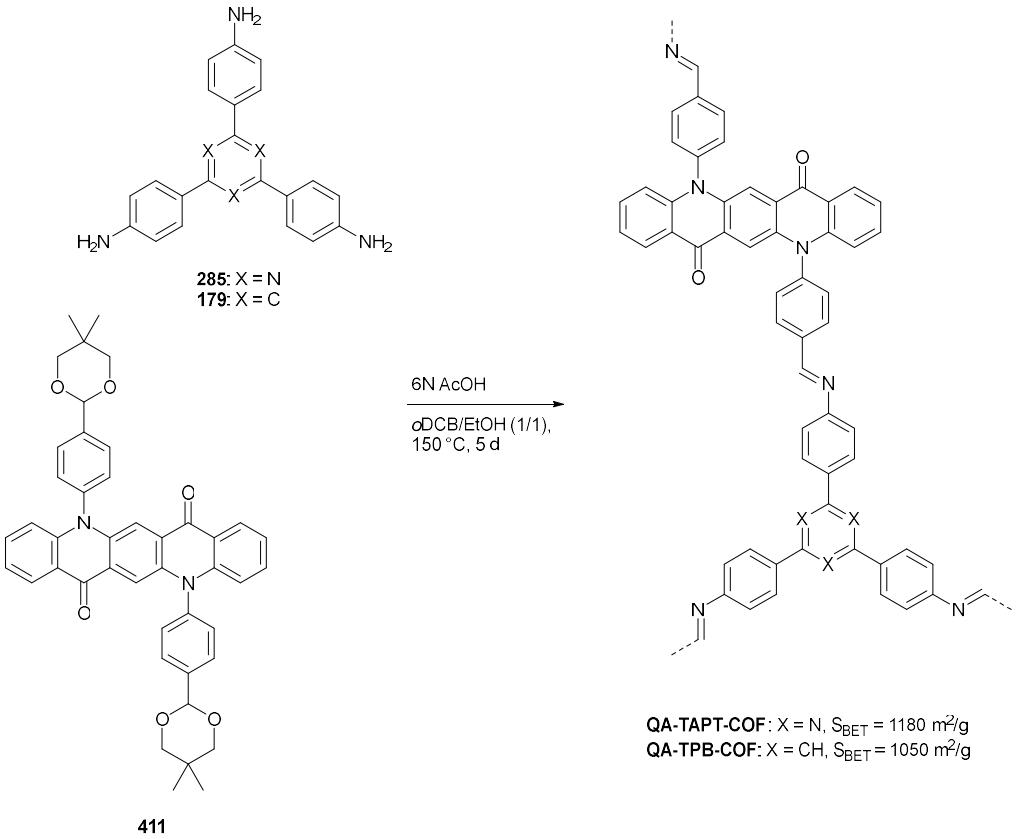

Scheme 118: Synthesis of quinacridone containing COFs.[347]

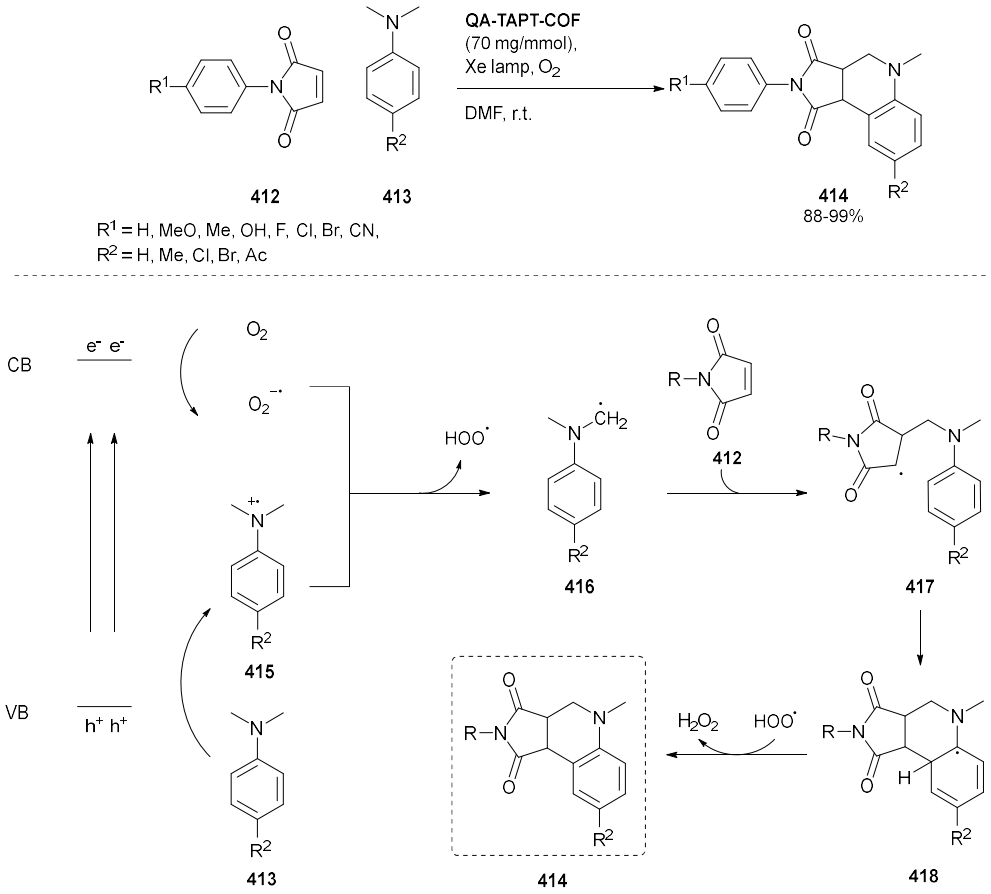

Scheme 119: The oxidative Povarov reaction between *N*-phenylmaleimides **412** and *N*,*N*-dimethylanilines **413** catalyzed by **QA-TAPT-COF**.[347]

1.8.2.3.6.2 Ugi reaction

The classical Ugi reaction is an important multicomponent reaction which allows for the synthesis of bis-amides by combination of a ketone/aldehyde with an amine, isocyanide, and a carboxylic acid. Zhang *et al*. prepared CMPs by Suzuki coupling or Lewis acid catalyzed crosslinking of building blocks **419**-**423**, containing a benzene or a phenothiazine core (Scheme 120). These materials were then applied for photocatalytic Ugi reactions, where the imine is formed by photochemical oxidation and not via Schiff base condensation like in the classical Ugi reaction. With the test reaction of *N*,*N*-4-trimethylaniline, *p*-toluene sulfonylmethyl isocyanide and H_2O yields of <5%, 42%, 72% and 84% were obtained for **CMP-CSU-2/3/6/8**, respectively. Using the most effective photocatalyst **CMP-CSU8** a wide range of products **430** could be obtained in generally good yields (45-86%) (Scheme 122). As in the previous example, this reaction occurs via the one-electron oxidation of dimethylaniline **427** by photogenerated holes. Simultaneously, photogenerated electrons will reduce O_2 to $O_2^{-\bullet}$. Abstraction of a hydrogen atom from the amine radical **431** by $O_2^{-\bullet}$ yields the iminium ion **432**. Photogenerated singlet oxygen also played a role, as $^1O_2$ can directly oxidize dimethylaniline **427** to the iminium ion **432**. In any case, the iminium ion will undergo nucleophilic attack by isocyanide **428** to give the nitrilium ion **433**. Reaction of this ion with a nucleophile **429**, a carboxylic acid or water, followed by rearrangement or proton transfer, gives the product **430**.[348] Interestingly, besides the photocatalytic Ugi reaction **CMP-CSU8** was also used for the aerobic selenation of indoles (Scheme 121). Using 1,2-

diphenyldiselane **425** and a variety of indoles **424** the selenated products **426** were obtained in very good yields (84-97%). The mechanism proposed by the authors seems to be unclear, as they suggest the generation of the phenylselenyl radical by oxidation of diphenyl diselenide. In the literature other mechanisms can be found, such as radical formation by direct energy transfer, followed by oxidation of the radical to the cation, which then reacts with the electron rich indole in an electrophilic aromatic substitution.[349]

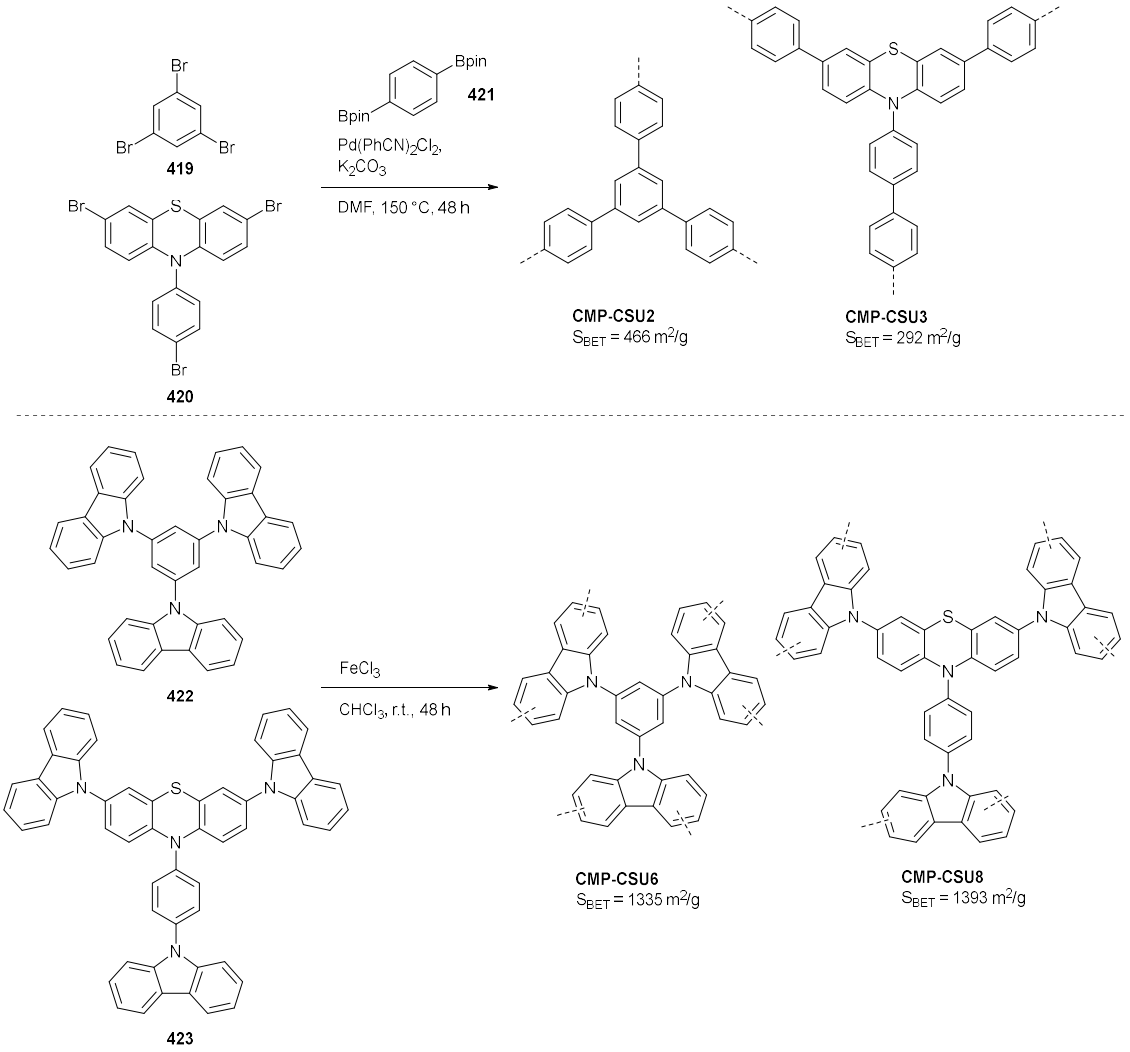

Scheme 120: Synthesis of CMPs by Suzuki cross-coupling or $FeCl_3$ catalyzed hypercrosslinking.[348]

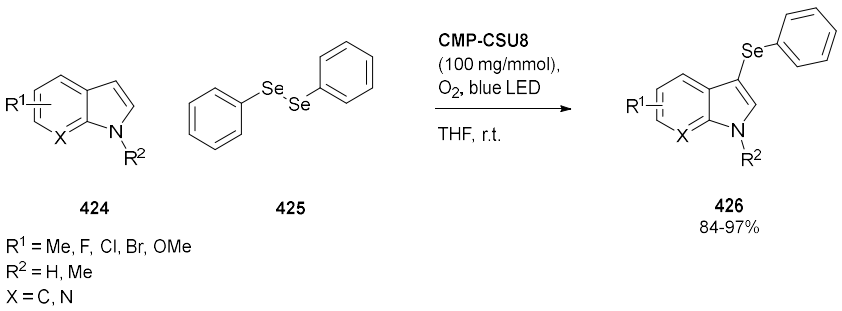

Scheme 121: Photocatalytic aerobic selenation of indoles catalyzed by **CMP-CSU8**.[348]

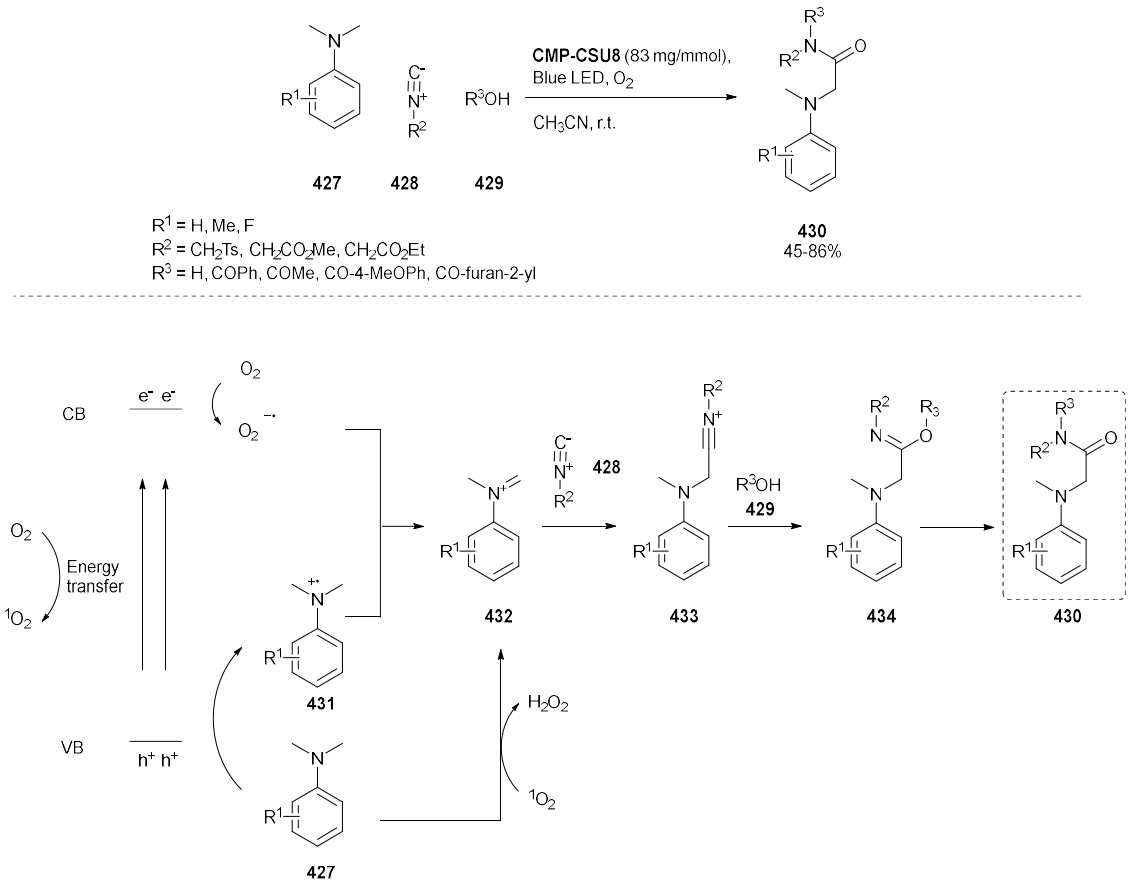

Scheme 122: Photocatalytic Ugi reactions catalyzed by **CMP-CSU8**.[348]

1.8.2.3.6.3 Thiocyanation of anilines

A direct reaction of the aniline radical cation with other radicals has also been reported. Zhang *et al*. synthesized porphyrin based CMPs by Sonogashira coupling between porphyrin bromides **435**-**436** and alkyne **437**, resulting in **CMP-1/2**. Interestingly, the morphology of the material, which was studied by optical microscopy, SEM and TEM, could be controlled by selection of the substitution on the porphyrin core. When the monomer **435** with straight alkyl chains was used **CMP-1** with a tubular morphology was obtained. The introduction of phenyl rings in monomer **436** led to a resulting material **CMP-2** which consisted of irregular solid granules (Scheme 123). These materials were used as photocatalysts for the thiocyanation of anilines. A wide range of anilines **438** could be converted, at room temperature, to the resulting thiocyanated products **439** in generally good yields (40-92%), with complete chemoselectivity for the 4-substituted product (Scheme 124). The tubular **CMP-1** performed much better than the granular **CMP-2** which the authors ascribe to its more accessible structure. This reaction occurs due to the CMP oxidizing both the aromatic amine **438** to the radical cation **440**, and the $^{-}$SCN anion to the $^{\bullet}$SCN free radical, with oxygen acting as an electron sink. The two radicals **441** and $^{\bullet}$SCN are combined, forming the cation **442**, which forms the final product **439** by loss of a proton.[350]

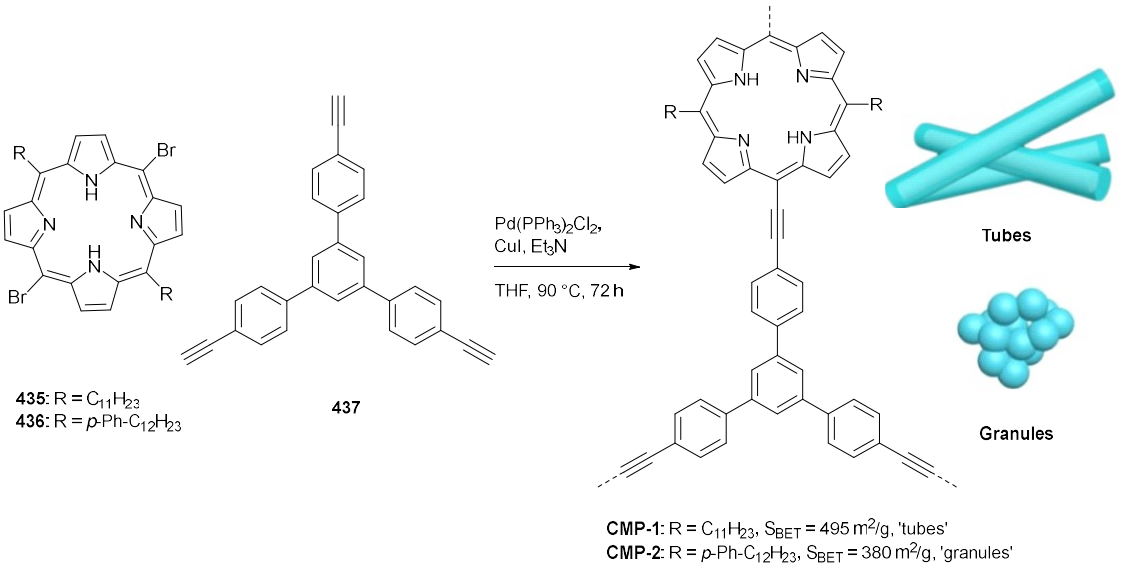

Scheme 123: Synthesis of porphyrin containing CMPs by Sonogashira coupling, depending on the substituents on the porphyrins CMPs with tubular (**CMP-1**) or irregular (**CMP-2**) morphology are formed.[350]

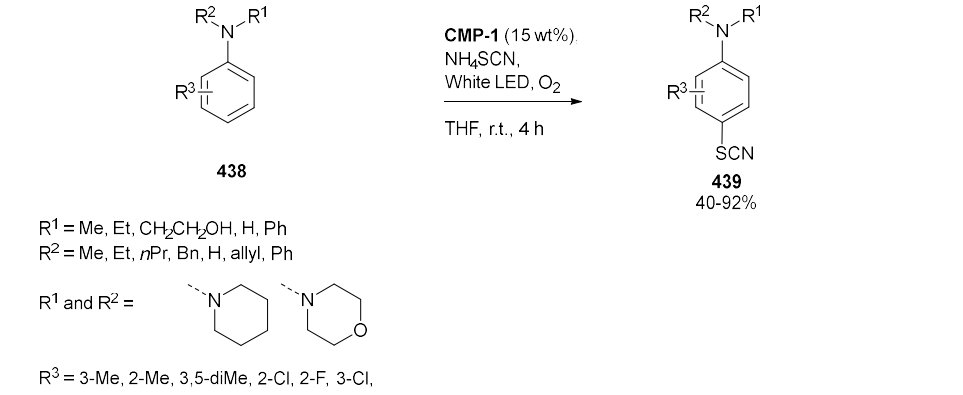

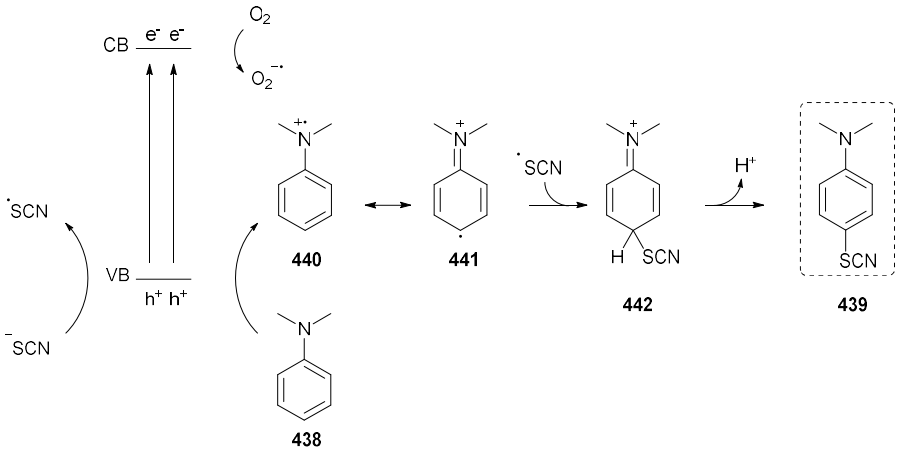

Scheme 124: Application of **CMP-1** as a photocatalyst for the 4-thiocyanation of annilines.[350]

1.8.2.4 Oxidation of C=C bonds

1.8.2.4.1 Cleavage of alkenes to aldehydes

The oxidative cleavage of alkenes to aldehydes is an important reaction in organic chemistry, and the textbook way to perform this transformation is ozonolysis followed by reductive work up, or dihydroxylation followed by cleavage of the diol.[351] Photocatalytic methods can form a convenient alternative, avoiding the use of dangerous ozone or toxic metals. Ayed *et al.* synthesized CMPs **BBT**, **BTh** and **BThBt** by Sonogashira coupling between 1,3,5-triethynylbenzene **7** and brominated monomers **443** and **444** using silica nanoparticles (SiO_2NPs) as a template (Scheme 125). These materials were applied as photocatalysts for the oxidative cleavage of C=C bonds. Using styrene **445** as a model substrate the main product was benzaldehyde **446**, along with side products such as acetophenone **447**, benzoic acid **321**, phenylacetaldehyde **448** and styrene oxide **248** (Scheme 126). **BBT** proved to be the most active of the three synthesized materials, reaching a conversion of 91% and a benzaldehyde yield of 86% when an optimized solvent mixture of CH_3CN/H_2O was used, as the solvent polarity had a pronounced influence on the reaction yield. Using meta- and ortho-substituted styrenes **445**, high conversions were also obtained (92-99%), however, the selectivities for the aldehyde were much lower (27-65%). (*E*)-Prop-1-en-1-ylbenzene **449** or cinnamyl alcohol **450** gave benzoic acid **321** as the main product in 42% and 60% yield, respectively. Interestingly, when 2-allylphenol **451** was used as the substrate, benzofuran **452** was obtained in a very high yield. Lastly, cyclohexene **453** could also be efficiently oxidized to cyclohexen-1-one **454**. According to quenching and electron paramagnetic resonance (EPR) measurements, both $O_2^{-\bullet}$ and $^1O_2$ played a role in the reaction. The first step in the reaction is the oxidation of the double bond of styrene **455** by the photogenerated holes producing the radical cation **456**. This intermediate can then react with $O_2^{-\bullet}$ to generate the dioxetane **457**. Alternatively, $^1O_2$ can directly undergo the [2 + 2] cycloaddition with styrene **455** to generate the same dioxetane intermediate **457**. Hydrolysis of the dioxetane **457** generates the diol **458**, which is further oxidatively cleaved into benzaldehyde **446** and formaldehyde. This last step was not further elaborated in this paper, but according to other literature[352] this proceeds via hydrogen atom transfer to generate radical intermediate **459**. This then undergoes β-scission to lose formaldehyde and generate radical **460**, which after transfer of another hydrogen atom gives the aldehyde product **446**.[353]

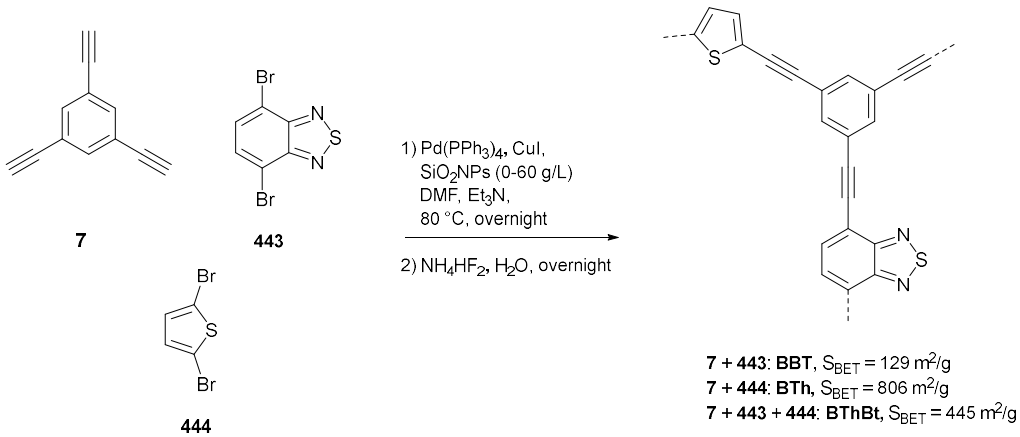

Scheme 125: Synthesis of thiophene and benzothiadiazole containing CMPs by Sonogashira coupling.[353]

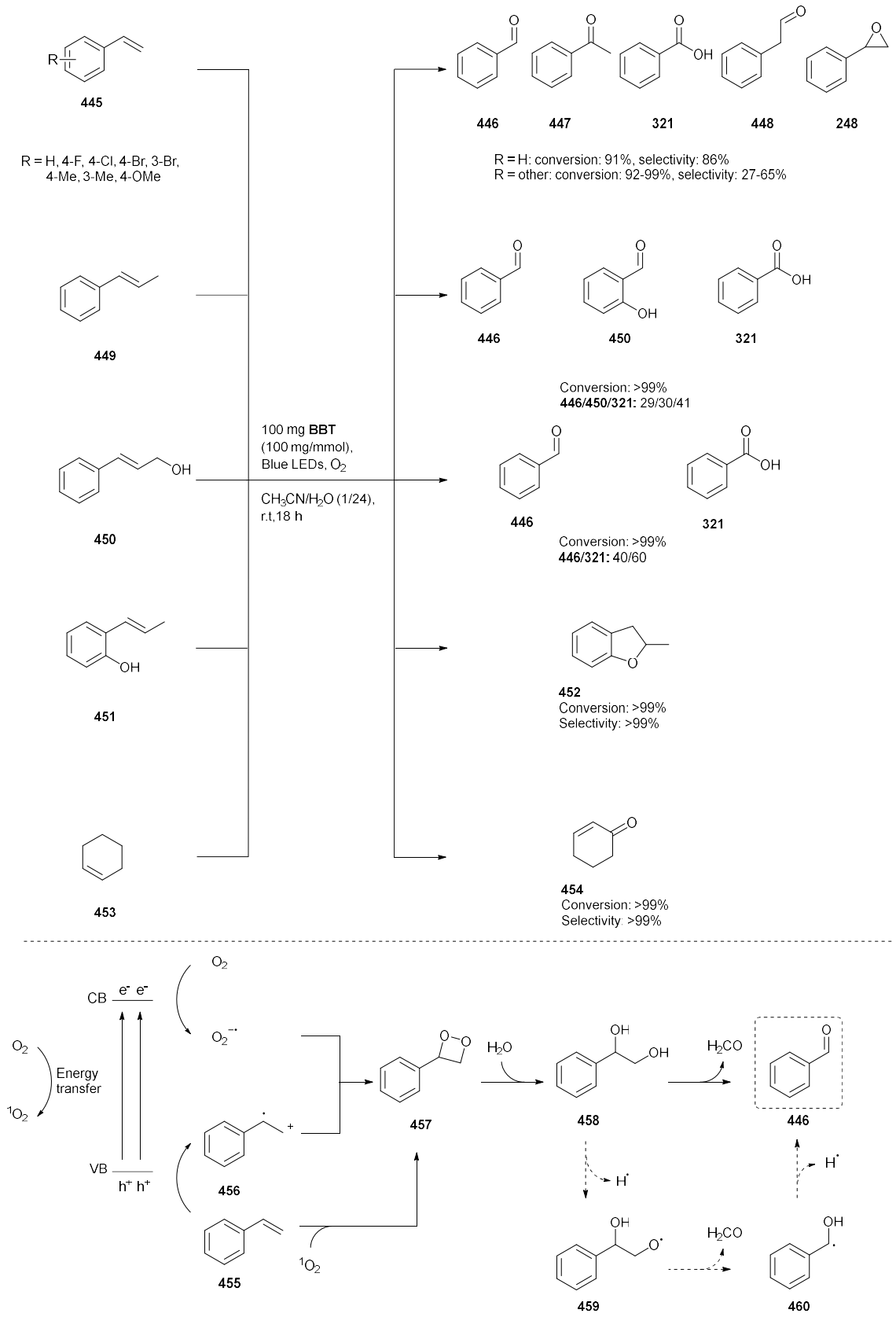

Scheme 126: Photocatalytic double bond cleavage catalyzed by **BBT**. [353]

1.8.2.4.2 Oxidation of α-terpinene to ascaridole

Using the same method as discussed in the previous paragraph, Zhang *et al*. incorporated benzothiadiazole, a strong electron acceptor, in CMPs by Sonogashira coupling of brominated benzothiadiazole **443** with 1,3,5-triethynylbenzene **7**. Different amounts of silica nanoparticles were used as templating agent, which were etched away with ammonium hydrogen difluoride. This resulted in **CMP_0-60** with surface areas ranging from 270 to 660 m^2/g, increasing as the amount of templating agent increased (Scheme 127). Interestingly, the surface area of the polymer without template removal corresponded with the surface area of the polymer made without template. This illustrates that the use of the template makes the micropores of the material more accessible through the formation of big mesopores, thus resulting in increased surface areas. The materials were able to photochemically generate singlet oxygen, which can undergo a cycloaddition reaction with α-terpinene **461**, producing ascaridole **462** (Scheme 128). The polymer was used in a flow setup, by dispersing it together with α-terpinene **461** and oxygen in $CDCl_3$ and pumping this mixture through a photoreactor made of tubing wrapped around a polycarbonate plate which was irradiated with blue LEDs. The CMP with the greatest surface area, **CMP_60**, resulted in the highest α-terpinene conversion of 96%. The selectivity for ascaridole **462** was around 86-88% with the main impurity being *p*-cymene **463** from the aromatization of α-terpinene **461**.[354]

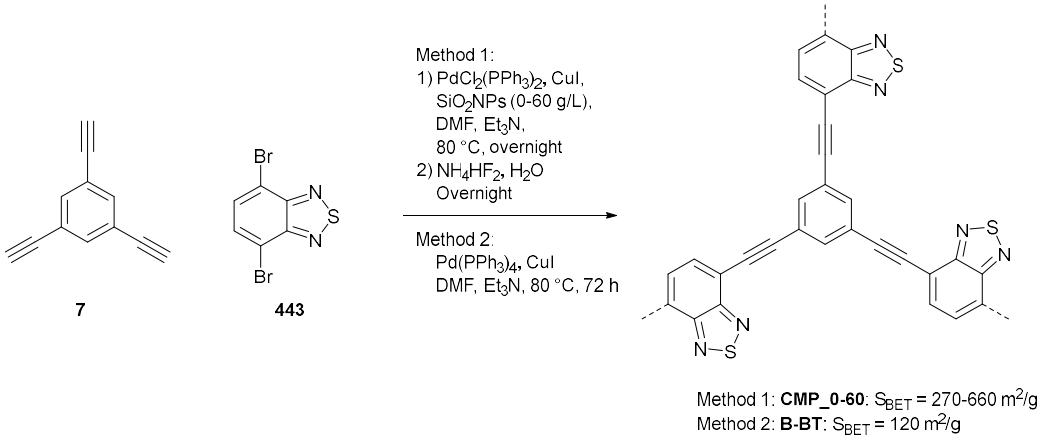

Scheme 127: Synthesis of benzothiadiazole containing CMPs by Zhang *et al.* (**CMP_0-60**) and *Li et al.* (**B-BT**).[354,355]

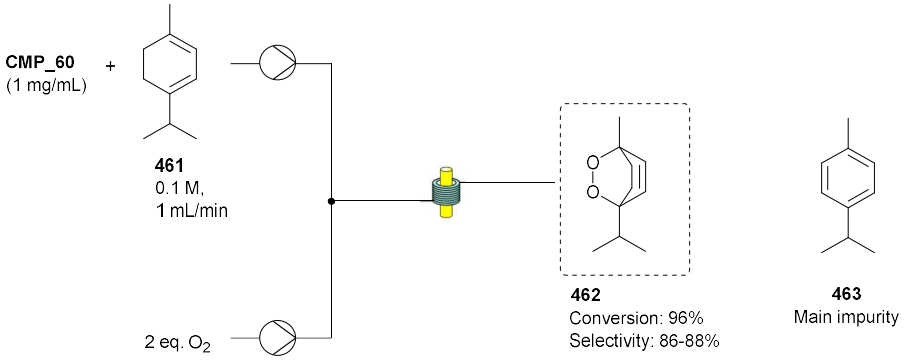

Scheme 128: Photocatalytic oxidation of α-terpinene **461** to ascaridole **426** in flow.[354]

1.8.2.4.3 Cycloaddition of styrenes to cyclobutanes

Li *et al.* synthesized the same material as in the previous paragraph without using a templating agent, and called this **B-BT** (Scheme 127). This material was applied for the photocatalytic [2 + 2] cycloaddition of styrene derivatives. Using **B-BT** under air in nitromethane the cycloadducts **466** of a range of styrene derivatives **465** were obtained in very good yields (87-96%). This transformation occurs through the direct oxidation of the electron rich double bond of the anethol derivative **464** (E_{ox} = 1.17 eV vs SCE) by the photogenerated hole of **B-BT** (E_{ox} = 1.73 V vs SCE). The alkene radical cation **467** then undergoes [2 + 2] cycloaddition with styrene derivative **465**, generating the cyclobutene substituted radical cation **468**. This is then reduced by one electron, either by oxidizing another equivalent of the anethole derivative, and thus propagating the chain, or by taking an electron from **B-BT** or $O_2^{-\bullet}$. Note that this mechanism is based on the original work by the Yoon group[356] and Crellin *et al.*[357] as the mechanism proposed by *Li et al.* contained a further oxidation of the radical cation **468**, which does not seem feasible.[355]

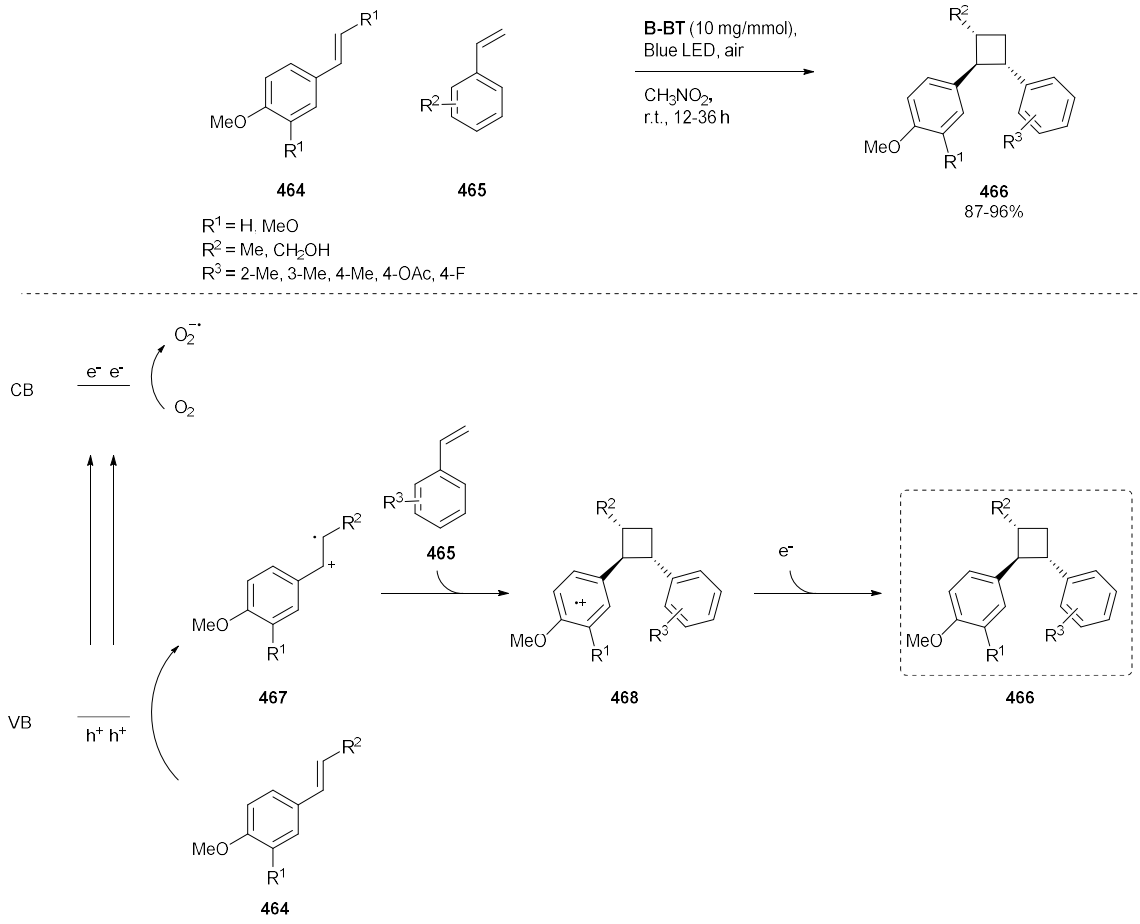

Scheme 129: Cycloaddition of styrenes catalyzed by **B-BT**.[355–357]

1.8.2.4.4 Oxidative alkylation of alkenes with dicarbonyl compounds

Song *et al.* synthesized 1,2,3-triazole based HCPs **PTPT**, **PCPT** and **PAPT** by $FeCl_3$ catalyzed hypercrosslinking of building blocks **469**-**471** (Scheme 130). The bandgaps of these materials were 2.73, 2.45 and 2.32 eV for **PAPT**, **PCPT** and **PTPT**, respectively. The efficiency of the charge separation in these materials was evaluated by photoluminescence spectroscopy, where the light emitted from the sample after irradiation is measured. Lower emission intensities point to improved charge separation and lower rates of charge recombination, which is advantageous for efficient photocatalysis. Of the three synthesized materials **PTPT** possessed the lowest emission intensity. Moreover, the authors used time-resolved photoluminescence (TRPL) spectroscopy to determine the photoluminescence lifetime, which was much longer for **PTPT** than for **PCPT** or **PAPT**. Lastly, transient photocurrent measurements were used to study the photoinduced charge generation, separation, and migration. Strong photocurrent signals were detected for all polymers, with **PTPT** showing the highest photocurrent response, again pointing to its more efficient charge separation. These materials were first applied towards the oxidative hydroxylation of phenylboronic acids (*vide supra*). **PTPT** was the best performer by far, giving 98% yield for phenylboronic acid, with **PCPT** and **PAPT** only furnishing the product in 85% and 51% yield, respectively. Next to this transformation, the authors studied the oxidative alkylation of vinylarenes using **PTPT** as a photocatalyst. A wide range of vinylarenes **472** could be alkylated with diethyl bromomalonate **473** or bromoacetonitrile **474** to the corresponding β-ketomalonates **475** or γ-ketonitriles **476** in good yields (70-86%) (Scheme 131). Interestingly, these authors also tested the viability of their catalysts on a larger scale, with a **PTPT** catalyzed synthesis of compounds **477** and **478** on a one-gram scale resulting in yields of 83% and 91%, respectively. The oxidative alkylation reaction starts by the reduction of diethyl bromomalonate **473** with a photogenerated electron, to form the bromide anion and the alkyl radical **479**. Addition of this radical to the styrene double bond results in intermediate **480**, which further reacts with molecular oxygen, giving peroxyl radical **481**. Radical combination between intermediates **480** and **481** gives the intermediary peroxide **482**, which after homolytic cleavage and 1,2 hydrogen atom transfer forms benzyl radical **484**. This then finally undergoes one-electron oxidation and loses a proton to give product **475**.[358]

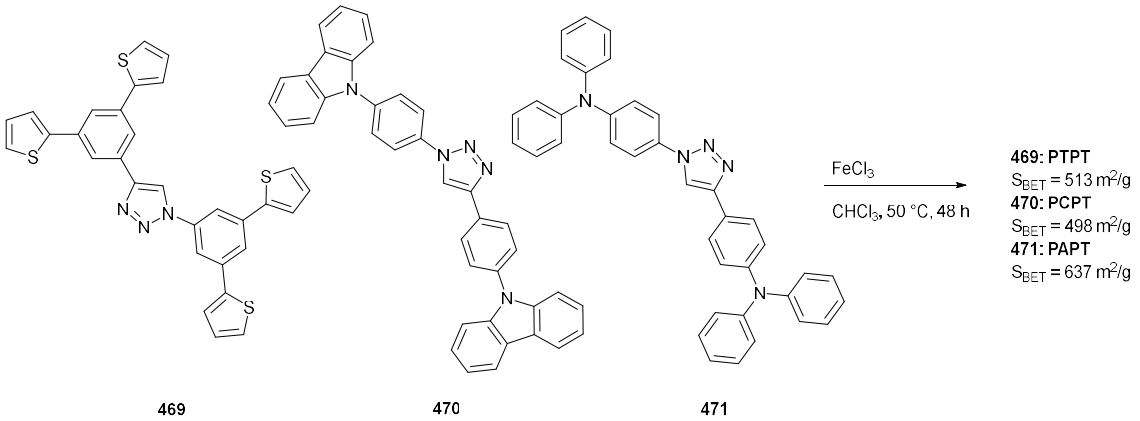

Scheme 130: Synthesis of 1,2,3-triazole containing HCPs by $FeCl_3$ catalyzed crosslinking.[358]

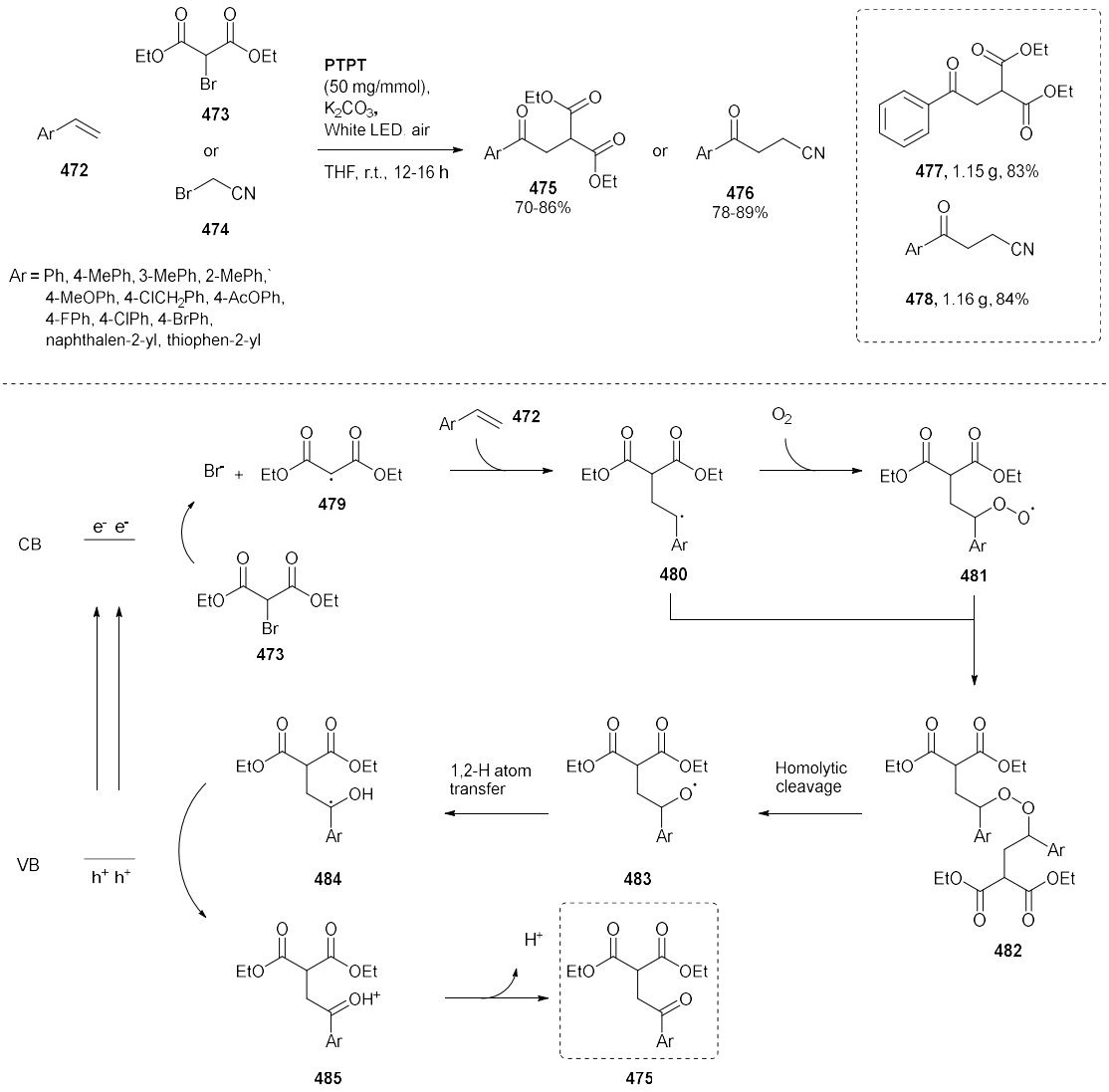

Scheme 131: Oxidative alkylation of vinylarenes catalyzed by **PTPT**.[358]

1.8.2.5 Oxidation of C-H bonds

1.8.2.5.1 Benzylic C-H oxidation

The direct oxidation of C-H bonds through photocatalytic methods allows for the convenient synthesis of functionalized molecules from simple substrates. In this light Chen *et al.* developed heptazine based COFs for the oxidation of benzylic C-H bonds. Heptazine is the primary active center in graphitic carbon nitride (*g*-C_3N_4), however, *g*-C_3N_4 possesses low crystallinity, which is detrimental to achieving efficient charge carrier separation and photocatalysis. The crystalline materials **HEP-TAPT-COF** and **HEP-TABP-COF** were synthesized by direct acid-promoted condensation of amines **285** and **179** with diacetate protected heptazine containing aldehyde **486** (Scheme 132). Interestingly, this gave much more crystalline materials then when the free aldehyde was used as a building block. The acetal first needs to deprotect to the free aldehyde, this slows down the reaction and provides materials with greater crystallinity. Using these materials different isochromans **487** could be selectively oxidized to give the isochroman-1-ones **488** in good yields and selectivities. Other benzylic hydrocarbons such as phthalane **489** and 9*H*-xanthene **491** were also efficiently oxidized (Scheme 133). As in previous examples, the triazine based material **HEP-TAPT-COF** was more effective than the benzene based **HEP-TABP-COF**. The authors proved through quenching experiments that singlet oxygen is the dominant ROS, which can undergo direct reaction with the benzylic C-H bonds to produce the corresponding ketones.[359]

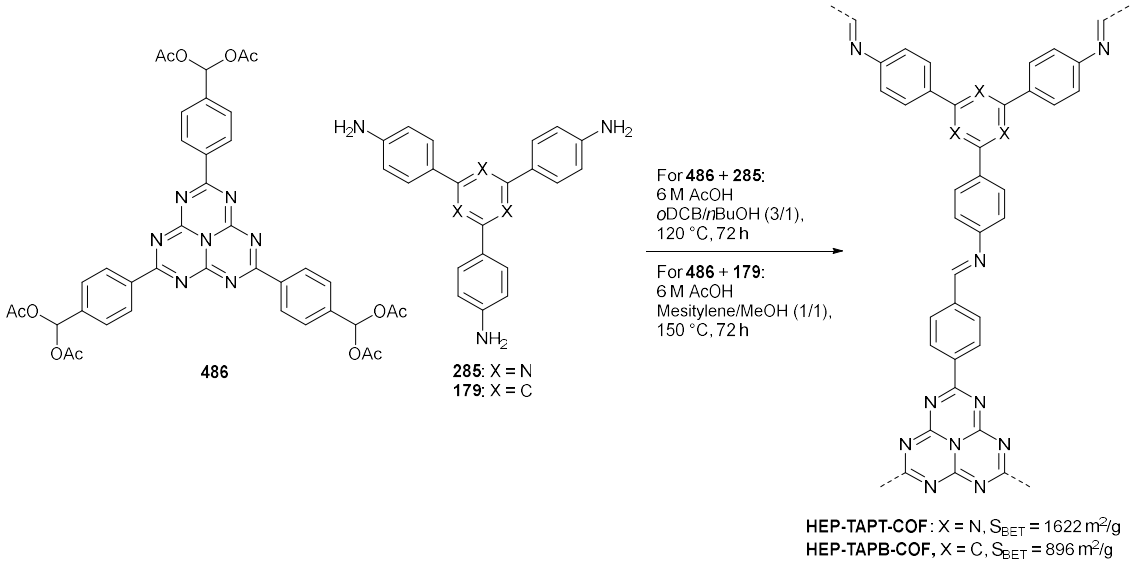

Scheme 132: Synthesis of heptazine based COFs.[359]

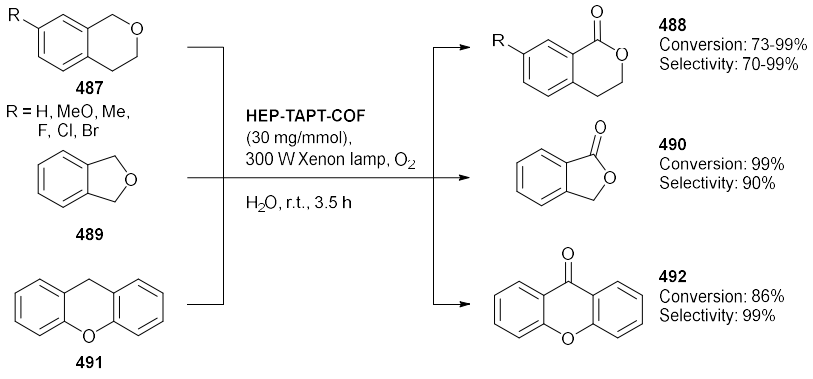

Scheme 133: Benzylic oxidation catalyzed by **HEP-TAPT-COF**.[359]

1.8.2.5.2 Bromination of aromatic compounds

Li *et al.* prepared HCPs by crosslinking of benzothiadiazole **493** with FDMA, resulting in **MOP-1b** and **MOP-1**. **MOP-1** was synthesized by repeating the synthesis procedures three times, each time cooling down to room temperature and adding new FDMA. This led to a higher degree of crosslinking, and thus a material with a much higher porosity was obtained (Scheme 134). These materials were applied as photocatalysts for the bromination of electron rich aromatics **394** with HBr as a bromine source and molecular oxygen as a clean oxidant (Scheme 135). In this way brominated compounds can be made while avoiding the use of highly toxic, corrosive, and volatile bromine. Moreover, iodination and chlorination using HI and HCl were also possible, but this gave lower yields. The reaction occurs through the oxidation of an electron rich aromatic **496** by the photogenerated holes, forming the cationic radical **497**, which then reacts with the bromide anion, forming radical **498** as an intermediate. A hydrogen atom is then abstracted from this intermediate **498** by $O_2^{-\bullet}$ or $^1O_2$, ultimately forming hydrogen peroxide and the product **499**.[360]

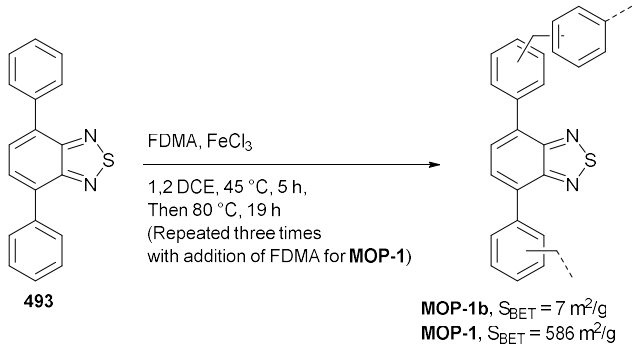

Scheme 134: Synthesis of benzothiadiazole containing HCPs by crosslinking with FDMA.[360]

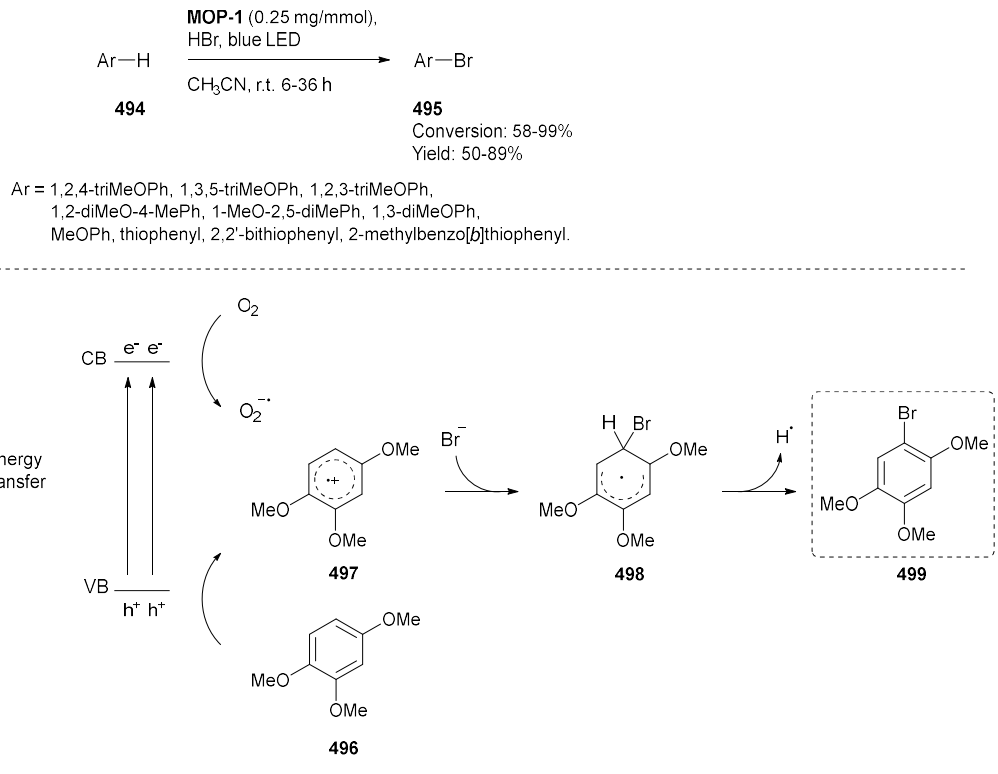

Scheme 135: Bromination of electron rich aromatics catalyzed by **MOP-1**.[360]

1.8.2.5.3 Oxidation of *N*-methylpyridinium salts

Sun *et al.* synthesized 'photoswitchable' CMPs by Sonogashira coupling of porphyrin **500** with fluorinated dithienylethene building block **501**. The resulting **AEDTE-H_2TIPP-POP** possessed a surface area of 90 m^2/g. Under UV light irradiation the dithienylethene moieties underwent ring closure, producing the 'closed' form. This was reversible, and under visible light irradiation the 'open' form could again be obtained, hence the 'photoswitchable' property of the material (Scheme 136). A range of *N*-methylpyridinium salts **502** could be converted into the corresponding quinoline-2(1*H*)-ones **503** in very high yields (99%) by the polymer in the 'open' form (Scheme 137). The 'closed' polymer was almost inactive in this transformation, due to energy transfer from the porphyrin to the dithienyl moieties in this form, suppressing the reaction with the substrate. Importantly, after irradiation with visible light, the reopened form of the material was active again. Mechanistically, this transformation occurs by one electron reduction of an *N*-methylpyridinium salt **502**, followed by reaction with oxygen to produce intermediate **511**. After H-atom shift and loss of an electron, intermediate **413** is produced, which then finally forms the quinoline-2(1*H*)-one **414** by treatment with Cs_2CO_3 and I^-.[361]

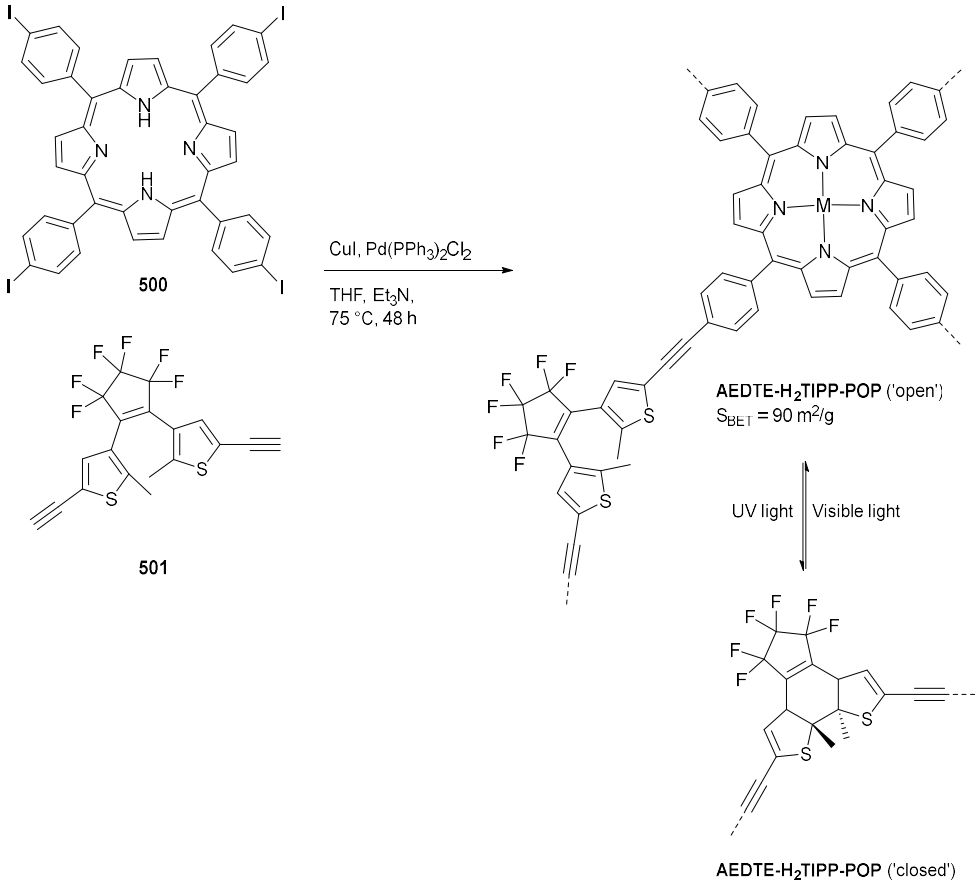

Scheme 136: Synthesis of photoswitchable **AEDTE-H_2TIPP-POP** by Sonogashira coupling, upon irradiation with UV light dithienylethene moieties of the material undergo ring closure, which can be reversed by irradiation with visible light.[361]

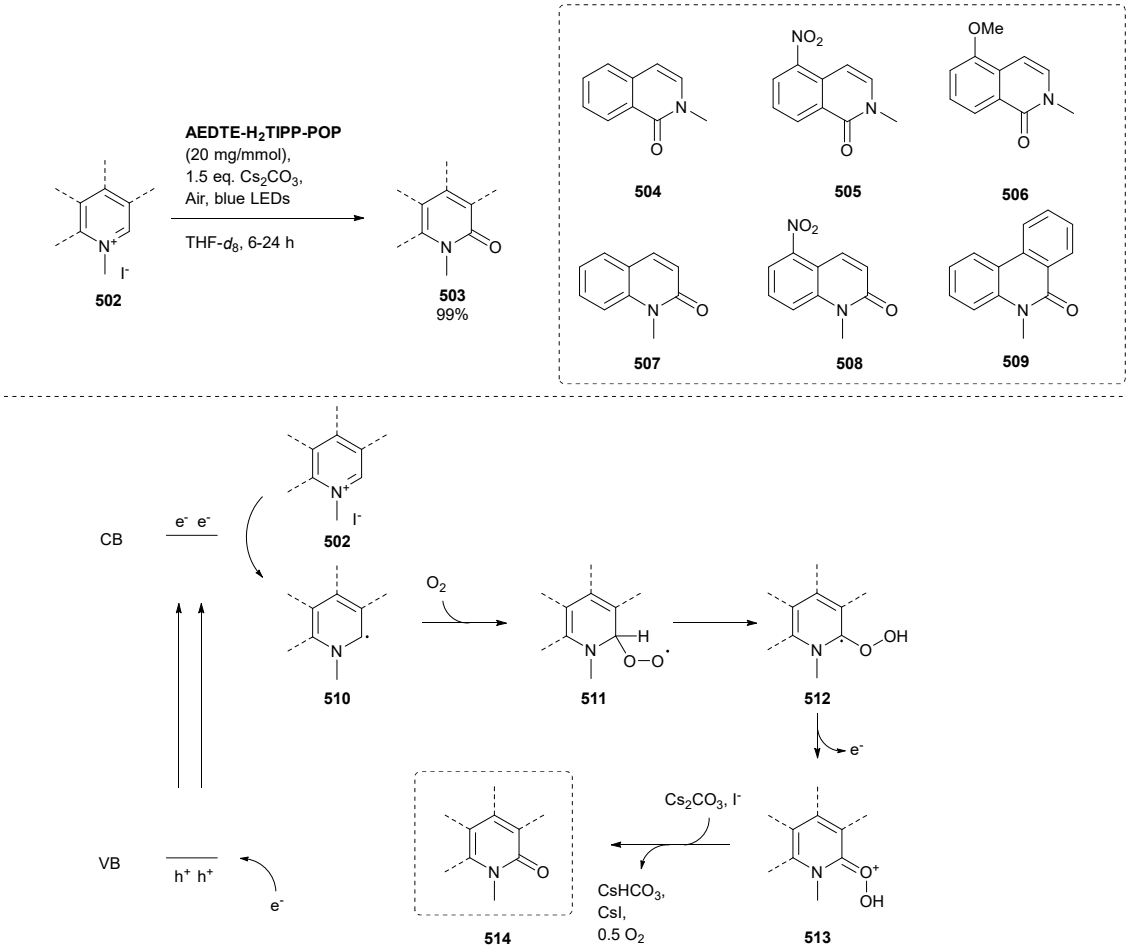

Scheme 137: The oxidation of *N*-methylpyridinium salts **502** catalyzed by **AEDTE-H_2TIPP-POP**.[361]

1.8.2.5.4 α-Oxyamination of 1,3-dicarbonyls

Liu *et al.* prepared donor-acceptor COFs **D_{Ph}/D_{TT}/D_{BDT}-A_{BBO}-COFs** by Schiff base condensation between electron poor benzobisoxazole **515** and electron rich aldehydes **46,516**-**517** (Scheme 138). These materials were applied towards the α-oxyamination of dicarbonyl compounds **518** with TEMPO (Scheme 139). The thienothiophene containing COF **D_{TT}-A_{BBO}-COF** was the most active, yielding 92% for the conversion of ethyl-3-oxo-3-phenylpropanoate, whilst the benzene and benzodithiophene based materials **D_{Ph}-A_{BBO}-COF** and **D_{BDT}-A_{BBO}-COF** only reached 68% and 79%, respectively. Interestingly, using a linear polymer analog of **D_{TT}-A_{BBO}-COF** greatly reduced yields of only 40% were obtained. The band gap of the **D_{TT}-A_{BBO}-COF** (1.96 eV) was smaller compared to the linear polymer (2.04), **D_{Ph}-A_{BBO}-COF** (2.20 eV) and **D_{BDT}-A_{BBO}-COF** (2.05 eV). Moreover, **D_{TT}-A_{BBO}-COF** possessed the most negative CB value and the strongest photocurrent response. Using **D_{TT}-A_{BBO}-COF** a wide range of dicarbonyl compounds **518** could be converted to their α-oxyaminated products **519** in good yields (83-99%). In general, the use of electron rich substrates led to lowered yields. The reaction goes via the oxidation of TEMPO **368** to $TEMPO^+$ **369** by the photogenerated holes, with simultaneous reduction of TEMPO **368** to $TEMPO^-$ **520** by the photogenerated electrons. The reduced $TEMPO^-$ **520** deprotonates the acidic α-proton of the dicarbonyl compound **518** to form TEMPOH and the enolate **521**. This enolate can finally react with $TEMPO^+$ **369** to give the α-oxyaminated product **519**.[362]

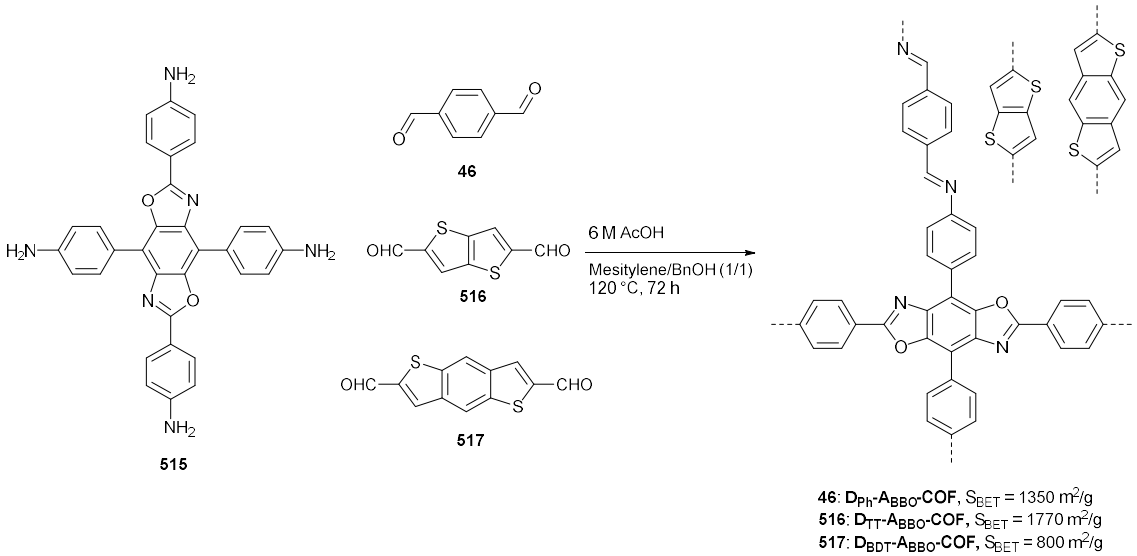

Scheme 138: Syntheses of donor-acceptor COFs based on electron poor benzobisoxazole **515** and electron rich benzene **46**, thienothiophene **516** and benzodithiophene **517**.[362]

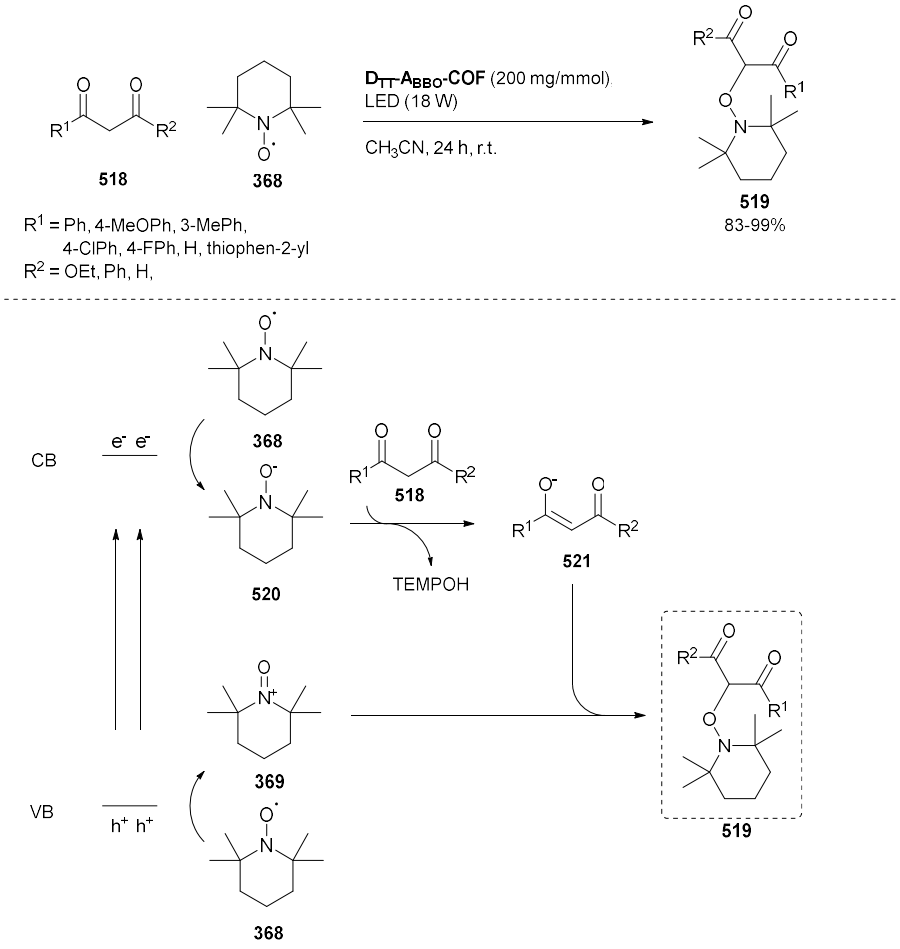

Scheme 139: Photocatalytic a-oxyamination of 1,3-dicarbonyls **518**.[362]

1.8.2.6 Oxidation of alcohols

The selective oxidation of alcohols to aldehydes is an extremely important and well researched transformation in organic chemistry. As described in Section 1.7.1, metal-free CTFs synthesized by ionothermal condensation have been used for this transformation by the Van Der Voort group, however these reactions occurred without light. Huang *et al.* reported a thiophene containing CTF, **CTF-Th@SBA-15**, which was synthesized by polymerization of 2,5-dicyanothiophene **522** with triflic acid vapors acting as the catalyst, using mesoporous silica SBA-165 as the template (Scheme 140). The hydrolysis of cyano groups and intermediates during the superacid catalyzed CTF synthesis can cause a low degree of polymerization and an accompanying low surface area. This was suppressed by polymerizing in the solid state using triflic acid vapors. **CTF-Th** and **CTF-Th@SBA-15** possessed a valence band energy level of +1.75 V (vs SCE), indicating their high oxidizing potential. The materials were therefore applied as catalysts for the photocatalytic oxidation of benzylic alcohols **523** to aldehydes **524** (Scheme 141). **CTF-Th@SBA-15**, due to its much higher surface area compared with **CTF-Th**, led to a greatly enhanced conversion of benzylalcohol to benzaldehyde (99% vs 17%). A wide range of alcohols could be reacted and gave high conversions and yields, with no side products being detected, except difenylmethanol leading to 13% of a coupled product **525**, and cinnamyl alcohol also undergoing cleavage of the double bond to produce benzaldehyde (27%). The reaction is thought to proceed via the activation of oxygen, producing the superoxide radical anion ($O_2^{-\bullet}$) and singlet oxygen ($^1O_2$). The radical anion can deprotonate the benzylic alcohol **523**, forming the benzyl anion **526**, which then is oxidized by the holes of the CTF to give radical **527**. Hydrogen abstraction from this radical **527**, by the $^{\bullet}$OOH species, yields the target aldehyde **524** and hydrogen peroxide as a side product.[363]

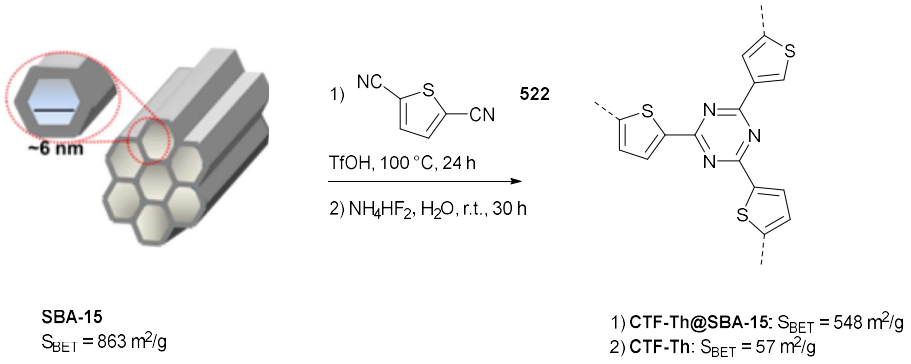

Scheme 140: Synthesis of a thiophene containing CTF by the superacid catalyzed trimerization of nitriles.[363]

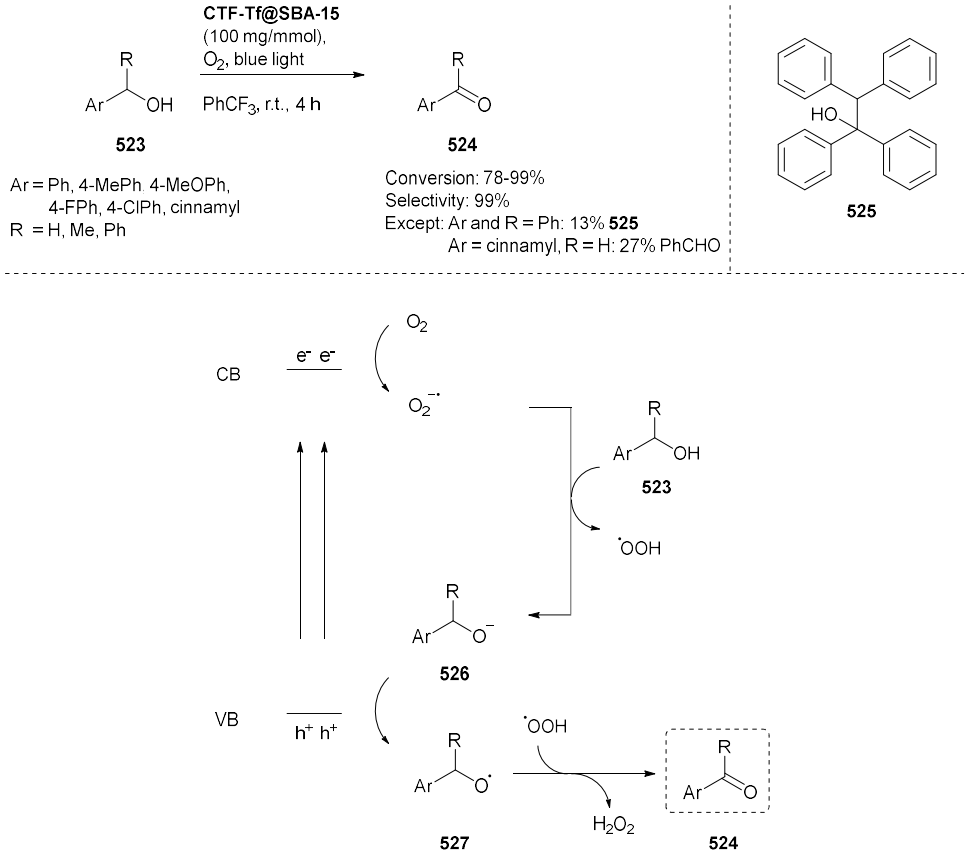

Scheme 141: The selective oxidation of benzylic alcohols to aldehydes catalyzed by **CTF-Tf@SBA-15.**[363]

1.8.2.7 Oxidation of a carbon – metal bond

Stille couplings are a convenient and widely used method to generate C-C bonds, however these reactions typically require palladium catalysts. Ghasimi *et al.* developed CMPs to perform metal-free, photocatalytic Stille couplings through the formation of aryl radicals by one-electron oxidation of aryl stannanes. The CMP **p_Az_B** was obtained by Suzuki cross-coupling between 1,3,5-phenyltriboronic acid tris(pinacol)ester **393** with 1,3-dibromoazulene **528** (Scheme 142). This material possessed a band gap of 2.03 eV and absolute positions of the valence and conducting band of +1.14 V and -1.10 V (vs SCE), respectively. First the authors evaluated the destannylation reaction of various aryl stannanes. For the stannanes with a low enough oxidation potential (< 1.14 V) both destannylation products **530** and the formation of dimers **531** were detected (Scheme 143). Aryl stannanes with phenyl, pyridyl or oxazolyl groups possess oxidation potentials higher than 1.14 V, therefore they cannot be oxidized by **p_Az_B** and do not show any reactivity. When aryl iodides **532** were also added to the reaction, the coupled products **533** could be isolated in generally good yields (49-93%). Importantly, only electron poor aryl halides reacted, with aryl chloride/bromides and electron neutral or rich aryl iodides being inert. Interestingly, in none of the reactions dehalogenation was observed, as the photogenerated electrons of **P-Az-B** do not possess enough energy to completely cleave the C-I bond. A CV-diagram of an aryl-iodide contains two reduction 'waves', for example 4-iodobenzonitril has a first 'wave' at -0.85 V (vs SCE) and the second one at -1.89 V (vs SCE). In the first 'wave' the formation of the activated state occurs, which is an anionic radical without full dissociation of the C-I bond. In the second 'wave' the aryl halide is completely disassociated. In the first wave the C-I bond already elongates greatly,

which enables a substitution reaction on the iodide. The authors therefore pose a mechanism that proceeds through the photogeneration of aryl radicals by oxidation of the aryl stannane **529**, together with the formation of activated aryl radical anions **536** by reduction of the aryl halide **532** with photogenerated electrons. Attack of the aryl radical **535** on the activated aryl halide **537**, followed by loss of the iodide anion, produces the final coupled product **533**.[364]

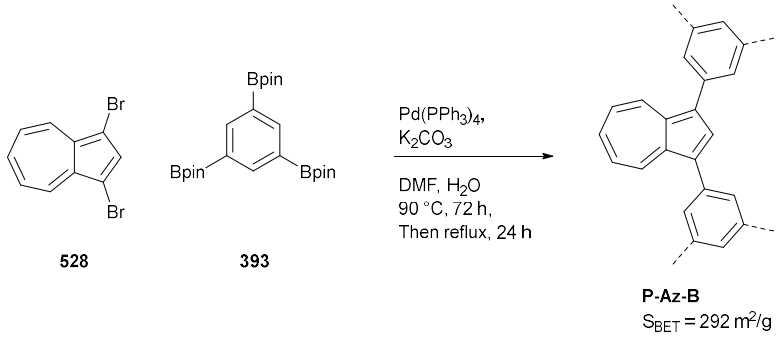

Scheme 142: Synthesis of an azulene containing CMP **P-Az-B** by Suzuki coupling.[364]

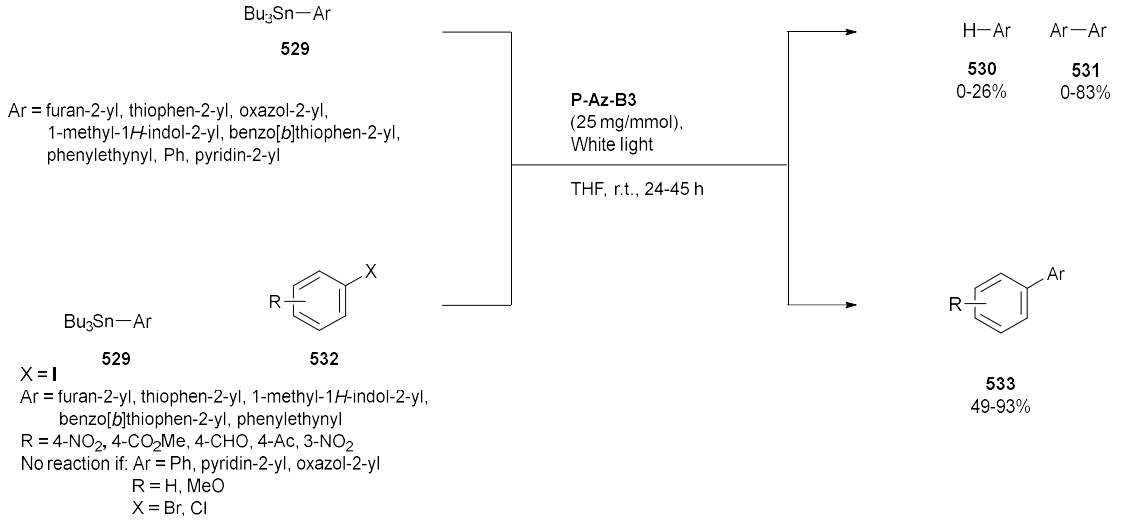

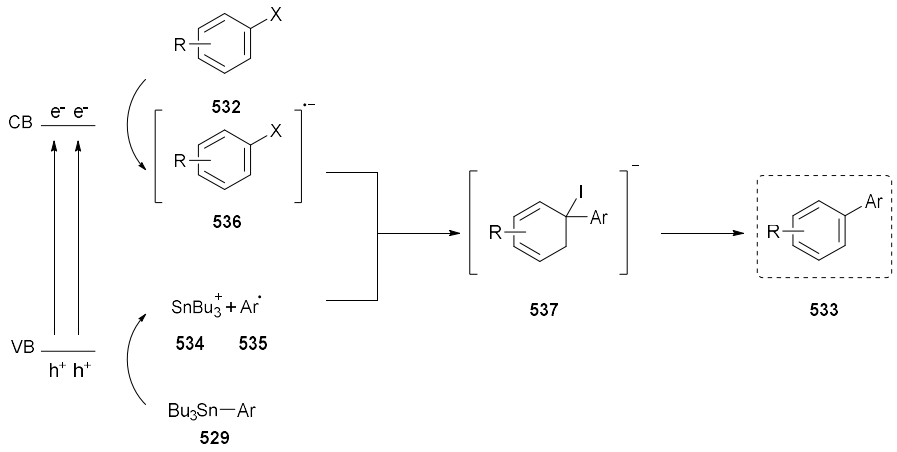

Scheme 143: Photocatalytic destannylation, dimerization and Stille coupling of aryl stannanes **529** catalyzed by **P-Az-B3**.[364]

1.8.3 Reduction reactions

1.8.3.1 Regeneration of NADH

As previously discussed, imine-linked COFs, while used widely, possess some clear disadvantages for use in photocatalysis. They generally possess rather low stabilities towards acids, bases or strong nucleophiles. In addition the imine linkage is relatively polarized, which leads to less effective conjugation and thus charge separation and migration. To help alleviate these shortcomings, Wang *et al.* reported an interesting strategy to improve the stability and conjugation of imine-linked COFs, by intramolecular cyclization between the imine bonds and neighboring thiophenes. Thiophene containing ditopic amine **538** was first condensed with triazine or benzene based tritopic aldehydes **209** and **344**, producing imine-linked **T-COF-1** and **B-COF-1**. Treatment of these materials with TFA under oxygen atmosphere led to a Pictet-Spengler reaction between the β-carbon of the thiophene and the imine carbon, furnishing the corresponding thieno[3,2-*c*]pyridine-linked **T-COF-2** and **B-COF-2** (Scheme 144). These materials were highly crystalline and stable towards both strong acids (12 M HCl) and bases (12 M NaOH). The authors tested them in the photocatalytic regeneration of nicotinamide adenine dinucleotide (NADH), a typical coenzyme (Scheme 145). Imine-linked **B-COF-1** showed no photoactivity, whilst the thieno[3,2-*c*]pyridine-linked **B-COF-2** only gave a yield of 6%. The triazine based material showed much higher activity, with **T-COF-2** giving 74% regeneration yield in only 10 minutes. In this reaction a rhodium complex is used as co-catalyst and tris(2-hydroxyethyl)amine (TEOA) as an electron donor. The COFs donate their excited electrons to $[Cp^*Rh(bpy)(H_2O)]^{2+}$ **543** to form the hydride rhodium $[Cp^*Rh(bpy)(H)]^+$ **542** after coupling with one proton. This complex then acts as a hydride transfer reagent, reducing NAD^+ **539** to NADH **540**. The authors suggest that nitrogen-rich triazine units can act as the active site for redox reactions with their free electron pairs and electron-poor nature, thus explaining the high activity of triazine containing **T-COF-2** when compared with **B-COF-2**. Interestingly, due to the strong π-π stacking interactions between the adenine of NAD^+ and the π-conjugated 2D surface of **T-COF-2** a charge transfer complex is formed. This complex can be considered a pre-state, which facilitates direct photoinduced electron transfer between the COF and NAD^+.[365] Therefore, when the reaction is done without the rhodium complex as a mediator, 44% yield was still obtained.[331]

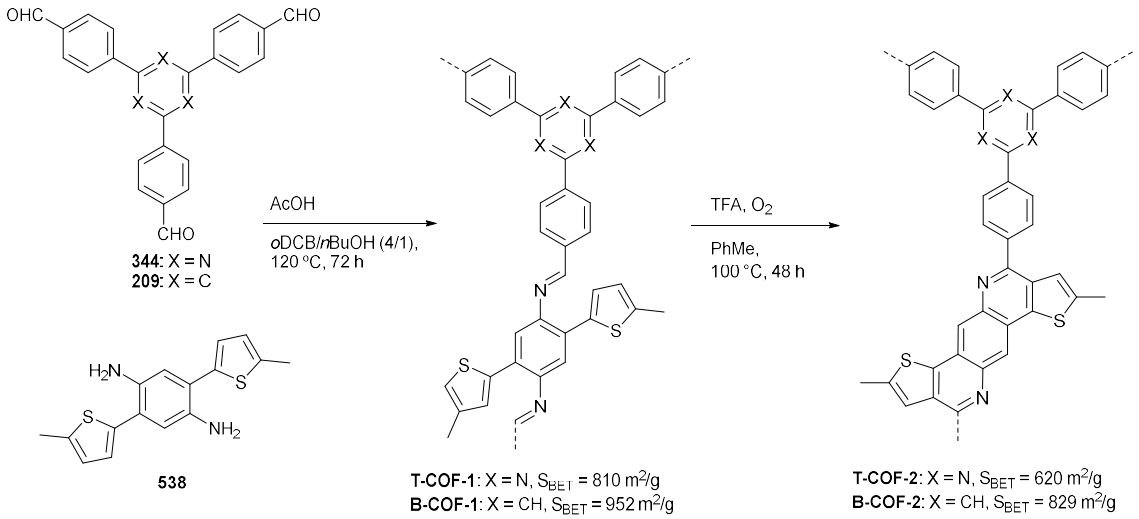

Scheme 144: Synthesis of thieno[3,2-*c*]pyridine-linked **T-COF-2** and **B-COF-2** by imine condensation followed by cyclization and oxidation.[331]

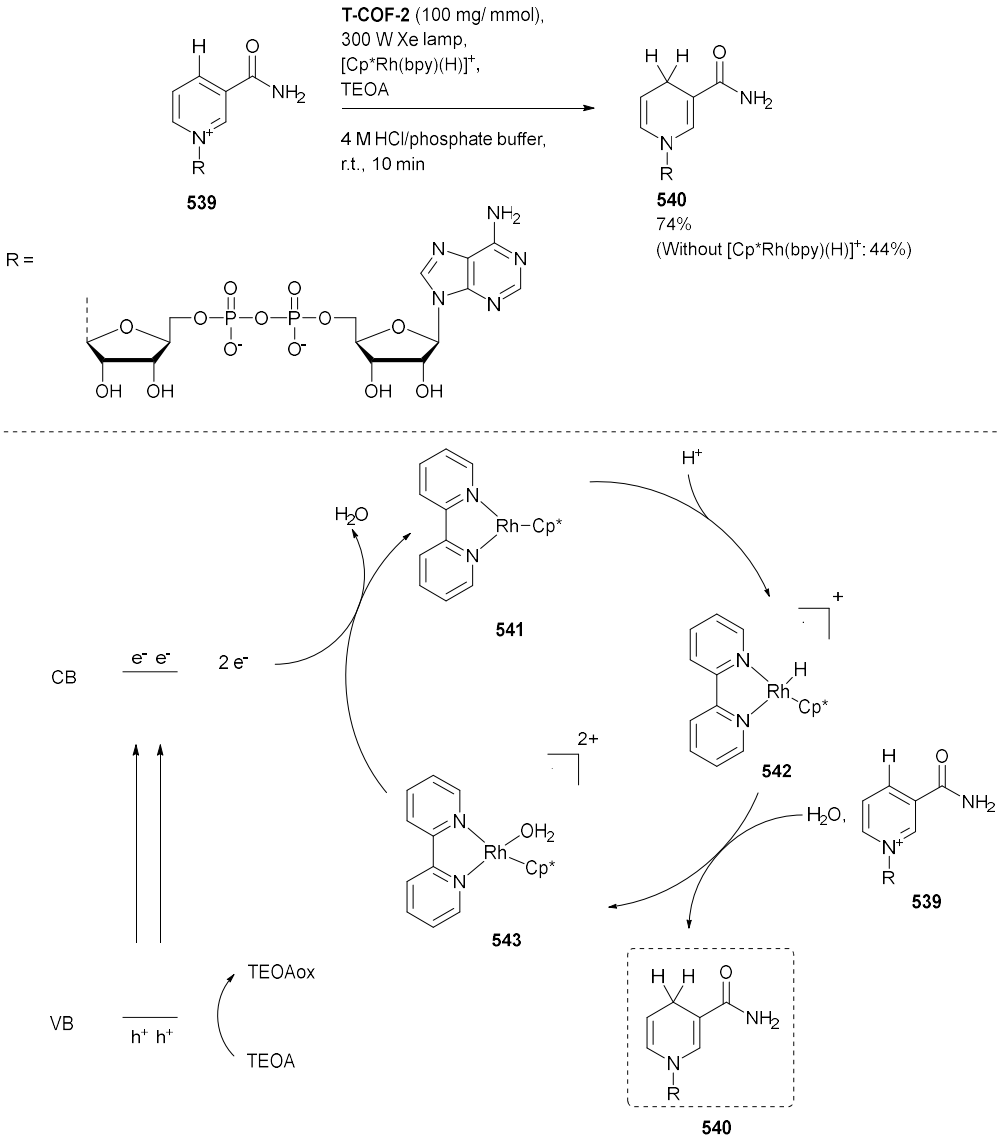

Scheme 145: **T-COF-2** catalyzed photocatalytic regeneration of NADH **539**.[331]

1.8.3.2 Reduction of carbon-halogen bonds

1.8.3.2.1 α-Alkylation of aldehydes

The materials described in Section 1.8.2.3.3 (**COF-1/2**, Scheme 112) as catalysts for the CDC were also used as catalysts for the enantioselective α-alkylation of aldehydes using the Macmillan imidazolidinone organocatalyst **546** as co-catalyst. To achieve satisfactory *ee*'s the temperature was lowered to -10 °C, as this increases the enantioselectivity, however this also required lengthening the reaction time to 40 hours. Nevertheless, a range of products were obtained in good yields and *ee*'s, and again **COF-1** and **COF-2** performed similarly (Scheme 146).[343] The reaction occurs via the reduction of the carbon-bromine bond with photogenerated electrons, generating the alkyl radical **548**. In the organocatalytic cycle the organocatalyst **546** condenses with the aldehyde **544** to forms the enamine **549**. This enamine then reacts with the alkyl radical, preferentially on one side of the molecule by

steric shielding by the Macmillan catalyst, producing the radical intermediate **550**. This undergoes one-electron oxidation to the iminium **551**, which after hydrolysis regenerates the organocatalyst **546** and liberates the alkylated product **547**.[343]

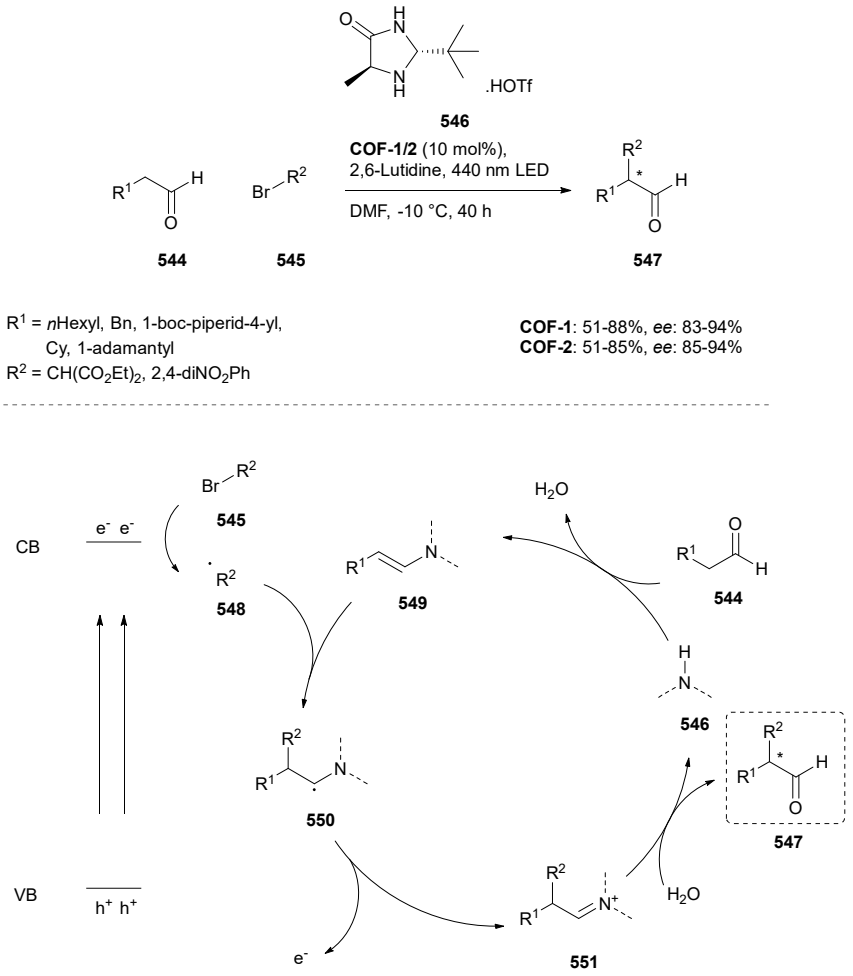

Scheme 146: Organocatalytic α-alkylation of aldehydes.[343]

1.8.3.2.2 Borylation of aryl iodides

Shang *et al.* reported the synthesis of three pyrene-based imine-linked COFs: **6N-COF**, **4N-COF** and **2N-COF** (Scheme 147) by solvothermal condensation between the pyrene amine **552** and tetrazine or benzene-based aldehydes **553-556**. These materials were applied for the borylation of aryl iodides **557**, where **6N-COF** was the most effective material and produced a wide range of products in high yields (76-99%) (Scheme 148). For the conversion of 4-iodo-anisole into 4-methoxybenzene boronic acid pinacol ester **6N-COF** reached 98%, whilst only 88%, 44% and 21% was obtained for **2N-COF**, **0N-COF** and **4N-COF**, respectively. The reaction occurs via the addition of water to bis(pinacolato)diboron **558** in the presence of DIPEA, giving the hydroxy adduct **560** and protonated DIPEA. The photogenerated holes of the COFs are quenched with DIPEA, a good electron donor, resulting in $DIPEA^+$. The photogenerated electrons reduce the aryl halide **557** to the radical anion **561**, which after elimination of the halide forms the aryl radical **562**. This will then react with the hydroxy adduct **560**,

forming the boric acid pinacol ester HOBpin and the aryl boronic ester radical anion **563**. Finally, this radical anion **563** will lose an electron to DIPEA or the COF to form the product **559**.[366]

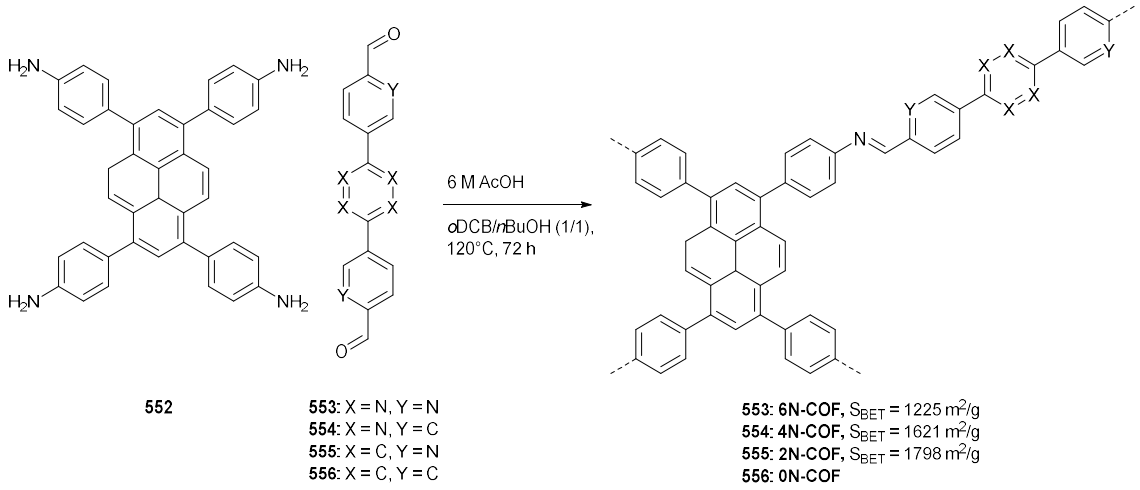

Scheme 147: Synthesis of COFs for the borylation of aryl halides.[366]

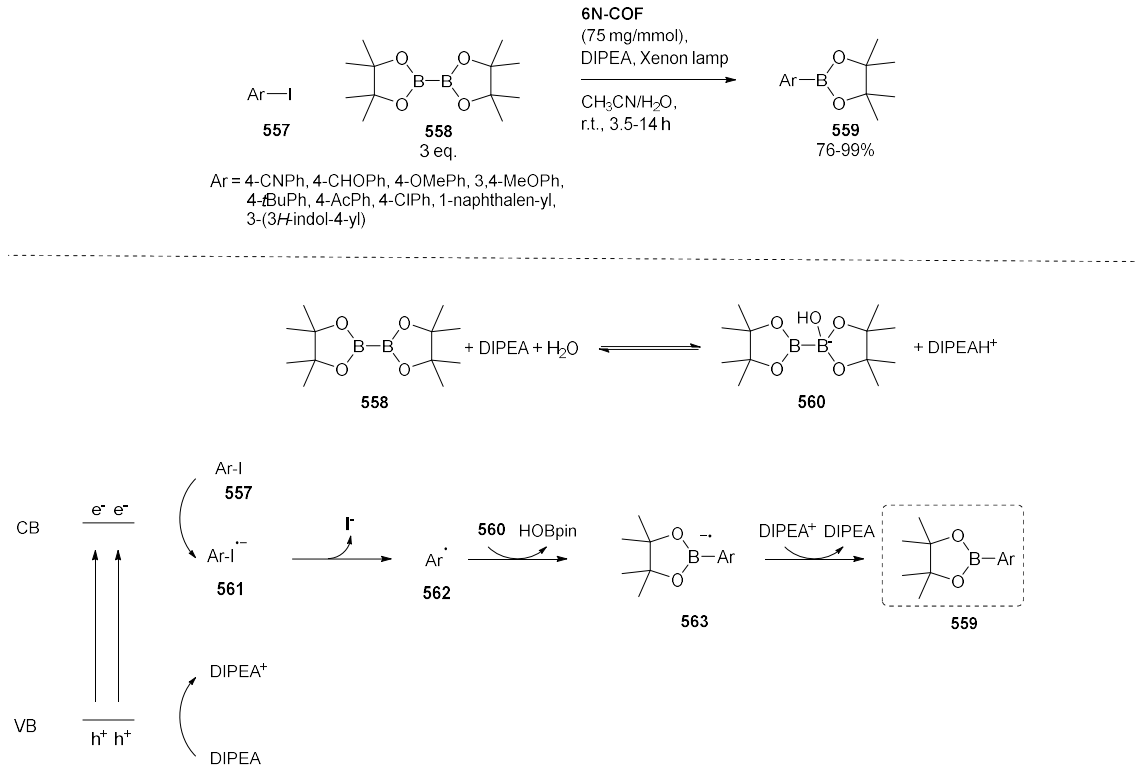

Scheme 148: Application of **6N-COF** as a photocatalyst for the borylation of aryl iodides.[366]

1.8.3.3 Reduction of nitro groups

Huang *et al.* synthesized **CTF-BT** based on the photoactive benzothiadiazole core by the superacid catalyzed trimerization and silica templating method that was discussed previously (Scheme 149). **CTF-BT** was used as a photocatalyst for the reduction of 4-nitrophenol (4-NP) **565** to 4-aminophenol (4-AP) **566** with $NaBH_4$ (Scheme 150). Using silica templated **CTF-BT** the reduction of 4-NP was complete after only 50 minutes. Bulk **CTF-BT**, synthesized without using the SiO_2NPs as template, resulted in a conversion of only 46% in the same time frame, despite the material possessing the same chemical composition and a similar BET surface area. The authors attribute this superior activity on the hollow structure of templated **CTF-BT**, which allows better mass transfer and enhanced light absorption via the multiple light reflections and absorptions inside the polymer itself. The mechanism of the reaction was probed via photoluminescence quenching experiments. When increasing concentrations of 4-NP were used, the emission intensity of **CTF-BT** gradually diminished, indicating electron transfer between the excited state of **CTF-BT** and 4-NP, producing an activated anionic radical intermediate of 4-NP. The role of $NaBH_4$, which can act as a hydride and electron donor was also studied. When sodium tetraphenylborate (NaTPB) was used, which can only act as an electron donor, the reduction was still successful. This points to the necessity of an electron donor, whilst the hydrogen species can also originate from a protic solvent. Therefore, in the proposed mechanism, the photogenerated holes of **CTF-BT** will oxidize an electron donor, $NaBH_4$ or NaTPB, and the electrons are transferred to 4-NP **565** to form the radical anion **567**, which is further reduced and takes up hydrogen to generate 4-AP **566**.[367]

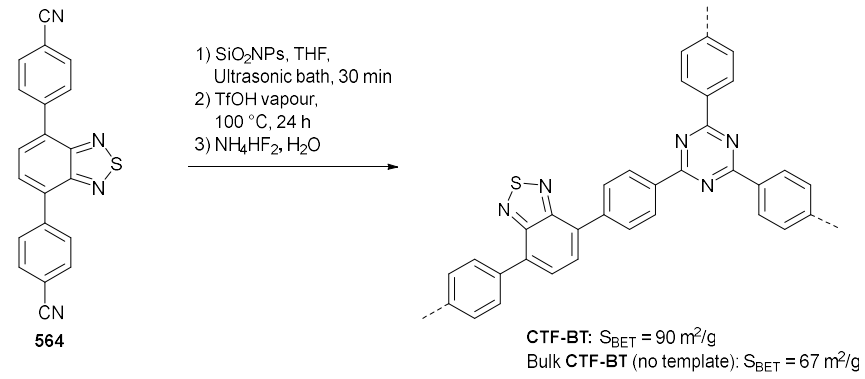

Scheme 149: Synthesis of **CTF-BT** by silica templated, superacid catalyzed nitrile trimerization.[367]

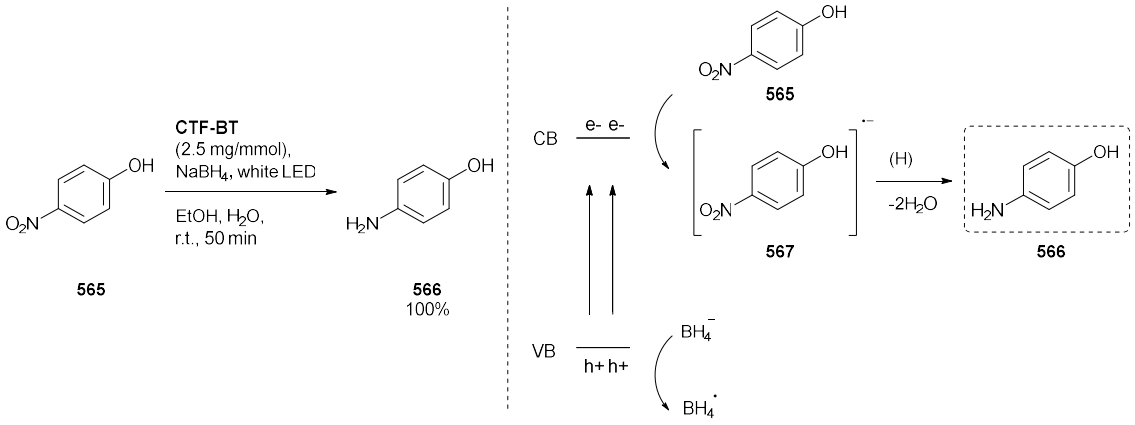

Scheme 150: Photocatalytic reduction of 4-nitrophenol.[367]

1.8.3.4 Reduction of alkenes

Chen *et al.* reported the synthesis of three CMPs: **pTTT-BTD**, **pTTT-Ben** and **pTTT-DMOB**, by palladium catalyzed, direct C-H arylation of 2,4,6-tri(thiophen-2-yl)-1,3,5-triazine (TTT) **568** and three different aryl bromides with varying electron density **443,569** and **570** (Scheme 151). 2,4,6-Tri(thiophen-2-yl)-1,3,5-triazine **568** possesses an inherent donor-acceptor structure due to its thiophene and triazine units. The three isomorphic linkers used were based on benzothiadiazole (BTD) **443**, benzene (Ben) **569** and dimethoxybenzene (DMOB) **570**. The materials possessed bandgaps of 2.01 eV, 2.50 eV and 2.23 eV for **pTTT-BTD**, **pTTT-Ben**, and **pTTT-DMOB**, respectively. The authors studied the photocatalytic hydrogenation of maleic acid **571** to succinic acid **572** using the synthesized CMPs as a photocatalyst and ascorbic acid as the sacrificial agent (Scheme 152). The production rates of succinic acid were 0.16 $mmolg^{-1}h^{-1}$ for **pTTT-BTD**, 2.44 $mmolg^{-1}h^{-1}$ for **pTTT-DMOB** and 4.66 $mmolg^{-1}h^{-1}$ for **pTTT-Ben** with a 40% yield of succinic acid for **pTTT-Ben** after 20 hours. Interestingly, the materials were also active for oxidation reactions. The authors reported the oxidation of hydroxymethylfurfural to 2,5-diformylfuran with **pTTT-Ben** again being the most performant. Using optimized conditions, a production rate of 0.53 mmol 2,5-diformylfuran $g^{-1}h^{-1}$ could be obtained.[368]

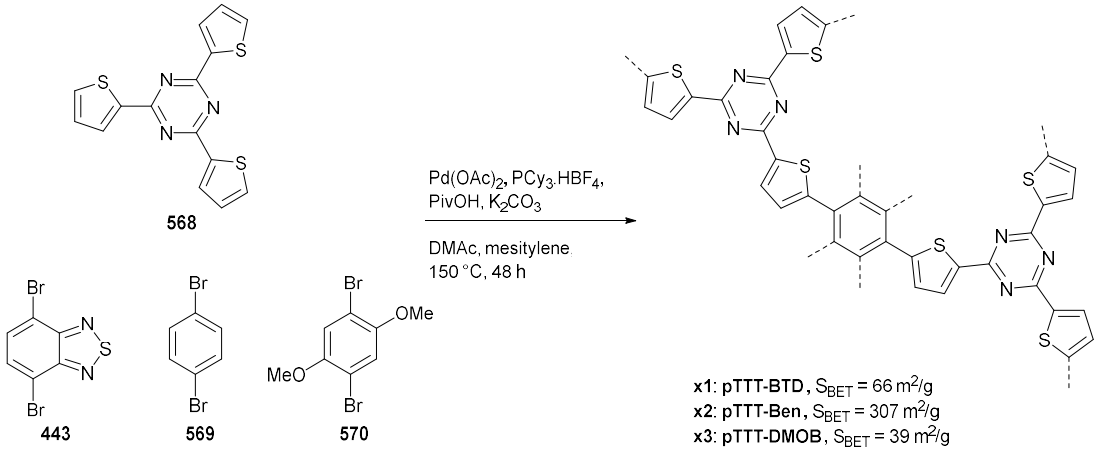

Scheme 151: Synthesis of CMPs by direct C-H arylation.[368]

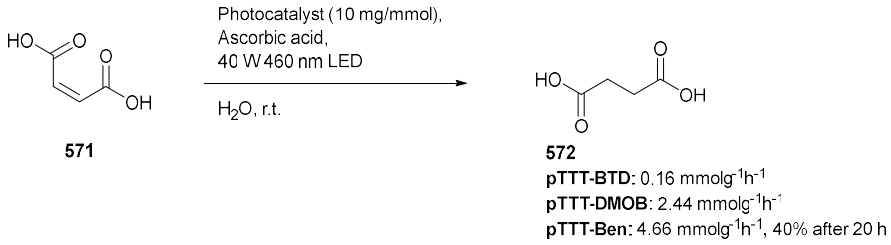

Scheme 152: Photocatalytic hydrogenation of maleic acid **571** to succinic acid **572**.[368]

1.8.4 Miscellaneous reactions

1.8.4.1 C-H trifluoromethylation

Yang *et al*. used the C=C linked 2D COF, **TTO-COF** (Scheme 104) for dye degradation and C-H trifluoromethylation. First, the degradation of methylene blue and methyl orange was studied, which was completed in 20 minutes by **TTO-COF**, much faster than g-C_3N_4 or an imine-linked analogue of **TTO-COF**, proving the superiority of olefin linkages when compared with imine linkages. Moreover, this material was an efficient catalyst for the C-H functionalization of arenes and heteroarenes by trifluoromethylation with Langlois' reagent (CF_3SO_2Na). A range of arenes could be trifluoromethylated in high yields (81-98%) and, interestingly, the trifluoromethylated pyrimidine derivative **583**, dimethyluracil **584**, and theophylline **585** could also be obtained in good yields (Scheme 153). Electron poor arenes reacted only sluggishly, with 1,3,5-trifluorobenzene and 1,3,5-trichlorobenzene only resulting in yields of 12% and 13%, respectively. This reaction occurs by oxidation of the Langlois' reagent **586** by the photogenerated holes and loss of SO_2 from the resulting CF_3SO_2 radicals **587**, producing CF_3 radicals **588**. Addition of these radicals to an arene, followed by aromatization, furnishes the trifluoromethylated products **574**.[369]

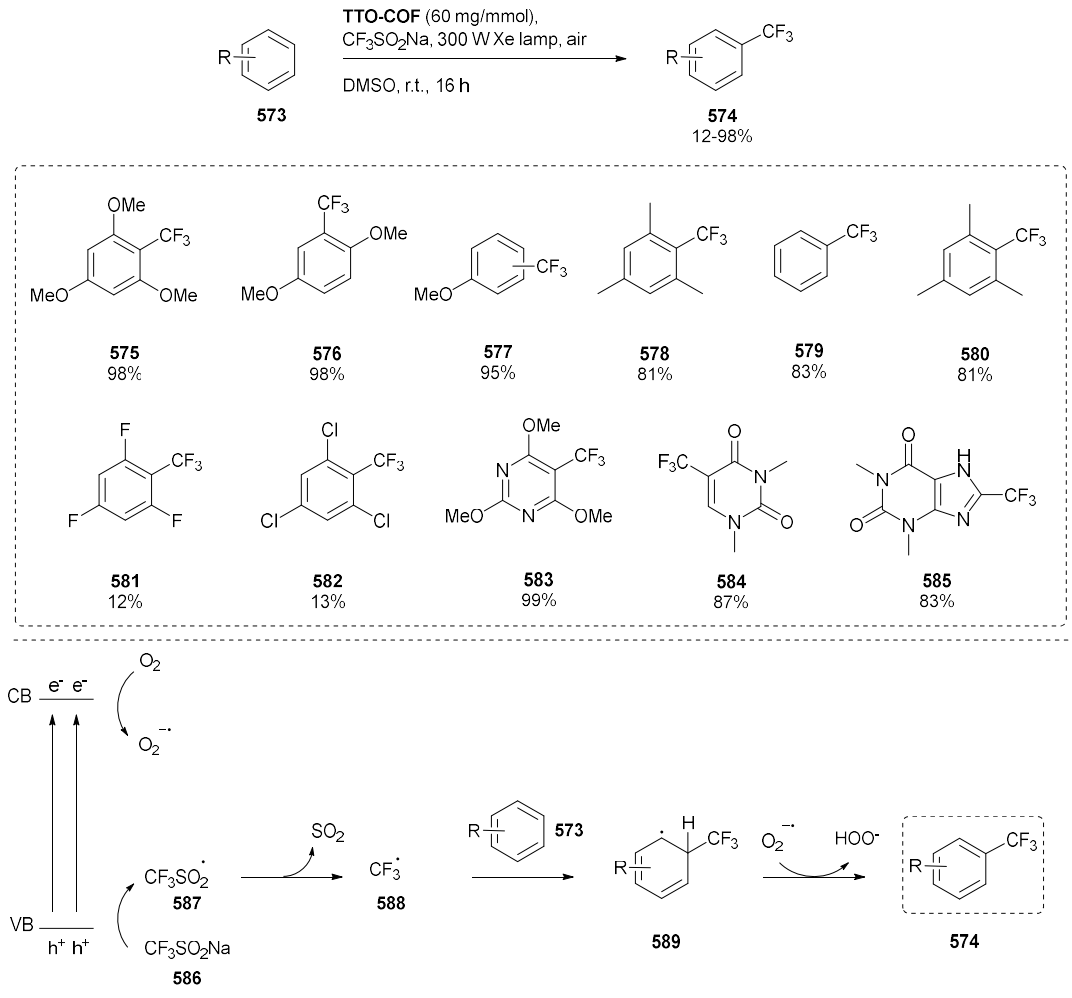

Scheme 153: **TTO-COF** catalyzed arene trifluoromethylation.[369]

1.8.4.2 Cyclization of 2-aryl phenyl isocyanides

Liu *et al*. prepared a hydrazone-linked COF, which are known for their great stability, by condensation of 2,5-dimethoxyterephthalohydrazide **587** with 1,3,5-triformylbenzene **48** (Scheme 154). This material was utilized for the tandem radical addition-cyclization of 2-aryl phenyl isocyanides **590** with various radical precursors **586,591-593** to deliver a wide range of 6-substituted phenanthridines **594**. Alkyl/aryl radicals could be installed via hydrazines **591**, trifluoromethyl radicals via Langlois' salt **586**, a P-centered radical from diphenylphosphine oxide **593** and lastly the phenylthiyl radical could be generated from diphenyl sulfide **592** (Scheme 155). The reaction between 2-isocyano-4'-methoxy-1,1'-biphenyl and diphenyl disulfide was scaled up to four mmol in continuous flow, giving the product in 79% yield. A plausible mechanism with trifluoromethylation as an example is given in Scheme 155. Initially, the photogenerated electrons will reduce the oxidant $K_2S_2O_8$, to its radical anion, which then in turn abstracts one electron from Langlois' reagent **586**, to produce the trifluoromethyl radical **588**. Radical addition to the isocyanide **590** affords intermediary radical **595**, which further cyclizes to intermediate **596**. Finally, this is oxidized and loses a proton to afford the final compound **594**.[370]

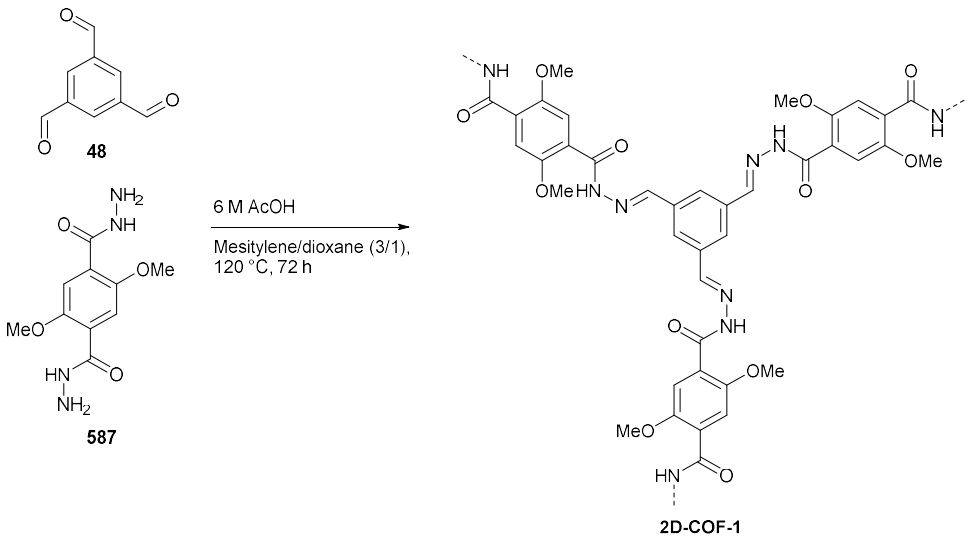

Scheme 154: Synthesis of hydrazone-linked **2D-COF-1**.[370]

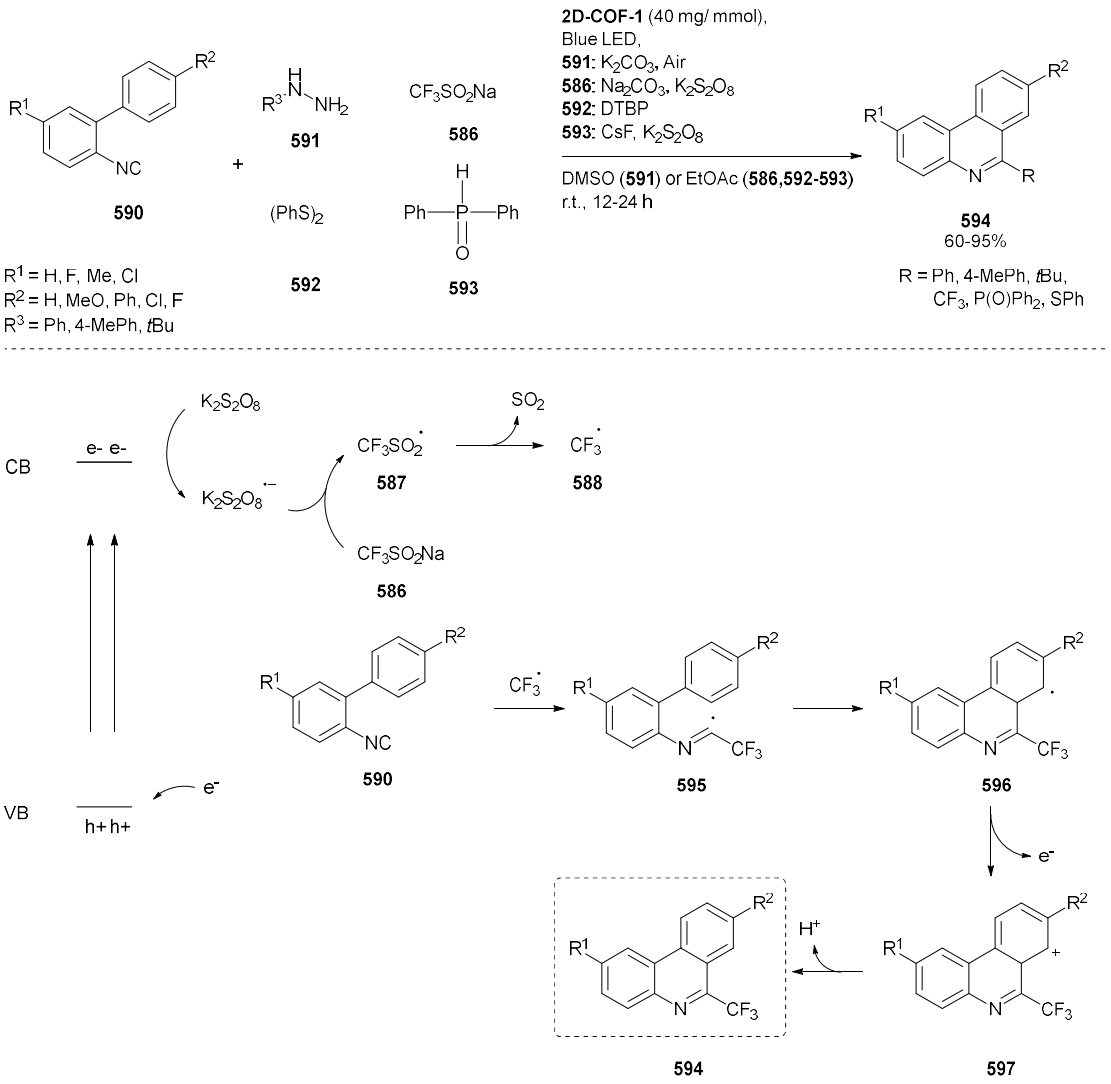

Scheme 155: Tandem radical addition-cyclization of 2-aryl phenyl isocyanides **590** to generate phenanthridines **594**.[370]

1.8.4.3 Alkene *E-Z* isomerization

In 2019 the Banerjee group reported a β-ketoenamine-linked COF **TpTt** that was effective as a photocatalyst for the *E-Z* isomerization of olefins. **TpTt** was synthesized by solvothermal Schiff base condensation and tautomerization of melamine **43** and triformylphloroglucinol **71** (Scheme 156). Melamine **43** is an attractive building block for COFs, as it is a cheap tritopic amine that is available on large scales, however, it possesses low reactivity and solubility. These authors were able to synthesize a moderately crystalline material by using a DMAc/DMSO (2/1) solvent mixture. Using this material a range of *trans*-stilbenes **598** could be converted into the corresponding *cis*-stilbenes **599** (Scheme 157). This reaction is catalyzed by the energy transfer from the excited **TpTt** material to the *trans*-stilbene, producing the biradical triplet intermediate state, which can undergo rotation and form the *cis*-stilbene product.[371]

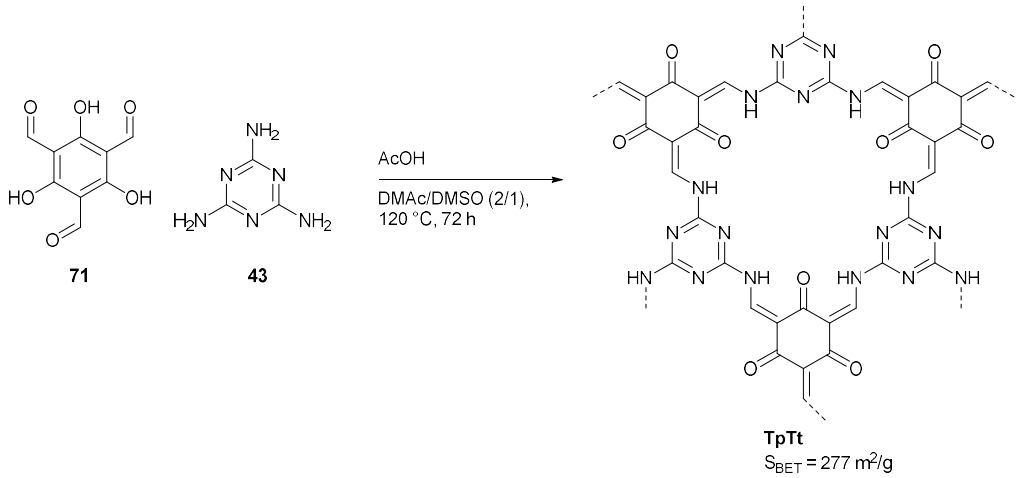

Scheme 156: Synthesis of **TpTt** by Schiff base condensation and tautomerization.[371]

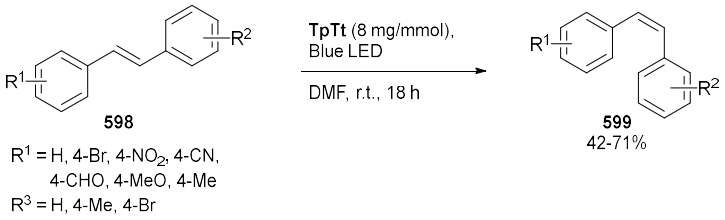

Scheme 157: Application of **TpTt** as a photocatalyst for the *E-Z* isomerization of olefins.[371]

1.8.4.4 Synthesis of benzophosphole oxides

Huang *et al*. synthesized a CTF by TfOH catalyzed trimerization of 5-(4-cyanophenyl)thiophene-2-carbonitrile **600**. The monomer **600** was coated on silica nanoparticles and then directly, in the solid state, polymerized by TfOH catalyzed trimerization at 100 °C. Finally, after etching of the silica template **asy-CTF** was obtained (Scheme 158). This material was applied as a photocatalyst for the synthesis of benzophosphole oxides **604** from phosphine oxides **601** and acetylene derivatives **602** (Scheme 159). With *N*-ethoxy-2-methylpyridinium tetrafluoroborate **603** as an oxidant in DMF a wide range of benzophosphole oxides **604** could be produced in generally good yields (31-95%). Remarkably, when asymmetric acetylenes were used the reaction occurred with very high regioselectivity. The first step in the reaction occurs through the reduction of the oxidant (E_{red} = -0.78 V vs SCE) by the photogenerated electrons (E_{red} = -1.30 V vs SCE), generating ethoxyl radicals **605**. Hydrogen abstraction by these radicals on the phosphine **601** results in the phosphinoyl radical **607**. This then undergoes addition onto the alkyne **602**, producing radical species **608**. After cyclization intermediate **609** is formed, which then loses an electron and a proton, thus generating the final product **604**.[372]

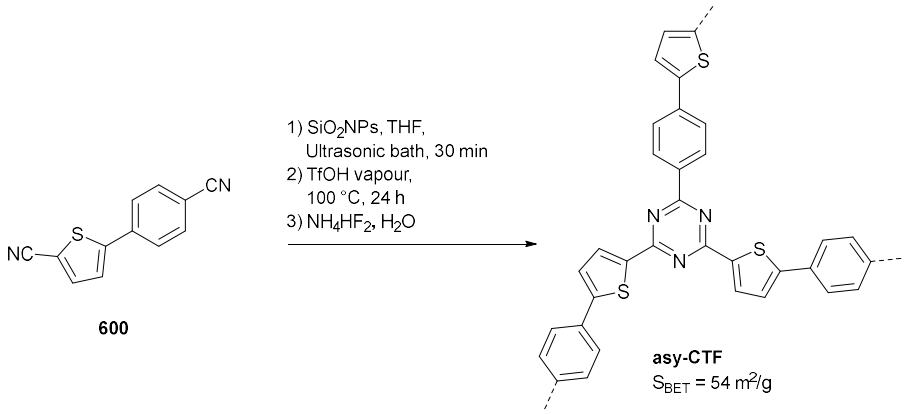

Scheme 158: Synthesis of **asy-CTF** by trimerization of nitrile containing linker **600**.[372]

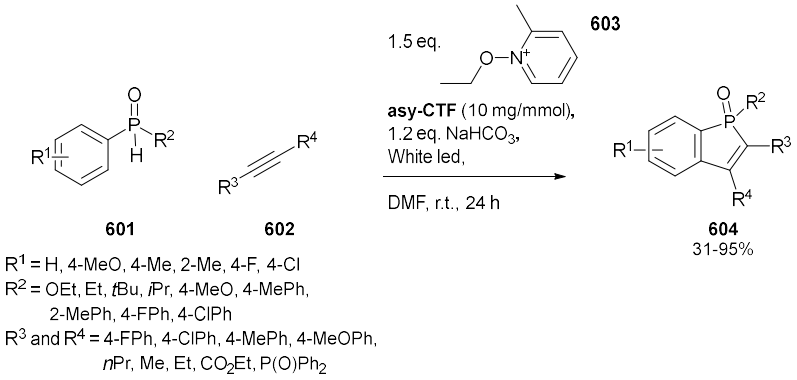

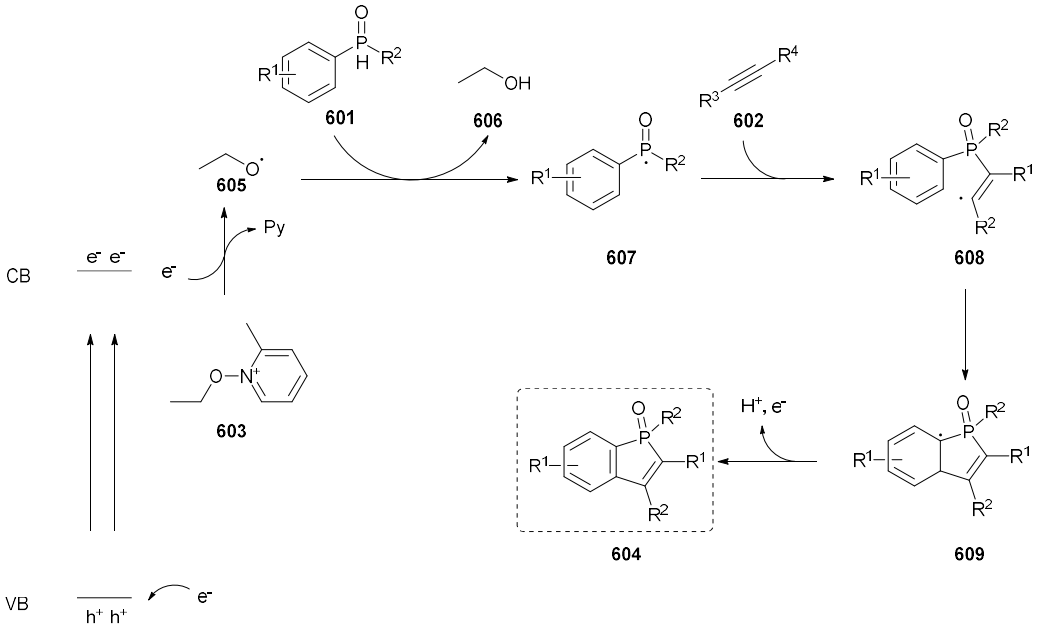

Scheme 159: Synthesis of benzophosphole oxides **604** catalyzed by **asy-CTF**.[372]

1.8.4.5 C-S coupling

In 2020 the Van Der Voort group reported the use of a nickel containing COF as a bifunctional catalyst, combining photocatalysis with metal catalysis. **Ace-COF** was synthesized by solvothermal condensation of tritopic amine **285** with acenaphthenequinone **610**. Importantly, the resulting 1,2-bisimines can chelate transition metals, such as nickel, thus forming **ACE-COF-Ni** (Scheme 160). This material was used for photocatalytic cross-couplings between aryl iodides **611** and thiols **612** giving sulfides **613** in good yields (79-96%) (Scheme 161). From emission quenching experiments with varying thiol or aryl iodide concentrations it became clear that the thiophenol was a much more effective luminescence quencher of **ACE-COF-Ni** than the aryl iodides. Furthermore, the lifetime of the exited state was measured using time-resolved emission spectroscopy, and adding the thiol resulted in a decrease of this lifetime. These experiments point to the generation of the thiophenol radical by oxidation, and this sulfur centered radical could also be observed with EPR. Using this information the proposed mechanism consists of oxidation of the thiol **612** by the excited COF, generating the thiol radical cation **621**, which after deprotonation with pyridine forms the thiol radical **617**. This will add to the Ni(I) complex **616** to form the Ni(II) complex **618**. The photogenerated electrons serve as a reducing agent, reducing this Ni(II) complex **618** to the Ni(I) complex **619**, which then undergoes oxidative addition with the aryl iodide **611**. Reductive elimination results in regeneration of the Ni(I) species **616** and the product **613**.[373]

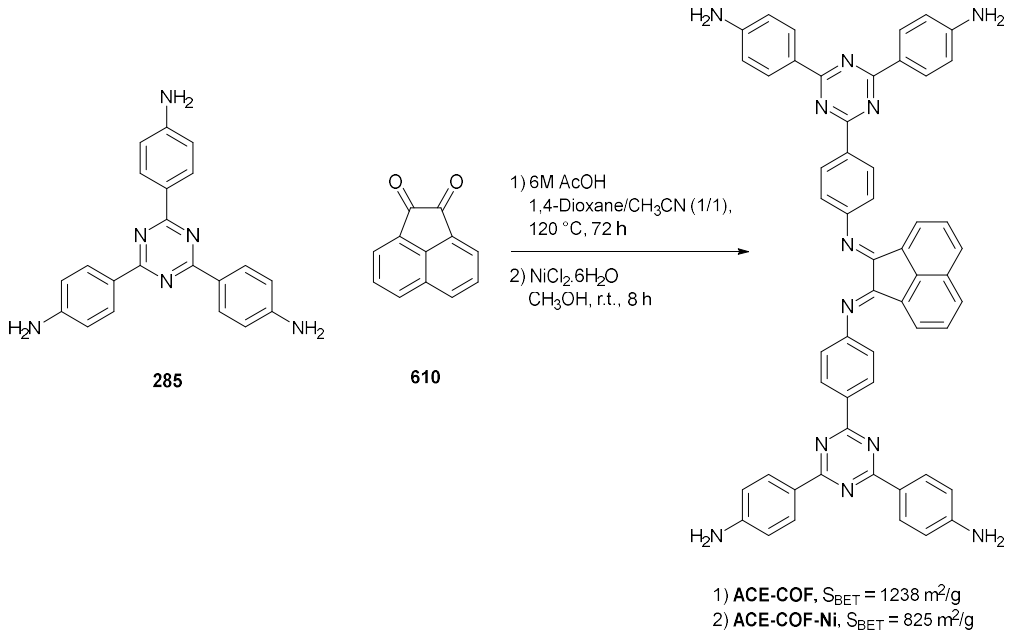

Scheme 160: Synthesis of a bifunctional nickel containing **ACE-COF-Ni**.[373]

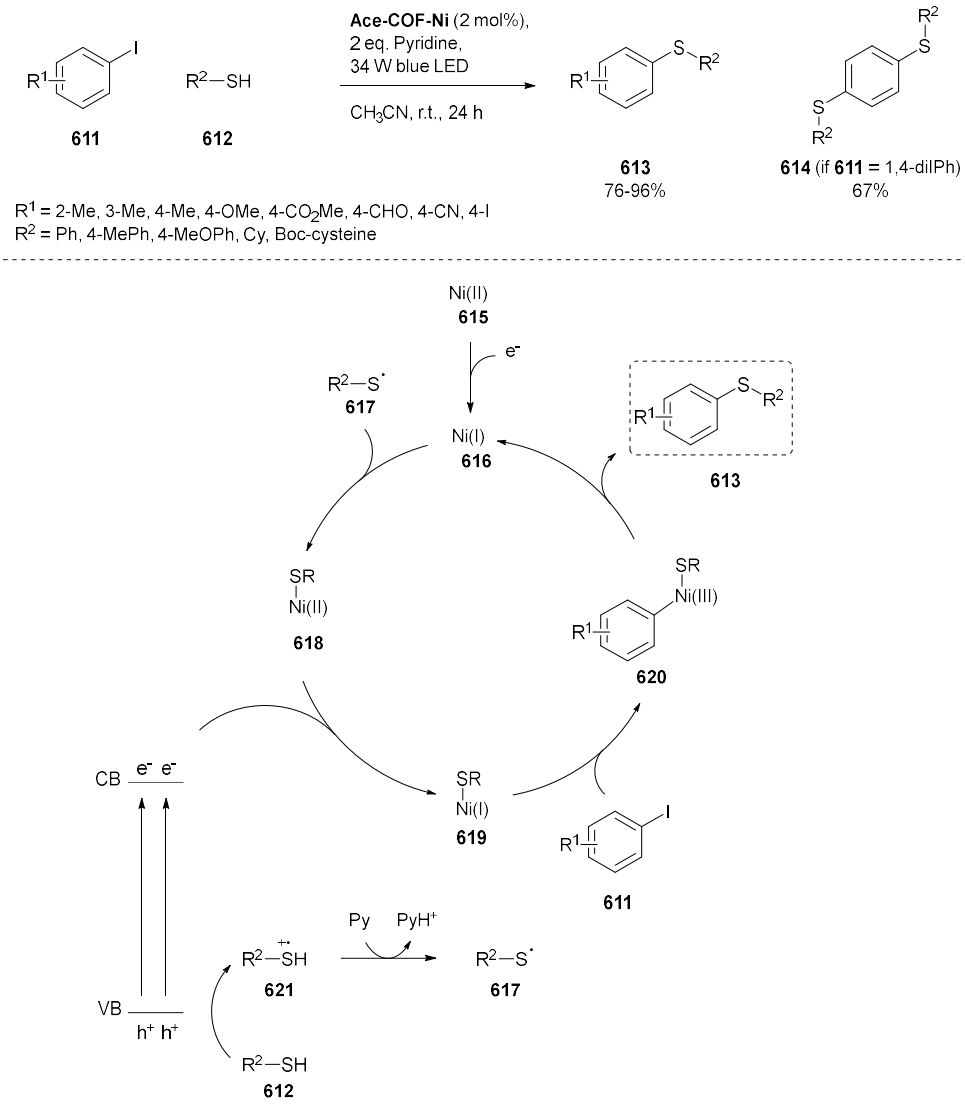

Scheme 161: Cross-coupling between aryl iodides **611** and sulfides **612** catalyzed by **Ace-COF-Ni**.[373]

1.8.4.6 Transformation of active methylene compounds to (*E*)-amino-2-thiocyanato-α,β-unsaturated olefins

Wan-kai *et al*. synthesized **BF-COFs** by the condensation between benzofurans **621-622** containing alkyl chains of different length and 1,3,5-triformylphloroglucinol **72** (Scheme 162). The two COFs, due to their extremely similar compositions, possessed analogous optical properties. The band gap was 1.87 eV and 1.88 eV for **BF-COF1** and **BF-COF2**, respectively, with the position of the CB at -0.81 V (vs SCE) for **BF-COF1** and -0.78 V (vs SCE) for **BF-COF2**. Using these materials an interesting transformation was reported, the difunctionalization of active methylene compounds **623** with ammonium thiocyanate, resulting in (*E*)-amino-2-thiocyanato-α,β-unsaturated olefins **624**. A wide range of substrates were converted, with 28 reported examples, and generally high yields were obtained (40-98%). This reaction was further applied towards the synthesis of chiral compounds **625**, which were then used as starting materials to prepare chiral aminothiazoles **626** (Scheme 163). In the proposed mechanism the COF generates $^1O_2$ and $O_2^{-\bullet}$ via energy transfer and SET, respectively. The easily oxidized SCN^- anion (E_{ox} = 0.61 V vs SCE) can be oxidized by the **BF-COFs** (E_{ox} = 1.06 V vs SCE), or by $^1O_2$ and $O_2^{-\bullet}$, forming the thiocyanate radical. This can then abstract a hydrogen atom from the substrate **623** to form intermediate **627**, which finally undergoes Schiff base reaction with ammonia, followed by isomerization to give the product **624**.[374]

1.8.4.7 Thiol-ene cross-coupling and acetamide formation

Chao *et al.* reported the synthesis of **3D TAPPy-TFPA** by Schiff base condensation between pyrene-based amine **552** and triphenylamine-based aldehyde **629**. As was discussed in Section 1.8.2.3.3, triphenylmethane is non-planar, and the resulting framework therefore adopts a 3D (fjh) topology (Scheme 164). The material was used to catalyze the thiol-ene cross-coupling and thiol radical mediated acetamide formation from potassium thioacetate **633** (Scheme 165). The mechanism consists of the oxidation of thiol **630** or potassium thioacetate **633** generating the thiyl radical cation **636** or the thioacetic radical **639**. The thiyl radical cation **636** is deprotonated to the thiyl radical **637**, which readily adds to double bonds, to furnish alkyl radical **638**. This radical can then abstract a hydrogen atom from an unreacted thiol, to give the product **632** and another thiyl radical **637**. For the acetamide formation, the thioacetic radical **639** will dimerize to the key intermediate **640**, which can react with an amine to form the product **635** and intermediate **641**, which can also undergo aminolysis to furnish the acetamide **635**.[375]

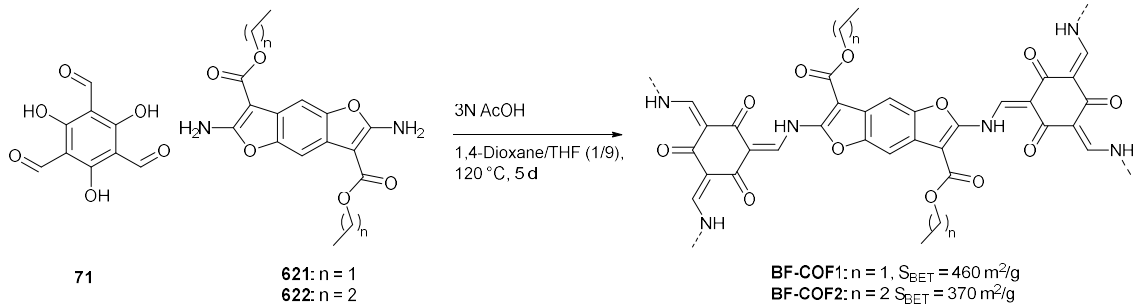

Scheme 162: Synthesis of benzofuran containing β-ketoenamine-linked COFs.[374]

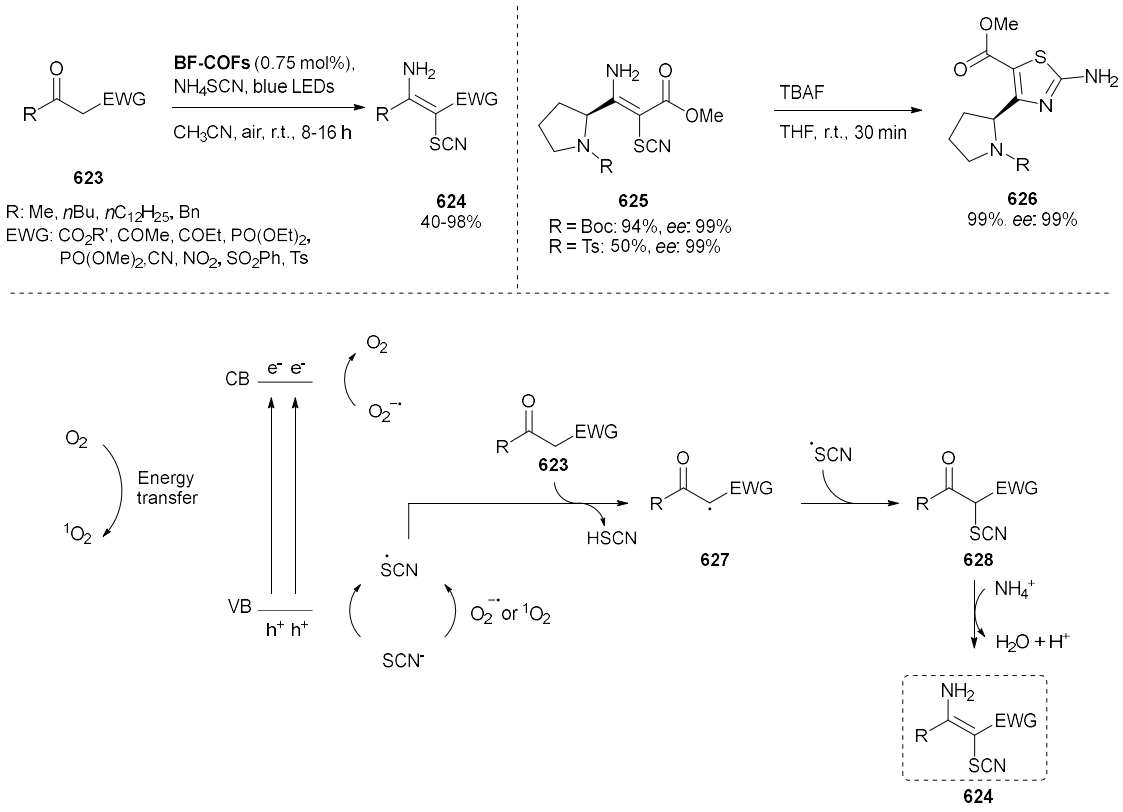

Scheme 163: Application of **BF-COFs** towards the photochemical difunctionalization of olefins.[374]

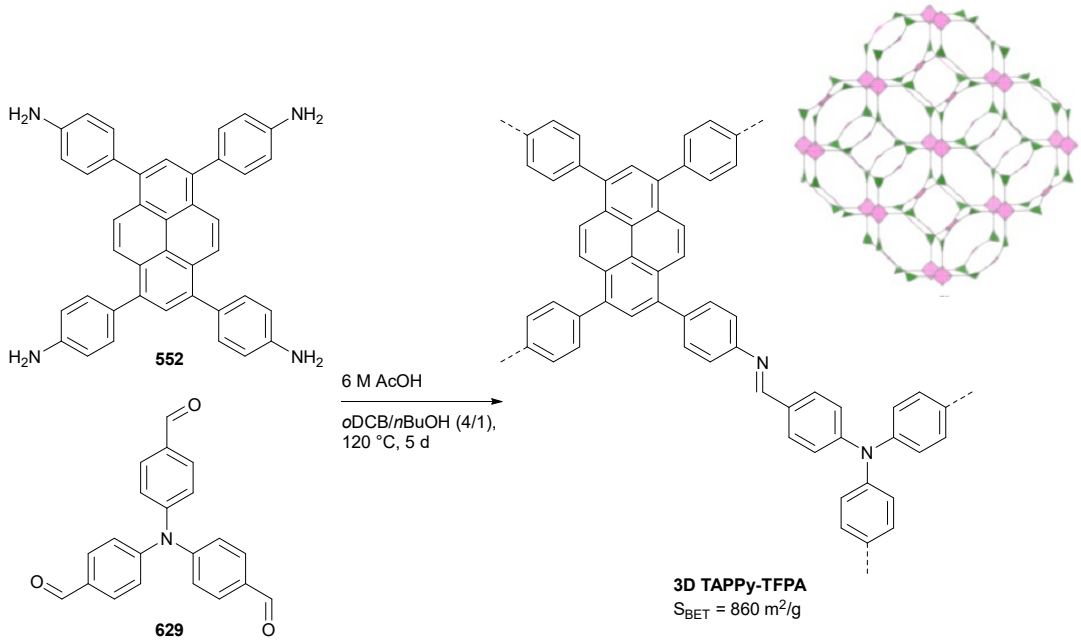

Scheme 164: Synthesis of a 3D imine-linked COF adopting a fjh topology.[375]

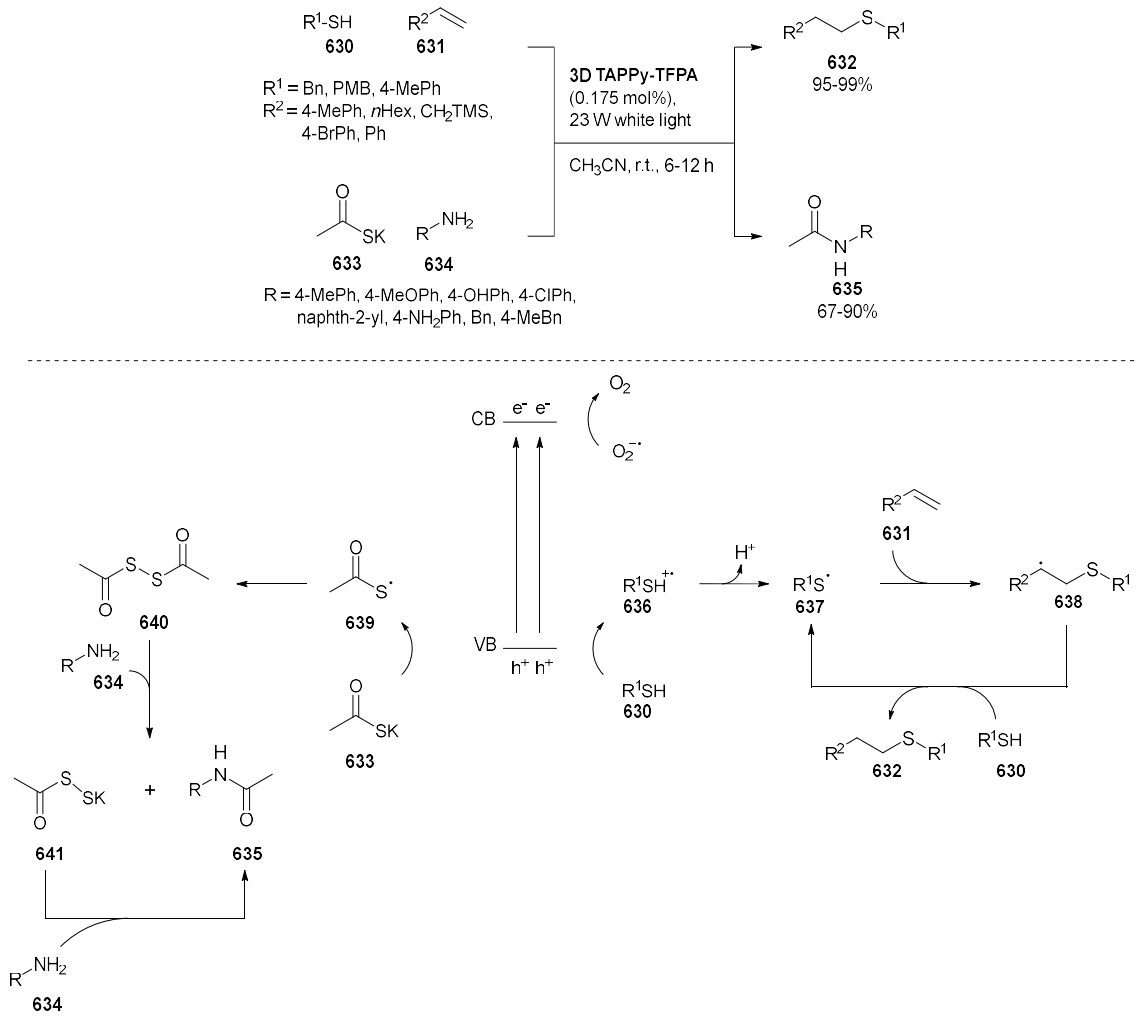

Scheme 165: Application of **3D TAPPy-TFPA** towards the thiol-ene cross-coupling and acetamide formation.[375]

1.8.5 Outlook on POPs as photocatalysts

A general comparison between POPs and other classes of photocatalysts is shown in Table 6 and some typical examples of these catalysts are shown in Figure 6. Homogeneous catalysts offer advantages over heterogeneous catalysts, such as their accessibility and simpler reaction setup and upscaling. They are typically more active, allowing for lower catalyst loading. However, homogeneous catalysts require a more difficult purification and are generally not recyclable.[376,377] Homogeneous photocatalysts can be divided into two main classes: metal complexes and organic dyes.

Metal complexes, of which tris(2,2′-bipyridine)ruthenium(II) [$Ru(bpy)_3$] and tris(2-phenylpyridine)iridium [$Ir(ppy)_3$] are typical examples, possess excellent light absorption, long-lived excited states and have been applied extensively in organic synthesis. A wide range of redox potentials is available by tuning the metal and ligands, allowing a multitude of transformations to occur.[377] However, these catalysts can be prohibitively expensive, particularly iridium-based catalysts due to the scarcity of the metal. Additionally, the potential for traces of toxic metals to remain in the product makes the application of these complexes unappealing in the later stages of a pharmaceutical synthesis.[378] The second main class of homogeneous photocatalysts, organic dyes, consists of compounds such as fluorenone and fluorescein. Numerous organic photocatalysts are available and they have gained widespread interest due to their typically low cost. However, they don't offer the same convenient fine-tuning potential by ligand modification as metal complexes.[379]

In comparison to homogeneous catalysts, heterogeneous catalysts have the advantage of being conveniently separable and recyclable.[376] Their more specialized nature, however, makes them more difficult to access by an average lab, as they may require advanced synthesis and characterization techniques.[136] They are also (generally) more expensive and more difficult to scale up, as light penetration into the suspensions becomes increasingly problematic on larger scales.[380] Moreover, in almost all cases higher catalysts loadings are needed, and stability issues can make reuse impractical.[381] Many different types of heterogeneous photocatalysts have been developed, such as carrier materials, inorganic semiconductors, carbon nitrides, MOFs and POPs.

Heterogeneous carriers for homogeneous catalysts such as resins, PMOs and silicas can be used to immobilize transition metal complexes or organic dyes.[382] These materials are typically cheaper than the more complex materials like MOFs, amorphous POPs, and COFs. The use of such carriers normally does not change the properties of the photocatalytic moieties, making their application more conceptually straightforward. However, the support generally does not offer any advantages to the reaction and is considered a 'dead weight'. Moreover, in the case of resins, adequate swelling may require the use of specific solvents.[136] Inorganic semiconductors, such as titanium dioxide (TiO_2), are known for their affordability, stability, and safety. These materials often have wide band gaps and a fast recombination of charge carriers, requiring metal doping or dye sensitization, making their synthesis more complex.[383] Furthermore, very high catalyst loadings are required in many cases.[384] Carbon nitrides are extremely stable and inexpensive to make. Their performance in a variety of photocatalyzed transformations has been reported to be comparable to that of ruthenium photocatalysts or organic dyes.[385] The exceptional stability of carbon nitrides makes them excellent candidates for transformations involving very reactive intermediates such as alkyl radicals. It is important to note that these materials possess limited porosity and also require high catalyst loadings.[385,386] MOFs exhibit excellent crystallinity, porosity, and accessibility of the active sites. However, the activity is still often lower than that of homogeneous catalysts. Additionally, the cost of producing MOFs can be high, and they frequently possess limited recycling stability.[387,388]

POPs, and especially COFs are promising materials to use as photocatalysts. The large degree of control over their structure facilitates the design of tailor made photocatalysts. The photochemical properties can be controlled, not only by selecting the chemistry of the linkers but also by controlling the geometry and even the interlayer interactions. However, POPs are often made from difficult to access building blocks, harsh conditions are used, and large-scale synthesis is usually not reported or even possible. Besides, a problem plaguing most semiconductors as photocatalysts is the rather large catalyst loading needed to efficiently catalyze a reaction, and even then, the reaction times are often very long. Moreover, the reactions themselves are frequently only done on very small scales (<1 mmol). The current generation of POPs enabled the identification of some clear 'privileged' structures such as pyrene, triazine, benzothiadiazole, etc. which are highly active. In the future other, new heterocycles could be explored with hereto underdeveloped photocatalytic applications. Next to this, to fully access the potential of these materials more information is needed on their structure-activity relationship, to enable the rational design of new photocatalysts.

Table 6: Advantages and disadvantages of commonly used classes of photocatalysts.[376–379,382,383,385–388]

	Advantages	Disadvantages
Homogeneous	- Accessible - High activity - Easy reaction setup	- Separation of catalyst needed - Hard to recycle
Metal complexes	- Large reaction scope - Easily tuned by choice of ligand/metal	- Can be very expensive - Often toxic - Metal residues in product
Organic dyes	- Generally inexpensive - Metal free	- More complicated to fine-tune
Heterogeneous	- Convenient recycling and separation	- Generally harder to access - Typically more expensive - Absolute stability needed for effective reuse - Harder to upscale - Higher catalyst loadings needed
Carriers (resins, PMOs, silicas…)	- Cheap - Easy to access - Conceptually simple	- Solvent compatibility - Carrier material itself is inactive
Inorganic semiconductors (*e.g.* TiO_2)	- Typically inexpensive, stable, safe	- Wide band gaps and fast recombination of charge carriers (can be solved by metal doping/dye sensitization) - Typically high catalyst loadings required
MOFs	- High crystallinity, very well-defined structures - High porosity, good accessibility of the active sites	- Stability (not always) - Can be expensive
Carbon nitrides	- Very good chemical stability - Cheap, simple to make	- Limited porosity
Amorphous POPs	- Typically highly porous - Less challenging to make than COFs	- Poorly defined structure - Can be expensive
COFs	- Crystalline: defined structures - Good porosity - Control over photochemical properties	- Stability (not always) - Scalability - Expensive

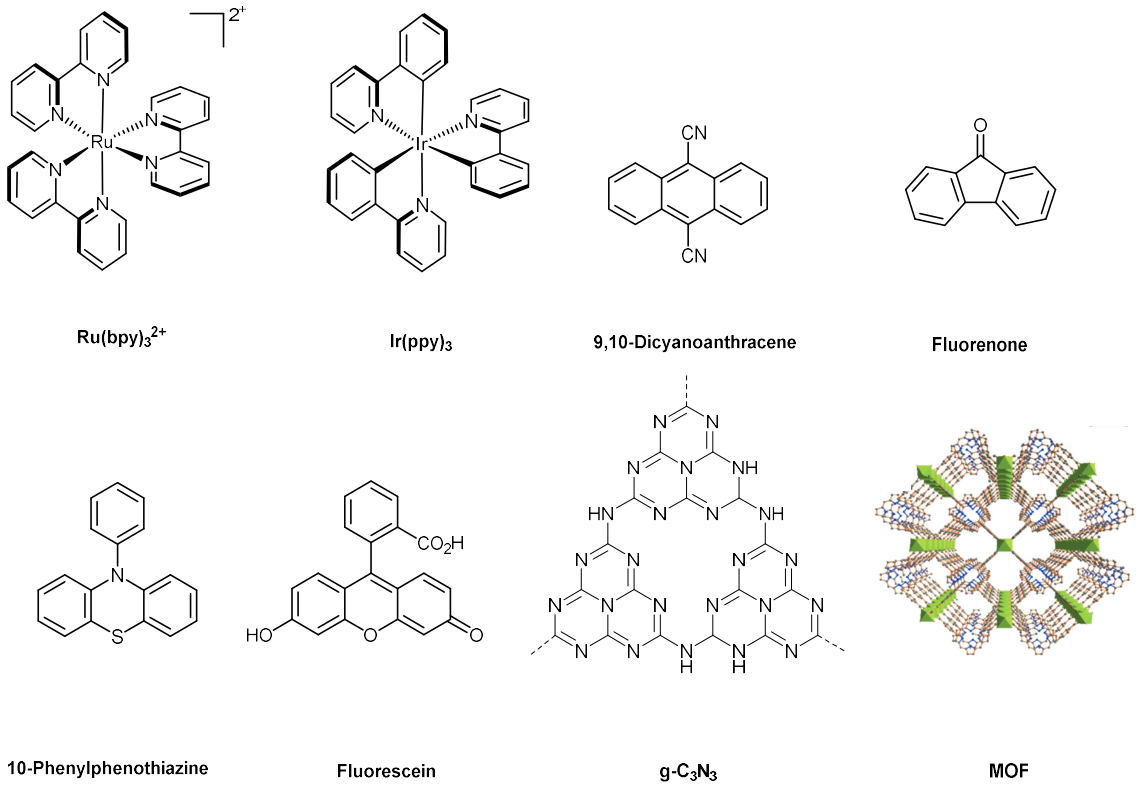

Figure 6: Some examples of the classes described in Table 6, the image of the MOF is taken from ref. [389].

1.9 Summary and perspectives

This review summarized the literature concerning metal-free porous organic polymers (POPs) as heterogeneous catalysts. POPs are a class of polymers that have attracted tremendous interest these past few years. POPs are being researched for many different applications: organic semiconductors, sensors, energy storage, proton conduction, gas adsorption and separation… and of course heterogeneous catalysis.

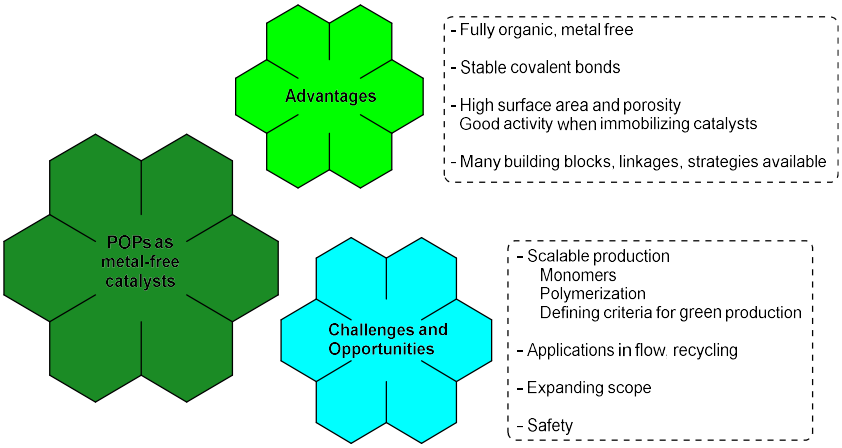

Figure 7: Advantages and future challenges applying POPs as metal-free organocatalysts.

Their attractive properties such as good stability, high surface areas and accompanying good mass transfer make POPs especially suited for catalysis and gas sorption applications. The tailorable design and functionality by the large choice of building blocks and linkages available, allows for an unprecedent control of the structure and function of these materials. A lot of research thus far has been focused on using POPs as a support for metal complexes or nanoparticles. However, when suitable building blocks or postsynthetic functionalization strategies are used, metal-free POPs can be highly effective heterogeneous catalysts. This literature review offered an in depth overview on the literature concerning POPs, including CTFs and COFs, as metal-free catalysts. The main topics covered concerned acid and base catalysis, chiral catalysis, the cycloaddition of CO_2 with epoxides and photocatalysis.

We have seen that metal-free POPs can be effective catalysts for a wide variety of transformations, forming an alternative for homogeneous catalysts and other types of heterogeneous materials. Often when immobilizing catalysts on carrier materials, such as polystyrene resins, the activity is lowered considerably, through mass transfer limitations and changes in the chemical environment. However, POPs generally possess good mass transfer, and do not require specific solvents to swell because of their permanent porosity. They also possess much finer control over the chemical environment than other carrier materials, allowing activities that are similar, and even in some cases higher than the corresponding homogeneous catalysts. Moreover, this fine control allows very advanced types of materials, combining catalytic units (*e.g.* Scheme 37) and providing an ideal chemical space for certain transformations (*e.g.* Scheme 3, 84 and 85).

Next to these advantages, many challenges remain on the way to more widespread (industrial) application, and to be able to speak of truly green or sustainable materials. In general, large-scale synthesis of the more complex materials is a big problem, especially for COFs. Expensive or

commercially unavailable monomers, toxic or expensive catalysts and the harsh conditions that are often used still form major hurdles towards large-scale applications.

Many POPs require very specific, highly functionalized, expensive or synthetically challenging building blocks. As mentioned several times in this overview many of the monomers are not commonly available and require multiple, often inefficient synthesis steps utilizing toxic and hazardous reagents, challenging the green potential of the materials themselves. For example, some of the monomers (**155** and **156**) for the discussed chiral phosphoric acid containing polymers required an up to ten step synthesis. But even more commonly used building blocks such as 5,5'-diamino-2,2'-bipyridine **282**, 2,4,6-triformylphloroglucinol **71**, 1,3,5-triformylbenzene **48** and many more require inefficient chemical synthesis using hazardous reagents. Moreover, not much effort has been made to incorporate building blocks based on renewable resources into these materials, for example, 2,5-furandicarboxaldehyde could be used to synthetize imine COFs, a further avenue for enhancing the sustainability of these materials.

The actual polymerization of the monomers into POPs is also, in many cases, not (yet) scalable or green. The synthesis of HCPs prepared through radical crosslinking is comparable to that of polystyrene resins and can be performed on larger scales, under relatively mild conditions. However, HCPs based on Friedel-Crafts crosslinking typically use DCE, a non-recommended solvent, and large excesses (up to more than ten equivalents) of corrosive Lewis acids such as $AlCl_3$ or $FeCl_3$. CMPs and PAFs are typically prepared by precious-metal based crosslinking in non-recommended solvents such as toluene, THF, DMF, Et_3N or DIPEA, etc. for several days at high temperatures.

COFs, and CTFs in particular, are in this case the biggest offenders, these are still mainly made in vacuum sealed glass ampoules placed in ovens at high temperatures (typically 120 °C for COFs) at very small scales (<100 mg). In the case of the CTFs extremely high temperatures (≥400 °C) are applied, which forms a safety hazard due to the possibility of the ampoules exploding. Moreover, these extremely high temperatures lead to carbonization of parts of the material making characterization difficult and obscuring their structure. To help solve these problems a lot of research has been done to improve the synthesis. For CTFs an alternative to the high temperature ionothermal reaction consists of superacid catalyzed trimerization at room temperature[390] or the condensation of alcohols or aldehydes with amidines in DMSO at 120 °C, with the latter method even capable of producing crystalline materials.[391,392]

Obtaining truly crystalline COFs still forms a tremendous challenge. Every new COF requires a large amount of trial and error based optimization of the reaction conditions to obtain a crystalline material, and even then the synthesis typically only works on a small scale.[393–395] Furthermore, many of the common solvents to synthetize COFs are non-recommended,[88] *e.g.* DMAc, DMF, mesitylene, 1,4-dioxane, *o*DCB, etc. Progress is being made to develop new synthetic strategies to help overcome these challenges, such as microwave or mechanochemical synthesis, linker exchange, multicomponent reaction and multistep synthesis.[395] However, a truly large-scale, green synthesis method for COFs (and most POPs in general) has not been found yet.

Similarly as with MOFs, POPs are touted as 'green materials' enabling sustainable technologies. For this to happen the availability of clean and sustainable synthesis methodologies that work on larger scales is of paramount importance. While criteria for green, sustainable and industrially-acceptable MOF synthesis have been developed,[396,397,398] for POPs this has not yet been done. These criteria include the costs and availability of raw materials, the space time yield (STY), reaction and work up (filtration-washing-drying) conditions, total cost and the safety or environmental concerns for all steps of the production process. For MOFs examples already exist of ton-scale production in a green way,

for example, Basolite A520.[397,399] For its production, DMF, the classical solvent for MOF synthesis, was replaced by water. The STY was increased by more than 500-fold, to more than 3600 kg/m^3/day and the synthesis was so easy and safe that it could be performed in a high school laboratory.[397] This does raise the hope that similar enhancements for POP synthesis could be possible, to enable the transition from the small, academic scale to the larger, industrial scale.

Next to the synthesis of the POPs another important aspect is their toxicity when handled or disposed. There is a lack of studies addressing these points. It is of course not unthinkable that porous (crystalline) powders such as POPs would form breathing hazards. The degradation of POPs in the environment is also uncharted terrain. While some, more unstable materials such as certain imine COFs, could degrade quite quickly, others such as CTFs could prove to be quite persistent.

Another important aspect is the exploration of the catalytic applications of POPs in flow chemistry. Almost all applications were reported in batch, whilst due to the insolubility of POPs they are perfectly suited for applications in flow. Continuous flow chemistry has several advantages over batch. The efficient mass and heat transfer allows a very precise temperature control over the reactor and thus avoids uncontrolled exotherms and ensures process safety. The quality of the end product is very consistent, and continuous production can lead to long term economic savings.[400,401] For this application the stability, recyclability or possibility of regeneration of the heterogeneous catalyst is extremely important. While for many of the discussed catalysts the activity was constant, even after many runs, this is not always the case. Especially in the case of the chiral POPs yields sometimes dropped dramatically. The production of these expensive heterogeneous catalysts is of course only justified if they can be recycled many times.

Furthermore, the reaction scope is still quite limited. In many papers the catalytic applications are only reported as an afterthought to probe, for example, the basicity of the material. For some transformations that are already well established with POPs, for example, Knoevenagel type reactions, CO_2 cycloadditions to epoxides, chiral amine organocatalysis, etc. it is time to move beyond these proof of concept studies into larger, scale-up studies, to truly establish these materials as an important class of catalysts for practical applications. Moreover, it is challenging to compare catalyst performance due to non-uniform reporting. The kinetics of the reactions should be studied and reported better: (initial) turnover frequencies and numbers should be determined under as uniform conditions as possible to enable clear comparisons between catalysts.

Next to this, more truly novel types of reactions should be performed with POPs. It may be time to move away from simply heterogenizing homogeneous catalysts on POPs for the increased stability and recyclability as a primary reason to investigate these catalysts. POPs can provide control of the shape and chemical environment of the pores and thus the catalytic moieties. This enables mechanisms and reactivities not possible with homogeneous catalysts and should be researched and developed further.[402] COFs especially enable truly unprecedented control of the microenvironment of fully organic extended materials. This allows for the construction of catalysts utilizing multiple substrate binding and transition state stabilizing interactions, enabling extremely efficient catalysis of new transformations.

As stated in the beginning of this literature review, efficient catalysis is essential to perform green chemistry and for the modern world in general. We have seen throughout this overview that as a class of materials metal-free POPs can have tremendous potential as heterogeneous catalysts, even though many challenges remain on the way to widespread adaptation.

1.10 Goals of this thesis

As clarified by this extensive literature review, the field of POPs has known substantial development in recent years. However, it is still in its infancy compared with other, more mature fields such as organic synthesis or 1D polymer chemistry. In this light, far more exploration of virtually any aspect concerning these materials is needed. The focal point of this thesis will be the synthesis of novel POPs and COFs as photocatalysts to catalyze organic transformations. Attention will be given to the synthesis of the building blocks, as to make these as sustainable as possible. The detailed characterization of these advanced materials is essential, and therefore we collaborated with the Centre for Ordered Materials, Organometallics and Catalysis (COMOC, Ghent University, Department of Chemistry) and the Center for Molecular Modeling (CMM, Ghent University, Department of Applied Physics).

Organic semiconductors, such as POPs and COFs, act as photocatalysts by absorption of light with an energy equal to, or greater than the band gap. This leads to charge separation to photogenerated holes and electrons, which can then participate in redox reactions. POPs can be tailor made for specific transformations, by careful design of their building blocks and linkages, to result in frameworks with ideal energy levels for a given transformation. However, no clear structure-activity relationships can be drawn yet, because of the limited number of detailed studies on the effects of small structural variations on the band gap and photocatalytic activity of these materials.

In the first part of this thesis the primary aim is the synthesis of isostructural frameworks. This allows us to study the effect of small variations in the linkage and linkers on the band gap and photocatalytic activity, to offer more insight in this important field. A range of COFs will be made using phenyl, phenylpyridine and bipyridine based linkers and different linkages such as vinylene, imine, β-ketoenamine or hydrazone (Scheme 166). These materials will then be used to catalyze oxidation reactions, starting with the oxidation of benzylamine **649** as a well-known test reaction. However, as stated in the conclusion to this literature review, there is already an overload of materials that catalyze the same, basic transformations. Therefore the focus will lie on the development of a more advanced reaction, where the oxidation is coupled to a cyclization reaction, and further oxidation to finally produce quinolines **652** (Scheme 166). This tandem oxidation/Povarov reaction has been reported using a ruthenium bipyridine complex as a photocatalyst.[403] This has disadvantages considering the high price of ruthenium, its toxicity and the difficulty of completely removing the catalyst. The development of a heterogeneous, metal-free photocatalyst for this transformation is therefore considered highly desirable.

Alongside this first major part, in a second part the photocatalytic applications of amorphous POPs will be explored. Whilst these POPs do not have the well-defined structure of COFs, they are generally easier to make and can be made on larger scales as well. However, as described in the literature review, most photoactive amorphous POPs are made by (precious) metal-catalyzed couplings of highly functionalized and difficult to access building blocks. A class of materials that are not constructed by metal based cross-couplings is that of the covalent triazine frameworks (CTFs), but still their synthesis is problematic. These materials are typically made by trimerization of nitriles at extremely high temperatures in molten $ZnCl_2$, resulting in partially degraded black powders, which are unsuitable for photocatalysis. The superacid catalyzed trimerization does give materials applicable for photocatalysis, but this method is not compatible with many building blocks, moreover, this requires the use of very corrosive chemicals such as triflic acid. CTF synthesis by the condensation of amidines and aldehydes has also attracted interest,[267] however, this still requires functionalized building blocks,

that are much less accessible than simple aromatics. Recently, a Friedel-Crafts alkylation based approach to CTFs was reported.[404] This new, mild, Lewis acid catalyzed synthesis should give suitable materials for photocatalysis, however, this application has not yet been reported. Moreover, in this method unfunctionalized aromatics are the building blocks, which are widely available, compared with the aromatic nitriles needed for the conventional CTF synthesis.

Using this method, electron rich aromatics **660-664** can be combined with the electron deficient triazine cores, which should give rise to potent photocatalysts. These materials will be used as catalysts for aromatization reactions of *N*-heterocycles such as dihydropyridines **656** and pyrazolines **657**, allowing for convenient access to pyridines **658** and pyrazines **659**, which are important aromatic moieties (Scheme 167). In literature stoichiometric oxidants (*e.g.* MnO_2, SeO_2, IBX, etc.[405]) are typically used for these transformations, which is much less desirable from a green chemistry perspective. The development of efficient, heterogeneous organic photocatalysts working at room temperature, using air as the oxidant, would be a significant step forwards for these important reactions.

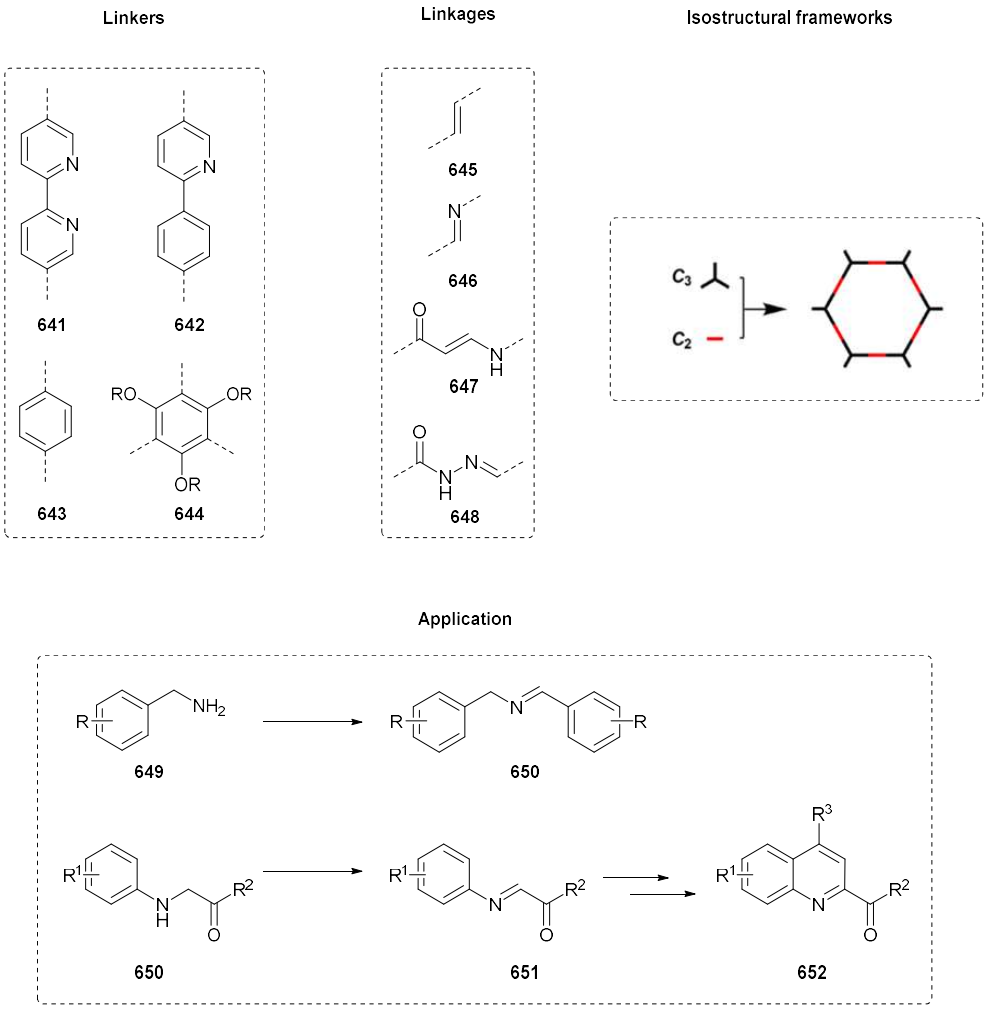

Scheme 166: Goals of the first major part of this thesis. The experimental work of this PhD thesis will focus in first instance on the synthesis of several isostructural COFs, using different (hetero)aromatics (phenyl, phenylpyridine, bipyridine) and linkages (vinylene, imine, β-ketoenamine, hydrazone). The photochemical properties of these similar materials will then be determined and compared. A first catalytic application that will be developed is the benzylamine oxidation, which is already well known. Then a similar reaction was envisaged by the oxidation of a glycine derivative **650**, to the corresponding imine **651**, which can undergo cycloaddition reactions and further oxidation to finally produce quinolines **652**.

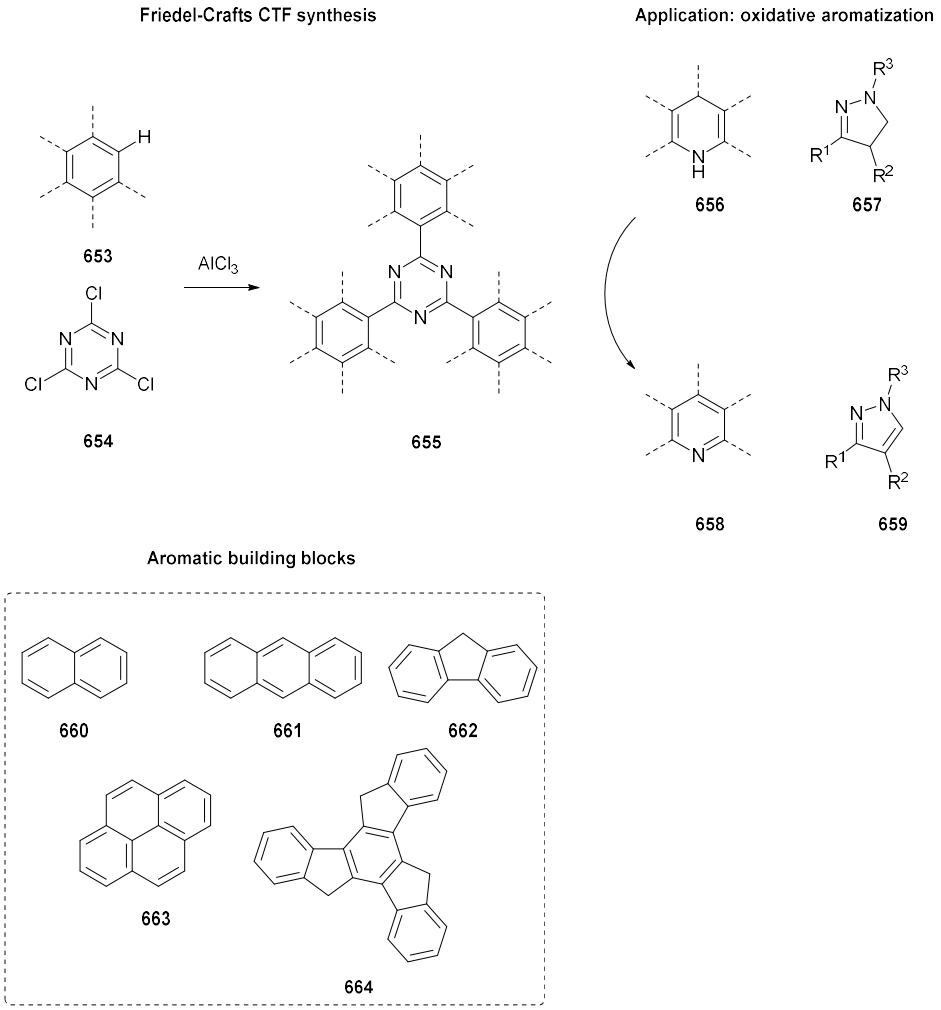

Scheme 167: Goals of the second major part of this thesis. Novel photoactive CTFs will be synthesized by the underexplored $AlCl_3$ catalyzed CTF synthesis. These materials will be used as photocatalysts for the aromatization of *N*-heterocycles such as dihydropyridines **656** and pyrazolines **657**.

The final objective of this PhD was the development of NHC-containing COFs, as these are important ligands for the coordination of metal complexes, and potent organocatalysts in their own right. Despite their great importance, NHC-containing COFs are severely underdeveloped. The imidazolium derivative **665** will therefore be synthesized, as a building block towards new imine- or β-ketoenamine-linked frameworks. Upon incorporation in a COF and deprotonation, these moieties can act as metal-free organocatalysts or as ligands to heterogenize transition metal complexes (Scheme 168).

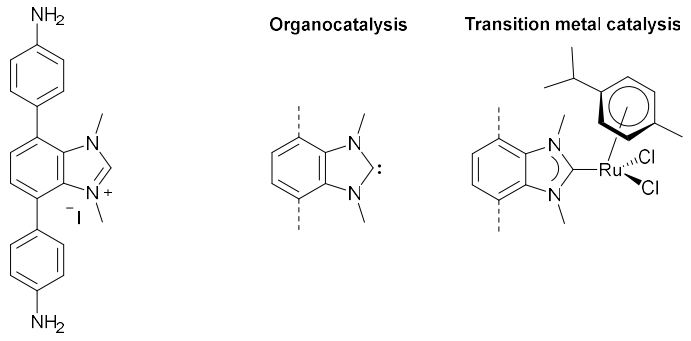

665 666 667

Figure 168: The last goal of this thesis was the development of new NHC-based COFs. Building block **665** will be synthesized and incorporated into COFs. This will be applied as an organocatalyst, or as a heterogeneous ligand to complex with metals such as ruthenium.

Overall, the work in this thesis should offer advances in the use of heterogeneous, porous organic materials as photocatalysts. On the one hand more insight will be gained in the structure-activity relationship of photo-active COFs. Next to this, an underexplored class of materials will be applied as photocatalysts. New applications for POPs as photocatalysts, predominantly as catalysts for oxidation reactions will be developed. All of this will hopefully contribute towards greener catalysts and chemical processes in the future, which are essential for a more sustainable chemical industry.

Chapter 2: Development of COFs as heterogeneous photocatalysts.

Manuscript in preparation: **Engineering of phenylpyridine- and bipyridine-based covalent organic frameworks for the photocatalytic tandem aerobic oxidation/Povarov cyclization.** M. Debruyne, S. Borgmans, J. De Vos, K. Sing Rawat, A. Laemont, H. Salemi, J. Everaert, F. Vanden Bussche, H. Vrielinck, K. Leus, R. Morent, N. De Geyter, D. Poelman, P. Van Der Voort, V. Van Speybroeck, C. V. Stevens.

Abstract: Covalent organic frameworks (COFs) are emerging as a new class of photoactive organic semiconductors, which possess crystalline ordered structures and high surface areas. COFs can be tailor-made towards specific (photocatalytic) applications and the size and position of their band gaps can be tuned by the choice of building blocks and linkages. However, to do this predictably it is essential to obtain more information about the relationship between the structure of the COF and the photocatalytic properties. Next to this, the scope of reactions that are reported to be photocatalyzed by COFs is still quite limited. We report the synthesis of three structurally similar bipyridine- or phenylpyridine-based COFs: **TpBpyCOF**, **TpOMeBpyCOF** and **TpPpyCOF**. The substitution of a nitrogen atom in bipyridine to a carbon in phenylpyridine led to a larger band gap, whilst replacing the hydroxyls with methoxy groups led to an imine-linked framework with a smaller band gap compared to its β-ketoenamine-linked analogue. Due to their good photocatalytic properties the materials could be applied as metal-free photocatalysts for the tandem aerobic oxidation/Povarov cyclization and α-oxidation of *N*-aryl glycine derivatives, with **TpBpyCOF**, possessing both bipyridine units and β-ketoenamine linkages possessing the highest activity. These results shed light on the design of COFs for photocatalytic applications and help pave the way towards the application of COFs as metal-free heterogeneous photocatalysts, as a convenient alternative for the commonly used homogeneous photocatalysts.

Contributions: All computational results were performed by S. Borgmans, J. De Vos and K. S. Rawat at the Center for Molecular Modeling (UGent, Department of Applied Physics). A. Laemont performed the CV measurements. F. Vanden Bussche, H. Salemi and J. Everaert helped with some experiments and BET and XRD analysis. K. Leus, R. Morent and N. De Geyter performed XPS and SEM measurements. Solid state UV-Vis measurements were performed under guidance of D. Poelman. EPR measurements were conducted with help from H. Vrielinck.

2.1 Goals and Scope

A booming world population and economy puts an ever-increasing pressure on the environment. Together with growing concerns about pollution, global warming, and the finite supply of fossil resources, this has led to the development of many different green technologies. One promising avenue is visible light photocatalysis, which utilizes the energy of visible light and converts it into chemical energy for organic reactions through a catalyst.[406–409] Based on whether the photocatalyst and the reactants exist in the same phase or not, it is classified as a homogeneous or heterogeneous photocatalyst, respectively. Typical examples of the former include metal complexes (mainly ruthenium and iridium complexes)[410,411] and organic dyes (fluorenone, acridinium-based photocatalysts, xanthene dyes, etc.),[412–415] whereas the latter category mainly contains inorganic semiconductors (TiO_2, CdSe, WO_3, ZnS, ZnO, etc.).[416–420] However, homogeneous catalysts, and especially the precious metal-based ones, have drawbacks such as high costs, difficult separation from the product, and low or no recyclability.

In recent years, new, heterogeneous, polymer-based photocatalysts such as graphitic carbon nitride (g-C_3N_4),[421,422] metal organic frameworks (MOFs),[423,424] and porous organic polymers (POPs)[407] have emerged to help eliminate these aforementioned deficiencies. Covalent organic frameworks (COFs) are a subclass of POPs, and like POPs, they are constructed completely from organic building blocks. Their defining characteristic is their long-range order and accompanying crystallinity. Due to their low weight, high specific surface area, and modular design they have found application in diverse fields, such as gas sorption and separation,[425,426] energy storage,[427,428] sensing[429–431] and heterogeneous catalysis.[323,432–434] COFs hold a lot of promise as heterogeneous photocatalysts, with great recyclability due to their insolubility. Their extended π-conjugated frameworks, regular pore structures, and high surface areas are beneficial for obtaining high photocatalytic activities due to the good light absorbing capacity and high accessibility of their active sites.[435–437] Despite these advantages and the great amount of research currently being done on COFs as photocatalysts, the scope of reactions that are catalyzed by photoactive COFs is still quite limited. Moreover, due to their tailor-made character the optical properties and photocatalytic efficiency can be easily adjusted by the choice of building blocks.[438–440] However, to do this rationally, more information towards this structure-activity relationship is needed. Therefore, the synthesis of isostructural frameworks was envisaged to allow the study of the effect of small structural changes on the photocatalytic properties of COFs.

In this chapter the synthesis of three isostructural bipyridine- or phenylpyridine-based COFs: **TpBpyCOF**, **TpOMeBpyCOF** and **TpPpyCOF** and their application as photocatalysts is described. Through the use of structurally similar amines (**Bpy** and **Ppy**) and aldehydes (**Tp** and **TpOMe**) the size and position of the band gap and the photocatalytic activity could be tailored. Substitution of a nitrogen atom in bipyridine to a carbon in phenylpyridine led to a larger band gap, whilst replacing the hydroxyls with methoxy groups led to a smaller band gap. To evaluate their efficacy as photocatalysts, these materials were applied in the COF-catalyzed photocatalytic aerobic oxidation/Povarov cyclization and the α-oxidation of *N*-aryl glycine derivatives, broadening the scope of COF-catalyzed photocatalytic reactions. These COFs were also applied as photocatalysts for benzylamine oxidations. Next to these successful results, the synthesis of other linkers and COFs was also attempted, which will be described in less detail. Moreover, a ruthenium complex was also anchored on **TpBpyCOF**, by bottom-up synthesis, to produce **Ru@TpBpyCOF** and this was used for the intermolecular aerobic oxidation/Povarov cyclization.

2.2 A brief introduction to COFs

2.2.1 Historical perspective

Covalent organic frameworks (COFs) are very important members of the class of porous (organic) materials. They can be viewed as the fully organic analogues of metal organic frameworks (MOFs), and consist of organic building blocks stitched together with strong covalent bonds to form crystalline structures. These materials are the pinnacle of organic material chemistry, as they allow precise control of the chemical architecture of extended 3D structures. In this part a short backstory is given to frame these extraordinary materials in their historical perspective (Figure 1).

In 1916, Lewis published 'The atom and the molecule', introducing the bonding of atoms in molecules through covalent bonds.[441] From there on, organic chemists developed methodologies for covalent molecular chemistry, leading to the development of total synthesis. Since its humble start with the total synthesis of urea, massive strides were made, and by the second half of the 20th century this science had already matured. In 1972 the art of organic synthesis to produce highly complex and intricate molecules was famously illustrated by the total synthesis of vitamin B12 by Woodward and Eschenmoser.[442] Similarly, polymer science, starting with Staudinger's 'Über Polymerisation'[443] in 1920, had quickly developed into a mature field with great importance. Whilst ever more intricate molecules could be made, getting molecules to organize themselves into more complex, extended, ordered systems was still uncharted territory. Even by the 1990s no ordered, extended organic 2D or 3D structures had been reported, which was keenly observed by Roald Hoffman in 1993: ''*Organic chemists are masterful at exercising control in zero dimensions. One subculture of organic chemists has learned to exercise control in one dimension. These are polymer chemists, the chain builders (…) But in two or three dimensions, it's a synthetic wasteland. The methodology for exercising control so that one can make unstable but persistent extended structures on demand is nearly absent*''.[444]

Nevertheless, developments in supramolecular chemistry had led to the production of sophisticated architectures such as crown ethers[445] and cryptands.[446] Furthermore, shape persistent cages were synthesized as permanently porous, fully organic materials.[447] This supramolecular chemistry was based on non-covalent interactions, which allow reversibility in the reaction, and thus thermodynamic control and error-correction. The used interactions, however, were weak and therefore extended structures were unstable. Error-correction over stronger, covalent bonds was finally realized with the advent of dynamic covalent chemistry (DCC).[448] This led to the synthesis of highly complex structures such as catenanes[449] and molecular Borromean rings.[450]

Building on these developments, reticular chemistry arose, which is defined as the chemistry of linking molecular building blocks by strong bonds, to make crystalline extended structures.[451] The stronger the bonds, the harder it is to achieve crystalline materials, as error-correction becomes progressively more difficult. However, only strong bonds lead to stable materials, which is essential for real-world applications. The first example of such a material was reported in 1995 by Yaghi, who coined the term metal organic framework (MOF) for the materials formed by coordination of charged organic linkers with metal ions or clusters.[452] Yaghi then took this one step further, by the synthesis of the first 2D and 3D COFs in 2005[25] and 2007.[26] This finally took the idea of Lewis beyond the molecule and into the framework, as a COF is a collection of molecules in a certain connectivity, geometry, and spatial arrangement, just as molecules are collections of atoms in a certain arrangement, which is illustrated in Scheme 1.[453]

Following this seminal work, the research in this area has increased dramatically. Other major important achievements were the synthesis of COFs with sufficient crystallinity to fully solve the crystal structure. Yaghi *et al.* reported the synthesis of COF-320 with crystals of up to 200 nm in size which were solved using Rotation Electron Diffraction (RED)[454] and Wuest *et al.* obtained 3D COFs as large crystals, that were visible to the naked eye, and whose crystal structure could be solved via Single Crystal X-Ray Diffraction (SXRD).[455]

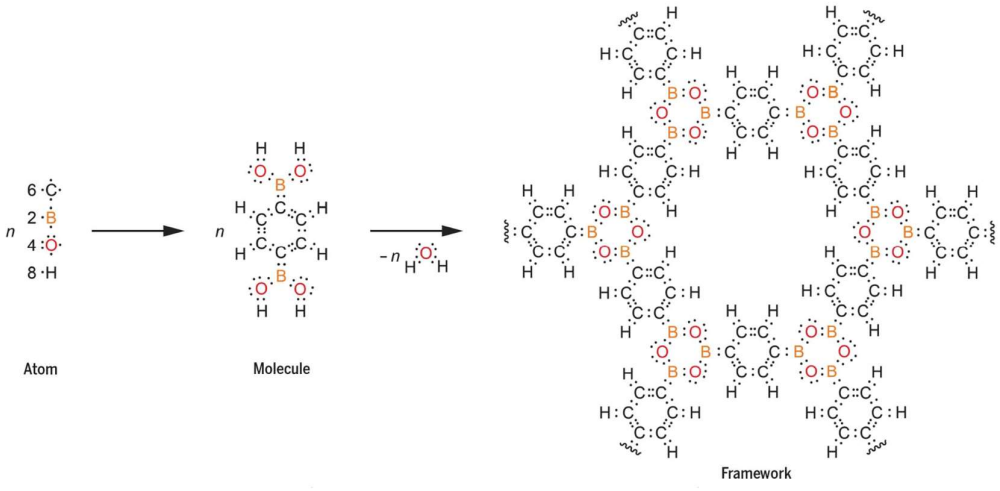

Scheme 1: 'The atom, the molecule and the covalent organic framework'. Reproduced from ref. [453].

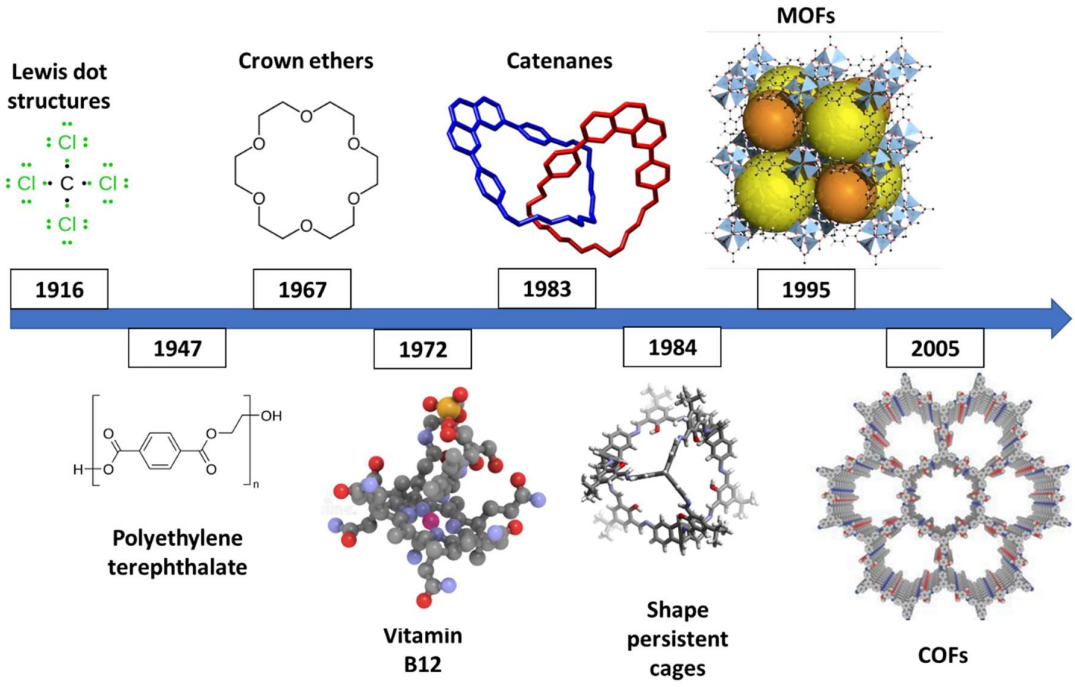

Figure 1: Milestones in COF history.

2.2.2 Linkages and linkers

Much further effort has gone into identifying new suitable reactions for the synthesis of COFs (Scheme 2). For every new reaction type suitable conditions have to be developed, ensuring the formation of crystalline materials. The reaction needs to be sufficiently reversible, so that self-correction of defects is possible. Without this high degree of reversibility and the related error-correction no ordered structures, but only amorphous polymers, will be obtained.

The first types of linkages were boron based, either via the self-condensation of boronic acids **1** or the condensation of boronic acids **1** with catechols **3** forming boroxine rings or boronate linkages, respectively.[25] Later on spiroborate[456] and borosilicate[457] linkages were also developed. These boron-based materials do have the disadvantage of being generally unstable to air/water. A second major type are the CTFs (covalent triazine frameworks), which are COFs linked through triazine rings. CTFs are typically formed through cyclotrimerization of nitriles **29** in $ZnCl_2$ at high temperatures (>400 °C).[29] Crystalline CTFs have also been reported by the condensation of amidines **30** with alcohols or aldehydes **11**.[391,392] A third major type of COFs are the imine-linked COFs,[458] and all the related linkages such as urea,[459] hydrazone,[460] squaraine,[461] azine,[462] phenazine,[463] benzoxazole,[464,465] benzimidazole,[466] benzothiazole,[467] β-ketoenamine[468], etc. In more recent years the development of C=C linked COFs has received considerable attention because of the high stability and good photochemical properties this linkage can provide. These C=C linked materials have been made by Knoevenagel condensations,[469,470] Horner-Waddsworth-Emmons[471] or Wittig reactions[472] and aldol like reactions with heterocycles such as trimethyltriazine **34**,[473,474] trimethyldicyanopyridine **36**,[475,476] trimethyltricyanobenzene **37**,[477] and dimethylpyrazine **38**.[473,474] Even more structural diversity is possible by the postmodification of COFs. The double bond of imines or alkenes can be reduced to give amine- and alkyl-linked COFs, the Povarov cyclization of imines results in quinoline-linked COFs, the oxidation of imines gives amides, etc.[478]

Besides the linkage type, the size, symmetry and geometry of the building blocks is important, as it will determine the topology of the framework. A representative overview of possible building block geometries and resulting topologies for 2D COFs is given in Figure 2. In this work the COFs were made through condensation of tritopic (C_3) and ditopic (C_2) building blocks, leading to COFs with a hexagonal (honeycomb, hcb) topology.

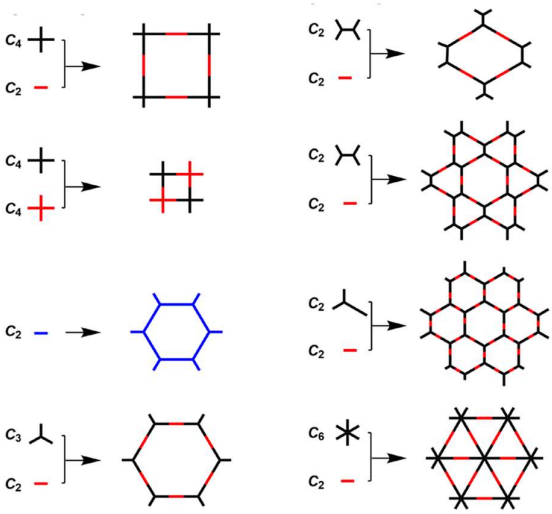

Figure 2: The relation between the symmetry and connectivity of the building blocks and the topology of the resulting (2D) COF. Reproduced from ref. [479].

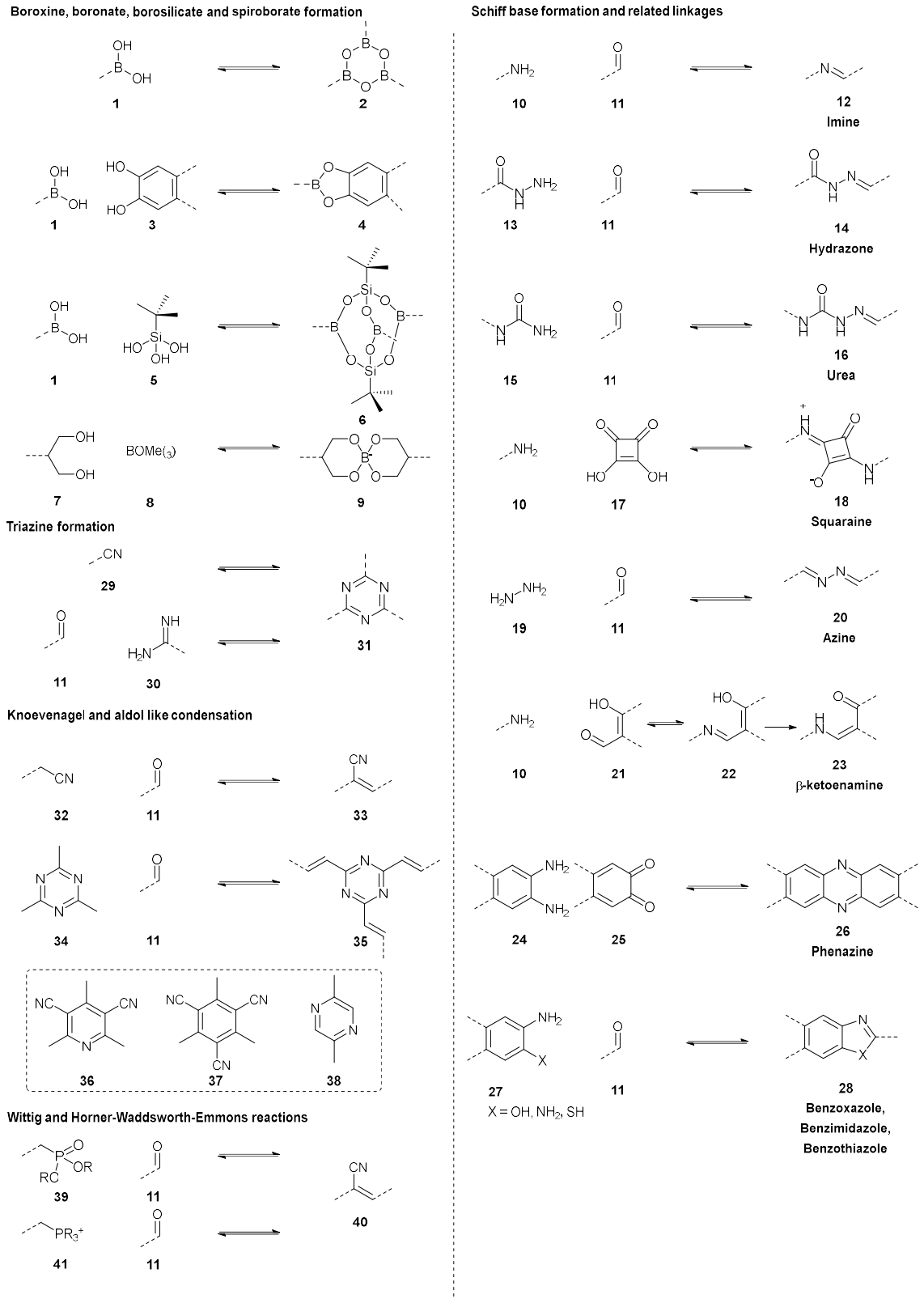

Scheme 2: Overview of the linkages that are commonly used in COF synthesis.

2.2.3 Characterization of COFs

As stated before, COFs are crystalline, porous, organic polymers that are completely insoluble in all common solvents. That is why typical characterization techniques used by organic (polymer) chemists, such as mass spectrometry (MS) or solution state nuclear magnetic resonance (NMR) cannot be used to analyze COFs. However, due to their crystallinity it is possible to obtain (powder) X-ray diffraction (XRD) spectra, which in conjunction with computational techniques can unambiguously define the atomic arrangement of these materials, a feat not possible with conventional polymers or amorphous POPs.[480] Next to XRD, other characterization techniques that are routinely used are Fourier transformed infrared (FTIR), solid state NMR, X-ray photoelectron spectroscopy (XPS), nitrogen or argon sorption and microscopy techniques. FTIR provides a convenient measurement to analyze the functional groups present in the materials. Using FTIR the completion of a COF-formation reaction can quickly be assessed, by analyzing the presence of typical functional groups (*e.g.* the presence of an aldehyde when making imine COFs). Using XPS the surface of materials can be analyzed to detect the elements present, and their chemical state. Solid state NMR is another powerful characterization technique, providing information on the chemical environments of the carbon and hydrogen atoms in the framework. Lastly, with nitrogen or argon sorption the porosity of the materials can be characterized, with the latter being especially useful in the case of microporous materials. Using sorption isotherms the surface areas of the materials can be calculated. Moreover, in conjunction with density-functional theory (DFT) calculations the pore size distributions can be derived from these isotherms, giving more information on the structure of the materials. Lastly, a range of optical techniques such as scanning electron microscopy (SEM) and transmission electron microscopy (TEM) can be used to characterize the morphology of the material.

Regarding the optical and photochemical properties of the materials, generally (and in this work) the optical band gaps are determined by diffuse reflectance UV-Vis spectroscopy. First the reflectance data is transformed, using the Kubelka-Munk function, to obtain the absorption spectra of these materials. The intersection of the linear part of the related Tauc plots with the x-axis then provides the optical band gap.[481] The use of (chopped light) cyclic voltammetry allows the indirect measurement of the energy level of conduction band, which in conjunction with the band gap allows for the full estimation of the band structure of the materials. Other techniques such as ultraviolet photoemission spectroscopy (UPS)[482] or valence band X-ray photoelectron spectroscopy[483] can be used to measure the electronic band structure directly, but were not applied in this work.

Other than the energy levels themselves, for efficient photocatalysts it is essential that the photogenerated charges have sufficient migration, separation and lifetime so that reactions can actually happen. To investigate charge carrier mobility time-resolved spectroscopic techniques can be used, such as laser-flash photolysis time-resolved microwave conductivity (FP-TRMC)[484] or femtosecond transient absorption (FS-TA) spectroscopy.[485] As these techniques are not routinely used, they were not applied in this work, and are therefore only mentioned briefly. Lastly, photoluminescence spectroscopy allows for an indication of the rate of charge recombination, as a higher rate of charge recombination results in a higher emission intensity.[485]

2.3 Results and discussion

2.3.1 Synthesis of building blocks for COFs

The objective of this chapter was the synthesis of isostructural frameworks, to examine how slight changes in linkages and linkers affect the band gap and photocatalytic activity, offering insights into this critical area of research. As the materials were to be used as recyclable photocatalysts, they should feature motifs conferring photocatalytic activity and exhibit high stability. A wide range of linkers was selected to produce photoactive COFs (Figure 3). Existing procedures towards these compounds have shortcomings, as discussed in the literature review. Often metal-based couplings with very high catalyst loadings, or oxidations using extremely undesirable reagents such as PCC are applied. Therefore, significant efforts were expended to make the synthesis of some linkers more green or scalable. Ultimately, the synthesis of **Ppy** could be remarkedly improved compared with published procedures, in the other cases literature routes were still found to be the most effective. Of the synthesized linkers **Ppy**, **Bpy**, **45**, **Tp** and **TpOMe** were successfully incorporated in COFs, resulting in **TpBpyCOF**, **TpOMeBpyCOF**, **TpPpyCOF** and **TpPa-1**.

The bipyridine and phenylpyridine linkers were selected for two reasons. Most importantly, nitrogen-rich moieties, when incorporated in extended frameworks, are known to confer significant photocatalytic activity. Whilst nitrogen-rich motifs such as triazines, porphyrins and benzothiadiazoles have been applied extensively in metal-free heterogeneous photocatalysts, bipyridines and phenylpyridines have not been explored in this way. Next to this, these moieties could serve as complexing agents for (iridium and ruthenium) metal complexes, to enhance the photocatalytic activity.

The condensation of bipyridine- and phenylpyridine-based amines **Bpy** and **Ppy** with the aldehyde **TpOMe** was envisioned, to produce exceptionally stable imine-linked materials, as the methoxy groups sterically shield the imine linkage from hydrolysis and provide stronger interlayer interactions.[486] Condensation of the amines **Bpy** and **Ppy** with **Tp** produces β-ketoenamine-linked frameworks, which are known for their high stability.[487] Ketoenamine **46** was synthesized as an alternative entry to β-ketoenamine-linked frameworks. Hydrazide **42** was selected, as upon condensation with aldehydes such as **Tp** or **TpOMe** it provides hydrazone-linked COFs, which are also highly stable.[488] The bisphosphonate **43** and the dicyano linker **44** were synthesized as building blocks for C=C linked COFs. Compared to imine-linked frameworks, these olefin-linked materials exhibit higher stability and photocatalytic activity, courtesy of their hydrolytically stable and unpolarized bond.[330] Finally, benzophenone-protected 1,4-diaminobenzene **45** was synthesized, to evaluate a nitrogen-poor linker, and to assess the effectiveness of the benzophenone-protected synthesis method, which has been reported as suitable for the large-scale synthesis of COFs.[489]

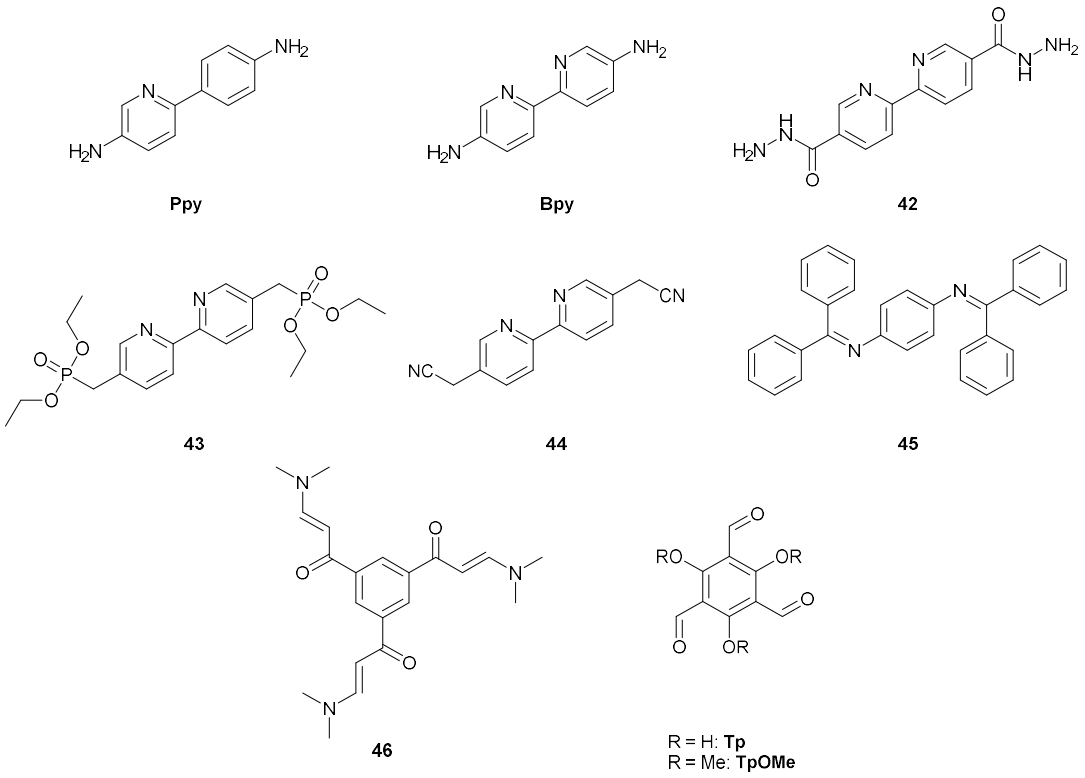

Figure 3: Overview of the synthesized linkers to produce photoactive COFs.

2.3.1.1 The synthesis of 6-(4-aminophenyl)pyridin-3-amine Ppy

Two synthesis routes were already described in literature for the synthesis of **Ppy**. One was based on the benzidine rearrangement, by reduction of diazo compound **50**, and the other route consisted of the reduction of 5-nitro-2-(4-nitrophenyl)pyridine **57**.[490,491,492] To evaluate the benzidine rearrangement the diazo compound **50** was first synthesized by the condensation of pyridin-3-amine **48** with nitrosobenzene **47**. Two main products were hereby formed, which were separated using reversed phase chromatography. This resulted in the isolation of the desired diazo compound **50** and a side product **49** in 36% and 12% yield, respectively. In the next step, the reduction and rearrangement of diazo compound **50**, a difficult to purify crude mixture, containing traces of the desired product **Ppy** with unidentified impurities was obtained. Using a lower amount of acid and reducing agent the intermediary 3-(2-phenylhydrazineyl)pyridine **51** could be isolated. The rearrangement of this compound to the desired **Ppy** was also undertaken, but again a complex and difficult to purify mixture was obtained.

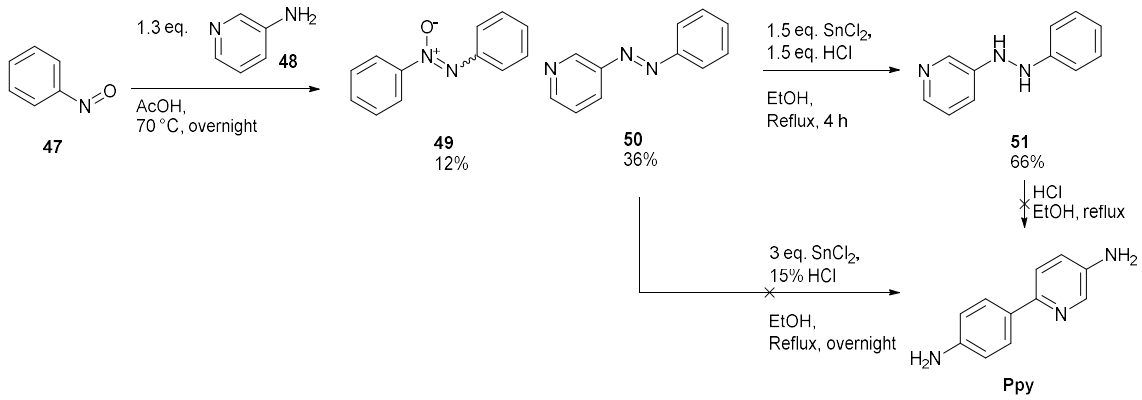

Scheme 3: Attemted synthesis of **Ppy** by reduction and benzidine rearangement of diazocompound **50**.

The other described route to this compound goes via the reduction of the corresponding nitro compound **57**, whose literature synthesis is shown in Scheme 4. Schiff base formation between dimethoxy acetal protected malondialdehyde **52**, followed by nitration gives compound **55**, which then undergoes cyclization with 4-nitroacetophenone **56** to produce 5-nitro-2-(4-nitrophenyl)pyridine **57**.[491,492] To avoid this long synthesis using hazardous reagents, a Suzuki coupling was used in this work to synthesize dinitro compound **57**. Using 1.1 equivalent of the nitro substituted pinacol ester **59**, 1 equivalent of the aryl bromide **58** and $Pd(PPh)_4$ as the catalyst, the resulting cross-coupled product **57** could be isolated in 63% yield after reversed phase chromatography. This was then reduced using hydrazine hydrate and palladium on carbon to give **Ppy**. To obtain a 100% pure product for the COF synthesis, the crude reaction mixture was further purified using reversed phase chromatography to obtain **Ppy** in 71% yield (Scheme 5).

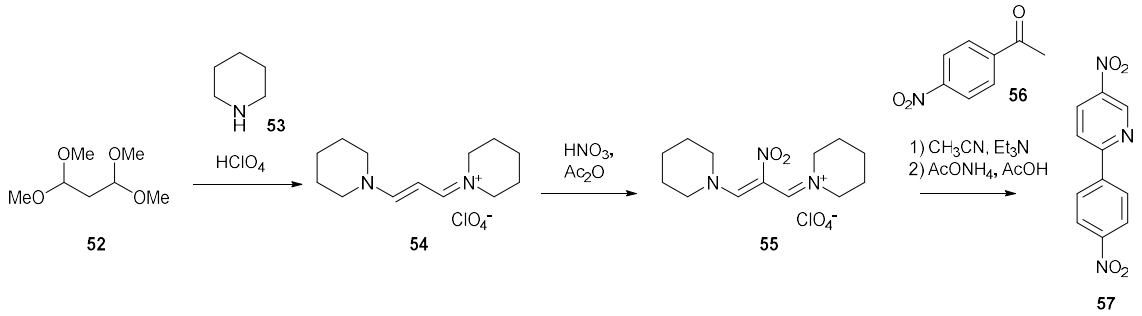

Scheme 4: Literature route towards 5-nitro-2-(4-nitrophenyl)pyridine **57**.[491,492]

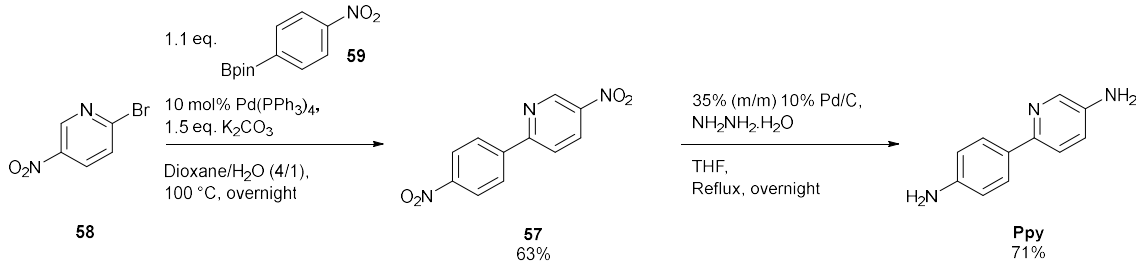

Scheme 5: Synthesis of **Ppy** by Suzuki coupling and reduction.

2.3.1.2 The synthesis of 2,2'-bipyridine-5,5'-diamine **Bpy**

Bpy is an important building block for the synthesis of functional materials. The synthesis that is generally used in literature is shown in Scheme 6 and was developed by Albrecht *et al.* in 2005.[493] In this route the nitrogen of 6-chloropyridin-3-amine **60a** is first protected as a dimethylpyrrole group using a Paal-Knorr synthesis. This can then be homocoupled using $NiBr_2(PPh_3)_2$, NEt_4I and zinc, resulting in the dimethylpyrrole protected **Bpy**, which is finally deprotected using hydroxylamine.

As stated in the literature review, the use of building blocks synthesized through unsustainable methods is a major factor preventing the application of POPs on larger, industrial scales. As this method required the use of the difficult to remove dimethylpyrrole protecting group, and the use of high catalyst loadings and stoichiometric reagents in the coupling step, other routes were also evaluated. The nickel catalyzed homocoupling was therefore tested using more easily cleaved protecting groups and using the free amine. Next to this, Pd-catalyzed couplings and the reduction and rearrangement of diazo compounds were also tried. However, the only route that was found reliable was the one reported by Albrecht *et al.*, and this was applied to produce the **Bpy** used during this project.

2.3.1.2.1 The synthesis of Bpy using the method described by Albrecht *et al.*

This route was evaluated using both the chloro- and bromo-substituted pyridines. In the first step, the Paal-Knorr synthesis, the resulting pyrrole protected amines could easily be made in high yields. The nickel catalyzed coupling itself gave yields ranging from 54% to 75%. It was found that activating the zinc powder prior to using it, by washing with HCl, was essential to obtain reliable results. The purification of the coupled product **63** using the reported purification, *i.e.* column chromatography in ethyl acetate/hexanes, proved quite challenging. The product had only a very limited solubility in this solvent system, resulting in tailing and a very tedious separation. This could be solved by using a CH_2Cl_2/hexanes system, in which the product was much more soluble. The third step, deprotection, also proved to be sensitive. On larger scales very long reaction times and the repeated addition of extra equivalents of hydroxylamine and triethylamine were needed. However, using this method **Bpy** could be reliably obtained on relatively large scales (~1 g).

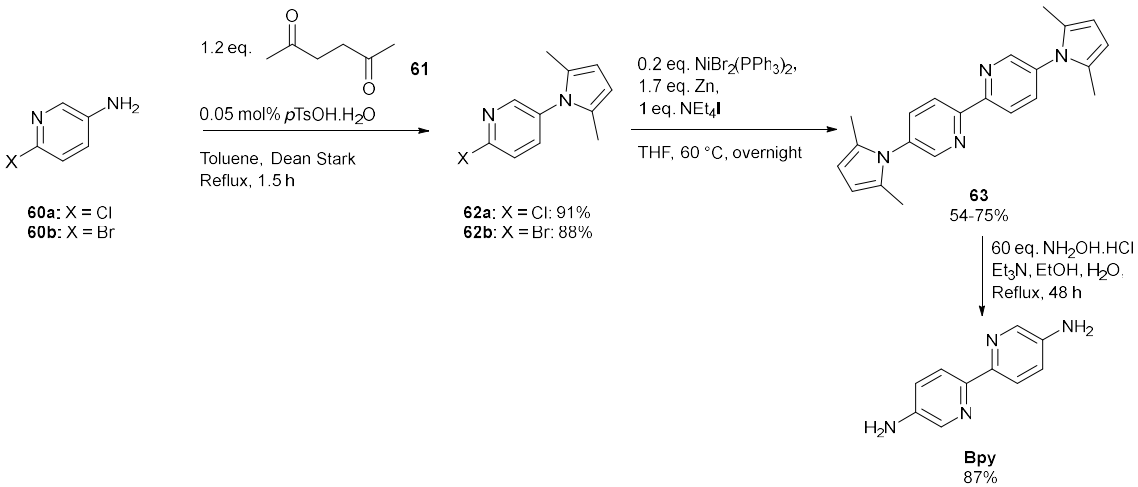

Scheme 6: Synthesis of **Bpy** using the method developed by Albrecht *et al.*, consisting of dimethylpyrrole protection, homocoupling and deprotection.

2.3.1.2.2 Attempted synthesis of Bpy by nickel catalyzed homocoupling using other protecting groups

The difficulty in using the dimethylpyrrole protecting group lies in its deprotection, requiring large excesses of toxic and corrosive hydroxylamine. Therefore, the same conditions, using $NiBr_2(PPh_3)_2$, zinc and NEt_4I were used with other, more easily cleaved, protecting groups. The synthesis of **Bpy** using the benzaldehyde imine (benzylidene) protecting group was reported by the Breslow group.[494] However, this protecting group gave no appreciable coupling for both the chloro- and bromopyridine **64a-b**. It was hypothesized that the more stable benzophenone imine could offer better results, but this also gave no product for both the aryl chloride **65a** and bromide **65b**. Finally, acetamide and trifluoroacetamide protecting groups were evaluated, as they provide easy protection and deprotection, however the coupling was also unsuccessful for these substrates **66-67** (Scheme 7).

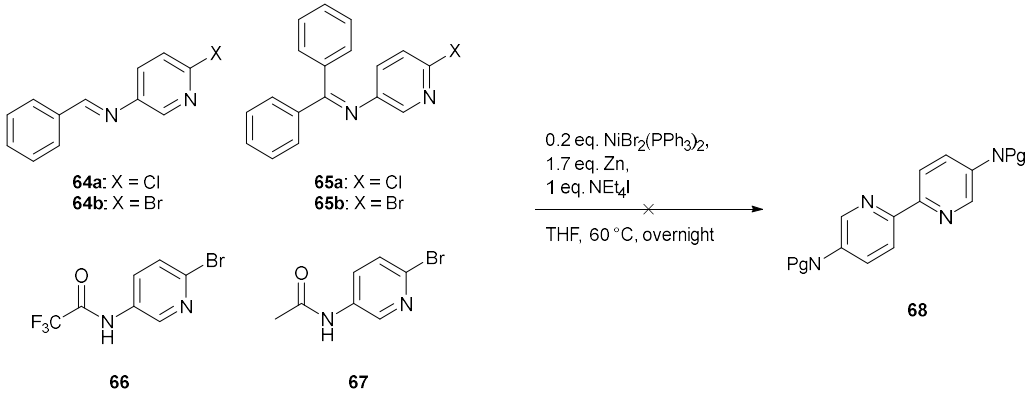

Scheme 7: Attempted nickel catalyzed reductive homocouplings using different protecting groups.

2.3.1.2.3 Attempted synthesis of Bpy by ligand-free nickel catalyzed homocoupling

In 2014 Liao *et al.* reported a ligand-free nickel catalyzed reductive coupling of 2-halopyridines using $NiCl_2.6H_2O$. This reaction has been successfully applied in our lab to synthesize [2,2'-bipyridine]-5,5'-dicarbonitrile, an important building block for bipyridine CTFs.[495] When these conditions were applied to the unprotected 6-bromopyridin-3-amine **60b** no reaction could be detected. Using the dimethylpyrrole protected pyridine **62b**, the coupled product was detected on LC-MS, however significant amounts of debromination and other unidentified side products were also observed. This method was therefore not pursued any further.

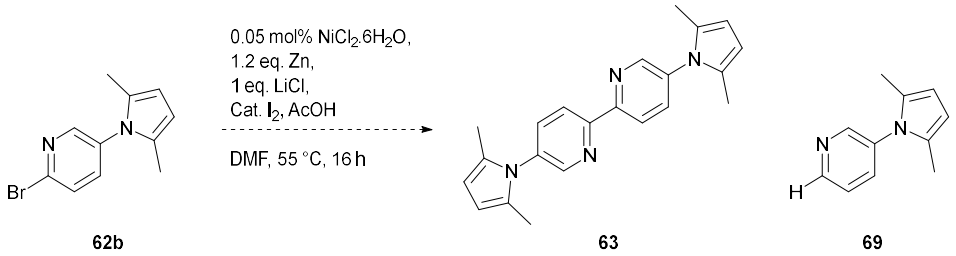

Scheme 8: Attempted ligand-free nickel catalyzed homocoupling.

2.3.1.2.4 Attempted synthesis of Bpy by palladium catalyzed couplings

Wang *et al.* reported a $Pd(OAc)_2$ catalyzed cross-coupling of aryl halides in PEG4000.[496] These conditions were applied to the dimethylpyrrole protected bromopyridine, and initially gave very promising results in a small-scale reaction (LC-MS). However, both upscaling and repetition of the small-scale reaction gave inconsistent results, and no product could be isolated. This reaction was also evaluated for benzylidene, trifluoroacetamide and acetamide protected 6-bromopyridin-3-amines **70**, which all gave no conversion. Another method, reported by Shao *et al.*, for the Pd-catalyzed homocoupling of pyridines using palladium on carbon and EtOH in DMSO was evaluated. No reaction was detected using these conditions, after which these palladium catalyzed approaches were abandoned (Scheme 9).

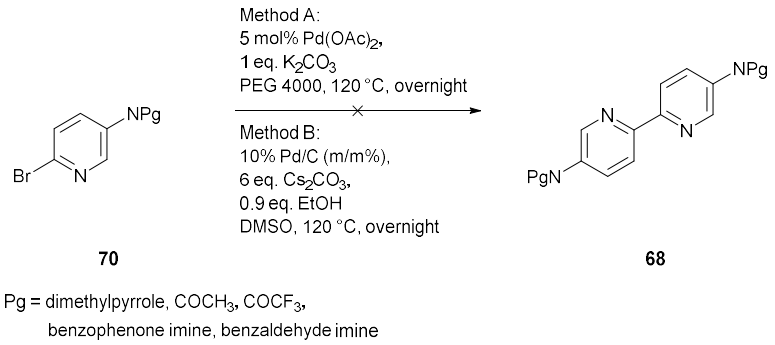

Scheme 9: Attempted synthesis of **63** through Pd-catalyzed homocouplings.

2.3.1.2.5 Attempted synthesis of Bpy by benzidine rearrangement

Similarly as in the synthesis of **Ppy**, the rearrangement of a diazo compound **71** was also evaluated. The diazo compound **71** was easily synthesized from 3-aminopyridine **48** using *N*-chlorosuccinimide (NCS) and 1,8-diazabicyclo[5.4.0]undec-7-ene (DBU) in dichloromethane, giving the product **71** with a yield of 54% after chromatography. However, upon reduction of this compound only the hydrazine derivative **72** could be obtained, and the rearranged product could not be detected (Scheme 10). This approach was therefore also abandoned.

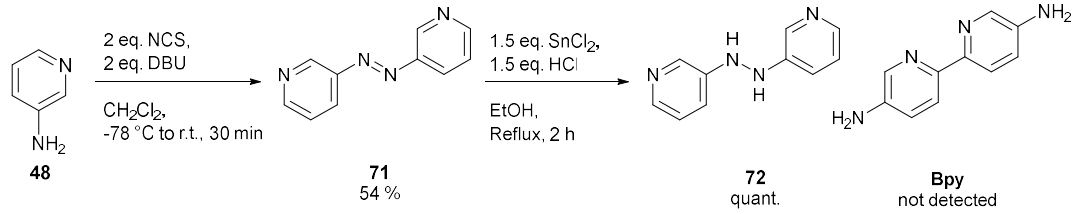

Scheme 10: Attemted synthesis of **Bpy** by reduction and benzidine rearangement of diazocompound **71**.

2.3.1.3 The synthesis of benzophenone-protected 1,4-diaminobenzene **45**

As stated in the literature review, the large-scale synthesis of COFs is still a challenge. In this light Vitaku *et al.* reported a new approach towards imine and β-ketoenamine-linked COFs, based on the transimination of *N*-aryl benzophenone imines.[489] To evaluate this attractive route, benzophenone-protected 1,4-diaminobenzene **45** was synthesized by $TiCl_4$ catalyzed Schiff-base formation (Scheme 11). The protected 1,4-diaminobenzene **45** was used to synthesize **TpPa-1**, a COF synthesis that was reported by Vitaku *et al.* on gram scale, which was successfully reproduced in this work (Section 2.3.2.2). As this type of benzophenone-protected building block proved quite promising to perform COF synthesis on larger scales, it was also attempted to protect **Bpy** in the same manner. Unfortunately, this proved unsuccessful as no imine product was formed, even after greatly elongated reaction times.

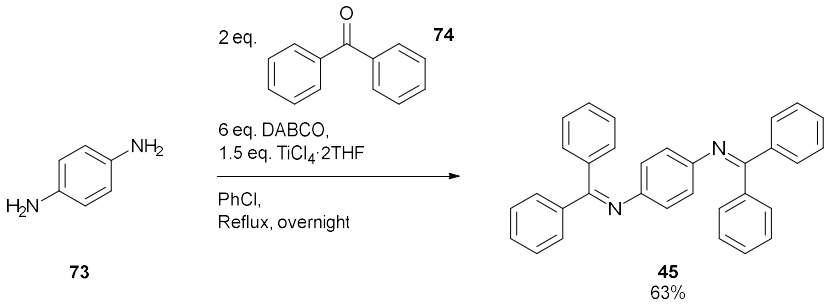

Scheme 11: Synthesis of benzophenone-protected 1,4-diaminobenzene **45**, a building block for the large-scale synthesis of **TpPa-1**.

2.3.1.4 The synthesis of [2,2'-bipyridine]-5,5'-dicarbohydrazide **12**

Hydrazone-linked COFs, first reported by Yaghi and coworkers, are known for their great chemical stability.[488] To explore this type of linkage for photocatalytic applications [2,2'-bipyridine]-5,5'-dicarbohydrazide **42** was synthesized in three steps from commercially available 5,5'-dimethyl-2,2'-bipyridine **75** using literature procedures.[497,498] Oxidation with potassium permanganate followed by esterification gave the ethyl ester **76** in 31% yield over two steps, which was then converted into the hydrazide by reaction with hydrazine hydrate (Scheme 12). It was attempted to synthesize COFs with this building block by condensation with **Tp**, however no crystalline materials could be obtained. The very limited solubility of the [2,2'-bipyridine]-5,5'-dicarbohydrazide **42** is a possible culprit for this disappointing result. Mechanochemical synthesis provides a possible solution for this problem, however this was not further explored in this work.

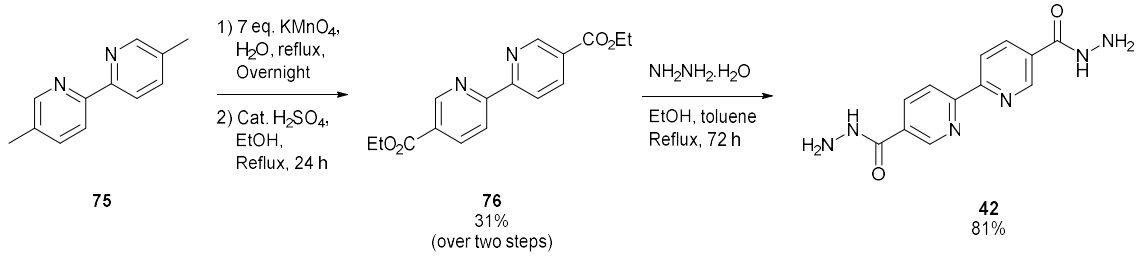

Scheme 12: Synthesis of [2,2'-bipyridine]-5,5'-dicarbohydrazide **42**, a building block for hydrazone-linked COFs.

2.3.1.5 The synthesis of functionalized bipyridines **43-44** as building blocks for C=C linked COFs

As discussed in the literature review on photocatalysis, the C=C linkage has many potential advantages for photocatalytic applications, as this linkage is both very stable and allows for extensive conjugation throughout the framework. To explore this linkage, two linkers were synthesized based on literature procedures: the dicyano linker **44** and the bisphosphonate **43** (Scheme 13).[499,500] Both these linkers can react with aldehydes to furnish C=C linked COFs by either Knoevenagel condensation or Horner-Wadsworth-Emmons reaction. Benzylic bromination of 5,5'-dimethyl-2,2'-bipyridine **75** using catalytic azobisisobutyronitrile (AIBN) in CCl_4 gave 5,5'-bis(bromomethyl)-2,2'-bipyridine **77**. The Arbuzov reaction with $P(OEt)_3$ afforded the bisphosphonate **43** whilst the dicyano linker **44** could be made with trimethylsilyl cyanide (TMSCN). Unfortunately, no crystalline materials could be produced using these linkers. The bond formation reactions to make C=C linked COFs are less reversible, compared with reactions such as boroxine or Schiff base formation, making the synthesis of C=C linked COFs more challenging.

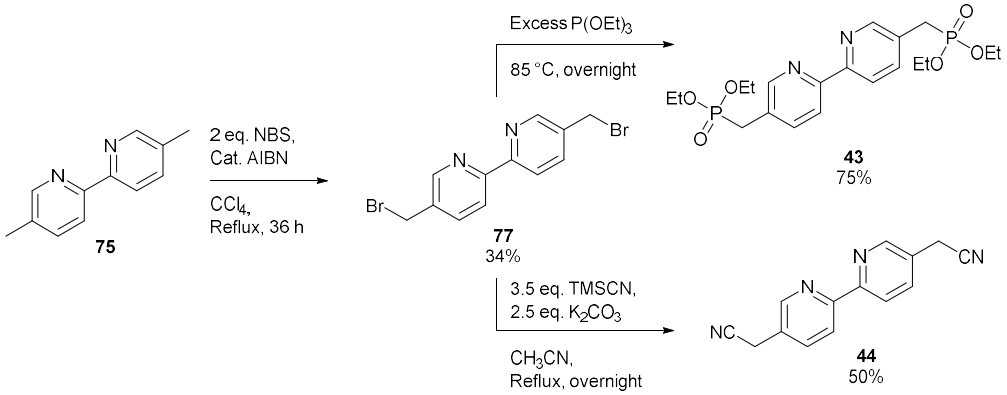

Scheme 13: Synthesis of bipyridine containing dicyano compound **44** and bisphosphonate **43**.

2.3.1.6 The synthesis of 1,3,5-triformylphloroglucinol **Tp**

1,3,5-triformylphloroglucinol **Tp** is a unique aldehyde used for COF synthesis, as it does not form imine linkages upon reacting with amines, but β-ketoenamine linkages. The resulting materials, first developed by the Banerjee group, are much more stable towards acids and bases than imine-linked materials.[487] **Tp** is typically synthesized by Duff formylation, using a large excess of hexamethylenetetramine (HMTA) in trifluoroacetic acid (TFA). The resulting imines are then hydrolyzed using aqueous HCl (Scheme 14). While this procedure reliably gives the product as a pure compound after aqueous work up, due to polymerization and other side reactions yields of only 15-20% are obtained. Moreover, the use of TFA as a solvent is undesirable due to its corrosiveness and expense. An alternative method has been described by Wang *et al.*, using formamidine acetate as a formylating agent.[501] This was attempted, but the described results could not be reproduced. Notably, other authors also reported mainly monoformylation using this method, and no polyformylation.[502] Lastly, formation of the diformylated phloroglucinol by Vilsmeier-Haack reaction, followed by installation of the final formyl group by Duff reaction has been reported to give higher yields.[503] However, the diformylated product could not reliably be obtained, and therefore this route was not evaluated further.

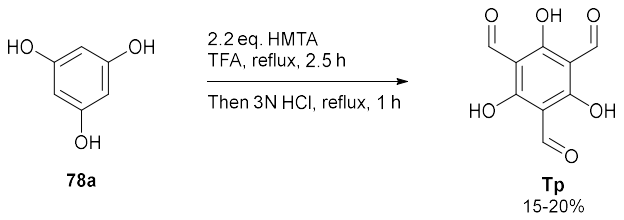

Scheme 14: Synthesis of **Tp** by Duff formylation.

2.3.1.7 The synthesis of 2,4,6-trimethoxybenzene-1,3,5-tricarbaldehyde TpOMe

Another unique aldehyde developed by the Banerjee group is **TpOMe**, the methylated analogue of **Tp**. Imine-linked COFs made with this building block are known to possess exceptional stability towards conc. H_2SO_4 (18 M), conc. HCl (12 M), and NaOH (9 M). This is explained by the presence of very strong interlayer C-H--N hydrogen bonding, providing steric hindrance and hydrophobic shielding around the imine C=N bonds.[486] The reported synthesis for **TpOMe** follows a four-step procedure from 1,3,5-trimethoxybenzene **78b**: bromomethylation using HBr and formaldehyde, nucleophilic substitution to the triacetate **80**, hydrolysis to form the triol **81** and finally oxidation to **TpOMe** (Scheme 15). While this route was used in this work to obtain **TpOMe**, it was not an attractive synthesis. Next to requiring four steps, this route also uses carcinogenic Cr(VI) reagents, which are extremely undesirable from an environmental and safety perspective. Two alternative routes: the methylation of **Tp** and the oxidation of bromomethylated compound **79** were evaluated to improve this synthesis.

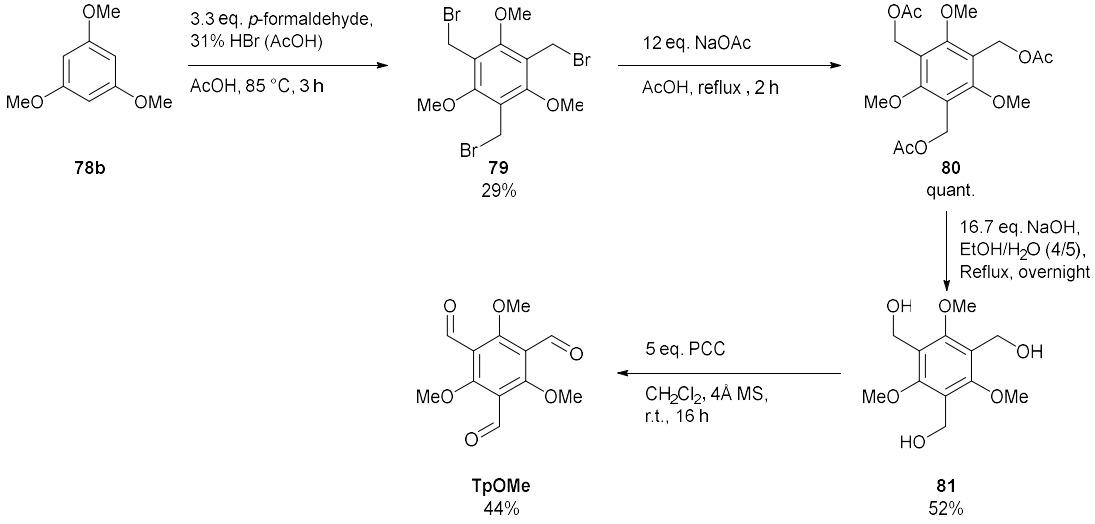

Scheme 15: Synthesis of **TpOMe**.

First, we evaluated the synthesis of **TpOMe** by direct methylation of **Tp**. Unfortunately, this alkylation of a phenol proved much more challenging than initially thought (Scheme 16). No reaction with methyl iodide was detected. Therefore, dimethyl sulfate (DMS), a stronger methylating agent, was used. When reacting **Tp** with DMS and K_2CO_3 in acetone, initially promising results were obtained. The crude ^{1}H-NMR of the product corresponded with that of **TpOMe**, and almost no impurities were detected. Unfortunately, this could not be reproduced, and in subsequent experiments mixtures of alkylated products were obtained.

Even after several optimization attempts, using other solvents such as DMF, CH_3CN or THF, a stronger base such as NaH, and different equivalents of K_2CO_3 or DMS, no reliable results were obtained. Varying the time and temperature or using a microwave still did not ensure a complete reaction. Lastly, an even stronger methylating agent, methyl triflate, was used. This also gave mixtures of products that were difficult to purify, and therefore this route was abandoned.

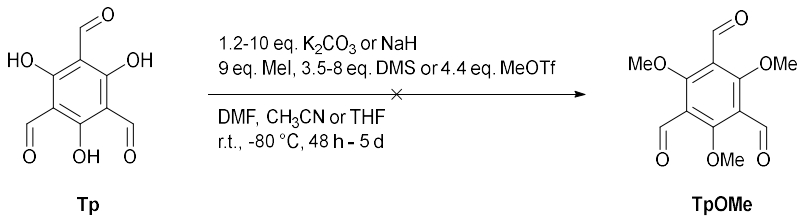

Tp **TpOMe**

Scheme 16: Attempted synthesis of **TpOMe** by direct methylation of **Tp**.

A second route that was evaluated was the direct oxidation of the bromomethylated compound **79** to **TpOMe**. Many conditions and name reactions exist for this particular type of transformation and were evaluated (Table 1). The Hass-Bender oxidation, using the sodium salt of 2-nitropropane as an oxidant in DMF, resulted in a very complex mixture (entry 1). The use of Ag_2O with pyridine-*N*-oxide also gave a complex mixture (entry 3). Using DMSO with Na_2CO_3 at 150°C a mixture of aldehydes was detected after two hours, while continuing the reaction overnight resulted in complete decomposition (entry 4). The reaction with 2-iodoxybenzoic acid (IBX) also resulted in a mixture of products (entry 5). Interestingly, when using 4.5 eq. $K_2Cr_2O_7$ in DMSO at 120 °C for one hour the dialdehyde was formed relatively pure (entry 2). It was reported in literature that the addition of the crown ether 18-crown-6 has a beneficial effect on these types of reactions, but in this case only complete decomposition was obtained (entry 6). Lastly, two approaches using periodic acid (H_5IO_6) in ionic liquids, called Ming A en B, were evaluated as these were reported to work particularly well for the oxidation of polyhalides to polyaldehydes.[504] However, applied on substrate **79** both reactions did not give an appreciable conversion towards the product. To conclude, no improved route towards **TpOMe** was found and the approach of the Banerjee group was used.

Table 1: Attempted synthesis of **TpOMe** by direct oxidation of bromomethyl derivative **79**.

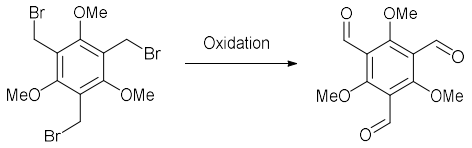

79 **TpOMe**

Entry	Conditions	Result
1	4.5 eq. NaH, 6 eq. *i*$PrNO_2$ DMF, 0 °C to r.t., overnight	Complex mixture
2	4.5 eq. $K_2Cr_2O_7$ DMSO, 120 °C, 1 h	Dialdehyde as the main product
3	1.5 eq. Ag_2O, 3 eq. pyridine-*N*-oxide CH_3CN, 50 °C, overnight	Complex mixture
4	5 eq. Na_2CO_3 DMSO, 150 °C, overnight	Complex mixture after two hours, decomposition overnight
5	4.5 eq. IBX DMSO, 65 °C, overnight	Complex mixture after two hours, similar mixture overnight
6	4.5 eq. $K_2Cr_2O_7$, 4.5 eq. 18-crown-6 DMSO, 100 °C, overnight	Decomposition
7	Ming A: 3.6 eq. H_5IO_6, [C12mim]$FeCl_4$, 50 °C, overnight	No product detected
8	Ming B: 3.6 eq. H_5IO_6, 0.105 eq. V_2O_5, [bmpy]PF_6, 50 °C, overnight	No product detected

2.3.1.8 The synthesis of enaminone linker 46

Liu *et al.* reported COFs with a different type of β-ketoenamine linkage, by Michael addition-elimination reaction of the tritopic enaminone linker **46** with aromatic amines.[505] This class of COFs has been very underdeveloped, as of September 2022 no other COFs have been produced this way, except for the original report in 2019. As it would be interesting to explore the photochemical properties of this linkage, the reproduction of a COF from the original paper was attempted. This COF, JUC-520 was made through condensation of linker **46** with 1,3,5-tris-(4-aminophenyl)triazine (TAPT). The linker itself could easily be produced through condensation 1,3,5-triacetylbenzene **82** with *N*,*N*-dimethylformamide dimethyl acetal (DMFDMA), using the reported procedure (Scheme 17).[505] However, even after multiple attempts JUC-520 could not be reproduced, as almost no solid material was obtained, and it was decided to not pursue COF synthesis with this linker anymore.

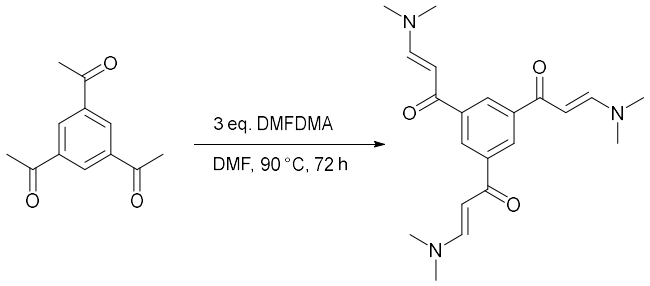

82 **46** 69%

Scheme 17: Synthesis of the tritopic enaminone linker **46** through condensation of 1,3,5-triacetylbenzene **82** with DMFDMA.

2.3.2 Synthesis and characterization of COFs

Whilst many linkers were synthesized, finally, four crystalline COFs were made: **TpBpyCOF**, **TpOMeBpyCOF**, **TpPPyCOF** and **TpPa-1**. To not overload this work with failed reactions, where only amorphous powders or black tars were obtained, only these materials will be discussed here. In Appendix 1 the attempted synthesis of an NHC-containing COF is discussed, which will shed more light on the difficulty of obtaining truly crystalline COFs.

2.3.2.1 The synthesis of TpBpyCOF, TpOMeBpyCOF and TpPPyCOF

Two-dimensional (2D) COFs with one-dimensional open channels were synthesized by condensing 2,2'-bipyridine-5,5'-diamine (**Bpy**) or 6-(4-aminophenyl)pyridin-3-amine (**Ppy**) with 1,3,5-triformylphloroglucinol (**Tp**) or 2,4,6-trimethoxybenzene-1,3,5-tricarbaldehyde (**TpOMe**) by solvothermal synthesis using AcOH as a catalyst in the DMAc/*o*DCB solvent mixture for three days at 120 °C (Scheme 18). **TpBpyCOF** is already well known in literature[506–510] and **TpOMeBpyCOF** has been synthesized via a mechanochemical reaction.[511] **TpPpyCOF** was a newly synthesized COF, and the first COF synthesized using **Ppy** as a building block. It has potential, not only as a photocatalyst, but also a platform to complex metals with its phenylpyridine moiety. Lastly, the polymer formed through condensation of **TpOMe** and **Ppy**: **TpOMePpyPOP** was also made, but whilst the material was porous (S_{BET} = 365 m^2/g) this was not a COF, as it possessed little to no crystallinity.

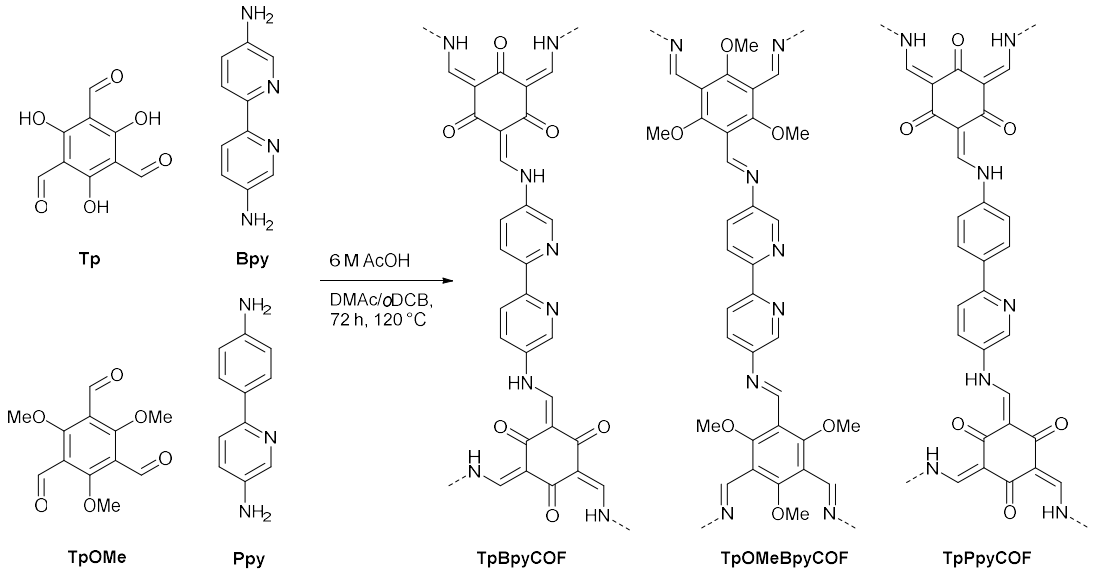

Scheme 18: Schematic illustration of the synthesized COFs.

A typical workflow of the COF synthesis used is shown in Figure 4. The synthesis of these materials was performed in GC-vials on a ~100 mg scale (Section 2.5.5). After additions of the monomers, solvents, and the catalyst the vials were capped, sonicated, degassed and put under argon. The vials were then placed in a pre-heated oven for a set amount of time. After the reaction the purification of the formed materials takes place via washing with a range of solvents followed by further Soxhlet extraction with MeOH. All unreacted building blocks or partly polymerized intermediates are hereby removed from the pores of the material. The materials are then activated, through removal of the remaining solvents by extensive drying under vacuum.

These materials were made through Schiff- base condensation, followed by tautomerization in the case of **TpBpyCOF** and **TpPpyCOF,** to form imine or β-ketoenamine-linked materials. The mechanism for the imine formation and subsequent tautomerization is shown in Scheme 19. Acetic acid is a typical catalyst that is added to enhance the reversibility of the reaction. Importantly, when all three imines have tautomerized the reaction is no longer an equilibrium, as the fully tautomerized compound is much more stable, and the structure becomes 'locked'.

Figure 4: Visual representation of the workflow to synthesize COFs. In the first picture the solid reagents are added to the vials, after which the solvents and the acid catalysts are added and the vials are capped (picture 2). Then the vials were sonicated (picture 3) after which they are repeatedly frozen in liquid nitrogen and pumped to remove all traces of oxygen from the reaction (picture 4). Finally, they are placed in a pre-heated oven at a set temperature for a pre-determined time (typically 120 °C, 72 h, picture 5). The vials are then opened, filtered over a membrane filter, and washed with a range of solvents (picture 6). The materials are then placed in a paper filter to use for Soxhlet extraction (picture 7 and 8). After Soxhlet extraction and drying under vacuum the COFs are stored in vials at room temperature (picture 9).

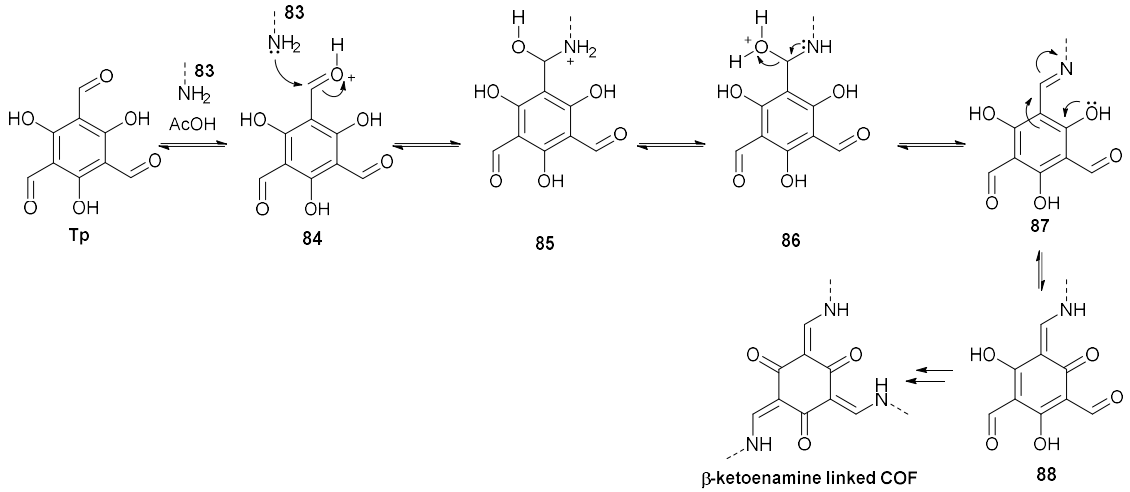

Scheme 19: Mechanism for the formation of imine and β-ketoenamine-linked COFs.

Characterization of these materials was performed by powder X-ray diffraction (PXRD), Fourier transform infrared spectroscopy (FTIR) and nitrogen sorption measurements. First FTIR was used to confirm the completion of the reaction and the formation of imine or β-ketoenamine linkages. As seen in Figure 5a, the characteristic absorption bands of the **Bpy** amino group (3180-3418 cm^{-1}) and the **Tp** carbonyl (1632 cm^{-1}) disappear in the resulting **TpBpyCOF**. New peaks corresponding with the keto functionality are observed at 1604 cm^{-1} (C=O) and 1564 cm^{-1} (C=C).[506] The peaks around 1260 cm^{-1} correspond with the C–N bond.[512] For the other β-ketoenamine-linked material, **TpPpyCOF**, similar results were obtained (Figure 5c), the characteristic amine absorption bands (3192-3443 cm^{-1}) disappear and new bands corresponding with the C=O and C=C absorption, which are nearly merged in this material, appear around 1595 and 1568 cm^{-1}. For the imine-linked **TpOMeBpyCOF** the N–H (3180-3418 cm^{-1}) and C=O (1680 cm^{-1}) absorptions fully disappeared and the stretching band of the newly formed C=N linkage appeared at 1565-1605 cm^{-1} (Figure 5b).[511]

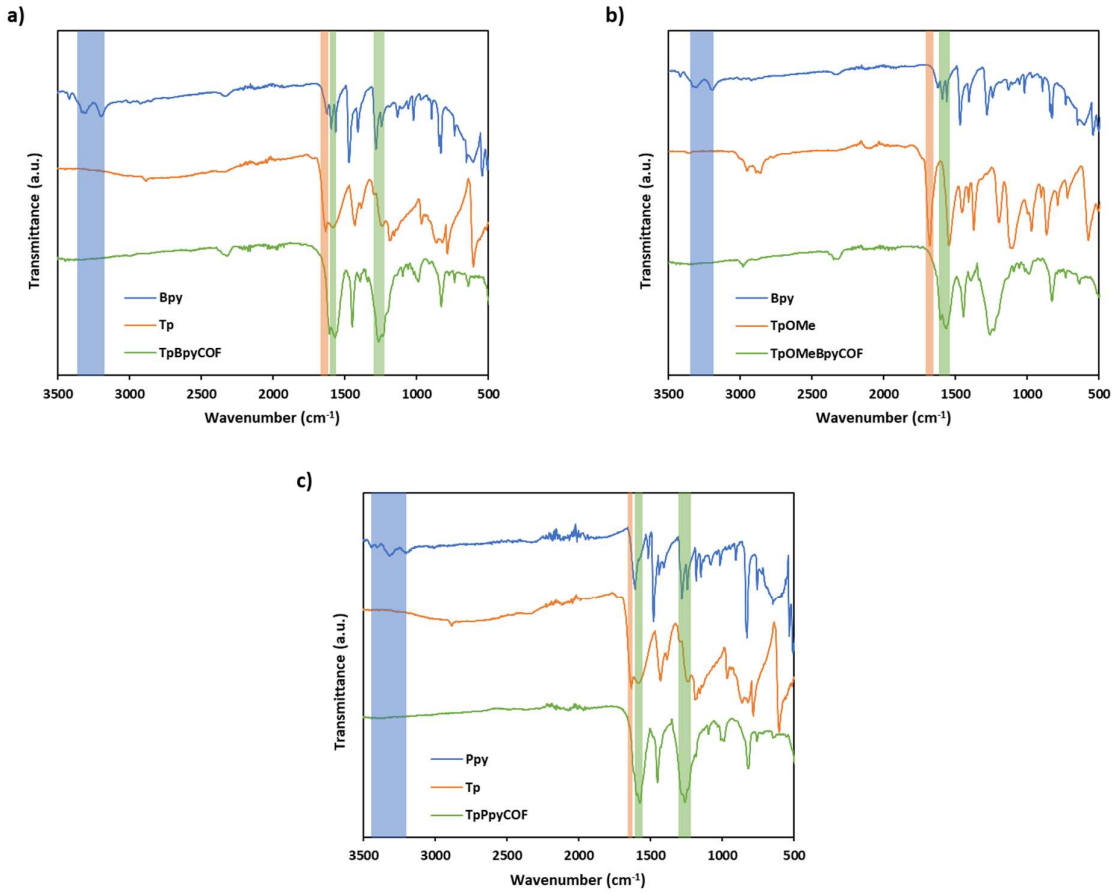

Figure 5: Overlay of the FTIR spectra of (a) **Bpy** (top, blue), **Tp** (middle, orange) and **TpBpyCOF** (bottom, green); (b) **Bpy** (top, blue), **TpOMe** (middle, orange) and **TpOMeBpyCOF** (bottom, green); and (c) **Ppy** (top, blue), **Tp** (middle, orange) and **TpPpyCOF** (bottom, green). Characteristic signals originating from the amino groups, aldehydes and imine/β-ketoenamine linkages are marked in blue, orange and green, respectively.

While FTIR gives information regarding the chemical functionalities in the materials, to conclude whether or not these materials where truly COFs XRDs are required. The relatively sharp diffraction peaks of the XRD patterns (Figure 6a-c) point to a good crystallinity of the resulting COFs. The peaks around 2θ = 4° are assigned to the (100) plane and the smaller peak around 7° to the (200) plane. The broad peak at around 25° corresponds to the (001) plane and originates from π- π stacking between the individual layers of the COF.

The atomic structures of the materials were determined through computational modelling (see Section 2.5.6), using the measured diffraction patterns as reference data. Through judicious comparison of the experimental diffraction patterns with a collection of calculated diffraction patterns, corresponding to different possible structure models, the most representative model was identified.[513] Moreover, by performing molecular dynamics (MD) simulations at operating conditions (1 bar, 300 K), peak broadening effects due to movement of the layers were effectively included in the calculated diffraction patterns for optimal comparison. The models were generated, starting from a hexagonal layer topology (**hcb**), combinatorically varying all flexible moieties in the layer geometry that might not be able to transition at operating conditions during the MD simulation, due to prohibitively large free energy barriers. Moreover, as typically only the nearest neighboring layer orientation is relevant due to screening effects, and to allow for different variations between subsequent layers, two-layer unit cells were constructed. For both the **Tp**- and **TpOMe**-based COFs, the orientations of both the pyridine (py) moieties and the imine/amine linkages were considered, and, for the **TpOMe**-based COF, the methoxy (OMe) groups as well (see Figure 30). The molecular interactions in these systems were modelled using system-specific force fields, derived using the QuickFF protocol (Section 2.1.5.6). Ultimately, this approach gave rise to a single optimal atomic structure for each of the materials, as visualized in Figure 6, with excellent agreement to the experimental PXRDs. For **TpBpyCOF** the optimal structural model has amine linkages with an identical orientation in the same layer, but inverted with respect to the layer above. The bipyridine is in a *trans* configuration and is inverted with respect to the layer above. For **TpOMeBpyCOF** the optimal structural model has imine linkages with different orientations in both the same layer as the layer above. The bipyridine is in a *trans* configuration and is inverted with respect to the layer above. The methoxy groups are not all aligned and are inverted with respect to the layer above. Lastly, for **TpPpyCOF** the optimal structural model has amine linkages with an identical orientation in the same layer, but inverted with respect to the layer above. The pyridine unit is inverted with respect to the layer above and also switches position. A small discrepancy for the **TpOMeBpyCOF** remains for larger 2θ values, corresponding to a smaller interlayer distance for the experiment. This might be due to some residual solvent allowing a smaller interlayer distance.

The orientation of asymmetric moieties in COFs, such as the linkage, configuration of bipyridine/phenylpyridine linkers, and methoxy groups are usually not modelled. However, by utilizing the methodology outlined in this study, we were able to obtain a more comprehensive understanding of these materials' configurations. Additionally, the good agreement observed between the modelled and experimental PXRDs provides further evidence of the crystallinity of these materials.

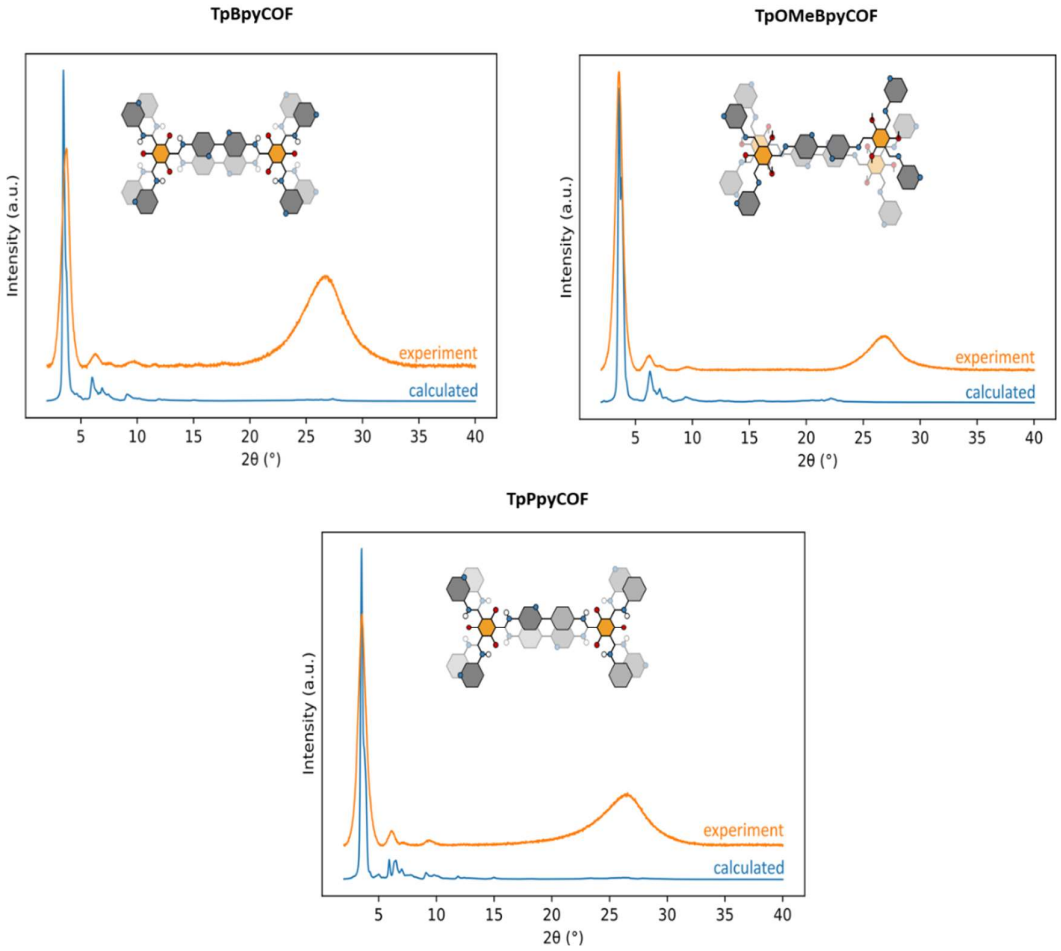

Figure 6: PXRD comparison for (a) **TpBpyCOF**; (b) **TpOMeBpyCOF**; and (c) **TpPpyCOF** between experimental measurements and calculated MD averages.

The permanent porosity of the synthesized COFs was assessed by N_2 sorption measurements at 77 K (Figure 7a). The calculated Brunauer−Emmett−Teller (BET) surface area for **TpBpyCOF**, **TpOMeBpyCOF** and **TpPpyCOF** were 879, 1322 and 755 m^2/g, respectively. The pore size distributions are given in Figure 7b and the pore diameters were 17.9, 17.3 and 18.5 Å for **TpBpyCOF**, **TpOMeBpyCOF** and **TpPpyCOF**, respectively.

SEM images of the COFs images are shown in Figure 7d-e. **TpBpyCOF** and **TpPpyCOF** form large aggregates with a relatively smooth surface in the case of **TpBpyCOF** and a more rough surface for **TpBpyCOF**, **TpOMeBpyCOF** adopts a flower like morphology.

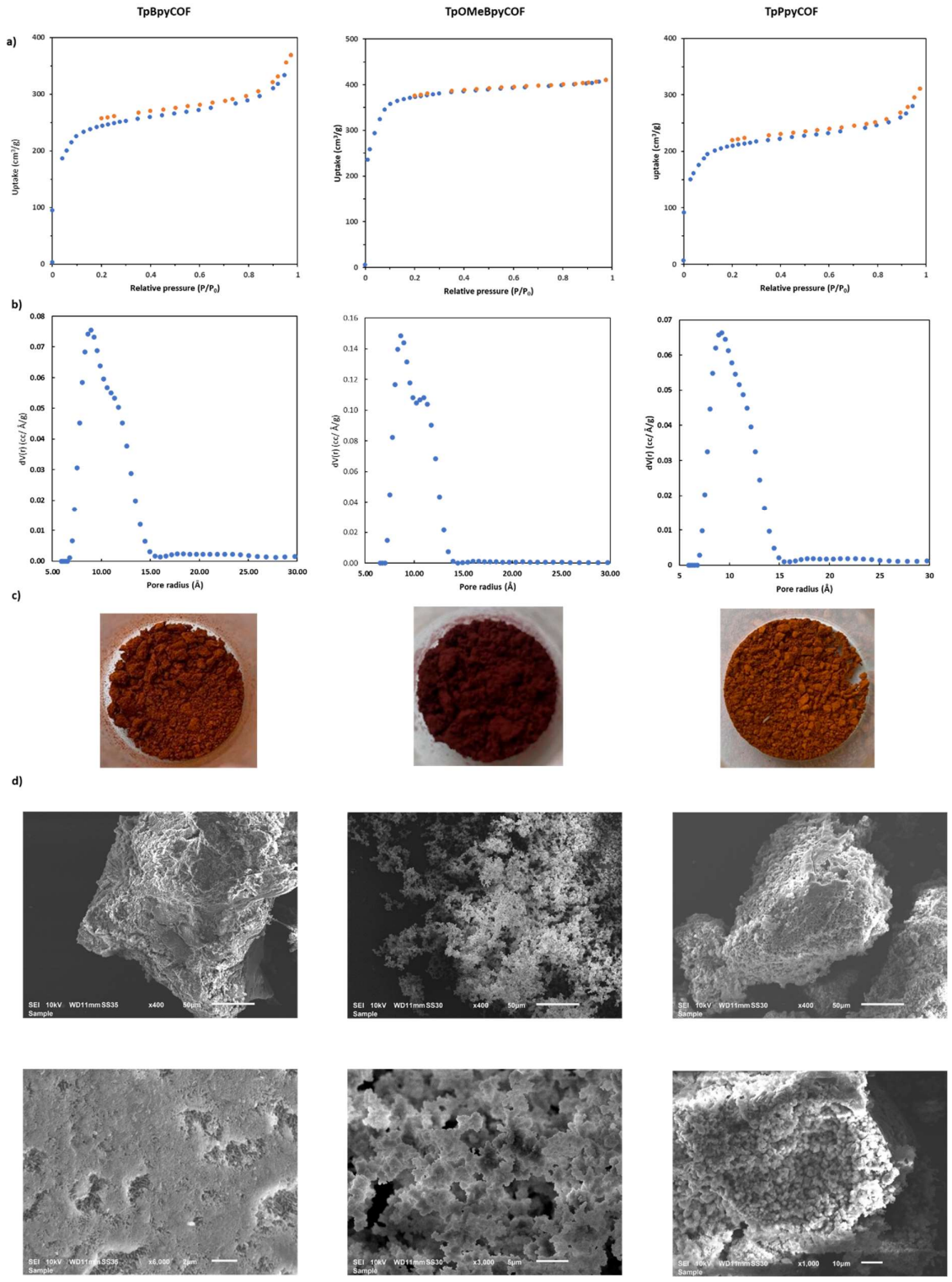

Figure 7: (a) Nitrogen adsorption/desorption isotherms at 77K; (b) Pore size distributions; (c) pictures (d) SEM images with x400 magnification and (e) 6000x, 3000x and 1000x magnification (from left to right) of **TpBpyCOF**, **TpOMeBpyCOF** and **TpPpyCOF**.

To further characterize the COFs, the optical properties of the materials were determined. The diffuse reflectance UV-Vis spectra of the COFs were measured and transformed through the Kubelka-Munk function to obtain the absorption spectra. These spectra exhibit absorption edges around 500-550 nm and the absorption tails extend beyond 850 nm (Figure 8a). It can be clearly seen that the absorption edges for **TpPpyCOF** and **TpOMeBpyCOF** are blue- and red-shifted, respectively, compared to **TpBpyCOF**. The related Tauc plots (Figure 8b) were used to estimate the band gaps, which amounted to 2.10, 1.95 and 2.23 eV for **TpBpyCOF**, **TpOMeBpyCOF** and **TpPpyCOF**, respectively.

As anticipated, these structurally similar materials also possessed similar band gaps. In earlier literature the band gaps of LZU1 and COF-TpPa, synthesized by condensation of 1,4-phenylenediamine with 1,3,5-triformylbenzene and 1,3,5-triformylphloroglucinol **Tp**, respectively, were compared.[337] The imine-linked LZU1 possessed a band gap that was 0.3 eV higher than the β-ketoenamine-linked COF-TpPa (2.1 vs. 2.4 eV), suggesting the band gap lowering effect of the β-ketoenamine linkage, however, this did not take into account the electronic differences between the two building blocks. In another report describing three acridine based COFs using mono-, di-, or tri-hydroxy triformylbenzene, the band gaps did not really change with increased β-ketoenamine tautomerism. Interestingly, the fully β-ketoenamine-linked material did possess greater photocatalytic activity.[514] In our findings the methoxy substitution of **TpOMe** led to a resulting imine-linked **TpOMeBpyCOF** with a band gap 0.15 eV smaller than the analogous β-ketoenamine-linked **TpBpyCOF**. The formed imine linkage could possibly allow for more conjugation than in the cross-conjugated β-ketoenamine-linked materials. The resulting trimethoxy-substituted imine core is also a stronger electron donor than the β-ketoenamine core, resulting in a material with more of a donor-acceptor character[515] and thus a lowered band gap. Substitution of a nitrogen atom in bipyridine to a carbon in phenylpyridine increased the band gap by 0.13 eV. Next to the electronic effects in the layers, variations in building blocks alter the interlayer alignment and thus the π-π interactions between subsequent layers, also effecting the band gap. The band gaps and density of states were calculated using the hybrid functional (HSE06) (Figure 34). The calculated band gaps were 2.09, 2.49 and 2.14 eV for **TpBpyCOF**, **TpOMeBpyCOF** and **TpPpyCOF**, respectively. Whilst the values for **TpBpyCOF** and **TpPpyCOF** are in good agreement with the experimental values, for **TpOMeBpyCOF** a large deviation was found. It is likely that the interlayer distance plays a significant role here, as the experimental interlayer distance was also lower than simulated. This points to strong interactions between the layers, and could explain the lower experimental band gap for **TpOMeBpyCOF**.[516] In all cases, the band gaps were quite small, allowing absorption of visible light and its conversion into useful chemical energy. It is clear from these findings that selecting different linkages and electron donating or accepting building blocks offers a way to fine-tune the band gaps of COFs.

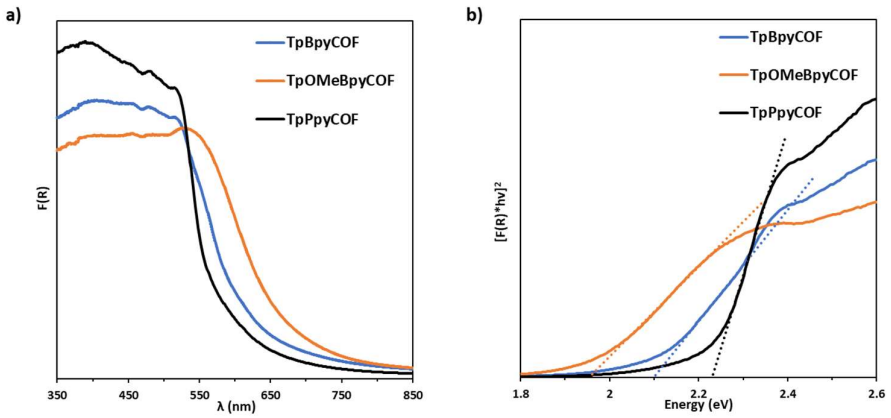

Figure 8: (a) Kubelka-Munk absorption spectra; and (b) Tauc plots of **TpBpyCOF**, **TpPpyCOF** and **TpOMeBpyCOF**.

Finally, the absolute positions of the valence band (VB) and conducting band (CB) of the three COFs were estimated by linear sweep voltammetry under chopped light illumination.[517,518] To this end, the COFs were mechanically exfoliated by grinding and coated on a working electrode. This was then used in a three-electrode setup, with an Ag/AgCl reference electrode and a Pt coil counter electrode. The anodic photocurrent was measured under chopped white light illumination and an applied bias which was swept from +0.4 V to -0.4 vs. Ag/AgCl. The resulting photocurrent decreased in magnitude and changed sign when going from +0.4 V to -0.4 V (Figure 9 a-c). The energy level of the conduction band can be determined from the potential at which this sign change occurs. The energy levels of the valence band can then be calculated using the equation: $E_{CB} = E_{VB} - E_g$.[519] The resulting band structure of the COFs is shown in Figure 9d.

To gain insight in the possible organic transformations that these COFs can catalyze, these values can be compared with known oxidation (E_{ox}) and reduction potentials (E_{red}) of relevant substrates. For example, the oxidation potential of benzylamine is 1.28 V (vs NHE),[520] meaning that the holes of **TpBpyCOF** and **TpPpyCOF** should be able to oxidize this substrate. The oxidation potential of another interesting substrate, ethyl *p*-tolylglycinate, is 1.30 V (vs. NHE),[521] in line with the oxidation potential of **TpBpyCOF** and **TpPpyCOF**. The reduction potential of O_2 is 0.62 V (vs. NHE),[520] therefore all three COFs can reduce oxygen to the superoxide radical anion ($O_2^{-\bullet}$). Moreover, these COFs could also act as photosensitizers to generate singlet oxygen ($^1O_2$) through direct energy transfer. Singlet oxygen is a powerful oxidizing agent, capable of oxidizing many organic substrates without further involvement of the COF.

By using EPR-spectroscopy and **TpBpyCOF** as the model catalyst, the ability of this material to create activated forms of oxygen ($O^{-\bullet}$ and $^1O_2$) was confirmed. By stirring a suspension of the COF in acetonitrile with 5,5-dimethyl-1-pyrroline-*N*-oxide (DMPO), under air and visible light irradiation, the DMPO-superoxide adduct could be detected in the EPR spectrum (Figure 9e). Using a similar methodology, with 2,2,6,6-tetramethylpiperidine (TEMP) as the spin trap, the production of singlet oxygen was demonstrated by the detection of the characteristic spectrum of the TEMPO free radical (Figure 9f).

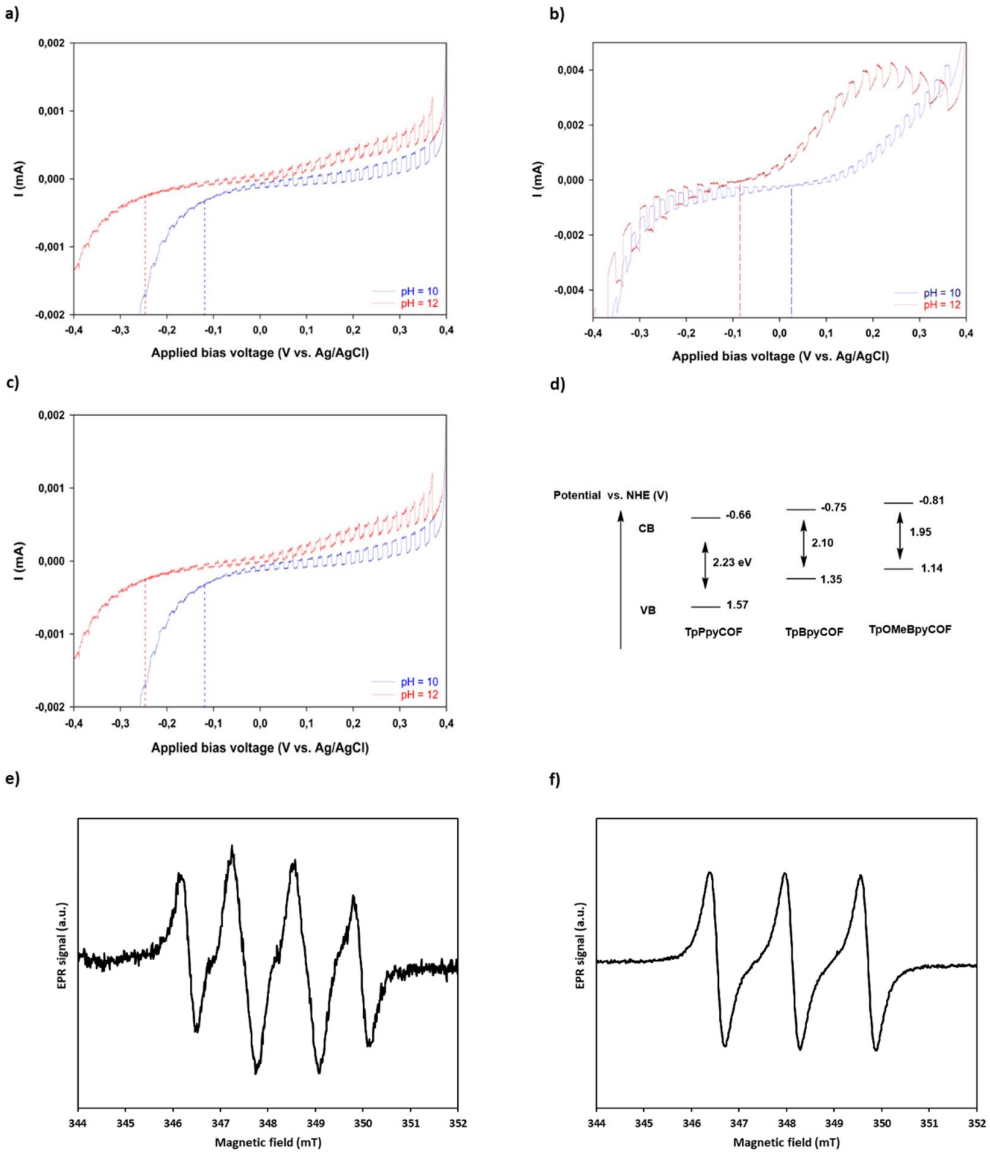

Figure 9: (a-c) Linear sweep voltammetry of **TpBpyCOF**, **TpPpyCOF** and **TpOMeBpyCOF** under chopped illumination in electrolytes at pH 10 or 12. The umklappotential is marked by the red and blue dotted lines; (d) Energy band structure of **TpBpyCOF**, **TpPpyCOF** and **TpOMeBpyCOF**. (e) EPR spectrum of DMPO-$O^{-\bullet}$ and (f) TEMPO produced by **CTF-Pyr** under light irradiation.

2.3.2.2 The synthesis of TpPa-1

TpPa-1 was mainly made to evaluate the feasibility of using benzophenone-protected building blocks to produce β-ketoenamine COFs on large scales as reported by Vitaku *et al.*[489] The large-scale synthesis worked well and almost a gram of a crystalline material could be made in a single batch (Scheme 20). In the IR spectrum the characteristic absorption of **Tp** at 1632 cm^{-1} had disappeared and the C=O and C=C stretch appeared (Figure 10a). These bands fall together around 1580 cm^{-1}, with the C=O band visible as a shoulder on the C=C stretch, which is typical for these types of materials. Furthermore, the C-N absorption bands are visible around 1250 cm^{-1}. The XRD spectrum of the material shows two small signals around 2θ = 5° and 7.5° together with a broad signal at 25°, pointing to a moderate degree of crystallinity and π-π stacking (Figure 10b). The nitrogen sorption isotherms are shown in Figure 10c, and the BET surface area was 688 m^2/g. The pore size distribution was calculated and is shown in Figure 10d. The distribution is narrow, and the material is clearly microporous as the average pore diameter was 14.53 Å. Lastly the diffuse reflectance UV-Vis spectra of **TpPa-1** were recorded to determine the band gap. The Kubelka-Munk transformed absorption spectra and the related Tauc plot are shown in Figure 10e-f. The band gap of **TpPa-1** with an unfunctionalized phenyl linker in conjunction with the β-ketoenamine linkage was 2.06 eV, which is intermediary between that of **TpBpyCOF** and **TpPpyCOF**.

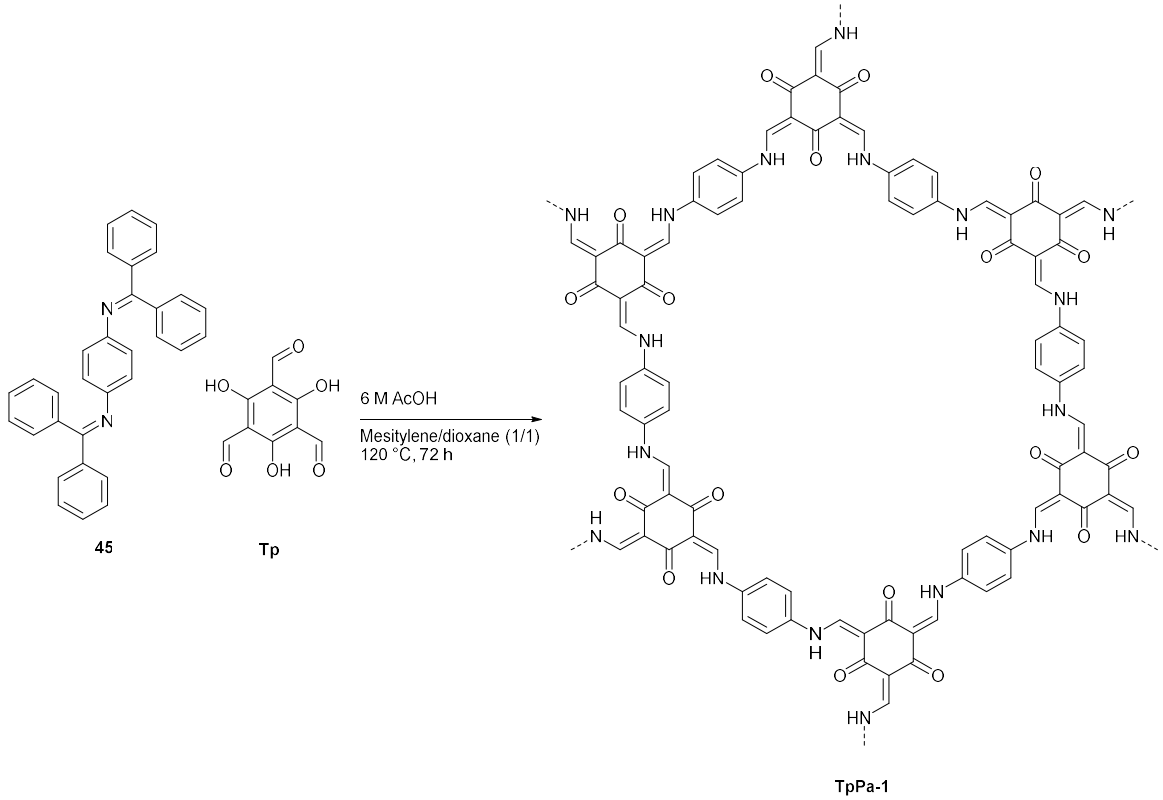

Scheme 20: Synthesis of **TpPa-1**.

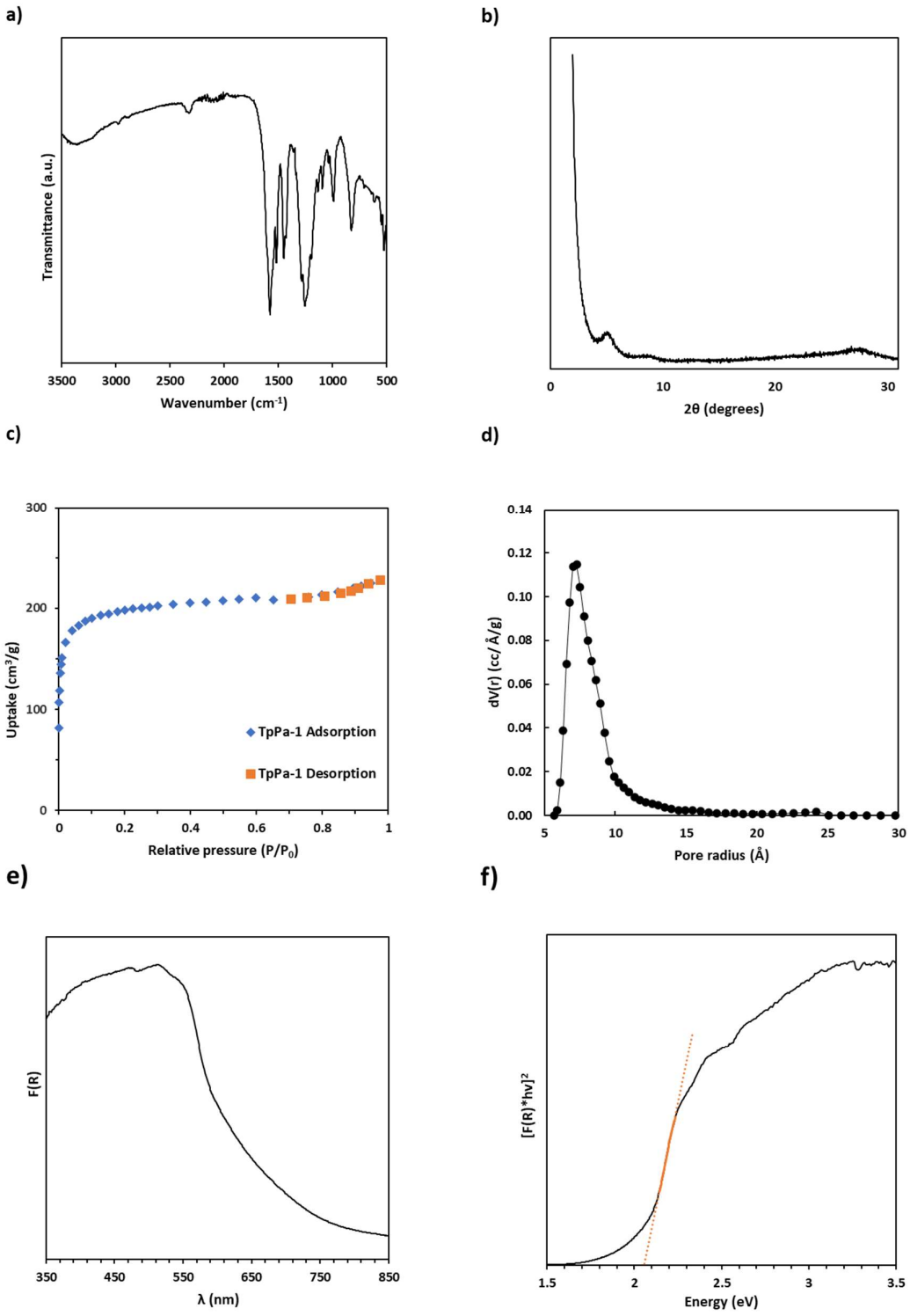

Figure 10: (a) FTIR spectrum; (b) XRD; (c) Nitrogen sorption isotherms; (d) Pore size distribution; (e) Kubelka-Munk transformed UV-Vis absorption spectrum; and (f) Tauc plot of **TpPa-1**.

2.3.3 Application of metal free COFs as photocatalysts

2.3.3.1 The hydroxylation of boronic acids

The first application that was evaluated for the photocatalytic COFs was the aerobic hydroxylation of aryl boronic acids. This proceeds through the excitation of molecular oxygen to superoxide anions[435] and produces phenols, which are building blocks for the chemical and pharmaceutical industries. The hydroxylation of phenylboronic acid **89** to phenol **90** was studied as a model reaction. Encouragingly, after sixteen hours the conversion reached 100% with full selectivity for the phenol product (Table 2). No reaction took place in absence of the COF or DIPEA.

This photoredox reaction has already been developed homogeneously with catalysts such as ruthenium(II) polypyridyl complexes or methylene blue.[522,523] Heterogeneously, there have been successes using MOFs with embedded ruthenium(II) polypyridyl complexes. It is worth noting that in the absence of ruthenium on the bipyridine-MOF the reactions also proceed, albeit with a very low yield (22%). This underscores the photocatalytic activity of bipyridine moieties when embedded in extended structures.[524]

An organic dye, anthraquinone, has been immobilized on a POP, to serve as a heterogeneous catalyst for this transformation. A low loading of 10 mg/mmol resulted in a yield of 93% after 27 hours.[525] Some COFs have also been reported as heterogeneous photocatalysts for this transformation. As described in the literature review (Section 1.8.2.2), Wei *et al.* synthesized benzoxazole-linked COFs to catalyze this transformation. The conversion of phenylboronic acid to phenol reached 88% after 72 hours using 100 mg/mmol loading.[435] An imine-linked COF with benzoxazole building blocks was also found active, as a 100 mg/mmol loading resulted in a yield of 99% after 96 hours.[436] **TpBpyCOF** was applied with 40 mg/mmol loading, and thus performed on par or better than these COFs, proving its potential as a heterogeneous photocatalyst. However, this reaction has been reported frequently using heterogeneous catalysts, and was therefore not developed further.

Table 2: Photocatalytic oxidation of phenyl boronic acid **89** to phenol **90**.[a]

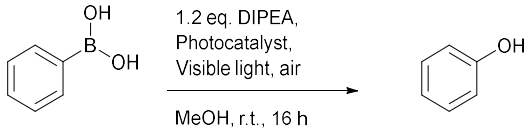

89 90

Entry	Catalyst	Conversion[b]
1	TpBpyCOF	100%
2	$Ru(bpy)_3Cl_2.6H_2O$	100%
3	No DIPEA	0
4	No COF	0

[a] Reaction conditions: 0.1 mmol phenyl boronic acid **89** (12 mg, 0.1 mmol, 1 eq.), DIPEA (15.5 mg, 0.12 mmol, 1.2 eq.), 4 mg catalyst, CFL (26 W), under air, 1 mL MeOH.
[b] Determined using ^{1}H-NMR.

2.3.3.2 The oxidation of benzylic amines into imines

The aerobic, photocatalytic, oxidative coupling of amines to imines is another typical test reaction for photocatalytic materials. Imines, which are important intermediates in organic synthesis, are traditionally prepared via the condensation of amines with ketones or aldehydes. However, the oxidative coupling of amines has received attention as an alternative pathway with great potential. This transformation can be performed with stoichiometric reagents such as *o*-iodoxybenzoic acid.[526] However, much work has been done to develop methods using oxygen or air as the oxidizing agent. Often these methods utilize transition metals such as gold,[527] iridium,[528] ruthenium,[529] etc. as catalysts. Not only are these catalysts very expensive and difficult to recycle, but the products can contain transition metal impurities and purification becomes more complicated. This forms a major downside to utilizing these methods for the synthesis of pharmaceutical compounds.[530] Highly efficient, metal free, heterogeneous and recyclable catalysts are therefore essential to render this transformation attractive.

As an initial test the dimerization of benzylamine **91a** to *N*-(benzylidene)benzylamine **92a** was studied. The three bipyridine/phenylpyridine based COFs all gave a high conversion after 24 hours (Table 3, entry 1-3), with **TpBpyCOF** being the best performer, reaching 98%. **TpPa-1**, which was recently reported as a photocatalyst for this transformation,[337,531] was also evaluated. However, **TpPa-1** reached only 74% conversion, indicating the beneficial effects of the extra nitrogen atoms in the framework for photocatalytic applications.

Table 3: COF catalyzed benzylamine oxidation.[a]

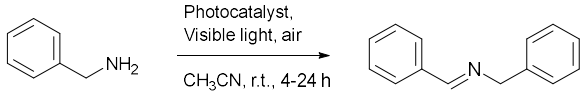

91a **92a**

Entry	Catalyst	Conversion (%)[b]	
		4 h	24 h
1	TpBpyCOF	49	98
2	TpOMeBpyCOF	41	86
3	TpPpyCOF	37	90
4	TpPa-1	32	74

[a] Reaction conditions: COF (5 mg), benzylamine **91a** (21 mg, 0.2 mmol, 1 eq.), CH_3CN (2 mL), CFL (26 W), r.t., 24 h.
[b] Determined via ^{1}H-NMR.

To investigate the mechanism, several control experiments were performed (Table 3). When inhibiting singlet oxygen or hydroxyl radicals with L-histidine,[532] or *i*PrOH[533] the conversion was not affected (Table 4, entry 2-3), suggesting that these oxygen species are not essential to the transformation. When inhibiting superoxide radicals with benzoquinone[534] the reaction was also unaffected (Table 4, entry 4). However, this quinone itself is an oxidising agent and therefore unsuited to probe the mechanism of this transformation.[319] A second experiment was therefore performed with nitroblue tetrazolium chloride (NBT),[535] another quencher of the superoxide radical. The reaction was significantly inhibited and the dark blue formazan was clearly formed (Table 4, right), indicating the presence and importance of superoxide radicals. Interestingly, TEMPO had no effect on the conversion (Table 4, entry 8). This suggests the absence of radical intermediaries, however TEMPO has also shown to be a mediater in this transformation,[341] and is therefore unsuited to quench radicals in this reaction. Quenching holes (KI)[536] or electrons ($AgNO_3$)[537] inhibited the reaction almost completely, pointing to the importance of both the holes and electrons (Table 4, entry 6-7). When oxygen was excluded from the reaction mixture, there was still some conversion, however the reaction was clearly supressed

(Table 4, entry 9). Suprisingly, in the dark, no real decrease in conversion was found (Table 4, entry 10), even after performing this experiment multiple times. This was of course a very intriguing result, suggesting an organocatalytic activation of oxygen at room temperature, and was therefore investigated further.

Table 4: Control experiments for the **TpBpyCOF** catalyzed oxidation of benzylamine under visible light. The picture shown on the right is of the reaction mixture containing NBT. The purple color originates from the formazan formed by reaction with the superoxide radicals.

Entry	Modification[a,]	Conversion (%)[b]
1	None	98
2	L-histidine	98
3	*i*PrOH	100
4	Benzoquinone	100
5	Nitroblue tetrazolium chloride (NBT)	30
6	$AgNO_3$	8
7	KI	11
8	TEMPO	100
9	Under argon	38
10	In the dark	92-98

[a] Reaction conditions: **TpBpyCOF** (5 mg), benzylamine **91a** (21 mg, 0.2 mmol, 1 eq.), CH_3CN (2 mL), CFL (26 W), r.t., 24 h
[b] Determined via ^{1}H-NMR.

First the reaction with benzylamine in the dark was repeated with the other COFs (Table 5, entry 2-4) and **TpOMeBpyCOF** and **TpPpyCOF** had similarly high conversions. However, when using **TpPa-1** a low conversion was detected. This suggests that while the bipyridine or phenylpyridine based COFs could act as organocatalysts for the activation of oxygen, **TpPa-1** with its phenyl linker could not.

Following this, the oxidation of dibenzylamine **93** was studied, as this has a much higher oxidation potential, which would make a photocatalytic oxidation at the holes more difficult. Besides, it is also a secondary amine, which would inhibit organocatalytic mechanisms that are reliant on imine formation. The results are shown in Table 6 and three observations can be made. First of all, whilst **TpBpyCOF** was able to catalyze this conversion quite well, as a conversion of 79% was reached, **TpOMeBpyCOF** and **TpPpyCOF** only reached 14% and 22% conversion and **TpPa**-1 was essentially not active. Secondly, the selectivity of the reaction was much lower, as in the **TpBpyCOF** catalyzed reaction a ratio of around 50/50 of the imine **92a** to benzaldehyde was formed. This is in contrast with the benzylamine oxidation, where generally very high selectivities were found (>99%, ^{1}H-NMR). Lastly, in contrast with the benzylamine oxidation, this reaction did not show any conversion in the dark. This means that for this substrate only a photocatalytic pathway is operating, whilst for benzylamine photocatalytic and organocatalytic (light-independent) pathways are occurring simultaneously.

To gain further information on the organocatalytic mechanism some of the quenching experiments were repeated in the dark, and similar results were found (Table 5, entry 5-9). TEMPO, benzoquinone, L-histidine and *i*PrOH showed no significant inhibition of the reaction. However, NBT completely inhibited the reaction, and again the dark purple formazan was formed, proving that $O^{-\bullet}$ is generated and is necessary for the reaction.

Lastly, three homogeneous control compounds **94**-**96** were made, by condensation of the corresponding amines with **Tp** (Figure 11). It should be noted that the **TpBpyCOF** analogue **96** possessed an extremely low solubility. The compound was therefore very hard to characterize or purify, and the crude product was used in the catalytic experiments. Interestingly, both compounds **95** and **96** were good homogeneous photocatalysts for this transformation when light was used. Compound **94**, possessing phenyls instead of pyridines or bipyridines, was much less active, pointing to the beneficial effects of these extra nitrogens in obtaining effective photocatalysts. Intriguingly, in

the dark, the catalytic activity of all three homogeneous catalysts was essentially non-existent, pointing to the necessity of a larger, extended system to obtain the activation of oxygen in the dark.

Table 5: Control experiments for the **TpBpyCOF** catalyzed oxidation of benzylamine in the dark.

Entry	Modification	Conversion (%)
1	None	92
2	TpOMeBpyCOF	94
3	TpPpyCOF	81
4	TpPa-1	19
5	TEMPO	100
6	Benzoquinone	>95[c]
7	L-histidine	93
8	*i*PrOH	91
9	NBT	9
10	**94**	0
11	**95**	4
12	**96**	2
13	**94**, light	42
14	**95**, light	100
15	**96**, light	97

[a] Reaction conditions: **TpBpyCOF** (5 mg), benzylamine **91a** (21 mg, 0.2 mmol, 1 eq.), CH_3CN (2 mL), in the dark, r.t., 24 h
[b] Determined via ^{1}H-NMR.
[c] Formation of a complex mixture.

Table 6: Investigation of the COF catalyzed dibenzylamine oxidation.

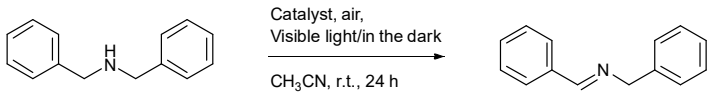

93 **92a**

Entry	Catalyst	Conversion (%)[b], ratio imine/aldehyde [b]	
		Light	Dark
1	TpBpyCOF	79 (0.50/0.50)	1.4 (0.77/0.23)
2	TpOMeBpyCOF	14 (0.75/0.25)	
3	TpPpyCOF	22 (0.68/0.32)	
4	TpPa-1	4 (0.74/0.26)	

[a] Reaction conditions: Catalyst (5 mg), dibenzylamine **93** (20 mg, 0.1 mmol, 1 eq.), CH_3CN (2 mL), CFL (26 W) or in the dark, r.t., 24 h
[b] Determined via ^{1}H-NMR.

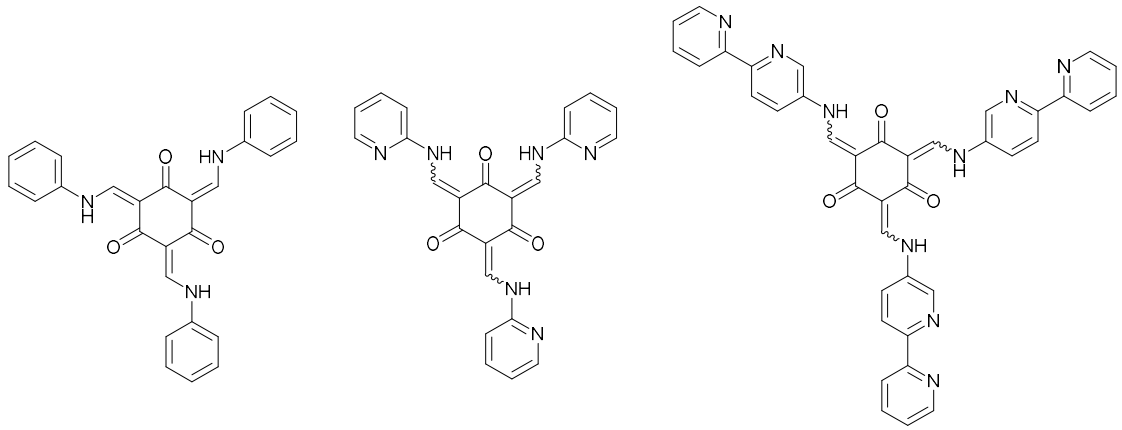

94 **95** **96**

Figure 11: The homogeneous control compounds that were made by condensation of the corresponding amine with **Tp** to further investigate the benzylamine oxidation.

Based on these results and existing literature, the following mechanism can be proposed for the oxidation pathway under visible light irradiation.[337,531,538,539] Electrons in the valence band of the COF will be excited to the conduction band. The excited electrons will reduce oxygen to the superoxide radical via single electron transfer. The generated positive holes will oxidize the amine **91** to its corresponding radical cation **97**, which will then react with the superoxide radical. H^+ and $H^\cdot$ transfer then generates the imine **98** and hydrogen peroxide. The generated hydrogen peroxide, a strong oxidizing agent, can also react with amines to produce another equivalent of imine and water. Nucleophilic attack of the amine **91** on the imine intermediate **98** followed by elimination of ammonia results in the final imine product being formed.

For the organocatalytical pathway that is operating irrespective of light, unfortunately, no real mechanism can be proposed at this time. Some examples of organocatalytic benzylamine oxidations are described in literature. For example, quinones[540] and salicylimines[541] have been reported as catalysts for this transformation. However, there is no explanation why the COFs would work in the dark, whereas the homogeneous controls were not active at all. Lastly, a bipyridine containing MOF has also been reported as a catalyst for the metal free activation of oxygen in the dark,[542] however at a very high temperature (150 °C), whilst the materials descriped in this work were active at room temperature.

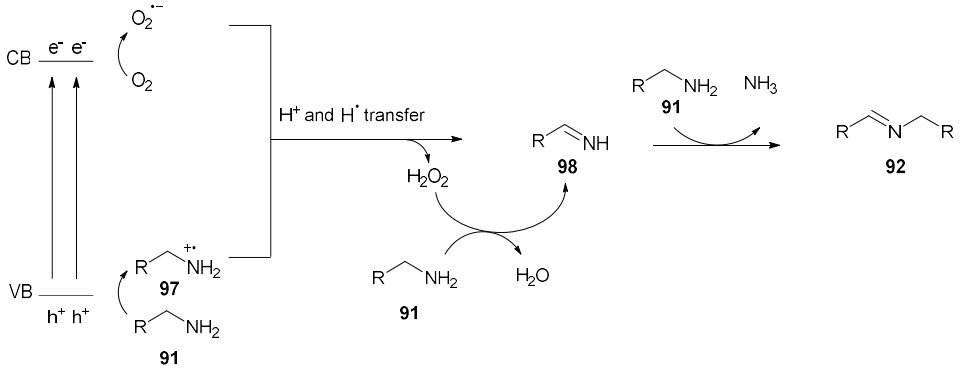

Scheme 21: Mechanism for the benzylamine oxidation pathway under visible light irradiation.

To probe the substrate scope a range of amines were reacted using **TpBpyCOF** as the catalyst, both using visible light as in the dark (Table 7). A wide range of substituents were tolerated and gave high conversions (73-99%). When the same reactions were performed in the dark, similar results were obtained, however generally longer reaction times were needed. This points out that while these reactions happen in the dark, the photocatalytic pathway enhances the reaction rate.

Table 7: COF catalyzed formation of imines **92a-f** from benzylamines **91a-f**, the reactions in the third column were performed under visible light irradiation, whilst the reactions in the last column were performed in the dark.[a]

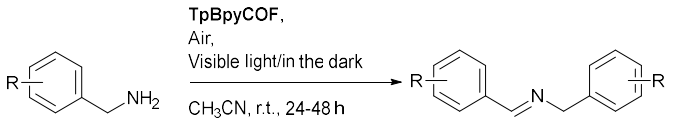

91a-f

92a-f
7 examples
73-99%

Entry	R	Conversion (%)	
		Under light irradiation, after 24 h	In the dark, after 24 h and 48 h
1	H	97	92[c]
2	4-Me	>99	96[c]
3	4-F	94	82, 98
4	2-Cl	80	47, 78
5	3-Br	92	50, 91
6	2-Br	73	38, 64
7	3-F	98	38, 94

[a] Reaction conditions: **TpBpyCOF** (5 mg), benzylamine **91a-f** (0.2 mmol), CH_3CN (2 mL), CFL (26 W)/in the dark, r.t., 24 h.
[b] Determined via ^{1}H-NMR.
[c] After 24 hours.

Lastly, recycling experiments were performed. Whilst in the second run the conversion was still largely unchanged (95%), after the third run the yield was lowered drastically (17%) and a lot of the material had degraded (Table 8). It was hypothesized that benzylamine reacts with the β-ketoenamine linkages, and thus degrades the material. A plausible mechanism in shown in Scheme 22. To further test this hypothesis, **TpBpyCOF** was stirred with cyclohexylamine in acetonitrile resutling in the complete degradation of the material, proving its instability towards strong amine nucleophiles. When the material was stirred with aniline, a weaker nucleophile, no degradation was detected. Some imine- or β-ketoenamine-linked COFs have been described in literature to catalyze this reaction and to be recyclable.[337,543] However, these results and other findings[338,544,545] do shed doubt on this recyclability. Recently, Jiménez-Almarza *et al.* synthesised three different POPs with triazine, imine and hydrazone linkages to use for the benzylamine oxidation. Both the imine and hydrazone-linked materials showed siginficant erosion upon reuse, while the CTF was stable. It can be concluded that β-ketoenamine-linked materials are similarly unstable to strong nucleophiles, and are therefore not suited for this transformation.

Table 8: Recycling of **TpBpyCOF** for the oxidation of benzylamine **91a**.[a]

Run	Conversion (%)	Remaining catalyst (mg)
1	98	30
2	95	8
3	17	Not determined

[a] Reaction conditions: **TpBpyCOF** (50 mg), benzylamine **91a** (214 mg, 2 mmol, 1 eq.), CH_3CN (20 mL), CFL (26 W), r.t., 24 h.

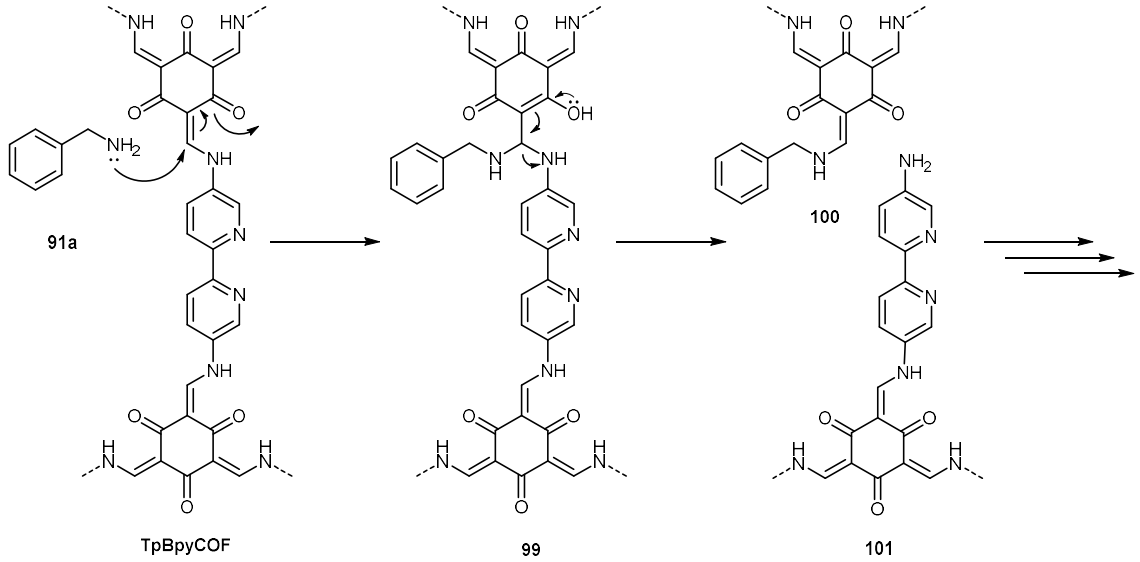

Scheme 22: Proposed mechanism for the observed degradation of the β-ketoenamine-linked **TpBpyCOF** during the benzylamine oxidation.

Next to the imine and β-ketoenamine-linked materials, which are clearly incompatible with strong nucleophiles such as benzylamines, other COFs have been reported in the literature for this transformation. Liu *et al.* utilized a highly hydrophilic hydrazine-based COF and obtained 99% conversion after 24 hours. However, these authors applied a very high loading of 200 mg/mmol.[520] A C=C linked COF with porphyrin knots has been reported, and obtained 96% yield after only 45 minutes using 85 mg/mmol loading.[546] The same porphyrin COF was discussed in Section 1.8.2.3.1, with TEMPO as co-catalyst. By applying 2 mol% TEMPO and 40 mg/mmol loading, a conversion of 94% could already be reached after 15 minutes, moreover, low-energy red light could be used.[341] Whilst **TpBpyCOF** performed better than the hydrazine-based material, these last two materials do possess superior activity, likely due to their less polarized C=C linkage and highly photoactive porphyrin moieties.

To conclude this section, four COFs were used as catalysts for the oxidation of benzylamines. **TpBpyCOF**, containing bipyridine moieties and β-ketoenamine linkages proved to be the most active. Using this material, a range of benzylamines could be oxidized. Interestingly, the reaction still worked in the dark, proving the existence of an unknown organocatalytical pathway for the activation of oxygen in these extended frameworks. Unfortunately, the exact mechanism that is operating is still unknown. From recycling experiments is is also clear that, unlike what is often reported in literature, these materials are not suited for this reaction, as they degrade through the unstability of the β-keto enamine linkage towards strong nucleophiles.

2.3.3.3 The tandem oxidation/Povarov cyclization

2.3.3.3.1 Introduction

The prepared photocatalysts were applied towards the tandem aerobic oxidation/Povarov cyclization, which allows the synthesis of quinoline-fused lactones and lactams **103** from cinnamyl 2-(arylamino)-acetates and acetamides **102** (Scheme 23). Quinoline-fused lactones and lactams are an important class of heterocycles and also serve as synthons for the synthesis of natural products and analogues such as Uncialamycin,[547–549] Luotonin A,[550] Camptothecin,[551] and quinolinecarboxamides[552,553] (Figure 12). The first report on this transformation used difficult-to-synthetize glyoxal imines **104** as starting materials with $BF_3{\cdot}Et_2O$ as a Lewis acid to catalyze the cyclization and stoichiometric DDQ to oxidize the intermediary tetrahydroquinoline **105**.[547] However, *in situ* generation of the imines from the corresponding, easily accessible and stable amines **102** is more convenient and can be achieved by a stoichiometric oxidant such as Oxone.[554] Tris(4-bromophenyl)ammoniumyl hexachloroantimonate, a radical cation salt, has also been used catalytically for this reaction with air as the terminal oxidant,[555] however, it is a moisture-sensitive irritant.[556] Moreover, tris(bipyridine)ruthenium/$BF_3{\cdot}Et_2O$[403] or rhodamine 6G/$HClO_4$[557] have been used as a photocatalyst/acid couple for this transformation. Nevertheless, a metal-free heterogeneous photocatalyst has not yet been reported for this reaction, whilst it can give many advantages, such as easy separation and catalyst recovery, avoiding toxic and expensive metals.

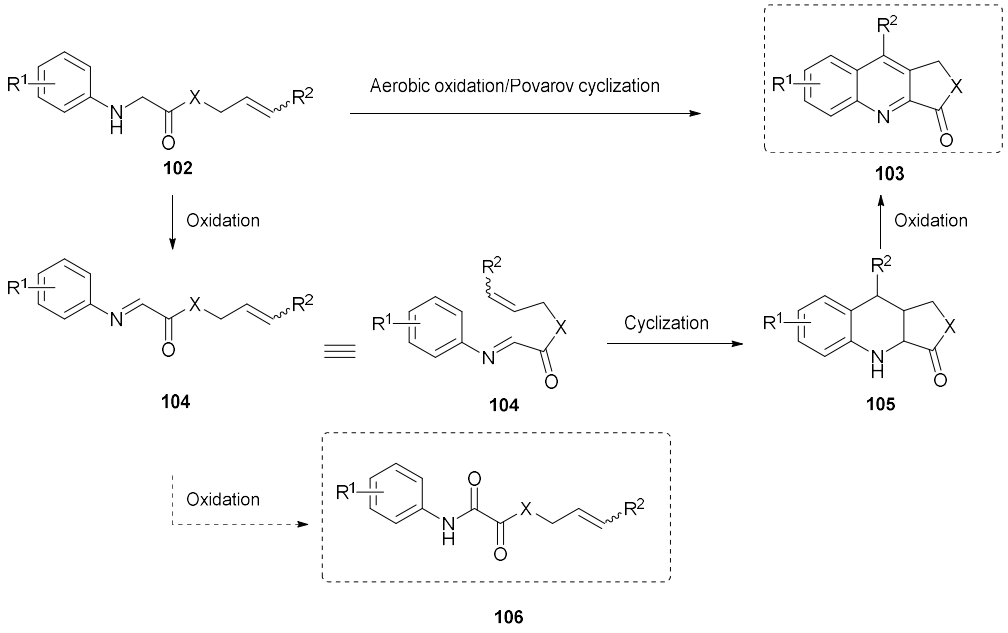

Scheme 23: One-pot oxidation-Povarov cyclization.

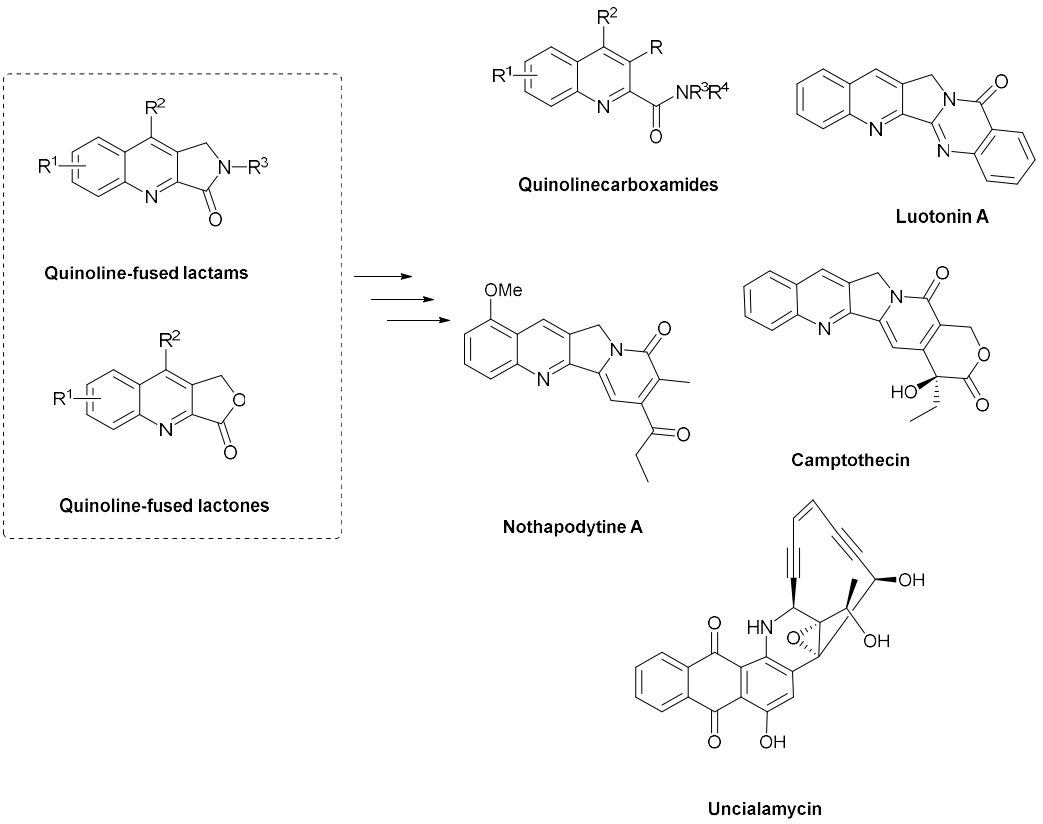

Figure 12: Utility of quinoline-fused lactams and lactones.

2.3.3.3.2 Optimalisation of the tandem oxidation-Povarov cyclization

The initial reaction conditions, using 10 mol% $BF_3{\cdot}Et_2O$ in acetonitrile at room temperature and exposed to air, were chosen based on literature data[403] (Table 9, entry 1-3). This gave moderate yields of 38%, 24% and 32% for **TpBpyCOF**, **TpOMeBpyCOF** and **TpPpyCOF**, respectively. When no Lewis acid was used, the formation of a side product, cinnamyl 2-oxo-2-(*p*-tolylamino)acetate **123a**, was detected in 42% yield (Table 9, entry 6). To further optimize the yield and to avoid the moisture- and air-sensitive $BF_3{\cdot}Et_2O$[558] many different Lewis and Brønsted acids were screened (Table 9, entry 7-31). First, the easier to handle and heterogeneous BF_3@silica was used, which also gave acceptable yields (Table 9, entry 8). However $Sc(OTf)_3$ gave the most promising results (Table 9, entry 15). When higher or lower amounts than the standard 10 mol% were used, lower yields were obtained (Table 9, entry 32 and 33). The screening of solvents other than acetonitrile such as $PhCF_3$, EtOH, THF, CH_2Cl_2, DMF, HFIP, or 1,2-DCE (Table 9, entry 35-41) all resulted in lower yields, except for nitromethane which also gave promising results, indicating that a polar, aprotic solvent is ideal for this reaction (Table 9, entry 42). Nitromethane was then also screened with some other Lewis acids (Table 9, entry 43-44), however, this did not improve the yields and finally CH_3CN was chosen because it is much less harmful than CH_3NO_2. Lastly, **TpOMeBpyCOF** and **TpPpyCOF** were again tested using $Sc(OTf)_3$, as well as $Ru(Bpy)_3(PF_6)_2$ and all gave worse results than **TpBpyCOF** (Table 9, entry 45-48). **TpBpyCOF**, possessing bipyridine units and β-ketoenamine linkages, was the most performant, which corroborates the earlier report on acridine based COFs, where the fully β-ketoenamine-linked material proved to be the most effective photocatalyst.[514]

Table 9: Optimization of the tandem oxidation-Povarov cyclization.[a]

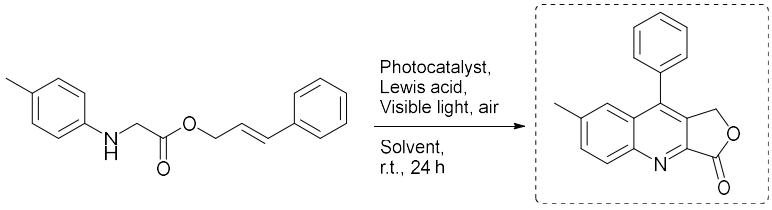

102a **103a**

Entry	Photocatalyst	Lewis acid	Solvent	Yield (%)[b]
1	TpBpyCOF	$BF_3{\cdot}Et_2O$	CH_3CN	38
2	TpOMeBpyCOF			24
3	TpPpyCOF			32
4	$[Ru(Bpy)_3](PF_6)_2$[c]			22
5	$[Ru(Bpy)_3](PF_6)_2$[d]			43
6	TpBpyCOF	No Lewis acid		/[e]
7	TpBpyCOF	$BF_3@SiO_2$		48
8		1 eq. $BF_3{\cdot}Et_2O$		26
9		$BF_3{\cdot}Et_2O$/TMSOTf		46
10		TMSOTf		55
11		$Cu(OTf)_2$		19
12		$Bi(OTf)_3$		38
13		TFA		41
14		$Dy(OTf)_3$		52
15		**$Sc(OTf)_3$**		**61**
16		$HN(OTf)_2$		45
17		$Zn(OTf)_2$		29
18		$AlCl_3$		25
19		$Ho(OTf)_3$		36
20		$Yb(OTf)_3$		49
21		$Er(OTf)_3$		40
22		$La(OTf)_3$		41
23		$Sm(OTf)_3$		49
24		$Eu(OTf)_3$		45
25		$HAuCl_4{\cdot}3H_2O$		33
26		$Gd(OTf)_3$		40
27		$In(OTf)_3$		40
28		$Ce(OTf)_3$		57
29		$CeCl_3{\cdot}7H_2O$		20
30		$TiCl_4{\cdot}2THF$		9
31		$B(PhF_5)_3$		14
32		5 mol% $Sc(OTf)_3$		32
33		30 mol% $Sc(OTf)_3$		39
34		10 mol% $Sc(OTf)_3$	CH_3CN[f]	52
35			$PhCF_3$	27
36			EtOH	5
37			THF	17
37			CH_2Cl_2	22
38			DMF	12
39			1,2-DCE	32
40			HFIP	n.r.[g]
41			CH_3NO_2	60
42		TMSOTf	CH_3NO_2	57
43		$B(PhF_5)_3$	CH_3NO_2	26
44	TpOMeBpyCOF	$Sc(OTf)_3$	CH_3CN	50
45	TpPpyCOF			49
46	$[Ru(Bpy)_3](PF_6)_2$[c]			12
47	$[Ru(Bpy)_3](PF_6)_2$[d]			42

[a] Reaction conditions: Cinnamyl *p*-tolylglycinate **102a** (28 mg, 0.1 mmol, 1 eq.), COF (10 mg) or $[Ru(Bpy)_3](PF_6)_2$ (1 or 10 mol%),[c,d] Lewis acid (10 mol%), 1 mL CH_3CN, 26 W CFL, 24 h, r.t.

[b] Determined by ^{1}H-NMR analysis using 1,3,5-trimethoxybenzene or mesitylene as an internal standard.

[c] 1 mol%, [d] 10 mol%.

[e] 42% cinnamyl 2-oxo-2-(*p*-tolylamino)acetate **123a** was detected.

[f] 5 mL CH_3CN.

[g] No reaction.

2.3.3.3.3 The synthesis of substrates for the Povarov reaction

*2.3.3.3.3.1 The synthesis of N-aryl glycine esters **102a-k***

To test the substrate scope of the Povarov reaction, a wide range of *N*-aryl glycine esters **102** were synthesized. Two different procedures based on literature were followed (Scheme 24). In both procedures the haloacetylated derivatives **110a-d** were synthesized by reaction of different allylic alcohols **107a-c** with chloroacetyl chloride **108** or bromoacetyl bromide **109**. Commercially available cinnamyl alcohol **107a** and (2*E*,4E)-hexa-2,4-dien-1-ol **107c** were used, whilst (*E*)-3-(naphthalen-2-yl)prop-2-en-1-ol **107b** was synthesized using a Horner-Wadsworth-Emmons olefination followed by DIBAL reduction of commercially available 2-naphthaldehyde. The haloacetylated derivatives **110a-d** were converted into the desired *N*-aryl glycine esters **102a-k** by alkylation with an aniline derivative in acetonitrile or DMF. For compounds **102a-d** method A[555] was used, however, it was found that this required long reaction times and did not allow for full conversion of starting materials in the case of more electron poor anilines. Therefore method B[554] was applied for the synthesis of the other substrates **102e-k**. Using these procedures eleven different *N*-aryl glycine esters **102a-k** were made in yields ranging from 23% to 59% over the two steps.

*2.3.3.3.3.2 The synthesis of N-aryl glycine amides **102l-n**.*

Whilst the synthesis of the *N*-aryl glycine esters **102a-k** went relatively well, and the desired compounds could easily be produced, the synthesis of *N*-aryl glycine amides **102l-n** proved more challenging, and no synthetic route was described in literature for these compounds. Based on the previously used route for the synthesis of the *N*-aryl glycine esters **102a-k** a three-step process starting from cinnamyl bromide **111** was used (Scheme 25).

The monosubstituted *N*-cinnamyl amines **112a-c** could be isolated in relatively low yields (22-41%), by reaction of cinnamyl bromide **111** with three equivalents of amine in EtOH. In all cases large amounts of overalkylated di- and trisubstituted sideproducts were obtained next to the desired monoalkylated amine. Using ammonia as a nucleophile only polyalkylated products were detected (LC-MS), and not the desired primary (*E*)-3-phenylprop-2-en-1-amine. The next step was the formation of the 2-bromophenylacetamides **113a-c** by amide formation with bromoacetyl bromide **109**. In this reaction more complex mixtures were obtained than in the synthesis of the ester derivatives, necessitating chromatography. Similarly, the final step also gave more difficulties than for the ester derivatives, with relatively low isolated yields for the phenyl and *p*-methoxybenzyl derivatives **102l-m** of 26% and 30%, respectively. For the isobutyl derivative **102n** only a very low amount of product could be isolated, and therefore this compound was not used in the following Povarov reaction.

2.3.3.3.4 The synthesis of substrates for the α-oxidation of glycine derivatives

Next to the oxidation/Povarov reaction, the COFs catalyzed the α-oxidation of *N*-aryl glycine derivatives to the corresponding *N*-aryl oxalic acid derivative when no Lewis acids present (Table 9, entry 6). To further explore this transformation a range of substrates were synthesized (Scheme 26). Ethyl *p*-tolylglycinate **116i** was synthesized, following a literature procedure, by alkylation of *p*-toluidine **114** with ethyl bromoacetate **115**.[559] In a similar manner *p*-tolylglycine **118** could be prepared, by hydrolysis of this ester.[560] 1-(*p*-Tolylamino)propan-2-one **116n** was prepared by alkylation of *p*-toluidine **114** with chloroacetone **121**.[561]

Some new amides **116j-l** and a thioester **116m** were prepared by a three step procedure starting from previously prepared *p*-tolylglycine **118**. First, this was Boc protected to the corresponding *N*-Boc derivative **119**. Using typical amide coupling conditions, *i.e.* hexafluorophosphate benzotriazole tetramethyl uronium (HBTU) and *N*-methylmorpholine (NMM) in DMF, amides **120a-c** were easily prepared in good yields (63-92%) after purification with reversed phase chromatography. For the thioester **120d**, hexafluorophosphate azobenzotriazole tetramethyl uronium (HATU) with DIPEA in DMF was used, as this was reported to be an optimal reagent for the synthesis of thioesters.[562] After Boc deprotection using TFA in CH_2Cl_2 the desired unprotected compounds **116j-m** were obtained. Lastly, to obtain an aliphatic analogue, ethyl cyclohexylglycinate **116o** was synthesized by reaction of cyclohexylamine **122** with ethyl bromoacetate **115**.[563]

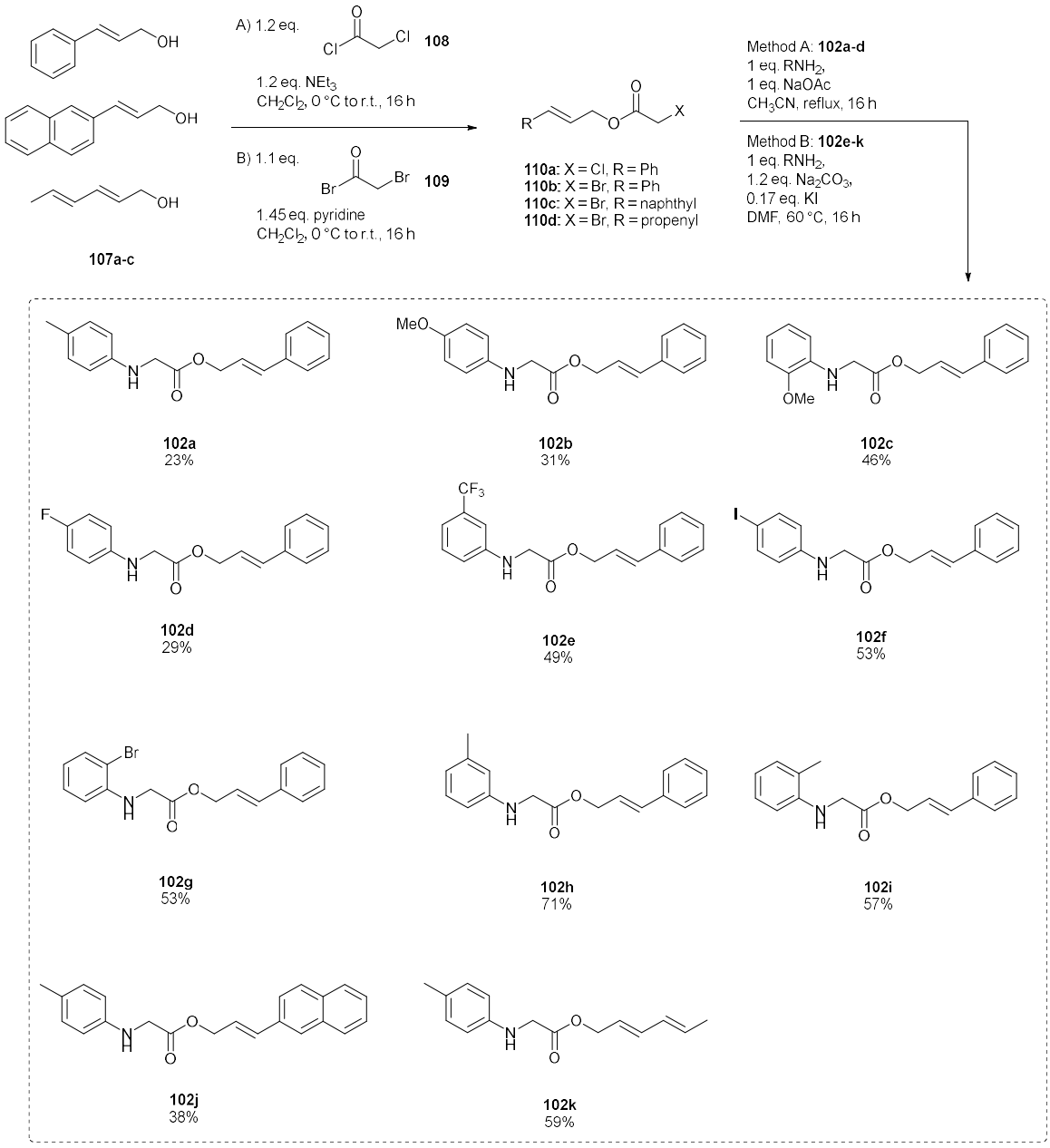

Scheme 24: Synthesis of *N*-aryl glycine esters **122a-k**.

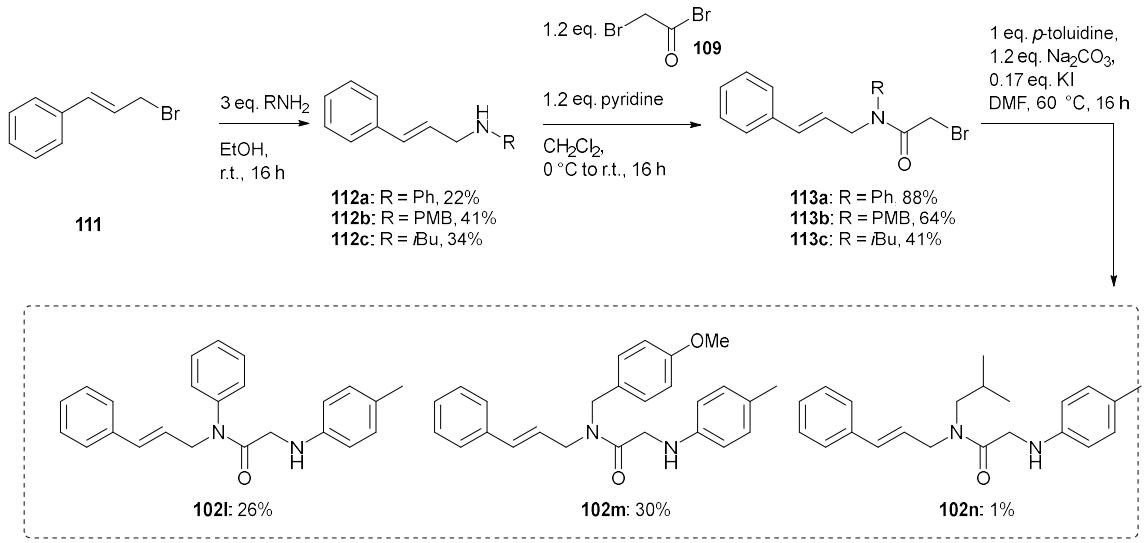

Scheme 25: Synthesis of *N*-aryl glycine amides **102l-n**.

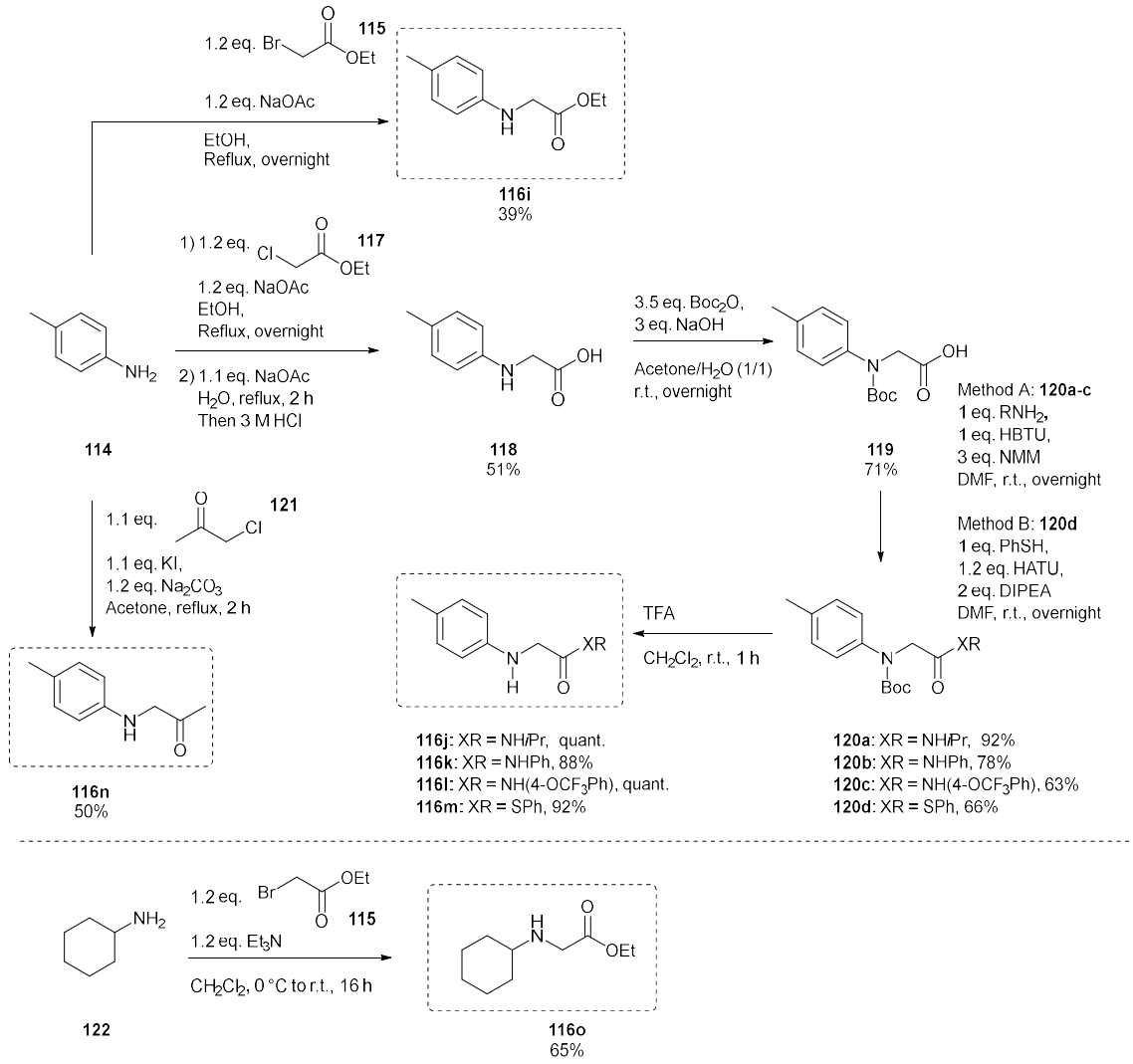

Scheme 26: Synthesis of glycine derivatives **116i-o** to use as substrates for the photocatalyzed α-oxidation.

2.3.3.3.5 Substrate scope and mechanism of the tandem oxidation-Povarov cyclization

With the optimal conditions at hand, the scope of the reaction was examined by reacting a wide range of substrates **102a-m** with both electron-withdrawing (F, CF_3, Br, I) and electron-donating (OMe, Me) substituents in various positions (*ortho*-, *meta*- and *para*-). The corresponding quinolines **103a-m** were obtained in moderate yields (Table 10, 27-62%). While full conversion of the starting materials was achieved in all cases, side reactions and losses during isolation resulted in moderate isolated yields. As major side products were generally not observed in ^{1}H-NMR and LC-MS analysis, it is thought that the substrates partly polymerize during the reaction to form insoluble oligomers, which lower the yield. When using *meta*-substituted aryls, mixtures of the 6- and 8-substituted regioisomers (6/8: 64/36 for **103h** and 87/13 for **103e**) were observed, of which only the isomer **103e** could be isolated in the case of the trifluoromethyl substituted quinoline. Substitution of the R^2-group was also tolerated and both naphthalene and vinylene substituted quinolines **103j** and **103k** could be isolated with acceptable yields (39% and 35%). The photochemical synthesis of quinoline fused lactams had not yet been reported, and to our delight quinoline fused lactams **103l-m** could also be synthesized and isolated in 47% and 31% yield.

Table 10: **TpBpyCOF** and $Sc(OTf)_3$ catalyzed synthesis of quinolines **103a-m**.[a,b]

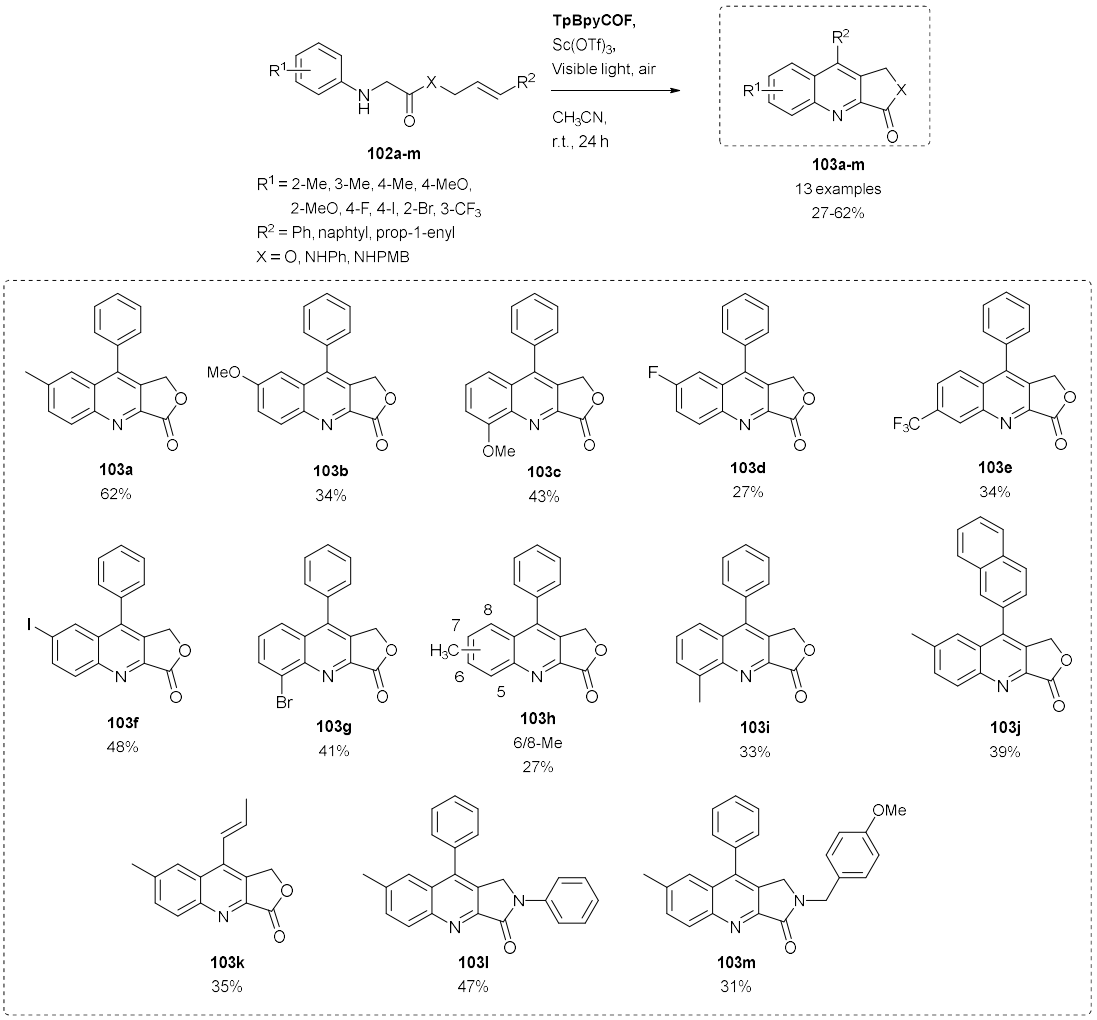

[a] Reaction conditions: Substrate **102a-m** (0.2 mmol, 1 eq.), 20 mg **TpBpyCOF**, $Sc(OTf)_3$ (10 mg, 0.02 mmol, 0.1 eq.), 2 mL CH_3CN, 26 W CFL, 24 h, r.t.

[b] Isolated yields are reported.

Next to these quinolines, a series of oxalic acid derivatives **123a-k** could be synthesized by photocatalytic α-oxidation of the glycine derivatives **116a-k** when no Lewis acid was present in the system (Table 11). A wide range of oxalic acid derivatives **123a-k** could be produced in this way, albeit in relatively low isolated yields (15-47%). These rather low yields were due to side reactions and losses by purification using reversed phase chromatography. For the trifluoromethoxy-substituted substrate **116l**, no product could be isolated, due to the low stability of the starting material in solution. For thioester **116m**, the oxidized end product was obtained, however, it could not be fully separated from impurities. The product resulting from oxidation of ketone **116n** was obtained in only a very low yield (6%). For compound **116o** no product was obtained, and degradation of the COF was observed as the nucleophilic amine attacks the β-ketoenamine linkage and solubilizes the COF.

Table 11: COF catalyzed synthesis of oxalic acid derivatives **116a-k**.[a,b]

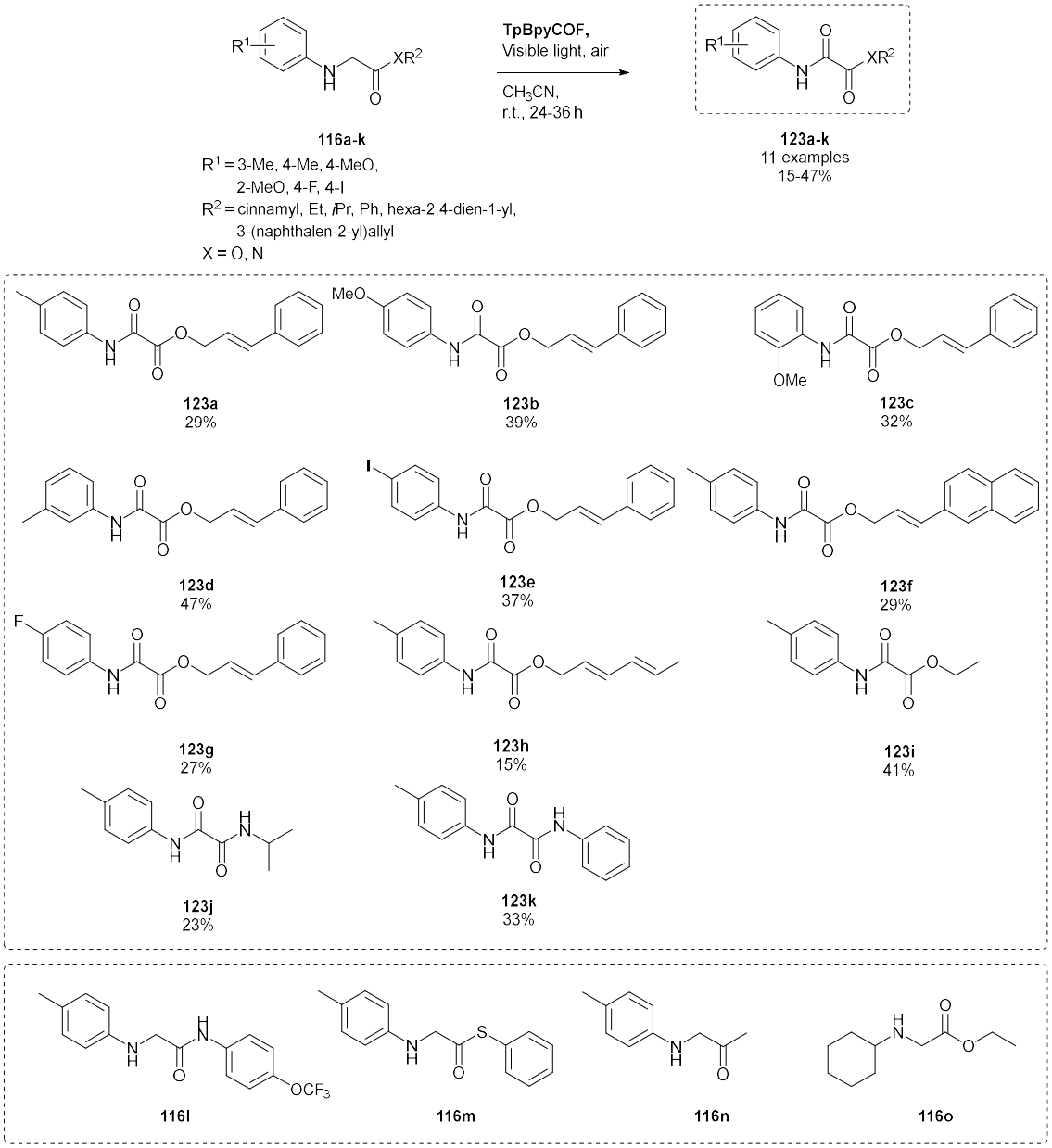

[a] Reaction conditions: substrate **116a-k** (0.2 mmol, 1 eq.), 20 mg **TpBpyCOF**, 2 mL CH_3CN, 26 W CFL, 24-36 h, r.t.
[b] Isolated yields are reported.

To probe the mechanism of the oxidation/Povarov cyclization, several control experiments were performed (Table 12). In the dark, under argon or without COF, no product was formed (Table 12, entry 2-4). In absence of a Lewis acid the oxalic acid derivative was formed (Table 12, entry 5). Thus oxygen, light, the COF and the Lewis acid were essential for the transformation. To study the role of oxygen, several quenchers were added (Table 12, entry 6-14). Using quenchers for the superoxide radical, *p*-benzoquinone[534] or nitro blue tetrazolium chloride,[535] only a slight decrease in yield was observed. Similarly, *i*PrOH, a quencher for hydroxyl radicals,[533] did not lower the yield significantly. However, when using quenchers for singlet oxygen, such as L-histidine,[532] DABCO[564] or sodium azide[565] the reaction was inhibited effectively. This leads us to conclude that the key driver for this transformation is singlet oxygen. When quenching holes and electrons using KI[536] and $AgNO_3$,[537] respectively, the yield was also lowered. In the presence of TEMPO,[566] a known radical scavenger, the yield lowered drastically (Table 12, entry 14), suggesting the involvement of radical processes.

Based on these control experiments and previous reports[403,554,567] the following mechanism is proposed (Scheme 27). Upon irradiation of the COF, singlet oxygen is produced by direct energy transfer[568–572] or by sequential oxidation/reduction of molecular oxygen.[573] The photogenerated singlet oxygen then oxidizes the amine **102** to the corresponding imine **104**, hereby generating H_2O_2.[574–576] In absence of a Lewis acid imine **102** is further oxidized to the oxalic derivative **106**. In presence of a Lewis acid, imine **104** undergoes an intramolecular aza-Diels-Alder reaction, which can either occur concerted (Path A) or stepwise (Path B).[577] The resulting tetrahydroquinoline **105** is then further oxidized to the quinoline product **103**. Lastly, reuse experiments were performed to ascertain the stability of **TpBpyCOF** in the reaction. Upon recycling the catalyst for five times, full conversion of the starting material was still achieved, however the yield had dropped to 45%, which is still 75% of the original activity (Figure 13a). This lowered yield is likely caused by the slow degradation of the material over the reaction cycles, causing an increased number of side reactions in the starting material, such as oligomerization. While the main chemical linkages of **TpBpyCOF** remained intact according to FTIR, the PXRD of the recycled material indicated that it had lost its crystallinity (Figure 13b-c). The loss of activity and crystallinity, while unfortunate, has been observed many times for photoactive COFs, and can be attributed to photobleaching, partial deactivation by singlet oxygen and also possibly side reactions with intermediates formed during the reaction.[347,374,514,578,579]

Table 12: Control experiments for the Povarov reaction.

Entry	Conditions[a]	Result (%)[b]
1	No modification	62
2	In the dark	n.r.
3	Under argon	n.r.
4	No COF	n.r.
5	No Lewis acid	42% **123a**
6	*p*-Benzoquinone	52
7	Nitro blue tetrazolium chloride[a]	53
8	*i*PrOH	51
9	L-histidine	6
10	DABCO	n.r.
11	NaN_3	n.r.
12	$AgNO_3$	27
13	KI	n.r.
14	TEMPO	10

[a] Reaction conditions: Cinnamyl *p*-tolylglycinate **102a** (28 mg, 0.1 mmol, 1 eq.), 10 mg **TpBpyCOF**, $Sc(OTf)_3$ (5 mg, 0.01 mmol, 0.1 eq.), quencher (0.1 mmol, 1 eq.), except NBT (12 mg, 0.015 mmol, 0.15 eq.).
[b] Determined by ^{1}H-NMR analysis using 1,3,5-trimethoxybenzene as an internal standard.

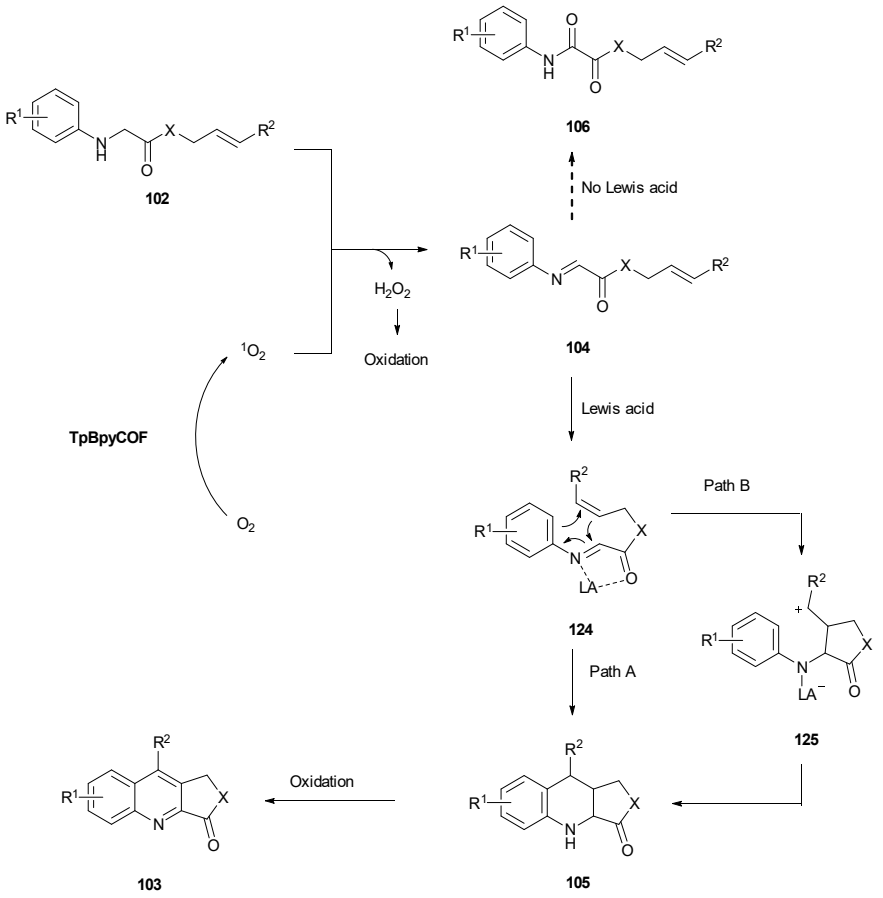

Scheme 27: Mechanism for the photocatalytic generation of quinolines **103** and glyoxal derivatives **106** by **TpBpyCOF**.

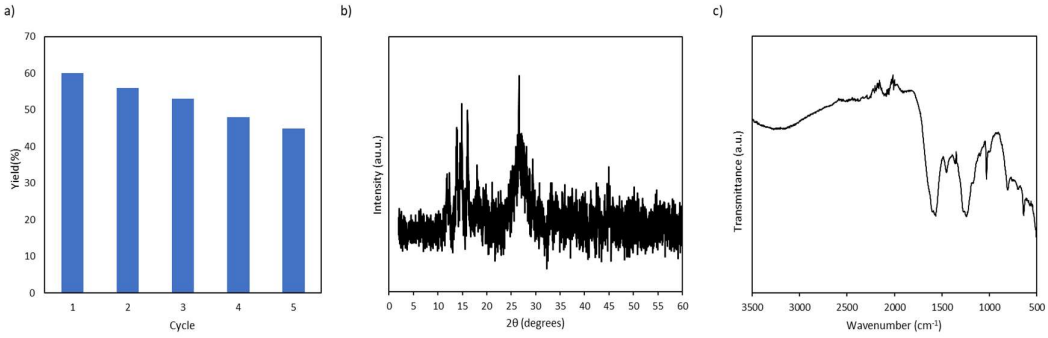

Figure 13: Recycling **TpBpyCOF**: (a) Yields of the cycling experiments; (b) PXRD; and (c) FTIR of recycled **TpBpyCOF** after five runs.

In this section the application of three structurally related COFs, **TpBpyCOF**, **TpOMeBpyCOF** and **TpPpyCOF**, was described towards the oxidation-Povarov cyclization and α-oxidation of *N*-aryl glycine derivatives. **TpBpyCOF**, containing bipyridine moieties and β-ketoenamine linkers was the most effective photocatalyst and a wide range of quinoline-fused lactones/lactams and glyoxal derivatives were successfully synthesized, which is a new application for photoactive COFs.

2.3.4 Anchoring of ruthenium on a COF

As stated in the literature review, a possible method to obtain more photoactive materials is the addition of photocatalytic metal complexes. Tris(2,2'-bipyridine)ruthenium(II) [$Ru(bpy)_3$], together with tris(2-phenylpyridine)iridium [$Ir(ppy)_3$] are prototypical visible light photocatalysts. A quick Scifinder search highlights this importance: as of September 2022 tris(bipyridine)ruthenium(II) chloride has been used in more than 2700 publications. However, homogeneous precious metal complexes possess many disadvantages, such as toxicity, cost, a difficult separation from the final product and a low to non-existent recyclability. Immobilizing ruthenium bipyridine complexes on a COF is therefore highly attractive, as it would make recycling easy, and prevent any leaching of the (toxic) metal into the product. The already synthesized **TpBpyCOF** was selected as the target material and two approaches were taken: bottom-up synthesis and postsynthetic metalation, to produce **Ru@TpBpyCOF**. This material was then used as a heterogeneous catalyst for the intermolecular tandem aerobic oxidation/Povarov reaction.

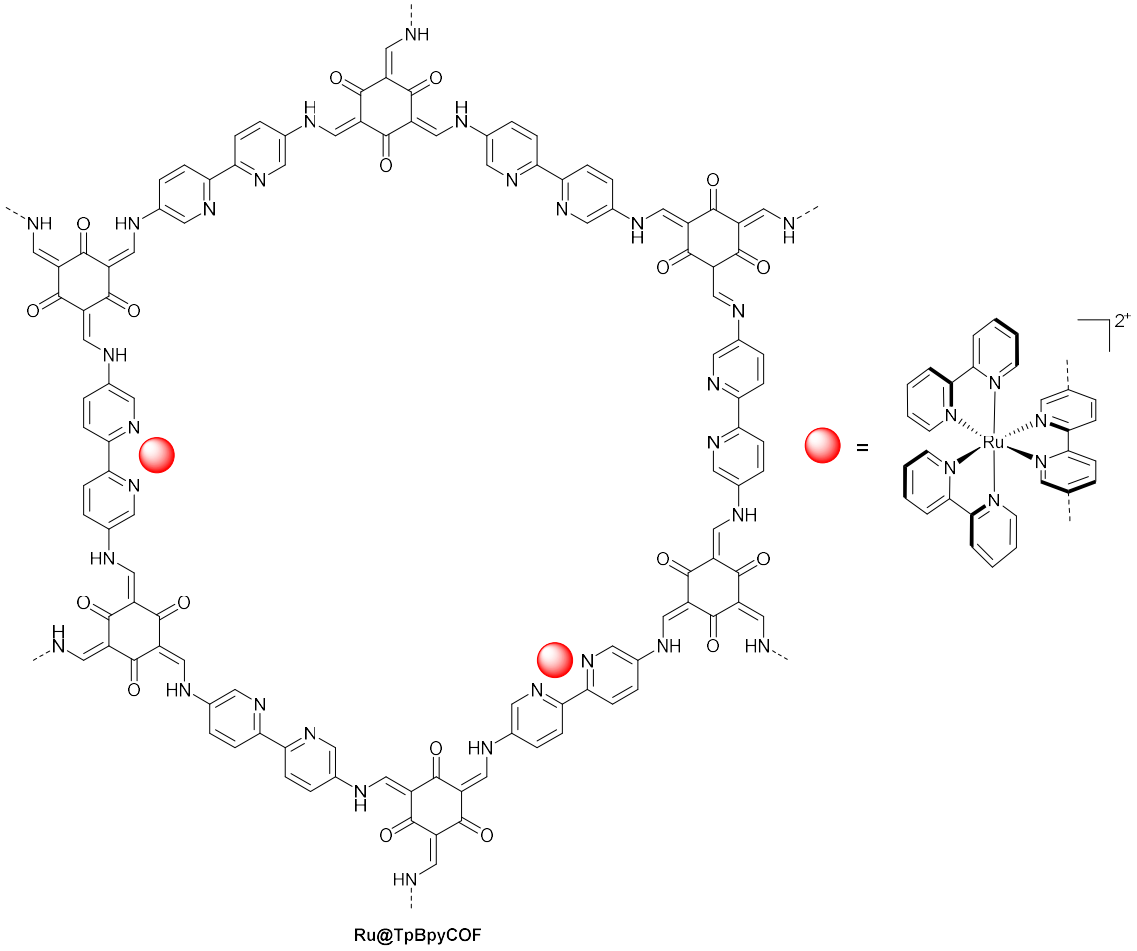

Figure 14: Structure of **Ru@TpBpyCOF**.

2.3.4.1 The synthesis of Ru@COF

2.3.4.1.1 Postsynthetic metalation of TpBpyCOF

TpBpyCOF was metalated with *cis*-dichlorobis(2,2'-bipyridine)ruthenium(II) **126** under a variety of conditions, using a postsynthetic metalation approach (Table 13). Quite disappointingly, no ruthenium loading was ever detected using X-ray fluorescence (XRF) as a qualitative method. It is possible that the complex is simply too sterically hindered to efficiently penetrate the pores to perform the desired metalation. Alternatively, the used metalation conditions were simply not suited to this material. Interestingly, an analogue of this material, but with iridium (Ir@TpBpyCOF) has been reported very recently, and this material was synthesized using postsynthetic metalation.[580] The iridium precursor used was $[Ir(ppy)_2(CH_3CN)_2]PF_6$, whose labile acetonitrile ligands possibly allowed for smoother anchoring. In any case, the postsynthetic metalation strategy was no longer pursued in this work, and a bottom-up strategy was therefore devised.

Table 13: Attempted synthesis of **Ru@TpBpyCOF** by postsynthetic metalation with complex **126**.

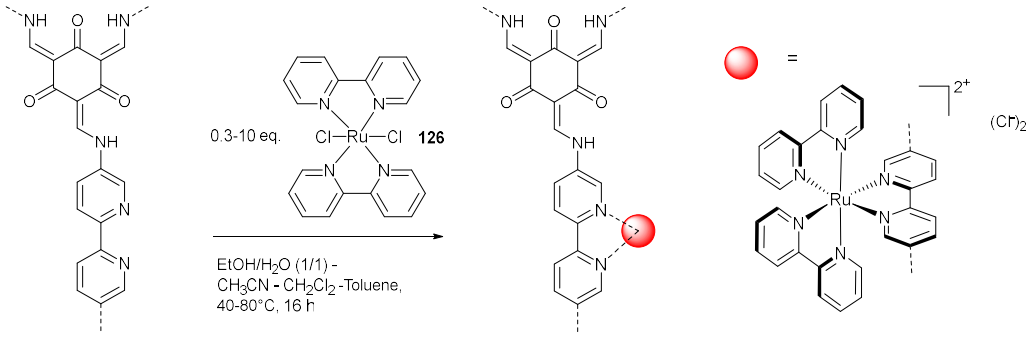

TpBpyCOF Ru@TpBpyCOF

Entry	Conditions[a]	Result
1	0.3 eq. *cis*-$Ru(bpy)_2Cl_2$, $EtOH/H_2O$ (1/1), 80 °C	/ (XRF)
2	10 eq. *cis*-$Ru(bpy)_2Cl_2$, $EtOH/H_2O$ (1/1), 80 °C	/ (XRF)
3	10 eq. *cis*-$Ru(bpy)_2Cl_2$, CH_3CN, 80 °C	/ (XRF)
4	1 eq. *cis*-$Ru(bpy)_2Cl_2$, CH_3CN, 80 °C	/ (XRF)
5	1 eq. *cis*-$Ru(bpy)_2Cl_2$, CH_2Cl_2, 40 °C	/ (XRF)
6	1 eq. *cis*-$Ru(bpy)_2Cl_2$, Toluene, 100 °C	0.262 m/m% (ICP-OES)

[a] Reaction conditions: **TpBpyCOF** (29 mg, 0.1 mmol bpy sites, 1 eq.), 2 mL solvent, 16 h

2.3.4.1.2 Bottom-up synthesis of Ru@TpBpyCOF

In a bottom-up synthesis a precursor of the material is already metalated. This can provide more reliable metal anchoring compared with postsynthetic metalation. Luckily, the synthesis of a precursor, complex **Ru@Bpy** was already described in the literature (Scheme 28).[581] **Ru@Bpy** could easily be prepared from **Bpy** by metalation with complex **126**. When ammonium hexafluorophosphate was added upon completion of the reaction, the product precipitated out, and it could be conveniently isolated by filtration to give the metalated linker in high yield (90%).

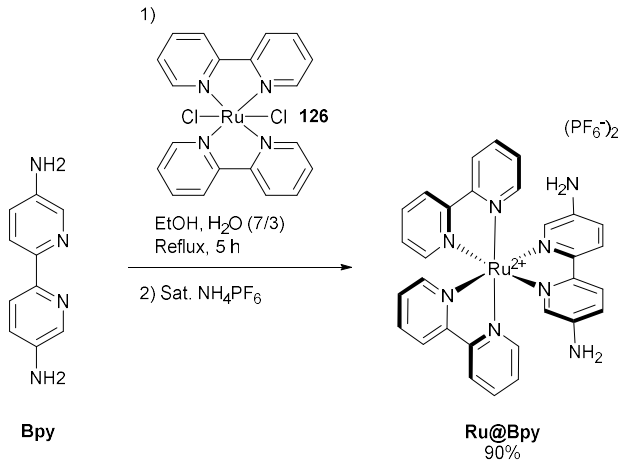

Scheme 28: The synthesis of **Ru@Bpy**, a metalated precursor for the bottom-up synthesis of **Ru@TpBpyCOF**.

Polymerizing varying amounts of this complex **Ru@Bpy**, together with unmetalated **Bpy** and **Tp**, resulted in **Ru_1-100@TpBpyCOF**. The ruthenium contents of these materials were measured with inductively coupled plasma optical emission spectroscopy (ICP-OES, Table 14). In all cases these metal contents were lower than the theoretical contents, which points out that the complex is preferentially not incorporated into the COF, in comparison with the much less sterically hindered **Bpy**. However, in **Ru_10@TpBpyCOF** 0.96% m/m% Ru was detected. This is a quite good loading, considering the high mass of the complex and the material in comparison with the ruthenium atom itself. The synthesis of a last material, **Ru_100@TpBpyCOF**, where only **Ru@Bpy** was used (x = 100) was also performed. This material was only obtained with very low yields, likely due to steric hindrance precluding efficient polymerization, and was not further used.

Table 14: Bottom-up synthesis of **Ru@TpBpyCOF**.[a]

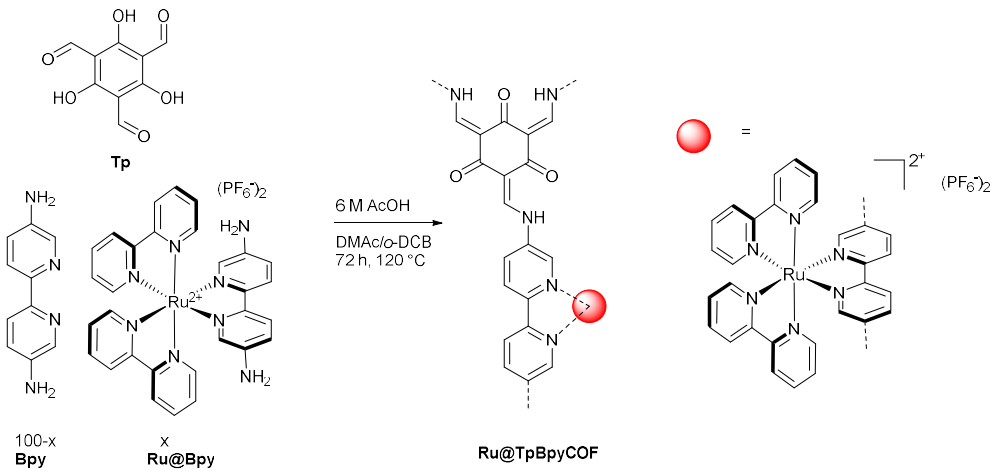

Material	x	Theoretical ruthenium content m/m(%)	Measured ruthenium content m/m (%)[a]
Ru_1@TpBpyCOF	1	0.36	0.262
Ru_2.5@TpBpyCOF	2.5	0.87	0.41
Ru_5@TpBpyCOF	5	1.64	0.78
Ru_10@TpBpyCOF	10	2.95	0.96
Ru_100@TpBpyCOF	100	6.78	5.57

[a] Reaction conditions: 1,3,5-triformylphloroglucinol **Tp** (63.0 mg, 0.3 mmol, 1 eq.), 2,2'-bipyridine-5,5'-diamine **Bpy** (100-x * 0.45 mmol), **Ru@Bpy** (x * 0.45 mmol), DMAc (4.5 mL), *o*DCB (1.5 mL), 6M AcOH (0.6 mL), 120 °C, 72 h.
[b] Measured by ICP-OES.

2.3.4.1.3 Characterization of Ru@TpBpyCOF

As a first characterization technique FTIR spectroscopy was used, and the IR spectrum of **Ru_10@TpBpyCOF** was virtually identical to that of pristine **TpBpyCOF** (Figure 14a). The nitrogen sorption isotherms also did not show a large difference between the two materials, with the surface area only dropping slightly, from 879 m^2/g to 811 m^2/g, in the metalated material (Figure 14b). Lastly, the PXRD pattern of **Ru_10@TpBpyCOF** corresponded well with that of **TpBpyCOF**, albeit with a lower intensity, indicating a lower degree of crystallinity (Figure 14c). XPS spectra were also taken, but given the relatively low abundance of ruthenium in the material, and overlap between the Ru 3d with the C 1s signals, no convolution could be obtained.

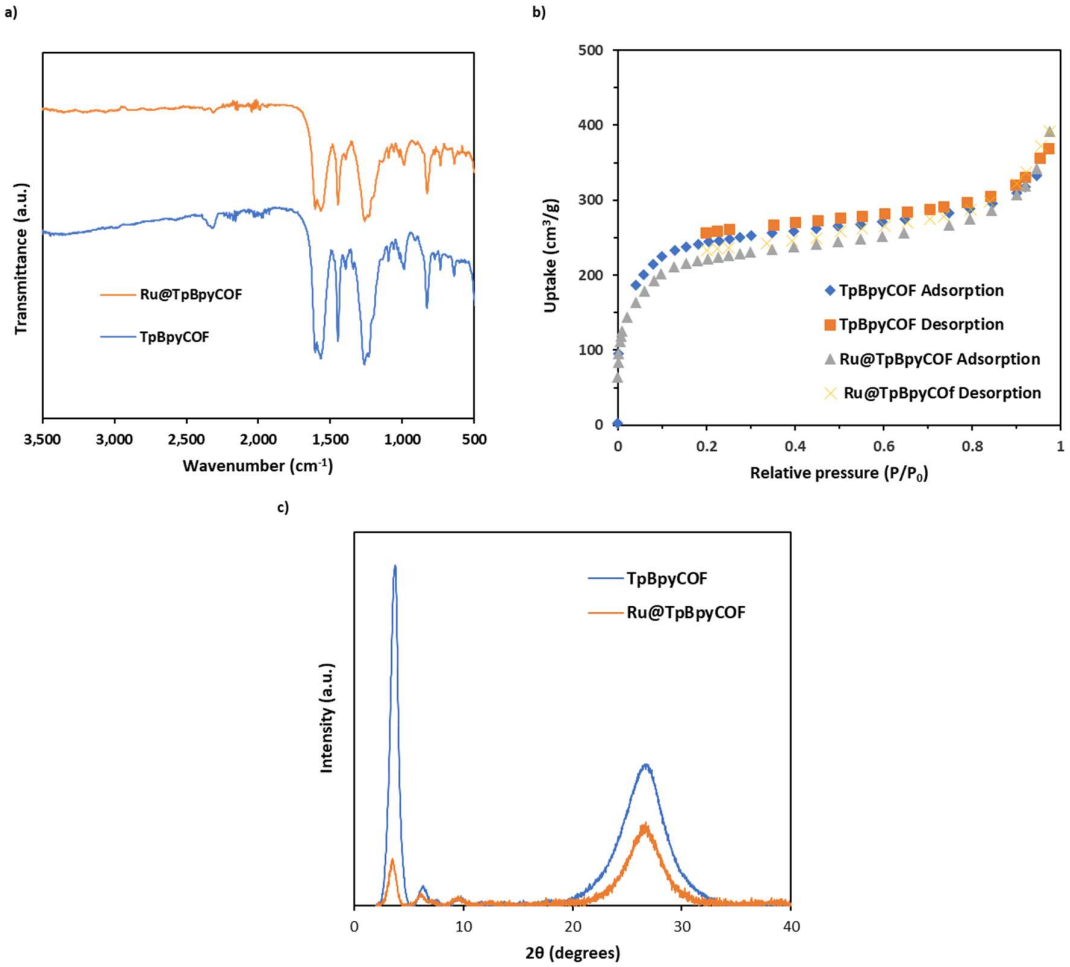

Figure 15: FTIR spectra (a); N_2 sorption curves (b) and XRD spectra (c) of **TpBpyCOF** and **Ru@TpBpyCOF**.

2.3.4.2 Application of Ru@TpBpyCOF as a catalyst in the tandem oxidation/intermolecular Povarov cyclization

The metalated **Ru@TpBpyCOF** was used for a similar application as **TpBpyCOF**, *i.e.* a tandem oxidation/Povarov cyclization, only this time the cyclization was intermolecular. This reaction was reported in literature to be working well with $Ru(bpy)_3Cl_2.6H_2O$ as a photocatalyst and $Cu(OTf)_2$ as a Lewis acid.[582] Like in the intramolecular oxidation/Povarov cyclization the *N*-aryl glycine derivative **116i** is oxidized to the corresponding imine **129**, which can then undergo Lewis acid catalyzed cyclization with styrene **127**. The resulting intermediary tetrahydroquinoline **130** is oxidized, *in situ*, to the quinoline **128**. Using a loading of 100 mg **Ru@TpBpyCOF** per mmol of substrate and conditions adapted from literature, $Cu(OTf)_2$ in acetonitrile,[582] a very encouraging yield of 77% was obtained (Table 15 entry 1). This corresponds well with the 78% reported in literature using $Ru(bpy)_3Cl_2{\cdot}6H_2O$ as a homogeneous photocatalyst (Table 15, entry 25).[582] Some other metal triflates and cupper salts ($Sc(OTf)_3$, $Cu(OAc)_2$, $InCl_3$, $Cu(acac)_2$, $Cu(hfac)_2$ and $Zn(OAc)_2$) were screened, however all gave worse results than $Cu(OTf)_2$ (Table 15, entry 2-7). A range of other solvents were screened, and just as in the intermolecular reaction, acetonitrile and nitromethane were the most effective (Table 15, entry 8-12). When using more catalyst (150 mg/mmol, entry 13) the yield was not increased significantly. The amount of catalyst could be lowered to 50 mg/mmol (entry 14), whilst still obtaining similar results, but decreasing further to 25 mg/mmol had an adverse effect (entry 15).

To gain more insight into the reaction some control experiments were performed (Table 15, entry 16-24). When no COF was present in the reaction, a yield of only 10% was obtained (entry 17). When no Lewis acid was present 50% of the α-oxidized product, ethyl 2-oxo-2-(*p*-tolylamino)acetate **123i**, was obtained (entry 18). Quenching superoxide radicals using 1,4-benzoquinone had a significant effect on the yield, lowering it to 34% (entry 19). The effect of singlet oxygen quencher L-histidine was even more pronounced, as under these conditions no reaction was detected (entry 22). Quenching holes or electrons using $AgNO_3$ or KI also led to (almost) no reaction (entry 21 and 23). On the other hand, quenching hydroxyl radicals had a much smaller effect (entry 20). To conclude, a similar mechanism as in the intramolecular reaction is probably taking place, but in this case the superoxide radical anion is also playing a role in oxidizing the substrates. Importantly, using unmetalated **TpBpyCOF** a yield of only 49% was obtained (entry 24), clearly proving the beneficial effect of the incorporated ruthenium complexes.

While these results were already compelling, due to time constraints it was decided to focus on the next chapter, where amorphous metal free POPs are used as photocatalysts. However, this material and its application as a photocatalyst is very promising and could definitely be further developed in future research. An especially interesting avenue would be to also immobilize the cupper complex onto the COF, to achieve a bifunctional material.

Table 15: Optimization and control experiments of the **Ru_10@TpBpyCOF** catalyzed oxidation/intermolecular cyclization[a]

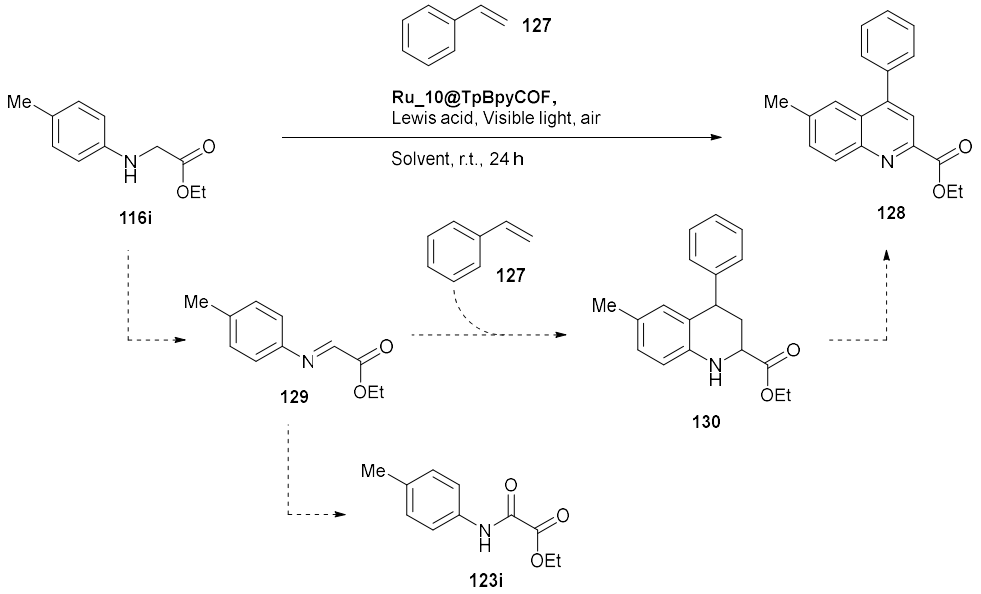

Entry	Lewis Acid	Solvent	Yield (%)[b]
1	$Cu(OTf)_2$	CH_3CN	77
2	$Sc(OTf)_3$		36
3	$Cu(OAc)_2$		24
4	$InCl_3$		15
5	$Cu(acac)_2$		/
6	$Zn(OAc)_2$		29
7	$Cu(hfac)_2$		/
8	$Cu(OTf)_2$	CH_3NO_2	72
9		THF	36
10		CH_2Cl_2	65
11		*i*PrOH	7
12		EtOH	8
13	$Cu(OTf)_2$[c]	CH_3CN	79
14	$Cu(OTf)_2$[d]		78
15	$Cu(OTf)_2$[e]		61
Entry	**Conditions[f]**		**Yield (%)[b]**
16	Unchanged		78
17	No COF		10
18	No LA		/[g]
19	1,4-benzoquinone		34
20	*i*PrOH		62
21	KI		n.r.[h]
22	L-histidine		0
23	$AgNO_3$		10
24	TpBpyCOF		49
25	$Ru(bpy)_3Cl_2{\cdot}6H_2O$		78[i]

[a] Standard conditions: Ethyl *p*-tolylglycinate **116i** (19 mg, 0.1 mmol, 1 eq.), styrene **127** (21 mg, 0.2 mmol, 2 eq.), 10 mol% Lewis acid, 10 mg **Ru_10@TpBpyCOF**, 1 mL solvent, r.t., 24 h.

[b] Determined by ^{1}H-NMR using 1,3,5-trimethoxybenzene as an internal standard.

[c,d,e] 15 - 5 - 2.5 mg **Ru_10@TpBpyCOF**.

[f] Standard conditions: Ethyl *p*-tolylglycinate **116i** (19 mg, 0.1 mmol, 1 eq.), 10 mol% $Cu(OTf)_2$, styrene (21 mg, 0.2 mmol, 2 eq.), 5 mg **Ru_10@TpBpyCOF**, 1 mL solvent, r.t., 24 h.

[h] No reaction.

[i] Taken from ref. [582]

2.4 Conclusions

The focal point of this work was the synthesis, characterization and photocatalytic application of isostructural COFs. Three structurally related COFs, **TpBpyCOF**, **TpOMeBpyCOF** and **TpPpyCOF**, were successfully synthesized and photochemically characterized. Through the use of structurally similar amines (**Bpy** and **Ppy**) and aldehydes (**Tp** and **TpOMe**) information on the relation between the structure and the properties of the COFs was obtained. The use of phenylpyridine led to a larger band gap compared with bipyridine, whilst replacing the hydroxyls of **Tp** with methoxy groups in **TpOMe** led to a smaller band gap. Importantly, **TpBpyCOF** possessing both bipyridine units and β-ketoenamine linkages was the most effective photocatalyst for the one-pot oxidation-Povarov cyclization. A wide range of quinoline-fused lactones/lactams and glyoxal derivatives could be synthesized, which is a new application for photoactive COFs.

These COFs, together with **TpPa-1**, which contained a phenyl linker and β-ketoenamine linkages were also evaluated as catalysts for the oxidation of benzylamines. Again **TpBpyCOF**, containing bipyridines and the β-ketoenamine linkage was the most active material and a wide range of benzylamines could be oxidized using this material. The main active oxygen species for this transformation was $O^{-\bullet}$. Intriguingly, **TpBpyCOF**, **TpPpyCOF** and **TpOMeBpyCOF** also showed significant catalytic activity in the dark, pointing to a hereto unknown and undescribed organocatalytic pathway for the activation of oxygen in these extended frameworks. Interestingly, the homogeneous counterparts of these COFs did work as photocatalysts, but not as organocatalysts. This signifies that the extended structure of the materials plays a large role, but the exact mechanism is still unknown.

Lastly, **TpBpyCOF** was functionalized with ruthenium complexes. Two avenues were evaluated: postsynthetic metalation and bottom-up synthesis. No significant ruthenium loading could be obtained by postsynthetic metalation, however, bottom-up synthesis was effective and **Ru@BpyCOF** containing 1% ruthenium could be obtained. Using this material preliminary work was done on the tandem aerobic oxidation/intermolecular Povarov cyclization. Yields of up to 78% were obtained, and the probable driver for this reaction was again photogenerated singlet oxygen. In further research this application could be developed further, especially if the used Lewis acid, $Cu(OTf)_2$, could also be immobilized on the COF to obtain a bifunctional, heterogeneous and recyclable material.

The field of COFs as photocatalysts has attracted considerable attention over the last years. However, in many cases, the same transformations are studied over and over again. This work entailed the development of the first heterogeneous photocatalyst for the aerobic oxidation/Povarov cyclization, an extremely useful reaction to generate highly substituted quinolines. In addition, for the α-oxidation of *N*-aryl glycine derivatives there had only been incidental reports of the occurrence of the α-dicarbonyl compounds as side products. **TpBpyCOF** is the first photocatalyst used (homogeneous or heterogeneous) to study this reaction in more detail and examine the substrate scope. The results described in this chapter shed light on the design and application of COFs as photocatalysts. This facilitates the advancement of these emerging materials as alternatives for homogeneous (metal-based) catalysts.

2.5 Experimental Part

2.5.1 General procedures

Unless stated otherwise all reagents and solvents were purchased from commercial sources and used without further purification. Dry tetrahydrofuran and dichloromethane were obtained using the MBraun SPS-800 solvent purification system. Dry *N*,*N*-dimethylformamide was obtained by drying over 4 Å molecular sieves and storing for at least two days prior to use.

IR spectra were obtained in neat form with a Shimadzu IRAffinity1S WL FTIR spectrophotometer. Nitrogen adsorption-desorption isotherms were obtained using a Micromeritics® Tristar II. The samples were activated at 120 °C under vacuum overnight before measurements. Pore size distributions were calculated from N_2 sorption isotherms with quenched solid density functional theory (QSDFT) using ASiQwin software (Quantachrome Instruments). Powder X-ray diffraction spectra were taken using a Bruker D8 Advance spectrometer with a copper Kα radiation source (λ = 1.54056 Å) at 40 kV and 45 Ma with 1 °/s scanning speed. UV-Vis absorption spectra were recorded in solid-state on a Perkin Elmer Lambda 1050 UV-Vis-NIR spectrophotometer. The measurement of the ruthenium content was done by ICP-OES. This was performed by the research group of prof. Tack (Ecochem, Department of Green Chemistry and Technology, Faculty of Bioscience Engineering, Ghent University) using a Varian Vista-MPXTM CCD Simultaneous ICP-OES instrument (ICap7400 Duo). Prior to analysis, the sample was digested in a microwave with nitric acid. The results were processed using Thermo Scientific™ Qtegra™ Intelligent Scientific Data Solution™ (ISDS) software. Photoelectrochemical measurements were performed in 0.2 M KCl/NaOH buffer (pH 12) or 0.06 M $Na_2B_4O_7{\cdot}10H_2O$/NaOH buffer (pH 10) using an ALS-Japan Ag/AgCl 3 M NaCl reference electrode (+0.195 V vs. SHE), ALS-Japan Pt coil as counter electrode and the photocatalyst-coated fluorine doped tin oxide (FTO) was used as working electrode. A Bio-Logic VSP potentiostat and EC-Lab software were used to record the measurements. White light was provided by a Philips Tornado T2 CFL (23 W, 1450 lumen). The EPR spectra were recorded with a Varian E-line spectrometer equipped with a HP 5342A microwave frequency counter. The magnetic fields were calibrated using the spectrum of diphenyl picryl hydrazyl (g = 2.0036). The spectra were taken from an aliquot of a stirred suspension of **TpBpyCOF** (3.75 mg), in 0.75 mL of a 200 mM spin trap solution (DMPO or TEMP), after illumination for 15 minutes. ^{1}H-NMR, ^{19}F-NMR and ^{13}C-NMR spectra were recorded with a Bruker Avance III HD-400 spectrophotometer at 25 °C at 400, 376 and 100 MHz, respectively. The NMR was equipped with 1H/BB z-gradient probe (BBO, 5 mm). All spectra were acquired through standard sequences available in the Bruker pulse program library and processed using TOPSPIN 4.1. An Agilent 1200 series HPLC system fitted with an Ascentis® Express C18 column (particle size 2.7 µm, length 30 mm, internal diameter 4.6 mm) was used for HPLC(-MS) using a mixture of acetonitrile/water (5 mM NH_4OAc) as the eluent. The HPLC was connected with a UV-Vis detector and an Agilent 1100 series LC/MSD-type SL mass spectrometer (ESI, 4000 V) using a mass-selective single quadrupole detector. Thin layer chromatography (TLC) for the analysis of reaction mixtures or gradient determination for chromatography was performed using glass-backed 0.25-mm Merck silica gel 60 F254 TLC plates, and visualized under UV light (254 nm). Column chromatography was performed with glass columns using silica gel (particle size 35-70 µm, pore diameter 6 nm) or on a Büchi Reveleris® X2 flash chromatography system (normal phase) or Grace Reveleris® X1 flash chromatography system (reversed phase), using prepacked Reveleris® silica or Reveleris® C18 cartridges.

2.5.2 Linker synthesis

2.5.2.1 Synthesis of 6-(4-aminophenyl)pyridin-3-amine Ppy

Step 1: Synthesis of 5-nitro-2-(4-nitrophenyl)pyridine **57**

2-Bromo-5-nitropyridine **58** (1.02 g, 5 mmol, 1 eq.), 4,4,5,5-tetramethyl-2-(4-nitrophenyl)-1,3,2-dioxaborolane **59** (1.37 g, 5.5 mmol, 1.1 eq.) and potassium carbonate (1.10 g, 7.5 mmol, 1.5 eq.) were added to a two necked flask equipped with a reflux condenser together with 80 mL dioxane and 20 mL water. Nitrogen was bubbled through this mixture for 30 minutes after which $Pd(PPh_3)_4$ (0.58 g, 0.5 mmol, 0.1 eq.) was added. The reaction mixture was refluxed overnight, filtered and rinsed thoroughly with EtOAc (2 x 75 mL). Water (150 mL) was added and the layers were separated. The water layer was further extracted with EtOAc (2 x 100 mL). The combined organic layers were concentrated and purified using column chromatography (C18, gradient CH_3CN/H_2O: 40/60 – 100/0) furnishing the product **57** as a light yellow solid (776 mg, 63%).

Step 2: Synthesis of 6-(4-aminophenyl)pyridin-3-amine **Ppy**

5-Nitro-2-(4-nitrophenyl)pyridine **57** (776 mg, 3.2 mmol, 1 eq.) was dissolved in 100 mL THF in a 250 mL round bottom flask equipped with a reflux condenser and put under a flow of nitrogen. Pd/C (270 mg) and 4.6 mL 80% $NH_2NH_2.H_2O$ were added and the resulting mixture was refluxed overnight. The catalyst was filtered of, rinsed with THF (50 mL) and the filtrate was concentrated under vacuum with a rotavapor in a fume hood. The product was purified using column chromatography (C18, gradient CH_3CN/H_2O: 10/90 – 40/60) and this furnished the product **Ppy** as a yellow to brown solid (426 mg, 71%).

5-Nitro-2-(4-nitrophenyl)pyridine 57

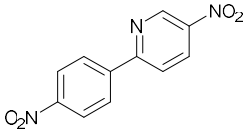

^{1}H-NMR (400 MHz, DMSO-d_6): δ 8.39-8.49 (5H, m, 5 x CH_{arom}); 8.75 (1H, d x d, J = 8.8 x 2.5 Hz, CH_{arom}); 9.51 (1H, d, J = 2.5 Hz, CH_{arom}). **^{13}C-NMR** (100 MHz, DMSO-d_6): δ 122.0 (CH_{arom}); 124.2 (2 x CH_{arom}); 128.9 (2 x CH_{arom}); 133.1 (CH_{arom}); 142.3 ($C_{arom,quat}$); 143.9 ($C_{arom,quat}$); 145.1 (CH_{arom}); 148.7 ($C_{arom,quat}$); 158.6 ($C_{arom,quat}$). Light yellow solid, 63%. Spectral data matched literature.[491]

6-(4-Aminophenyl)pyridin-3-amine Ppy

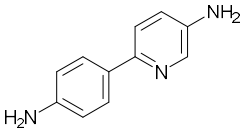

^{1}H-NMR (400 MHz, DMSO-d_6): δ 5.11 (2H, s, NH_2); 5.16 (2H, s, NH_2); 6.55-6.58 (2H, m, 2 x CH_{arom}); 6.92 (1H, d x d, J = 8.5 x 2.7 Hz, CH_{arom}); 7.41 (1H, d, J = 8.5 Hz, CH_{arom}); 7.57-7.60 (2H, m, 2 x CH_{arom}); 7.92 (1H, d, J = 2.7 Hz, CH_{arom}). **^{13}C-NMR** (100 MHz, DMSO-d_6): δ 113.8 (2 x CH_{arom}); 118.7 (CH_{arom}); 121.4 (CH_{arom}); 126.0 (2 x CH_{arom}); 127.0 ($C_{arom,quat}$); 135.1 (CH_{arom}); 142.6 ($C_{arom,quat}$); 144.9 ($C_{arom,quat}$); 148.1 ($C_{arom,quat}$). **IR** (ATR, cm^{-1}): ν_{max} = 3443, 3318, 3192, 1605, 1477, 1281, 1242, 826, 465, 449. **MS** (ESI): *m/z* (%) 186 ($[M + 1]^+$, 100). Yellow to brown solid, 71%. Spectral data matched literature.[491]

2.5.2.2 Synthesis of 2,2'-bipyridine-5,5'-diamine Bpy

Bpy was synthesized according to literature procedures, in three steps, starting from 2-bromo/chloro -5-amino-pyridine **60a/b**.

Step 1: Synthesis of dimethylpyrrole protected amines **62a-b**

This synthesis was based on a literature procedure.[583] To a 100 mL flask was added 5-amino-2-bromopyridine **60b** (5.92 g, 29 mmol, 1 eq.), 50 mL toluene, 4.1 mL hexane-2,5-dione **61** (3.97 g, 34.8 mmol, 1.2 eq.) and *p*-toluenesulfonic acid monohydrate (276 mg, 1.5 mmol, 0.05 eq.). This mixture was heated in a Dean- Stark apparatus for 1.5 hours until completion of the reaction (LC-MS). After cooling to room temperature the mixture was quenched with a saturated aqueous solution of $NaHCO_3$ (50 mL) and separated. The organic layer was washed with water (50 mL) and dried over $MgSO_4$. After removing the solvent by rotary evaporation the resulting crude product was purified by column chromatography (SiO_2, PE/EtOAc: 20/1) to yield to product **62b** as a pale pink solid (6.35 g, 88%). Using the same procedure the pyrrole protected chloropyridine **62a** was obtained as a yellow solid in 91% yield.

Step 2: Coupling to bipyridine **63**

This procedure was based on literature.[584,585] In a 250 mL two necked flask activated zinc powder (2.64 g, 40.4 mmol, 1.7 eq.), tetraethylammonium iodide (6.10 g, 23.7 mmol, 1 eq.) and $NiBr_2(PPh_3)_2$ (3.53 g, 4.8 mmol, 0.2 eq.) were suspended in 25 mL dry THF and stirred at 60 °C under argon for one hour. Pyrrole protected bromopyridine **62b** (5.96 g, 23.7 mmol, 1 eq.) was dissolved in dry THF (60 mL) and slowly added to this mixture with an addition funnel and the reaction mixture was stirred overnight at 60 °C, after which it was allowed to cool down to room temperature. Then concentrated ammonia (25%, 100 mL), water (50 mL), and CH_2Cl_2 (100 mL) were added, and this mixture was stirred for 15 minutes after which it was filtered over Celite®. The phases were separated, and the aqueous phase was extracted twice with 100 mL CH_2Cl_2. The combined organic phases were evaporated under reduced pressure and the crude product was purified by column chromatography (SiO_2, hexane/EtOAc/Et_3N: 10/1/0.05) as eluent to obtain the product **63** (2.23 g, 54%) as a light-yellow solid.

Using the same procedure, but with the protected chloropyridine **62a** a yield of 75% was obtained. To eliminate the large amount of tailing due to the limited solubility of the product during the chromatograpy, it was found to be easier to first elute the triphenylphospine oxide with ~5-10 Column volumes of 9/1 PE/CH_2Cl_2, and then elute the product with 100% CH_2Cl_2. The obtained product is slightly less pure, but can easily be cleaned up by stirring in boiling *i*PrOH (100 mL/gram of product), cooling in a freezer overnight and then filtering of the product.

Step 3: Deprotection to 2,2'-bipyridine-5,5'-diamine **Bpy**

To a 100 mL flask were added: 5,5'-bis(2,5-dimethyl-1*H*-pyrrole)-2,2'-bipyridine **63** (2.23 g, 6.53 mmol, 1 eq.), hydroxylamine hydrochloride (13.61 g, 196 mol, 30 eq.), 20 mL H_2O, 50 mL absolute EtOH and 8 mL triethylamine. This mixture was refluxed for 24 hours after which another 30 eq. of hydroxylamine hydrochloride and 4 mL triethylamine were added and the reaction was continued for another 24 hours. If LC-MS analysis then indicated complete conversion of the starting material, the reaction was stopped, if not another 30 eq. of $NH_2OH.HCl$ and 8 mL of triethylamine were added, and the reaction was stirred for another 24 hours. Upon completion, the reaction was allowed to cool down to room temperature and then 30 mL 3 N HCL was added followed by 100 mL EtOH. The mixture was stored in the freezer overnight and was filtered off, to obtain the hydrochloride salt of the product as an orange powder. This powder was dissolved in water (100 mL) and sodium hydroxide solution

(3N) was added until the mixture was highly alkaline (pH 11). This was then extracted multiple times with dichloromethane (5 x 100 mL), dried over $MgSO_4$, filtered and the solvent was removed under reduced pressure to obtain the product **Bpy** as a light-yellow solid (1.06 g, 87%). It can also (more conveniently) be obtained in a similar yield by allowing the product to precipitate from the basic solution. The precipitate can then be filtered off and washed with water, followed by extensive drying under vacuum to remove residual water.

1-1-(2-Chloropyridine-5-yl)-2,5-dimethyl-1*H*-pyrrole 62a

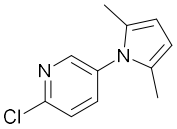

^{1}H-NMR (400 MHz, $CDCl_3$): δ 2.04 (6H, s, 2 x CH_3); 5.94 (2H, s, 2 x CH_{arom}); 7.46 (1H, d, *J* = 8.3 Hz, CH_{arom}); 7.53 (1H, d x d, *J* = 8.3 x 2.6 Hz, CH_{arom}); 8.30 (1H, d, *J* = 2.6 Hz, CH_{arom}). **^{13}C-NMR** (100 MHz, $CDCl_3$): δ 13.1 (2 x CH_3); 107.2 (2 x CH_{arom}); 124.7 (CH_{arom}); 129.0 (2 x $C_{arom,quat}$); 134.7 ($C_{arom,quat}$); 138.3 (CH_{arom}); 149.1 (CH_{arom}); 150.5 (2 x $C_{arom,quat}$). Yellow solid, 91%. Spectral data matched literature.[584]

1-1-(2-Bromopyridine-5-yl)-2,5-dimethyl-1*H*-pyrrole 62b

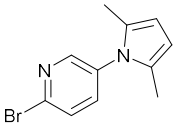

^{1}H-NMR (400 MHz, $CDCl_3$): δ 2.04 (6H, s, 2 x CH_3); 5.94 (2H, s, 2 x CH_{arom}); 7.43 (1H, d x d, *J* = 8.3 x 2.1 Hz, CH_{arom}); 7.61 (1H, d, *J* = 8.3 Hz, CH_{arom}); 8.29 (1H, ~d, *J* = 2.1 Hz, CH_{arom}). **^{13}C-NMR** (100 MHz, $CDCl_3$): δ 13.1 (2 x CH_3); 107.3 (2 x CH_{arom}); 128.5 (CH_{arom}); 129.0 (2 x $C_{arom,quat}$); 135.2 ($C_{arom,quat}$); 138.1 (CH_{arom}); 140.9 ($C_{arom,quat}$); 149.6 (CH_{arom}). Pale pink solid, 88%. Spectral data matched literature.[586]

5,5'-Bis(2,5-dimethyl-1*H*-pyrrol-1-yl)-2,2'-bipyridine 63

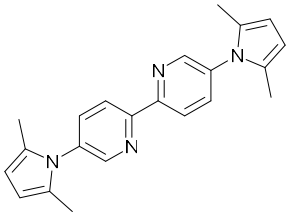

^{1}H-NMR (400 MHz, $CDCl_3$): δ 2.10 (12H, s, CH_3); 5.98 (4H, s, 4 x CH_{arom}); 7.72 (2H, d x d, *J* = 8.4 x 2.5 Hz, 2 x CH_{arom}); 8.57-8.60 (4H, m, 4 x CH_{arom}). **^{13}C-NMR** (100 MHz, $CDCl_3$): δ 13.2 (4 x CH_3); 107.0 (4 x CH_{arom}); 121.5 (2 x CH_{arom}); 129.1 (4 x $C_{arom,quat}$); 135.9 (2 x $C_{arom,quat}$); 136.5 (2 x CH_{arom}); 148.6 (2 x CH_{arom}); 154.5 (2 x $C_{arom,quat}$). Light yellow solid, 54-75%. Spectral data matched literature.[584]

2,2'-Bipyridine-5,5'-diamine Bpy

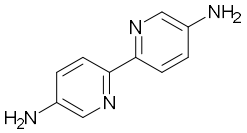

^{1}H-NMR (400 MHz, DMSO-d_6): δ 5.32 (4H, s, 2 x NH_2); 6.95 (2H, d x d, *J* = 8.5 x 2.6 Hz, 2 x CH_{arom}); 7.86 (2H, d, J = 8.5 Hz, 2 x CH_{arom}); 7.91 (2H, d, *J* = 2.5 Hz, 2 x CH_{arom}). **^{13}C-NMR** (100 MHz, DMSO-d_6): δ 119.1 (2 x CH_{arom}); 120.6 (2 x CH_{arom}); 135.0 (2 x CH_{arom}); 143.8 ($C_{arom,quat}$); 144.8 ($C_{arom,quat}$). **IR** (ATR, cm^{-1}): ν_{max} = 3308, 3198, 1626, 1593, 1562, 1470, 1408, 1281, 841, 503. **MS** (ESI): *m/z* (%) 395 ($[2M + 23]^+$, 20); 187 ($[M + 1]^+$, 100). Yellow solid, 87%. Spectral data matched literature.[584]

2.5.2.3 Attempted synthesis of Ppy and Bpy through reduction and rearrangement of diazocompounds

Synthesis of (*E*)-3-(phenyldiazenyl)pyridine **50**

Nitrosobenzene **47** (1.07 g, 10 mmol, 1 eq.) and 3-aminopyridine **48** (1.22 g, 13 mmol, 1.3 eq.) were added to a flask containing 25 mL glacial AcOH, and this was stirred overnight at 70 °C. The reaction mixture was concentrated under vacuum and purified using column chromatography (C18, H_2O/CH_3CN 70/30 – 0/100) to give (*E*)-3-(phenyldiazenyl)pyridine **50** as a red solid (657 mg, 36%) in the first fraction. In the second fraction 1,2-diphenyldiazene 1-oxide **49** could be isolated as an orange solid (246 mg, 12%).

(*E*)-3-(Phenyldiazenyl)pyridine 50

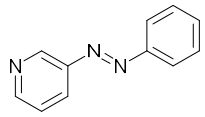

^{1}H-NMR (400 MHz, $CDCl_3$): δ 7.45 (1H, d x d, *J* = 7.9 x 4.7 Hz, CH_{arom}); 7.52-7.56 (3H, m, 3 x CH_{arom}); 7.95 (2H, d, *J* = 7.4 Hz, 2 x CH_{arom}); 8.15 (1H, d, *J* = 7.9 Hz, CH_{arom}); 8.71 (1H, d, *J* = 4.7 Hz, CH_{arom}); 9.21 (1H, s, CH_{arom}). **^{13}C-NMR** (100 MHz, $CDCl_3$): δ 123.2 (2 x CH_{arom}); 124.1 (CH_{arom}); 127.0 (CH_{arom}); 129.4 (2 x CH_{arom}); 131.9 (CH_{arom}); 147.5 (CH_{arom}); 148.0 ($C_{arom,quat}$); 151.9 (CH_{arom}); 152.7 ($C_{arom,quat}$). **MS** (ESI): *m/z* (%) 184 ([M + 1]$^+$, 100). Red solid, 36%.

1,2-Diphenyldiazene 1-oxide 49

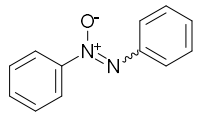

^{1}H-NMR (400 MHz, $CDCl_3$): δ 7.40 (1H, t, *J* = 7.2 Hz, CH_{arom}); 7.48-7.59 (5H, m, 5 x CH_{arom}); 8.18 (2H, d, *J* = 8.0 Hz, 2 x CH_{arom}); 8.32 (2H, d, *J* = 7.7 Hz, CH_{arom}). **^{13}C-NMR** (100 MHz, $CDCl_3$): δ 122.5 (2 x CH_{arom}); 125.7 (2 x CH_{arom}); 128.8 (2 x CH_{arom}); 128.9 (2 x CH_{arom}); 129.7 (CH_{arom}); 131.7 (CH_{arom}); 144.2 ($C_{arom,quat}$); 148.5 ($C_{arom,quat}$). **MS** (ESI): *m/z* (%) 199 ([M + 1]$^+$, 100). Orange solid, 12%. Spectral data matched literature.[587]

Synthesis of 3-(2-phenylhydrazineyl)pyridine **51**

(*E*)-3-(phenyldiazenyl)pyridine **50** (183 mg, 1 mmol, 1 eq.) was dissolved in 5 mL EtOH, $SnCl_2{\cdot}2H_2O$ (339 mg, 1.5 mmol, 1.5 eq.) and 120 µL conc. HCl (53 mg, 1.5 mmol, 1.5 eq.) were added. This was refluxed for two hours, cooled down to room temperature and brought to pH 11 with 6N NaOH. Water (15 mL) was added and the mixture was extracted with CH_2Cl_2 (3 x 15 mL). The organic layer was evaporated and purified using column chromatography (SiO_2, gradient PE/Et_2O/acetone: 75/12.5/12.5 – 1/1/1) to give the title product **51** as a white solid (122 mg, 66%).

3-(2-Phenylhydrazineyl)pyridine 51

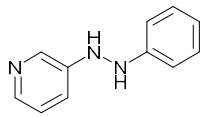

^{1}H-NMR (400 MHz, DMSO-d_6): δ 6.67 (1H, t, *J* = 7.3 Hz, CH_{arom}); 6.73 (2H, d, *J* = 8.1 Hz, 2 x CH_{arom}); 7.02-7.04 (1H, m, CH_{arom}); 7.09-7.14 (3H, m, 3 x CH_{arom}); 7.72 (1H, s, NH); 7.86-7.89 (2H, m, NH and CH_{arom}); 8.08 (1H, d, *J* = 2.3 Hz, CH_{arom}). **^{13}C-NMR** (100 MHz, DMSO-d_6): δ 111.8 (2 x CH_{arom}); 117.9 (CH_{arom}); 118.1 (CH_{arom}); 123.6 (CH_{arom}); 128.9 (2 x CH_{arom}); 134.6 (CH_{arom}); 138.9 (CH_{arom}); 145.8 ($C_{arom,quat}$); 149.3 ($C_{arom,quat}$). **MS** (ESI): *m/z* (%) 186 ([M + 1]$^+$, 100). White solid, 66%.

Synthesis of (*E*)-1,2-di(pyridin-3-yl)diazene **71**

3-Aminopyridine **48** (94 mg, 1 mmol, 1 eq.) and 0.3 mL DBU (304 mg, 2 mmol, 2 eq.) were added to a flask containing 15 mL dry CH_2Cl_2 and this was cooled to -84 °C. NCS (267 mmol, 2 mmol, 2 eq.) was added and the reaction was stirred for half an hour. This was quenched using aq. $NaHCO_3$ (15 mL) and the layers were separated. The organic layer was further washed with water (15 mL). The water layers were discarded, and the organic layer was acidified using 1N HCl (15 mL). The layers were separated, and the water layer was finally made basic again using 6N NaOH, and extracted with CH_2Cl_2 (15 mL). This final organic layer gave the product **71** after evaporation as a brown oil (50 mg, 54%).

(*E*)-1,2-Di(pyridin-3-yl)diazene 71

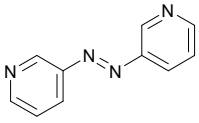

^{1}H-NMR (400 MHz, $CDCl_3$): δ 7.46 (2H, d x d, *J* = 7.7 x 4.5 Hz, 2 x CH_{arom}); 8.16 (2H, d, *J* = 7.7 Hz, 2 x CH_{arom}); 8.73 (2H, d, *J* = 4.5 Hz, 2 x CH_{arom}); 9.22 (2H, s, 2 x CH_{arom}). **MS** (ESI): *m/z* (%) 185 ([M + 1]$^+$, 100). Brown oil, 54%. Spectral data matched literature.[588]

Synthesis of 1,2-di(pyridin-3-yl)hydrazine **72**

(*E*)-1,2-di(pyridin-3-yl)diazene **71** (35 mg, 0.19 mmol, 1 eq.) was dissolved in 1 mL EtOH, $SnCl_2{\cdot}2H_2O$ (54 mg, 0.29 mmol, 1.5 eq.) and 24 µL conc. HCl (11 mg, 0.29 mmol, 1.5 eq.) were added. This was refluxed for 1.5 hours, cooled down to room temperature and brought to pH 11 with 6N NaOH. Water was added (10 mL) and the mixture was extracted with CH_2Cl_2 (3 x 10 mL). The organic layers were evaporated to give the title product **72** as a white solid (35 mg, quant).

1,2-Di(pyridin-3-yl)hydrazine 72

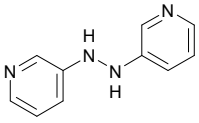

^{1}H-NMR (400 MHz, DMSO-d_6): δ 7.05 (2H, d, *J* = 8.2 Hz, 2 x CH_{arom}); 7.13 (2H, d x d, *J* = 8.2 x 4.5 Hz, 2 x CH_{arom}); 7.91 (2H, d, *J* = 4.5 Hz, 2 x CH_{arom}); 7.99 (2H, br s, NH); 8.09 (2H, s, 2 x CH_{arom}). **^{13}C-NMR** (100 MHz, DMSO-d_6): δ 118.1 (2 x CH_{arom}); 123.7 (2 x CH_{arom}); 134.7 (2 x CH_{arom}); 139.4 (2 x CH_{arom}); 145.3 (2 x $C_{arom,quat}$). **MS** (ESI): *m/z* (%) 187 ([M + 1]$^+$, 100). White solid, quant.

2.5.2.4 Synthesis of protected 6-halopyridin-3-amines

Benzaldehyde imine protection

(*E*)-*N*-(6-bromopyridin-3-yl)-1-phenylmethanimine **64b** was synthesized according to a literature procedure.[589] Benzaldehyde (106 mg, 1 mmol, 1 eq.) and 6-bromopyridin-3-amine **60b** (173 mg, 1 mmol, 1 eq.) were added to a vial containing 1 mL of abs. EtOH and stirred at room temperature for five hours. The solvent was removed by rotary evaporation to give the imine **64b** as a beige solid (261 mg, quant.).

For the synthesis of (*E*)-*N*-(6-chloropyridin-3-yl)-1-phenylmethanimine **64a** the same procedure was used with benzaldehyde (531 mg, 5 mmol, 1 eq.) and 6-chloropyridin-3-amine **60a** (643 mg, 5 mmol, 1 eq.) in 5 mL EtOH with stirring for 24 hours. After evaporation of the solvent the crude was purified via recrystallisation in ether to give the imine **64a** as an off white solid (635 mg, 59%).

(*E*)-*N*-(6-Bromopyridin-3-yl)-1-phenylmethanimine 64b

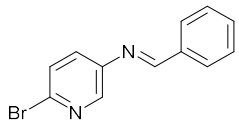

^{1}H-NMR (400 MHz, $CDCl_3$): δ 7.40-7.42 (1H, m, CH_{arom}); 7.49-7.54 (4H, m, 4 x CH_{arom}); 7.91 (2H, d, *J* = 7.4 Hz, 2 x CH_{arom}); 8.24 (1H, d, *J* = 1.9 Hz, CH_{arom}); 8.45 (1H, s, HC=N). **^{13}C-NMR** (100 MHz, $CDCl_3$): δ 128.3 (CH_{arom}); 129.1 (2 x CH_{arom}); 129.3 (2 x CH_{arom}); 131.0 (CH_{arom}); 132.4 (CH_{arom}); 135.6 ($C_{arom,quat}$); 138.6 ($C_{arom,quat}$); 142.7 (CH_{arom}); 147.5 ($C_{arom,quat}$); 162.7 (C=N). **MS** (ESI): *m/z* (%) 261 ([M + 1]$^+$, 100); 263 ([M + 1]$^+$, 100). Beige solid, quant. Spectral data matched literature.[589]

(*E*)-*N*-(6-Chloropyridin-3-yl)-1-phenylmethanimine 64b

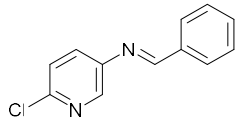

^{1}H-NMR (400 MHz, $CDCl_3$): δ 7.35 (2H, d, *J* = 8.4 Hz, 2 x CH_{arom}); 7.48-7.55 (4H, m, 4 x CH_{arom}); 7.91 (2H, d, *J* = 7.1 Hz, 2 x CH_{arom}); 8.26 (1H, s, CH_{arom}); 8.45 (1H, s, HC=N). **^{13}C-NMR** (100 MHz, $CDCl_3$): δ 124.5 (CH_{arom}); 129.1 (2 x CH_{arom}); 129.3 (2 x CH_{arom}); 131.1 (CH_{arom}); 132.4 (CH_{arom}); 135.6 ($C_{arom,quat}$); 142.2 (CH_{arom}); 147.1 ($C_{arom,quat}$); 148.4 ($C_{arom,quat}$); 162.6 (C=N). **MS** (ESI): *m/z* (%) 217 ([M + 1]$^+$, 100). Off white solid, 59%.

Benzophenone imine protection

For the synthesis of *N*-(6-bromopyridin-3-yl)-1,1-diphenylmethanimine **65b** a flask was charged with 6-bromopyridin-3-amine **60b** (259 mg, 1.5 mmol, 1.5 eq.), benzophenone **74** (182 mg, 1 mmol, 1 eq.), toluene (5 mL) and *p*TsOH (1.9 mg, 0.01 mmol, 0.01 eq.). The flask was equipped with a Dean-Stark apparatus and the reaction was refluxed for 72 hours. The reaction was cooled down to room temperature and EtOAc was added (15 mL). The mixture was transferred to an extraction funnel and washed with water (20 mL), and brine (20 mL). The organic layer was dried over $MgSO_4$ and the solvent was removed by rotary evaporation. The crude product was purified using crystallization in Et_2O/hexanes followed by recrystallisation in Et_2O, finally giving *N*-(6-bromopyridin-3-yl)-1,1-diphenylmethanimine **65b** as yellow crystals (140 mg, 40%).

For the synthesis of *N*-(6-chloropyridin-3-yl)-1,1-diphenylmethanimine **65a** the same procedure was used, with 6-chloropyridin-3-amine **60a** (964 mg, 7.5 mmol, 1.5 eq.), benzophenone **74** (910 mg, 5 mmol, 5 eq.) and *p*TsOH (10 mg, 0.05 mmol, 0.01 eq.) in 25 mL Toluene. The crude was purified using column chromatography (SiO_2, PE/EA: 10/1), giving the title product **65a** as yellow crystals (40 mg, 3%).

***N*-(6-Bromopyridin-3-yl)-1,1-diphenylmethanimine 65b**

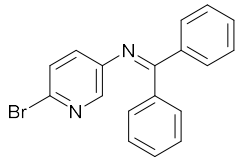

^{1}H-NMR (400 MHz, $CDCl_3$): δ 6.92 (1H, d, *J* = 8.3 Hz, CH_{arom}); 7.10 (2H, d, *J* = 6.9 Hz, 2 x CH_{arom}); 7.24-7.26 (1H, m, CH_{arom}); 7.31-7.34 (1H, m, CH_{arom}); 7.41-7.45 (3H, m, 3 x CH_{arom}); 7.50-7.54 (2H, m, CH_{arom}); 7.76 (2H, d, *J* = 7.6 Hz, 2 x CH_{arom}); 7.81 (1H, s, CH_{arom}). **^{13}C-NMR** (100 MHz, $CDCl_3$): δ 127.6 (CH_{arom}); 128.5 (2 x CH_{arom}); 128.6 (2 x CH_{arom}); 129.4 (2 x CH_{arom}); 129.5 (CH_{arom}); 129.7 (2 x CH_{arom}); 131.3 (CH_{arom}); 131.6 (CH_{arom}); 135.3 ($C_{arom,quat}$); 135.6 ($C_{arom,quat}$); 138.9 ($C_{arom,quat}$); 142.8 (CH_{arom}); 146.8 ($C_{arom,quat}$); 171.1 (C=N). **MS** (ESI): *m/z* (%) 337 ([M + 1]$^+$, 100); 339 ([M + 1]$^+$, 100). Yellow crystals, 40%.

***N*-(6-Chloropyridin-3-yl)-1,1-diphenylmethanimine 65a**

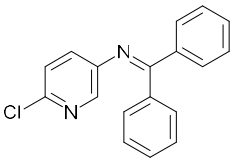

^{1}H-NMR (400 MHz, $CDCl_3$): δ 7.00-7.02 (1H, m, CH_{arom}); 7.09-7.11 (3H, m, CH_{arom}); 7.29-7.36 (3H, m, CH_{arom}); 7.41-7.44 (2H, m, 2 x CH_{arom}); 7.49-7.52 (1H, m, CH_{arom}); 7.74 (1H, d, *J* = 7.5 Hz, CH_{arom}); 7.81 (1H, s, CH_{arom}). **^{13}C-NMR** (100 MHz, $CDCl_3$): δ 123.8 (CH_{arom}); 128.51 (2 x CH_{arom}); 128.57 (2 x CH_{arom}); 129.4 (3 x CH_{arom}); 129.6 (2 x CH_{arom}); 131.4 (CH_{arom}); 131.6 (CH_{arom}); 135.3 ($C_{arom,quat}$); 138.9 ($C_{arom,quat}$); 142.2 (CH_{arom}); 145.5 ($C_{arom,quat}$); 146.4 ($C_{arom,quat}$); 171.2 (C=N). **MS** (ESI): *m/z* (%) 293 ([M + 1]$^+$, 100). Yellow crystals, 3%.

Trifluoroacetamide protection

N-(6-bromopyridin-3-yl)-2,2,2-trifluoroacetamide **66** was produced according to a modified literature procedure.[590] 6-Bromopyridin-3-amine **60b** (173 mg, 1 mmol, 1 eq.), 153 µL Et_3N (111 mg, 1.1 mmol, 1.1 eq.) and DMAP (6 mg, 0.05 mmol, 0.05 eq.) were added to a flame dried flask containing 7.5 mL dry CH_2Cl_2 under argon. Following this, 0.28 mL trifluoroacetic acid anhydride (420 mg, 2 mmol, 2 eq.) was carefully added and this was stirred for three hours at room temperature. The reaction was quenched with saturated ammonium chloride (10 mL), the layers were separated and extracted with CH_2Cl_2 (3 x 10 mL). The combined organic layers were washed with brine (50 mL) and dried over $MgSO_4$, filtered, and evaporated to give the title product **66** as a brown solid (245 mg, 91%).

***N*-(6-Bromopyridin-3-yl)-2,2,2-trifluoroacetamide 66**

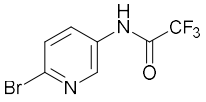

^{1}H-NMR (400 MHz, $CDCl_3$): δ 7.55 (1H, d, *J* = 8.6 Hz, CH_{arom}); 8.04 (1H, br s, NH); 8.06 (1H, d x d, *J* = 8.6 x 2.4 Hz, CH_{arom}); 8.50 (1H, d, *J* = 2.4 Hz, CH_{arom}). **^{19}F-NMR** (376 MHz, $CDCl_3$): δ -75.48 (CF_3). **^{13}C-NMR** (100 MHz, $CDCl_3$): δ 128.6 (CH_{arom}); 130.5 (CH_{arom}); 131.9 ($C_{arom,quat}$); 138.6 ($C_{arom,quat}$); 142.0 (CH_{arom}).* **MS** (ESI): *m/z* (%) 269 ([M + 1]$^+$, 100); 271 ([M + 1]$^+$, 100). Brown solid, 91%.

*C=O and CF_3 not detected due to insufficient concentration.

Acetamide protection

6-Bromopyridin-3-amine **60b** (173 mg, 1 mmol, 1 eq.) and 113 µL acetic anhydride (122.5 mg, 1.2 mmol, 1.2 eq.) were added to a flask containing 2.5 mL dry CH_2Cl_2 under argon. This was stirred for three hours at room temperature. The reaction was quenched with saturated aqueous $NaHCO_3$ and the organic layer was dried to give the title product **67** as a brown solid (195 mg, 91%).

***N*-(6-Bromopyridin-3-yl)acetamide 67**

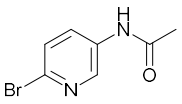

^{1}H-NMR (400 MHz, $CDCl_3$): δ 2.21 (3H, s, CH_3); 7.30 (1H, br s, NH); 7.44 (1H, d, *J* = 8.5 Hz, CH_{arom}); 8.07 (1H, d x d, *J* = 8.5 x 2.1 Hz, CH_{arom}); 8.32 (1H, d, *J* = 2.1 Hz, CH_{arom}). **^{13}C-NMR** (100 MHz, $CDCl_3$): δ 24.6 (CH_3); 128.2 (CH_{arom}); 130.0 (CH_{arom}); 134.4 ($C_{arom,quat}$); 136.1 ($C_{arom,quat}$); 141.1 (CH_{arom}); 168.7 (C=O). **MS** (ESI): *m/z* (%) 215 ([M + 1]$^+$, 100); 217 ([M + 1]$^+$, 100). Brown solid, 91%.

2.5.2.5 Synthesis of *N*,*N*'-(1,4-phenylene)bis(1,1-diphenylmethanimine) 45

This synthesis was modified from a literature procedure.[591] 1,4-Phenylenediamine **73** (0.50 g, 4.625 mmol, 1 eq.), benzophenone **74** (1.70 g, 9.25 mmol, 2 eq.) and DABCO (3.10 g, 27.75 mmol, 6 eq.) were added to a flame dried flask containing 50 mL chlorobenzene. To this mixture $TiCl_4$·2THF (2.30 g, 6.94 mmol, 1.5 eq.) was added slowly (portion wise, over 15 min), and this was refluxed overnight under a nitrogen atmosphere. The reaction was filtered whilst hot over Celite® and rinsed thoroughly with toluene (100 mL). Water (100 mL) was added and the layers were separated. The organic layer was evaporated under reduced pressure and recrystallized from EtOH/H_2O to give the product **45** as shiny yellow flakes (1.273 g, 63%).

***N*,*N*'-(1,4-Phenylene)bis(1,1-diphenylmethanimine) 45**

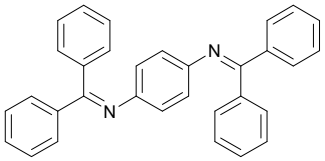

^{1}H-NMR (400 MHz, $CDCl_3$): δ 6.52 (4H, s, 4 x CH_{arom}); 7.06 (4H, d, *J* = 7.4 Hz, 4 x CH_{arom}); 7.23-7.31 (6H, m, 6 x CH_{arom}); 7.37-7.40 (4H, m, 4 x CH_{arom}); 7.44-7.47 (2H, m, 2 x CH_{arom}); 7.71 (4H, d, *J* = 7.8 Hz, 4 x CH_{arom}). **^{13}C-NMR** (100 MHz, $CDCl_3$): δ 121.6 (4 x CH_{arom}); 128.1 (4 x CH_{arom}); 128.3 (4 x CH_{arom}); 128.6 (2 x CH_{arom}); 129.4 (4 x CH_{arom}); 129.7 (4 x CH_{arom}); 130.7 (2 x CH_{arom}); 136.4 (2 x $C_{arom,quat}$); 139.9 (2 x $C_{arom,quat}$); 147.0 (2 x $C_{arom,quat}$); 168.3 (2 x C=N). **MS** (ESI): *m/z* (%) 437 ([M + 1]$^+$, 100). Yellow flakes, 63%.

2.5.2.6 Synthesis of [2,2'-bipyridine]-5,5'-dicarbohydrazide 42

The synthesis of these compounds was undertaken according to modified literature procedures.[497,498]

Step 1: Synthesis of [2,2'-Bipyridine]-5,5'-dicarboxylic acid **131**

5,5'-Dimethyl-2,2'-dipyridyl **75** (2.00 g, 10.86 mmol, 1 eq.) and $KMnO_4$ (12.00 g, 75.93 mmol, 7 eq.) were refluxed overnight in 70 mL H_2O. The brown reaction mixture was filtered and the solvent was removed by rotary evaporation until about 10 mL remained, after which the mixture was acidified using 35% HCl and stored in a freezer overnight. The precipitate was filtered off, washed with water, and dried to give the product as a white solid, which was used without further purification.

Step 2: Synthesis of Diethyl [2,2'-bipyridine]-5,5'-dicarboxylate **76**

The 2,2'-bipyridine-5,5'-dicarboxylic acid from the previous step was suspended in 30 mL EtOH. Concentrated sulfuric acid (4 mL) was carefully dropped to this reaction mixture, and this was refluxed for 24 hours. Upon completion of the reaction (LC-MS) the reaction was allowed to cool down to room temperature and poured into ice water. The precipitate was filtered off, washed with water, and dried under vacuum to give the diethyl ester **76** as a white solid (1.02 g, 31% over two steps).

Step 3: Synthesis of [2,2'-Bipyridine]-5,5'-dicarbohydrazide **42**

Diethyl [2,2'-bipyridine]-5,5'-dicarboxylate (1.02 g, 3.40 mmol, 1 eq.) **76** was dissolved into 20 mL EtOH and 5 mL toluene. The reaction was refluxed in an oil bath set at 120 °C for 72 hours. The reaction was then filtered, washed with CH_2Cl_2, and dried under vacuum to yield the product **42** as a white solid (0.75 g, 81%).

[2,2'-Bipyridine]-5,5'-dicarboxylic acid 131

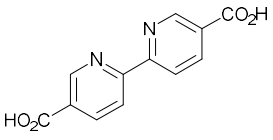

^{1}H-NMR (400 MHz, DMSO-d_6): δ 8.45 (2H, d x d, J = 8.3 x 1.5 Hz, 2 x CH_{arom}); 8.57 (2H, d, J = 8.3 Hz, 2 x CH_{arom}); 9.19 (2H, s, 2 x CH_{arom}). **^{13}C-NMR** (100 MHz, DMSO-d_6): δ 121.2 (2 x CH_{arom}); 127.2 (2 x $C_{arom,quat}$); 138.6 (2 x CH_{arom}); 150.3 (2 x CH_{arom}); 157.3 (2 x $C_{arom,quat}$); 166.0 (2 x C=O). **MS** (ESI): *m/z* (%) 245 ([M + 1]$^+$, 100). White solid.

Diethyl [2,2'-bipyridine]-5,5'-dicarboxylate 76

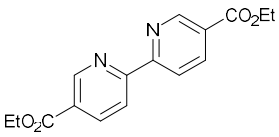

^{1}H-NMR (400 MHz, DMSO-d_6): δ 1.37 (6H, t, J = 7.1 Hz, 2 x CH_3); 4.39 (4H, q, J = 7.1 Hz, 2 x CH_2); 8.50 (2H, d, J = 8.3 Hz, 2 x CH_{arom}); 8.60 (2H, d, J = 8.3 Hz, 2 x CH_{arom}); 9.22 (2H, s, 2 x CH_{arom}). **^{13}C-NMR** (100 MHz, DMSO-d_6): δ 14.1 (2 x CH_3); 61.4 (2 x CH_2); 121.3 (2 x CH_{arom}); 126.4 (2 x $C_{arom,quat}$); 138.4 (2 x CH_{arom}); 150.1 (2 x CH_{arom}); 157.4 ($C_{arom,quat}$); 164.4 (2 x C=O). **MS** (ESI): *m/z* (%) 301 ([M + 1]$^+$, 100). White solid, 31% over two steps. Spectral data matched literature.[497]

[2,2'-Bipyridine]-5,5'-dicarbohydrazide 42

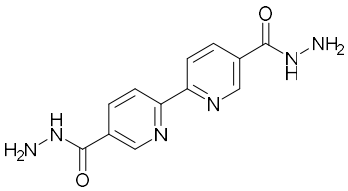

^{1}H-NMR (400 MHz, DMSO-d_6): δ 4.62 (4H, br s, 2 x NH_2); 8.33-8.36 (2H, m, 2 x CH_{arom}); 8.49-8.51 (2H, m, 2 x CH_{arom}); 9.10 (2H, s, 2 x CH_{arom}); 10.08 (2H, s, 2 x NH).* **MS** (ESI): *m/z* (%) 273 ([M + 1]$^+$, 100). White solid, 81%. Spectral data matched literature.[497]

*Insufficient solubility to obtain ^{13}C-NMR data.

2.5.2.7 Synthesis of tetraethyl ([2,2'-bipyridine]-5,5'-diylbis(methylene))bis(phosphonate) 43 and 2,2'-([2,2'-bipyridine]-5,5'-diyl)diacetonitrile 44

Synthesis of 5,5'-Bis(bromomethyl)-2,2'-bipyridine **77**

5,5'-Bis(bromomethyl)-2,2'-bipyridine **77** was synthesized according to a modified literature procedure.[500] To 150 mL of carbon tetrachloride was added of 5,5'-dimethyl-2,2'-bipyridine **75** (2.80 g, 15.4 mmol, 1 eq.), *N*-bromosuccinimide (5.06 g, 30.8 mmol, 2 eq.) and AIBN (58 mg, 0.35 mmol, 0.02 eq.). The reaction mixture was refluxed for 36 hours, until no more monobrominated product and starting material were present (LC-MS) and then filtered while still hot. The filtrate was evaporated and the crude was purified by recrystallization in CH_2Cl_2, giving 5,5'-bis(bromomethyl)-2,2'-bipyridine **77** as white crystals (1.77 g, 34%).

Synthesis of tetraethyl ([2,2'-bipyridine]-5,5'-diylbis(methylene))bis(phosphonate) **43**

The bisphosphonate **43** was synthesized according to a modified literature procedure.[500] To 5,5'-bis(bromomethyl)-2,2'-bipyridine **77** (214 mg, 0.63 mmol, 1 eq.) was added a large excess of $P(OEt)_3$ (1 mL) and this was stirred overnight at 85 °C. The reaction mixture was evaporated under high vacuum, and to finally remove all traces of $P(OEt)_3$ the crude was purified using column chromatography (C18, H_2O/CH_3CN: 80/20 – 0/100) to give the product **43** as white crystals (215 mg, 75%).

Synthesis of 2,2'-([2,2'-bipyridine]-5,5'-diyl)diacetonitrile **44**

2,2'-([2,2'-Bipyridine]-5,5'-diyl)diacetonitrile **44** was synthesized according to a literature procedure.[499] A two-necked flask was charged with: 5,5'-bis(bromomethyl)-2,2'-bipyridine **77** (611 mg, 1.79 mmol, 1 eq.), K_2CO_3 (623 mg, 4.5 mmol, 2.5 eq.) and 10 mL dry acetonitrile. A reflux condenser was equipped, and the reaction was put under nitrogen flow, with the exhaust gas going through a wash bottle containing concentrated NaOH solution. Finally, 0.8 mL TMSCN (622 mg, 6.27 mmol, 3.5 eq.) was carefully (!) added and the reaction was refluxed overnight. The reaction was then allowed to cool down to room temperature after which it was quenched with 15 mL 1N NaOH. Water (50 mL) and EtOAc (50 mL) were added and the layers were separated. The water layer was further extracted with EtOAc (3 x 50 mL). Finally, the crude was purified using column chromatography (SiO_2, CH_2Cl_2/MeOH: 50/1) giving the product **44** as white crystals (207 mg, 50%).

5,5'-Bis(bromomethyl)-2,2'-bipyridine 77

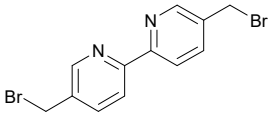

^{1}H-NMR (400 MHz, $CDCl_3$): δ 4.54 (4H, s, 2 x CH_2); 7.86 (2H, d x d, *J* = 8.2 x 2.2 Hz, 2 x CH_{arom}); 8.41 (2H, d, *J* = 8.2 Hz, 2 x CH_{arom}); 8.68 (2H, d, *J* = 2.2 Hz, 2 x CH_{arom}). **^{13}C-NMR** (100 MHz, $CDCl_3$): δ 29.7 (2 x CH_2); 121.3 (2 x CH_{arom}); 134.0 (2 x $C_{arom,quat}$); 137.8 (2 x CH_{arom}); 149.5 (2 x CH_{arom}); 155.6 (2 x $C_{arom,quat}$). White crystals, 34%. Spectral data matched literature.[500]

Tetraethyl ([2,2'-bipyridine]-5,5'-diylbis(methylene))bis(phosphonate) 43

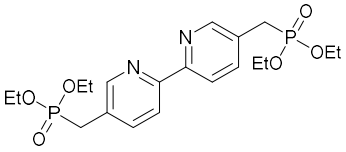

^{1}H-NMR (400 MHz, $CDCl_3$): δ 1.27 (12H, t, *J* = 7.1 Hz, 4 x CH_3); 3.19 (4H, d, *J* = 21.7 Hz, 2 x $C_{arom,quat}CH_2$); 4.03-4.10 (8H, m, 4 x OCH_2); 7.79 (2H, d x t, *J* = 8.2 x 2.3 Hz, 2 x CH_{arom}); 8.33 (2H, d, *J* = 8.2 Hz, 2 x CH_{arom}); 8.56 (2H, t, *J* = 2.3 Hz, 2 x CH_{arom}). **^{13}C-NMR** (100 MHz, $CDCl_3$): δ 16.6 (d, *J* = 6.2 Hz, 4 x CH_3); 31.2 (d, *J* = 139.3 Hz, 2 x $C_{arom,quat}\underline{C}H_2$); 62.5 (d, *J* = 6.9 Hz, 4 x OCH_2); 120.9 (2 x CH_{arom}); 128.2 (d, *J* = 9.2 Hz, 2 x $C_{arom,quat}$); 138.2 (d, *J* = 5.9 Hz, 2 x CH_{arom}); 150.1 (d, *J* = 7.5 Hz, 2 x CH_{arom}); 154.8 (2 x $C_{arom,quat}$). **MS** (ESI): *m/z* (%) 457 ($[M + 1]^+$, 100). White crystals. Spectral data matched literature.[500]

2,2'-([2,2'-Bipyridine]-5,5'-diyl)diacetonitrile 44

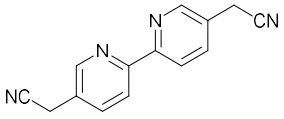

^{1}H-NMR (400 MHz, $CDCl_3$): δ 3.84 (4H, s, 2 x CH_2); 7.85 (2H, d x d, *J* = 8.2 x 2.0 Hz, 2 x CH_{arom}); 8.46 (2H, d, *J* = 8.2 Hz, 2 x CH_{arom}); 8.64 (2H, d, *J* = 2.0 Hz, 2 x CH_{arom}). **^{13}C-NMR** (100 MHz, $CDCl_3$): δ 21.2 (2 x CH_2); 121.3 (2 x CH_{arom}); 126.3 (2 x $C_{arom,quat}$); 136.6 (2 x CH_{arom}); 148.5 (2 x CH_{arom}); 155.4 (2 x $C_{arom,quat}$). White crystals, 50%. **MS** (ESI): *m/z* (%) 235 ($[M + 1]^+$, 100). Spectral data matched literature.[499]

2.5.2.8 Synthesis of 1,3,5-triformylphloroglucinol Tp

This procedure was taken from literature.[592] A 500 mL flask was charged with HMTA (18.64 g, 133 mmol, 2.2 eq.), phloroglucinol **78a** (7.56 g, 60 mmol, 1 eq.) and 120 mL trifluoroacetic acid. A reflux condenser was attached to the flask, and it was heated in an oil bath at 100 °C for 2.5 hours under nitrogen atmosphere. Then 250 mL 3N HCl was slowly added to the reaction mixture and this reaction was kept in the oil bath at 100 °C for one hour. After cooling to room temperature, the reaction mixture was filtered and then extracted with dichloromethane (5 x 200 mL). The combined extracts were dried over $MgSO_4$, filtered and the solvent was removed by rotary evaporation yielding an orange sludge. This solid could be further purified by washing it with ethanol, yielding 1,3,5-triformylphloroglucinol **Tp** as a salmon-colored powder (1.83 g, 15%).

1,3,5-Triformylphloroglucinol Tp

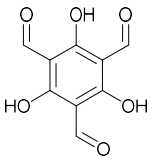

^{1}H-NMR (400 MHz, $CDCl_3$): δ 10.16 (3H, s, 3 x CHO); 14.12 (3H, s, 3 x OH). **^{13}C-NMR** (100 MHz, $CDCl_3$): δ 103.0 (3 x $C_{arom,quat}$); 173.7 (3 x $C_{arom,quat}$); 192.2 (3 x C=O). **IR** (ATR, cm^{-1}): $\nu_{C=O}$ = 1632; ν_{max} = 2886, 1584, 1427, 1240, 1153, 964, 820, 783, 604. **MS** (ESI): m/z (%) 209 ($[M-1]^-$, 100). Salmon colored powder, 15%. Spectral data matched literature.[592]

2.5.2.9 Synthesis of 2,4,6-trimethoxybenzene-1,3,5-tricarbaldehyde TpOMe

Step 1: Synthesis of 1,3,5-tris(bromomethyl)-2,4,6-trimethoxybenzene **79**

The procedure was adapted from literature.[593,594] 1,3,5-Trimethoxybenzene **78b** (5.00 g, 29.7 mmol, 1 eq.) and paraformaldehyde (3.33 g, 110.9 mmol, 3.3 eq.) were added with 11 mL AcOH to a pressure tube and stirred at room temperature for one hour. Then 30 mL of 33% HBr in AcOH was slowly added and this was stirred at 85 °C for three hours. This was allowed to cool to room temperature and dichloromethane (150 mL) and water (150 mL) were added. The phases were separated, and the organic layer was washed three times with water (3 x 100 mL). The organic layer was concentrated and purified using column chromatography (SiO_2, PE/EtOAc: 20/1), to give the product **79** as a white solid (3.87 g, 29%).

Step 2: Synthesis of 2,4,6-trimethoxybenzene-1,3,5-triyl)tris(methylene) triacetate **80**

The procedures for step 2 to 4 were based on literature.[511] 1,3,5-tris(bromomethyl)-2,4,6-trimethoxybenzene **79** (3.87 g, 8.7 mmol, 1 eq.) and NaOAc (8.53 g, 104 mmol, 12 eq.) were added to a round bottom flask containing 100 mL AcOH and refluxed for two hours until completion of the reaction (LC-MS). The reaction mixture was allowed to come to room temperature and 200 mL CH_2Cl_2 was added. This was then filtered, and the filtrate was concentrated under vacuum. To this crude solid EtOAc (100 mL) and aqueous $NaHCO_3$ (100 mL) were added. The phases were separated, and the organic phase was further extracted with aqueous $NaHCO_3$, H_2O and brine (100 mL each). The organic phase was concentrated to give the crude triacetate **80** as a white solid in quantitative yield, which was used without further purification.

Step 3: Synthesis of (2,4,6-trimethoxybenzene-1,3,5-triyl)trimethanol **81**

NaOH (5.78 g, 144.6 mmol, 16.7 eq.) was dissolved in water (50 mL). The crude triacetate **80** from the previous step was dissolved in EtOH (40 mL). The sodium hydroxide solution was added and the reaction was refluxed overnight. After cooling to room temperature, the ethanol was removed via rotary evaporation and 1 N HCl was added until the pH was neutral. Brine (75 mL) was added and the solution was extracted five times with ethyl acetate (5 x 50 mL), furnishing the triol **81** as a white solid (1.167 g, 52%).

Step 4: Synthesis of 2,4,6-trimethoxybenzene-1,3,5-tricarbaldehyde **TpOMe**

The triol **81** (608 mg, 4.5 mmol, 1 eq.) was dissolved in 30 mL dry CH_2Cl_2 under argon and powdered 4 Å molecular sieves were added. To this PCC (4.85 g, 22.5 mmol, 5 eq.) was added and the resulting suspension was stirred overnight. This was filtered over Celite®, the filter cake was rinsed with CH_2Cl_2 (2 x 100 mL), and the filtrate was concentrated under vacuum. The crude was purified using column chromatography (SiO_2, PE/EtOAc: 3/2) resulting in **TpOMe** as a beige solid (150 mg, 44%).

1,3,5-Tris(bromomethyl)-2,4,6-trimethoxybenzene 79

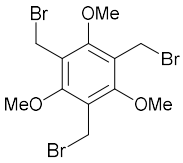

^{1}H-NMR (400 MHz, $CDCl_3$): δ 4.15 (9H, s, 3 x CH_3); 4.60 (6H, s, 3 x CH_2). **^{13}C-NMR** (100 MHz, $CDCl_3$): δ 22.6 (3 x CH_2); 62.8 (3 x CH_3); 123.4 (3 x $C_{arom,quat}$); 160.2 (3 x $C_{arom,quat}$). White solid, 29%. Spectral data matched literature.[594]

(2,4,6-Trimethoxybenzene-1,3,5-triyl)tris(methylene) triacetate 80

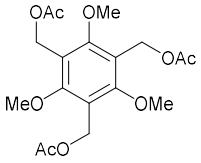

^{1}H-NMR (400 MHz, $CDCl_3$): δ 2.08 (9H, s, 3 x CH_3C=O); 3.84 (9H, s, 3 x CH_3O); 5.17 (6H, s, 3 x CH_2). **^{13}C-NMR** (100 MHz, $CDCl_3$): δ 21.2 (3 x CH_3C=O); 56.9 (3 x CH_2O); 64.0 (3 x CH_3O); 120.0 (3 x $C_{arom,quat}$); 162.2 (3 x $C_{arom,quat}$); 170.9 (3 x C=O). White solid, quantitative.

(2,4,6-Trimethoxybenzene-1,3,5-triyl)trimethanol 81

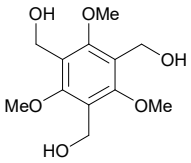

^{1}H-NMR (400 MHz, DMSO-d_6): δ 3.86 (9H, s, 3 x CH_3); 4.45 (6H, d, J = 4.1 Hz, 3 x CH_2); 4.76 (3H, t, J = 4.1 Hz, 3 x OH). **^{13}C-NMR** (100 MHz, DMSO-d_6): δ 52.9 (3 x CH_2O); 63.7 (3 x CH_3O); 124.3 (3 x $C_{arom,quat}$); 159.1 (3 x $C_{arom,quat}$). White solid, 52%. Spectral data matches literature.[511]

2,4,6-Trimethoxybenzene-1,3,5-tricarbaldehyde TpOMe

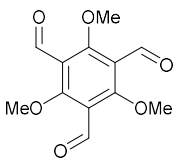

^{1}H-NMR (400 MHz, $CDCl_3$): δ 4.03 (9H, s, 3 x CH_3); 10.35 (3H, s, 3 x CHO). **^{13}C-NMR** (100 MHz, $CDCl_3$): δ 65.7 (3 x CH_3); 120.3 (3 x $C_{arom,quat}$); 169.9 (3 x $C_{arom,quat}$); 187.2 (3 x C=O). **IR** (ATR, cm^{-1}): $\nu_{C=O}$ = 1680; ν_{max} = 2953, 2889, 2860, 1545, 1373, 1198, 1117, 866, 575. **MS** (ESI): m/z (%) 253 ([M + 1]$^+$, 100). Beige solid, 44%. Spectral data matches literature.[511]

2.5.2.10 The synthesis of enaminone linker 46

This synthesis was adapted from a literature reference.[505] 1,3,5-Triacetyl benzene **82** (0.93 g, 4.6 mmol, 1 eq.) was dissolved in 10 mL DMF and 1.8 mL *N*,*N*-dimethylformamide dimethyl acetal (1.64 g, 13.8 mmol, 3 eq.) was added. The mixture was heated at 90 °C overnight, under argon. After cooling down to room temperature, ether (50 mL) was added and the resulting crystals were filtered and washed with hexane (3 x 25 mL) to give the product **46** as an orange powder (1.176 g, 69%).

(2*E*,2'*E*,2''*E*)-1,1',1''-(Benzene-1,3,5-triyl)tris(3-(dimethylamino)prop-2-en-1-one) 46

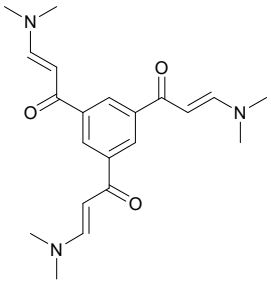

^{1}H-NMR (400 MHz, $CDCl_3$) δ 2.95 (9H, s, 3 x NCH_3); 3.16 (9H, s, 3 x NCH_3); 5.87 (3H, d, *J* = 12.3 Hz, 3 x HC=CHN); 7.83 (3H, d, *J* = 12.3 Hz, 3 x HC=CHN); 8.54 (3H, s, 3 x CH_{arom}). **^{13}C-NMR** (100 MHz, $CDCl_3$): δ 36.6 (3 x CH_3); 45.3 (CH_3); 92.6 (HC=CHN); 126.1 (3 x CH_{arom}); 140.5 (3 x $C_{arom,quat}$); 154.7 (3 x HC=CHN); 188.0 (3 x C=O). **MS** (ESI): *m/z* (%) 370 ([M + 1]$^+$, 100). Orange powder, 69%. Spectral data matched literature.[505]

2.5.2.11 Synthesis of Ru@Bpy

Ru@Bpy was synthesized according to a modified literature procedure.[581] **Bpy** (67 mg, 0.36 mmol, 1.2 eq.) and $[RuCl_2(bpy)_2]\cdot 2H_2O$ **126** (150 mg, 0.29 mmol, 1 eq.) were added to a flask containing 25 mL of a $EtOH/H_2O$ (7/3) solution, and this reaction mixture was refluxed under argon for five hours. The flask was allowed to cool down to room temperature, kept at room temperature for 20 minutes and filtered. A saturated aqueous NH_4PF_6 solution was added to the filtrate, resulting in the formation of a dark red precipitate. The NH_4PF_6 solution was added until no more precipitate was formed, and the mixture was then kept at room temperature for 20 minutes. The solid was then filtered off and washed with water and ether (25 mL each). After drying under vacuum the title complex **Ru@Bpy** was obtained as a red powder (233 mg, 90%).

Bis(2,2'-bipyridine-κ*N*^{1},κ*N*$^{1'}$)([2,2'-bipyridine]-5,5'-diamine-κ*N*^{1},κ*N*$^{1'}$)ruthenium di(hexafluorophosphate) Ru@Bpy

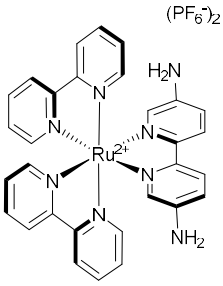

^{1}H-NMR (400 MHz, $CDCl_3$) δ 5.96 (4H, s, 2 x NH_2); 6.87 (2H, d, *J* = 2.3 Hz, 2 x CH_{arom}); 7.10 (2H, d x d, *J* = 8.9 x 2.3 Hz, 2 x CH_{arom}); 7.49 (2H, d x d x d, *J* = 7.3 x 5.5 x 1.2 Hz, 2 x CH_{arom}); 7.61 (2H, d x d x d, *J* = 7.3 x 5.7 x 1.1 Hz, 2 x CH_{arom}); 7.69 (2H, d x d, *J* = 5.5 x 1.1 Hz, 2 x CH_{arom}); 7.78 (2H, d x d, *J* = 5.7 x 1.2 Hz, 2 x CH_{arom}); 8.06 (2H, d, *J* = 8.9 Hz, 2 x CH_{arom}); 8.14 (2H, d x d x d, *J* = 7.7 x 7.3 x 1.4 Hz, 2 x CH_{arom}); 8.18 (2H, d x d x d, *J* = 7.6 x 7.3 x 1.5 Hz, 2 x CH_{arom}); 8.82 (2H, d, *J* = 7.7 Hz, 2 x CH_{arom}); 8.85 (2H, d, *J* = 7.6 Hz, 2 x CH_{arom}). **IR** (ATR, cm^{-1}): ν_{max} = 3379, 1601, 1485, 1466, 1314, 1265, 835, 760, 557, 536. Red powder, 90%. Spectral data matched literature.[581]

2.5.3 Synthesis of control compounds

For the synthesis of model compound **94** a literature procedure was followed.[595] Triformylphloroglucinol **Tp** (0.163 g, 0.78 mmol, 1 eq.) was dissolved in a flask containing 70 mL EtOH. Anniline (0.500 g, 5.37 mmol, 6.9 eq.) was added and the mixture was refluxed for 24 hours. The reaction was allowed to cool down to room temperature and filtered. The solid was washed with EtOH and dried under vacuum to give (*Z*)-2,4,6-tris((phenylamino)methylene)cyclohexane-1,3,5-trione **94** as a yellow solid (0.243 g, 72%). The same procedure was used for the synthesis of (*Z*)- and (2*E*,4*E*,6*E*)-2,4,6-tris((pyridin-2-ylamino)methylene)cyclohexane-1,3,5-trione **95**, using 2-aminopyridine (0.505 mg, 5.37 mmol, 6.9 eq.) and the product **95** was obtained as a yellow solid (0.229 g, 67%)

(2*E*,4*E*,6*E*)-2,4,6-Tris((phenylamino)methylene)cyclohexane-1,3,5-trione

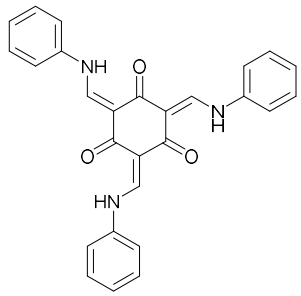

^{1}H-NMR (400 MHz, $CDCl_3$) δ 7.22 (3H, ~t, *J* = 7.4 Hz, 3 x CH_{arom}); 7.30-7.32 (6H, m, 6 x CH_{arom}); 7.40-7.44 (6H, m, 6 x CH_{arom}); 8.79 (3H, d, *J* = 13.1 Hz, 3 x C=CH); 13.41 (3H, d, *J* = 13.1 Hz, 3 x NH). **^{13}C-NMR** (100 MHz, $CDCl_3$): δ 106.9 (3 x C=CH); 117.8 (3 x 2 x CH_{arom}); 125.8 (3 x CH_{arom}); 130.1 (3 x 2 x CH_{arom}); 139.2 (3 x $C_{arom,quat}$); 149.5 (3 x C=CH); 185.7 (3 x C=O). **IR** (ATR, cm^{-1}): $\nu_{C=O}$ = 1615; $\nu_{C=C}$ = 1574 and 1545; ν_{C-N} = 1273 and 1231; ν_{max} = 1441, 816, 687, 486, 467. **MS** (ESI): *m/z* (%) 436 ([M + 1]$^+$, 100). Yellow solid, 72%. Spectral data matched literature.[595]

(*Z*) and (2*E*,4*E*,6*E*)-2,4,6-Tris((pyridin-2-ylamino)methylene)cyclohexane-1,3,5-trione 95ab

This compound was isolated as the mixture of two diastereomers **95a** and **95b**; ratio a/b: 49/51 (^{1}H-NMR, $CDCl_3$)

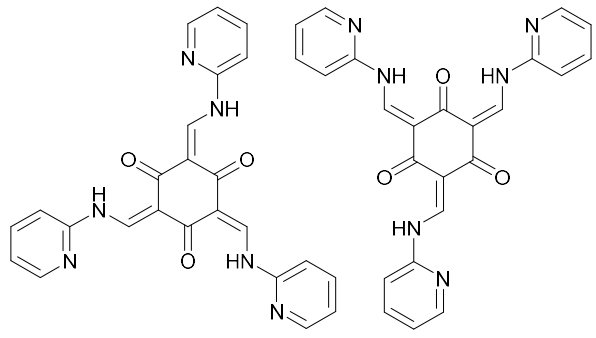

95a 95b

^{1}H-NMR (400 MHz, $CDCl_3$) δ 7.00-7.04 (4H, m, 4 x CH_{arom}); 7.07-7.14 (8H, m, 8 x CH_{arom}); 7.68-7.75 (6H, m, 6 x CH_{arom}); 8.42-8.43 (6H, m, 6 x CH_{arom}); 9.33 (1H, d, *J* = 12.8 Hz, C=CH); 9.36 (1H, d, *J* = 12.7 Hz, C=CH); 9.43 (1H, d, *J* = 12.5 Hz, C=CH); 9.45 (3H, d, *J* = 12.4 Hz, 3 x C=CH); 13.04 (1H, ~t, *J* = 11.8 Hz, 2 x NH); 13.39 (1H, d, *J* = 12.2 Hz, NH); 13.40 (3H, d, *J* = 12.2 Hz, 3 x NH). **^{13}C-NMR** (100 MHz, $CDCl_3$): δ 108.3 (3 x C=CH); 112.9 (3 x CH_{arom}); 120.5 (3 x CH_{arom}); 138.7 (3 x CH_{arom}); 148.7 (3 x C=CH); 149.2 (3 x CH_{arom}); 150.8 (3 x $C_{arom,quat}$); 186.5 (3 x C=O).* **IR** (ATR, cm^{-1}): $\nu_{C=O}$ = 1607; $\nu_{C=C}$ = 1564 and 1555; ν_{C-N} = 1269 and 1231; ν_{max} = 1466, 1417, 1142, 768, 474. **MS** (ESI): *m/z* (%) 439 ([M + 1]$^+$, 100). Yellow solid, 67%.

*Given the very low solubility of compound **95**, only the ^{13}C peaks of the symmetric compound (**95a**) were assigned.

For the synthesis of (*Z*)-2,4,6-tris(([2,2'-bipyridin]-5-ylamino)methylene)cyclohexane-1,3,5-trione **96** a literature procedure was followed.[506] 1,3,5-Triformylphloroglucinol **Tp** (0.51 mg, 0.24 mmol, 1 eq.) and 5-amino-2,2'-bipyridine (166 mg, 0.97 mmol, 4 eq.) were refluxed in 15 mL EtOH for 48 hours. The solution was then cooled down to room temperature, the precipitate was filtered and washed with EtOH. The filter cake was dried to give the title product **96** as red-purple flakes (109 mg, 68%). The product thus obtained possessed an extremely poor solubility in all solvents. It was used as such in catalytic experiments, without further purification or characterization.

2.5.4 Synthesis of substrates for photocatalysis

2.5.4.1 Synthesis of (*E*)-3-(naphthalen-2-yl)prop-2-en-1-ol **107b**

The synthesis was adapted from a literature procedure.[596] 2-Naphthaldehyde (2.34 g, 15 mmol, 1 eq.) was added to a flame dried flask, under argon, containing 30 mL dry CH_2Cl_2. To this ethyl (triphenylphosphoranylidene)acetate (5.75 g, 16.5 mmol, 1.1 eq.) was added and the mixture was stirred overnight at room temperature. The solvent was then removed, and 150 mL of PE/EtOAc (10/1) was added. This was then filtered to remove triphenylphosphine oxide and the solvent was removed to give ethyl (*E*)-3-(naphthalen-2-yl)acrylate as a white solid (2.99 g, 88%) which was used without further purification.

Ethyl (*E*)-3-(naphthalen-2-yl)acrylate (2.625 g, 11.6 mmol, 1 eq.) was dissolved in 100 mL dry CH_2Cl_2, under argon, and 29 mL 1N DIBAL-H in toluene (29 mmol, 2.5 eq.) was added dropwise at -84 °C. This mixture was allowed to come to room temperature and stirred overnight. To quench the reaction the flask was placed in an ice bath and 150 mL 1N HCl was slowly (!) added and this was allowed to stir for 15 minutes. The phases were separated and the aqueous phase was further extracted with CH_2Cl_2 (2 x 100 mL). The combined organic phases were washed with $NaHCO_3$ (250 mL), dried over $MgSO_4$ and evaporated. The crude was purified using column chromatography (SiO_2, PE/EtOAc: 1/7) furnishing (*E*)-3-(naphthalen-2-yl)prop-2-en-1-ol **107b** as a white solid (1.20 g, 56%).

(*E*)-3-(Naphthalen-2-yl)prop-2-en-1-ol 107b

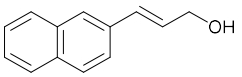

^{1}H-NMR (400 MHz, $CDCl_3$): δ 1.52 (1H, t, *J* = 5.8 Hz, OH); 4.39 (2H, d x d x d, *J* = 5.8 x 5.8 x 1.3 Hz, CH_2); 6.50 (1H, d_{AB} x t, *J* = 15.9 x 5.8 Hz, $CH_2C\underline{H}$=CH); 6.79 (1H, br d_{AB}, *J* = 15.9 Hz, CH_2CH=C$\underline{H}$); 7.42-7.49 (2H, m, 2 x CH_{arom}); 7.61 (1H, d x d, *J* = 8.6 x 1.7, CH_{arom}); 7.40-7.82 (4H, m, 4 x CH_{arom}). **^{13}C-NMR** (100 MHz, $CDCl_3$): 64.0 (CH_2); 123.7, 126.1, 126.4, 126.6, 127.8, 128.1 and 128.4 (7 x CH_{arom}); 129.0 ($CH_2\underline{C}$H=CH); 131.4 (CH_2CH=$\underline{C}$H); 133.2, 133.7 and 134.2 (3 x $C_{arom,quat}$). **IR** (ATR, cm^{-1}): ν_{OH} = 3302; ν_{max} = 1090, 1007, 962, 905, 862, 826, 812, 739, 517. **MS** (ESI): *m/z* (%) 167 [$C_{13}H_{11}^+$, 100]. White solid, 56%. Spectral data matched literature.[597]

2.5.4.2 Synthesis of *N*-aryl glycine esters **102a-k**

For the synthesis of the *N*-aryl glycine esters **102a-k** two different procedures based on literature were followed. For compounds **102a-d** procedure 1[555] was followed, however it was found that this required long reaction times and did not allow for full conversion of starting materials in the case of more electron poor anilines. Therefore procedure 2[554] was followed for the synthesis of the other substrates **102e**-**k**.

Procedure 1[555]

The synthesis of cinnamyl *p*-tolylglycinate **102a** is described as a representative example for the synthesis of compounds **102a-d**.

Step 1:

To a flame dried flask equipped with a pressure equalized addition funnel, under nitrogen, 1.3 mL cinnamyl alcohol **107a** (1.34 g, 10 mmol, 1 eq.) was added together with 1.7 mL triethylamine (1.21 g, 12 mmol, 1.2 eq.) and 20 mL dry CH_2Cl_2. To this reaction mixture 0.96 mL chloroacetyl chloride **108** (1.36 g, 12 mmol, 1.2 eq.) in 10 mL CH_2Cl_2 was slowly added over five minutes, at 0 °C. After addition the mixture was allowed to come to room temperature, after which it was stirred overnight. The mixture was then filtered, 30 mL water was added to the filtrate and the two phases were separated. The aqueous phase was further extracted twice with 30 mL CH_2Cl_2. The combined organic phases were dried over $MgSO_4$, filtered and concentrated under vacuum. The resulting crude cinnamyl 2-chloroacetate **110a** was taken to the next step without additional purification.

Step 2:

The crude cinnamyl 2-chloroacetate **110a** was dissolved in 5 mL CH_3CN. *p*-Toluidine (1.07 g, 10 mmol, 1 eq.) and NaOAc (0.82 g, 10 mmol, 1 eq.) were added. This mixture was refluxed overnight, filtered and purified using column chromatography (SiO_2, PE/EtOAc: 20/1) followed by recrystallisation in EtOH furnishing cinnamyl *p*-tolylglycinate **102a** as a yellow solid (0.66 g, 23%). For compounds **102b-d** the reaction was refluxed for 48 hours to ensure full conversion and the crudes were purified using column chromatography (C18, gradient H_2O/CH_3CN: 50/50 – 0/100).

Procedure 2[554]

The synthesis of cinnamyl (4-iodophenyl)glycinate **102f** is described as a representative example for compounds **102e-k**.

Step 1:

To a flame dried flask equipped with a pressure equalized addition funnel, under nitrogen, 3.2 mL cinnamyl alcohol **107a** (3.35 g, 25 mmol, 1 eq.) was dissolved in 50 mL dry CH_2Cl_2 and 2.9 mL pyridine (2.85 g, 36 mmol, 1.45 eq.) was added. To this reaction mixture 2.4 mL bromo acetylbromide **109** (5.55 g, 27.5 mmol, 1.1 eq.) in 15 mL dry CH_2Cl_2 was slowly added over five minutes, at 0 °C. The mixture was then allowed to come to room temperature, after which it was stirred overnight. Water (50 mL) was added and the two phases were separated. The aqueous phase was further extracted twice with 50 mL CH_2Cl_2. The combined organic phases were dried over $MgSO_4$, filtered and concentrated under vacuum resulting in the crude cinnamyl 2-bromoacetate **110b** (5.17 g, 81%), which was used without additional purification.

Step 2:

Cinnamyl 2-bromoacetate **110b** (740 mg, 2.9 mmol, 1 eq.), Na_2CO_3 (369 mg, 3.5 mmol, 1.2 eq.), 4-iodoaniline (635 mg, 2.9 mmol, 1 eq.) and potassium iodide (86 mg, 0.5 mmol, 0.17 eq.) were added to a flask containing 15 mL DMF. The resulting suspension was stirred at 60 °C until consumption of starting material (LC-MS). Upon completion of the reaction 100 mL of water was added and the mixture was extracted with EtOAc (3 x 100 mL), dried over $MgSO_4$ and the solvent removed in vacuo. The product was purified using column chromatography (SiO_2, PE/EtOAc: 10/1) resulting in cinnamyl (4-iodophenyl)glycinate **110f** as a yellow powder (602 mg, 53%).

For the 2-haloacetates **110a-d** the spectral data is derived from the crude mixture.

Cinnamyl 2-chloroacetate 110a

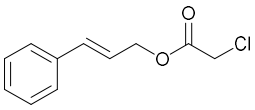

^{1}H-NMR (400 MHz, $CDCl_3$): δ 4.11 (2H, s, CH_2Cl); 4.85 (2H, d, *J* = 6.6 Hz, CH_2O); 6.29 (1H, d x t, *J* = 15.7 x 6.6 Hz, $CH_2C\underline{H}$=CH); 6.70 (1H, br d, *J* = 15.7 Hz, CH_2CH=C<u>H</u>); 7.28-7.41 (5H, m, 5 x CH_{arom}). **^{13}C-NMR** (100 MHz, $CDCl_3$): δ 41.0 (CH_2Cl); 66.9 (CH_2O); 122.1, 126.9, 128.5, 128.8, 135.6 (5 x CH_{arom} and $CH_2\underline{C}H$=<u>C</u>H); 136.0 ($C_{arom,quat}$); 167.3 (C=O).

Cinnamyl 2-bromoacetate 110b

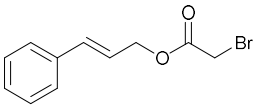

^{1}H-NMR (400 MHz, $CDCl_3$): δ 3.88 (2H, s, CH_2Br); 4.83 (2H, d, *J* = 6.4 Hz, CH_2O); 6.29 (1H, d x t, *J* = 15.9 x 6.4 Hz, $CH_2C\underline{H}$=CH); 6.70 (1H, br d, *J* = 15.9 Hz, CH_2CH=C<u>H</u>); 7.27-7.41 (5H, m, 5 x CH_{arom}).**^{13}C-NMR** (100 MHz, $CDCl_3$): δ 25.9 (CH_2Br); 66.9 (CH_2O); 122.2 ($CH_2\underline{C}H$=CH); 126.8 (2 x CH_{arom}); 128.5 (CH_{arom}); 128.8 (2 x CH_{arom}); 135.4 (CH_2CH=<u>C</u>H); 136.1 ($C_{arom,quat}$); 167.2 (C=O).

(*E*)-3-(Naphthalen-2-yl)allyl 2-bromoacetate 110c

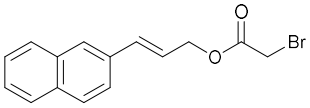

^{1}H-NMR (400 MHz, $CDCl_3$): 3.90 (2H, s, CH_2Br); 4.89 (2H, d x d, *J* = 6.6 x 1.2 Hz, CH_2O); 6.37-6.45 (1H, m, $CH_2C\underline{H}$=CH); 6.86 (1H, br d, *J* = 15.9 Hz, CH_2CH=C<u>H</u>); 7.44-7.48 (2H, m, 2 x CH_{arom}); 7.58-7.61 (1H, m, CH_{arom}); 7.72-7.82 (4H, m, 4 x CH_{arom}).

(2*E*,4*E*)-Hexa-2,4-dien-1-yl 2-bromoacetate 110d

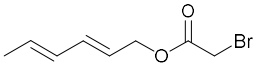

^{1}H-NMR (400 MHz, $CDCl_3$): δ 1.77 (3H, d, *J* = 6.7 Hz, CH_3); 3.84 (2H, s CH_2Br); 4.67 (2H, d, *J* = 6.7 Hz, CH_2O); 5.58-5.65 (1H, m, C<u>H</u>=CH-CH=CHCH_3); 5.74 - 5.84 (1H, m, CH=CH-CH=C<u>H</u>CH_3); 6.02-6.09 (1H, m, CH=CH-C<u>H</u>=CHCH_3); 6.26-6.35 (1H, m, CH=C<u>H</u>-CH=CHCH_3).

Cinnamyl *p*-tolylglycinate 102a

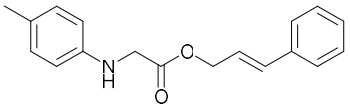

^{1}H-NMR (400 MHz, $CDCl_3$): δ 2.24 (3H, s, CH_3); 3.95 (2H, d, *J* = 5.6 Hz, NCH_2); 4.16 (1H, br s, NH); 4.83 (2H, d, *J* = 6.5 Hz, OCH_2); 6.28 (1H, d_{AB} x t, *J* = 15.7 x 6.5 Hz, $CH_2C\underline{H}$=CH); 6.56 (2H, d, *J* = 7.7 Hz, 2 x C<u>H</u>$_{arom}$); 6.65 (1H, br d_{AB}, *J* = 15.7 Hz, CH_2CH=C<u>H</u>); 7.01 (2H, d, *J* = 7.7 Hz, 2 x CH_{arom}); 7.29-7.39 (5H, m, 5 x CH_{arom}). **^{13}C-NMR** (100 MHz, $CDCl_3$): δ 20.5 (CH_3); 46.4 (NCH_2); 65.9 (OCH_2); 113.4 (2 x CH_{arom}); 122.6 ($CH_2\underline{C}H$=CH); 126.8 (2 x CH_{arom}); 127.7 ($C_{arom,quat}$); 128.4 (CH_{arom}); 128.8 (2 x CH_{arom}); 130.0 (2 x CH_{arom}); 134.9 (CH_2CH=<u>C</u>H); 136.1 ($C_{arom,quat}$); 144.9 ($C_{arom,quat}$); 171.3 (C=O). **IR** (ATR, cm^{-1}): ν_{NH} = 3395; $\nu_{C=O}$ = 1728; ν_{max} = 1526, 1196, 1184, 972, 953, 802, 691, 507. **MS** (ESI): *m/z* (%) 282 ($[M + 1]^+$, 100). Light yellow solid, 23%. Spectral data matched literature.[403]

Cinnamyl (4-methoxyphenyl)glycinate 102b

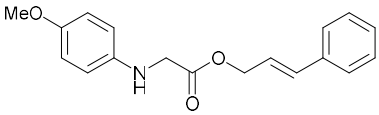

^{1}H-NMR (400 MHz, $CDCl_3$): δ 3.74 (3H, s, CH_3); 3.93 (2H, s, NCH_2); 4.03 (1H, br s, NH); 4.83 (2H, d, *J* = 6.4 Hz, OCH_2); 6.27 (1H, d_{AB} x t, *J* = 15.8 x 6.4 Hz, $CH_2C\underline{H}$=CH); 6.60 (2H, d_{AB}, *J* = 8.3 Hz, 2 x C<u>H</u>$_{arom}$); 6.65 (1H, br d_{AB}, *J* = 15.8 Hz, CH_2CH=C<u>H</u>); 6.79 (2H, d_{AB}, *J* = 8.3 Hz, 2 x C<u>H</u>$_{arom}$); 7.29-7.39 (5H, m, 5 x CH_{arom}). **^{13}C-NMR** (100 MHz, DMSO-d_6): 45.5 (NCH_2); 55.3 (OCH_3); 64.4 (OCH_2); 113.2 (2 x CH_{arom}); 114.5 (2 x CH_{arom}); 123.7 ($CH_2C\underline{H}$=CH); 126.4 (2 x CH_{arom}); 128.0 (CH_{arom}); 128.6 (2 x CH_{arom}); 132.8 (CH_2CH=C<u>H</u>); 136.0 ($C_{arom,quat}$); 142.2 ($C_{arom,quat}$); 151.1 ($C_{arom,quat}$); 171.4 (C=O).

IR (ATR, cm^{-1}): ν_{NH} = 3387; $\nu_{C=O}$ = 1726; ν_{max} = 1514, 1190, 970, 935, 820, 745, 692, 503. **MS** (ESI): *m/z* (%) 298 ($[M + 1]^+$, 100). Brown solid, 31%. Spectral data matched literature.[403*]

*In $CDCl_3$ ^{13}C-NMR did not match the literature, in DMSO however the expected signals were obtained.

Cinnamyl (2-methoxyphenyl)glycinate 102c

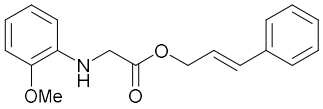

^{1}H-NMR (400 MHz, $CDCl_3$): δ 3.87 (3H, s, CH_3); 3.99 (2H, s, NCH_2); 4.84 (3H, d, *J* = 6.4 Hz, OCH_2 and NH); 6.29 (1H, d_{AB} x t, *J* = 16.0 x 6.4 Hz, $CH_2C\underline{H}$=CH); 6.51 (1H, d, *J* = 7.8 Hz, CH_{arom}); 6.66 (1H, br d_{AB}, *J* = 16.0 Hz, CH_2CH=C$\underline{H}$); 6.70-6.88 (3H, m, 3 x CH_{arom}); 7.29-7.39 (5H, m, 5 x CH_{arom}). **^{13}C-NMR** (100 MHz, $CDCl_3$): δ 45.9 (NCH_2); 55.6 (OCH_3); 65.9 (OCH_2); 109.8, 110.2, 117.7 and 121.3 (4 x CH_{arom}); 122.8 ($CH_2\underline{C}$H=CH); 126.8 (2 x CH_{arom}); 128.3 (CH_{arom}); 128.8 (2 x CH_{arom}); 134.9 ($CH_2CH=\underline{C}H$); 136.2, 137.2 and 147.3 (3 x $C_{arom,quat}$); 171.1 (C=O). **IR** (ATR, cm^{-1}): ν_{NH} = 3420; $\nu_{C=O}$ = 1734; ν_{max} = 1600, 1510, 1190, 1177, 1026, 964, 736, 692. **MS** (ESI): *m/z* (%) 298 ($[M + 1]^+$, 100). Brown solid, 46%.

Cinnamyl (4-fluorophenyl)glycinate 102d

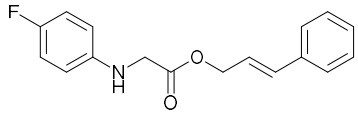

^{1}H-NMR (400 MHz, $CDCl_3$): δ 3.93 (2H, s, NCH_2); 4.18 (1H, br s, NH); 4.84 (2H, d, *J* = 6.5 Hz, OCH_2); 6.28 (1H, d_{AB} x t, *J* = 15.8 x 6.5 Hz, $CH_2C\underline{H}$=CH); 6.55-6.58 (2H, m, 2 x CH_{arom}); 6.67 (1H, br d_{AB}, *J* = 15.8 Hz, CH_2CH=C$\underline{H}$); 6.91 (2H, t, *J* = 8.5 Hz, 2 x C$\underline{H}_{arom}$); 7.28-7.39 (5H, m, 5 x CH_{arom}). **^{19}F-NMR** (376 MHz, $CDCl_3$): δ -127.03 (1F, m). **^{13}C-NMR** (100 MHz, $CDCl_3$): δ 46.7 (NCH_2); 66.0 (OCH_2); 114.1 (d, *J* = 7.6 Hz, 2 x CH_{arom}); 116.0 (d, *J* = 22.4 Hz, 2 x CH_{arom}); 122.5 ($CH_2\underline{C}$H=CH); 126.8 (2 x CH_{arom}); 128.4 (CH_{arom}); 128.8 (2 x CH_{arom}); 135.1 ($CH_2CH=\underline{C}H$); 136.1 ($C_{arom,quat}$), 143.5 (d, *J* = 1.1 Hz, $C_{arom,quat}$), 156.5 (d, *J* = 235.9 Hz, $C_{arom,quat}$), 171.1 (C=O). **IR** (ATR, cm^{-1}): ν_{NH} = 3387; $\nu_{C=O}$ = 1724; ν_{max} = 1512, 1190, 1140, 972, 818, 752, 692, 503. **MS** (ESI): *m/z* (%) 117 ($[C_9H_9]^+$, 100); 286 ($[M + 1]^+$, 30). Brown solid, 29%. Spectral data matched literature.[598]

Cinnamyl (3-(trifluoromethyl)phenyl)glycinate 102e

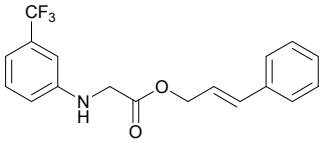

^{1}H-NMR (400 MHz, $CDCl_3$): δ 3.98 (2H, d, *J* = 5.4 Hz, NCH_2); 4.51 (1H, br s, NH); 4.86 (2H, d, *J* = 6.5 Hz, OCH_2); 6.29 (1H, d_{AB} x t, *J* = 15.8 x 6.5 Hz, $CH_2C\underline{H}$=CH); 6.68 (1H, br d_{AB}, *J* = 15.8 Hz, CH_2CH=C$\underline{H}$); 6.75-6.81 (2H, m, 2 x CH_{arom}); 6.99 (1H, d, *J* = 7.6 Hz, CH_{arom}); 7.28-7.40 (6H, m, 6 x CH_{arom}). **^{19}F-NMR** (376 MHz, $CDCl_3$): δ -62.87 (3F, s). **^{13}C-NMR** (100 MHz, $CDCl_3$): δ 45.7 (NCH_2); 66.2 (OCH_2); 109.3 (q, *J* = 3.9 Hz, CH_{arom}); 114.8 (q, *J* = 3.9 Hz, CH_{arom}); 116.1 (~d, *J* = 0.9 Hz, CH_{arom}); 122.3 ($CH_2\underline{C}$H=CH); 124.4 (q, *J* = 272.8 Hz, CF_3); 126.8 (2 x CH_{arom}); 128.5 (CH_{arom}); 128.8 (2 x CH_{arom}); 129.9 (CH_{arom}); 131.8 (q, *J* = 31.8 Hz, $C_{arom,quat}$); 135.3 ($CH_2CH=\underline{C}H$); 136.1 ($C_{arom,quat}$); 147.2 ($C_{arom,quat}$); 170.6 (C=O). **IR** (ATR, cm^{-1}): ν_{NH} = 3391; $\nu_{C=O}$ = 1722; ν_{max} = 1614, 1522, 1364, 1171, 1113, 1069, 787, 698. **MS** (ESI): *m/z* (%) 117 ($[C_9H_9]^+$, 100); 336 ($[M + 1]^+$, 20). White-yellow crystals, 49%.

Cinnamyl (4-iodophenyl)glycinate 102f

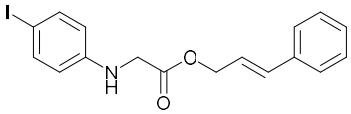

^{1}H-NMR (400 MHz, $CDCl_3$): δ 3.92 (2H, d, *J* = 5.6 Hz, NCH_2); 4.33 (1H, br t, *J* = 5.3 Hz, NH); 4.84 (2H, d x d, *J* = 6.5 x 1.0 Hz, OCH_2); 6.27 (1H, d_{AB} x t, *J* = 15.9 x 6.5 Hz, $CH_2C\underline{H}$=CH); 6.39-6.42 (2H, m, 2 x C$\underline{H}_{arom}$); 6.66 (1H, br d_{AB}, *J* = 15.9 Hz, CH_2CH=C$\underline{H}$); 7.28-7.46 (7H, m, 7 x CH_{arom}). **^{13}C-NMR** (100 MHz, $CDCl_3$): δ 45.8 (NCH_2); 66.1 (OCH_2); 79.3 ($C_{arom,quat}$); 115.3 (2 x CH_{arom}); 122.4 ($CH_2\underline{C}$H=CH); 126.8 (2 x CH_{arom}); 128.4 (CH_{arom}); 128.8 (2 x CH_{arom}); 135.2 ($CH_2CH=\underline{C}H$); 136.1 ($C_{arom,quat}$), 138.1 (CH_{arom}), 146.7 ($C_{arom,quat}$), 170.7 (C=O). **IR** (ATR, cm^{-1}): ν_{NH} = 3391; $\nu_{C=O}$ = 1726; ν_{max} = 1589, 1508, 1443, 1381, 1202, 1180, 968, 689. **MS** (ESI): *m/z* (%) 267 ($[M – I + 1]^+$, 100). Yellow powder, 53%.

Cinnamyl (2-bromophenyl)glycinate 102g

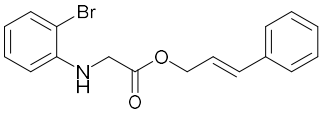

^{1}H-NMR (400 MHz, $CDCl_3$): δ 4.01 (2H, d, *J* = 5.4 Hz, NCH_2); 4.86 (2H, d x d, *J* = 6.5 x 1.2 Hz, OCH_2); 4.99 (1H, t, *J* = 5.4 Hz, NH); 6.29 (1H, d_{AB} x t, *J* = 15.9 x 6.5 Hz, $CH_2C\underline{H}$=CH); 6.53 (1H, d x d, *J* = 8.1 x 1.3 Hz, $C\underline{H}_{arom}$); 6.63 (1H, t x d, *J* = 7.8 x 1.4 Hz, CH_{arom}); 6.68 (1H, br d_{AB}, *J* = 15.9 Hz, CH_2CH=$C\underline{H}$); 7.16-7.20 (1H, m, CH_{arom}); 7.27-7.40 (5H, m, 5 x CH_{arom}); 7.45 (1H, d x d, *J* = 7.8 x 1.4 Hz, CH_{arom}). **^{13}C-NMR** (100 MHz, $CDCl_3$): δ 45.9 (NCH_2); 66.1 (OCH_2); 110.2 ($C_{arom,quat}$); 111.5 (CH_{arom}); 118.9 (CH_{arom}); 122.5 ($CH_2\underline{C}H$=CH); 126.8 (2 x CH_{arom}); 128.4 (CH_{arom}); 128.7 (CH_{arom}); 128.8 (2 x CH_{arom}); 132.8 (CH_{arom}); 135.1 (CH_2CH=$\underline{C}H$); 136.1 ($C_{arom,quat}$); 144.1 ($C_{arom,quat}$); 170.4 (C=O). **IR** (ATR, cm^{-1}): ν_{NH} = 3397; $\nu_{C=O}$ = 1738; ν_{max} = 1595, 1508, 1443, 1196, 1018, 961, 739, 661. **MS** (ESI): *m/z* (%) 117 ($[C_9H_9]^+$, 100); 346 ($[M + 1]^+$, 15); 348 ($[M + 1]^+$, 15). Colorless oil, 53%.

Cinnamyl m-tolylglycinate 102h

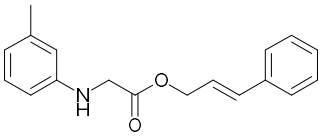

^{1}H-NMR (400 MHz, $CDCl_3$): δ 2.28 (3H, s, CH_3); 3.96 (2H, d, *J* = 5.4 Hz, NCH_2); 4.23 (1H, br s, NH); 4.84 (2H, d, *J* = 6.4 Hz, OCH_2); 6.28 (1H, d_{AB} x t, *J* = 15.9 x 6.4 Hz, $CH_2C\underline{H}$=CH); 6.43-6.45 (2H, m, 2 x $C\underline{H}_{arom}$); 6.59 (1H, d, *J* = 7.4 Hz, $C\underline{H}_{arom}$); 6.67 (1H, br d_{AB}, *J* = 15.9 Hz, CH_2CH=$C\underline{H}$); 7.09 (1H, t, *J* = 7.6 Hz, $C\underline{H}_{arom}$); 7.29-7.40 (5H, m, 5 x CH_{arom}). **^{13}C-NMR** (100 MHz, $CDCl_3$): δ 21.7 (CH_3); 46.1 (NCH_2); 65.9 (OCH_2); 110.3, 114.0 and 119.4 (3 x CH_{arom}); 122.6 ($CH_2\underline{C}H$=CH); 126.8 (2 x CH_{arom}); 128.4 (CH_{arom}); 128.8 (2 x CH_{arom}); 135.0 (CH_2CH=$\underline{C}H$); 136.2, 139.3 and 147.2 (3 x $C_{arom,quat}$); 171.2 (C=O). **IR** (ATR, cm^{-1}): ν_{NH} = 3387; $\nu_{C=O}$ = 1730; ν_{max} = 1587, 1493, 1447, 1348, 1331, 1204, 964, 987. **MS** (ESI): *m/z* (%) 282 ($[M + 1]^+$, 100). White to yellow crystals, 71%.

Cinnamyl o-tolylglycinate 102i

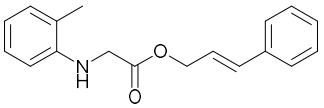

^{1}H-NMR (400 MHz, $CDCl_3$): δ 2.22 (3H, s, CH_3); 4.01 (2H, d, *J* = 5.2 Hz, NCH_2); 4.20 (1H, br t, *J* = 5.2 Hz, NH); 4.86 (2H, d, *J* = 6.5 Hz, OCH_2); 6.30 (1H, d_{AB} x t, *J* = 15.8 x 6.5 Hz, $CH_2C\underline{H}$=CH); 6.50 (1H, d, *J* = 8.0 Hz, CH_{arom}); 6.66-6.73 (2H, m, CH_2CH=$C\underline{H}$ and CH_{arom}); 7.08-7.15 (2H, m, 2 x CH_{arom}); 7.28-7.40 (5H, m, 5 x CH_{arom}). **^{13}C-NMR** (100 MHz, $CDCl_3$): δ 17.5 (CH_3); 46.1 (NCH_2); 66.0 (OCH_2); 110.1 (CH_{arom}), 118.0 (CH_{arom}); 122.6 ($CH_2\underline{C}H$=CH); 122.7 ($C_{arom,quat}$); 126.8, 127.3, 128.4, 128.8 and 130.4 (7 x CH_{arom}); 135.0 (CH_2CH=$\underline{C}H$); 136.1 ($C_{arom,quat}$); 145.1 ($C_{arom,quat}$); 171.3 (C=O). **IR** (ATR, cm^{-1}): ν_{NH} = 3421; $\nu_{C=O}$ = 1736; ν_{max} = 1607, 1587, 1514, 1193, 1150, 962, 743, 691. **MS** (ESI): *m/z* (%) 282 ($[M + 1]^+$, 100). Light yellow oil, 57%. Spectral data matched literature.[598]

(*E*)-3-(Naphthalen-2-yl)allyl p-tolylglycinate 102j

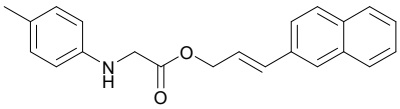

^{1}H-NMR (400 MHz, $CDCl_3$): δ 2.24 (3H, s, CH_3); 3.97 (2H, d, *J* = 5.6 Hz, CH_2N); 4.17 (1H, br s, NH); 4.89 (2H, d x d, *J* = 6.5 x 1.1 Hz, CH_2O); 6.40 (1H, d x t, 15.9 x 6.5 Hz, $CH_2C\underline{H}$=CH); 6.56-6.59 (2H, m, 2 x CH_{arom}); 6.82 (1H, br d, *J* = 15.9 Hz, CH_2CH=$C\underline{H}$); 7.00-7.03 (2H, m, 2 x CH_{arom}); 7.44-7.50 (2H, m, 2 x CH_{arom}); 7.58 (1H, d x d, *J* = 8.6 x 1.6 Hz, CH_{arom}); 7.74-7.82 (4H, m, 4 x CH_{arom}). **^{13}C-NMR** (100 MHz, $CDCl_3$): δ 20.6 (CH_3); 46.5 (CH_2N); 65.9 (CH_2O); 113.4 (2 x CH_{arom}); 123.0 ($CH_2\underline{C}H$=CH); 123.6, 126.3, 126.5 and 127.1 (4 x CH_{arom}); 127.75 ($C_{arom,quat}$); 127.84 (CH_{arom}); 128.2 (CH_{arom}); 128.5 (CH_{arom}); 130.0 (2 x CH_{arom}); 133.4 ($C_{arom,quat}$); 133.6 (CH_{arom}); 135.0 (CH_2CH=$\underline{C}H$); 144.9 ($C_{arom,quat}$); 171.3 (C=O). **IR** (ATR, cm^{-1}): ν_{NH} = 3397; $\nu_{C=O}$ = 1724; ν_{max} = 1520, 1358, 1200, 1180, 1138, 806, 739, 476. **MS** (ESI): *m/z* (%) 167 ($[C_{13}H_{11}]^+$, 100); 332 ($[M + 1]^+$, 5); 354 ($[M + 23]^+$, 5). Beige solid, 38%.

(*E*)-Penta-2,4-dien-1-yl p-tolylglycinate 102k

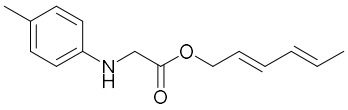

^{1}H-NMR (400 MHz, $CDCl_3$): δ 1.77 (3H, d, *J* = 6.7 Hz, C<u>H</u>$_3$CH=CH); 2.24 (3H, s, $CH_3C_{arom,quat}$); 3.90 (2H, s, NCH_2); 4.13 (1H, br s, NH); 4.67 (2H, d, *J* = 6.7 Hz, CH_2O); 5.59-5.66 (1H, m, C<u>H</u>=CH-CH=CHCH$_3$); 5.72-5.81 (1H, m, CH=CH-CH=C<u>H</u>CH$_3$); 6.02-6.09 (1H, m, CH=CH-C<u>H</u>=CHCH$_3$); 6.23-6.29 (1H, m, CH=C<u>H</u>-CH=CHCH$_3$); 6.52-6.57 (2H, m, 2 x CH_{arom}); 7.00-7.01 (2H, m, 2 x CH_{arom}). **^{13}C-NMR** (100 MHz, $CDCl_3$): δ 18.3 (<u>C</u>H$_3$CH=CH); 20.5 (<u>C</u>H$_3$C$_{arom,quat}$); 46.4 (CH_2N); 65.8 (CH_2O); 113.4 (2 x CH_{arom}); 123.1 (<u>C</u>H=CH-CH=CHCH$_3$); 127.6 ($C_{arom,quat}$); 130.0 (2 x CH_{arom}); 130.4 (CH=CH-<u>C</u>H=CHCH$_3$); 131.9 (CH=CH-CH=<u>C</u>HCH$_3$); 135.7 (CH=<u>C</u>H-CH=CHCH$_3$); 144.9 ($C_{arom,quat}$); 171.3 (C=O). **IR** (ATR, cm^{-1}): ν_{NH} = 3383; $\nu_{C=O}$ = 1728; ν_{max} = 1618, 1522, 1352, 1204, 1182, 988, 802, 505. **MS** (ESI): *m/z* (%) 246 ([M + 1]$^+$, 100). Red crystals, 59%. Spectral data matched literature.[403]

2.5.4.3 Synthesis of *N*-aryl glycine amides 102l-m

<u>Step 1: Synthesis of cinnamyl amines **112a-c**.</u>

The synthesis of *N*-cinnamylaniline **112a** is described as a representative example for **112a-c**.

Aniline (2.79 g, 30 mmol, 3 eq.) was added to a flask containing 30 mL EtOH. Cinnamyl bromide **111** (1.98 g, 10 mmol, 1 eq.), dissolved in 15 mL EtOH, was added dropwise to this flask at 0 °C. After stirring at room temperature for 16 hours, 30 mL 1N NaOH and 150 mL water were added, and the mixture was extracted using ethyl acetate (3 x 100 mL). The organic phases were concentrated under vacuum and purified using column chromatography (SiO_2, PE/EtOAc: 99/1) giving the product **112a** as yellow oil (464 mg, 22%).

***N*-Cinnamylaniline 112a**

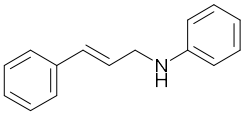

^{1}H-NMR (400 MHz, $CDCl_3$): δ 3.84 (1H, br s, NH); 3.94 (2H, d, *J* = 5.1 Hz, CH_2); 6.33 (1H, d_{AB} x t, *J* = 15.7 x 5.1 Hz, CH_2C<u>H</u>=CH); 6.61-6.74 (4H, m, CH_2CH=CH and 3 x CH_{arom}); 7.17-7.38 (7H, m, 7 x CH_{arom}). **^{13}C-NMR** (100 MHz, $CDCl_3$): δ 46.4 (CH_2); 113.2 (2 x CH_{arom}); 117.8 (CH_{arom}); 126.5 (2 x CH_{arom}); 127.2 (CH_2<u>C</u>H=CH); 127.7 (CH_{arom}); 128.7 (2 x CH_{arom}); 129.4 (2 x CH_{arom}); 131.7 (CH_2CH=<u>C</u>H); 137.0 ($C_{arom,quat}$); 148.2 ($C_{arom,quat}$). Yellow oil, 22%. Spectral data matched literature.[599]

(*E*)-*N*-(4-Methoxybenzyl)-3-phenylprop-2-en-1-amine 112b

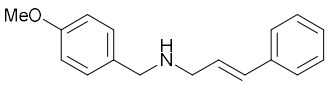

^{1}H-NMR (400 MHz, $CDCl_3$): δ 3.43 (2H, d x d, *J* = 6.3 x 1.4 Hz, C<u>H</u>$_2$CH=CH); 3.78 (2H, s, $CH_2C_{arom,quat}$); 3.80 (3H, s, CH_3); 6.32 (1H, d_{AB} x t, *J* = 15.9 x 6.3 Hz, CH_2C<u>H</u>=CH); 6.54 (1H, br d_{AB}, *J* = 15.9 Hz, CH_2CH=C<u>H</u>); 6.86-6.89 (2H, m, 2 x CH_{arom}); 7.20-7.32 (5H, m, 5 x CH_{arom}); 7.36-7.38 (2H, m, 2 x CH_{arom}). **^{13}C-NMR** (100 MHz, $CDCl_3$): δ 51.3 (<u>C</u>H$_2$CH=CH); 52.9 (<u>C</u>H$_2$C$_{arom,quat}$); 55.4 (CH_3); 114.0 (2 x CH_{arom}); 126.4 (2 x CH_{arom}); 127.5 (CH_{arom}); 128.7 (2 x CH_{arom} and CH_2<u>C</u>H=CH); 129.5 (2 x CH_{arom}); 131.5 (CH_2CH=<u>C</u>H); 132.6 ($C_{arom,quat}$); 137.3 ($C_{arom,quat}$); 158.8 ($C_{arom,quat}$). Yellow oil, 41%. Spectral data matched literature.[600]

(*E*)-*N*-Isobutyl-3-phenylprop-2-en-1-amine 112c

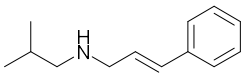

^{1}H-NMR (400 MHz, $CDCl_3$): δ 0.93 (6H, d, *J* = 6.6 Hz, 2 x CH_3); 1.65 (1H, br s, NH); 1.78 (1H, ~nonet, *J* = 6.7 Hz C<u>H</u>$(CH_3)_2$); 2.48 (2H, d, *J* = 6.8 Hz, C<u>H</u>$_2$CH$(CH_3)_2$); 3.41 (2H, d x d, *J* = 6.3 x 1.3 Hz, C<u>H</u>$_2$CH=CH); 6.31 (1H, d_{AB} x t, *J* = 15.9 x 6.3 Hz, CH_2C<u>H</u>=CH); 6.53 (1H, d_{AB}, *J* = 15.9 Hz, CH_2CH=C<u>H</u>); 7.20-7.24 (1H, m, CH_{arom}); 7.29-7.32 (2H, m, 2 x CH_{arom}); 7.37-7.39 (2H, m, 2 x CH_{arom}). **^{13}C-NMR** (100 MHz, $CDCl_3$): δ 20.9 (2 x CH_3); 28.5 (<u>C</u>H$(CH_3)_2$); 52.2 (<u>C</u>H_2CH=CH); 57.7 (<u>C</u>H_2CH$(CH_3)_2$); 126.4 (2 x CH_{arom}); 127.4 (1 x CH_{arom}); 128.7 (2 x CH_{arom}); 128.9 (CH_2<u>C</u>H=CH); 131.3 (CH_2CH=<u>C</u>H); 137.4 ($C_{arom,quat}$). Yellow oil, 34%. Spectral data matched literature.[601]

<u>Step 2: Synthesis of 2-bromophenylacetamides **113a-c**</u>

The synthesis of 2-bromo-*N*-cinnamyl-*N*-phenylacetamide **113a** is described as an example for compounds **113a-c**.

N-cinnamylaniline **112a** (464 mg, 2.20 mmol, 1 eq.) was dissolved in 15 mL dry CH_2Cl_2 in a flame dried flask under nitrogen and NEt_3 (267 mg, 2.64 mmol, 1.2 eq.) was added. Bromo acetylbromide **109** (533 mg, 2.64 mmol, 1.2 eq.) in 5 mL dry CH_2Cl_2 was slowly added over five minutes to this reaction, at 0 °C. The mixture was then allowed to come to room temperature, after which it was stirred overnight. Water (25 mL) was added, and the two phases were separated. The aqueous phase was further extracted twice with 25 mL CH_2Cl_2. The combined organic phases were dried over $MgSO_4$, filtered, and purified using column chromatography (SiO_2, PE/EtOAc: 10/1) yielding the title product **113a** as a light-yellow oil (635 mg, 88%).

2-Bromo-*N*-cinnamyl-*N*-phenylacetamide 113a

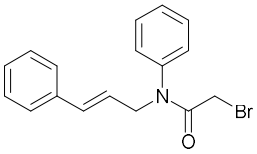

^{1}H-NMR (400 MHz, $CDCl_3$): δ 3.67 (2H, s, CH_2Br); 4.46 (2H, d, *J* = 6.7 Hz, CH_2N); 6.26 (1H, d_{AB} x t, *J* = 15.8 x 6.7 Hz, CH_2C<u>H</u>=CH); 6.40 (1H, br d_{Ab}, *J* = 15.8 Hz, CH_2CH=C<u>H</u>); 7.21-7.45 (10H, m, 10 x CH_{arom}). **^{13}C-NMR** (100 MHz, $CDCl_3$): δ 27.4 (CH_2Br); 52.6 (CH_2N); 123.4 (CH_2C<u>H</u>=CH); 126.6 (2 x CH_{arom}); 128.0 (CH_{arom}); 128.3 (2 x CH_{arom}); 128.7 (2 x CH_{arom}); 128.9 (CH_{arom}); 130.0 (2 x CH_{arom}); 134.2 (CH_2CH=<u>C</u>H); 136.6 ($C_{arom,quat}$); 141.5 ($C_{arom,quat}$); 166.3 (C=O). Light-yellow oil, 88%.

2-Bromo-*N*-cinnamyl-*N*-(4-methoxybenzyl)acetamide 113b

Found as a mixture of two rotamers (60/40 in $CDCl_3$).

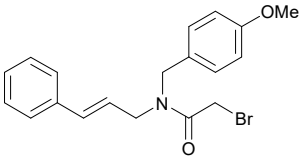

^{1}H-NMR (400 MHz, $CDCl_3$): δ 3.80 and 3.82 (3H, 2 x s, OCH_3); 3.91 and 3.94 (2H, 2 x s, CH_2Br); 4.07 and 4.15 (2H, 2 x d, *J* = 5.5 x 1.4 Hz and 6.5 x 0.7 Hz, C<u>H</u>$_2$CH=CH); 4.57 and 4.61 (2H, 2 x s, NCH_2PMP); 6.08-6.18 (1H, m, CH_2C<u>H</u>=CH); 6.42-6.48 (1H, m, CH_2CH=C<u>H</u>); 6.86-6.92 (2H, m, 2 x CH_{arom}); 7.14-7.16 (2H, m, 2 x CH_{arom}); 7.24-7.36 (5H, m, 5 x CH_{arom}). **^{13}C-NMR** (100 MHz, $CDCl_3$): δ 26.5 and 26.6 (CH_2Br); 47.8 (C<u>H</u>$_2$CH=$CH_{rotameric}$); 48.2 ($NCH_2PMP_{rotameric}$); 49.4 (C<u>H</u>$_2$CH=$CH_{rotameric}$); 50.7 ($NCH_2PMP_{rotameric}$); 55.4 and 55.5 (OCH_3); 114.3 and 114.6 (2 x CH_{arom}); 123.6 and 123.8 (CH_2<u>C</u>H=CH); 126.6 (2 x CH_{arom}); 127.90, 127.96, 127.99, 128.3, 128.7, 128.9 and 129.7 (2 x (2 x CH_{arom}), CH_{arom} and $C_{arom,quat}$); 132.6 and 133.6 (CH_2CH=<u>C</u>H); 136.0 and 136.6 ($C_{arom,quat}$); 159.3 and 159.5 ($C_{arom,quat}$); 167.15 and 167.27 (C=O). Yellow oil, 64%

2-Bromo-*N*-cinnamyl-*N*-isobutylacetamide 113c

Found as a mixture of two rotamers (59/41 in $CDCl_3$).

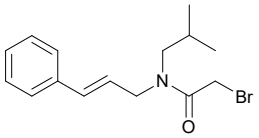

^{1}H-NMR (400 MHz, $CDCl_3$): δ 0.93 and 0.96 (6H, 2 x d, *J* = 6.7 Hz, 2 x $CH_2CH(\underline{C}H_3)_2$); 1.96-2.10 (1H, m, $CH_2\underline{C}H(CH_3)_2$); 3.17 and 3.26 (2H, 2 x d, *J* = 7.6 Hz, $C\underline{H}_2CH(CH_3)_2$); 3.88 and 3.92 (2H, 2 x s, CH_2Br); 4.15-4.18 (2H, m, $C\underline{H}_2CH{=}CH$); 6.12-6.20 (1H, m, $CH_2C\underline{H}{=}CH$); 6.45-6.54 (1H, m, $CH_2CH{=}C\underline{H}$); 7.22-7.38 (5H, m, 5 x CH_{arom}). **^{13}C-NMR** (100 MHz, $CDCl_3$): δ 20.2 (CH_3); 26.62 and 26.68 (CH_2Br); 27.1 and 27.8 ($CH_2C\underline{H}(CH_3)_2$); 48.2 and 51.0 ($\underline{C}H_2CH{=}CH$); 53.4 and 55.7 ($C\underline{H}_2CH(CH_3)_2$); 123.9 and 124.1 ($CH_2C\underline{H}{=}CH$); 126.6 (2 x CH_{arom}); 127.9 and 128.3 (CH_{arom}); 128.7 and 128.9 (2 x CH_{arom}); 132.1 and 132.9 ($CH_2CH{=}C\underline{H}$); 136.0 and 136.7 ($C_{arom,quat}$); 167.0 and 167.5 (C=O). Yellow oil, 41%.

Step 3: Synthesis of *N*-aryl glycine amides **102l-n**

The synthesis of *N*-cinnamyl-*N*-phenyl-2-(*p*-tolylamino)acetamide **102l** is described as an example for the synthesis of compounds **102l-n**.

2-Bromo-*N*-cinnamyl-*N*-phenylacetamide **113a** (635 mg, 1.93 mmol, 1 eq.), Na_2CO_3 (245 mg, 2.31 mmol, 1.2 eq.), *p*-toluidine (206 mg, 1.93 mmol, 1 eq.) and potassium iodide (58 mg, 0.39 mmol, 0.2 eq.) were added to a flask containing 20 mL DMF. The resulting suspension was stirred at 60°C for 16 hours. Upon completion of the reaction water (100 mL) was added and the mixture was extracted with EtOAc (3 x 100 mL), dried over $MgSO_4$ and the solvent removed in vacuo. The product was purified using column chromatography (SiO_2, PE/EtOAc: 92/8) resulting in *N*-cinnamyl-*N*-phenyl-2-(*p*-tolylamino)acetamide **102l** as a yellow solid (176 mg, 26%).

***N*-Cinnamyl-*N*-phenyl-2-(*p*-tolylamino)acetamide 102l**

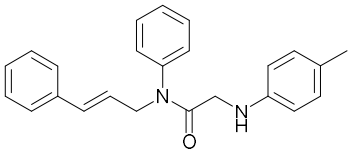

^{1}H-NMR (400 MHz, $CDCl_3$): δ 2.18 (3H, s, CH_3); 3.54 (2H, s, CH_2N); 4.46 (2H, d x d, *J* = 6.6 x 0.5 Hz, $C\underline{H}_2CH{=}CH$); 4.59 (1H, br s, NH); 6.24 (1H, d_{AB} x t, *J* = 15.8 x 6.6 Hz, $CH_2C\underline{H}{=}CH$); 6.35-6.40 (3H, m, $CH_2CH{=}CH$ and 2 x CH_{arom}); 6.93 (2H, d, *J* = 8.2 Hz, 2 x CH_{arom}); 7.18-7.31 (7H, m, 7 x CH_{arom}); 7.39-7.44 (3H, m, 3 x CH_{arom}). **^{13}C-NMR** (100 MHz, $CDCl_3$): δ 20.4 (CH_3); 46.7 (CH_2N); 52.1 ($\underline{C}H_2CH{=}CH$); 113.2 (CH_{arom}); 123.8 ($CH_2C\underline{H}{=}CH$); 126.5 (2 x CH_{arom}); 126.8 ($C_{arom,quat}$); 127.8 (CH_{arom}); 128.3 (2 x CH_{arom}); 128.6 (2 x CH_{arom}); 128.7 (CH_{arom}); 129.7 (2 x CH_{arom}); 130.0 (2 x CH_{arom}); 133.8 ($CH_2CH{=}\underline{C}H$); 136.6 ($C_{arom,quat}$); 140.8 ($C_{arom,quat}$); 145.2 ($C_{arom,quat}$); 169.4 (C=O). **IR** (ATR, cm^{-1}): ν_{NH} = 3375; ν_{CO} = 1657; ν_{max} = 1493, 1393, 1393, 1244, 966, 802, 700, 687. **MS** (ESI): *m/z* (%) 357 ($[M + 1]^+$, 100); 713 ($[2M + 1]^+$, 5); 735 $[2M + 23]^+$, 10). Yellow solid, 26%.

***N*-Cinnamyl-*N*-(4-methoxybenzyl)-2-(*p*-tolylamino)acetamide 102m**

Found as a mixture of two rotamers (52/48 in $CDCl_3$).

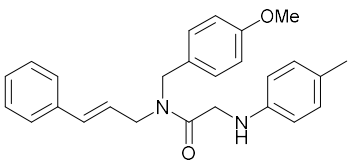

^{1}H-NMR (400 MHz, $CDCl_3$): δ 2.22 (3H, s, $CH_3C_{arom,quat}$); 3.77 and 3.78 (3H, 2 x s, OCH_3); 3.94-3.97 (4H, m, $NHC\underline{H}_2$ and $C\underline{H}_2CH{=}CH_{rotameric}$); 4.19 (2H, d, *J* = 6.5 Hz, $C\underline{H}_2CH{=}CH_{rotameric}$); 4.46 and 4.63 (2H, 2 x s, $NC\underline{H}_2PMP$); 6.04 and 6.14 (1H, 2 x d x t, *J* = 15.9 x 5.5 Hz and 15.8 x 6.6 Hz, $CH_2C\underline{H}{=}CH$); 6.46-6.58 (3H, m, 2 x CH_{arom} and $CH_2CH{=}C\underline{H}$); 6.84-6.89 (2H, m, 2 x CH_{arom}); 6.96-6.99 (2H, m, 2 x CH_{arom}); 7.10-7.13 (1H, m, CH_{arom}); 7.19-7.33 (5H, m, 5 x CH_{arom}). **^{13}C-NMR** (100 MHz, $CDCl_3$): δ 20.5 ($\underline{C}H_3C_{arom,quat}$); 45.8 and 45.9 ($NH\underline{C}H_2CO$); 47.6 and 47.7 ($N\underline{C}H_2CH{=}CH$); 48.2 and 48.7 ($CH_2PMP$); 55.3 and 55.4 ($OCH_3$); 113.3 (2 x CH_{arom}); 114.1 and 114.5 (2 x CH_{arom}); 123.4 and 124.0 ($NHCH_2\underline{C}H{=}CH$); 126.49 and 126.51 (2 x CH_{arom}); 126.8, 127.7, 127.87,

127.91, 128.2, 128.6, 128.8, 129.1, 129.8 (2 x $C_{arom,quat}$, 3 x (2 x CH_{arom}) and CH_{arom}); 132.6 and 133.6 ($CH_2CH=\underline{C}H$); 136.0 and 136.5 ($C_{arom,quat}$); 145.2 and 145.3 ($C_{arom,quat}$); 159.2 and 159.4 ($C_{arom,quat}$); 169.5 and 169.6 (C=O). **IR** (ATR, cm^{-1}): ν_{NH} = 3401; ν_{CO} = 1641; ν_{max} = 1611, 1510, 1252, 1161, 1030, 818, 739, 692. **MS** (ESI): *m/z* (%) 401 ($[M + 1]^+$, 100). Yellow solid, 30%.

_N_-Cinnamyl-_N_-isobutyl-2-(_p_-tolylamino)acetamide 102n

Found as a mixture of two rotamers (53/47 in $CDCl_3$).

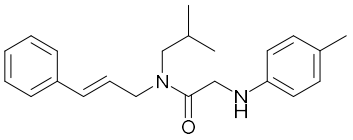

^{1}H-NMR (400 MHz, $CDCl_3$): δ 0.93 and 0.98 (6H, 2 x d, *J* = 6.7 and 6.6 Hz, 2 x $CH_2CH(C\underline{H}_3)_2$); 2.01-2.09 (1H, m, $CH_2C\underline{H}(CH_3)_2$); 2.23 and 2.25 (3H, 2 x s, $C_{arom,quat}C\underline{H}_3$); 3.11 and 3.32 (2H, 2 x d, *J* = 7.6 and 7.5 Hz, $C\underline{H}_2CH(CH_3)_2$); 3.91 and 3.95 (2H, 2 x s, NCH_2); 4.09 and 4.22 (2H, 2 x d, *J* = 5.4 x 1.5 Hz and 6.5 x 1.1 Hz; $C\underline{H}_2CH=CH$); 6.09-6.22 (1H, m, $CH_2C\underline{H}=CH$); 6.48-6.59 (3H, m, $CH_2CH=C\underline{H}$ and 2 x CH_{arom}); 6.97-7.02 (2H, m, 2 x CH_{arom}); 7.23-7.38 (5H, m, 5 x CH_{arom}). **^{13}C-NMR** (100 MHz, $CDCl_3$): δ 20.3 and 20.4 ($CH_2CH(\underline{C}H_3)_2$); 20.53 and 20.54 ($C_{arom,quat}\underline{C}H_3$); 27.2 and 27.5 ($CH_2C\underline{H}(CH_3)_2$); 48.2 and 49.3 ($\underline{C}H_2CH=CH$); 53.66 and 55.68 ($C\underline{H}_2CH(CH_3)_2$); 113.3 (2 x CH_{arom}); 123.7 and 124.5 ($CH_2C\underline{H}=CH$); 126.56 and 126.59 (2 x CH_{arom}); 126.89 and 126.94 (2 x CH_{arom}); 126.89 and 126.94 ($C_{arom,quat}$); 127.9 and 128.2 (CH_{arom}); 128.7 and 128.9 (2 x CH_{arom}); 129.89 and 129.91 (2 x CH_{arom}); 132.3 and 133.1 ($CH_2CH=C\underline{H}$); 136.1 and 136.6 ($C_{arom,quat}$); 145.40 and 145.44 ($C_{arom,quat}$); 169.5 and 169.8 (C=O). **IR** (ATR, cm^{-1}): ν_{NH} = 3374; ν_{CO} = 1645; ν_{max} = 2959, 1618, 1521, 1433, 1126, 966, 808, 737. **MS** (ESI): *m/z* (%) 337 ($[M + 1]^+$, 100). Yellow oil, 1%.

2.5.4.4 Synthesis of Ethyl *p*-tolylglycinate **116i**

Ethyl *p*-tolylglycinate **116i** was synthesized according to literature.[559] *p*-Toluidine **114** (2.14 g, 20 mmol, 1 eq.) and sodium acetate (3.28 g, 40 mmol, 2 eq.) were brought in a flask containing 50 mL EtOH. To this mixture was added 2.44 mL ethyl bromoacetate **115** (3.67 g, 22 mmol, 1.1 eq.) and this was refluxed overnight. The reaction was allowed to cool down to room temperature and water (200 mL) was added. The resulting precipitate was filtered off and purified via recrystallisation from EtOH/H_2O to give the title compound **116i** as grey needles (1.543 g, 39%).

Ethyl _p_-tolylglycinate 116i

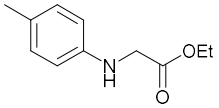

^{1}H-NMR (400 MHz, $CDCl_3$): δ 1.29 (3H, t, *J* = 7.1 Hz, $C\underline{H}_3CH_2$); 2.24 (3H, s, $CH_3C_{arom,quat}$); 3.88 (2H, d, *J* = 5.60 Hz, CH_2N); 4.15 (1H, br s, NH); 4.23 (2H, q, *J* = 7.1 Hz, $CH_3C\underline{H}_2$); 6.54 (2H, d, *J* = 7.8 Hz, 2 x CH_{arom}); 7.01 (2H, d, *J* = 7.8 Hz, 2 x CH_{arom}). **^{13}C-NMR** (100 MHz, $CDCl_3$): δ 14.3 ($\underline{C}H_3CH_2$); 20.5 ($\underline{C}H_3C_{arom,quat}$); 46.4 ($CH_2N$); 61.4 ($CH_2O$); 113.3 (2 x CH_{arom}); 127.6 ($C_{arom,quat}$); 130.0 (2 x CH_{arom}); 144.9 ($C_{arom,quat}$); 171.5 (C=O). **IR** (ATR, cm^{-1}): ν_{NH} = 3379; ν_{CO} = 1724; ν_{max} = 2978, 2905, 1516, 1508, 1449, 1364, 1339, 806. **MS** (ESI): *m/z* (%) 194 ($[M + 1]^+$, 100). Grey needles, 39%. Spectral data matched literature.[602]

2.5.4.5 Synthesis of 1-(*p*-tolylamino)propan-2-one 116n

1-(*p*-Tolylamino)propan-2-one **116n** was synthesized according to literature.[561] *p*-Toluidine **114** (1.071 g, 10 mmol, 1 eq.), K_2CO_3 (1.66 g, 12 mmol, 1.2 eq.) and KI (1.83 g, 11 mmol, 1 eq.) were added to a 50 mL flask containing 20 mL acetone. To this mixture 0.91 ml chloroacetone (1.018 g, 11 mmol, 1.1 eq.) was added, at room temperature, and the mixture was then refluxed overnight under a nitrogen atmosphere. The solvent was evaporated under vacuum, CH_2Cl_2 (100 mL) was added and the solution was washed with aq. $NaHCO_3$ (2 x 100 mL). The crude mixture was purified via column chromatography (SiO_2, EtOAc/PE: 20/80) to give the title compound **116n** as yellow-orange crystals (0.824 g, 50%).

1-(*p*-Tolylamino)propan-2-one 116n

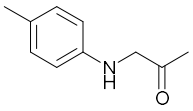

^{1}H-NMR (400 MHz, $CDCl_3$): δ 2.24 (3H, s, CH_3); 2.25 (3H, s, CH_3); 3.99 (2H, s, CH_2); 4.43 (1H, br s, NH); 6.51-6.54 (2H, m, 2 x CH_{arom}); 7.00-7.02 (2H, m, 2 x CH_{arom}). **^{13}C-NMR** (100 MHz, $CDCl_3$): δ 20.5 ($\underline{C}H_3C_{arom,quat}$); 27.5 ($CH_3CO$); 54.8 ($CH_2$); 113.1 (2 x CH_{arom}); 127.2 ($C_{arom,quat}$); 130.0 (2 x CH_{arom}); 144.8 ($C_{arom,quat}$); 204.5 (C=O). **IR** (ATR, cm^{-1}): ν_{NH} = 3379; $\nu_{C=O}$ = 1724; ν_{max} = 2978, 2905, 2860, 1516, 1508, 1449, 1364, 806. **MS** (ESI): *m/z* (%) 164 ($[M + 1]^+$, 100) Yellow crystals, 50%. Spectral data matched literature.[561]

2.5.4.6 Synthesis of *p*-tolylglycine 118

p-Tolylglycine **118** was synthesized according to a literature procedure.[560] *p*-Toluidine **114** (16.1 g, 150 mmol, 1 eq.), 19.2 mL ethyl chloroacetate **117** (22.1 g, 180 mmol, 1.2 eq.) and sodium acetate (14.8 g, 180 mmol, 1.2 eq.) were added to a flask containing 50 mL EtOH and the resulting mixture was refluxed overnight. The mixture was then poured on ice, filtered and dried. The filter cake was added to a flask together with 75 mL H_2O and NaOH (6.60 g, 165 mmol, 1.1 eq.) and this was refluxed for 30 minutes. The mixture was allowed to come to room temperature and the pH was adjusted by slow addition of 3N HCl until it was about 2. The resulting precipitate was filtered and washed with water. The crude was purified by recrystallisation from EtOH/water giving the title compound **118** as a brown solid (12.56 g, 51%).

***p*-Tolylglycine 118**

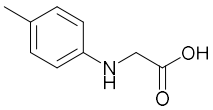

^{1}H-NMR (400 MHz, $CDCl_3$): δ 2.25 (3H, s, CH_3); 3.94 (2H, s, CH_2); 6.57 (2H, d, *J* = 8.3 Hz, 2 x CH_{arom}); 7.02 (2H, d, *J* = 8.3 Hz, 2 x CH_{arom}). **^{13}C-NMR** (100 MHz, $CDCl_3$): δ 20.6 (CH_3); 46.5 (CH_2); 113.7 (2 x CH_{arom}); 128.5 ($C_{arom,quat}$); 129.9 (2 x CH_{arom}); 144.4 ($C_{arom,quat}$); 174.9 (C=O). **IR** (ATR, cm^{-1}): ν_{max} = 3347, 1653, 1510, 1381, 1310, 812, 712, 644, 565, 453. **MS** (ESI): *m/z* (%) 166 ($[M + 1]^+$, 100). Brown solid, 51%. Spectral data matched literature.[560]

2.5.4.7 Synthesis of glycine derivatives 116j-m

Step 1: Synthesis of *N*-(*tert*-butoxycarbonyl)-*N*-(*p*-tolyl)glycine **119**

p-Tolylglycine **118** (4.29 g, 25.9 mmol, 1 eq.) was dissolved in 50 mL acetone/H_2O (1/1) and sodium hydroxide (4.66 g, 116.6 mmol, 4.5 eq.) was added. Di-*tert*-butyl dicarbonate (16.98 g, 77.8 mmol, 3 eq.) was dissolved in 15 mL acetone and added to the *p*-tolylglycine **118** solution. The reaction was stirred at room temperature overnight. The acetone was then removed via rotary evaporation and the mixture was extracted with diethyl ether (25 mL). The water layer was acidified using 3N HCl until the pH was about 3 and then extracted with CH_2Cl_2 (3 x 50 mL). After evaporation the crude was further purified using column chromatography (C18, gradient CH_3CN/H_2O: 10/100 – 100/0) furnishing compound **119** as a yellow oil/off white solid (4.91 g, 71%).

***N*-(*Tert*-butoxycarbonyl)-*N*-(*p*-tolyl)glycine 119**

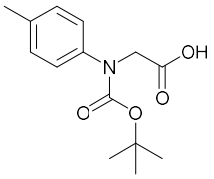

^{1}H-NMR (400 MHz, $CDCl_3$): δ 1.43 (9H, br s, $(CH_3)_3CO$); 2.33 (3H, s, $CH_3C_{arom,quat}$); 4.31 (2H, s, CH_2); 7.11-7.15 (4H, m, 4 x CH_{arom}). **^{13}C-NMR** (100 MHz, $CDCl_3$): δ 21.1 ($\underline{C}H_3C_{arom,quat}$); 28.3 (($\underline{C}H_3)_3CO$); 52.3 ($CH_2N$); 81.4 ($(CH_3)_3\underline{C}O$); 126.4 ($C_{arom,quat}$); 129.6 (2 x CH_{arom}); 136.4 (2 x CH_{arom}); 140.1 ($C_{arom,quat}$); 154.8* (NC=O); 175.5* (C(O)OH). **IR** (ATR, cm^{-1}): $\nu_{C=O}$ = 1705; ν_{max} = 2980, 1512, 1366, 1246, 1233, 1152, 1046, 870, 764. **MS** (ESI): *m/z* (%) 166 ($[M - C_4H_8 - CO_2 + 1]^+$, 75); 210 ($[M - C_4H_8 + 1]^+$, 100); 553 ($[2 x M + 23]^+$, 5); 834 ($[3 x M + 39]^+$, 10). Yellow oil/off white solid, 71%.
*peak broadening

Step 2: Synthesis of Boc protected compounds **120a-d**

The synthesis of *tert*-butyl (2-(isopropylamino)-2-oxoethyl)(*p*-tolyl)carbamate **120a** is described as a representative example for the synthesis of amides **120a-c**.

N-(*Tert*-butoxycarbonyl)-*N*-(*p*-tolyl)glycine **119** (805 mg, 3.03 mmol, 1 eq.), HBTU (1.150 g, 3.03 mmol, 1 eq.) and 1 mL NMM (919 mg, 9.09 mmol, 3 eq.) were added to a flask containing 15 mL dry DMF under argon. The flask was stirred for 10 minutes at room temperature and then 260 µL isopropylamine (179 mg, 3.03 mmol, 1 eq.) was added. This was stirred at room temperature overnight, then water (100 mL) and EtOAc (100 mL) were added and the layers were separated. The organic layer was further washed with brine (2 x 100 mL), evaporated and purified using column chromatography (C18, gradient CH_3CN/H_2O: 30/100 – 100/0)* to furnish the title compound **120a** as a white solid (855 mg, 92%).
*For **120b**: C18, CH_3CN/H_2O: 50/50. For **120c**: C18, gradient CH_3CN/H_2O: 60/100 – 100/0.

For the synthesis of compound **120d** the following procedure was used. *N*-(*Tert*-butoxycarbonyl)-*N*-(*p*-tolyl)glycine **119** (505 mg, 1.9 mmol, 1 eq.), HATU (868 mg, 2.3 mmol, 1.2 eq.) and 662 µL DIPEA (491 mg, 3.8 mmol, 2 eq) were stirred in 10 mL dry DMF under argon for 10 minutes. To this 194 µl thiophenol (209 mg, 1.9 mmol, 1 eq.) was added and the mixture was stirred at room temperature overnight. Water (100 mL) and ethyl acetate (100 mL) were added and the organic layer was further washed with brine (2 x 100 mL). The organic layer was evaporated and purified via column chromatography (C18, gradient CH_3CN/H_2O: 60/100 – 100/0) to give the title compound **120d** as a colorless oil (445 mg, 66%).

***Tert*-butyl (2-(isopropylamino)-2-oxoethyl)(*p*-tolyl)carbamate 120a**

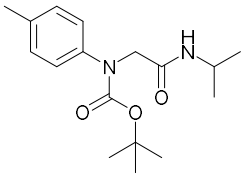

^{1}H-NMR (400 MHz, $CDCl_3$): 1.15 (6H, d, *J* = 6.6 Hz, $(C\underline{H}_3)_2CH$); 1.45 (9H, s, $(C\underline{H}_3)_3CO$); 2.31 (3H, s, $CH_3C_{arom,quat}$); 4.06-4.13 (1H, m, $(CH_3)_2C\underline{H}$); 4.15 (2H, s, CH_2); 6.02 (1H, br s, NH); 7.12 (4H, s, 4 x CH_{arom}). **^{13}C-NMR** (100 MHz, $CDCl_3$): δ 21.0 ($\underline{C}H_3C_{arom,quat}$); 22.9 ($(\underline{C}H_3)_2CH$); 28.3 ($(\underline{C}H_3)_3CO$); 41.5 ($(CH_3)_2\underline{C}H$); 54.8 ($CH_2$); 81.6 ($(CH_3)_3\underline{C}$); 125.6 (2 x CH_{arom}); 129.6 (2 x CH_{arom}); 136.1 ($C_{arom,quat}$); 140.1 ($C_{arom,quat}$); 154.9 (NC(O)O); 168.6 (NC=O). **IR** (ATR, cm^{-1}): ν_{NH} = 3348; $\nu_{C=O}$ = 1678; ν_{max} = 2976, 2934, 1678, 1516, 1381, 1366, 1223, 1175. **MS** (ESI): *m/z* (%) 207 ($[M - C_4H_8 - CO_2 + 1]^+$, 80); 251 ($[M - C_4H_8 + 1]^+$, 100); 307 ($[M + 1]^+$, 20); 635 ($[2 x M + 23]^+$, 10). White solid, 92%.

***Tert*-butyl (2-oxo-2-(phenylamino)ethyl)(*p*-tolyl)carbamate 120b**

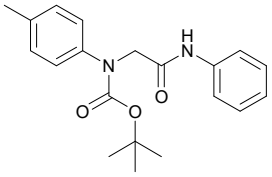

^{1}H-NMR (400 MHz, $CDCl_3$): δ 1.46 (9H, s, $(CH_3)_3CO$); 2.33 (3H, s, $CH_3C_{arom,quat}$); 4.32 (2H, s, CH_2); 7.10-7.18 (5H, m, 5 x CH_{arom}); 7.33 (2H, t, *J* = 7.9 Hz, 2 x CH_{arom}); 7.52 (2H, d, *J* = 7.9 Hz, 2 x CH_{arom}); 8.28 (1H, br s, NH). **^{13}C-NMR** (100 MHz, $CDCl_3$): δ 21.1 ($\underline{C}H_3C_{arom,quat}$); 28.4 ($(\underline{C}H_3)_3CO$); 55.8 ($CH_2$); 82.0 ($(CH_3)_3\underline{C}O$); 119.9 (2 x CH_{arom}); 124.5 (CH_{arom}); 125.9 (2 x CH_{arom}); 129.2 (2 x CH_{arom}); 129.8 (2 x CH_{arom}); 136.5 ($C_{arom,quat}$); 137.8 ($C_{arom,quat}$); 140.0 ($C_{arom,quat}$); 155.5 (NC(O)O); 167.9 (HNC=O). **IR** (ATR, cm^{-1}): ν_{NH} = 3285; $\nu_{C=O}$ = 1692 and 1672; ν_{max} = 2970, 1516, 1429, 1385, 1152, 826, 519. **MS** (ESI): *m/z* (%) 241 ($[M - C_4H_8 - CO_2 + 1]^+$, 100); 285 ($[M - C_4H_8 + 1]^+$, 40); 703 ($[2 x M + 23]^+$, 10). White solid, 78%.

***Tert*-butyl (2-oxo-2-((4-(trifluoromethoxy)phenyl)amino)ethyl)(p-tolyl)carbamate 120c**

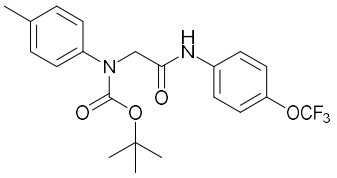

^{1}H-NMR (400 MHz, $CDCl_3$): δ 1.45 (9H, s, $(CH_3)_3CO$); 2.33 (3H, s, $CH_3C_{arom,quat}$); 4.32 (2H, s, CH_2); 7.12-7.18 (6H, m, 6 x CH_{arom}); 7.54 (2H, d, *J* = 9.0 Hz, 2 x CH_{arom}); 8.51 (1H, br s, NH). **^{19}F-NMR** (376 MHz, $CDCl_3$): -58.1 (CF_3) **^{13}C-NMR** (100 MHz, $CDCl_3$): δ 21.1 ($\underline{C}H_3C_{arom,quat}$); 28.4 ($(\underline{C}H_3)_3CO$); 55.8 ($CH_2$); 82.1 ($(CH_3)_3\underline{C}O$); 119.3 ($CF_3$);* 121.0 (2 x CH_{arom}); 121.9 (2 x CH_{arom}); 125.9 (2 x CH_{arom}); 129.8 (2 x CH_{arom}); 136.5 ($C_{arom,quat}$); 136.7 ($C_{arom,quat}$); 139.9 ($C_{arom,quat}$); 145.4 ($C_{arom,quat}$); 155.7 (NC(O)O); 168.1 (HNC=O). **IR** (ATR, cm^{-1}): ν_{NH} = 3292; $\nu_{C=O}$ = 1697 and 1672; ν_{max} = 1541, 1508, 1248, 1221, 1200, 1150, 826. **MS** (ESI): *m/z* (%) 325 ($[M - C_4H_{8+} - CO_2 + 1]^+$, 100); 369 ($[M - C_4H_8 + 1]^+$, 45); 447 ($[M + 23]^+$, 5); 871 ($[2 x M + 23]^+$, 10). White solid, 63%.

*rest of CF_3 quartet not visible

***S*-Phenyl 2-((*tert*-butoxycarbonyl)(*p*-tolyl)amino)ethanethioate 120d**

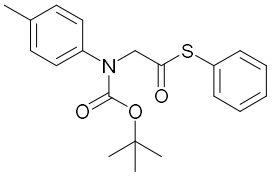

^{1}H-NMR (400 MHz, $CDCl_3$): δ 1.48 (9H, br s, $(CH_3)_3CO$); 2.34 (3H, s, $CH_3C_{arom,quat}$); 4.52 (2H, s, CH_2); 7.14-7.16 (2H, m, 2 x CH_{arom}); 7.23-7.26 (2H, m, 2 x CH_{arom}); 7.42 (5H, s, 5 x CH_{arom}). **^{13}C-NMR** (100 MHz, $CDCl_3$): δ 21.0 ($\underline{C}H_3C_{arom,quat}$); 28.2 ($(\underline{C}H_3)_3CO$); 60.0 ($CH_2$); 81.4 ($(CH_3)_3\underline{C}O$); 126.3 (2 x CH_{arom}); 126.9 (CH_{arom}); 129.3, 129.4 and 129.5 (5 x CH_{arom}); 134.7 (2 x CH_{arom}); 136.2 ($C_{arom,quat}$); 139.3 ($C_{arom,quat}$); 154.3 (NC=O); 195.7 (SC=O). **IR** (ATR, cm^{-1}): $\nu_{C=O}$ = 1697; ν_{max} = 2976, 1514, 1366, 1225, 1150, 1016, 745, 729, 583. **MS** (ESI): *m/z* (%) 258 ($[M - C_4H_8 - CO_2 + 1]^+$, 100); 737 ($[2 x M + 23]^+$, 5). Colorless oil, 66%.

Step 3: Synthesis of Boc deprotected compounds **116j-m**

The synthesis of compound **116j** is described as an example for the synthesis of compounds **116j-m**.

The Boc protected amine **120a** (855 mg, 2.8 mmol, 1 eq.) was dissolved in 7.5 mL dry CH_2Cl_2 under nitrogen and TFA (2.5 mL) was added. This was stirred at room temperature for one hour until completion (LC-MS). The reaction mixture was evaporated and the residue was redissolved in CH_2Cl_2 (10 mL) and washed with saturated $NaHCO_3$ solution (10 mL). The water phase was further extracted with CH_2Cl_2 (10 mL), the combined organic layers were washed with brine (20 mL), dried over $MgSO_4$, filtered and evaporated to give the product **116j** as a colorless oil (577 mg, quant.).

***N*-Isopropyl-2-(*p*-tolylamino)acetamide 116j**

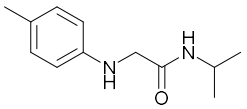

^{1}H-NMR (400 MHz, $CDCl_3$): δ 1.12 (6H, d, *J* = 6.6 Hz, $(C\underline{H}_3)_2CH$); 2.25 (3H, s, $CH_3C_{arom,quat}$); 3.72 (2H, s, CH_2); 4.06-4.19 (2H, m, $C\underline{H}(CH_3)_2$ and $N\underline{H}CH_2$); 6.53 (2H, d, *J* = 8.3 Hz, 2 x CH_{arom}); 6.57 (1H, br s, NHCO); 7.02 (2H, d, *J* = 8.3 Hz, 2 x CH_{arom}). **^{13}C-NMR** (100 MHz, $CDCl_3$): δ 20.5 ($\underline{C}H_3C_{arom,quat}$); 22.8 ($(\underline{C}H_3)_2CH$); 41.2 ($(CH_3)_2\underline{C}H$); 49.7 ($CH_2$); 113.5 (2 x CH_{arom}); 128.6 ($C_{arom,quat}$); 130.0 (2 x CH_{arom}); 145.2 ($C_{arom,quat}$); 169.9 (C=O). **IR** (ATR, cm^{-1}): ν_{NH} = 3337; $\nu_{C=O}$ = 1649; ν_{max} = 2972, 1616, 1516, 1312, 1258, 1171, 806, 513. **MS** (ESI): *m/z* 207 ($[M + 1]^+$, 100). Colorless oil, quant.

***N*-Phenyl-2-(*p*-tolylamino)acetamide 116k**

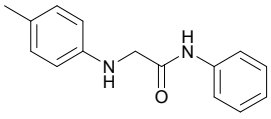

^{1}H-NMR (400 MHz, $CDCl_3$): δ 2.26 (3H, s, CH_3); 3.88 (2H, s, CH_2); 6.62 (2H, d, *J* = 8.2 Hz, 2 x CH_{arom}); 7.05 (2H, d, *J* = 8.2 Hz, 2 x CH_{arom}); 7.11 (1H, t, *J* = 7.7 Hz, CH_{arom}); 7.31 (2H, d x d, *J* = 7.8 x 7.7 Hz, 2 x CH_{arom}); 7.53 (2H, d, *J* = 7.8 Hz, 2 x CH_{arom}); 8.64 (1H, br s, NH). **^{13}C-NMR** (100 MHz, $CDCl_3$): δ 20.5 (CH_3); 50.4 (CH_2); 113.8 (2 x CH_{arom}); 120.0 (2 x CH_{arom}); 124.6 (CH_{arom}); 129.1 (2 x CH_{arom}); 129.3 ($C_{arom,quat}$); 130.2 (2 x CH_{arom}); 137.4 ($C_{arom,quat}$); 144.8 ($C_{arom,quat}$); 169.2 (C=O). **IR** (ATR, cm^{-1}): ν_{NH} = 3410 and 3314; $\nu_{C=O}$ = 1655; ν_{max} = 1620, 1599, 1508, 1441, 1315, 1258, 806. **MS** (ESI): *m/z* 241 ($[M + 1]^+$, 100). Light brown solid, 88%.

2-(*p*-Tolylamino)-*N*-(4-(trifluoromethoxy)phenyl)acetamide 116l

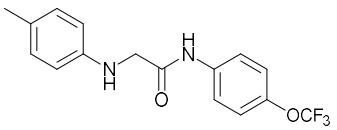

^{1}H-NMR (400 MHz, $CDCl_3$): δ 2.27 (3H, s, CH_3); 3.89 (2H, s, CH_2); 6.59-6.63 (2H, m, 2 x CH_{arom}); 7.05 (2H, d, *J* = 8.3 Hz, 2 x CH_{arom}); 7.16 (2H, d, *J* = 8.3 Hz, 2 x CH_{arom}); 7.54-7.58 (2H, m, 2 x CH_{arom}); 8.72 (1H, br s, NH). **^{19}F-NMR** (376 MHz, $CDCl_3$): -58.14 (CF_3). **^{13}C-NMR** (100 MHz, $CDCl_3$): δ 20.5 (CH_3); 50.4 (CH_2); 113.8 (2 x CH_{arom}); 119.3 (CF_3);* 121.1 (2 x CH_{arom}); 121.9 (2 x CH_{arom}); 129.5 ($C_{arom,quat}$); 130.3 (2 x CH_{arom}); 136.1 ($C_{arom,quat}$); 144.7 ($C_{arom,quat}$); 145.6 ($C_{arom,quat}$); 169.3 (C=O). **IR** (ATR, cm^{-1}): ν_{NH} = 3379; $\nu_{C=O}$ = 1697; ν_{max} = 1614, 1508, 1171, 1155, 1130, 1109, 816, 532. **MS** (ESI): *m/z* 325 ($[M + 1]^+$, 100). White solid, quant.

*rest of CF_3 quartet not visible

***S*-Phenyl 2-(*p*-tolylamino)ethanethioate 116m**

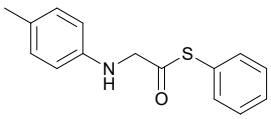

^{1}H-NMR (400 MHz, $CDCl_3$): δ 2.28 (3H, s, CH_3); 4.13 (2H, s, CH_2); 4.30 (1H, br s, NH); 6.60 (2H, d, *J* = 8.1 Hz, 2 x CH_{arom}); 7.06 (2H, d, *J* = 8.1 Hz, 2 x CH_{arom}); 7.41 (5H, s, 5 x CH_{arom}). **^{13}C-NMR** (100 MHz, $CDCl_3$): δ 20.6 (CH_3); 54.7 (CH_2); 113.2 (2 x CH_{arom}); 127.6 ($C_{arom,quat}$); 128.2 ($C_{arom,quat}$); 129.3 (2 x CH_{arom}); 129.5 (CH_{arom}); 130.0 (2 x CH_{arom}); 134.7 (2 x CH_{arom}); 144.4 ($C_{arom,quat}$); 199.7 (C=O). **IR** (ATR, cm^{-1}): ν_{NH} = 3418; $\nu_{C=O}$ = 1692; ν_{max} = 2920, 1520, 1304, 1263, 1057, 806, 756, 579. **MS** (ESI): *m/z* 258 ($[M + 1]^+$, 100). White crystals, 92%

2.5.4.8 Synthesis of ethyl cyclohexylglycinate 116n

Ethyl cyclohexylglycinate **116n** was synthesized according to a modified literature procedure.[563] Cyclohexylamine **122** (0.99 g, 10 mmol, 1 eq.) and triethylamine (1.21 g, 12 mmol, 1.2 eq.) were added to a flame dried flask containing 25 mL dry CH_2Cl_2 under nitrogen. Ethyl bromoacetate **115** (2.00 g, 12 mmol, 1.2 eq.) in 10 mL CH_2Cl_2 was added dropwise at 0 °C. This mixture was stirred at room temperature for 16 hours and then water was added (50 mL) and the layers separated. The water layer was further extracted with CH_2Cl_2 (2 x 50 mL), the combined organic fractions were concentrated and purified by column chromatography (SiO_2, PE/EtOAc: 66/33) to obtain **116o** as a brown oil (1.20 g, 65%).

Ethyl cyclohexylglycinate 116o

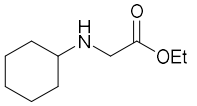

^{1}H-NMR (400 MHz, $CDCl_3$): δ 1.04-1.29 (8H, m, $OCH_2C\underline{H}_3$ and NHCHC(H)HC(H)HC(H)H); 1.58-1.63 (2H, m, NH and $NHCHCH_2CH_2C(H)\underline{H}$); 1.71-1.76 (2H, m, $NHCHCH_2C(H)\underline{H}CH_2$); 1.83-1.87 (2H, m, $NHCHC(H)\underline{H}CH_2CH_2$); 2.40 (1H, t x t, *J* = 15.5 x 3.8 Hz, $NHC\underline{H}CH_2CH_2CH_2$), 3.42 (2H, $NHC\underline{H}_2CO$); 4.19 (2H, t, *J* = 7.1 Hz, $OC\underline{H}_2CH_3$) **^{13}C-NMR** (100 MHz, $CDCl_3$): δ 14.4 ($\underline{C}H_3CH_2O$); 25.0 ($NHCHCH_2\underline{C}H_2CH_2$); 26.2 ($NHCHCH_2CH_2\underline{C}H_2$); 33.5 ($NHCH\underline{C}H_2CH_2CH_2$); 48.5 ($NH\underline{C}H_2CO$); 56.6 ($NH\underline{C}HCH_2CH_2CH_2$); 60.9 ($CH_3\underline{C}H_2O$); 173.1 (C=O). **IR** (ATR, cm^{-1}): $\nu_{C=O}$ = 1736; ν_{max} = 2926, 2853, 1449, 1373, 1182, 1152, 1024, 891, 692. **MS** (ESI): *m/z* 186 ($[M + 1]^+$, 100). Brown oil, 65%. Spectral data matched literature.[563]

2.5.5 Synthesis of COFs

2.5.5.1 Synthesis of TpBpyCOF, TpPpyCOF and TpOMeBpyCOF

The procedure to synthesize **TpBpyCOF** was modified from a literature procedure.[506] An Agilent GC vial (size: 22.75 mm x 75 mm; 20 mm cap) was charged with 1,3,5-triformylphloroglucinol **Tp** (63.0 mg, 0.3 mmol, 1 eq.) and 2,2'-bipyridine-5,5'-diamine **Bpy** (83.7 mg, 0.45 mmol, 1.5 eq.). Dimethylacetamide (4.5 mL) and *o*-dichlorobenzene (1.5 mL) were added via the sides of the vial, to flush the remaining solids from the walls. Then 0.6 mL of 6.0 M aqueous acetic acid was added and the vial was capped. This mixture was then sonicated for ten minutes, flash frozen at 77 K in liquid N_2 and degassed by three freeze-pump-thaw cycles, after which the vial was put under argon. After warming to room temperature the vial was placed in an oven pre-heated at 120 °C. The resulting red powder was collected via filtration and washed sequentially with copious DMAc-DMF-H_2O-acetone-ethanol-THF. Further purification was done by Soxhlet extraction with methanol for 72 hours. Finally, the material was dried under vacuum overnight giving **TpBpyCOF** as a red powder (113 mg, 86%). Similarly, using **Bpy** (83.7 mg, 0.45 mmol, 1.5 eq.) and **TpOMe** (76 mg, 0.3 mmol, 1 eq.) **TpOMeBpyCOF** was obtained as a dark red powder (115 mg, 80%) and using **Ppy** (83 mg, 0.45 mmol, 1.5 eq.) and **Tp** (63.0 mg, 0.3 mmol, 1 eq.) **TpPpyCOF** was obtained as an orange powder (103 mg, 79%).

2.5.5.2 Synthesis of TpPa-1

This synthesis was performed according to a literature reference.[489] Benzophenone-protected diamine **45** (982 mg, 2.25 mmol, 1.5 eq.) and **Tp** (315 mg, 1.5 mmol, 1 eq.) were added to a 25 mL Schlenk flask. Mesitylene/dioxane (1/1, 15 mL) and 6 M AcOH (2.5 mL) were added via the sides of the flask, to flush down remaining solids. The mixture was then sonicated for ten minutes. The flask was degassed through three freeze-pump-thaw cycles, after which it was put under argon. This was heated in an oil bath at 120 °C for three days. The resulting dispersion was added to hot DMF (90 °C) and stirred for an hour, this was then filtered and repeated one more time. The filter cake was then also thoroughly rinsed with acetone and EtOH, and further purified via Soxhlet extraction with MeOH to obtain **TpPa-1** as a red powder (0.90 g, 74%).

2.5.5.3 Synthesis of Ru_xx@TpBpyCOF

The synthesis of **Ru_10@TpBpyCOF** is given as a representative example for the synthesis of **Ru_xx@TpBpyCOF**.

An Agilent GC vial (size: 22.75 x 75 mm; 20 mm cap) was charged with 1,3,5-triformylphloroglucinol **Tp** (63.0 mg, 0.3 mmol, 1 eq.), 2,2'-bipyridine-5,5'-diamine **Bpy** (75 mg, 0.40 mmol, 1.34 eq.) and **Ru@Bpy** (40 mg, 0.045 mmol, 0.15 eq.). Dimethylacetamide (4.5 mL) and *o*-dichlorobenzene (1.5 mL) were added via the sides of the vial, to flush the remaining solids from the walls. Then 0.6 mL of 6.0 M aqueous acetic acid was added, and the vial was capped. This mixture was then sonicated for 10 minutes, flash frozen at 77 K in liquid N_2 and degassed by three freeze-pump-thaw cycles, after which the vial was put under argon. The vial was warmed to room temperature and then placed in an oven pre-heated at 120 °C. The resulting red powder was collected via filtration and washed sequentially with copious DMAc-DMF-H_2O-acetone-ethanol-THF. Further purification was done by Soxhlet extraction with methanol for 72 hours. Finally, the material is dried under vacuum overnight giving **Ru_10@TpBpyCOF** as a dark red powder (114 mg, 70%).

2.5.6 Computational modelling

All computational experiments were performed by Sander Borgmans, Juul De Vos and Kuber Sing Rawat at the Center for Molecular Modeling (UGent, Department of Applied Physics) and this section was largely written by these authors.

2.5.6.1 Construction of system-specific force fields

2.5.6.1.1 Cluster force fields

A system specific force field is derived for each of the materials from the cluster force fields of the underlying building blocks.[603–611] The cluster models are terminated properly as such that they mimic the periodic structure. The used cluster models and their termination are visualized in Figure 16. As the Bpy linker is both combined with the Tp and TpOMe building blocks, which form an amine or imine linkage respectively, two different clusters are defined for which the termination differs to mimic the correct neighboring cluster. The Tp and TpOMe clusters are terminated with a phenyl ring, linked by an amine and imine linkage respectively. It is assumed that the nitrogen atoms in the Bpy and Ppy do not influence the resulting covalent and electrostatic parameters of these clusters significantly.

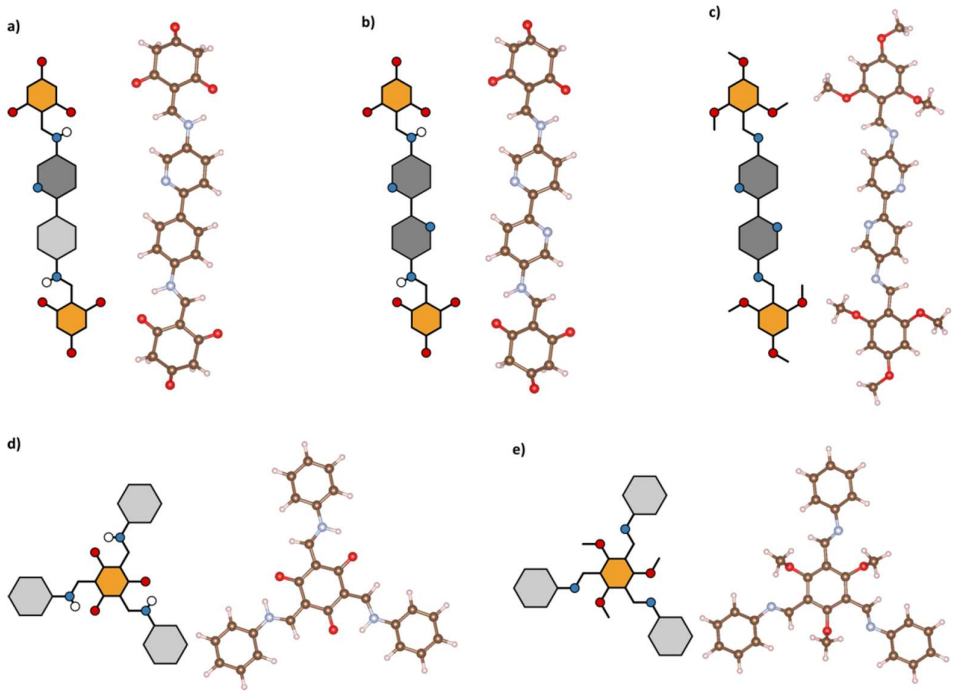

Figure 16: Atomic and abstract visualization of the cluster models that are used to derive the cluster force fields. a) Ppy with a Tp termination (Ppy_amine), b) Bpy with a Tp termination (Bpy_amine), c) Bpy with a TpOMe termination (Bpy_imine), d) Tp with an amine linkage (Tp_amine), e) TpOMe with an imine linkage (TpOMe_imine). The color code that was used: (white) hydrogen, (brown) carbon, (blue) nitrogen, (red) oxygen.

After an optimization, the *ab initio* hessian of each cluster is derived with Gaussian16[612] using the B3LYP exchange-correlation functional[613–615] extended with Grimme D3 dispersion corrections[616] and the 6-311++G(d,p) Pople basis set.[617] For the optimization, the default convergence criteria were

adopted and the NoSymm keyword is used. The YQC self-consistent field procedure was followed for both optimization and hessian calculations.

Subsequently, the partial charges are derived from the electron density distribution with the MBIS partitioning scheme,[618] as implemented in HORTON,[619] and adopted by QuickFF[620,621] to determine the electrostatic force field parameters, using Gaussian charge distributions[622] and bond charge increments.[623] Finally, QuickFF[620,621] fits the covalent parameters as such that the force field derived hessian reproduces the *ab initio* hessian as accurately as possible. Besides the covalent and electrostatic interactions, the force field also comprises Van der Waals interactions, as dispersion corrections are included in the *ab initio* calculations. These are described by a Buckingham potential using the fully transferable MM3 parameters.[624]

2.5.6.1.2 Validation

Once the cluster force fields are derived, their capability in reproducing both the *ab initio* relaxed structure and the *ab initio* frequencies is examined. The clusters are first optimized using yaff,[625] after which a normal mode analysis (NMA)[626] is performed with TAMkin[627] to derive the vibrational frequencies. These force field derived frequencies are compared with the earlier derived *ab initio* frequencies in Figure 17. In Figure 18, the internal coordinates (bonds, bends, dihedral angles and out-of-plane distances) from the force field and *ab initio* relaxed structures are compared. For both the frequency and geometry comparison, the mean deviation (MD) and root mean square deviation (RMSD) have been indicated.

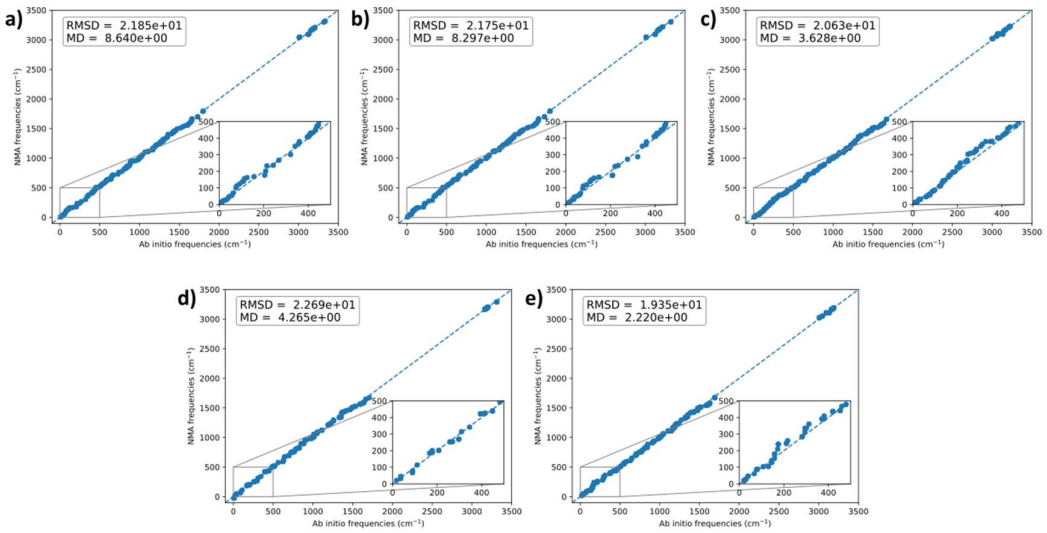

Figure 17: Comparison of the *ab initio* (AI) and force field (FF) derived vibrational frequencies, with an inset of the low frequencies. The dashed lines correspond to perfect agreement. Both the mean deviation (MD) and root mean square deviation (RMSD) are reported. Alphabetical labels correspond to the cluster models in Figure 15.

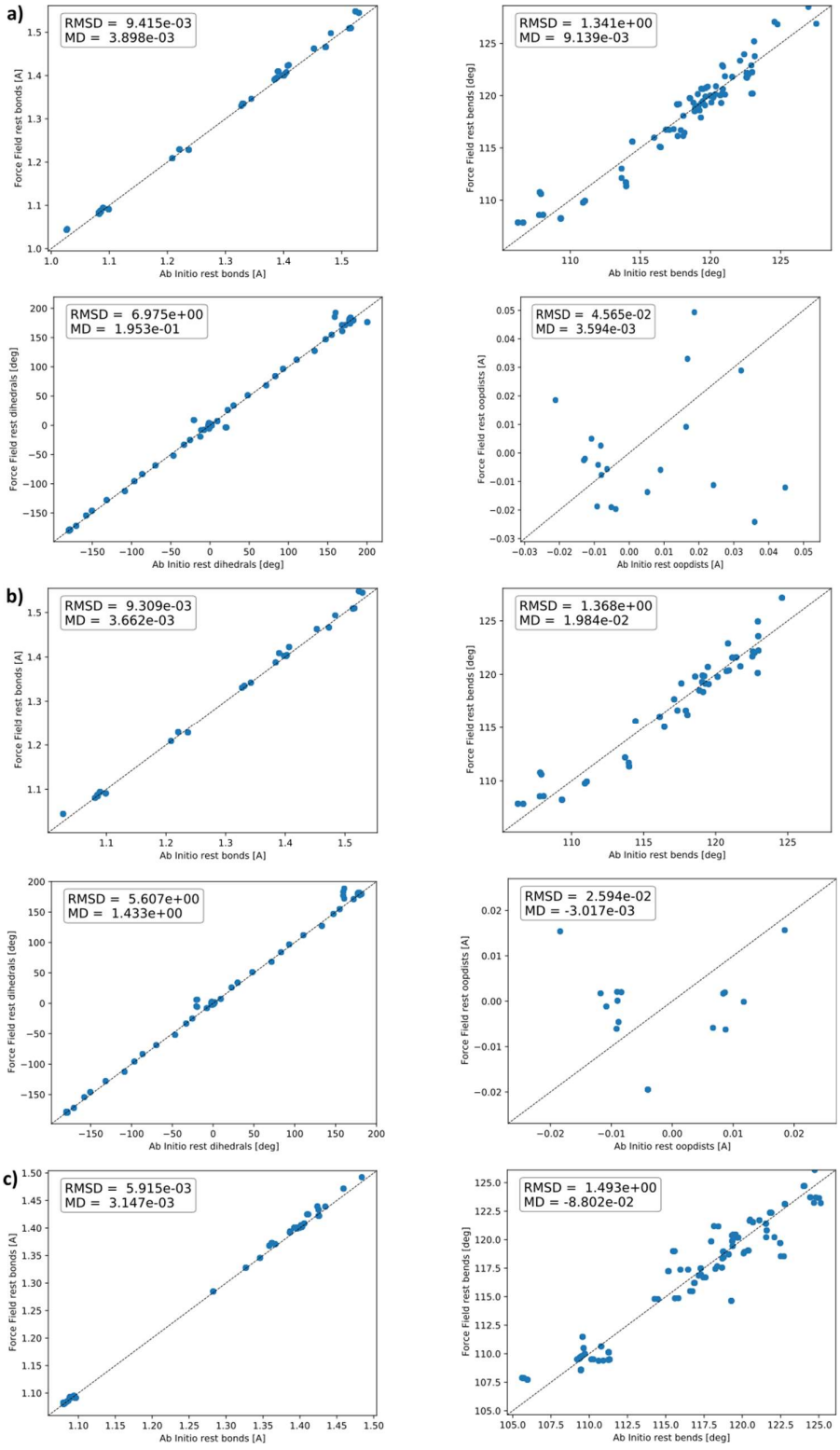
a)
RMSD = 9.415e-03
MD = 3.898e-03
Force Field rest bonds [A]
Ab Initio rest bonds [A]
RMSD = 1.341e+00
MD = 9.139e-03
Force Field rest bends [deg]
Ab Initio rest bends [deg]
RMSD = 6.975e+00
MD = 1.953e-01
Force Field rest dihedrals [deg]
Ab Initio rest dihedrals [deg]
RMSD = 4.565e-02
MD = 3.594e-03
Force Field rest oopdists [A]
Ab Initio rest oopdists [A]
b)
RMSD = 9.309e-03
MD = 3.662e-03
Force Field rest bonds [A]
Ab Initio rest bonds [A]
RMSD = 1.368e+00
MD = 1.984e-02
Force Field rest bends [deg]
Ab Initio rest bends [deg]
RMSD = 5.607e+00
MD = 1.433e+00
Force Field rest dihedrals [deg]
Ab Initio rest dihedrals [deg]
RMSD = 2.594e-02
MD = -3.017e-03
Force Field rest oopdists [A]
Ab Initio rest oopdists [A]
c)
RMSD = 5.915e-03
MD = 3.147e-03
Force Field rest bonds [A]
Ab Initio rest bonds [A]
RMSD = 1.493e+00
MD = -8.802e-02
Force Field rest bends [deg]
Ab Initio rest bends [deg]

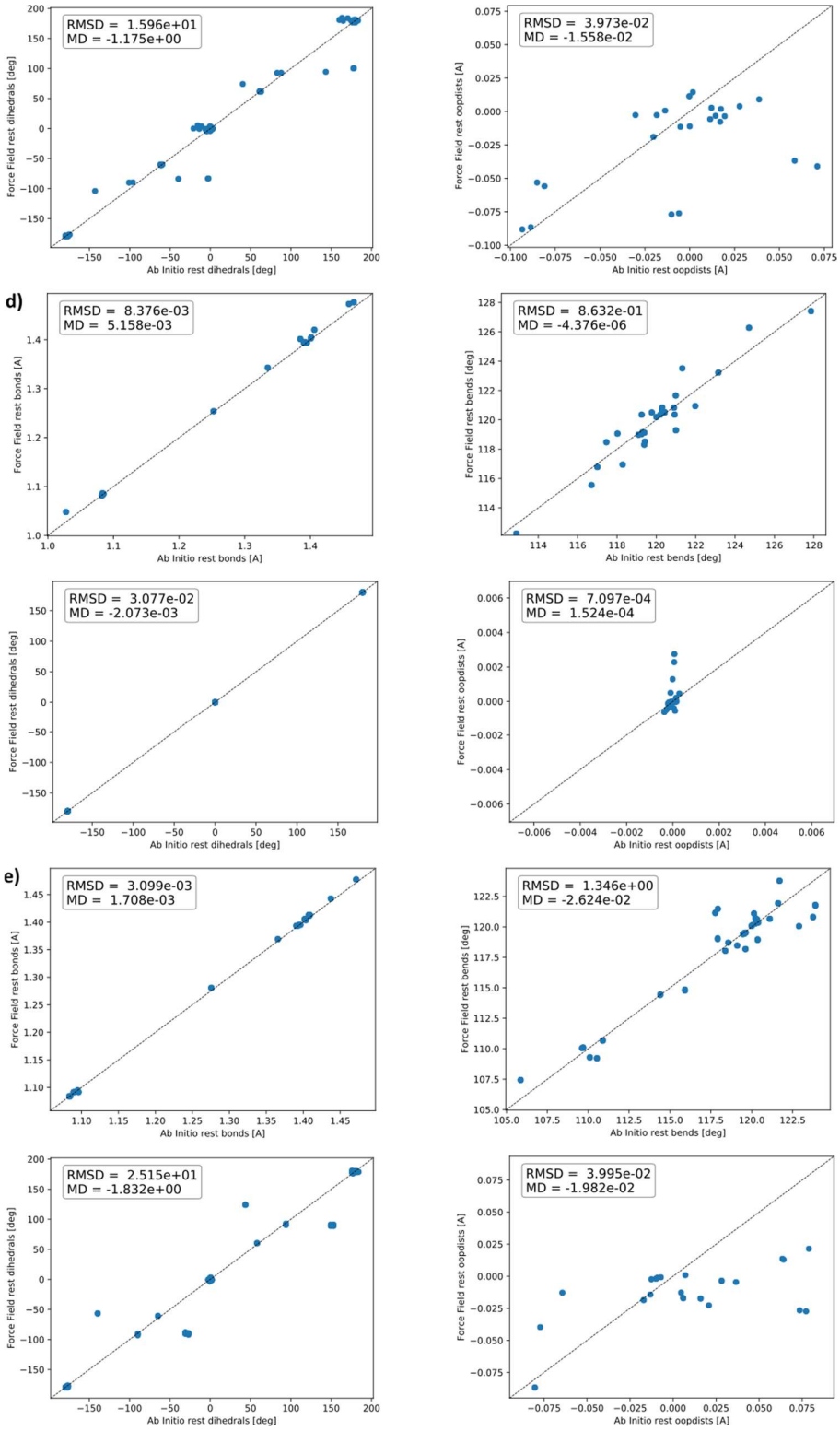

Figure 18: Comparison of the *ab initio* (AI) and force field (FF) derived relaxed internal coordinates. The dashed lines correspond to perfect agreement. Both the mean deviation (MD) and root mean square deviation (RMSD) are reported. Alphabetical labels correspond to the cluster models in Figure 16. For each cluster, the bonds, bends, dihedral angles, and out-of-plane distances are visualized from top left to bottom right respectively.

2.5.6.1.3 Additional dihedral terms

When considering the deviations in the dihedral angles after optimizing the optimal *ab initio* geometry with the force field, it is clear that the clusters force field needs to be adapted to better account for the rotational barrier of the imine/amine linkage and the phenyl/pyridine rotations. This is facilitated by *ab initio* rotational scans, such that the relevant force field terms can be replaced by more accurate sixth order polynomials. As evidenced by Figures 19-29, it is clear that the new force field significantly improves the reproduction of this rotational barrier.

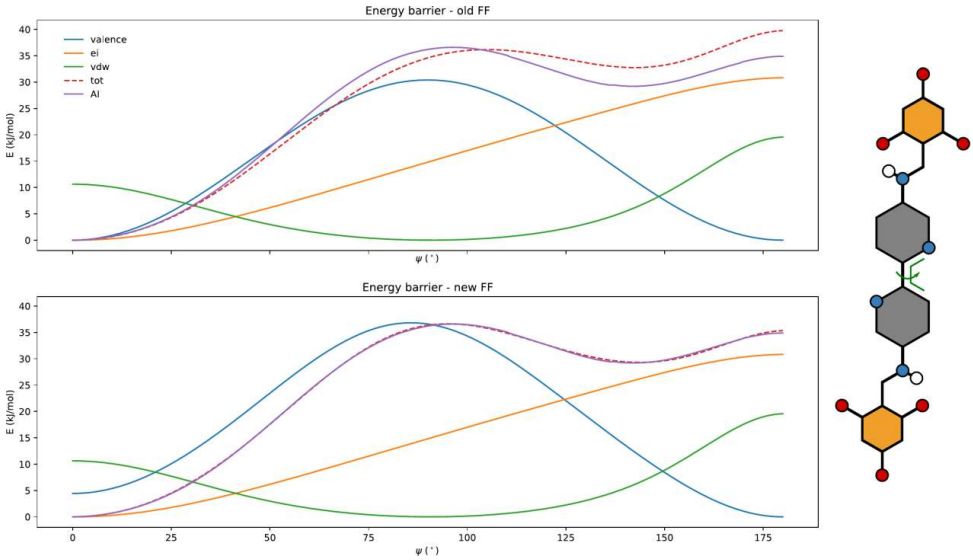

Figure 19: Force field contributions of the old and newly fitted force field for the rotational barrier of the bipyridine unit, with an amine linkage (Bpy_amine), compared to the corresponding *ab initio* barrier. The total (tot) contribution is equal to the sum of the covalent contributions (valence), the electrostatic interactions (ei), and the dispersion interactions (vdw).

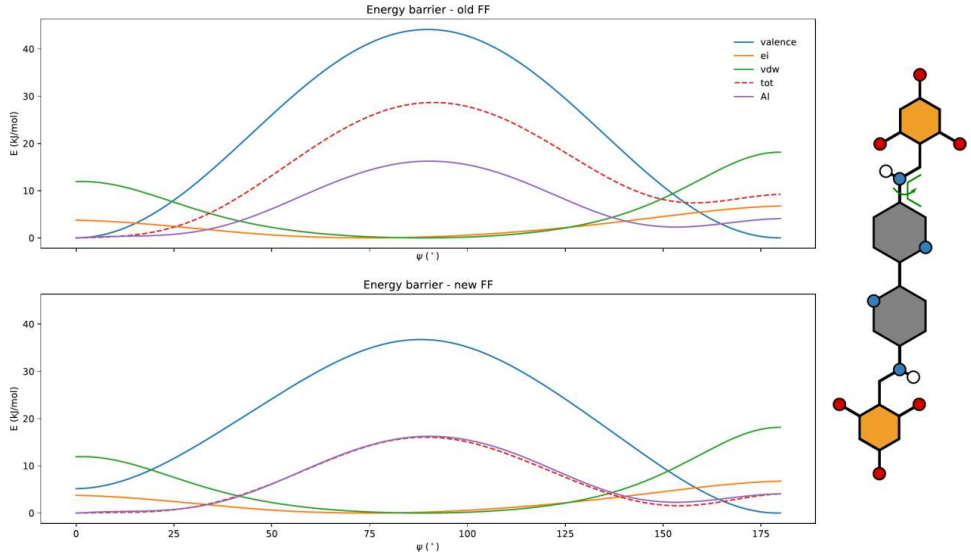

Figure 20: Force field contributions of the old and newly fitted force field for the rotational barrier of the amine linkage, linked to the bipyridine unit (Bpy_amine), compared to the corresponding *ab initio* barrier. The total (tot) contribution is

equal to the sum of the covalent contributions (valence), the electrostatic interactions (ei), and the dispersion interactions (vdw).

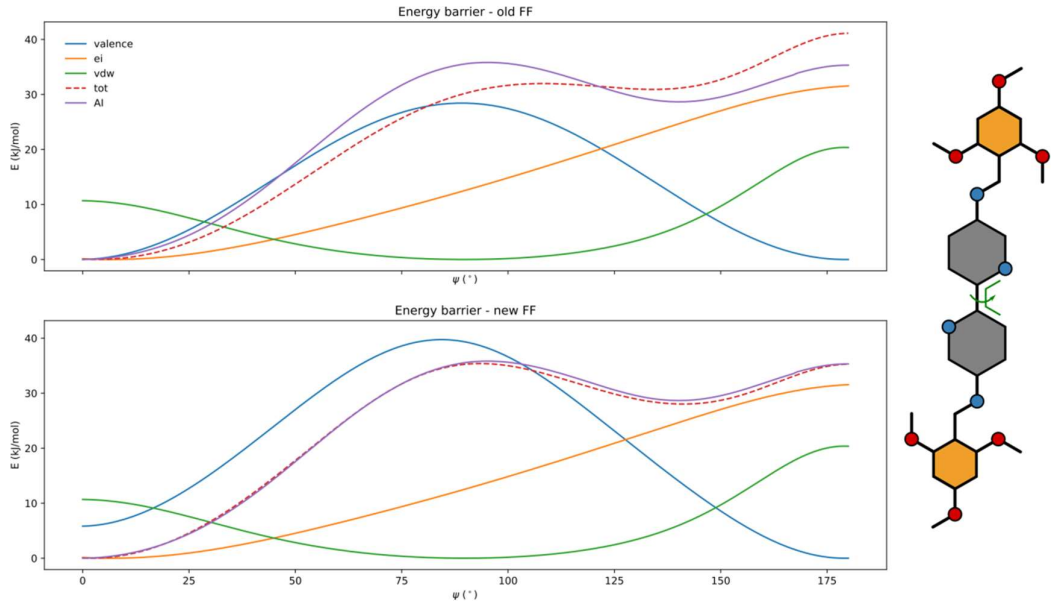

Figure 21: Force field contributions of the old and newly fitted force field for the rotational barrier of the bipyridine unit, with an imine linkage (Bpy_imine), compared to the corresponding *ab initio* barrier. The total (tot) contribution is equal to the sum of the covalent contributions (valence), the electrostatic interactions (ei), and the dispersion interactions (vdw).

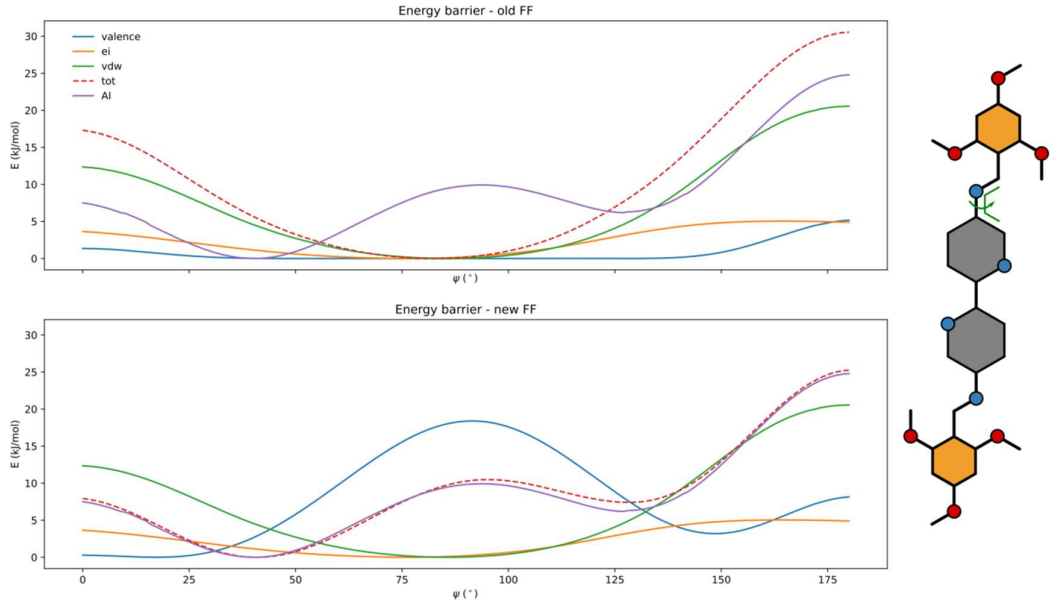

Figure 22: Force field contributions of the old and newly fitted force field for the rotational barrier of the imine linkage, linked to the bipyridine unit (Bpy_imine), compared to the corresponding *ab initio* barrier. The total (tot) contribution is equal to the sum of the covalent contributions (valence), the electrostatic interactions (ei), and the dispersion interactions (vdw).

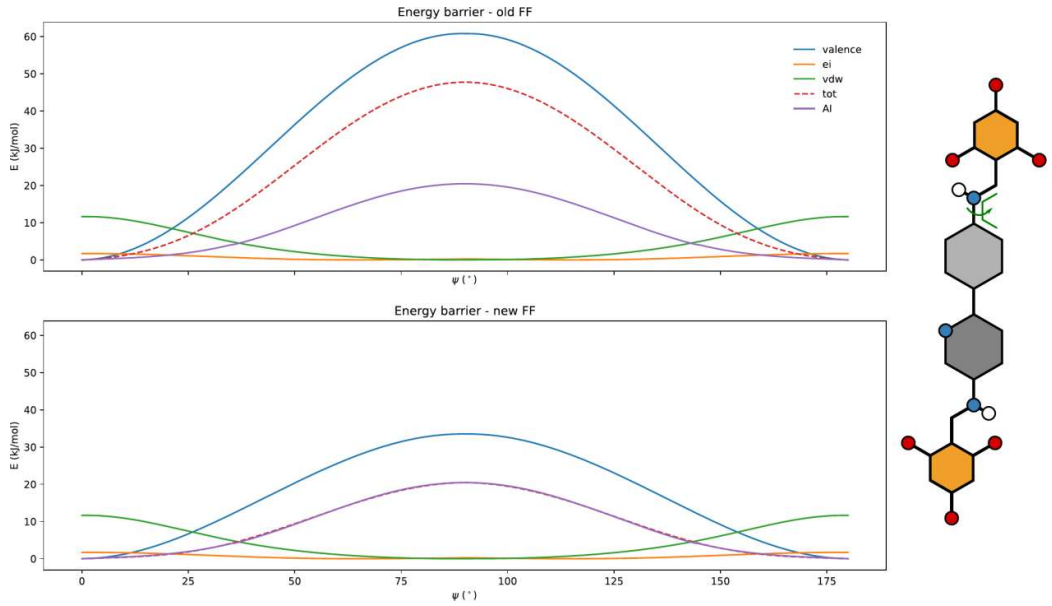

Figure 23: Force field contributions of the old and newly fitted force field for the rotational barrier of the amine linkage, linked to the phenylpyridine unit (Ppy_amine), compared to the corresponding *ab initio* barrier. The total (tot) contribution is equal to the sum of the covalent contributions (valence), the electrostatic interactions (ei), and the dispersion interactions (vdw).

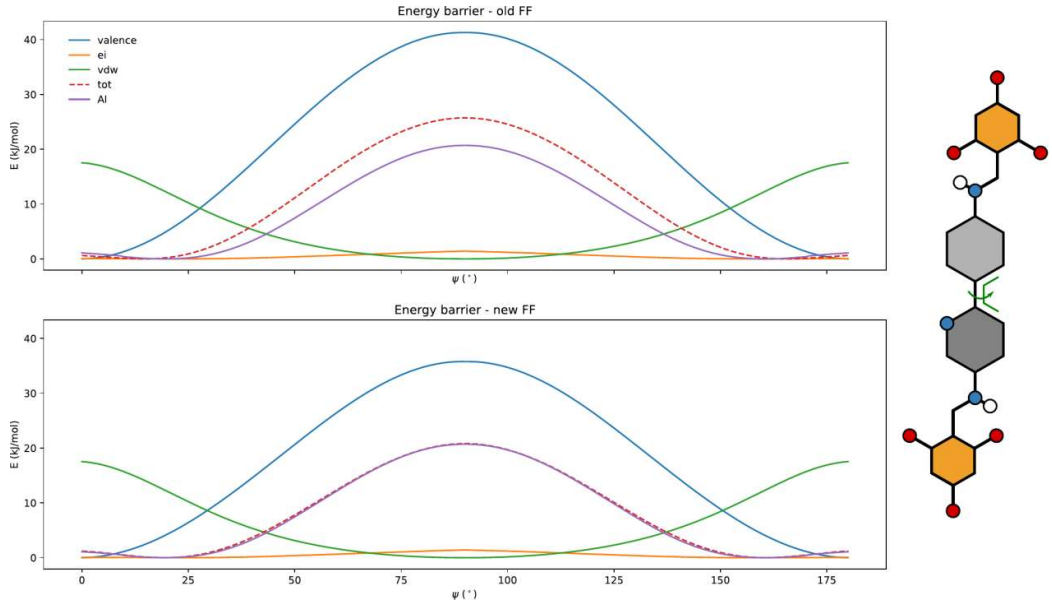

Figure 24: Force field contributions of the old and newly fitted force field for the rotational barrier of the phenylpyridine unit, with an amine linkage (Ppy_amine), compared to the corresponding *ab initio* barrier. The total (tot) contribution is equal to the sum of the covalent contributions (valence), the electrostatic interactions (ei), and the dispersion interactions (vdw).

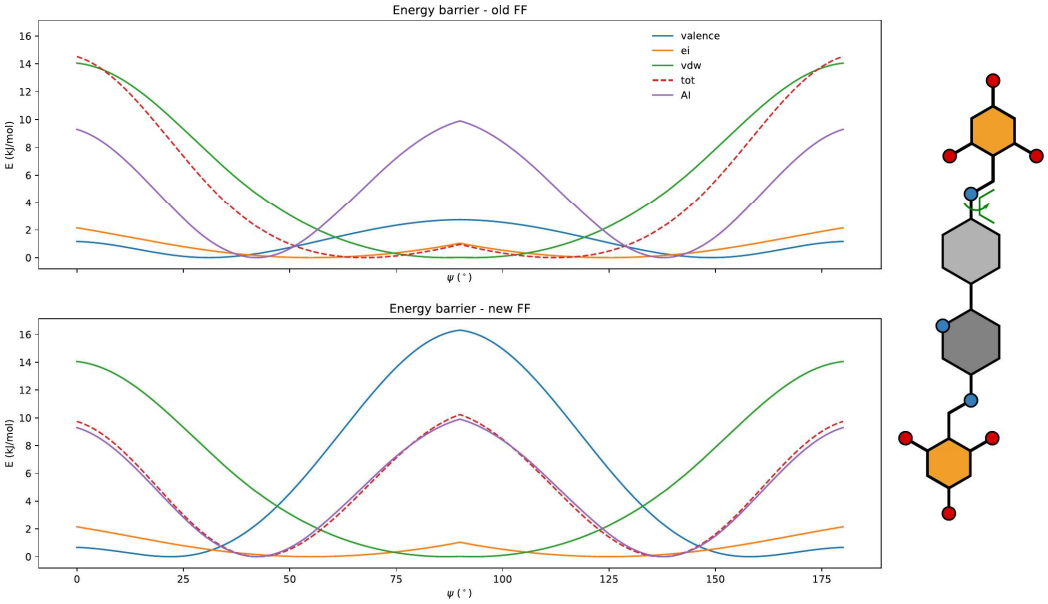

Figure 25: Force field contributions of the old and newly fitted force field for the rotational barrier of the imine linkage, linked to the phenylpyridine unit (Ppy_imine), compared to the corresponding *ab initio* barrier. The total (tot) contribution is equal to the sum of the covalent contributions (valence), the electrostatic interactions (ei), and the dispersion interactions (vdw).

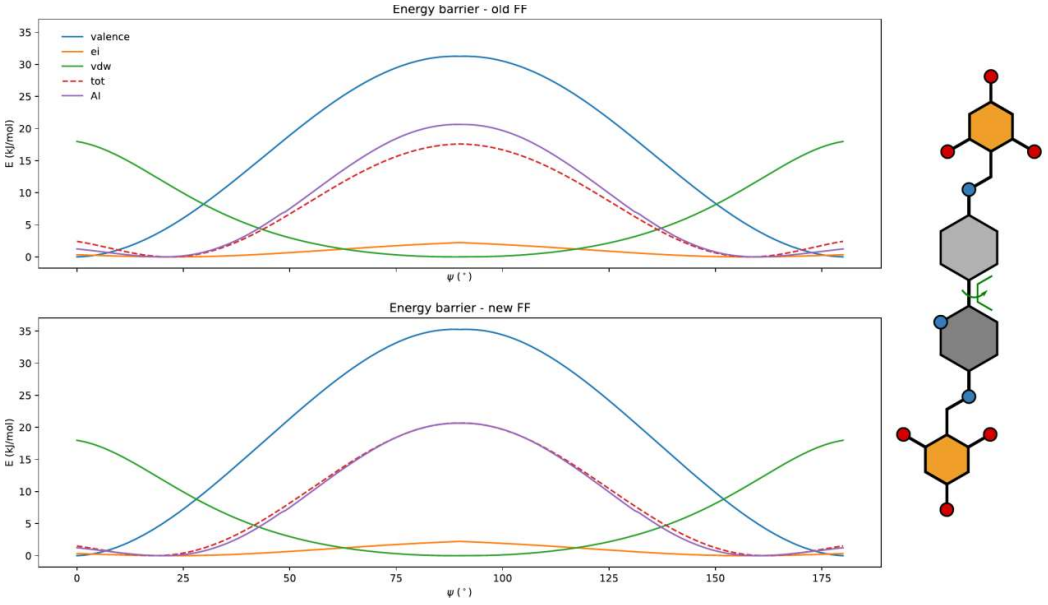

Figure 26: Force field contributions of the old and newly fitted force field for the rotational barrier of the phenylpyridine unit, with an imine linkage (Ppy_imine), compared to the corresponding *ab initio* barrier. The total (tot) contribution is equal to the sum of the covalent contributions (valence), the electrostatic interactions (ei), and the dispersion interactions (vdw).

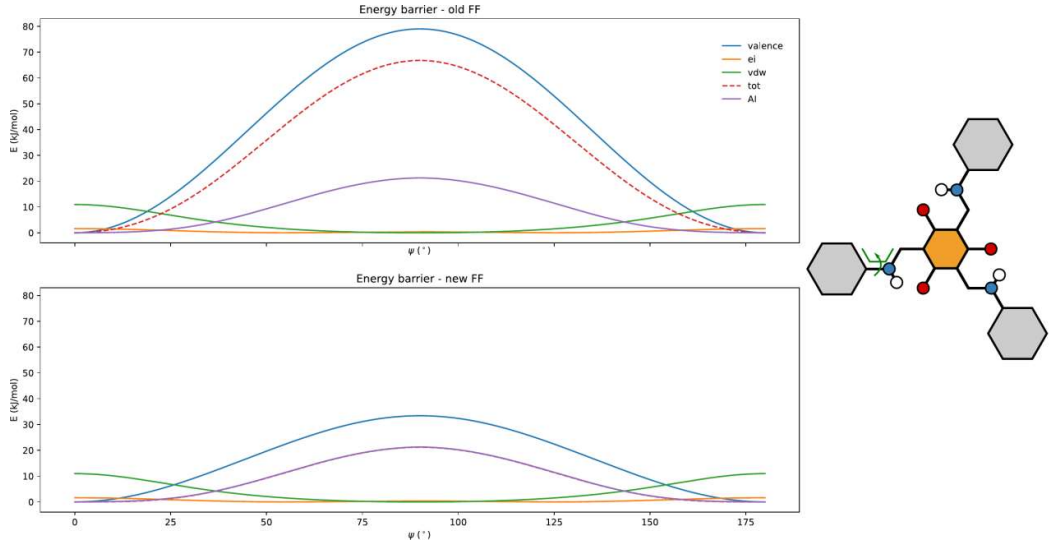

Figure 27: Force field contributions of the old and newly fitted force field for the rotational barrier of the amine linkage, with respect to the Tp unit (Tp_amine), compared to the corresponding *ab initio* barrier. The total (tot) contribution is equal to the sum of the covalent contributions (valence), the electrostatic interactions (ei), and the dispersion interactions (vdw).

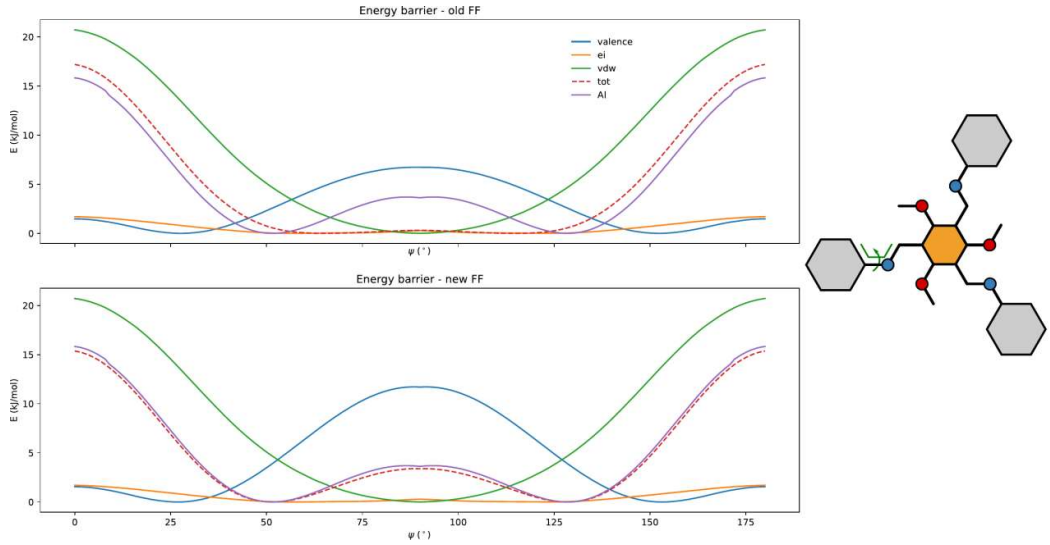

Figure 28: Force field contributions of the old and newly fitted force field for the rotational barrier of the imine linkage for the TpOMe building unit with respect to the linker (TpOMe_imine), compared to the corresponding *ab initio* barrier. The total (tot) contribution is equal to the sum of the covalent contributions (valence), the electrostatic interactions (ei), and the dispersion interactions (vdw).

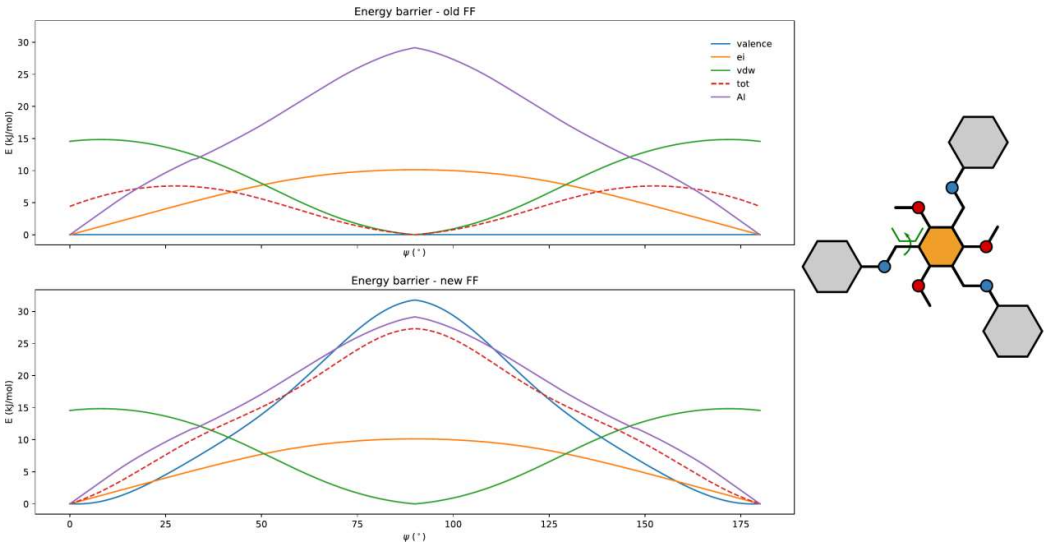

Figure 29: Force field contributions of the old and newly fitted force field for the rotational barrier of the imine linkage for the TpOMe building unit with respect to the vertex (TpOMe_imine), compared to the corresponding *ab initio* barrier. The total (tot) contribution is equal to the sum of the covalent contributions (valence), the electrostatic interactions (ei), and the dispersion interactions (vdw).

2.5.6.1.4 Combining cluster force field into periodic force fields

Following a procedure established earlier at the CMM,[610,611] accurate, system-specific periodic force fields can be generated from the cluster force field of their underlying building blocks, on the condition that their framework environment is properly mimicked in the cluster termination. This cluster approximation has the smallest impact on the covalent terms that are embedded fully in the cluster. Therefore, these terms are directly adopted from the cluster force field. On the other hand, overlap terms that span two building blocks are described most accurately in the force field of the building block with the majority of the atoms. The parameters of these overlap terms are defined by a weighted average over the respective terms in both constituent cluster force fields.

Similarly, the bond charge increments of bonds between atoms that are assigned to different building blocks is formed by an average of the bond charge increments in the two respective clusters. Charge neutrality is guaranteed as bond charge increments are used. The Van der Waals interactions can be adopted directly as the parameters of the Buckingham potential are derived from atomic parameters.

2.5.6.2 Structural models

The initial structural models are generated *in silico* with our in-house structure assembly software, which is based on a top-down approach.[628] This requires a predefined topology, which is in this work always the honeycomb **hcb** lattice, and a set of building blocks that can be placed on its nodes. TpBpy, TpPpy, and TpOMeBpy are generated using a combination of clusters d and b, clusters d and a, and clusters e and c, respectively (see Figure 16), similar to their synthesis procedure. For each cluster, an appropriate set of points of extension is defined as the points where the building block can link with other building blocks. The points of extension are here always chosen in the center of the C=N imine bond or C-N amine bond. The termination of the clusters, *i.e.* all atoms beyond the points of extension, are omitted in the building procedure.

After careful selection of the building blocks and the topology, the topological nodes are decorated in a three-step procedure. Initially, the unit cell of the topology is isotropically rescaled to accommodate the building blocks. Secondly, the configurations of each building block are selected for which the points of extension are nicely oriented towards the neighboring topological nodes. The symmetry of the atomic representation of the building blocks can be lower than the symmetry of the points of extension. In these cases, multiple configurations that result in the same alignment within the topology, have a different atomic representation. In the final step, one configuration for each building block is chosen from the remaining ones based on an energetical descriptor that defines the energy penalty introduced by inserting the building blocks in this configuration. Once all topological nodes are decorated with the appropriate building blocks, a two-layer structure is obtained by taking a 1,1,2-supercell with a sub-optimal interlayer distance of 10 Å. The initial models are realized by relaxing these structures with the periodic force fields as derived in Section 2.5.6.1.

Within the materials discussed in the main text, several asymmetric moieties are present, which might give rise to variations in the PXRD pattern depending on their relative orientations. Moreover, as the emergent behavior of 2D COFs is typically dependent on the behavior of subsequent layers, variations in these orientations of subsequent layers is also taken into account. Although molecular dynamics (MD) simulations are performed to sample the relevant parts of the potential energy surface (PES), the stacking of the layers might inhibit variations in the orientations of these moieties to occur, such that they have to be modelled explicitely.

Here, we explicitly take the orientation of the following units into account:

- Imine/amine linkage
- Bipyridine/phenylpyridine linker
- Methoxy groups on TpOMe

Within one layer their orientation can be either parallel or antiparallel, whereas between subsequent layers their orientation can be either symmetric or antisymmetric. Moreover, the relative sequence of the phenyl ring and pyridine ring in phenylpyridine can be switched between subsequent rings, which will be denoted as either aligned or alternating. Finally, the methoxy groups can either all be aligned with each other, or they can be adapted such that one out of three is aligned differently. These variations are all abstractly visualized in Figure 30 for clarity.

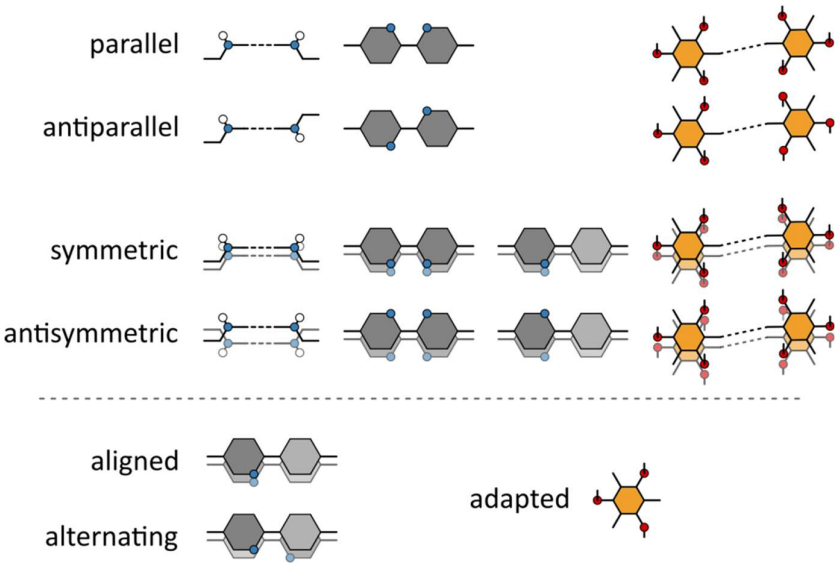

Figure 30: Abstract illustration of the terminology for the different structural models. (Top) General labels which are applicable to most building units. As the imine and amine linkage behave identically (terminology wise) only the amine examples are provided. The parallel/antiparallel label is based on the single layer orientation, whereas the symmetric/antisymmetric label is based on the two layer orientation. (Bottom) The aligned/alternating label is a specific label for the phenylpyridine moiety to account for the relative position of the pyridine ring, whereas the adapted label indicates a change in the orientation of a single methoxy group for a single vertex instead of all methoxy groups at the same time.

2.5.6.3 PXRD generation

As in our previous work,[513] all structural models were first optimized for a static approach to the PXRD pattern, sampling the PES at zero Kelvin. However, in general, this is a poor approximation for reproducing the experimental reference pattern when dealing with 2D COFs with dynamically shearing layers. Instead, simulating at the elevated pressures and temperatures that occur during the experimental measurement, results in small dynamic fluctuations of the reflection planes that mimic the peak broadening effects that occur during the inherently time-averaged diffraction measurement. As such, by averaging the PXRDs calculated at 50 uniformly distributed snapshots throughout the MD simulation, a much better agreement is obtained. In accordance with our previously reported workflow[513] a metric comparison was performed to identify the optimal models, as illustrated in Figures 31-33.

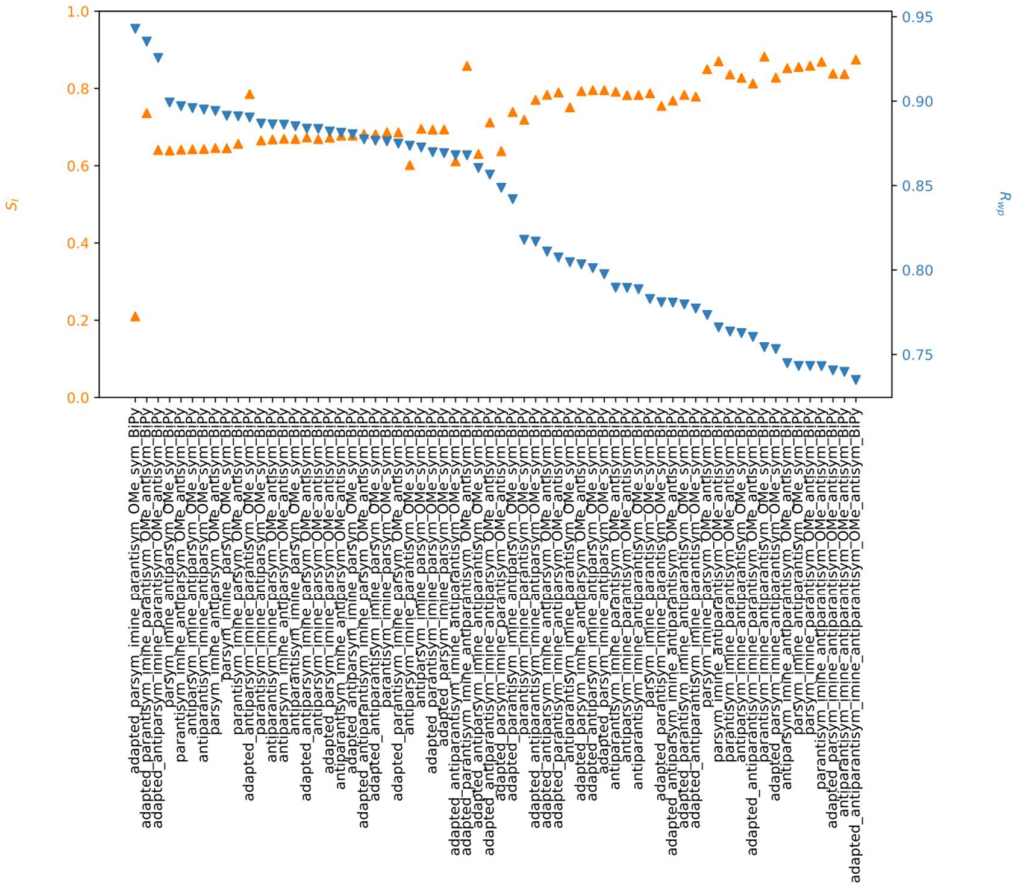

Figure 31: Metric ranking for **TpOMeBpyCOF** to identify the optimal model, based on the MD averaged PXRD pattern.

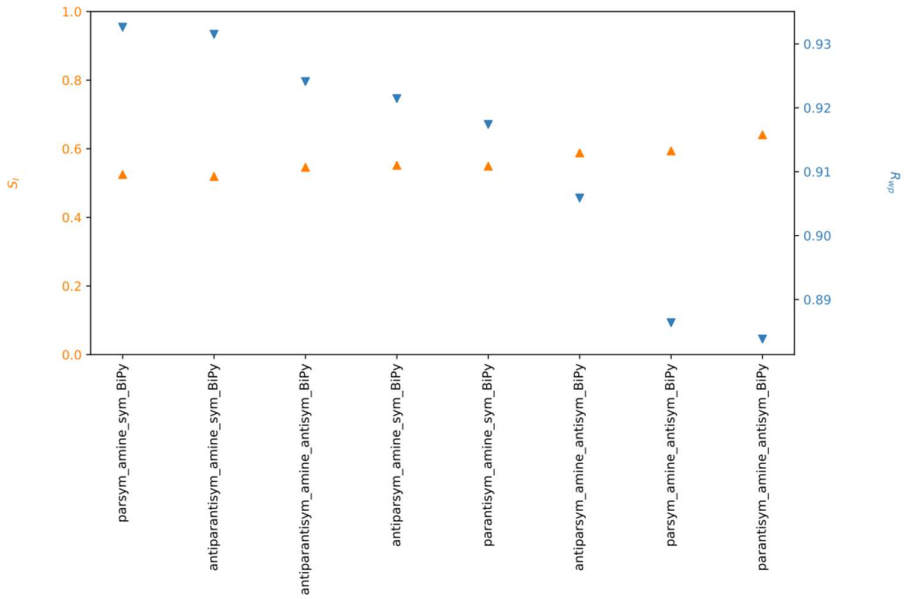

Figure 32: Metric ranking for **TpBpyCOF** to identify the optimal model, based on the MD averaged PXRD pattern.

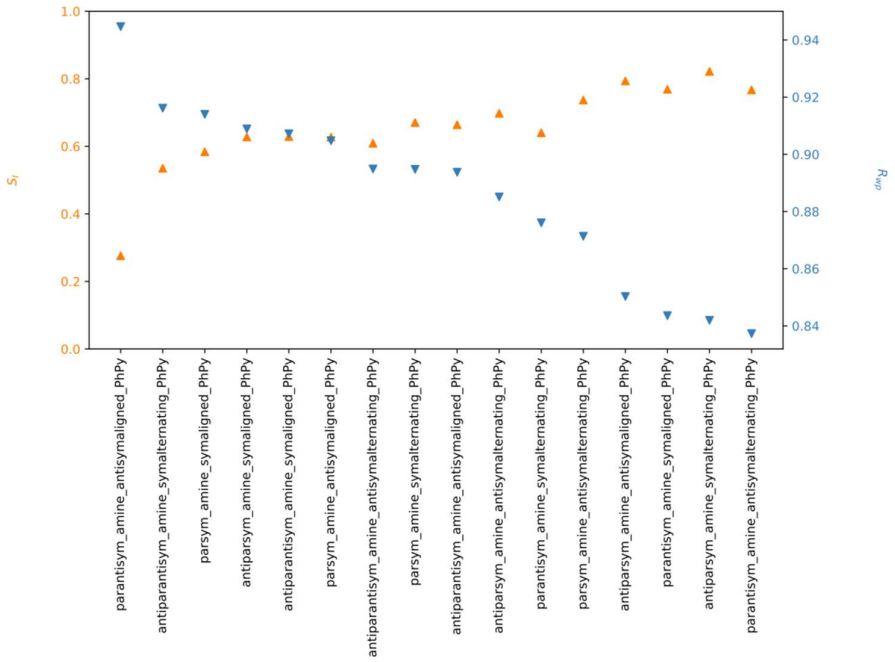

Figure 33: Metric ranking for **TpPpyCOF** to identify the optimal model, based on the MD averaged PXRD pattern.

2.5.6.4 Computational details: Structural modelling

The PXRD patterns were calculated using the pyobjcryst python package, which is a wrapper for the ObjCryst++ Object-Oriented Crystallographic Library.[629] The program settings were chosen in accordance with the experimental settings, taking 1.54056 Å as the scattering wavelength for Cu K_α. A pseudo-Voigt peak shape was employed, with equal parts of a Gaussian and a Lorentzian peak shape function, and a full width at half maximum of 0.14°.

The interactions in our molecular systems were evaluated with the aforementioned system-specific force fields (Section 2.5.6.1), using the Yaff[625] package (v1.6.0) interfaced with LAMMPS[630] (stable_3Mar2020) to efficiently calculate the long range interactions. The long-range electrostatic interactions were calculated through Ewald summations, with a real space cut-off r_{cut} of 12 Å, a scaling factor α of 0.267 $Å^{-1}$, a reciprocal space cut-off k_{max} of 0.4 $Å^{-1}$, and tail corrections. For the van der Waals interactions a real space cut-off of 15 Å was used. Both cut-offs were smoothed by a truncation model.

The geometric optimizations were performed using the following criteria: *gpos_rms*=*grvecs_rms*=1e-8 and *dpos_rms*=*drvecs_rms*=1e-6. The subsequent molecular dynamics simulations were performed in the (N,P,$\boldsymbol{\sigma_\alpha}$ = $\boldsymbol{0}$,T) ensemble,[631] integrated through a velocity verlet integration scheme with a timestep of 0.5 fs. The temperature was controlled by a thermostat at 300 K, employing the Nosé-Hoover chain thermostat[632–634] with three beads and a relaxation time of 0.1 ps, whereas the pressure was controlled at 1 bar, using the Martyna-Tuckerman-Tobias-Klein barostat[635,636] with a relaxation time of 1 ps. To account for sufficient layer dynamics throughout the simulations, supercells were constructed, starting from the single two layer unit cell from the geometric optimization, and periodically extending them to a ten layer unit cell for the molecular dynamics simulation.

2.5.6.5 Computational details: Simulation of bandgaps and density of states

Density functional theory (DFT) calculations were carried out using a projector augmented wave (PAW)[637] with the Vienna ab initio simulation package (VASP).[638–640] The electron exchange-correlational functional was considered via the generalized gradient approximation with the Perdew-Burke-Ernzerhof (PBE)[641] functional with Grimme's D3 corrections with Becke-Johnson damping.[642,643] The Brillouin zone was sampled using 1 × 1 × 4 Γ-centered grids. A kinetic energy cutoff at 600 eV was considered to describe the electronic wave function. All the structures were optimized until the convergence criteria of energy becomes less than 1×10^{-5} eV. The hybrid functional (HSE06) was used for the better estimation of the electronic band gap.[644]

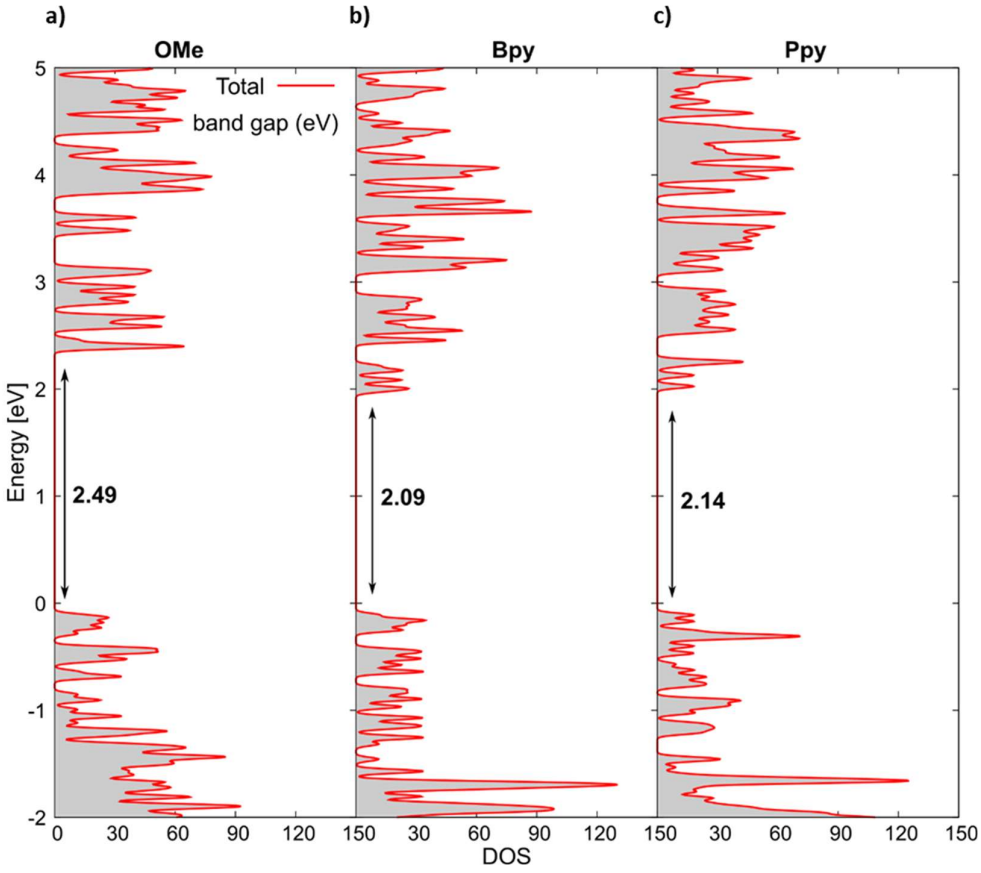

Figure 34: Band structure and density of states of a) **TpOMeBpyCOF** b) **TpBpyCOF** and c) **TpPpyCOF**.

2.5.7 Photocatalysis

2.5.7.1 Hydroxylation of phenylboronic acid

TpBpyCOF (4 mg) and phenylboronic acid **89** (12 mg, 0.1 mmol, 1 eq.) were added to a small round bottom flask equipped with a reflux condenser, followed by 1 mL MeOH. After addition of 21 µL DIPEA (15.5 mg, 0.12 mmol, 1.2 eq.) the mixture was stirred under irradiation from a 26 W compact fluorescent lamp (CFL; ~10 cm distance) for 24 hours. A sample was taken from the reaction mixture, the solvent evaporated and the conversion was determined via ^{1}H-NMR (CD_3OD).

2.5.7.2 Benzylamine oxidation

2.5.7.2.1 Procedure

The catalyst (5 mg) was added to a small glass test tube, followed by 2 mL CH_3CN after which the benzylamine **91** (0.2 mmol) was added. This was stirred under air and irradiated with a 26 W CFL (~10 cm distance) for 24 hours. A sample was directly taken from the reaction mixture, diluted with $CDCl_3$ and analyzed using ^{1}H-NMR by integration of the benzyl protons of the imine and the benzyl protons of residual benzylamine. When the reactions were shielded from light aluminium foil was wrapped around the test tubes and the same procedure was used.

2.5.7.2.2 Recycling experiments

Benzylamine **91a** (214 mg, 2 mmol, 1 eq.), 20 mL CH_3CN and 50 mg **TpBpyCOF** were added to a flask and stirred for 24 hours under air and irradiation of a 26 W CFL. A sample was taken from the reaction mixture, diluted with $CDCl_3$ and the conversion was determined using ^{1}H-NMR. The reaction was filtered and washed with CH_3CN. The filtrate was evaporated to obtain the imine **92a** and the filter cake was dried and used for the next cycle.

2.5.7.3 The tandem aerobic oxidation/Povarov cyclization and α-oxidation

2.5.7.3.1 Screening and control experiments

To a small glass test tube were added the photocatalyst (10 mg), Lewis acid (0.1 eq.) and cinnamyl *p*-tolylglycinate* **102a** (28 mg, 0.1 mmol, 1 eq.)* after which 1 mL solvent was added. This was stirred under air and irradiation from a 26 W CFL (~10 cm distance) for 24 hours. The reaction mixture was filtered over filter paper and the filter was rinsed thoroughly with acetone. The filtrate was evaporated under vacuum and the internal standard, 1,3,5-trimethoxybenzene (17 mg, 0.1 mmol, 1 eq.)* or mesitylene (12 mg, 0.1 mmol, 1 eq.)* was added. The NMR yield was determined by integration of the aromatic signals of the internal standard (3H) and the CH_2 of the lactone **103a** at δ = 5.36 ppm (^{1}H-NMR, $CDCl_3$).

*To make the yield determination using NMR more precise these quantities were weighed exactly using a Mettler Toledo ME204/M Analytical balance.

2.5.7.3.2 Tandem aerobic oxidation/Povarov reaction of *N*-aryl glycine derivatives

Typically, 20 mg **TpBpyCOF**, $ScOTf_3$ (10 mg, 0.02 mmol, 0.1 eq.), 0.2 mmol of substrate **102** and 2 mL CH_3CN were added to a small glass test tube. This was stirred under air and irradiated with a 26 W CFL (~10 cm distance) for 24 hours. The reaction mixture was filtered over a filter paper and washed with acetone. The filtrate was then evaporated and the product **103** was purified using column chromatography (SiO_2, hexane/acetone: 10/1 or C18, gradient CH_3CN/H_2O: 30/70 – 100/0).
*Reversed phase chromatography was used for compounds **103c,e,h,k**.

2.5.7.3.3 α-Oxidation of *N*-aryl glycine derivatives.

Typically, 20 mg **TpBpyCOF**, 0.2 mmol of substrate **116** and 2 mL CH_3CN were added to a small glass test tube. This was stirred under air and irradiated with a 26 W CFL (~10 cm distance) for 24-36 hours. The reaction mixture was filtered through a filter paper and rinsed thoroughly with acetone. The filtrate was then evaporated and the crude product **123** was purified using column chromatography (C18, gradient CH_3CN/H_2O: 40/60 – 100/0 or 50/50 – 100/0).

2.5.7.3.4 Recycling of TpBpyCOF for the tandem aerobic oxidation/Povarov reaction

To a small glass test tube were added: 20 mg **TpBpyCOF**, $ScOTf_3$ (10 mg, 0.02 mmol, 0.1 eq.), cinnamyl *p*-tolylglycinate **102a** (56 mg, 2 mmol, 1 eq.) and 2 mL CH_3CN. This was stirred under air and irradiation from a 26 W CFL (~10 cm distance) for 24 hours. The reaction mixture was filtered over a membrane filter and washed with acetone. The filtrate was then evaporated and the internal standard, 1,3,5-trimethoxybenzene (33.6 mg, 0.2 mmol, 1 eq.) was added. The NMR yield was determined by integration of the aromatic signals of the internal standard (3H) and the CH_2 of the lactone **103a** at δ = 5.36 ppm (^{1}H-NMR, $CDCl_3$). The filter cake was dried, scraped off, and used for the next cycle.

2.5.7.3.5 Characterization of products

7-Methyl-9-phenylfuro[3,4-*b*]quinolin-3(1*H*)-one 103a

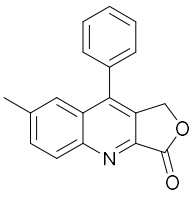

^{1}H-NMR (400 MHz, $CDCl_3$): δ 2.51 (3H, s, CH_3); 5.36 (2H, s, OCH_2); 7.43-7.45 (2H, m, 2 x CH_{arom}); 7.55-7.64 (4H, m, 4 x CH_{arom}); 7.67 (1H, d x d, *J* = 8.7 x 1.8 Hz, CH_{arom}); 8.31 (1H, d, *J* = 8.7 Hz, CH_{arom}). **^{13}C-NMR** (100 MHz, $CDCl_3$): δ 22.3 (CH_3); 67.9 (CH_2); 124.4 (CH_{arom}); 128.1 ($C_{arom,quat}$); 129.0 (2 x CH_{arom}); 129.4 (2 x CH_{arom}); 129.5 (CH_{arom}); 131.2 (CH_{arom}); 132.6 ($C_{arom,quat}$); 133.3 (CH_{arom}); 133.9, 140.1, 143.0, 143.5 and 149.6 (5 x $C_{arom,quat}$); 169.0 (C=O). **IR** (ATR, cm^{-1}): $\nu_{C=O}$ = 1776; ν_{max} = 2922, 1371, 1132, 1057, 826, 725, 700, 538, 453. **MS** (ESI): *m/z* (%) 276 ($[M + 1]^+$, 100). White solid, 62%. Spectral data matched literature.[403]

7-Methoxy-9-phenylfuro[3,4-*b*]quinolin-3(1*H*)-one 103b

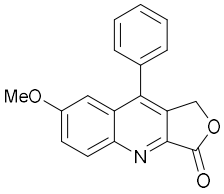

^{1}H-NMR (400 MHz, $CDCl_3$): δ 3.81 (3H, s, CH_3); 5.34 (2H, s, CH_2); 7.10 (1H, d, *J* = 2.8 Hz, CH_{arom}); 7.44-7.46 (2H, m, 2 x CH_{arom}); 7.51 (1H, d x d, *J* = 9.3 x 2.8 Hz, CH_{arom}); 7.55-7.63 (3H, m, 3 x CH_{arom}); 8.33 (1H, d, *J* = 9.3 Hz, CH_{arom}).**^{13}C-NMR** (100 MHz, $CDCl_3$): δ 55.6 (CH_3); 67.7 (CH_2); 102.9 (CH_{arom}); 123.9 (CH_{arom}); 128.6 (2 x CH_{arom}); 129.4 (CH_{arom} and 1 x (2 x CH_{arom})); 129.6 ($C_{arom,quat}$), 132.9 (CH_{arom}), 133.1, 133.9, 141.7, 141.9, 147.1 and 160.2 (6 x $C_{arom,quat}$); 169.0 (C=O). **IR** (ATR,

cm^{-1}): $\nu_{C=O}$ = 1775; ν_{max} = 1620, 1582, 1371, 1242, 1225, 1126, 1018, 837, 745. **MS** (ESI): *m/z* (%) ([M + 1]$^+$, 292). Beige solid, 34%. Spectral data matched literature.[547]

5-Methoxy-9-phenylfuro[3,4-*b*]quinolin-3(1*H*)-one 103c

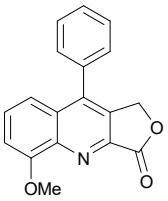

^{1}H-NMR (400 MHz, $CDCl_3$): δ 4.14 (3H, s, CH_3); 5.37 (2H, s, CH_2); 7.17 (1H, d, *J* = 7.8 Hz, CH_{arom}); 7.42-7.44 (3H, m, 3 x CH_{arom}); 7.56-7.62 (4H, m, 4 x CH_{arom}). **^{13}C-NMR** (100 MHz, $CDCl_3$): δ 56.4 (CH_3); 67.7 (CH_2); 108.5 (CH_{arom}); 117.3 (CH_{arom}); 129.0 (2 x CH_{arom}); 129.3 ($C_{arom,quat}$); 129.4 (2 x CH_{arom}); 129.6 (CH_{arom}); 129.9 (CH_{arom}); 133.3, 134.0, 143.1, 143.2, 143.8 and 156.9 (6 x $C_{arom,quat}$); 168.4 (C=O). **IR** (ATR, cm^{-1}): $\nu_{C=O}$ = 1773; ν_{max} = 1510, 1400, 1368, 1256, 1136, 1049, 1007, 743, 706. **MS** (ESI): *m/z* (%) 292 ([M + 1]$^+$, 100). **HRMS** (ESI): calcd. for $C_{18}H_{14}NO_3^+$: 292.0968 [M + H]$^+$, found: 292.0960. White solid, 43%.

7-Fluoro-9-phenylfuro[3,4-*b*]quinolin-3(1*H*)-one 103d

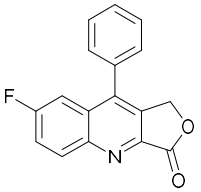

^{1}H-NMR (400 MHz, $CDCl_3$): δ 5.40 (2H, s, CH_2); 7.42-7.45 (2H, m, 2 x CH_{arom}); 7.50 (1H, d x d, *J* = 9.8 x 2.7 Hz, CH_{arom}); 7.59-7.65 (4H, m, 4 x CH_{arom}); 8.44 (1H, d x d, *J* = 9.3 x 5.6 Hz, CH_{arom}). **^{19}F-NMR** (376 MHz, $CDCl_3$): -107.1 (1F, m). **^{13}C-NMR** (100 MHz, $CDCl_3$): δ 67.9 (CH_2); 109.3 (d, *J* = 23.7 Hz, CH_{arom}); 121.6 (d, *J* = 26.4 Hz, CH_{arom}); 128.8 (2 x CH_{arom}); 129.3 (d, *J* = 10.1 Hz, $C_{arom,quat}$); 129.7 (2 x CH_{arom}); 130.0 (CH_{arom}); 133.1 ($C_{arom,quat}$); 133.2 ($C_{arom,quat}$); 134.2 (d, *J* = 9.6 Hz, CH_{arom}); 143.5 (d, *J* = 6.3 Hz, $C_{arom,quat}$); 144.1 (d, *J* = 2.9 Hz, $C_{arom,quat}$); 148.0 ($C_{arom,quat}$); 162.5 (d, *J* = 253.2 Hz, $C_{arom,quat}$); 168.6 (C=O). **IR** (ATR, cm^{-1}): $\nu_{C=O}$ = 1773; ν_{max} = 1508, 1495, 1456, 1229, 1200, 1134, 1051, 1009, 737. **MS** (ESI): *m/z* (%) 280 ([M + 1]$^+$, 100). Beige solid, 27%. Spectral data matched literature.[547]

9-Phenyl-6-(trifluoromethyl)furo[3,4-*b*]quinolin-3(1*H*)-one 103e

Crude contained a mixture of regio-isomers (6/8-CF_3: 87/13). Only 9-phenyl-6-(trifluoromethyl)furo[3,4-*b*]quinolin-3(1*H*)-one **103e** could be isolated and characterized after reversed phase chromatography.

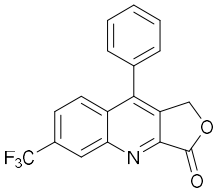

^{1}H-NMR (400 MHz, $CDCl_3$): δ 5.44 (2H, s, OCH_2); 7.44-7.46 (2H, m, 2 x CH_{arom}); 7.62-7.66 (3H, m, 3 x CH_{arom}); 7.82 (1H, d x d, *J* = 8.9 x 1.8, CH_{arom}); 8.06 (1H, d, *J* = 8.9 Hz, CH_{arom}); 8.75 (1H, s, CH_{arom}). **^{13}C-NMR** (100 MHz, $CDCl_3$): δ 67.9 (CH_2), 122.3* (CF_3), 125.0 (q, *J* = 3.0 Hz, CH_{arom}), 127.4 (CH_{arom}); 128.9 (2 x CH_{arom}); 129.3 (q, *J* = 4.4 Hz, CH_{arom}); 129.4 ($C_{arom,quat}$); 129.7 (2 x CH_{arom}); 130.2 (CH_{arom}); 132.7 (q, *J* = 33.2 Hz, $C_{arom,quat}$); 132.9, 134.0, 144.5, 146.0, 149.9 (5 x $C_{arom,quat}$); 168.0 (C=O). **IR** (ATR, cm^{-1}): $\nu_{C=O}$ = 1771; ν_{max} = 1335, 1317, 1296, 1125, 1107, 1065, 903, 700, 681. **MS** (ESI): *m/z* (%) 330 ([M + 1]$^+$, 100). **HRMS** (ESI): calcd. for $C_{18}H_{11}F_3NO_2^+$: 330.0736 [M + H]$^+$, found: 330,0732. White solid, 34%.

*Rest of CF_3 quartet not visible

7-Iodo-9-phenylfuro[3,4-*b*]quinolin-3(1*H*)-one 103f

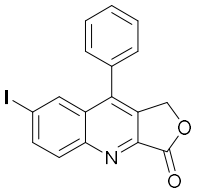

^{1}H-NMR (400 MHz, $CDCl_3$): δ 5.39 (2H, s, CH_2O); 7.42-7.44 (2H, m, 2 x CH_{arom}); 7.60-7.64 (3H, m, 3 x CH_{arom}); 8.07 (1H, d_{AB} x d, *J* = 9.0 x 1.6 Hz, CH_{arom}); 8.12 (1H, d_{AB}, *J* = 9.0 Hz, CH_{arom}); 8.26 (1H, *J* = 1.6 Hz, CH_{arom}). **^{13}C-NMR** (100 MHz, $CDCl_3$): δ 67.9 (CH_2); 96.6 ($C_{arom,quat}$); 128.9 (2 x CH_{arom}); 129.3 ($C_{arom,quat}$); 129.7 (2 x CH_{arom}); 130.0 (CH_{arom}); 132.8 (CH_{arom}); 133.0 ($C_{arom,quat}$); 133.1 ($C_{arom,quat}$); 134.7 (CH_{arom}); 139.8 (CH_{arom}); 142.9, 144.8 and 149.6 (3 x $C_{arom,quat}$); 168.4 (C=O). **IR** (ATR, cm^{-1}): $\nu_{C=O}$ = 1773; ν_{max} = 2930, 1574, 1485, 1369, 1132, 1007, 831, 708, 534. **MS** (ESI): *m/z* (%) 388 ([M + 1]$^+$, 100). **HRMS** (ESI): calcd. for $C_{17}H_{11}INO_2^+$: 387.9829 [M + H]$^+$, found: 387.9817. White solid, 48%.

5-Bromo-9-phenylfuro[3,4-*b*]quinolin-3(1*H*)-one 103g

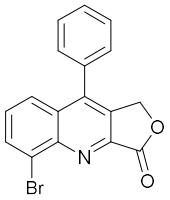

^{1}H-NMR (400 MHz, $CDCl_3$): δ 5.39 (2H, s, CH_2); 7.42-7.45 (2H, m, 2 x CH_{arom}); 7.49 (1H, d x d, *J* = 8.5 x 7.4 Hz, 1H); 7.59-7.62 (3H, m, 3 x CH_{arom}); 7.87 (1H, d x d, *J* = 8.5 x 1.2 Hz, CH_{arom}); 8.20 (1H, d x d, *J* = 7.4 x 1.2 Hz, CH_{arom}). **^{13}C-NMR** (100 MHz, $CDCl_3$): δ 67.7 (CH_2); 125.8 (CH_{arom}); 127.2 ($C_{arom,quat}$); 129.0 (2 x CH_{arom}); 129.47 ($C_{arom,quat}$); 129.54 (2 x CH_{arom}); 129.6 (CH_{arom}); 129.9 (CH_{arom}); 133.3 ($C_{arom,quat}$); 133.4 ($C_{arom,quat}$); 134.7 (CH_{arom}); 144.9, 145.1 and 148.0 (3 x $C_{arom,quat}$); 168.1 (C=O). **IR** (ATR, cm^{-1}): $\nu_{C=O}$ = 1782; ν_{max} = 1485, 1454, 1121, 1047, 1007, 768, 760, 712, 700, 629. **MS** (ESI): *m/z* (%) 342 ([M + 1]$^+$, 98); 340 ([M + 1]$^+$, 100). **HRMS** (ESI): calcd. for $C_{17}H_{11}BrNO_2^+$: 339.9968 [M + H]$^+$, found: 339.9955. White solid, 41%.

8- and 6-Methyl-9-phenylfuro[3,4-*b*]quinolin-3(1*H*)-one 103h

Spectral data derived from the mixture of the two regio-isomers (6/8-Me: 64/36).

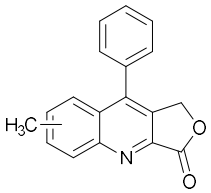

^{1}H-NMR (400 MHz, $CDCl_3$): δ 2.10 (3H, s, CH_3); 2.62 (3H, s, CH_3); 5.16 (2H, s, OCH_2); 5.38 (2H, s, OCH_2); 7.31-7.34 (2H, m, 2 x 1 x CH_{arom}); 7.43-7.62 (5H, m, 2 x 5 x CH_{arom}); 7.73 (1H, d x d, *J* = 8.3 x 7.2 Hz, CH_{arom}); 7.80 (1H, d, *J* = 8.7 Hz, CH_{arom}); 8.22 (1H, s, CH_{arom}); 8.34 (1H, d, *J* = 8.3 Hz, CH_{arom}). **^{13}C-NMR** (100 MHz, $CDCl_3$): 21.9 (CH_3); 24.6 (CH_3); 67.9 (CH_2); 68.1 (CH_2); 125.5 (CH_{arom}); 126.2 ($C_{arom,quat}$); 127.2 ($C_{arom,quat}$); 128.0 (CH_{arom}); 129.0 (2 x CH_{arom}); 129.07 (2 x CH_{arom}); 129.12 (CH_{arom}); 129.4 (2 x CH_{arom}); 129.6 (2 x CH_{arom}); 130.3 (CH_{arom}); 130.4 (CH_{arom}); 130.7 (CH_{arom}); 131.9 ($C_{arom,quat}$); 132.0 (CH_{arom}); 132.7 (CH_{arom}); 133.9 ($C_{arom,quat}$); 134.4 ($C_{arom,quat}$); 136.1 ($C_{arom,quat}$); 137.8 ($C_{arom,quat}$); 141.5 ($C_{arom,quat}$); 143.4 ($C_{arom,quat}$); 144.35 ($C_{arom,quat}$); 144.44 ($C_{arom,quat}$); 151.2 ($C_{arom,quat}$); 152.2 ($C_{arom,quat}$); 168.9 (C=O); 169.0 (C=O). **IR** (ATR, cm^{-1}): $\nu_{C=O}$ = 1777; ν_{max} = 2926, 1585, 1445, 1371, 1236, 1173, 1125, 1007, 704. **MS** (ESI): *m/z* (%) 276 ([M + 1]$^+$, 100). **HRMS** (ESI): calcd. for $C_{18}H_{14}NO_2^+$: 276.1019 [M + H]$^+$, found: 276.1011. Colorless oil, 27%.

5-Methyl-9-phenylfuro[3,4-*b*]quinolin-3(1*H*)-one 103i

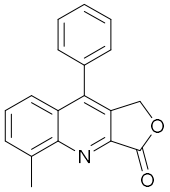

^{1}H-NMR (400 MHz, $CDCl_3$): δ 2.97 (3H, s, CH_3); 5.37 (2H, s, OCH_2); 7.41-7.44 (2H, m, 2 x CH_{arom}); 7.52-7.60 (4H, m, 4 x CH_{arom}); 7.69-7.74 (2H, m, 2 x CH_{arom}). **^{13}C-NMR** (100 MHz, $CDCl_3$): δ 18.8 (CH_3); 67.8 (CH_2); 123.8 (CH_{arom}); 128.1 ($C_{arom,quat}$); 129.0 (2 x CH_{arom}); 129.3 (CH_{arom}); 129.4 (2 x CH_{arom}); 129.5 (CH_{arom}); 130.8 (CH_{arom}); 132.3, 134.2, 139.9, 143.2, 144.0 and 150.1 (6 x $C_{arom,quat}$); 169.2 (C=O). **IR** (ATR, cm^{-1}): $\nu_{C=O}$ = 1767; ν_{max} = 1393, 1273, 1236, 1207, 1194, 1136, 1003, 841, 770. **MS** (ESI): *m/z* (%) 276 ([M + 1]$^+$, 100). White solid, 33%. Spectral data matched literature.[598]

7-Methyl-9-(naphthalen-2-yl)furo[3,4-*b*]quinolin-3(1*H*)-one 103j

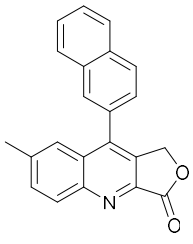

^{1}H-NMR (400 MHz, $CDCl_3$): δ 2.48 (3H, s, CH_3); 5.33-5.44 (2H, m, OCH_2); 7.53 (1H, d x d, *J* = 8.4 x 1.5 Hz, CH_{arom}); 7.62-7.70 (4H, m, 4 x CH_{arom}); 7.93-8.01 (2H, m, CH_{arom}); 8.09 (1H, d, *J* = 8.4 Hz, CH_{arom}); 8.34 (1H, d, *J* = 8.6 Hz, CH_{arom}). **^{13}C-NMR** (100 MHz, $CDCl_3$): δ 22.2 (CH_3); 68.0 (OCH_2); 124.5, 126.2, 127.3, 127.5 and 128.1 (5 x CH_{arom}); 128.2 ($C_{arom,quat}$); 128.4, 128.5, 129.3 and 131.2 (4 x CH_{arom}); 131.3 ($C_{arom,quat}$); 132.9 ($C_{arom,quat}$); 133.3 (CH_{arom}); 133.4, 133.5, 140.2, 143.0, 143.5 and 149.5 (6 x $C_{arom,quat}$); 169.0 (C=O). **IR** (ATR, cm^{-1}): $\nu_{C=O}$ = 1771; ν_{max} = 2930, 1574, 1449, 1371, 1132, 1057, 1049, 1001, 827. **MS** (ESI): *m/z* (%) 326 ([M + 1]$^+$, 100). **HRMS** (ESI): calcd. for $C_{22}H_{16}NO_2^+$: 326.1176 [M + H]$^+$, found: 326.1169. Light yellow solid, 39%.

(*E*)-7-Methyl-9-(prop-1-en-1-yl)furo[3,4-*b*]quinolin-3(1*H*)-one 103k

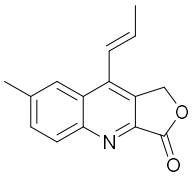

^{1}H-NMR (400 MHz, $CDCl_3$): δ 2.14 (3H, d x d, *J* = 6.6 x 1.7 Hz, $C\underline{H}_3CH$=CH); 2.62 (3H, s, $CH_3C_{arom,quat}$); 5.55 (2H, s, CH_2); 6.28 (1H, d x q, *J* = 16.1 x 6.6 Hz, $CH_3C\underline{H}$=CH); 7.06 (1H, d x q, *J* = 16.1 x 1.7 Hz, CH_3CH=C$\underline{H}$); 7.66 (1H, d x d, *J* = 8.7 x 1.8 Hz, CH_{arom}); 7.96 (1H, s, CH_{arom}); 8.25 (1H, d, *J* = 8.7 Hz, CH_{arom}). **^{13}C-NMR** (100 MHz, $CDCl_3$): δ 19.9 (CH_3); 22.4 (CH_3); 68.6 (OCH_2); 122.9 (CH_{arom}); 124.1 ($\underline{C}H$=$CHCH_3$); 127.2 ($C_{arom,quat}$); 130.9 ($C_{arom,quat}$); 131.4 (CH_{arom}); 133.0 (CH_{arom}); 137.1 (CH=$CHCH_3$); 138.3, 139.7, 143.5 and 149.2 (4 x $C_{arom,quat}$); 169.1 (C=O). **IR** (ATR, cm^{-1}): $\nu_{C=O}$ = 1778; ν_{max} = 3056, 2914, 1574, 1503, 1443, 1140, 1080, 959, 843. **MS** (ESI): *m/z* (%) 240 ([M + 1]$^+$, 100). White solid, 35%. Spectral data matched literature.[403]

7-Methyl-2,9-diphenyl-1,2-dihydro-3*H*-pyrrolo[3,4-*b*]quinolin-3-one 103l

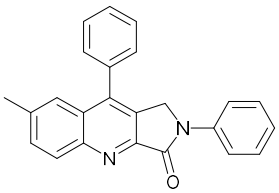

^{1}H-NMR (400 MHz, $CDCl_3$): δ 2.48 (3H, s, CH_3); 4.80 (2H, s, CH_2); 7.19 (1H, t x t, *J* = 7.5 x 1.1 Hz, CH_{arom}); 7.39-7.43 (2H, m, CH_{arom}); 7.46-7.50 (2H, m, 2 x CH_{arom}); 7.55 (1H, s, CH_{arom}); 7.59-7.66 (4H, m, 4 x CH_{arom}); 7.87-7.79 (2H, m, 2 x CH_{arom}); 8.34 (1H, d, *J* = 8.7 Hz, CH_{arom}). **^{13}C-NMR** (100 MHz, $CDCl_3$): δ 22.2 (CH_3); 48.3 (CH_2); 119.8 (2 x CH_{arom}); 124.5 (CH_{arom}); 125.3 (CH_{arom}); 127.7 ($C_{arom,quat}$); 128.0 ($C_{arom,quat}$); 129.16 (2 x CH_{arom}); 129.20 (CH_{arom}); 129.32 (2 x CH_{arom}); 129.34 (2 x CH_{arom}); 131.0 (CH_{arom}); 132.5 (CH_{arom}); 134.7, 138.8, 139.4, 142.8, 148.7 and 150.0 (6 x $C_{arom,quat}$); 165.6 (C=O). **IR** (ATR, cm^{-1}): $\nu_{C=O}$ = 1709; ν_{max} = 1597, 1493, 1385, 1300, 1267, 1173, 824, 754, 704. **MS** (ESI): *m/z* (%) 351 ([M + 1]$^+$, 100). Off white solid, 47%. Spectral data matched literature.[554]

2-(4-Methoxybenzyl)-7-methyl-9-phenyl-1,2-dihydro-3*H*-pyrrolo[3,4-*b*]quinolin-3-one 103m

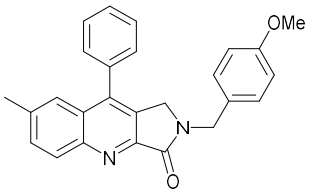

^{1}H-NMR (400 MHz, $CDCl_3$): δ 2.46 (3H, s, $CH_3C_{arom,quat}$); 3.77 (3H, s, CH_3O); 4.18 (2H, s, $NCH_2C_{quinoline}$); 4.82 (2H, s, NCH_2PMP); 6.82-6.84 (2H, m, 2 x CH_{arom}); 7.23-7.25 (2H, m, 2 x CH_{arom}); 7.35-7.37 (2H, m, 2 x CH_{arom}); 7.49-7.57 (4H, m, 4 x CH_{arom}); 7.62 (1H, d x d, *J* = 8.7 x 1.9 Hz, CH_{arom}); 8.32 (1H, d, *J* = 8.7 Hz, CH_{arom}). **^{13}C-NMR** (100 MHz, $CDCl_3$): δ 22.1 ($\underline{C}H_3C_{arom,quat}$); 44.6 and 46.8 ($NCH_2$PMP and $NCH_2C_{quinoline}$); 55.4 (CH_3O); 114.3 (2 x CH_{arom}); 124.4 (CH_{arom}); 127.6 ($C_{arom,quat}$); 128.5 ($C_{arom,quat}$); 128.6 ($C_{arom,quat}$); 129.0 (CH_{arom}); 129.10 (2 x CH_{arom}); 129.11 (2 x CH_{arom}); 129.8 (2 x CH_{arom}); 130.8 (CH_{arom}); 132.3 (CH_{arom}); 134.7 ($C_{arom,quat}$); 138.4 ($C_{arom,quat}$); 142.7 ($C_{arom,quat}$); 148.3 ($C_{arom,quat}$); 150.1 ($C_{arom,quat}$); 159.4 ($C_{arom,quat}$); 166.5 (C=O). **IR** (ATR, cm^{-1}): $\nu_{C=O}$ = 1692; ν_{max} = 1512, 1242, 1175, 1032, 908, 827, 729, 702, 546. **MS** (ESI): *m/z* (%) 395 ([M + 1]$^+$, 100); 789 ([2M + 1]$^+$, 45); 811 ([2M + 23]$^+$, 10). **HRMS** (ESI): calcd. for $C_{26}H_{23}N_2O_2^+$: 395.1754 [M + H]$^+$, found: 395.1735. Light pink solid, 31%.

Cinnamyl 2-oxo-2-(*p*-tolylamino)acetate 123a

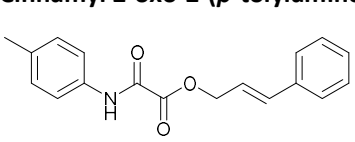

^{1}H-NMR (400 MHz, $CDCl_3$): δ 2.34 (3H, s, CH_3); 4.99 (2H, d x d, *J* = 6.7 x 1.1 Hz, CH_2); 6.36 (1H, d x t, *J* = 15.9 x 6.7 Hz, $CH_2C\underline{H}$=CH); 6.77 (1H, br d, *J* = 15.9 Hz, CH_2CH=C$\underline{H}$); 7.18 (2H, d, *J* = 8.4 Hz, 2 x CH_{arom}); 7.28-7.36 (3H, m, 3 x CH_{arom}); 7.40-7.42 (2H, m, 2 x CH_{arom}); 7.52 (2H, d, *J* = 8.4 Hz, 2 x CH_{arom}); 8.81 (1H, br s, NH). **^{13}C-NMR** (100 MHz, $CDCl_3$): δ 21.1 (CH_3); 68.1 (CH_2); 120.0 (2 x CH_{arom}); 121.4 ($CH_2\underline{C}H$=CH); 126.9, 128.6, 128.8 and 129.9 (7 x CH_{arom}); 133.9, 135.5 and 135.9 (3 x $C_{arom,quat}$); 136.4 (CH_2CH=$\underline{C}H$); 153.7 (NC=O); 161.0 (OC=O). **IR** (ATR, cm^{-1}): ν_{NH} = 3300; $\nu_{C=O}$ = 1732 and 1695; ν_{max} = 1595, 1526, 1513, 1271, 1161, 964, 941. **MS** (ESI): *m/z* (%) 117 ([C_9H_9]$^+$, 100); 613 ([2M + 23]$^+$, 10). Red oil, 29%.

Cinnamyl 2-((4-methoxyphenyl)amino)-2-oxoacetate 123b

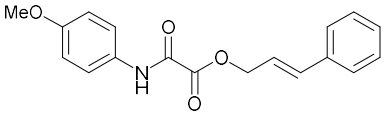

^{1}H-NMR (400 MHz, $CDCl_3$): δ 3.81 (3H, s, CH_3); 5.00 (2H, d x d, *J* = 6.7 x 1.0 Hz, CH_2); 6.36 (1H, d x t, *J* = 15.9 x 6.7 Hz, $CH_2C\underline{H}$=CH); 6.77 (1H, br d, *J* = 15.9 Hz, CH_2CH=C<u>H</u>); 6.89-6.92 (2H, m, 2 x CH_{arom}); 7.28-7.35 (3H, m, 3 x CH_{arom}); 7.55-7.57 (2H, m, 2 x CH_{arom}); 8.78 (1H, br s, NH). **^{13}C-NMR** (100 MHz, $CDCl_3$): δ 55.6 (CH_3); 68.1 (CH_2); 114.5 (2 x CH_{arom}); 121.4 ($CH_2\underline{C}H$=CH); 121.6 (2 x CH_{arom}); 126.8 (2 x CH_{arom}); 126.9 (CH_{arom}); 128.6 (2 x CH_{arom}); 128.8 ($C_{arom,quat}$); 129.6 ($C_{arom,quat}$); 135.9 ($C_{arom,quat}$); 136.4 (CH_2CH=C<u>H</u>); 153.6 (NC=O); 157.4 ($C_{arom,quat}$); 161.2 (OC=O). **IR** (ATR, cm^{-1}): ν_{NH} = 3345; $\nu_{C=O}$ = 1722 and 1695; ν_{max} = 1541, 1508, 1279, 1171, 941, 692, 515. **MS** (ESI): *m/z* (%) 117 ($[C_9H_9]^+$, 100); 334 ($[M + 23]^+$, 5); 645 ($[2M + 23]^+$, 15). Yellow solid, 39%.

Cinnamyl 2-((2-methoxyphenyl)amino)-2-oxoacetate 123c

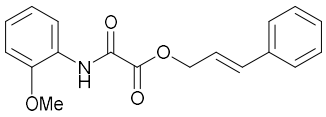

^{1}H-NMR (400 MHz, $CDCl_3$): δ 3.92 (3H, s, CH_3); 5.00 (2H, d x d, *J* = 6.7 x 1.1 Hz, CH_2); 6.37 (1H, d x t, *J* = 15.9 x 6.7 Hz, $CH_2C\underline{H}$=CH); 6.78 (1H, br d, *J* = 15.9 Hz, CH_2CH=C<u>H</u>); 6.91 (1H, d x d, *J* = 8.0 x 1.0 Hz, CH_{arom}); 7.00 (1H, d x d x d, *J* = 7.9 x 7.8 x 1.0 Hz, CH_{arom}); 7.13 (1H, d x d x d, *J* = 8.0 x 7.8 x 1.5 Hz, CH_{arom}); 7.28-7.35 (3H, m, 3 x CH_{arom}); 7.40-7.42 (2H, m, 2 x CH_{arom}); 8.41 (1H, d x d, *J* = 7.9 x 1.5 Hz, CH_{arom}); 9.51 (1H, br s, NH). **^{13}C-NMR** (100 MHz, $CDCl_3$): δ 55.9 (CH_3); 68.0 (CH_2); 110.3 (CH_{arom}); 120.1 (CH_{arom}); 121.2 (CH_{arom}); 121.5 ($CH_2C\underline{H}$=CH); 125.4 (CH_{arom}); 126.2 ($C_{arom,quat}$); 126.9 (2 x CH_{arom}); 128.5 (CH_{arom}); 128.8 (2 x CH_{arom}); 135.9 ($C_{arom,quat}$); 136.3 (CH_2CH=C<u>H</u>); 148.6 ($C_{arom,quat}$); 153.7 (NC=O); 160.8 (OC=O). **IR** (ATR, cm^{-1}): ν_{NH} = 3383; $\nu_{C=O}$ = 1705; ν_{max} = 1601, 1528, 1279, 1250, 1159, 1113, 745, 691. **MS** (ESI): *m/z* (%) 117 ($[C_9H_9]^+$, 100); 645 ($[2M + 23]^+$, 10). Brown oil, 32%.

Cinnamyl 2-oxo-2-(*m*-tolylamino)acetate 123d

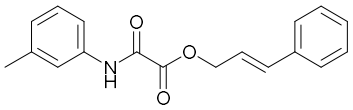

^{1}H-NMR (400 MHz, $CDCl_3$): δ 2.37 (3H, s, CH_3); 5.00 (2H, d x d, *J* = 6.7 x 1.0 Hz, CH_2); 6.36 (1H, d x t, *J* = 15.8 x 6.7 Hz, $CH_2C\underline{H}$=CH); 6.77 (1H, br d, *J* = 15.8 Hz, CH_2CH=C<u>H</u>); 7.01 (2H, d, J = 7.6 Hz, 2 x CH_{arom}); 7.24-7.36 (4H, m, 4 x CH_{arom}); 7.40-7.46 (4H, m, 4 x CH_{arom}); 8.81 (1H, br s, NH). **^{13}C-NMR** (100 MHz, $CDCl_3$): δ 21.6 (CH_3); 68.2 (CH_2); 117.1 (CH_{arom}); 120.6 (CH_{arom}); 121.3 ($CH_2\underline{C}H$=CH); 126.5 (CH_{arom}); 126.9 (2 x CH_{arom}); 128.6 (CH_{arom}); 128.8 (2 x CH_{arom}); 129.2 (CH_{arom}); 135.9 ($C_{arom,quat}$); 136.3 ($C_{arom,quat}$); 136.4 (CH_2CH=<u>C</u>H); 139.4 ($C_{arom,quat}$); 153.8 (NC=O); 161.0 (OC=O). **IR** (ATR, cm^{-1}): ν_{NH} = 3329; $\nu_{C=O}$ = 1726 and 1697; ν_{max} = 1551, 1491, 1275, 1190, 1158, 789, 689. **MS** (ESI): *m/z* (%) 117 ($[C_9H_9]^+$, 100); 613 ($[2M + 23]^+$, 10). Brown oil, 47%.

Cinnamyl 2-((4-iodophenyl)amino)-2-oxoacetate 123e

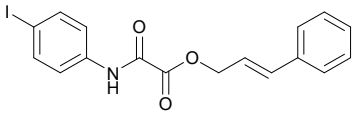

^{1}H-NMR (400 MHz, $CDCl_3$): δ 4.99 (2H, d x d, *J* = 6.8 x 0.9 Hz, CH_2); 6.35 (1H, d x t, *J* = 15.8 x 6.8 Hz, $CH_2C\underline{H}$=CH); 6.77 (1H, br d, *J* = 15.8 Hz, CH_2CH=C<u>H</u>); 7.27-7.44 (7H, m, 7 x CH_{arom}); 7.66-7.70 (2H, m, 2 x CH_{arom}); 8.56 (1H, br s, NH). **^{13}C-NMR** (100 MHz, $CDCl_3$): δ 68.3 (CH_2); 89.3 ($C_{arom,quat}$); 121.1 ($CH_2\underline{C}H$=CH); 121.7 (2 x CH_{arom}); 126.9 (2 x CH_{arom}); 128.7 (CH_{arom}); 128.8 (2 x CH_{arom}); 135.8 ($C_{arom,quat}$); 136.2 ($C_{arom,quat}$); 136.7 (CH_2CH=<u>C</u>H); 138.4 (2 x CH_{arom}); 153.9 (NC=O); 160.7 (OC=O). **IR** (ATR, cm^{-1}): ν_{NH} = 3398; $\nu_{C=O}$ = 1738 and 1688; ν_{max} = 1565, 1483, 1271, 1173, 945, 818, 683. **MS** (ESI): *m/z* (%) 117 ($[C_9H_9]^+$, 100); 430 ($[M + 23]^+$, 10); 837 ($[2M + 23]^+$, 15). Brown oil, 37%.

(*E*)-3-(Naphthalen-2-yl)allyl 2-oxo-2-(*p*-tolylamino)acetate 123f

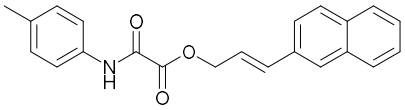

^{1}H-NMR (400 MHz, $CDCl_3$): δ 2.34 (3H, s, CH_3); 5.05 (2H, d, *J* = 6.7 Hz, CH_2); 6.49 (1H, d x t, 15.8 x 6.7 Hz, $CH_2C\underline{H}$=CH); 6.93 (1H, br d, *J* = 15.8 Hz, CH_2CH=C$\underline{H}$); 7.18 (2H, d, *J* = 8.4 Hz, 2 x CH_{arom}); 7.46-7.48 (2H, m, 2 x CH_{arom}); 7.53 (2H, d, *J* = 8.4 Hz, 2 x CH_{arom}); 7.61 (1H, d x d, *J* = 8.6 x 1.5 Hz, CH_{arom}); 7.78-7.83 (4H, m, 4 x CH_{arom}); 8.81 (1H, br s, NH). **^{13}C-NMR** (100 MHz, $CDCl_3$): δ 21.1 (CH_3); 68.2 (CH_2O); 120.0 (2 x CH_{arom}); 121.7 ($CH_2\underline{C}$H=CH); 123.6, 126.5, 126.6, 127.5, 127.9, 128.3, and 128.6 (7 x CH_{arom}); 129.9 (2 x CH_{arom}); 133.4, 133.5, 133.6, 133.9 and 135.5 (5 x $C_{arom,quat}$); 136.5 ($CH_2CH=\underline{C}H$); 153.7 (NC=O); 161.1 (C=O). **IR** (ATR, cm^{-1}): ν_{NH} = 3273; $\nu_{C=O}$ = 1730 and 1690; ν_{max} = 2982, 1597, 1531, 1514, 1275, 1165, 816. **MS** (ESI): *m/z* (%) 167 ($[C_{13}H_{11}]^+$, 100); 713 ([2M + 23]$^+$, 20). Off white solid, 29%

Cinnamyl 2-((4-fluorophenyl)amino)-2-oxoacetate 123g

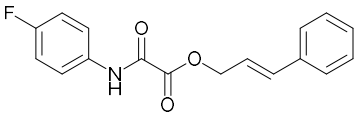

^{1}H-NMR (400 MHz, $CDCl_3$): δ 5.00 (2H, d x d, *J* = 6.7 x 0.9 Hz, CH_2); 6.36 (1H, d x t, *J* = 15.8 x 6.7 Hz, $CH_2C\underline{H}$=CH); 6.77 (1H, br d, *J* = 15.8 Hz, CH_2CH=C$\underline{H}$); 7.04-7.10 (2H, m, 2 x CH_{arom}); 7.27-7.42 (5H, m, 5 x CH_{arom}); 7.60-7.64 (2H, m, 2 x CH_{arom}); 8.86 (1H, br s, NH). **^{19}F-NMR** (376 MHz, $CDCl_3$): -115.88 (1F, m). **^{13}C-NMR** (100 MHz, $CDCl_3$): δ 68.3 (CH_2); 116.2 (d, *J* = 22.7 Hz, 2 x CH_{arom}); 121.2 ($CH_2\underline{C}$H=CH); 121.8 (d, *J* = 8.1 Hz, 2 x CH_{arom}); 126.9 (2 x CH_{arom}); 128.7 (CH_{arom}); 128.8 (2 x CH_{arom}); 132.5 (d, *J* = 2.7 Hz, $C_{arom,quat}$); 135.8 ($CH_2CH=\underline{C}H$); 136.6 ($C_{arom,quat}$); 153.8 (NC=O); 160.2 (d, *J* = 245.4 Hz, $C_{arom,quat}$); 160.9 (OC=O). **IR** (ATR, cm^{-1}): ν_{NH} = 3362; $\nu_{C=O}$ = 1705 and 1694; ν_{max} = 1551, 1508, 1279, 1171, 837, 692, 503. **MS** (ESI): *m/z* (%) 117 ($[C_9H_9]^+$, 100); 322 ([M + 23]$^+$, 15); 621 ([2M + 23]$^+$, 15). Brown solid, 27%.

(2*E*,4*E*)-Hexa-2,4-dien-1-yl 2-oxo-2-(*p*-tolylamino)acetate 123h

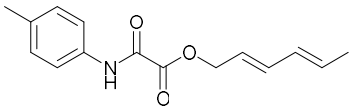

^{1}H-NMR (400 MHz, $CDCl_3$): δ 1.78 (2H, d, *J* = 6.5 Hz, $C\underline{H}_3CH$=CH); 2.33 (3H, s, $CH_3C_{arom,quat}$); 4.83 (2H, d, *J* = 7.1 Hz, CH_2); 5.70 (1H, d x t, *J* = 14.5 x 7.2 Hz, C$\underline{H}$=CH-CH=CHCH$_3$); 5.77-5.85 (1H, m, CH=CH-CH=C$\underline{H}$CH$_3$); 6.03-6.10 (1H, m, CH=CH-C$\underline{H}$=CHCH$_3$); 6.32-6.39 (1H, m, CH=C$\underline{H}$-CH=CHCH$_3$); 7.17 (2H, d, *J* = 8.3 Hz, 2 x CH_{arom}); 7.51 (2H, m, *J* = 8.3 Hz, 2 x CH_{arom}). **^{13}C-NMR** (100 MHz, $CDCl_3$): δ 18.3 ($\underline{C}H_3CH$=CH); 21.1 ($\underline{C}H_3C_{arom,quat}$); 68.2 ($CH_2O$); 119.9 (2 x CH_{arom}); 121.8 ($\underline{C}$H=CH-CH=CHCH$_3$); 129.9 (2 x CH_{arom}); 130.3 (CH=CH-$\underline{C}$H=CHCH$_3$); 132.7 (CH=CH-CH=$\underline{C}$HCH$_3$); 134.0 ($C_{arom,quat}$); 135.5 ($C_{arom,quat}$); 137.1 (CH=$\underline{C}$H-CH=CHCH$_3$); 153.8 (NC=O); 161.0 (OC=O). **IR** (ATR, cm^{-1}): ν_{NH} = 3362; $\nu_{C=O}$ = 1703 and 1690; ν_{max} = 1526, 1279, 1165, 989, 937, 820, 696. **MS** (ESI): *m/z* (%) 81 ($[C_6H_9]^+$, 100); 541 ([2M + 23]$^+$, 15). Brown to orange solid, 15%.

Ethyl 2-oxo-2-(*p*-tolylamino)acetate 123i

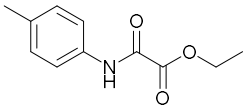

^{1}H-NMR (400 MHz, $CDCl_3$): δ 1.42 (3H, t, *J* = 7.1 Hz, $C\underline{H}_3CH_2$); 2.33 (3H, s, $CH_3C_{arom,quat}$); 4.41 (2H, q, *J* = 7.1 Hz, $CH_3C\underline{H}_2$); 7.17 (2H, d, *J* = 8.4 Hz, 2 x CH_{arom}); 7.52 (2H, d, *J* = 8.4 Hz, 2 x CH_{arom}); 8.83 (1H, br s, NH). **^{13}C-NMR** (100 MHz, $CDCl_3$): δ 14.1 ($\underline{C}H_3CH_2$); 21.1 ($\underline{C}H_3C_{arom,quat}$); 63.8 ($CH_3\underline{C}H_2$); 119.9 (2 x CH_{arom}); 129.8 (2 x CH_{arom}); 134.0 ($C_{arom,quat}$); 135.4 ($C_{arom,quat}$); 153.9 (NC=O); 161.2 (OC=O). **IR** (ATR, cm^{-1}): ν_{NH} = 3337; $\nu_{C=O}$ = 1703 and 1697; ν_{max} = 2980, 1551, 1491, 1275, 1190, 1157, 691, 496. **MS** (ESI): *m/z* (%) 208 ([M + 1]$^+$, 100). Yellow solid, 41%. Spectral data matched literature.[645]

N^1-Isopropyl-N^2-(*p*-tolyl)oxalamide 123j

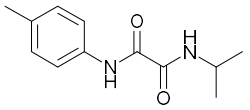

^{1}H-NMR (400 MHz, $CDCl_3$): δ 1.25 (6H, d, *J* = 6.6 Hz, $(C\underline{H}_3)_2CH$); 2.34 (3H, s, $CH_3C_{arom,quat}$); 4.04-4.16 (1H, m, $C\underline{H}(CH_3)_2$); 7.17 (2H, d, *J* = 8.3 Hz, 2 x CH_{arom}); 7.41 (1H, br s, $NHC_{arom,quat}$); 7.51 (2H, d, *J* = 8.3 Hz, 2 x CH_{arom}); 9.23 (1H, br s, $N\underline{H}CH(CH_3)_2$). **^{13}C-NMR** (100 MHz, $CDCl_3$): δ 21.1 ($\underline{C}H_3C_{arom,quat}$); 22.5 ($(\underline{C}H_3)_2CH$); 42.5 ($(CH_3)_2\underline{C}H$); 119.9 (2 x CH_{arom}); 129.9 (2 x CH_{arom}); 134.1 ($C_{arom,quat}$); 135.2 ($C_{arom,quat}$); 157.6 (C=O); 159.2 (C=O). **IR** (ATR, cm^{-1}): ν_{NH} = 3339; $\nu_{C=O}$ = 1655; ν_{max} = 2974, 1518, 1504, 1406, 812, 747, 729, 511. **MS** (ESI): *m/z* (%) 221 ($[M + 1]^+$, 40). Off white solid, 23%. Spectral data matched literature.[646]

N^1-Phenyl-N^2-(*p*-tolyl)oxalamide 123k

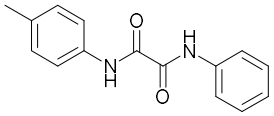

^{1}H-NMR (400 MHz, $CDCl_3$): δ 2.36 (3H, s, CH_3); 7.19-7.23 (3H, m, 3 x CH_{arom}); 7.38-7.42 (2H, m, 2 x CH_{arom}); 7.56 (2H, d, *J* = 8.4 Hz, 2 x CH_{arom}); 7.66-7.69 (2H, m, 2 x CH_{arom}); 9.31 (1H, br s, NH); 9.37 (1H, br s, NH).**^{13}C-NMR** (100 MHz, $CDCl_3$): δ 21.1 (CH_3); 119.99 (2 x CH_{arom}); 120.00 (2 x CH_{arom}); 125.7 (CH_{arom}); 129.4 (2 x CH_{arom}); 129.9 (2 x CH_{arom}); 133.9 ($C_{arom,quat}$); 135.5 ($C_{arom,quat}$); 136.4 ($C_{arom,quat}$); 157.5 (C=O); 157.8 (C=O). **IR** (ATR, cm^{-1}): ν_{NH} = 3306; $\nu_{C=O}$ = 1665; ν_{max} = 2972, 2922, 1593, 1516, 1501, 1443, 727, 689. **MS** (ESI): *m/z* (%) 255 ($[M + 1]^+$, 35). Beige solid, 33%.

***S*-Phenyl 2-oxo-2-(*p*-tolylamino)ethanethioate 123m**

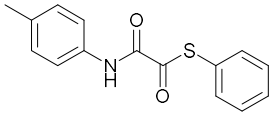

^{1}H-NMR (400 MHz, $CDCl_3$): δ 2.35 (3H, s, CH_3); 7.19 (2H, d, *J* = 8.3 Hz, 2 x CH_{arom}); 7.48 (5H, s, 5 x CH_{arom}); 7.53 (2H, d, *J* = 8.3 Hz, 2 x CH_{arom}); 8.48 (1H, br s, NH). **^{13}C-NMR** (100 MHz, $CDCl_3$): δ 21.1 (CH_3); 120.1 (2 x CH_{arom}); 126.7 ($C_{arom,quat}$); 129.2 ($C_{arom,quat}$); 129.7 (2 x CH_{arom}); 130.0 (2 x CH_{arom}); 130.1 (CH_{arom}); 134.5 (2 x CH_{arom}); 135.7 ($C_{arom,quat}$); 156.2 (NC=O); 190.9 (SC=O). **IR** (ATR, cm^{-1}): ν_{NH} = 3348; $\nu_{C=O}$ = 1688 and 1678; ν_{max} = 2920, 1526, 1225, 999, 806, 687, 453. **MS** (ESI): *m/z* (%) 272 ($[M + 1]^+$, 100). White solid, 22%, purity ~90%.

2-Oxo-*N*-(p-tolyl)propenamide 123n

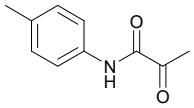

^{1}H-NMR (400 MHz, $CDCl_3$): δ 2.34 (3H, s, $CH_3C_{arom,quat}$); 2.56 (3H, s, CH_3CO); 7.17 (2H, d, *J* = 8.3 Hz, 2 x CH_{arom}); 7.52 (2H, d, *J* = 8.3 Hz, 2 x CH_{arom}); 8.66 (1H, br s, NH). **^{13}C-NMR** (100 MHz, $CDCl_3$): δ 21.1 ($\underline{C}H_3C_{arom,quat}$); 24.2 ($\underline{C}H_3CO$); 119.8 (2 x CH_{arom}); 129.9 (2 x CH_{arom}); 133.9 ($C_{arom,quat}$); 135.2 ($C_{arom,quat}$); 157.6 (NC=O); 197.6 (CH_3C=O). **IR** (ATR, cm^{-1}): ν_{NH} = 3333; $\nu_{C=O}$ = 1682; ν_{max} = 2922, 1533, 1508, 1256, 1136, 816, 691, 604. **MS** (ESI): *m/z* (%) 178 ($[M + 1]^+$, 70). Off white solid, 6%. Spectral data matched literature.[647]

Chapter 3: Development of amorphous POPs as heterogeneous photocatalysts

Manuscript in preparation. **Development of porous organic polymers as metal-free photocatalysts for the aromatization of *N*-heterocycles.** M. Debruyne, N. Raeymackers, A. Laemont, H. Vrielinck, K. Leus, D. Poelman, R. Morent, N. De Geyter, P. Van Der Voort, V. Van Speybroeck, C. V. Stevens, T. Heugebaert.

Abstract: Porous organic polymers (POPs), and covalent triazine frameworks (CTFs) in particular, are being developed as the next generation metal-free heterogeneous photocatalysts. However, many of the current synthetic routes to obtain these photoactive POPs require expensive monomers and rely on precious metal catalysts, thus hindering their widespread implementation. In this work, a range of POPs was made from simple unfunctionalized aromatic building blocks, through alkylation with cyanuric chloride or crosslinking/Scholl coupling. The obtained materials were applied, for the first time, as heterogeneous photocatalysts for the aromatization of *N*-heterocycles. With the use of the most active material, denoted as **CTF-Pyr**, which consists of photoactive pyrene and triazine moieties, a wide range of pyridines, dihydroquinoline-5-ones, tetrahydroacridine-1,8-diones and pyrazoles were obtained in excellent yields (70-99%). Moreover, these reactions were carried out under very mild conditions using air and at room temperature, highlighting the potential of these materials as catalysts for green transformations.

Contributions: The synthesis of the dihydropyridines **2a-c**, tetrahydroquinoline-5-ones **2d-j** and hexahydroacridine-1,8-diones **2k-n** was performed by N. Raeymackers and are described in more detail in his Master thesis.[648] A. Laemont performed CV measurements. K. Leus, R. Morent, N. De Geyter performed the XPS analysis. Solid state UV-Vis measurements were performed under guidance of D. Poelman. EPR measurements were conducted with help from H. Vrielinck.

3.1 Introduction

As described already in the previous chapter, visible light photocatalysis has become an increasingly important tool in organic synthesis. The use of photons as reagents allows the occurrence of unique transformations under mild conditions.[649] Traditionally, high energy UV light was used, and despite the advances made in this area[650,651] the requirements for specialized, expensive equipment and the side reactions caused by the use of these high energy photons preclude more widespread, industrial adoption.[652] Photocatalysts allows for the use of low-energy photons, in the visible light spectrum, to drive chemical transformations, providing green opportunities in both academic and industrial chemistry.[653] However, as mentioned in the previous chapters, the traditional homogeneous photocatalysts (*e.g.* ruthenium and iridium complexes) with their high prices, toxicity, a difficult separation from the final product and their low to non-existent recyclability, compromise the sustainability of the reactions.

Heterogeneous photocatalysts such as POPs are being developed to combat these deficiencies. The photoactive POPs currently described in literature are mostly made by precious metal catalyzed couplings of highly functionalized and difficult to access building blocks. Notably, a special subclass of POPs, the covalent triazine frameworks (CTFs) have a particularly problematic synthesis. These materials are predominantly made by trimerization of aromatic nitriles in molten zinc chloride at extreme temperatures (400-500 °C), causing significant degradation. The resulting black materials are unsuitable for photocatalysis. Moreover, the aromatic nitriles require two steps to synthesize, bromination and cyanation, from the unfunctionalized building blocks. Two other ways to produce CTFs have been described to give suitable materials for photocatalysis: the superacid catalyzed trimerization of nitriles and the condensation of amidines and aldehydes. The superacid is often triflic acid, which is incompatible with many building blocks and is also highly corrosive. The amidine-aldehyde condensation is much more mild, but still requires functionalized building blocks. The typical CTFs synthesis therefore severely limits the green character of the materials and precludes more widespread application development.[381]

On the contrary, the synthesis of POPs through Lewis acid catalyzed alkylation or crosslinking/Scholl coupling allows the generation of highly porous materials without the use of expensive catalysts or building blocks.[654] Importantly, when alkylating aromatics with cyanuric chloride, this grants the formation of CTFs from cheap and easily available building blocks, under relatively mild conditions. Whilst the application of these 'Friedel-Crafts' CTFs have been described for gas storage, separation, sensing and iodine capture,[404,655–657] to the best of our knowledge no photocatalytic applications have been described for these materials.

In this chapter POPs were synthesized using the Lewis acid catalyzed alkylation or crosslinking/Scholl coupling of simple, low cost, unfunctionalized aromatic building blocks and their photocatalytic applications were studied. Materials with very high surface areas, up to 1457 m^2/g, were generated. These were applied as photocatalysts for the oxidative aromatization of a very wide range of *N*-heterocycles. These reactions typically require the use of stoichiometric oxidants such as MnO_2, SeO_2, IBX, etc.,[405] which produces a lot of waste and lowers the atom economy of the reaction. The material containing both photoactive pyrene and triazine moieties, denoted as **CTF-Pyr**, was identified as the most effective photocatalyst. By using **CTF-Pyr** 21 pyridines, quinolines, acridines and pyrazoles were produced in excellent yields (70-99%), under air and at room temperature. These results demonstrate that these easily synthesized porous organic materials are powerful heterogeneous photocatalysts for green transformations.

3.2 Results and discussion

3.2.1 Synthesis and characterization of the POPs

To develop new POPs for photocatalytic applications, electron rich unfunctionalized aromatic building blocks were coupled with cyanuric chloride **CC** through Friedel-Crafts alkylation. It should be noted that this Friedel-Crafts alkylation does not work for electron poor building blocks such as bipyridine, phenanthroline, etc. The selected aromatic building blocks were truxene **Trux**, hexamethyltruxene **HMTrux**, fluorene **Fl** and pyrene **Pyr**. Truxene and pyrene are electron rich moieties that are known to have attractive photophysical and semiconductive properties.[658,659] The triazine core possesses free electron pairs, which combined with its electron poor nature facilitates redox reactions,[331] and is generally known to enhance photocatalysis. Combining the electron rich aromatics with the electron poor triazine cores should give rise to donor-acceptor polymers. These typically possess narrow bandgaps and high photocatalytic activities, allowing the use of visible light as a force to drive chemical transformations.[515]

Whilst pyrene and fluorene are commercially available on large scales, truxene and hexamethyltruxene had to be synthesized, which was done using literature procedures (Scheme 1).[660,661] Truxene was conveniently prepared by acid catalyzed trimerization of indanone **1** and could be precipitated from the reaction mixture, filtered off and used without further purification. Hexamethyltruxene was synthesized by exhaustive methylation with KO*t*Bu and MeI, and was isolated using column chromatography to give **HMTRux** in 66% yield.

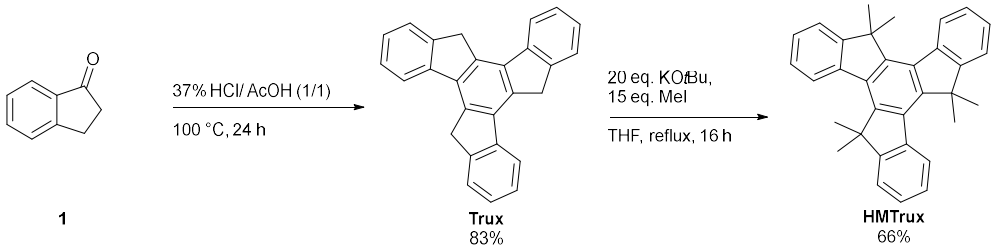

Scheme 1: Synthesis of **Trux** and **HMTrux**.

The synthesis of **CTF-Fl** using Friedel Crafts alkylation, as previously described in literature, was included as a reference (Scheme 2).[404] **CTF-Fl** was obtained as a dark red powder, in almost quantitative yield, with an FTIR spectrum and BET surface area corresponding to the literature. By using an analogous procedure for **Trux**, **HMTrux** and **Pyr** three new materials were obtained with high permanent porosities (383-1277 m^2/g). However, surprisingly, whilst for pyrene the resulting **CTF-Pyr** possessed a good nitrogen content (6.7%), for the truxene and hexamethyltruxene based materials the amount of nitrogen was only 0.8% and 0.7%, respectively, according to elemental analysis (Table 1). Moreover, the FTIR spectra showed no typical triazine absorptions. Therefore, for **Trux** and **HMTrux** almost no reaction with cyanuric chloride had taken place, and the porous materials were formed through Scholl coupling and/or crosslinking with the solvent, dichloromethane.[654] Given the applied reaction conditions, the occurrence of Scholl coupling seems less likely, as this generally requires very high temperatures (>100 °C).[662] However, due to the amorphous nature of the materials it could not be ruled out completely.

To further explore this, the four aromatic building blocks were subjected to the same reaction conditions, only this time cyanuric chloride was omitted. Four polymers **pTrux**, **pHMTrux, pFl** and **pPyr**

were obtained, of which **pHMTrux** was already described in the literature[663] (Scheme 2). **pTrux** and **pHMTrux** largely corresponded to the 'failed' CTFs synthesized from **Trux** and **HMTrux**. These 'failed' CTFs are renamed accordingly as **aza-pTrux** and **aza-pHMTrux**, as these do have some nitrogen doping. In contrast to this, **pFl** and **pPyr** were two completely distinct materials from **CTF-Fl** and **CTF-Pyr**. The materials synthesized in this study were analyzed through FTIR, N_2-sorption, elemental analysis and PXRD. The optical bandgaps of the materials were determined using solid state UV-Vis diffuse reflectance measurements. Furthermore, for the most photocatalytically active material, **CTF-Pyr**, the absolute band gap positions were determined, and further structural characterization was performed by means of XPS.

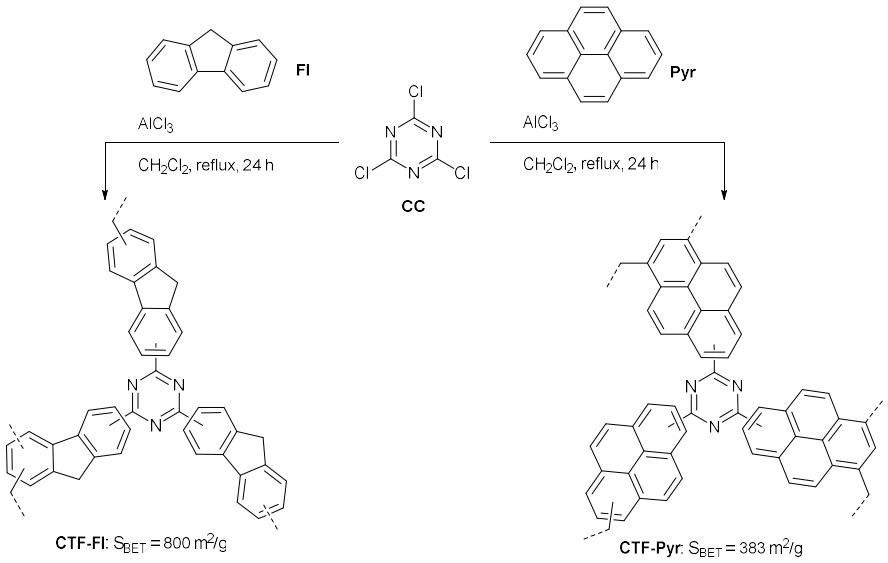

Scheme 2: Synthesis of CTFs: **CTF-Fl** and **CTF-Pyr**. Using analogous procedures with **Trux** and **HMTrux**, no real CTFs were obtained. These materials were therefore denoted as **aza-pTrux/pHMTRux** and are not shown on the scheme. Their chemical structures largely correspond with that of **pTrux/HMTRux**.

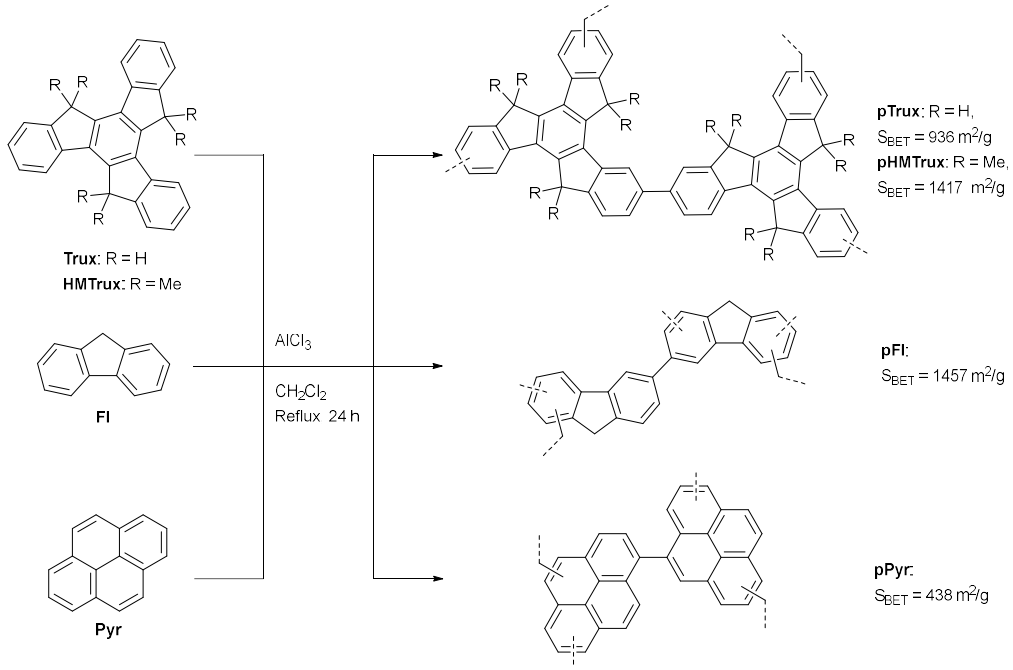

Scheme 3: Synthesis of POPs: **pTrux**, **pHMTRux**, **pFl** and **pPyr** by Scholl coupling and crosslinking with dichloromethane.

To obtain insights into the chemical functionalities present within these eight materials, the FTIR spectra were recorded (Figure 1). The FTIR spectrum of **CTF-Fl** largely corresponds to the one reported in literature.[404] The vibrations at approximately 1514 cm^{-1} and 1350-1358 cm^{-1} originate from the triazine rings.[664] Similarly, **CTF-Pyr** possesses large absorption bands at 1360 cm^{-1} and 1503 cm^{-1}, which are assigned to the triazine rings. Moreover, the main absorption bands of pyrene itself, at 835 cm^{-1} and 708 cm^{-1} could still be distinguished in the material at 812-839 cm^{-1} and 716 cm^{-1}. For the truxene and hexamethyltruxene based materials **pTrux** and **pHMTrux** more complex spectra were obtained. The monomers **Trux** and **HMTrux** exhibit one big absorption band at 733 cm^{-1} and 739 cm^{-1}, respectively. These bands are still present, but are slightly shifted, to 756 cm^{-1} in **pTrux** and 748 cm^{-1} in **pHMTrux**. However new absorption bands are observed at 1607 cm^{-1}, 1387 cm^{-1}, 1261 cm^{-1} and 1078 cm^{-1} for **pTrux**, and 1449 cm^{-1}, 1050-1159 cm^{-1} and 903 cm^{-1} for **pHMTrux**, which are assigned to the crosslinked aromatic moieties.[663] In the case of **pHMTrux** the very pronounced bands at 2868-2961 cm^{-1} can be assigned to the methyl groups and the alkyl crosslinks, the band at 1360 cm^{-1} is assigned to the geminal dimethyl groups in the material. The FTIR spectra for **aza-pTrux** and **aza-pHMTrux** matched with the FTIR spectra of **pTrux** and **pHMTrux**, as these had very similar chemical compositions. On the contrary, for the **pFl** and **pPyr** materials very different spectra were obtained compared to **CTF-Fl** and **CTF-Pyr**. The stretches around 1607 cm^{-1}, 1443 cm^{-1}, 1063 cm^{-1} and 889 cm^{-1}; and 1587 cm^{-1}, 1381 cm^{-1}, 1157 cm^{-1} and 839 cm^{-1} are assigned to the crosslinked aromatic moieties of **pFl** and **pPyr**, respectively. All the materials obtained by self-condensation in the absence of cyanuric chloride possess pronounced absorptions around 2850-2980 cm^{-1}, indicating the presence of methylene bridges, due to the Friedel-Crafts reaction with the solvent, dichloromethane.

The porosity and the pore size distribution of the synthesized materials was determined by means of N_2 sorption measurements (Figure 2-3). As seen from Table 2, the synthesized materials possess a permanent porosity with BET surface areas ranging from 383 m^2/g to 1457 m^2/g. The steep increase at relative pressures $P/P_0 < 0.1$ point to the pronounced microporous character of the materials (Type I isotherms). The isotherms show another increase above $P/P_0 = 0.8$, which is probably due to interparticle porosity.[665,666] Moreover, the isotherms do not fully close, which indicate a swelling of the materials in liquid nitrogen, typically observed for microporous polymers.[667,668] The surface area of **CTF-Fl** is 800 m^2/g, which is in good agreement with the reported value (773 m^2/g).[404] Similarly, the value for the **pHMTRux** material (1417 m^2/g) corresponds to the value reported by Guadeloupe *et al.* (1688 m^2/g).[663] In addition, the pore size distributions were determined using the quenched solid density functional theory (QSDFT) on the adsorption branch, and the average pore diameter ranged from 13.6 to 17.9 Å (Table 2, Figure 4-5). It should be noted that because of the swelling of the materials the pore size distributions of these flexible organic microporous materials should not be taken at face value, as the calculations are not optimized for this type of materials.[669]

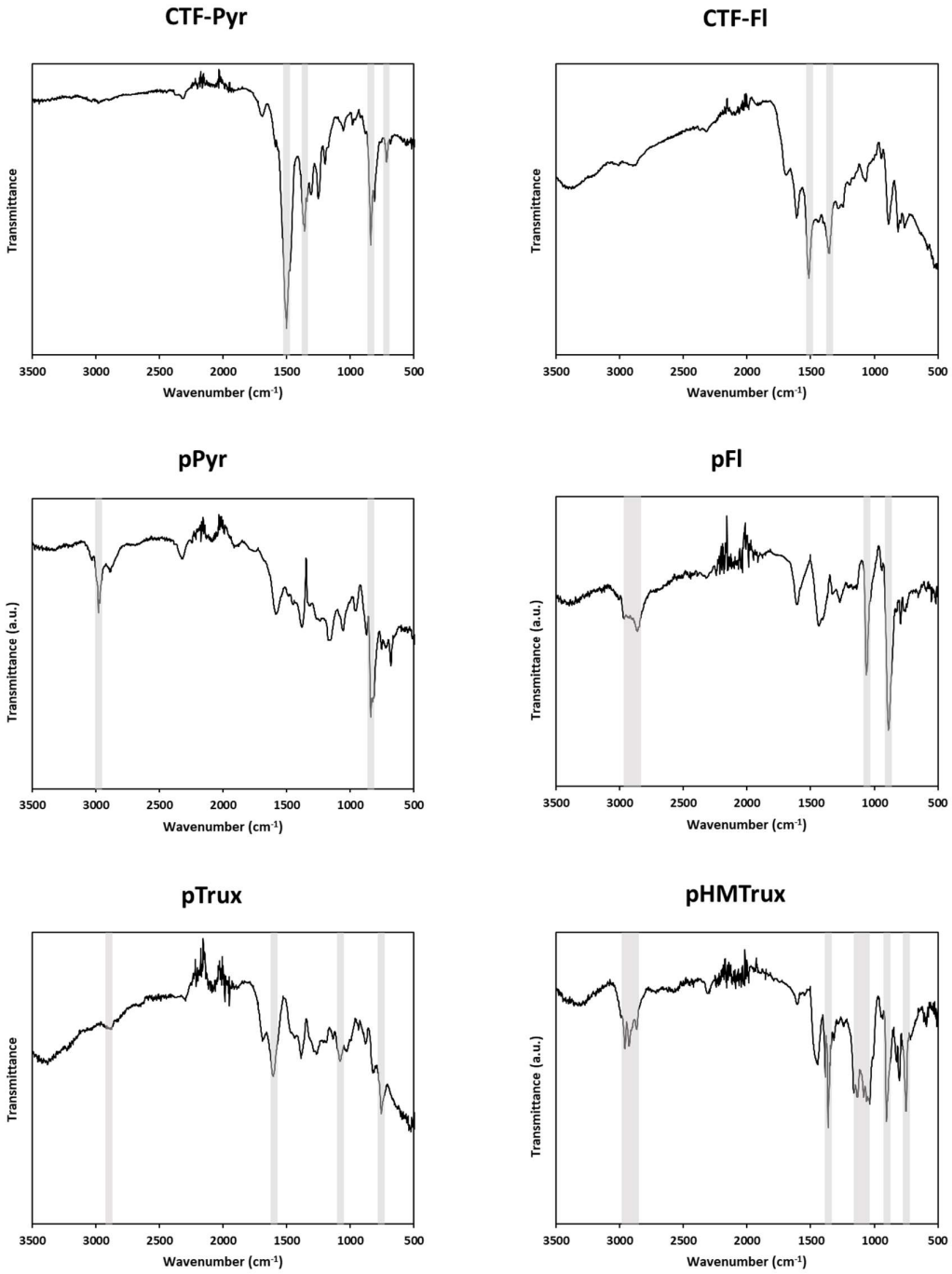

Figure 1: FTIR spectra of the obtained polymers. Noticeable features are indicated in grey. The spectra for **aza-pTrux** and **aza-pHMTrux** essentially corresponded to those of **pTrux** and **pHMTrux** and are not shown.

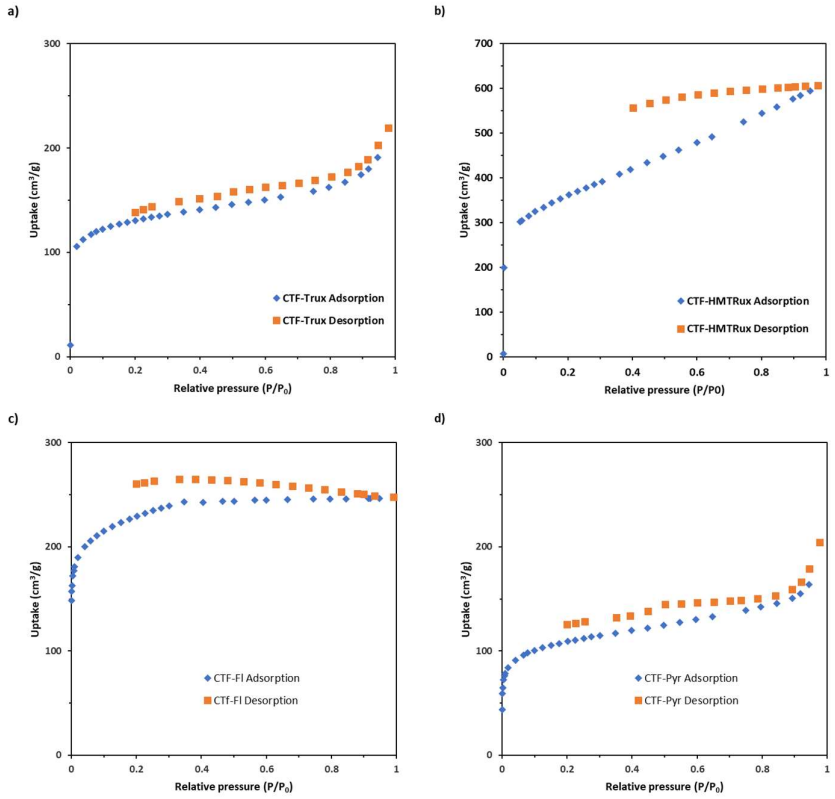

Figure 2: Nitrogen sorption isotherms for (a) **CTF-Trux**; (b) **CTF-HMTRux**; (c) **CTF-Fl**; and (d) **CTF-Pyr**.

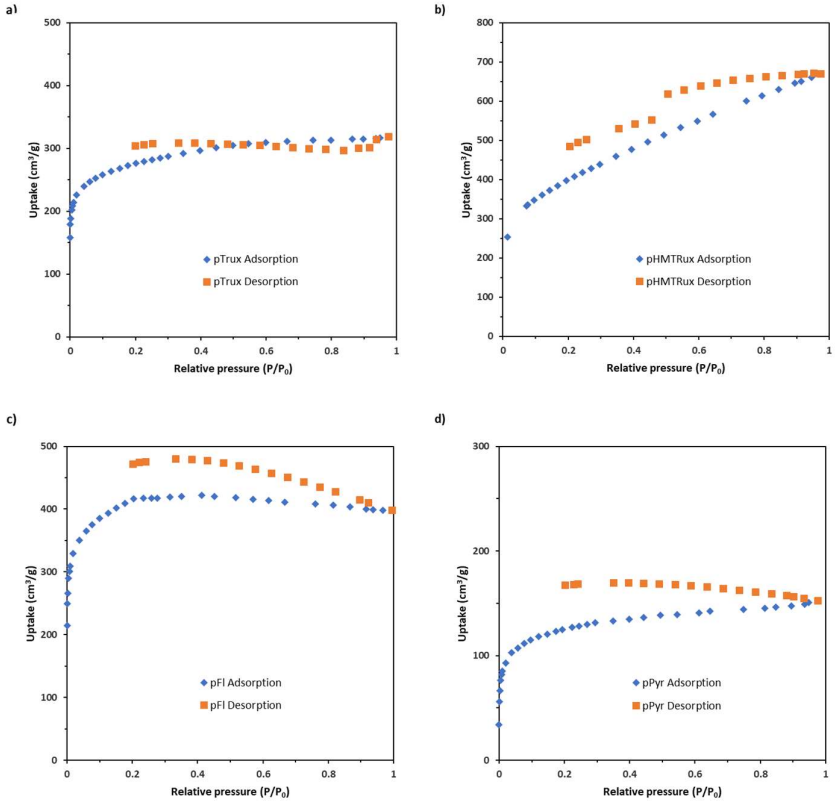

Figure 3: Nitrogen sorption isotherms for a) **pTrux**; b) **pHMTRux**; c) **pFl**; and d) **pPyr**.

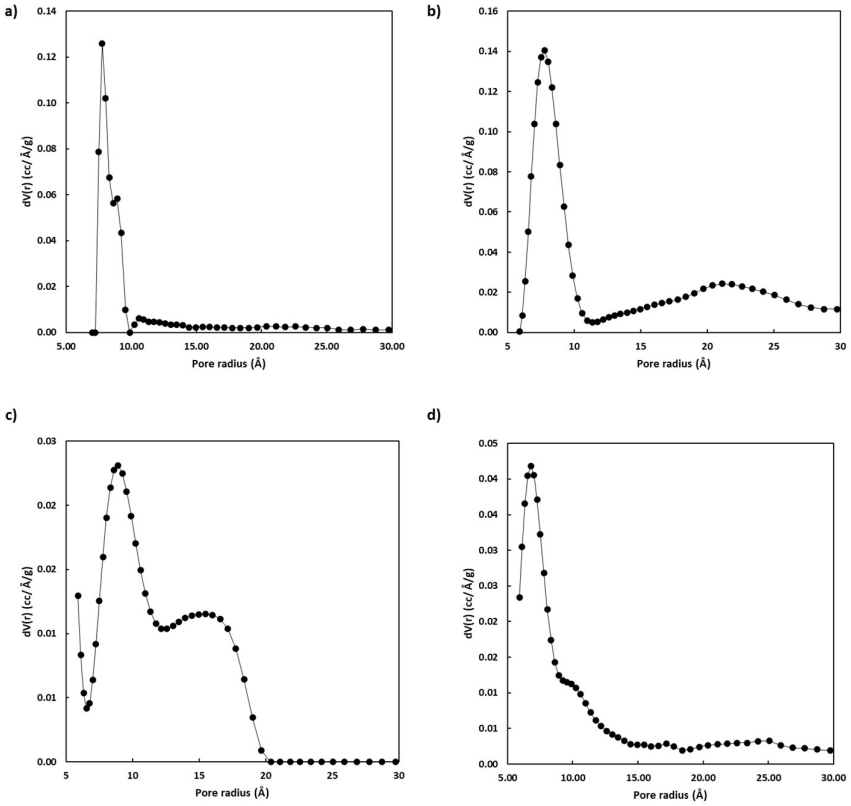

Figure 4: Pore size distributions for (a) **CTF-Trux**; (b) **CTF-HMTRux**; (c) **CTF-Fl**; and (d) **CTF-Pyr**.

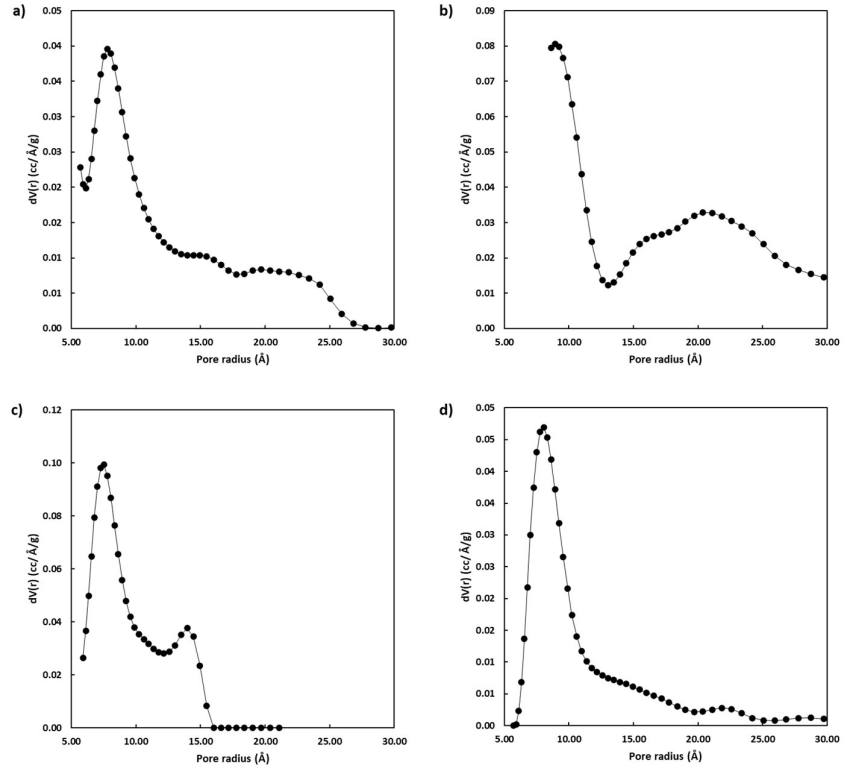

Figure 5: Pore size distributions for (a) **pTrux**; (b) **pHMTRux**; (c) **pFl**; and (d) **pPyr**.

The crystallinity was analyzed by means of PXRD, which showed that, as expected, amorphous networks were formed, indicated by the largely featureless spectra (Figure 6-7). The spectrum of **CTF-Pyr** possessed a broad peak centered around 2θ = 22°, which could imply stacking in the (001) plane.[29] Elemental analysis was used to further determine the chemical structures of the materials, and the results are presented in Table 1. The experimentally obtained values of C, H and N are lower than expected, which is a common feature for porous organic polymers.[31,670] This can be caused by the difficulty in achieving a complete combustion, or by residual solvents in the pores.[663] As mentioned before, the envisaged Friedel-Crafts alkylation between cyanuric chloride and truxene or hexamethyltruxene was not effective, and the nitrogen contents of these two materials were only 0.8% and 0.7%, respectively. The nitrogen contents for **CTF-Fl** and **CTF-Pyr** are significantly better, 3.2% and 6.7%, but are still lower than their theoretical nitrogen contents of 13.0% and 18.5%, respectively. This indicates that in addition to Friedel-Crafts alkylation, also self-condensation of the aromatic monomers takes place via Scholl coupling and/or crosslinking with CH_2Cl_2.

Table 1: EA of the synthesized polymers.

Material	C (%)	H (%)	N (%)	Atom C/H	Atom C/N
aza-pTrux	70.600	3.994	0.757	1.5	/
aza-pHMTrux	88.063	6.629	0.653	1.1	/
CTF-Fl	76.818	4.480	3.204	1.4	28.0
CTF-Pyr	70.094	3.214	6.700	1.8	12.2
pTRux	77.461	4.408	0	1.5	/
pHMTRux	84.214	6.245	0	1.1	/
pFl	84.400	4.950	0	1.4	/
pPyr	85.235	3.837	0	1.9	/

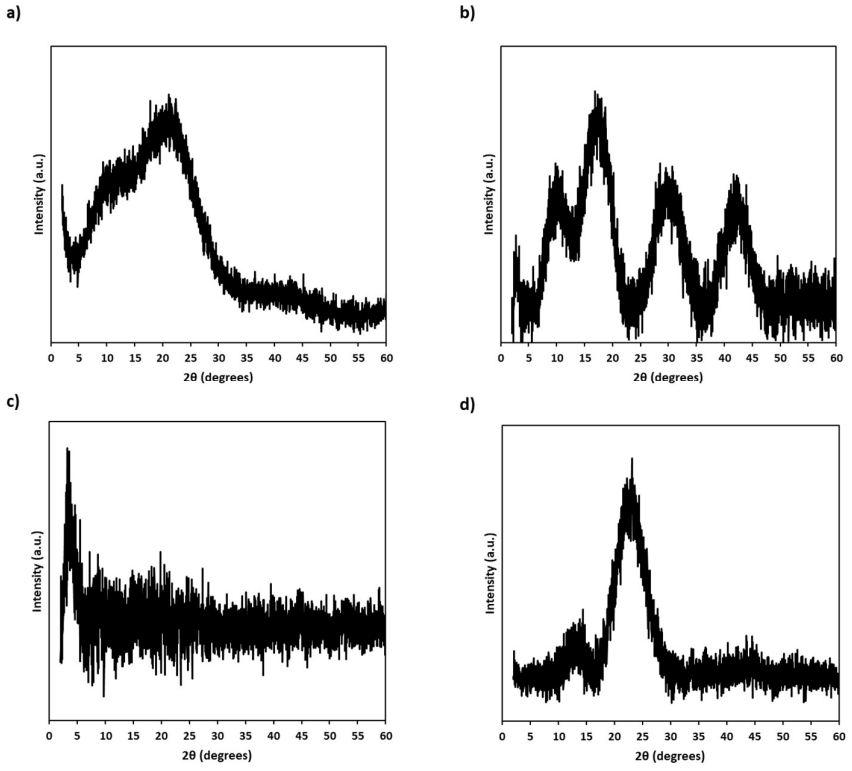

Figure 6: XRD spectra of a) **aza-pTrux**; b) **aza-pHMTrux**; c) **CTF-Fl**; and d) **CTF-Pyr**.

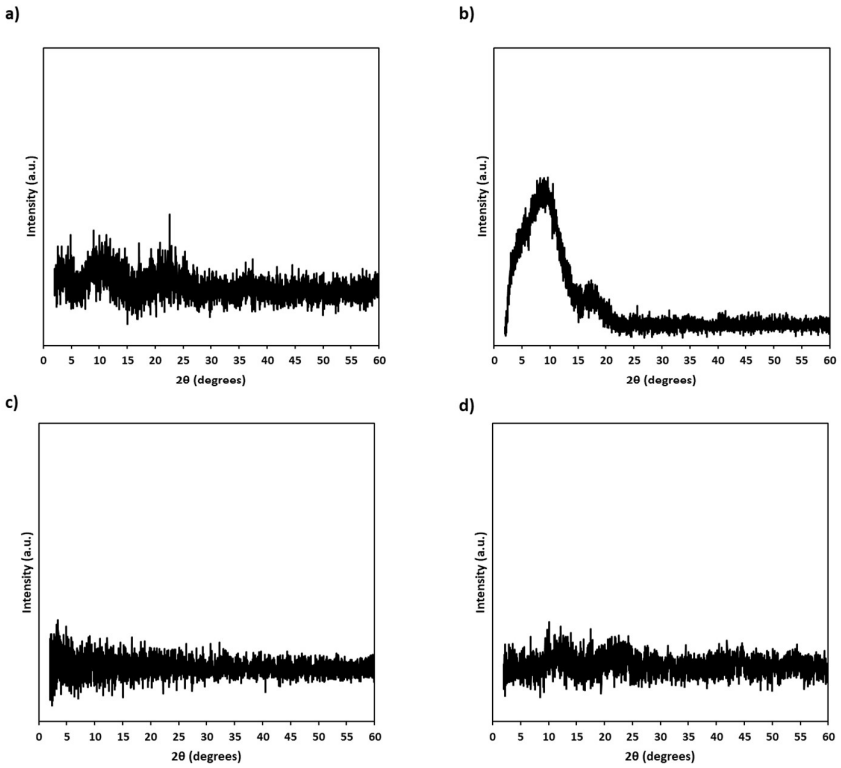

Figure 7: XRD spectra of a) **pTrux**; b) **pHMTRux**; c) **pFl**; and d) **pPyr**.

For these two CTF materials, the N 1s X-ray photoelectron spectroscopy (XPS) spectra were measured. The N 1s spectrum of **CTF-Pyr** could be deconvoluted into two peaks (Figure 8a). The major peak at 399.3 eV corresponds to the triazine moieties, and the smaller, secondary peak at 400.9 eV is assigned to the quaternary nitrogens, formed by side reactions or protonation. For the **CTF-Fl** material, the spectrum was deconvoluted into three signals (Figure 8b). The major peak at 399.1 eV corresponds to the triazine nitrogens, whereas the smaller peaks at 400.2 eV and 401.2 eV originate from the pyrrolic nitrogens and quaternary nitrogens, respectively.[671] Regarding the pyrrolic nitrogens, we hypothesize that the unreacted cyanuric C-Cl bonds can react with water during the work up of the reaction, producing hydroxytriazines, which are in a tautomeric equilibrium with their corresponding pyridinone, thus resulting in the observed pyrrolic signal.

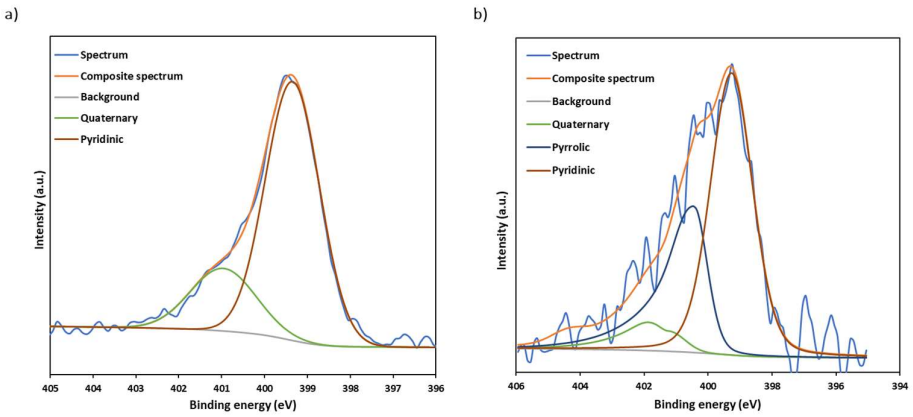

Figure 8: N 1s XPS spectra of (a) **CTF-Pyr**; and (b) **CTF-Fl**.

Given their intended application as photocatalysts, the optical properties of the synthesized materials were determined by means of diffuse reflectance UV-Vis spectrometry. The obtained spectra were transformed through the Kubelka-Munk function to obtain the absorption spectra. These spectra exhibit absorption edges around 400-500 nm and absorption tails that extend beyond 850 nm (Figure 9-10). The related Tauc plots were used to estimate the band gaps (Table 2), which ranged from 1.82-2.40 eV. The band gaps of the materials containing nitrogen was slightly larger than those of the nitrogen-free materials. In any case, the band gaps correspond with the energy of visible light, pointing to the ability of these polymers to harvest visible light, and convert this into usable chemical energy.

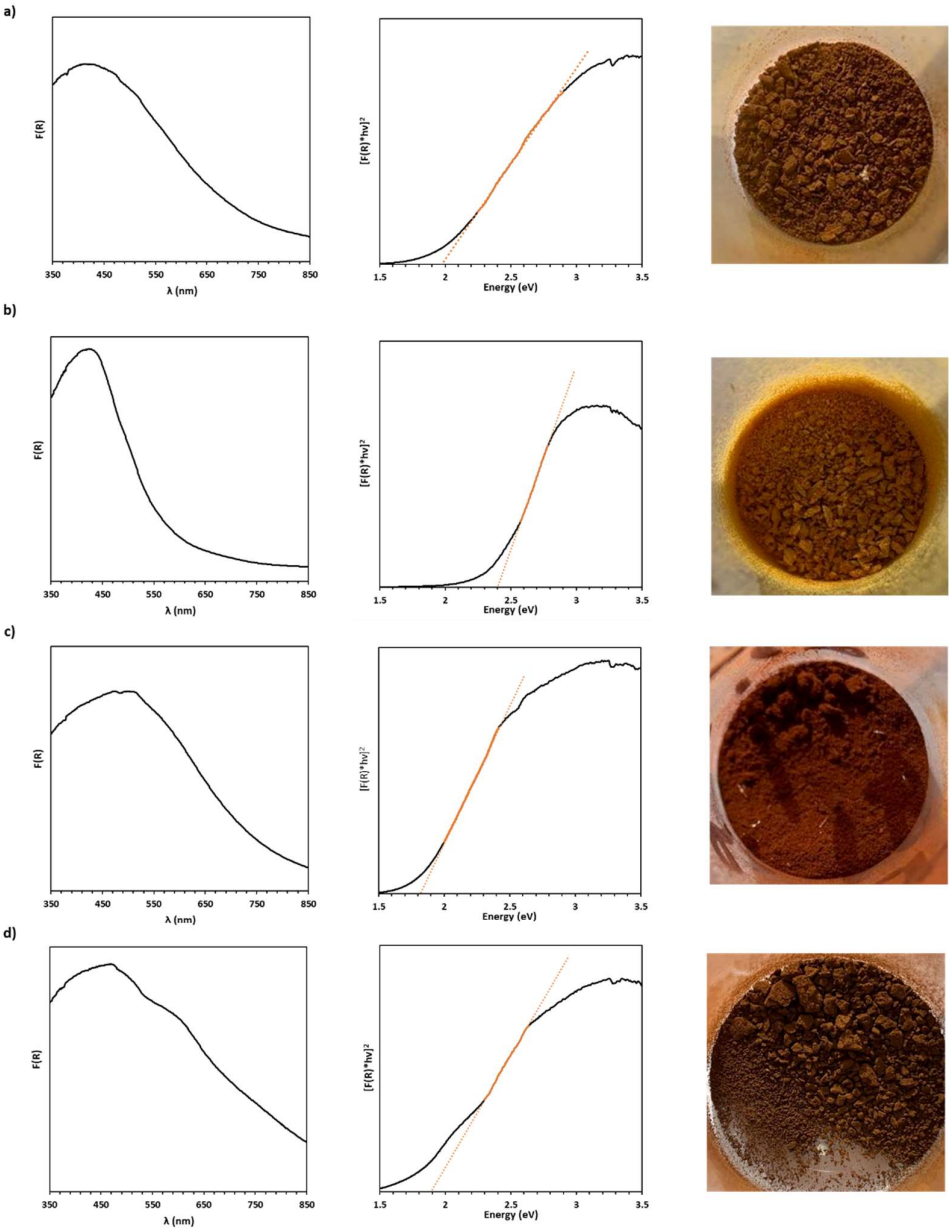

Figure 9: Kubelka-Munk transformed absorption spectra, Tauc plots and picture of (a) **aza-pTrux**; (b) **aza-pHMTrux**; (c) **CTF-Fl**; and (d) **CTF-Pyr**.

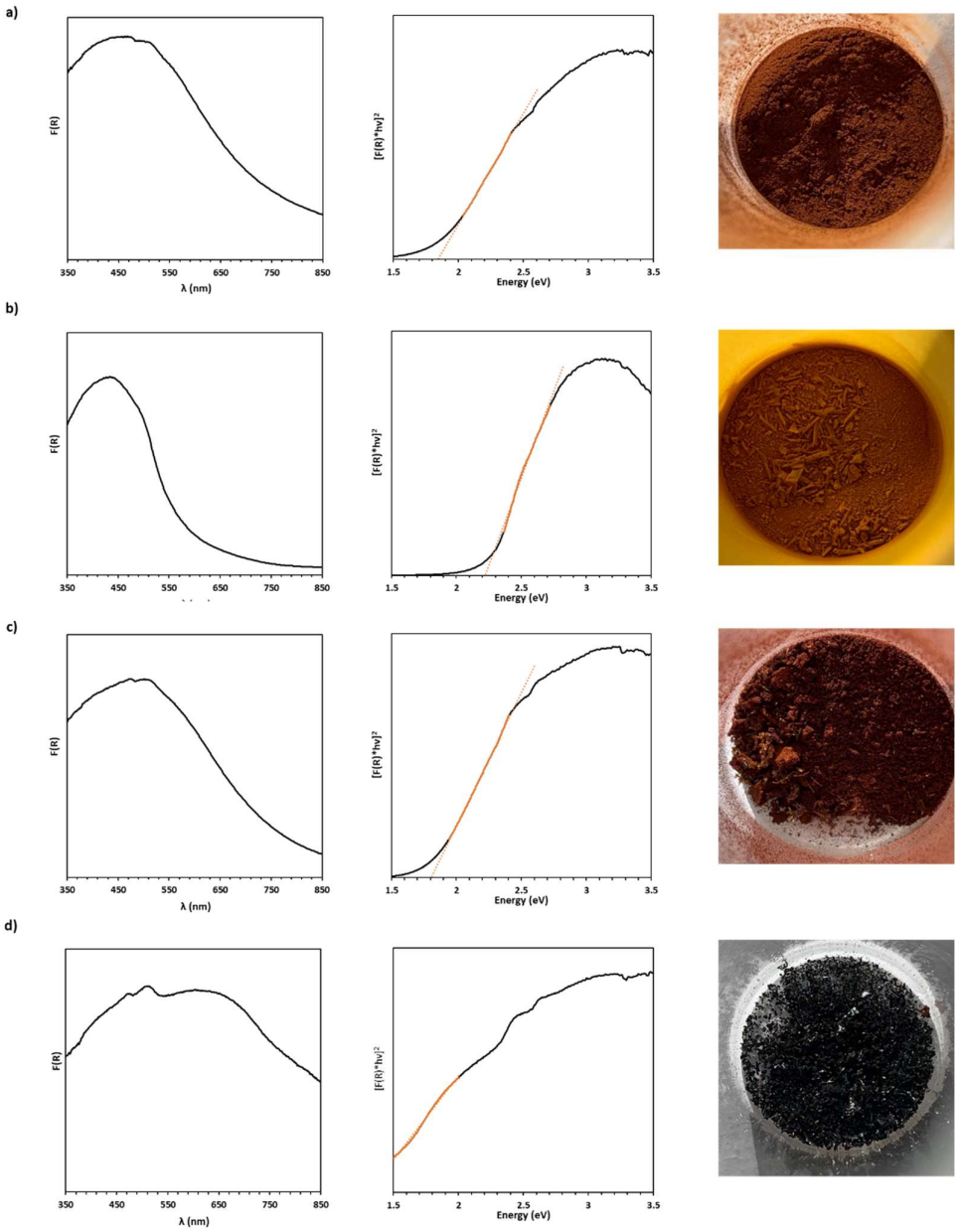

Figure 10: Kubelka-Munk transformed absorption spectra, Tauc plots and picture of (a) **pTrux**; (b) **pHMTRux**; (c) **pCTF-Fl**; and (d) **pCTF-Pyr**.

Table 2: BET surface area, average pore diameter and band gaps of the synthesized materials.

Material	S_{BET} (m^2)	Average pore diameter (Å)	Eg (eV)
aza-pTrux	456	15.6	1.97
aza-pHMTrux	1277	15.6	2.40
CTF-Fl	800	17.9	1.82
CTF-Pyr	383	13.6	1.89
pTRux	963	15.0	1.84
pHMTrux	1417	17.9	2.22
pFl	1457	15.0	1.81
pPyr	438	15.6	/[a]

[a] The method used to measure the band gap is not suited for black materials such as **pPyr**.

3.2.2 Application as photocatalysts for the aromatization of *N*-heterocycles

3.2.2.1 Introduction

To evaluate the potential of the synthesized materials as heterogeneous photocatalysts, we focused on the oxidative aromatization of *N*-heterocycles **2** and **4**, hereby producing a broad range of pyridines **3**, pyrazoles **5** and related compounds (Scheme 4). The pyridine core is one of the most widespread moieties in natural products, pharmaceuticals, dyes, drugs, reagents, ligands… and therefore its synthesis receives considerable attention.[672–674] A very convenient way to produce highly substituted pyridines is through the Hantzsch dihydropyridine (-like) synthesis followed by aromatization.[675] The existing methods to perform this last oxidation step mainly rely on stoichiometric oxidants such as $KMnO_4$,[676] HNO_3,[677] $K_2S_2O_8$,[678] *t*BuOOH,[679] CrO_2,[680] MnO_2,[681] $FeCl_3.6H_2O$,[682] etc. From a green chemistry perspective the use of stoichiometric oxidants is not desirable, and for this reason catalytic methods utilizing oxygen or air and a catalyst such as $Fe(ClO_4)_3$,[683] or *N*-hydroxyphthalimide (NHPI)[684] have been developed. Moreover, photocatalysts such as eosin Y bis(tetrabutyl ammonium salt) (TBA-eosin Y)[685] and acridinium dyes[686] have recently been described. Although these methods do not require the addition of stoichiometric oxidants, the catalysts still need to be separated from the reaction mixture and in most cases they are not recyclable. The development of a heterogeneous photocatalyst for this transformation is therefore highly desirable.

Next to the dihydropyridine derivatives a POP catalyzed oxidative aromatization of pyrazolines **4** to give the corresponding pyrazoles **5** was also envisaged. Pyrazoles are important moieties in *e.g.* pharmaceuticals, insecticides, herbicides, etc.[687–691] They can conveniently be obtained by the condensation between enones and hydrazines, resulting in pyrazolines, which can then be oxidized. A wide variety of methods has been described for this reaction.[692] However, mostly stoichiometric oxidizing agents or metals are used, and to the best of our knowledge an efficient heterogeneous photocatalyst for this transformation has not been described.

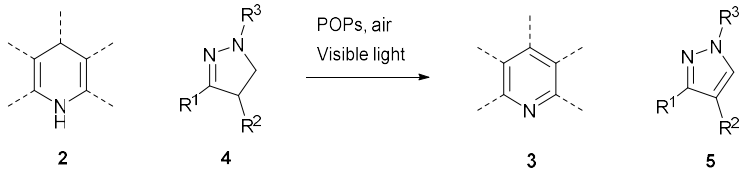

Scheme 4: Overview of the envisaged transformations.

3.2.2.2 Initial screening

In the initial screening of the photocatalysts the conversion of the model substrate **2d** was studied. Conversions ranging from 10 to 100% were obtained by using acetonitrile as a solvent, at room temperature, in air and under visible light irradiation (Table 3). Especially **CTF-Pyr**, which consists of electron rich pyrene chromophores, and electron poor, redox-active triazine moieties exhibited a good performance. Interestingly, the **aza-pTrux** and **aza-pHMTrux** materials also showed quite good activity (74-86%), which was much higher than for **pTrux** and **pHMTrux** (42-46%), signifying that even the low amount of nitrogen in these materials (0.65-0.76%) still has a beneficial effect on the activity. Similarly, **pFl** and **pPyr** possess very low activities, due to the absence of any nitrogen containing functionality.

Surprisingly, **CTF-Fl** also possessed a low activity, probably due to the fluorene moieties being worse chromophores in comparison to pyrene. Importantly, pyrene itself also gave a negligible conversion, proving the importance of the extended conjugated system in the CTF for photocatalytic activity.

To our delight, the oxidation reaction of the pyrazoles also worked well with **CTF-Pyr**. Using CH_3CN as a solvent full conversion was obtained, however some unknown side products were also detected. Other solvents were therefore screened (Table 4), showing that ethyl acetate was the most effective.

Table 3: Catalyst screening for the oxidation of tetrahydroquinoline-5-one **2d** to dihydroquinoline-5-one **3d**.[a]

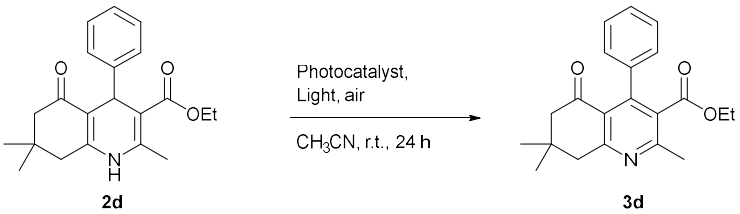

Entry	Catalyst	Conversion (%)[b]
1	CTF-Fl	25
2	aza-pTrux	86
3	aza-pHMTrux	74
4	**CTF-Pyr**	**95-100**
5	pFl	31
6	pTrux	42
7	pHMTrux	46
8	pPyr	10
9	Pyrene	7

[a] Reaction conditions: Ethyl 2,7,7-trimethyl-5-oxo-4-phenyl-1,4,5,6,7,8-hexahydroquinoline-3-carboxylate **2d** (33.7 mg, 0.1 mmol, 1 eq), photocatalyst (5 mg), 2.5 mL CH_3CN, open to the air, 26 W CFL, 24 h, r.t.
[b] Determined by ^{1}H-NMR.

Table 4: Optimalization of the **CTF-Pyr** catalyzed oxidation of 1,3,5-triphenyl-4,5-dihydro-1*H*-pyrazole **4a** and 3-methyl-1,5-diphenyl-4,5-dihydro-1*H*-pyrazole **4d** [a]

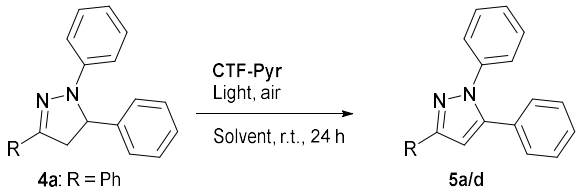

Entry	Substrate	Solvent	Yield (%)[b]	
			6 h	24 h
1	**4a**	CH_3CN	47	91
2		EtOAc	48	97
3		CH_3CN/H_2O (4/1)	42	86
4		Toluene	47	99
5		CF_3CF_2OH	13	40
6		CH_3CN[c]	5	35
7	**4d**	CH_3CN	n.m.[d]	84
8		EtOAc	n.m.	89
9		Toluene	n.m.	89

[a] Reaction conditions: Pyrazoline **4a/d** (0.1 mmol, 1 eq.), CTF-Pyr (5 mg), 2.5 mL solvent, open to the air, 26 W CFL, 24 h, r.t.
[b] Determined using ^{1}H-NMR with 1,3,5-trimethoxybenzene as an internal standard.
[c] No catalyst.
[d] Not measured.

3.2.2.3 Screening of other reactions

Next to the aforementioned reactions, some other transformations were screened (Scheme 5 and 6). Under the same reaction conditions as for the oxidation of tetrahydroquinoline-5-one **2** the aromatization of the dihydroisoxazole **8** and triazolidine-3,5-dione **6** gave no reaction to the corresponding isoxazole **9** or triazole-3,5(4*H*)-dione **7**, respectively, and the starting materials were recuperated unchanged. The reaction of pyrazolidin-3-one **10** to the 2,4-dihydro-3*H*-pyrazol-3-one **11** showed full conversion of the starting material, however, very complex mixtures were formed, and this was not pursued any further.

Some further derivatizations of the Hantzsch ester (analogues) were also explored. It is known that alkyl substituted Hantzsch esters such as compound **2h'**, can act as radical donors, thus serving as alkylating agents.[693] This reaction was assessed with dimethyl fumarate **12** as the radical acceptor. Using strict oxygen-free reaction conditions, no reactivity was observed. When oxygen was allowed in the reaction mixture, full conversion of the starting material was obtained, mainly to the dealkylated pyridine **3h**, and the desired product was not detected. Lastly, the [2 + 2] cycloaddition of dihydropyridine **2a** with styrene **14** was performed, a reaction that has been reported with $Ir(ppy)_3$ as a homogeneous photocatalyst via energy transfer of the excited state to styrene.[694] This transformation did not give any product, after which it was decided to focus on the oxidation reactions of 1,4 dihydropyridines, their derivatives and pyrazolines.

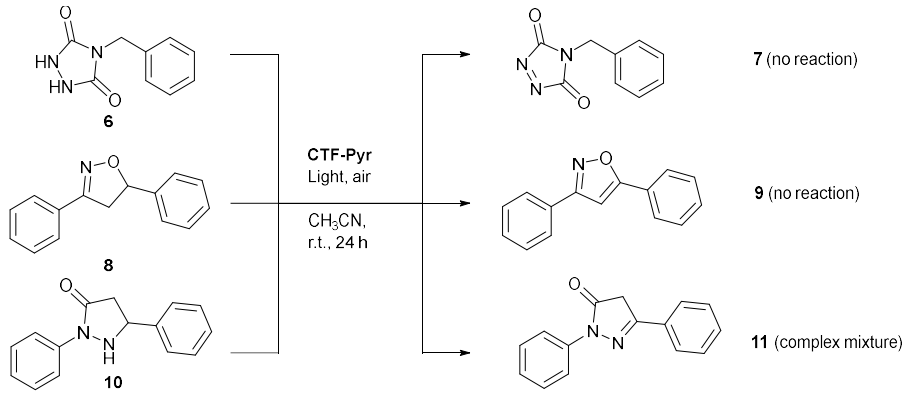

Scheme 5: Attempted oxidation of dihydroisoxazole **8**, triazolidine-3,5-dione **6** and pyrazolidin-3-one **10**.

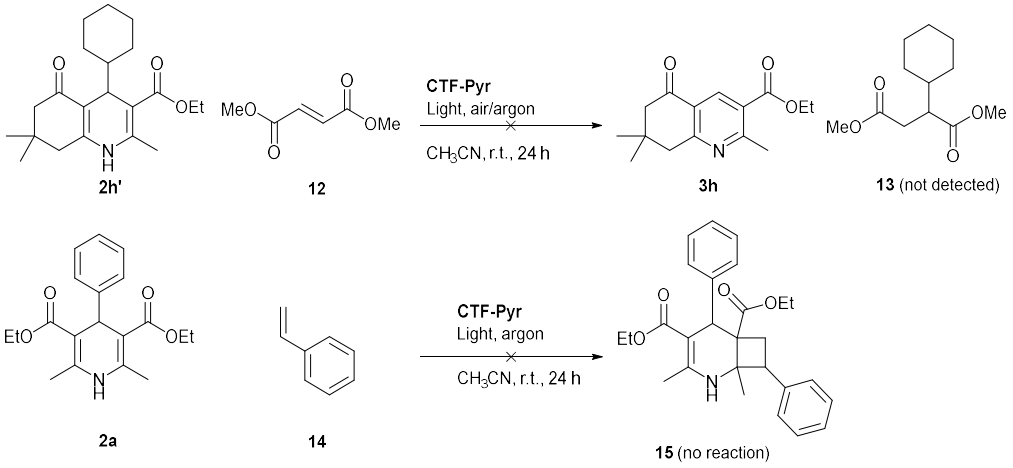

Scheme 6: Attempted use of alkyl substituted tetrahydroquinoline-5-one **2h'** as a radical donor, and attempted [2 + 2] cycloaddition of 1,4-dihydropyridine **2a**.

3.2.2.4 Synthesis of substrates

A small library of structurally resembling heterocycles were synthesized using the Hantzsch-like multicomponent condensation. Two different procedures based on the literature[695,696] were used to synthesize 1,4-dihydropyridines **2a-c**, tetrahydroquinoline-5-ones **2d-k** and hexahydroacridine-1,8-diones **2l-o** (Scheme 7). The procedure with KH_2PO_4 as catalyst[696] was used for compounds **2d-g** and **2k-o**: the tetrahydroquinoline-5-ones and hexahydroacridine-1,8-diones with an aromatic substitution on the dihydropyridine ring, by using an aromatic aldehyde. In most cases the crude product was pure which led to high yields, although in some cases recrystallization was needed, lowering the yield. On the other hand, the procedure with choline chloride as catalyst[695] was used for compounds **2a-c** and **2h-j**: the 1,4-dihydropyridines and the tetrahydroquinoline-5-ones with an aliphatic substitution on the dihydropyridine ring. In this procedure a recrystallisation was always needed, which led to lower yields. More details regarding these procedures can be found in the experimental section and in the Master thesis of Nathan Raeymackers.[648]

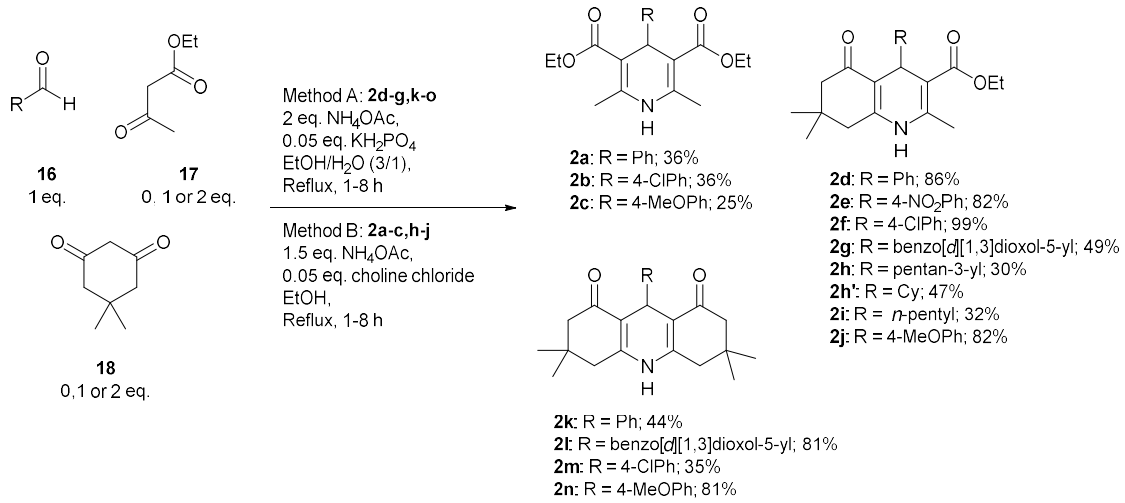

Scheme 7: Synthesis of 1,4-dihydropyridines **2a-c**, tetrahydroquinoline-5-ones **2d-2k** and hexahydroacridine-1,8-diones **2l-o**.

Pyrazolines **4a-g** could conveniently be synthesized by the reaction between α,β-unsaturated carbonyl compounds **19** and hydrazines (Scheme 8). Two modified literature procedures were used for the synthesis of pyrazolines **4a-g**, using either the hydrochloride salt of the hydrazine with acetic acid in methanol, or the hydrazine with sulfuric acid as catalyst in ethanol.[697,698] The products were isolated in yields ranging from 50% to 95% by recrystallisation or chromatography.

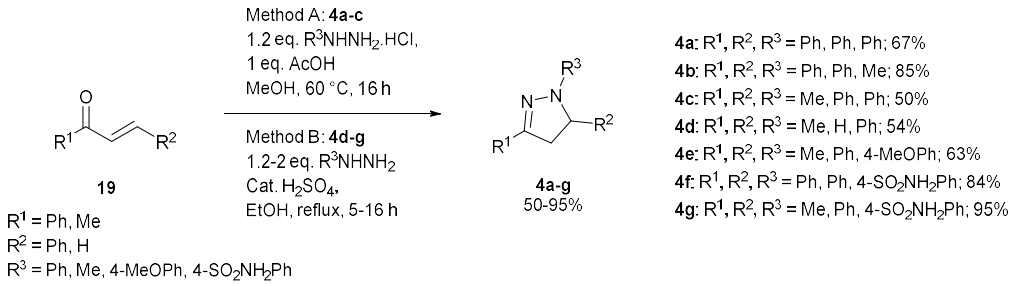

Scheme 8: Synthesis of pyrazolines **4a-g**.

3.2.2.5 Substrate scope, mechanism and recycling experiments

Using **CTF-Pyr** as the most promising material, the substrate scope for this reaction was extended (Scheme 9). Pyridines **3a-c**, dihydroquinoline-5-ones **3d-j** and tetrahydroacridine-1,8-diones **3k-n** were obtained in good to excellent yields (76-99%) with electron donating and withdrawing substituents being well tolerated. For the alkyl substituted substrates, in the case of cyclohexyl or pentan-3-yl substitution, the dealkylated dihydroquinoline-5-one **3h** was isolated. In the case of the *n*-pentyl substituted substrate the corresponding dihydroquinoline-5-one **3i** was formed, without dealkylation, which is likely due to the lower stability of the primary *n*-pentyl radical. To evaluate the application of **CTF-Pyr** on a larger scale the reaction was performed on a one mmol scale (0.34 g), with substrate **2d**. Due to a smaller surface to volume ratio a slightly longer reaction time was needed (40 hours), but the product **3d** was still obtained in 85% isolated yield.

Moreover, using **CTF-Pyr** in ethyl acetate, at room temperature and in air a range of pyrazoles **5a-g** could be produced in good yields (71-96%). Both electron rich (methoxy) and poor (sulfonamide) aryl substituted pyrazolines gave satisfactory results, and alkyl substitution on the pyrazoline core was also tolerated (Scheme 10).

Many systems have been reported to perform these transformations, including the use of dyes as homogeneous photocatalysts (see Section 3.2.2.1). However, there has been a lack of reports on the use of heterogeneous photocatalysts for this transformation. A recent study by Huang *et al*. described the use of a polyoxometalate-based open framework for both dihydropyridine synthesis and oxidation in a one-pot reaction. While this approach is attractive due to its one-pot nature and the relatively low catalyst loading of 10 mg/mmol (compared to 50 mg/mmol in this work), the required reaction times were significantly longer (two days). Additionally, the products were obtained as mixtures of dihydropyridines and pyridines, with only low yields (11-25%) of isolated pyridines, compared with the yields of 70-99% that were obtained in this work. Moreover, the substrate scope was quite narrow, only covering the synthesis of (dihydro)pyridines, and not the more difficult-to-oxidize dihydroquinoline-5-ones and tetrahydroacridine-1,8-diones.

To obtain more insights into the mechanism of the oxidation reaction several control experiments were performed (Table 5). In the dark or in the absence of a photocatalyst (almost) no product was detected (Table 5, entry 2 and 3). Under argon a very low conversion was detected (Table 5, entry 4), indicating the importance of oxygen as the terminal oxidant. Oxygen, a good photocatalyst, and light are thus essential for this transformation. To understand the role of oxygen several quenchers were added (Table 5, entry 5-13). Quenching of the superoxide radical ($O_2^{-\bullet}$) with *p*-benzoquinone[534] or nitro blue tetrazolium chloride (NBT)[535] lowered the conversion drastically to 42% and 45%, respectively (Table 5, entry 5-6). Similarly, when adding quenchers for singlet oxygen ($^1O_2$), such as L-histidine,[532] DABCO[564] or sodium azide[565] (Table 5, entry 7-9) the conversions were reduced to 71%, 62% and 42%, respectively. This indicates that both singlet oxygen and the superoxide anion are active contributors to this reaction. In contrast, when quenching hydroxyl radicals with *i*PrOH [533] the reaction was not significantly affected (Table 5, entry 10). When quenching holes using KI[536] the conversion was drastically lowered to 19% (Table 5, entry 10). Interestingly, $AgNO_3$ (Table 5, entry 11), a typical electron scavenger,[537] did not affect the reaction very much. This is probably due to the oxidizing effect of $AgNO_3$, which itself has been reported as a reagent for this transformation.[699–701] Lastly, in the presence of TEMPO,[566] a known radical scavenger, the yield also lowered drastically (Table 5, entry 14), signifying the involvement of radical processes. Importantly, as shown in Figure 11, hydrogen peroxide was clearly detected with its characteristic peak at 10.20 ppm (^{1}H-NMR, DMSO-d_6),[702] indicating its formation during the reaction.

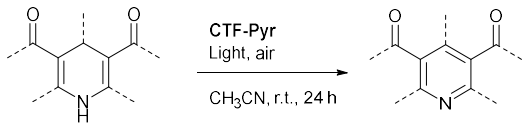

2a-n

3a-n
14 examples
70-99%

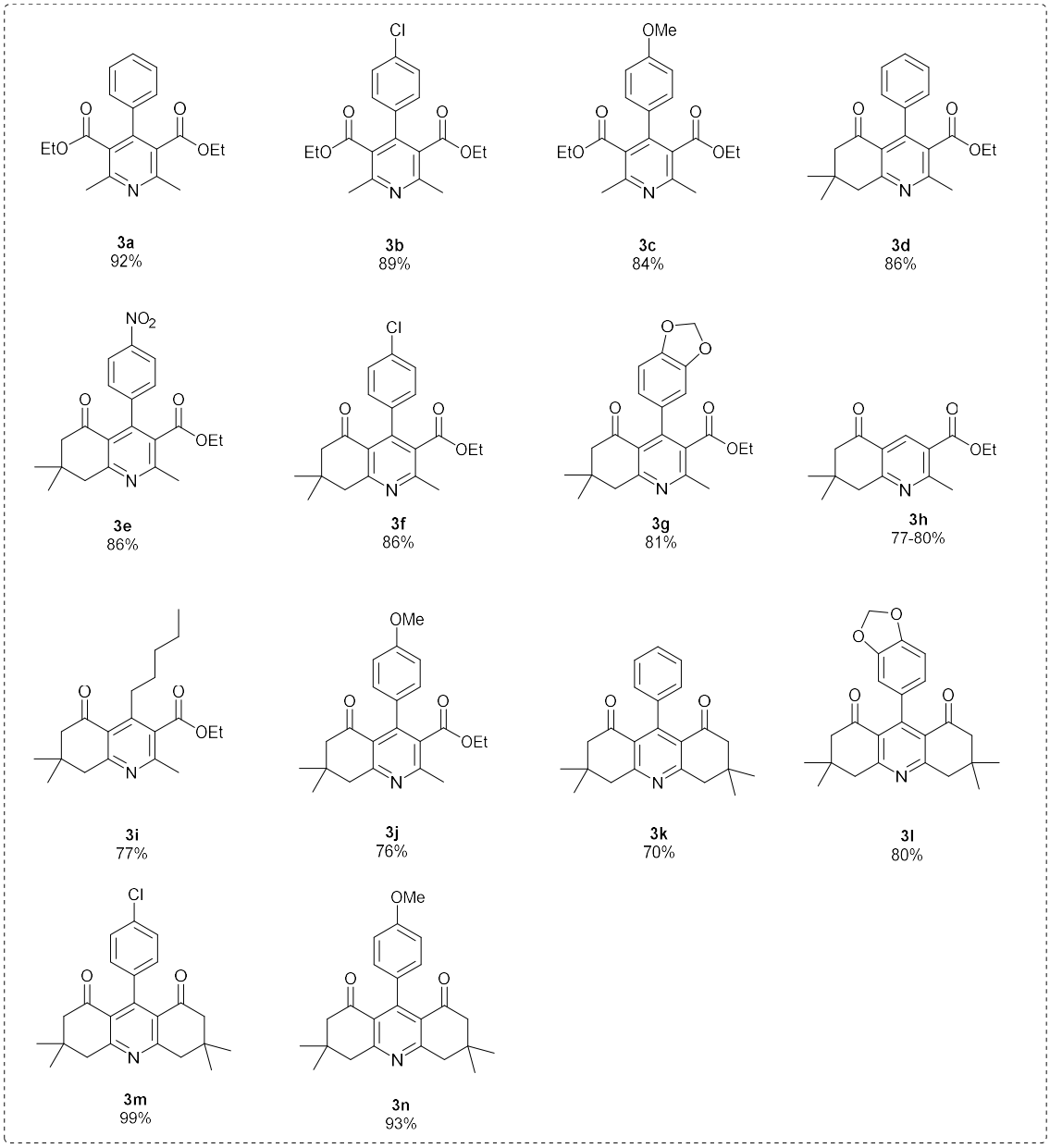

Scheme 9: **CTF-Pyr** catalyzed photocatalytic oxidation of dihydropyridines, tetrahydroquinoline-5-ones and hexahydroacridine-1,8-diones.[a,b]

[a] Reaction conditions: Substrate **2** (0.2 mmol), **CTF-Pyr** (10 mg), 5 mL CH_3CN, open to the air, 26 W CFL, 24 h, r.t.

[b] Isolated yields.

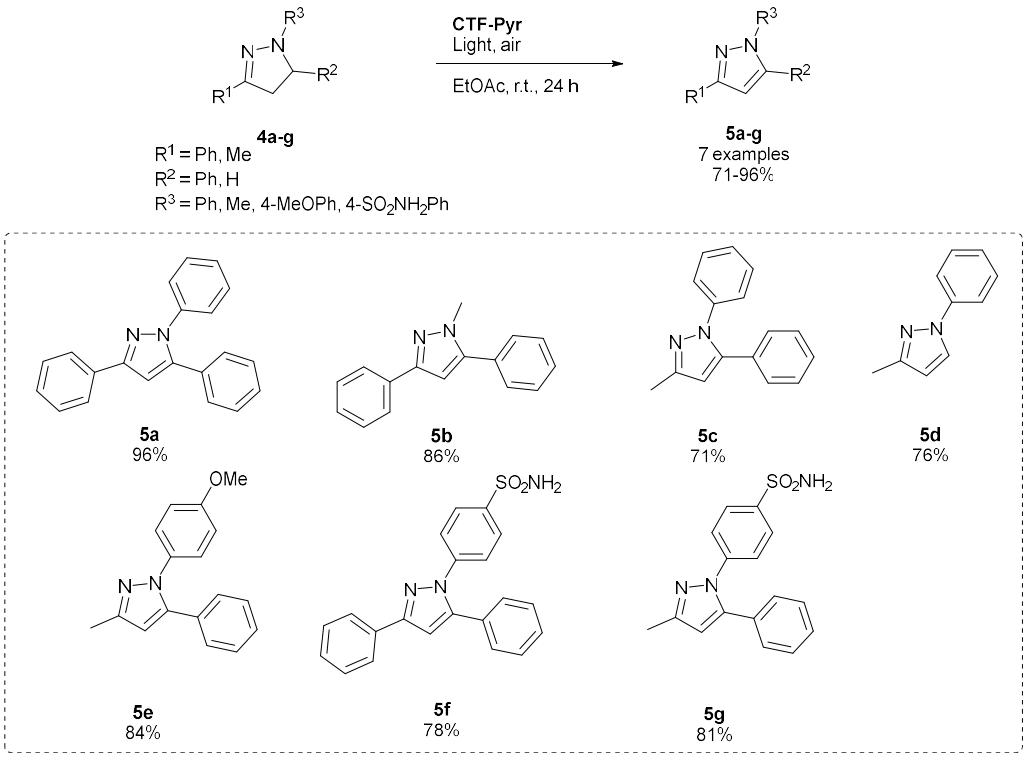

Scheme 10: **CTF-Pyr** catalyzed oxidation of pyrazolines.[a,b]

[a] Reaction conditions: Substrate **4** (0.2 mmol), **CTF-Pyr** (10 mg), 5 mL EtOAc, open to the air, 26 W CFL, 24 h, r.t.

[b] Isolated yields.

Table 5: Control experiments for the **CTF-Pyr** catalyzed oxidation of tetrahydroquinoline-5-one **2d**.[a]

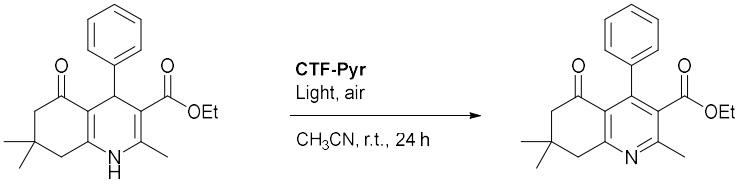

Entry	Conditions	Conversion[b]
1	No modification	95-100
2	Dark	0
3	No catalyst	3
4	Argon	18
5	*p*-Benzoquinone	42
6	Nitro blue tetrazolium chloride	45
7	L-Histidine	71
8	DABCO	62
9	NaN_3	42
10	*i*PrOH	95
11	KI	19
12	$AgNO_3$	88
13	TEMPO	11

[a] Reaction conditions: Ethyl 2,7,7-trimethyl-5-oxo-4-phenyl-1,4,5,6,7,8-hexahydroquinoline-3-carboxylate **2d** (33.7 mg, 0.1 mmol, 1 eq), **CTF-Pyr** (5 mg), 2.5 mL CH_3CN, open to the air, 26 W CFL, 24 h, r.t.

[b] Determined by ^{1}H-NMR.

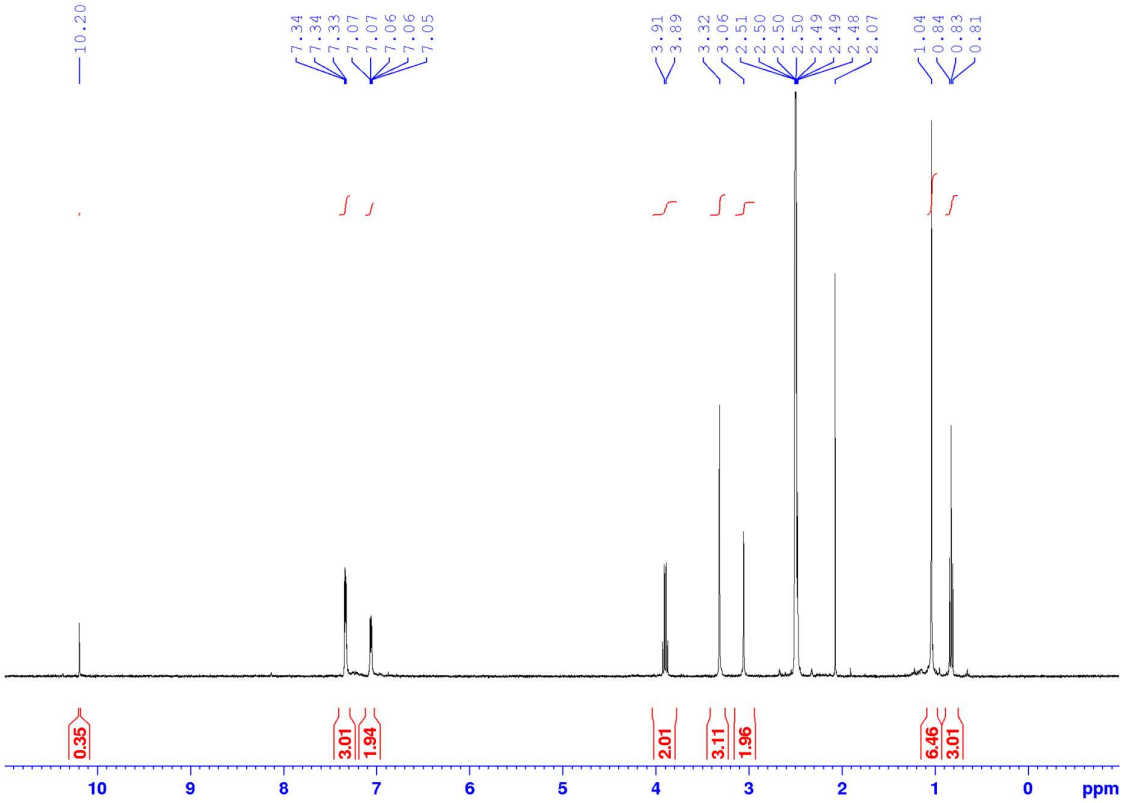

Figure 11: ^{1}H-NMR spectra of the reaction mixture after stirring substrate **2d** with **CTF-Pyr**, in acetonitrile, under irradiation for 24 hours. Next to signals originating from the product and the solvent (DMSO), residual CH_3CN is visible at 2.07 ppm, H_2O at 3.32 ppm and, importantly, H_2O_2 at 10.20 ppm.[702,703]

To determine whether **CTF-Pyr** is thermodynamically able to perform the required photoredox reactions the energy band structure of **CTF-Pyr** was determined and the oxidation potentials of a range of substrates were measured. The energy level of the valence band (VB) of **CTF-Pyr** was calculated from the oxidation onset potential as determined by cyclic voltammetry (Figure 12a-b). Using the obtained values for the VB the energy level of the conduction band (CB) is then calculated using the equation $E_{CB} = E_{VB} - E_g$,[519] resulting in a E_{CB} = -0.81 V (vs. NHE) and E_{VB} = 1.08 V (vs. NHE) (Figure 12c). The reduction potential of O_2 is 0.62 V (vs. NHE),[520] indicating the ability of **CTF-Pyr** to reduce oxygen to the superoxide radical anion ($O_2^{-\bullet}$). The measured oxidation potentials of the substrates ranged from 1.36 V to 1.64 V (vs. NHE, Figure 13) and are clearly higher than the oxidation potential of **CTF-Pyr**. However, the superoxide radical anion is capable of deprotonating dihydropyridines, hereby forming their corresponding anions, which possess a lowered oxidation potential by ~1 V,[704] thus falling in range of the oxidation potential of **CTF-Pyr**. Moreover, singlet oxygen, a powerful oxidizing agent, is also able to aromatize dihydropyridines to the corresponding pyridines.[705,706] The ability of **CTF-Pyr** to produce activated forms of oxygen, i.e. $O^{-\bullet}$ and $^{1}O_2$ was confirmed by EPR-spectroscopy. By stirring 5,5-dimethyl-1-pyrroline-*N*-oxide (DMPO) under air and irradiation with visible light, the generation of DMPO-superoxide adducts was demonstrated in the resulting EPR spectrum (Figure 14a).[707] Similarly, using 2,2,6,6-tetramethylpiperidine (TEMP) as a spin trap, the generation of singlet oxygen was confirmed, as the free radical TEMPO was generated (Figure 14b).[708,709]

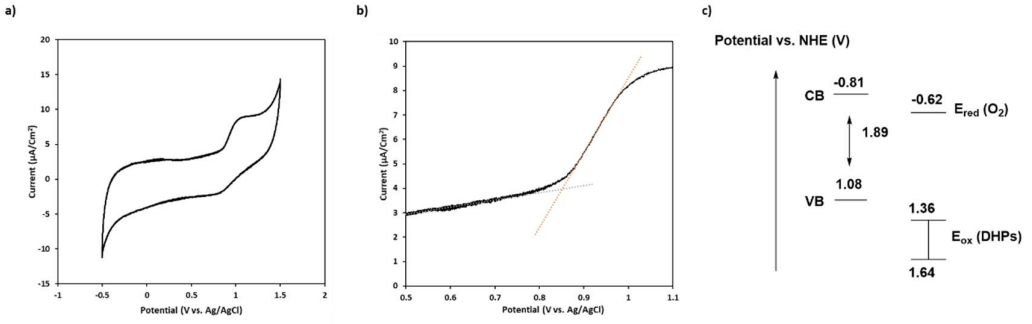

Figure 12: (a) Cyclic voltammogram (CV); (b) Inset of the CV used to calculate the energy level of the VB; (c) Band structure of **CTF-Pyr**.

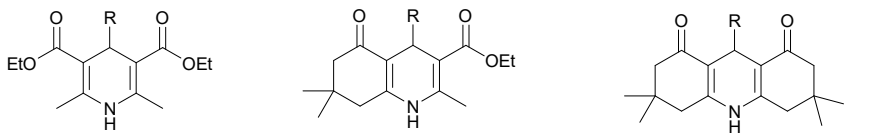

2a: R = Ph, E_{ox} = 0.73 V
2b: R = 4-ClPh, E_{ox} = 0.79 V
2c: R = 4-MeOPh, E_{ox} = 0.81 V

2d: R = Ph, E_{ox} = 0.86 V
2f: R = 4-ClPh, E_{ox} = 0.85 V
2j: R = 4-MeOPh, E_{ox} = 0.80 V
2e: R = 4-NO_2Ph, E_{ox} = 0.96 V

xxl: R = Ph, E_{ox} = 0.96 V
2m: R = 4-ClPh, E_{ox} = 0.96 V
2n: R = 4-MeOPh, E_{ox} = 1.01 V

Figure 13: The measured oxidation potential for a range of substrates. 1,4-Dihydropyridines **2a-c** possess the lowest oxidation potentials, followed by the tetrahydroquinoline-5-ones **2d,k,f,e** and finally the hexahydroacridine-1,8-diones **2l,n,o** which are the hardest to oxidize. The values were measured relative to ferrocene (Fc), to convert these to the NHE, 0.63 V is added[710] resulting in oxidation potentials ranging from 1.36-1.64 V (vs. NHE).

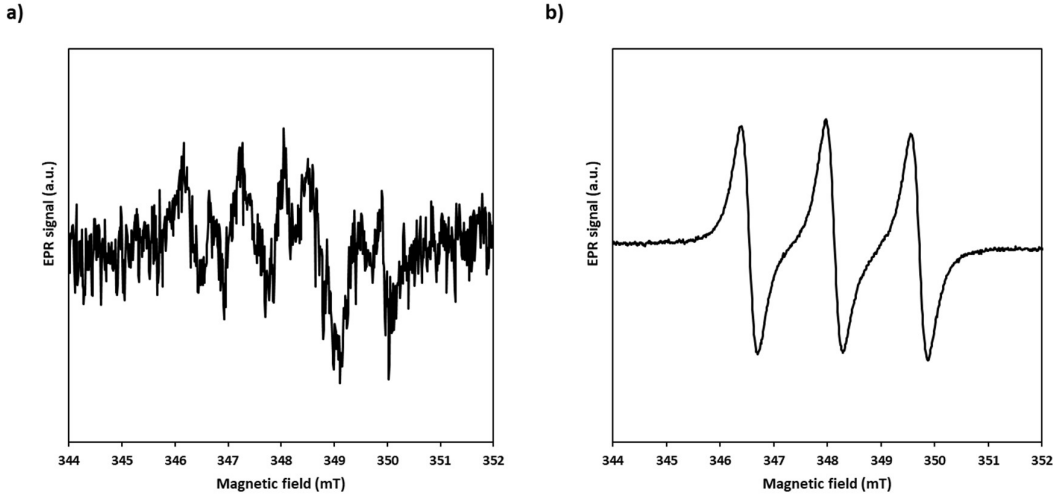

Figure 14: (a) EPR spectrum of DMPO-$O^{-\bullet}$ and (e) TEMPO produced by **CTF-Pyr** under light irradiation.

Based on these experiments and on previous literature reports, [686,704,711,712] the following mechanism was proposed (Scheme 11). Under irradiation, the electrons in the CTF will be excited, resulting in a transfer of electrons from the valence band to the conduction band. These excited electrons will reduce oxygen to the superoxide radical via single electron transfer (SET). This superoxide radical will then deprotonate the dihydropyridine **2** to its corresponding anion **20**, which is oxidized at the photogenerated holes to form radical **21**. The formed hydroperoxyl radical (HOO•) abstracts the hydrogen atom in the 4 position, generating the pyridine product **3** and hydrogen peroxide. The hydrogen peroxide side product is also able to act as an oxidizing agent in this reaction.[713] Next to the route mediated by the superoxide radical, photogenerated singlet oxygen also plays a role in this transformation. Singlet oxygen can be generated in two ways, either via a direct energy transfer from the CTF to oxygen[568–572] or via one electron oxidation of the superoxide radical.[573] Singlet oxygen is able to react with the dihydropyridine **2** via an ene reaction, producing the intermediary hydroperoxyl compound **22**, which then loses hydrogen peroxide to form the pyridine product **3**.[705,706]

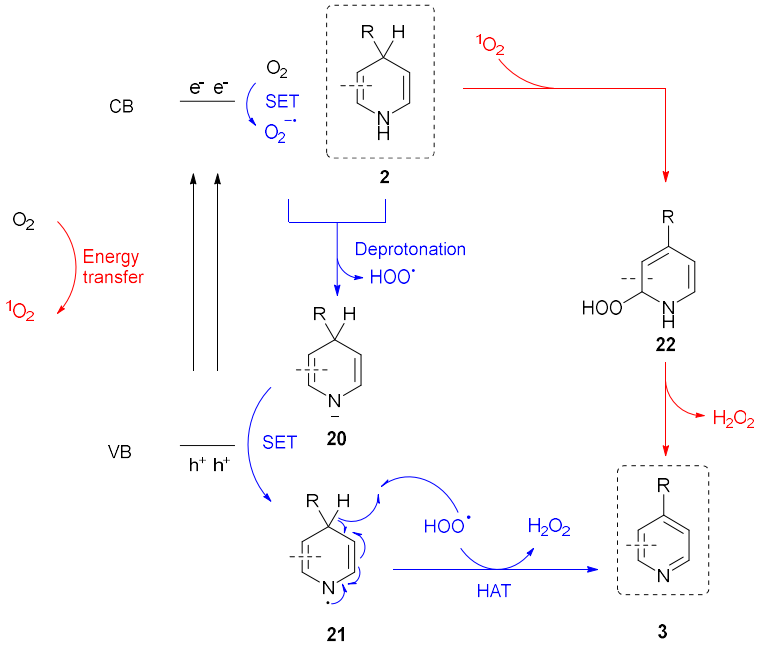

Scheme 11: Proposed mechanism for the **CTF-Pyr** catalyzed photooxidation of dihydropyridines.

Finally, recycling experiments were performed, to examine the stability of the catalyst. Whilst the second and third run still gave conversions of 96% and 91% after 24 hours, the conversion dropped in the fourth run, and only 59% conversion was reached. When prolonging the reaction time to 48 hours, 91% conversion was again reached (Figure 15a). This loss in activity has been observed for many photoactive POPs, and in most cases it is attributed to photobleaching, *i.e.* deactivation by reaction with reactive oxygen species (ROS).[347,374,514,520,578,579] In the FTIR spectrum of the recycled material new absorptions around 1701 cm^{-1}, typical for carbonyl functionalities, are observed, probably due to oxidation of the methylidene bridges which were formed by crosslinking with CH_2Cl_2 (Figure 15b). As such, future improvements should focus on the synthesis of similar materials under solvent-free conditions,[669] avoiding the oxidation prone methylidene crosslinks.

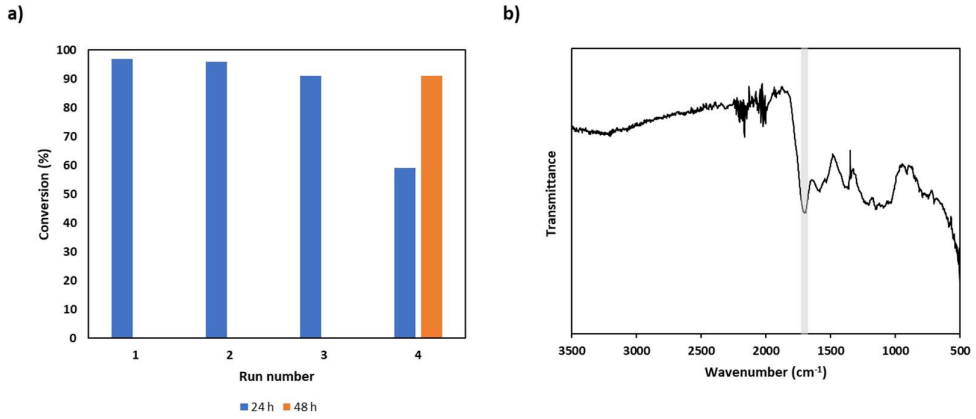

Figure 15: (a) Yields of the recycling experiments. After three runs a yield of 91% was still achieved. However, in the fourth run a longer reaction time (48 h) was needed to achieve a high conversion (91%). (b) FT-IR spectra of **CTF-Pyr** after four runs, new absorptions originating from carbonyl moieties can clearly be seen.

3.3 Conclusion

In summary, we studied the photocatalytic application of POPs made by Lewis acid catalyzed alkylation or crosslinking/Scholl coupling of simple, unfunctionalized aromatic building blocks. Four aromatic building blocks: fluorene, pyrene, truxene and hexamethyltruxene were polymerized through $AlCl_3$ catalyzed alkylation with cyanuric chloride. Surprisingly, in the case of truxene and hexamethyltruxene the materials were mainly formed through self-condensation, but in the case of fluorene and truxene true CTFs were formed. While the Lewis acid catalyzed CTF synthesis is an attractive method, it does have limitations that were previously undescribed. Not every electron rich aromatic building block reacted with cyanuric chloride, which was unexpected. Scholl coupling and the formation of methylene bridges by reaction with dichloromethane were side reactions that were not acknowledged in earlier literature. To study this more, another series of materials were made solely through crosslinking of aromatics with CH_2Cl_2/Scholl coupling, without cyanuric chloride present.

All synthesized materials were evaluated as catalysts for the aromatization of *N*-heterocycles. **CTF-Pyr**, containing both photoactive pyrene and triazine moieties was the most effective photocatalyst, once again proving the beneficial effects of triazine and pyrene moieties in the construction of effective photocatalysts. Using this material a wide range of 21 *N*-heterocycles including pyridines, dihydroquinoline-5-ones, tetrahydroacridine-1,8-diones and pyrazoles were made in good to excellent yields (70-99%). Mechanistic investigation point to the importance of both photogenerated singlet oxygen and the superoxide anion. These photocatalytic aromatizations were carried out under exceptionally mild conditions, at room temperature and under air.

The materials described in this chapter were new (except for **CTF-Fl** and **pHMTrux**), and provide more insights into POP synthesis, especially in the case of the Lewis acid catalyzed CTF synthesis (**CTF-Fl** and **CTF-Pyr**). **CTF-Pyr** is the first CTF synthesized by Friedel-Crafts alkylation to be used as a photocatalyst, and is one of the first heterogeneous catalysts for the aromatization of dihydropyridines and pyrazolines. The results described in this chapter further develop these easily synthesized porous organic materials as a new class of heterogeneous photocatalysts, paving the way for a greener chemical industry.

3.4 Experimental

3.4.1 General procedures

Unless stated otherwise all reagents and solvents were purchased from commercial sources and used without further purification. Dichloromethane and tetrahydrofuran were dried using the MBraun SPS-800 solvent purification system. The acetonitrile for the electrochemical measurements of the CTF was dried with 3Å molecular sieves 72 hours prior to use and stored under argon.

IR spectra of the materials and compounds were measured in neat form using a Shimadzu IRAffinity1S WL FTIR spectrophotometer. Nitrogen adsorption-desorption isotherms were obtained with a Micromeritics® Tristar II, after activating the samples at 120 °C under vacuum overnight. Pore size distributions were calculated from N_2 sorption isotherms using quenched solid density functional theory (QSDFT) on the adsorption branch, assuming cylindrical pores. The elemental analysis was performed using a Thermo Flash 2000 analyser. The powder X-ray diffraction (PXRD) spectra were measured with a Bruker D8 Advance spectrometer using a copper Kα radiation source (λ = 1.54056 Å) at 40 kV and 45 Ma with 1 °/s scanning speed. The UV-Vis absorption spectra were recorded in solid-state on a Perkin Elmer Lambda 1050 UV-Vis-NIR spectrophotometer. Photoelectrochemical measurements were performed by dispersing 2 mg of the material in 1 mL *i*PrOH containing 5 wt% Nafion®, dropcasting 50 µL of this dispersion on a glassy carbon electrode (0.197 cm^2) and drying this in an oven at 120°C. CV curves were recorded on a Bio-logic VSP electrochemical workstation in a three electrode setup with the coated glassy carbon as the working electrode, Pt coil as counter electrode and a leak-free Ag/AgCl electrode as the reference electrode. The experiments were carried out in anhydrous acetonitrile with 1 M tetra-n-butylammonium hexafluorophosphate ($TBAPF_6$) as the supporting electrolyte at a scan rate of 20 mV s^{-1}. A Bio-Logic SP50 potentiostat was used for the cyclic voltammetry experiments to determine the oxidation potential of a set of substrates. A Varian E-line spectrometer, equipped with a HP 5342A microwave frequency counter, was used to record the EPR spectra. The magnetic fields were calibrated using the diphenyl picryl hydrazyl spectrum (g = 2.0036). The spectra were obtained by illuminating a stirred suspension of **CTF-Pyr** (3.75 mg) in 0.75 mL of a 200 mM spin trap solution (DMPO or TEMP) for 15 minutes. XPS was used to investigate the chemical composition of the surface of the materials, using the PHI 5000 VersaProbe II spectrometer. This was equipped with a monochromatic Al Kα X-ray source (hν = 1486.6 eV) operating with a beam diameter of 200 µm at 50 W. All measurements were taken using an angle of 45° between the beam and the sample and under a pressure of 10^{-6} Pa or less. The binding energies were calibrated with respect to the C-C/C-H peak of the C 1s spectrum at 285.0 eV. Survey scans and high-resolution spectra were analyzed using Multipak (v 9.6.1) software. The high-resolution spectra were deconvoluted as Gaussian-Lorentzian peaks to identify the corresponding chemical bonds. A Bruker Avance III HD-400 spectrophotometer was used to measure ^{1}H-NMR and ^{13}C-NMR spectra at 400 and 100 MHz, respectively, using a 1H/BB z-gradient probe (BBO, 5 mm). The spectra were acquired using standard sequences available in the Bruker pulse program library and further processed using TOPSPIN 4.1. The HPLC used was an Agilent 1200 series HPLC system fitted with an Ascentis® Express C18 column (particle size 2.7 µm, length 30 mm, internal diameter 4.6 mm). A mixture of acetonitrile/water (5 mM NH_4OAc) was used as the eluent. As detectors for the HPLC a UV-Vis detector and an Agilent 1100 series LC/MSD-type SL mass spectrometer (ESI, 4000 V) using a mass-selective single quadrupole were used. Thin layer chromatography (TLC) was used to determine suitable solvent systems for chromatography, using glass-backed 0.25-mm Merck silica gel 60 F254 TLC plates, and visualized under UV light (254 nm). The chromatography itself was done using glass columns and silica gel (particle size

35-70 µm, pore diameter 6 nm) or on a Büchi Reveleris® X2 flash chromatography system (normal phase) or Grace Reveleris® X1 flash chromatography system (reversed phase), using prepacked Reveleris® silica or Reveleris® C18 cartridges.

3.4.2 Synthesis of building blocks and substrates

3.4.2.1 Synthesis of Truxene and Hexamethyltruxene

Truxene was prepared according to a literature procedure.[660] 1-Indanone **1** (5.5 g, 41.6 mmol, 1 eq.) was added to a mixture of acetic acid (30 mL) and concentrated (37%) hydrochloric acid (30 mL). This solution was stirred for 24 hours at 100 °C, allowed to cool to room temperature and then poured into ice water (400 mL). This was stirred for one hour, and the resulting principate was filtered and washed with water, EtOH and CH_2Cl_2 to give the product **Trux** as a white powder (3.926 g, 83%).

10,15-Dihydro-5*H*-diindeno[1,2-*a*:1',2'-*c*]fluorene Trux

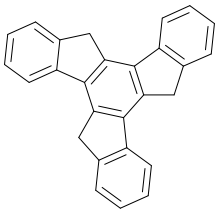

^{1}H-NMR (400 MHz, $CDCl_3$): δ 4.30 (6H, s, 3 x CH_2); 7.40 (3H, ~t, *J* = 7.3 Hz, 3 x CH_{arom}), 7.51 (3H, ~t, *J* = 7.4 Hz, 3 x CH_{arom}), 7.71 (3H, d, *J* = 7.4 Hz, 3 x CH_{arom}), 7.97 (3H, d, *J* = 7.6 Hz, 3 x CH_{arom}). **^{13}C-NMR** (100 MHz, $CDCl_3$): δ 36.7 (3 x CH_2); 122.1 (3 x CH_{arom}); 125.3 (3 x CH_{arom}); 126.5 (3 x CH_{arom}); 127.1 (3 x CH_{arom}); 135.4 (3 x $C_{arom,quat}$); 137.3 (3 x $C_{arom,quat}$); 141.9 (3 x $C_{arom,quat}$); 144.0 (3 x $C_{arom,quat}$). **IR** (ATR, cm^{-1}): ν_{max} = 2982, 2882, 1472, 1389, 1348, 1026, 775, 733, 669, 419. White powder, 83%. Spectral data matched literature.[660]

Hexamethyltruxene was prepared according to a literature procedure.[661] Truxene **Trux** (0.76 g, 2.2 mmol, eq.) was dissolved in 60 mL dry THF and *t*BuOK (5.00 g, 44.6 mmol, 20 eq.) were mixed in dry THF (60 mL) under argon. This was cooled in an ice bath and 2.05 mL methyl iodide (4.68 g, 33 mmol, 15 eq.) was slowly added, after which the reaction was allowed to reflux overnight. After cooling to room temperature the solvent was evaporated and water (50 mL) and CH_2Cl_2 (50 mL) were added. The layers were separated and the organic layer was further washed with brine (50 mL). The extract was then evaporated and purified using column chromatography (SiO_2, hexane/CH_2Cl_2: 15/85), giving the product **HMTrux** as a white solid (412 mg, 66%).

5,5,10,10,15,15-Hexamethyl-10,15-dihydro-5*H*-diindeno[1,2-*a*:1',2'-*c*]fluorene HMTrux

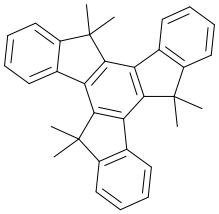

^{1}H-NMR (400 MHz, $CDCl_3$): δ 1.89 (18H, s, 6 x CH_3); 7.37-7.45 (6H, m, 6 x CH_{arom}), 7.55 (3H, d, *J* = 7.0 Hz, 3 x CH_{arom}), 8.31 (3H, d, *J* = 7.4 Hz, 3 x CH_{arom}). **^{13}C-NMR** (100 MHz, $CDCl_3$): δ 24.2 (6 x CH_3); 47.0 (3 x $\underline{C}_{quat}CH_3$); 122.6 (3 x CH_{arom}); 125.8 (3 x CH_{arom}); 126.4 (3 x CH_{arom}); 126.9 (3 x CH_{arom}); 135.8 (3 x $C_{arom,quat}$); 136.9 (3 x $C_{arom,quat}$); 148.4 (3 x $C_{arom,quat}$); 157.7 (3 x $C_{arom,quat}$). **IR** (ATR, cm^{-1}): ν_{max} = 2995, 2992, 2864, 1383, 1362, 1155, 1032, 739, 575, 486. White solid, 66%. Spectral data matched literature.[661]

3.4.2.2 Synthesis of dihydropyridines, tetrahydroquinoline-5-ones and hexahydroacridine-1,8-diones

The synthesis of the compounds **2a-o** was performed by Nathan Raeymackers and are described in more detail in his Master thesis.[648] The procedures written are given as representative examples of the synthesis of a tetrahydroquinoline-5-one. For the synthesis of the 1,4-dihydropyridines **2a-c** or hexahydroacridine-1,8-diones **2l-2o** two equivalents of respectively ethyl acetoacetate **17** or dimedone **18** were used.

Procedure 1 (KH_2PO_4): compounds **2d-g** and **2k-o**[696]

In a 25 ml round bottom flask the aromatic aldehyde **16** (3 mmol, 1 eq.), dimedone **18** (420 mg, 3 mmol, 1 eq.), ethyl acetoacetate **17** (390 mg, 3 mmol, 1 eq.), ammonium acetate (432 mg, 6 mmol, 2 eq.) and potassium dihydrogen phosphate (21 mg, 0.15 mmol, 0.05 eq.) were dissolved in an EtOH/H_2O mixture (3/1, 6 mL). The reaction was refluxed until maximum conversion was achieved (one to eight hours, ^{1}H-NMR). Subsequently, cold water was added to the reaction mixture. The product **2** precipitates and can be filtered off. If needed, the crude product can be recrystallized in ethanol.

Procedure 2 (choline chloride): compounds **2a-c** and **2h-j**[695]

In a 25 ml round bottom flask the aldehyde **16** (3 mmol, 1 eq.), dimedone **18** (420 mg, 3 mmol, 1 eq.), ethyl acetoacetate **17** (390 mg, 3 mmol, 1 eq.), ammonium acetate (347 mg, 4.5 mmol, 1.5 eq.) and choline chloride (21 mg, 0.15 mmol, 0.05 eq.) were dissolved in EtOH (7 mL). The reaction was refluxed until maximum conversion was achieved (one to eight hours, ^{1}H-NMR). Subsequently, cold water was added to the reaction mixture. If solids precipitated, these were filtered off. Otherwise, the crude mixture was extracted with saturated $NaHCO_3$ and ethyl acetate. To purify the crude product **2**, it was recrystallized in acetone, ethyl acetate or ethanol.

Compounds **2a-n**, with exception of the pentan-3-yl substituted tetrahydroquinoline-5-one **2h**, were already described in the literature,[695,696,714–718] but in general $CDCl_3$ was used as the solvent for NMR analysis. In this work DMSO-d_6 was used, as it generally was a better solvent for these products.

Diethyl 2,6-dimethyl-4-phenyl-1,4-dihydropyridine-3,5-dicarboxylate 2a

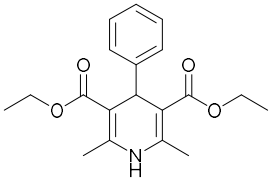

^{1}H-NMR (400 MHz, DMSO-d_6): δ 1.13 (6H, t, J = 7.1 Hz, 2 x $OCH_2C\underline{H}_3$); 2.28 (6H, s, 2 x $NHC_{quat}C\underline{H}_3$); 3.94-4.04 (4H, m, 2 x $OC\underline{H}_2CH_3$); 4.87 (1H, s, $C\underline{H}C_{arom,quat}$); 7.09 (1H, m, CH_{arom}); 7.14-7.24 (4H, m, 4 x CH_{arom}); 8.80 (1H, s, NH). **^{13}C-NMR** (100.6 MHz, DMSO-d_6): δ 14.6 (2 x $OCH_2\underline{C}H_3$); 18.7 (2 x $NHC_{quat}\underline{C}H_3$); 39.4 ($\underline{C}HC_{arom,quat}$); 59.4 (2 x $O\underline{C}H_2CH_3$); 102.3 (2 x $\underline{C}_{quat}CO$); 126.3 (CH_{arom}); 127.8 (2 x CH_{arom}); 128.3 (2 x CH_{arom}); 145.8 (2 x $NH\underline{C}_{quat}CH_3$); 148.7 ($C_{arom,quat}$); 167.4 (2 x C=O). **IR** (ATR, cm^{-1}): ν_{max} = 3339, 1686, 1649, 1487, 1207, 1090, 1032, 1018, 766, 702. **MS** (ESI): m/z (%) 330 ($[M+1]^+$, 100). Yellow crystals, 36%.

Diethyl 4-(4-chlorophenyl)-2,6-dimethyl-1,4-dihydropyridine-3,5-dicarboxylate 2b

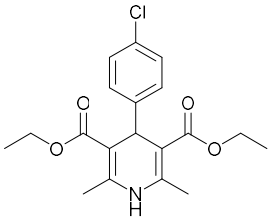

^{1}H-NMR (400 MHz, DMSO-d_6): δ 1.13 (6H, t, J = 7.1 Hz, 2 x $OCH_2C\underline{H}_3$); 2.27 (6H, s, 2 x $NHC_{quat}C\underline{H}_3$); 3.94-4.05 (4H, m, 2 x $OC\underline{H}_2CH_3$); 4.87 (1H, s, $CHC_{arom,quat}$); 7.16 (2H, d_{AB}, J = 8.4 Hz, 2 x CH_{arom}); 7.25 (2H, d_{AB}, J = 8.4 Hz, 2 x CH_{arom}); 8.86 (1H, s, NH). **^{13}C-NMR** (100.6 MHz, DMSO-d_6): δ 14.6 (2 x $OCH_2\underline{C}H_3$); 18.7 (2 x $NHC_{quat}\underline{C}H_3$); 39.1 ($\underline{C}HC_{arom,quat}$); 59.5 (2 x $O\underline{C}H_2CH_3$); 102.0 (2 x $\underline{C}_{quat}CO$); 128.3 (2 x CH_{arom}); 129.7 (2 x CH_{arom}) 130.9 ($C_{arom,quat}$); 146.1 (2 x $NH\underline{C}_{quat}CH_3$); 147.6 ($C_{arom,quat}$); 167.2 (2 x C=O). **IR** (ATR, cm^{-1}): ν_{max} = 3354, 1694, 1649, 1485, 1371, 1209, 1117, 1088, 1049, 1015. **MS** (ESI): m/z (%) 364 ([M+1]$^+$, 100); 366 ([M+1]$^+$, 38). Yellow crystals, 36%.

Diethyl 4-(4-methoxyphenyl)-2,6-dimethyl-1,4-dihydropyridine-3,5-dicarboxylate 2c

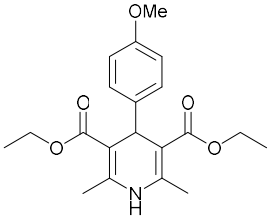

^{1}H-NMR (400 MHz, DMSO-d_6): δ 1.14 (6H, t, J = 7.1 Hz, 2 x $OCH_2C\underline{H}_3$); 2.25 (6H, s, 2 x $NHC_{quat}C\underline{H}_3$); 3.68 (3H, s, OCH_3); 3.94-4.04 (4H, m, 2 x $OC\underline{H}_2CH_3$); 4.80 (1H, s, $CHC_{arom,quat}$); 6.76 (2H, d, J = 8.6 Hz, CH_{arom}); 7.05 (2H, d, J = 8.6 Hz, CH_{arom}); 8.75 (1H, s, NH). **^{13}C-NMR** (100.6 MHz, DMSO-d_6): δ 14.7 (2 x $OCH_2\underline{C}H_3$); 18.7 (2 x $NHC_{quat}\underline{C}H_3$); 38.4 ($\underline{C}HC_{arom,quat}$); 55.3 ($OCH_3$); 59.4 (2 x $O\underline{C}H_2CH_3$); 102.6 (2 x $\underline{C}_{quat}CO$); 113.7 (2 x CH_{arom}); 128.8 (2 x CH_{arom}); 141.0 ($C_{arom,quat}$); 145.4 (2 x $NH\underline{C}_{quat}CH_3$); 158.0 ($C_{arom,quat}$); 167.5 (2 x C=O). **IR** (ATR, cm^{-1}): ν_{max} = 3339, 1688, 1647, 1489, 1207, 1173, 1119, 1088, 1030, 1020. **MS** (ESI): m/z (%) 252 ([M – $C_6H_4OCH_3$]$^+$, 100); 360 ([M+1]$^+$, 20). Yellow crystals, 25%.

Ethyl 2,7,7-trimethyl-5-oxo-4-phenyl-1,4,5,6,7,8-hexahydroquinoline-3-carboxylate 2d

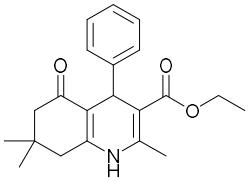

^{1}H-NMR (400 MHz, DMSO-d_6): δ 0.85 (3H, s, $CH_3C_{quat}C\underline{H}_3$); 1.02 (3H, s, $C\underline{H}_3C_{quat}CH_3$); 1.15 (3H, *t*, J = 7.1 Hz, $OCH_2C\underline{H}_3$); 1.98 (1H, d_{AB}, J = 16.2 Hz, $C(\underline{H})HC{=}O$); 2.16 (1H, d_{AB}, J = 16.2 Hz, $C(H)\underline{H}C{=}O$); 2.28 (3H, s, $NHC_{quat}C\underline{H}_3$); 2.29 (1H, d_{AB}, J = 17.1 Hz, $NHC_{quat}C(\underline{H})H$); 2.42 (1H, d_{AB}, J = 17.1 Hz, $NHC_{quat}C(H)\underline{H}$); 3.97 (2H, q, J = 7.1 Hz, $OC\underline{H}_2CH_3$); 4.86 (1H, s, $CHC_{arom,quat}$); 7.06 (1H, m, CH_{arom}); 7.17 (4H, m, 4 x CH_{arom}); 9.06 (1H, s, NH). **^{13}C-NMR** (100.6 MHz, DMSO-d_6): δ 14.6 ($OCH_2\underline{C}H_3$); 18.8 ($NHC_{quat}\underline{C}H_3$); 26.9 ($CH_3C_{quat}\underline{C}H_3$); 29.6 ($\underline{C}H_3C_{quat}CH_3$); 32.6 ($CH_3\underline{C}_{quat}CH_3$); 36.3 ($\underline{C}HC_{arom,quat}$); 39.9 ($NHC_{quat}\underline{C}H_2$); 50.7 ($\underline{C}H_2C{=}O$); 59.5 ($O\underline{C}H_2CH_3$); 104.1 ($\underline{C}_{quat}C(O)O$); 110.5 ($\underline{C}_{quat}C(O)CH_2$); 126.2 ($CH_{arom}$); 127.9 (2 x CH_{arom}); 128.2 (2 x CH_{arom}); 145.5 ($NH\underline{C}_{quat}CH_3$); 148.1 ($\underline{C}_{arom,quat}$); 150.0 ($CH_2\underline{C}_{quat}NH$); 167.4 (OC=O); 194.8 ($CH_2\underline{C}{=}O$). **IR** (ATR, cm^{-1}): ν_{max} = 3283, 1697, 1609, 1479, 1379, 1366, 1207, 1069, 696, 529. **MS** (ESI): m/z (%) 340 ([M+1]$^+$, 100). Yellow crystals, 86%.

Ethyl 2,7,7-trimethyl-4-(4-nitrophenyl)-5-oxo-1,4,5,6,7,8-hexahydroquinoline-3-carboxylate 2e

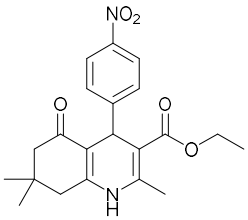

^{1}H-NMR (400 MHz, DMSO-d_6): δ 0.82 (3H, s, $CH_3C_{quat}C\underline{H}_3$); 1.01 (3H, s, $C\underline{H}_3C_{quat}CH_3$); 1.11 (3H, t, J = 7.0 Hz, $OCH_2C\underline{H}_3$); 1.98 (1H, d_{AB}, J = 16.0 Hz, $C(\underline{H})HC{=}O$); 2.19 (1H, d_{AB}, J = 16.0 Hz, $C(\underline{H})HC{=}O$); 2.32 (1H, d_{AB}, J = 17.1 Hz, $NHC_{quat}C(\underline{H})H$); 2.33 (3H, s, $NHC_{quat}C(H)\underline{H}$); 2.44 (1H, d_{AB}, J = 17.1 Hz, $NHC_{quat}C(H)\underline{H}$); 3.97 (2H, q, J = 7.0 Hz, $OC\underline{H}_2CH_3$); 4.98 (1H, s, $CHC_{arom,quat}$); 7.42 (2H, d, J = 8.1 Hz, 2 x CH_{arom}); 8.10 (2H, d, J = 8.1 Hz, 2 x CH_{arom}); 9.23 (1H, s, $N\underline{H}$). **^{13}C-NMR** (100.6 MHz, DMSO-d_6): δ 14.6 ($OCH_2\underline{C}H_3$); 18.8 ($NHC_{quat}\underline{C}H_3$); 27.0 ($CH_3C_{quat}\underline{C}H_3$); 29.5 ($\underline{C}H_3C_{quat}CH_3$); 32.6 ($CH_3\underline{C}_{quat}CH_3$); 37.1 ($\underline{C}HC_{arom,quat}$); 39.9 ($NHC_{quat}\underline{C}H_2$); 50.5 ($\underline{C}H_2C{=}O$); 59.7 ($O\underline{C}H_2CH_3$); 102.8 ($\underline{C}_{quat}C(O)O$); 109.5 ($\underline{C}_{quat}C(O)CH_2$); 123.6 (2 x CH_{arom}); 129.2 (2 x CH_{arom}); 146.2 ($C_{arom,quat}$); 146.6 ($NH\underline{C}_{quat}CH_3$); 150.6 ($CH_2\underline{C}_{quat}NH$); 155.4 ($C_{arom,quat}$); 166.9 (OC=O); 194.7

($CH_2\underline{C}$=O). **IR** (ATR, cm^{-1}): ν_{max} = 1701, 1605, 1489, 1342, 1211, 1150, 1107, 1070, 829, 532. **MS** (ESI): m/z (%) 385 ($[M+1]^+$, 100). Yellow crystals, 82%.

Ethyl 4-(4-chlorophenyl)-2,7,7-trimethyl-5-oxo-1,4,5,6,7,8-hexahydroquinoline-3-carboxylate 2f

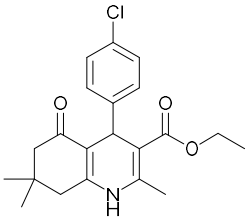

^{1}H-NMR (400 MHz, DMSO-d_6): δ 0.83 (3H, s, $CH_3C_{quat}C\underline{H}_3$); 1.01 (3H, s, $C\underline{H}_3C_{quat}CH_3$); 1.12 (3H, t, *J* = 6.9 Hz, $OCH_2C\underline{H}_3$); 1.98 (1H, d_{AB}, *J* = 16.1 Hz, C(H)$\underline{H}$C=O); 2.16 (1H, d_{AB}, *J* = 16.1 Hz, C($\underline{H}$)HC=O); 2.28 (1H, d_{AB}, *J* = 17.1 Hz, $NHC_{quat}C(\underline{H})H$); 2.30 (3H, s, $NHC_{quat}C\underline{H}_3$); 2.42 (1H, d_{AB}, *J* = 17.1 Hz, $NHC_{quat}C(H)\underline{H}$); 3.97 (2H, q, *J* = 6.9 Hz, $OC\underline{H}_2CH_3$); 4.85 (1H, s, $CHC_{arom,quat}$); 7.16 (2H, d_{AB}, *J* = 7.9 Hz, 2 x CH_{arom}); 7.25 (2H, d_{AB}, *J* = 7.9 Hz, 2 x CH_{arom}); 9.13 (1H, s, N$\underline{H}$). **^{13}C-NMR** (100.6 MHz, DMSO-d_6): δ 14.6 ($OCH_2\underline{C}H_3$); 18.8 ($NHC_{quat}\underline{C}H_3$); 26.9 ($CH_3C_{quat}\underline{C}H_3$); 29.6 ($\underline{C}H_3C_{quat}CH_3$); 32.6 ($CH_3\underline{C}_{quat}CH_3$); 36.1 ($\underline{C}HC_{arom,quat}$); 39.8 ($NHC_{quat}\underline{C}H_2$); 50.6 ($\underline{C}H_2C$=O); 59.6 ($O\underline{C}H_2CH_3$); 103.6 ($\underline{C}_{quat}C(O)O$); 110.1 ($\underline{C}_{quat}C(O)CH_2$); 128.2 (2 x CH_{arom}); 129.8 (2 x CH_{arom}); 130.7 ($C_{arom,quat}$); 145.9 ($NH\underline{C}_{quat}CH_3$); 147.0 ($C_{arom,quat}$); 150.1 ($CH_2\underline{C}_{quat}NH$); 167.1 (OC=O); 194.7 ($CH_2\underline{C}$=O). **IR** (ATR, cm^{-1}): ν_{max} = 1705, 1603, 1487, 1379, 1279, 1211, 1190, 1070, 534. **MS** (ESI): m/z (%) 374 ($[M+1]^+$, 100); 376 ($[M+1]^+$, 34). Yellow crystals, 99%.

Ethyl 4-(benzo[d][1,3]dioxol-5-yl)-2,7,7-trimethyl-5-oxo-1,4,5,6,7,8-hexahydroquinoline-3-carboxylate 2g

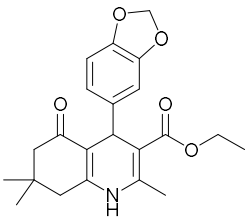

^{1}H-NMR (400 MHz, DMSO-d_6): δ 0.87 (3H, s, $CH_3C_{quat}C\underline{H}_3$); 1.01 (3H, s, $C\underline{H}_3C_{quat}CH_3$); 1.15 (3H, t, *J* = 7.0 Hz, $OCH_2C\underline{H}_3$); 2.00 (1H, d_{AB}, *J* = 16.1 Hz, C($\underline{H}$)HC=O); 2.17 (1H, d_{AB}, *J* = 16.1 Hz, C(H)$\underline{H}$C=O); 2.28 (3H, s, $NHC_{quat}C\underline{H}_3$); 2.30 (1H, d_{AB}, *J* = 17.1 Hz, $NHC_{quat}C(\underline{H})H$); 2.40 (1H, d_{AB}, *J* = 17.1 Hz, $NHC_{quat}C(H)\underline{H}$); 3.99 (2H, q, *J* = 7.0 Hz, $OC\underline{H}_2CH_3$); 4.78 (1H, s, $CHC_{arom,quat}$); 5.90 (1H, s, $OC\underline{H}_2O$); 5.92 (1H, s, $OC\underline{H}_2O$); 6.56-6.77 (3H, m, $C\underline{H}_{arom}$); 9.04 (1H, s, N$\underline{H}$). **^{13}C-NMR** (100.6 MHz, DMSO-d_6): δ 14.6 ($OCH_2\underline{C}H_3$); 18.8 ($NHC_{quat}\underline{C}H_3$); 27.0 ($CH_3C_{quat}\underline{C}H_3$); 29.5 ($\underline{C}H_3C_{quat}CH_3$); 32.6 ($CH_3\underline{C}_{quat}CH_3$); 36.0 ($\underline{C}HC_{arom,quat}$); 39.9 ($NHC_{quat}\underline{C}H_2$); 50.7 ($\underline{C}H_2C$=O); 59.5 ($O\underline{C}H_2CH_3$); 101.0 ($O\underline{C}H_2O$); 104.2 ($\underline{C}_{quat}C(O)O$); 108.1 ($CH_{arom}$); 108.4 ($CH_{arom}$); 110.5 ($\underline{C}_{quat}C(O)CH_2$); 120.7 ($CH_{arom}$); 142.4 ($C_{arom,quat}$); 145.3 ($NH\underline{C}_{quat}CH_3$); 145.6 ($C_{arom,quat}$); 147.2 ($C_{arom,quat}$); 149.8 ($CH_2\underline{C}_{quat}NH$); 167.3 (OC=O); 194.8 ($CH_2\underline{C}$=O). **IR** (ATR, cm^{-1}): ν_{max} = 1688, 1601, 1485, 1379, 1281, 1231, 1209, 1148, 1070, 1032. **MS** (ESI): m/z (%) 384 ($[M+1]^+$, 100). Yellow crystals, 49%.

Ethyl 2,7,7-trimethyl-5-oxo-4-(pentan-3-yl)-1,4,5,6,7,8-hexahydroquinoline-3-carboxylate 2h

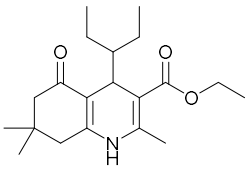

^{1}H-NMR (400 MHz, DMSO-d_6): δ 0.83 (6H, q, *J* = 7.2 Hz, $C\underline{H}_3CH_2CHCH_2C\underline{H}_3$); 0.87-1.17 (5H, m, $CH_3C\underline{H}_2C\underline{H}C\underline{H}_2CH_3$); 1.02 (6H, s, $C\underline{H}_3C_{quat}C\underline{H}_3$); 1.21 (3H, t, *J* = 7.2 Hz, $OCH_2C\underline{H}_3$); 2.05-2.40 (7H, m, $C\underline{H}_2C_{quat}C\underline{H}_2$ and $NHC_{quat}C\underline{H}_3$); 3.80 (1H, m, $C\underline{H}CH(Et)_2$); 4.06 (2H, m, $OC\underline{H}_2CH_3$); 8.84 (1H, s, NH). **^{13}C-NMR** (100.6 MHz, DMSO-d_6): δ 12.5 ($\underline{C}H_3CH_2CHCH_2CH_3$); 12.6 ($CH_3CH_2CHCH_2\underline{C}H_3$); 14.7 ($OCH_2\underline{C}H_3$); 18.5 ($NHC_{quat}\underline{C}H_3$); 21.9 ($CH_3\underline{C}H_2CHCH_2CH_3$); 22.0 ($CH_3CH_2C\underline{H}C\underline{H}_2CH_3$); 26.9 ($CH_3C_{quat}\underline{C}H_3$); 30.0 ($\underline{C}H_3C_{quat}CH_3$); 31.2 ($\underline{C}HCH(Et)_2$); 32.1 ($CH_3\underline{C}_{quat}CH_3$); 40.1 ($NHC_{quat}\underline{C}H_2$); 50.5 ($CH_3CH_2\underline{C}HCH_2CH_3$); 51.1 ($\underline{C}H_2C$=O); 59.4 ($O\underline{C}H_2CH_3$); 102.6 ($\underline{C}_{quat}C(O)O$); 108.6 ($\underline{C}_{quat}C(O)CH_2$); 145.6 ($NH\underline{C}_{quat}CH_3$); 151.7 ($CH_2\underline{C}_{quat}NH$); 168.4 (OC=O); 195.3 ($CH_2\underline{C}$=O). **IR** (ATR, cm^{-1}): ν_{max} = 3285, 3201, 1601, 1477, 1381, 1366, 1169, 1150, 1103, 1070. **MS** (ESI): m/z (%) 334 ($[M+1]^+$, 100). Yellow crystals, 30%.

Ethyl 4-cyclohexyl-2,7,7-trimethyl-5-oxo-1,4,5,6,7,8-hexahydroquinoline-3-carboxylate 2i

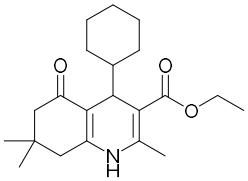

^{1}H-NMR (400 MHz, DMSO-d_6): δ 0.80 (2H, m, $C_{cyclohexyl}\underline{H}_2$); 0.89-1.16 (4H, m, 2 x $C_{cyclohexyl}\underline{H}_2$); 1.03 (6H, s, $C\underline{H}_3C_{quat}C\underline{H}_3$); 1.20 (3H, t, *J* = 7.0 Hz, $OCH_2C\underline{H}_3$); 1.40-1.66 (5H, m, 2 x $C_{cyclohexyl}\underline{H}_2$ and $C_{cyclohexyl}\underline{H}$); 2.05-2.40 (7H, m, $C\underline{H}_2C_{quat}C\underline{H}_2$ and $NHC_{quat}C\underline{H}_3$); 3.80 (1H, m, $C\underline{H}C_{cyclohexyl}$); 4.06 (2H, m, $OC\underline{H}_2CH_3$); 8.87 (1H, s, N<u>H</u>). **^{13}C-NMR** (100.6 MHz, DMSO-d_6): δ 14.8 ($OCH_2\underline{C}H_3$); 18.8 ($NHC_{quat}\underline{C}H_3$); 26.6 ($C_{cyclohexyl}\underline{H}_2$); 26.7 ($C_{cyclohexyl}\underline{H}_2$); 26.8 ($C_{cyclohexyl}\underline{H}_2$); 27.1 ($CH_3C_{quat}\underline{C}H_3$); 29.2 (2 x $C_{cyclohexyl}\underline{H}_2$); 30.0 ($\underline{C}H_3C_{quat}CH_3$); 32.3 ($CH_3\underline{C}_{quat}CH_3$); 34.7 ($\underline{C}HC_{cyclohexyl}$); 40.1 ($NHC_{quat}\underline{C}H_2$); 46.1 ($C_{cyclohexyl}\underline{H}$); 51.0 ($\underline{C}H_2C{=}O$); 59.3 ($O\underline{C}H_2CH_3$); 101.9 ($\underline{C}_{quat}C(O)O$); 108.3 ($\underline{C}_{quat}C(O)CH_2$); 145.8 ($NH\underline{C}_{quat}CH_3$); 151.4 ($CH_2\underline{C}_{quat}NH$); 168.3 (OC=O); 195.3 ($CH_2\underline{C}{=}O$). **IR** (ATR, cm^{-1}): ν_{max} = 1695, 1603, 1479, 1383, 1364, 1211, 1167, 1152, 1092, 1078. **MS** (ESI): m/z (%) 345 ([M+1]$^+$, 100). Yellow crystals, 47%.

Ethyl 2,7,7-trimethyl-5-oxo-4-pentyl-1,4,5,6,7,8-hexahydroquinoline-3-carboxylate 2j

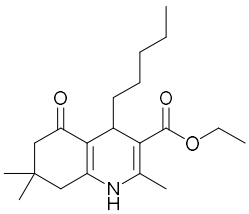

^{1}H-NMR (400 MHz, DMSO-d_6): δ 0.80 (3H, m, $C_{pentyl}\underline{H}_3$); 1.00 (3H, s, $C\underline{H}_3C_{quat}CH_3$); 1.02 (3H, s, $CH_3C_{quat}C\underline{H}_3$); 1.05-1.21 (8H, m, 4 x $C_{pentyl}\underline{H}_2$); 1.20 (3H, *t*, *J* = 7.1 Hz, $OCH_2C\underline{H}_3$); 2.02-2.38 (7H, m, $C\underline{H}_2C_{quat}C\underline{H}_2$ and $NHC_{quat}C\underline{H}_3$); 3.80 (1H, m, $C\underline{H}C_{pentyl}$); 4.07 (2H, m, $OC\underline{H}_2CH_3$); 8.83 (1H, s, N<u>H</u>). **^{13}C-NMR** (100.6 MHz, DSMO-d_6): δ 14.3 ($C_{pentyl}\underline{H}_3$); 14.8 ($OCH_2\underline{C}H_3$); 18.7 ($NHC_{quat}\underline{C}H_3$); 22.6 ($C_{pentyl}\underline{H}_2$); 24.5 ($C_{pentyl}\underline{H}_2$); 26.8 ($CH_3C_{quat}\underline{C}H_3$); 29.7 ($\underline{C}HC_{pentyl}$); 29.9 ($\underline{C}H_3C_{quat}CH_3$); 32.0 ($C_{pentyl}\underline{H}_2$); 32.5 ($CH_3\underline{C}_{quat}CH_3$); 36.5 ($C_{pentyl}\underline{H}_2$); 40.1 ($NHC_{quat}\underline{C}H_2$); 50.9 ($\underline{C}H_2C{=}O$); 59.3 ($O\underline{C}H_2CH_3$); 103.3 ($\underline{C}_{quat}C(O)O$); 109.7 ($\underline{C}_{quat}C(O)CH_2$); 146.0 ($NH\underline{C}_{quat}CH_3$); 151.0 ($CH_2\underline{C}_{quat}NH$); 167.7 (OC=O); 195.0 ($CH_2\underline{C}{=}O$). **IR** (ATR, cm^{-1}): ν_{max} = 1695, 1599, 1479, 1466, 1393, 1385, 1215, 1146, 1092, 1067. **MS** (ESI): m/z (%) 334 ([M+1]$^+$, 100). Yellow crystals, 32%.

Ethyl 4-(4-methoxyphenyl)-2,7,7-trimethyl-5-oxo-1,4,5,6,7,8-hexahydroquinoline-3-carboxylate 2k

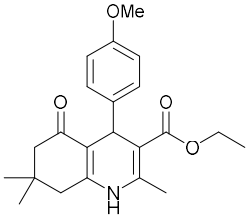

^{1}H-NMR (400 MHz, DMSO-d_6): δ 0.86 (3H, s, $CH_3C_{quat}C\underline{H}_3$); 1.01 (3H, s, $C\underline{H}_3C_{quat}CH_3$); 1.13 (3H, t, *J* = 7.0 Hz, $OCH_2C\underline{H}_3$); 1.97 (1H, d_{AB}, *J* = 16.1 Hz, $C(\underline{H})HC{=}O$); 2.16 (1H, d_{AB}, *J* = 16.1 Hz, $C(H)\underline{H}C{=}O$); 2.27 (3H, s, $NHC_{quat}C\underline{H}_3$); 2.28 (1H, d_{AB}, *J* = 17.0 Hz, $NHC_{quat}C(\underline{H})H$); 2.41 (1H, d_{AB}, *J* = 17.0 Hz, $NHC_{quat}C(H)\underline{H}$); 3.67 (3H, s, $OC\underline{H}_3$); 3.97 (2H, q, *J* = 7.0 Hz, $OC\underline{H}_2CH_3$); 4.79 (1H, s, $CHC_{arom,quat}$); 6.74 (2H, d_{AB}, *J* = 8.5 Hz, CH_{arom}); 7.05 (2H, d_{AB}, *J* = 8.5 Hz, CH_{arom}); 9.02 (1H, s, NH). **^{13}C-NMR** (100.6 MHz, DMSO-d_6): δ 14.6 ($OCH_2\underline{C}H_3$); 18.8 ($NHC_{quat}\underline{C}H_3$); 27.0 ($CH_3C_{quat}\underline{C}H_3$); 29.6 ($\underline{C}H_3C_{quat}CH_3$); 32.6 ($CH_3\underline{C}_{quat}CH_3$); 35.4 ($\underline{C}HC_{arom,quat}$); 39.9 ($NHC_{quat}\underline{C}H_2$); 50.8 ($\underline{C}H_2C{=}O$); 55.3 ($OCH_3$); 59.5 ($O\underline{C}H_2CH_3$); 104.4 ($\underline{C}_{quat}C(O)O$); 110.7 ($\underline{C}_{quat}C(O)CH_2$); 113.6 (2 x CH_{arom}); 128.9 (2 x CH_{arom}); 140.5 ($C_{arom,quat}$); 145.1 ($NH\underline{C}_{quat}CH_3$); 149.7 ($CH_2\underline{C}_{quat}NH$); 157.7 ($C_{arom,quat}$); 167.4 (OC=O); 194.8 ($CH_2\underline{C}{=}O$). **IR** (ATR, cm^{-1}): ν_{max} = 3275, 1699, 1603, 1485, 1377, 1211, 1167, 1070, 1030, 534. **MS** (ESI): m/z (%) 370 ([M+1]$^+$, 100). Yellow crystals, 82%.

3,3,6,6-Tetramethyl-9-phenyl-3,4,6,7,9,10-hexahydroacridine-1,8(2*H*,5*H*)-dione 2l

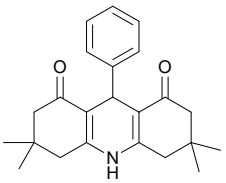

^{1}H-NMR (400 MHz, DMSO-d_6): δ 0.87 (6H, s, 2 x $CH_3C_{quat}C\underline{H}_3$); 1.02 (6H, s, 2 x $C\underline{H}_3C_{quat}CH_3$); 1.99 (2H, d_{AB}, *J* = 16.1 Hz, 2 x C(<u>H</u>)HCO); 2.18 (2H, d_{AB}, *J* = 16.1 Hz, 2 x C(H)<u>H</u>CO); 2.34 (2H, d_{AB}, *J* = 17.1 Hz, 2 x $NHC_{quat}C(\underline{H})H$); 2.45 (2H, d_{AB}, *J* = 17.1 Hz, 2 x $NHC_{quat}C(H)\underline{H}$); 4.82 (1H, s, $CHC_{arom,quat}$); 7.04 (1H, m, CH_{arom}); 7.15 (4H, m, 4 x CH_{arom}); 9.28 (1H, s, NH). **^{13}C-NMR** (100.6 MHz, DMSO-d_6): δ 26.9 (2 x $CH_3C_{quat}\underline{C}H_3$); 29.6 (2 x $\underline{C}H_3C_{quat}CH_3$); 32.6 (2 x $CH_3\underline{C}_{quat}CH_3$); 33.3 ($\underline{C}HC_{arom,quat}$); 40.1 (2 x $NHC_{quat}\underline{C}H_2$); 50.8 (2 x $\underline{C}H_2C{=}O$); 111.9 (2 x $\underline{C}_{quat}C(O)CH_2$); 125.9 ($CH_{arom}$); 128.2 (4 x CH_{arom}); 147.7 ($C_{arom,quat}$); 149.9 (2 x $CH_2\underline{C}_{quat}NH$); 194.8 (2 x C=O). **IR** (ATR, cm^{-1}): ν_{max} = 3279, 1638, 1603, 1476, 1366, 1215, 1138, 700, 557, 517. **MS** (ESI): m/z (%) 350 ($[M+1]^+$, 100). Yellow crystals, 44%.

9-(Benzo[*d*][1,3]dioxol-5-yl)-3,3,6,6-tetramethyl-3,4,6,7,9,10-hexahydroacridine-1,8(2*H*,5*H*)-dione 2m

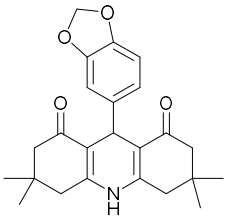

^{1}H-NMR (400 MHz, DMSO-d_6): δ 0.89 (6H, s, 2 x $CH_3C_{quat}C\underline{H}_3$); 1.01 (6H, s, 2 x $C\underline{H}_3C_{quat}CH_3$); 2.01 (2H, d_{AB}, *J* = 16.1 Hz, 2 x C(<u>H</u>)HCO); 2.17 (2H, d_{AB}, *J* = 16.1 Hz, 2 x C(H)<u>H</u>CO); 2.33 (2H, d_{AB}, *J* = 17.1 Hz, 2 x $NHC_{quat}C(\underline{H})H$); 2.44 (2H, d_{AB}, *J* = 17.1 Hz, 2 x $NHC_{quat}C(H)\underline{H}$); 4.73 (1H, s, $C\underline{H}C_{arom,quat}$); 5.90 (2H, s, $OC\underline{H}_2O$); 6.58-6.72 (3H, m, 3 x CH_{arom}); 9.28 (1H, s, NH). **^{13}C-NMR** (100.6 MHz, DMSO-d_6): δ 27.0 (2 x $CH_3C_{quat}\underline{C}H_3$); 29.5 (2 x $\underline{C}H_3C_{quat}CH_3$); 32.6 (2 x $CH_3\underline{C}_{quat}CH_3$); 32.9 ($\underline{C}HC_{arom,quat}$); 40.1 (2 x $NHC_{quat}\underline{C}H_2$); 50.7 (2 x $\underline{C}H_2C{=}O$); 101.0 ($O\underline{C}H_2O$); 107.9 (CH_{arom}); 108.8 (CH_{arom}); 112.0 (2 x $\underline{C}_{quat}C(O)CH_2$); 108.8 ($CH_{arom}$); 120.9 ($CH_{arom}$); 141.9 ($C_{arom,quat}$); 145.4 ($C_{arom,quat}$); 147.0 ($C_{arom,quat}$); 149.5 (2 x $CH_2\underline{C}_{quat}NH$); 194.9 (2 x C=O). **IR** (ATR, cm^{-1}): ν_{max} = 1643, 1601, 1479, 1362, 1221, 1171, 1144, 1125, 1036, 571. **MS** (ESI): m/z (%) 394 ($[M+1]^+$, 100). Yellow crystals, 81%.

9-(4-Chlorophenyl)-3,3,6,6-tetramethyl-3,4,6,7,9,10-hexahydroacridine-1,8(2H,5H)-dione 2n

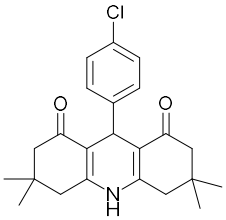

^{1}H-NMR (400 MHz, DMSO-d_6): δ 0.87 (6H, s, 2 x $CH_3C_{quat}C\underline{H}_3$); 1.01 (6H, s, 2 x $C\underline{H}_3C_{quat}CH_3$); 1.99 (2H, d_{AB}, *J* = 16.1 Hz, 2 x C(<u>H</u>)HCO); 2.18 (2H, d_{AB}, *J* = 16.1 Hz, 2 x C(H)<u>H</u>CO); 2.33 (2H, d_{AB}, *J* = 17.1 Hz, 2 x $NHC_{quat}C(\underline{H})H$); 2.46 (2H, d_{AB}, *J* = 17.1 Hz, 2 x $NHC_{quat}C(H)\underline{H}$); 4.79 (1H, s, $C\underline{H}C_{arom,quat}$); 7.16 (2H, d_{AB}, *J* = 8.5 Hz, 2 x CH_{arom}); 7.23 (2H, d_{AB}, *J* = 8.5 Hz, 2 x CH_{arom}); 9.34 (1H, s, NH).**^{13}C-NMR** (100.6 MHz, DMSO-d_6): δ 27.0 (2 x $CH_3C_{quat}\underline{C}H_3$); 29.5 (2 x $\underline{C}H_3C_{quat}CH_3$); 32.6 (2 x $CH_3\underline{C}_{quat}CH_3$); 33.2 ($\underline{C}HC_{arom,quat}$); 40.1 (2 x $NHC_{quat}\underline{C}H_2$); 50.6 (2 x $\underline{C}H_2C{=}O$); 111.5 (2 x $\underline{C}_{quat}C(O)CH_2$); 128.0 (2 x $C_{arom}H$); 130.0 (2 x $C_{arom}H$); 130.4 ($C_{arom,quat}$); 146.6 ($C_{arom,quat}$); 150.0 (2 x $CH_2\underline{C}_{quat}NH$); 194.8 (2 x C=O). **IR** (ATR, cm^{-1}): ν_{max} = 1647, 1607, 1487, 1364, 1219, 1146, 1090, 843, 565, 529. **MS** (ESI): m/z (%) 384 ($[M+1]^+$, 100); 386 ($[M+1]^+$, 40). Yellow crystals, 35%.

9-(4-Methoxyphenyl)-3,3,6,6-tetramethyl-3,4,6,7,9,10-hexahydroacridine-1,8(2H,5H)-dione 2o

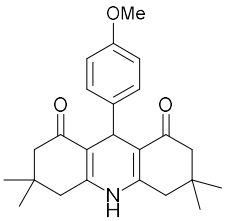

^{1}H-NMR (400 MHz, DMSO-d_6): δ 0.87 (6H, s, 2 x $CH_3C_{quat}C\underline{H}_3$); 1.01 (6H, s, 2 x $C\underline{H}_3C_{quat}CH_3$); 1.98 (2H, d_{AB}, *J* = 16.1 Hz, 2 x C(<u>H</u>)HCO); 2.17 (2H, d_{AB}, *J* = 16.1 Hz, 2 x C(H)<u>H</u>CO); 2.32 (2H, d, *J* = 17.1 Hz, 2 x $NHC_{quat}C(\underline{H})H$); 2.44 (2H, d, *J* = 17.1 Hz, 2 x $NHC_{quat}C(H)\underline{H}$); 3.66 (3H, s, $OC\underline{H}_3$); 4.76 (1H, s, $C\underline{H}C_{arom,quat}$); 6.72 (2H, d, *J* = 8.5 Hz, 2 x CH_{arom}); 7.06 (2H, d, *J* = 8.5 Hz, 2 x CH_{arom}); 9.24 (1H, s, $N\underline{H}$). **^{13}C-NMR** (100.6 MHz, DMSO-d_6): δ 27.0 (2 x $CH_3C_{quat}\underline{C}H_3$); 29.6 (2 x $\underline{C}H_3C_{quat}CH_3$); 32.3 ($\underline{C}HC_{arom,quat}$); 32.6 (2 x $CH_3\underline{C}_{quat}CH_3$); 40.1 (2 x $NHC_{quat}\underline{C}H_2$); 50.8 (2 x $\underline{C}H_2C{=}O$); 55.3 ($O\underline{C}H_3$); 112.2 (2 x $\underline{C}_{quat}C(O)CH_2$); 113.4 (2 x CH_{arom}); 129.0 (2 x CH_{arom}); 140.0 ($C_{arom,quat}$); 149.5 (2 x $CH_2\underline{C}_{quat}NH$); 157.6 ($C_{arom,quat}$); 194.8 (2 x C=O). **IR** (ATR, cm^{-1}): ν_{max} = 1643, 1605, 1479, 1364, 1219, 1171, 1144, 833, 665, 557. **MS** (ESI): m/z (%) 380 ($[M+1]^+$, 100). Yellow crystals, 81%.

3.4.2.3 Synthesis of pyrazolines

Two modified literature procedures were used for the synthesis of pyrazolines **4a-g**.

Procedure 1[697]

The synthesis of 1,3,5-triphenyl-4,5-dihydro-1*H*-pyrazole **4a** is given as a representative example for the synthesis of pyrazolines **4a-c**. Chalcone **19** (2.08 g, 10 mmol, 1 eq.) was added to a 250 mL round bottom flask containing 150 mL EtOH. Phenylhydrazine (1.190 g, 11 mmol, 1.1 eq.) was added, followed by a drop of sulfuric acid. The reaction mixture was then stirred overnight at reflux under a nitrogen atmosphere. The reaction was allowed to cool to room temperature after which it was placed in a freezer for two hours. The resulting precipitate was filtered and rinsed with cold EtOH and water to give the title compound **4a** as a light yellow solid (1.99 g, 67%).

For compounds **4b-c** the crude reaction mixture was evaporated and purification took place via column chromatography (SiO_2, hexane/EtOAc: 98/2).

Procedure 2[698]

The synthesis of **4f** is given as a representative example for the synthesis of compounds **4d-g**. Chalcone **19** (624 mg, 3 mmol, 1 eq.) and 4-sulfonamidophenylhydrazine hydrochloride (805 mg, 3.6 mmol, 1.2 eq.) were added to a flask containing 15 mL MeOH. Glacial acetic acid (180 mg, 3 mmol, 1 eq.) was added and the reaction was stirred under argon for five hours at 60 °C. The reaction was allowed to cool to room temperature and placed in a freezer overnight. The resulting precipitate was filtered and rinsed with cold MeOH to give the title compound **4f** as white crystals (0.95 g, 84%).

For compounds **4d,e,g**: the crude reaction mixture was evaporated and purification took place via column chromatography (C18, gradient CH_3CN/H_2O: 30/70 – 100/0), (SiO_2, gradient hexane/EtOAc: 98/2 – 90/10) and (SiO_2, gradient hexane/EtOAc: 98/2 – 0/100), respectively.

1,3,5-Triphenyl-4,5-dihydro-1*H*-pyrazole 4a

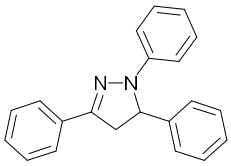

^{1}H-NMR (400 MHz, $CDCl_3$): δ 3.15 (1H, d x d, *J* = 17.1 x 7.3 Hz, NCHC(H)H); 3.85 (1H, d x d, *J* = 17.1 x 12.4 Hz, NCHC(H)H); 5.28 (1H, d x d, *J* = 12.4 x 7.3 Hz, NCHC(H)H); 6.76-6.80 (1H, m, CH_{arom}); 7.06-7.09 (2H, m, 2 x CH_{arom}); 7.16-7.20 (2H, m, 2 x CH_{arom}); 7.25-7.39 (6H, m, 6 x CH_{arom}); 7.37-7.41 (2H, m, 2 x CH_{arom}); 7.72-7.74 (2H, m, 2 x CH_{arom}). **^{13}C-NMR** (100 MHz, $CDCl_3$): δ 43.7 ($NCHCH_2$); 64.6 ($NCHCH_2$); 113.5 (2 x CH_{arom}); 119.2 (CH_{arom}); 125.9 (2 x CH_{arom}); 126.0 (2 x CH_{arom}); 127.7 (CH_{arom}); 128.66 (2 x CH_{arom}); 128.71 (CH_{arom}); 129.0 (2 x CH_{arom}); 129.3 (2 x CH_{arom}); 132.9 ($C_{arom,quat}$); 142.7 ($C_{arom,quat}$); 145.0 ($C_{arom,quat}$); 149.8 (C=N). **IR** (ATR, cm^{-1}): ν_{max} = 1595, 1489, 1323, 1123, 872, 758, 745, 704, 691, 529. **MS** (ESI): m/z (%) 299 ($[M+1]^+$, 100). Light yellow solid, 67%. Spectral data matched literature.[719]

1-Methyl-3,5-diphenyl-4,5-dihydro-1*H*-pyrazole 4b

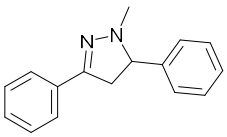

^{1}H-NMR (400 MHz, $CDCl_3$): δ 2.84 (3H, s, CH_3); 3.00 (1H, d x d, *J* = 16.1 x 14.4 Hz, NCHC(H)H); 3.48 (1H, d x d, *J* = 16.1 x 10.0 Hz, NCHC(H)H); 4.12 (1H, d x d, *J* = 14.4 x 10.0 Hz, NCHC(H)H); 7.32-7.41 (6H, m, 6 x CH_{arom}); 7.47-7.49 (2H, m, 2 x CH_{arom}); 7.63-7.66 (2H, m, 2 x CH_{arom}). **^{13}C-NMR** (100 MHz, $CDCl_3$): δ 41.7 (CH_3); 43.5 ($NCHCH_2$); 73.7 ($NCHCH_2$); 125.9 (2 x CH_{arom}); 127.6 (2 x CH_{arom}); 128.0 (CH_{arom}); 128.6 (2 x CH_{arom}); 128.75 (CH_{arom}); 128.82 (2 x CH_{arom}); 133.1 ($C_{arom,quat}$); 140.5 ($C_{arom,quat}$); 149.8 (C=N). **IR** (ATR, cm^{-1}): ν_{max} = 1445, 1128, 1036, 937, 750, 689, 671, 664, 602, 548. **MS** (ESI): m/z (%) 237 ($[M+1]^+$, 100). Colorless oil, 85%. Spectral data matched literature.[720]

3-Methyl-1,5-diphenyl-4,5-dihydro-1*H*-pyrazole 4c

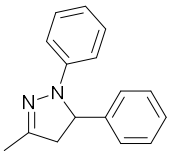

^{1}H-NMR (400 MHz, $CDCl_3$): δ 2.07 (3H, s, CH_3); 2.72 (1H, ~d x d x d, *J* = 17.4 x 8.1 x 1.1 Hz, NCHC(H)H); 3.41 (1H, ~d x d x d, *J* = 17.4 x 11.9 x 1.1 Hz, NCHC(H)H); 5.01 (1H, d x d, *J* = 11.9 x 8.1 Hz, NCHC(H)H); 6.73 (1H, ~t x t, *J* = 7.3 x 1.0 Hz, CH_{arom}); 6.90-6.93 (2H, m, 2 x CH_{arom}); 7.11-7.16 (2H, m, 2 x CH_{arom}); 7.23-7.27 (1H, m, CH_{arom}); 7.29-7.35 (4H, m, 4 x CH_{arom}). **^{13}C-NMR** (100 MHz, $CDCl_3$): δ 16.0 (CH_3); 48.0 ($NCHCH_2$); 64.9 ($NCHCH_2$); 113.2 (2 x CH_{arom}); 118.8 (CH_{arom}); 126.0 (2 x CH_{arom}); 127.5 (CH_{arom}); 129.0 (2 x CH_{arom}); 129.2 (2 x CH_{arom}); 143.2 ($C_{arom,quat}$); 146.2 ($C_{arom,quat}$); 148.6 (C=N). **IR** (ATR, cm^{-1}): ν_{max} = 1595, 1501, 1451, 1402, 1360, 1314, 866, 745, 691, 503. **MS** (ESI): m/z (%) 161 ($[M+1]^+$, 100). Orange crystals, 50%. Spectral data matched literature.[721]

3-Methyl-1-phenyl-4,5-dihydro-1*H*-pyrazole 4d

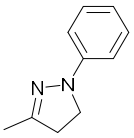

^{1}H-NMR (400 MHz, $CDCl_3$): δ 2.08 (3H, s, CH_3); 2.83 (2H, ~t x d, *J* = 10.0 x 1.0 Hz, NCH_2CH_2); 3.67 (2H, t, *J* = 10.0 Hz, NCH_2CH_2); 6.81 (1H, t x t, *J* = 11.0 x 1.0 Hz, CH_{arom}); 6.99-7.01 (2H, m, 2 x CH_{arom}); 7.23-7.27 (2H, m, 2 x CH_{arom}). **^{13}C-NMR** (100 MHz, $CDCl_3$): δ 16.1 (CH_3); 36.3 (NCH_2CH_2); 48.5 (NCH_2CH_2); 112.8 (2 x CH_{arom}); 118.6 (CH_{arom}); 129.0 (2 x CH_{arom}); 147.1 ($C_{arom,quat}$); 150.8 (C=N). **IR** (ATR, cm^{-1}): ν_{max} = 1595, 1501, 1393, 1175, 1101, 1040, 748, 691, 662, 505. **MS** (ESI): m/z (%) 237 ($[M+1]^+$, 100). Yellow solid 54%. Spectral data matched literature.[722]

1-(4-Methoxyphenyl)-3-methyl-5-phenyl-4,5-dihydro-1*H*-pyrazole 4e

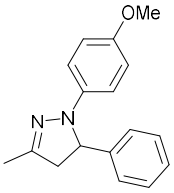

^{1}H-NMR (400 MHz, $CDCl_3$): δ 2.06 (3H, s, CH_3C=N); 2.72 (1H, ~d x d x d, *J* = 17.4 x 9.5 x 1.2 Hz, NCHC(H)H); 3.36 (1H, ~d x d x d, *J* = 17.4 x 11.6 x 1.0 Hz, NCHC(H)H); 3.71 (3H, s, OCH_3); 4.88 (1H, d x d, *J* = 11.6 x 9.5 Hz, NCHC(H)H); 6.71-6.74 (2H, m, 2 x CH_{arom}); 6.85-6.89 (2H, m, 2 x CH_{arom}); 7.25-7.28 (1H, m, CH_{arom}); 7.33-7.34 (4H, m, 4 x CH_{arom}). **^{13}C-NMR** (100 MHz, $CDCl_3$): δ 15.9 (CH_3C=N); 48.0 ($NCHCH_2$); 55.6 (CH_3O); 66.4 ($NCHCH_2$); 114.4 (2 x CH_{arom}); 115.0 (2 x CH_{arom}); 126.2 (2 x CH_{arom}); 127.4 (CH_{arom}); 129.0 (2 x CH_{arom}); 141.2 ($C_{arom,quat}$); 143.2 ($C_{arom,quat}$); 148.3 (C=N); 153.2 ($C_{arom,quat}$). **IR** (ATR, cm^{-1}): ν_{max} = 1506, 1493, 1242, 1036, 868, 814, 760, 700, 552, 517. **MS** (ESI): m/z (%) 267 ($[M+1]^+$, 100). Yellow solid, 63%. Spectral data matched literature.[723]

4-(3,5-Diphenyl-4,5-dihydro-1*H*-pyrazol-1-yl)benzenesulfonamide 4f

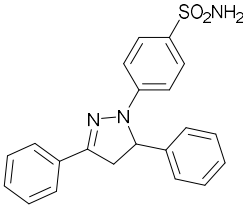

^{1}H-NMR (400 MHz, $CDCl_3$): δ 3.22 (1H, d x d, *J* = 17.3 x 5.9 Hz, NCHC(H)H); 3.91 (1H, d x d, *J* = 17.3 x 12.2 Hz, NCHC(H)H); 4.63 (2H, s, NH_2); 5.37 (1H, d x d, *J* = 12.2 x 5.9 Hz, NCHC(H)H); 7.07-7.10 (2H, m, 2 x CH_{arom}); 7.25-7.30 (3H, m, 3 x CH_{arom}); 7.33-7.44 (5H, m, 5 x CH_{arom}); 7.67-7.71 (2H, m, 2 x CH_{arom}); 7.73-7.76 (2H, m, 2 x CH_{arom}). **^{13}C-NMR** (100 MHz, $CDCl_3$): δ 43.8 ($NCHCH_2$); 63.7 ($NCHCH_2$); 112.7 (2 x CH_{arom}); 125.8 (2 x CH_{arom}); 126.3 (2 x CH_{arom}); 128.2 (2 x CH_{arom} and CH_{arom}); 128.8 (2 x CH_{arom}); 129.55 (2 x CH_{arom}); 129.63 (CH_{arom}); 130.4, 132.1, 141.3 and 147.5 (4 x $C_{arom,quat}$); 146.9 (C=N). **IR** (ATR, cm^{-1}): ν_{NH} = 3387 and 3279; ν_{max} = 1325, 1307, 1150, 1132, 810, 754, 602, 536. **MS** (ESI): m/z (%) 378 ($[M+1]^+$, 100). Light yellow crystals, 84%. Spectral data matched literature.[724]

4-(3-Methyl-5-phenyl-4,5-dihydro-1*H*-pyrazol-1-yl)benzenesulfonamide 4g

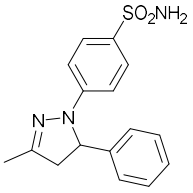

^{1}H-NMR (400 MHz, DMSO-d_6): δ 2.05 (3H, s, CH_3); 2.70 (1H, ~d x d x d, *J* = 17.9 x 5.5 x 0.7 Hz, NCHC(H)H); 3.58 (1H, ~d x d x d, *J* = 17.9 x 11.9 x 1.1 Hz, NCHC(H)H); 5.34 (1H, d x d, *J* = 11.9 x 5.5 Hz, NCHC(H)H); 6.85-6.87 (2H, m, 2 x CH_{arom}); 6.95 (2H, s, NH_2); 7.20-7.26 (3H, m, 3 x CH_{arom}); 7.32-7.35 (2H, m, 2 x CH_{arom}); 7.50-7.52 (2H, m, 2 x CH_{arom}). **^{13}C-NMR** (100 MHz, DMSO-d_6): δ 15.5 (CH_3); 47.1 (NCH$\underline{C}$H$_2$); 61.9 (N$\underline{C}$HCH$_2$); 111.2 (2 x CH_{arom}); 125.7 (2 x CH_{arom}); 127.1 (2 x CH_{arom}); 127.4 (CH_{arom}); 129.0 (2 x CH_{arom}); 132.0, 142.0 and 146.6 (3 x $C_{arom,quat}$); 151.8 (C=N). **IR** (ATR, cm^{-1}): ν_{NH} = 3325 and 3246; ν_{max} = 1591, 1323, 1169, 1099, 756, 702, 544, 536. **MS** (ESI): m/z (%) 316 ([M+1]$^+$, 100). Off white solid, 95%.

3.4.3 Synthesis of POPs

The synthesis of **CTF-Fl**

CTF-Fl was synthesized according to a slightly modified literature procedure.[404] Fluorene (249 mg, 1.5 mmol, 1.5 eq.) and cyanuric chloride (184 mg, 1 mmol, 1 eq.) were added to a flame dried flask equipped with a reflux condenser, containing 100 mL dry CH_2Cl_2, under argon. Aluminium chloride (600 mg, 4.5 mmol, 4.5 eq.) was added and the mixture was stirred for 24 hours. The resulting suspension was filtered and washed sequentially with CH_2Cl_2, DMF, H_2O, 3N HCl, H_2O, MeOH, THF and acetone and purified further via Soxhlet extraction with MeOH for 72 hours to give **CTF-Fl** as a brown – dark red powder (308 mg, 95%).

The synthesis of **CTF-Pyr**

Pyrene (152 mg, 0.75 mmol, 0.75 eq.) and cyanuric chloride (184 mg, 1 mmol, 1 eq.) were added to a flame dried flask equipped with a reflux condenser, containing 100 mL dry CH_2Cl_2, under argon. Aluminium chloride (600 mg, 4.5 mmol, 4.5 eq.) was slowly added*, over the course of 30 minutes, and the mixture was stirred at reflux for 24 hours. The resulting suspension was filtered and washed sequentially with CH_2Cl_2, DMF, H_2O, 3N HCl, H_2O, MeOH, THF and acetone and purified further via Soxhlet extraction with MeOH for 72 hours to give **CTF-Pyr** as a brown powder (153 mg, 68%).
*If the $AlCl_3$ is added all at once, a black material is obtained.

The synthesis of **aza-pTrux**

Truxene (257 mg, 0.75 mmol, 1 eq.) and cyanuric chloride (138 mg, 0.75 mmol, 1 eq.) were added to a flame dried flask equipped with a reflux condenser, containing 100 mL dry CH_2Cl_2, under argon. Aluminium chloride (450 mg, 3.4 mmol, 4.5 eq.) was added and the mixture was stirred for 24 hours. The resulting suspension was filtered and washed sequentially with CH_2Cl_2, DMF, H_2O, 3N HCl, H_2O, MeOH, THF and acetone and purified further via Soxhlet extraction with MeOH for 72 hours to give **aza-pTrux** as a brown powder (131 mg, 42%).

The synthesis of **aza-pHMTrux**

Hexamethyltruxene (320 mg, 0.75 mmol, 1 eq.) and cyanuric chloride (138 mg, 0.75 mmol, 1 eq.) were added to a flame dried flask equipped with a reflux condenser, containing 100 mL dry CH_2Cl_2, under argon. Aluminium chloride (450 mg, 3.4 mmol, 4.5 eq.) was added and the mixture was stirred at reflux for 24 hours. The resulting suspension was filtered and washed sequentially with CH_2Cl_2, DMF, H_2O,

3N HCl, H_2O, MeOH, THF and acetone and purified further via Soxhlet extraction with MeOH for 72 hours to give **aza-pHMTrux** as a yellow powder (183 mg, 49%).

The synthesis of **pFl**

Fluorene (249 mg, 1.5 mmol, 1 eq.) was added to a flame dried flask equipped with a reflux condenser, containing 100 mL dry CH_2Cl_2, under argon. To this aluminium chloride (600 mg, 4.5 mmol, 4.5 eq.) was added and the mixture was stirred at reflux for 24 hours. The resulting suspension was filtered and washed sequentially with CH_2Cl_2, DMF, H_2O, 3N HCl, H_2O, MeOH, THF and acetone and purified further via Soxhlet extraction with MeOH for 72 hours to give **pFl** as a brown – dark red powder (283 mg, >100%).*

*Likely extra mass from crosslinking with CH_2Cl_2.

The synthesis of **pTrux**

Truxene (342 mg, 1 mmol, 1 eq.) was added to a flame dried flask equipped with a reflux condenser, containing 100 mL dry CH_2Cl_2, under argon. To this aluminium chloride (600 mg, 4.5 mmol, 4.5 eq.) was added and the mixture was stirred at reflux for 24 hours. The resulting suspension was filtered and washed sequentially with CH_2Cl_2, DMF, H_2O, 3N HCl, H_2O, MeOH, THF and acetone and purified further via Soxhlet extraction with MeOH for 72 hours to give **pTrux** as a brown powder (303 mg, 89%).

The synthesis of **pHMTRux**

Hexamethyltruxene (427 mg, 1.5 mmol, 1 eq.) was added to a flame dried flask equipped with a reflux condenser, containing 100 mL dry CH_2Cl_2, under argon. To this aluminium chloride (600 mg, 4.5 mmol, 4.5 eq.) was added and the mixture was stirred at reflux for 24 hours. The resulting suspension was filtered and washed sequentially with CH_2Cl_2, DMF, H_2O, 3N HCl, H_2O, MeOH, THF and acetone and purified further via Soxhlet extraction with MeOH for 72 hours to give **pHMTrux** as a yellow powder (351 mg, 82%).

The synthesis of **pPyr**

Pyrene (202 mg, 1 mmol, 1 eq.) was added to a flame dried flask equipped with a reflux condenser, containing 100 mL dry CH_2Cl_2, under argon. To this aluminium chloride (800 mg, 6 mmol, 6 eq.) was added and the mixture was stirred at reflux for 24 hours. The resulting suspension was filtered and washed sequentially with CH_2Cl_2, DMF, H_2O, 3N HCl, H_2O, MeOH, THF and acetone and purified further via Soxhlet extraction with MeOH for 72 hours to give **pPyr** as shiny black flakes (53 mg, 26%).

3.4.4 Photocatalysis

3.4.4.1 Procedure for the screening and control experiments

The photocatalyst (5 mg) and ethyl 2,7,7-trimethyl-5-oxo-4-phenyl-1,4,5,6,7,8-hexahydroquinoline-3-carboxylate **2d** (33.7 mg, 0.1 mmol, 1 eq) were added to a small glass test tube, followed by addition of 2.5 mL CH_3CN. This was stirred under air and irradiation from a 26 W CFL (~10 cm distance) for 24 hours. The conversion was determined directly from the reaction mixture by taking a small aliquot and evaporating this under a stream of nitrogen. This was then analyzed using ^{1}H-NMR in DMSO-d_6. The conversion was determined via integration of the $CH_3C_{arom,quat}$ of the pyridine product **3d** and the CH of the dihydropyridine ring.

For the aromatization of pyrazolines **4** an analogous procedure was applied, using 1,3,5-triphenyl-4,5-dihydro-1*H*-pyrazole **4a** (29.8 mg, 0.1 mmol, 1 eq.) or 3-methyl-1,5-diphenyl-4,5-dihydro-1*H*-pyrazole **4d** (23.6 mg, 0.1 mmol, 1 eq.) and 1,3,5-trimethoxybenzene (16.8 mg, 0.1 mmol, 1 eq.) was added as the internal standard. The yield of the product was determined by integration of the aromatic proton of the pyrazole **4** and the aromatic protons of 1,3,5-trimethoxybenzene.

3.4.4.2 CTF-Pyr as a photocatalyst for the aromatization of dihydropyridines 2a-c, tetrahydroquinoline-5-ones 2d-k and hexahydroacridine-1,8-diones 2l-o

A small glass test tube was charged with: **CTF-Pyr** (10 mg), the substrate **2** (0.2 mmol) and CH_3CN (5 mL). This was stirred under air and irradiation from a 26 W CFL (~10 cm distance) for 24 hours. The reaction mixture was then filtered and rinsed with acetone to remove the catalyst. The crude mixture was purified by column chromatography (SiO_2, hexane/EtOAc: 4/1) to obtain the product **3**.

Diethyl 2,6-dimethyl-4-phenylpyridine-3,5-dicarboxylate 3a

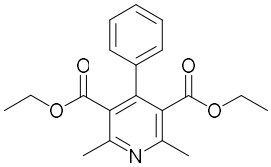

^{1}H-NMR (400 MHz, $CDCl_3$): δ 0.88 (6H, t, *J* = 7.1 Hz, 2 x $OCH_2C\underline{H}_3$); 2.59 (6H, s, 2 x $C\underline{H}_3C_{arom,quat}$); 3.98 (4H, q, *J* = 7.1 Hz, 2 x $OC\underline{H}_2CH_3$); 7.22-7.26 (2H, m, 2 x CH_{arom}); 7.33-7.36 (3H, m, 3 x CH_{arom}). **^{13}C-NMR** (100 MHz, $CDCl_3$): δ 13.6 (2 x $\underline{C}H_3CH_2O$); 23.0 (2 x $\underline{C}H_3C_{arom,quat}$); 61.4 (2 x $CH_3\underline{C}H_2O$); 127.0 (2 x $C_{arom,quat}$); 128.18 (2 x CH_{arom}); 128.21 (2 x CH_{arom}); 128.5 (CH_{arom}); 136.7 ($C_{arom,quat}$); 146.2 ($C_{arom,quat}$); 155.5 (2 x $C_{arom,quat}$); 168.0 (2 x C=O). **IR** (ATR, cm^{-1}): $\nu_{C=O}$ = 1715; ν_{max} = 1510, 1383, 1231, 1099, 1086, 837, 750, 700, 509. **MS** (ESI): *m/z* (%) 328 ($[M + 1]^+$, 100). Colorless oil, 92%. Spectral data matched literature.[686]

Diethyl 4-(4-chlorophenyl)-2,6-dimethylpyridine-3,5-dicarboxylate 3b

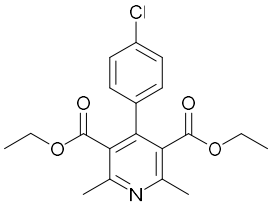

^{1}H-NMR (400 MHz, $CDCl_3$): δ 0.96 (6H, t, *J* = 7.1 Hz, 2 x $OCH_2C\underline{H}_3$); 2.58 (6H, s, 2 x $C\underline{H}_3C_{arom,quat}$); 4.02 (4H, q, *J* = 7.1 Hz, 2 x $OC\underline{H}_2CH_3$); 7.17-7.20 (2H, m, 2 x CH_{arom}); 7.32-7.35 (3H, m, 3 x CH_{arom}). **^{13}C-NMR** (100 MHz, $CDCl_3$): δ 13.8 (2 x $\underline{C}H_3CH_2O$); 23.0 (2 x $\underline{C}H_3C_{arom,quat}$); 61.6 (2 x $CH_3\underline{C}H_2O$); 126.9 (2 x $C_{arom,quat}$); 128.4 (2 x CH_{arom}); 129.7 (2 x CH_{arom}); 134.8 ($C_{arom,quat}$); 135.1 ($C_{arom,quat}$); 144.9 ($C_{arom,quat}$); 155.7 (2 x $C_{arom,quat}$); 167.7 (2 x C=O). **IR** (ATR, cm^{-1}): $\nu_{C=O}$ = 1715; ν_{max} = 1493, 1227, 1211, 1088, 1043, 1015, 866, 827, 561. **MS** (ESI): *m/z* (%) 362 ($[M + 1]^+$, 100); 364 ($[M + 1]^+$, 35). Colorless oil, 89%. Spectral data matched literature[684]

Diethyl 4-(4-methoxyphenyl)-2,6-dimethylpyridine-3,5-dicarboxylate 3c

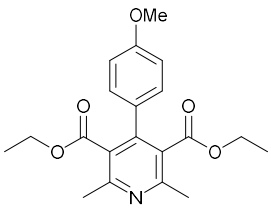

^{1}H-NMR (400 MHz, $CDCl_3$): δ 0.97 (6H, t, *J* = 7.1 Hz, 2 x $OCH_2C\underline{H}_3$); 2.57 (6H, s, 2 x $C\underline{H}_3C_{arom,quat}$); 3.81 (3H, s, CH_3O); 4.03 (4H, q, *J* = 7.1 Hz, 2 x $OC\underline{H}_2CH_3$); 6.86-6.90 (2H, m, 2 x CH_{arom}); 7.16-7.19 (2H, m, 2 x CH_{arom}). **^{13}C-NMR** (100 MHz, $CDCl_3$): δ 13.8 (2 x $\underline{C}H_3CH_2O$); 23.0 (2 x $\underline{C}H_3C_{arom,quat}$); 55.4 ($CH_3O$); 61.4 (2 x $CH_3\underline{C}H_2O$); 113.7 (2 x CH_{arom}); 127.4 (2 x $C_{arom,quat}$); 128.8 ($C_{arom,quat}$); 129.6 (2 x CH_{arom}); 145.9 ($C_{arom,quat}$); 155.3 (2 x $C_{arom,quat}$); 159.9 ($C_{arom,quat}$); 168.2 (2 x C=O). **IR** (ATR, cm^{-1}): $\nu_{C=O}$ = 1717; ν_{max} = 1514, 1292, 1233, 1207, 1177, 1105, 1028, 831, 559. **MS** (ESI): *m/z* (%) 358 ($[M + 1]^+$, 100). Colorless oil, 84%. Spectral data matched literature.[686]

Ethyl 2,7,7-trimethyl-5-oxo-4-phenyl-5,6,7,8-tetrahydroquinoline-3-carboxylate 3d

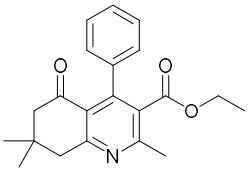

^{1}H-NMR (400 MHz, $CDCl_3$): δ 0.91 (3H, t, *J* = 7.1 Hz, $C\underline{H}_3CH_2O$); 1.11 (6H, s, $(CH_3)_2C_{quat}$); 2.46 (2H, s, $CH_2C{=}O$); 2.60 (3H, s, $CH_3C_{arom,quat}$); 3.08 (2H, s, $CH_2C_{arom,quat}$); 3.95 (2H, q, *J* = 7.1 Hz, $CH_3C\underline{H}_2O$); 7.11-7.13 (2H, m, 2 x CH_{arom}); 7.34-7.36 (2H, m, 2 x CH_{arom}). **^{13}C-NMR** (100 MHz, $CDCl_3$): δ 13.7 ($OCH_2\underline{C}H_3$); 23.4 ($\underline{C}H_3C_{arom,quat}$); 28.3 ($(\underline{C}H_3)_2C_{quat}$); 32.6 $(CH_3)_2\underline{C}_{quat}$); 47.6 ($\underline{C}H_2C_{arom,quat}$); 53.8 ($\underline{C}H_2C{=}O$); 61.6 ($O\underline{C}H_2CH_3$); 123.1 ($C_{arom,quat}$); 127.7 (2 x CH_{arom}); 127.8 (3 x CH_{arom}); 130.3, 137.5, 148.7, 158.4 and 163.3 (5 x $C_{arom,quat}$); 167.7 (OC=O); 197.2 ($CH_2\underline{C}{=}O$). **IR** (ATR, cm^{-1}): $\nu_{C=O}$ = 1715; ν_{max} = 1508, 1383, 1229, 1213, 1101, 1082, 837, 698, 507. **MS** (ESI): *m/z* (%) 338 ($[M + 1]^+$, 100). Yellow solid, 86%. Spectral data matched literature.[675]

Ethyl 2,7,7-trimethyl-4-(4-nitrophenyl)-5-oxo-5,6,7,8-tetrahydroquinoline-3-carboxylate 3e

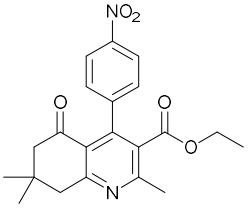

^{1}H-NMR (400 MHz, $CDCl_3$): δ 0.96 (3H, t, *J* = 7.1 Hz, $C\underline{H}_3CH_2O$); 1.11 (6H, s, $(C\underline{H}_3)_2C_{quat}$); 2.46 (2H, s, $CH_2C{=}O$); 2.61 (3H, s, $CH_3C_{arom,quat}$); 3.10 (2H, s, $CH_2C_{arom,quat}$); 3.98 (2H, q, *J* = 7.1 Hz, $CH_3C\underline{H}_2O$); 7.27-7.30 (2H, m, 2 x CH_{arom}); 8.21-8.24 (2H, m, 2 x CH_{arom}).**^{13}C-NMR** (100 MHz, $CDCl_3$): δ 13.8 ($OCH_2\underline{C}H_3$); 23.5 ($\underline{C}H_3C_{arom,quat}$); 28.2 ($(\underline{C}H_3)_2C_{quat}$); 32.6 ($(CH_3)_2\underline{C}_{quat}$); 47.5 ($\underline{C}H_2C_{arom,quat}$); 53.5 ($\underline{C}H_2C{=}O$); 61.9 ($O\underline{C}H_2CH_3$); 122.4 ($C_{arom,quat}$); 123.1 (2 x CH_{arom}); 128.8 (2 x CH_{arom}); 129.4, 144.8, 146.2, 147.4, 159.2 and 163.7 (6 x $C_{arom,quat}$); 166.9 (OC=O); 197.1 ($CH_2\underline{C}{=}O$). **IR** (ATR, cm^{-1}): $\nu_{C=O}$ = 1715; ν_{max} = 1508, 1383, 1229, 1101, 1082, 837, 748, 696, 507. **MS** (ESI): *m/z* (%) 383 ($[M + 1]^+$, 100). Colorless oil, 86%. Spectral data matched literature.[675]

Ethyl 4-(4-chlorophenyl)-2,7,7-trimethyl-5-oxo-5,6,7,8-tetrahydroquinoline-3-carboxylate 3f

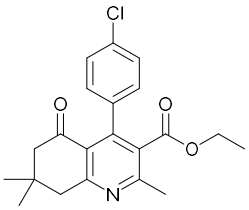

^{1}H-NMR (400 MHz, $CDCl_3$): δ 0.97 (3H, t, *J* = 7.1 Hz, $C\underline{H}_3CH_2O$); 1.10 (6H, s, $(C\underline{H}_3)_2C_{quat}$); 2.45 (2H, s, $CH_2C{=}O$); 2.59 (3H, s, $CH_3C_{arom,quat}$); 3.07 (2H, s, $CH_2C_{arom,quat}$); 3.99 (2H, q, *J* = 7.1 Hz, $CH_3C\underline{H}_2O$); 7.04-7.07 (2H, m, 2 x CH_{arom}); 7.31-7.34 (2H, m, 2 x CH_{arom}). **^{13}C-NMR** (100 MHz, $CDCl_3$): δ 13.8 ($OCH_2\underline{C}H_3$); 23.3 ($\underline{C}H_3C_{arom,quat}$); 28.2 ($(\underline{C}H_3)_2C_{quat}$); 32.5 ($(CH_3)_2\underline{C}_{quat}$); 47.5 ($\underline{C}H_2C_{arom,quat}$); 53.7 ($\underline{C}H_2C{=}O$); 61.7 ($O\underline{C}H_2CH_3$); 122.9 ($C_{arom,quat}$); 128.1 (2 x CH_{arom}); 129.1 (2 x CH_{arom}); 130.1, 133.9, 135.9, 147.3, 158.7 and 163.4 (6 x $C_{arom,quat}$); 167.4 (OC=O); 197.2 ($CH_2\underline{C}{=}O$). **IR** (ATR, cm^{-1}): $\nu_{C=O}$ = 1721 and 1686; ν_{max} = 2957, 1549, 1263, 1209, 1088, 1032, 1015, 729. **MS** (ESI): *m/z* (%) 372 ($[M + 1]^+$, 100); 374 ($[M + 1]^+$, 35). Colorless oil, 86%. Spectral data matched literature.[675]

Ethyl 4-(benzo[*d*][1,3]dioxol-5-yl)-2,7,7-trimethyl-5-oxo-5,6,7,8-tetrahydroquinoline-3-carboxylate 3g

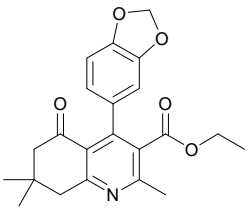

^{1}H-NMR (400 MHz, $CDCl_3$): δ 1.04 (3H, t, *J* = 7.1 Hz, $C\underline{H}_3CH_2O$); 1.09 (3H, s, $C\underline{H}_3C_{quat}CH_3$); 1.10 (3H, s, $CH_3C_{quat}C\underline{H}_3$); 2.46 (2H, s, $CH_2C{=}O$); 2.57 (3H, s, $CH_3C_{arom,quat}$); 3.06 (2H, s, $CH_2C_{arom,quat}$); 4.06 (2H, q, *J* = 7.1 Hz, $CH_3C\underline{H}_2O$); 5.96 (1H, s, $OC(\underline{H})HO$); 5.97 (1H, s, $OC(H)\underline{H}O$); 6.56 (1H, d x d, *J* = 7.9 x 1.6 Hz, CH_{arom}); 6.60 (2H, d, *J* = 1.6 Hz, CH_{arom}); 6.79 (1H, d, *J* = 7.9 Hz, CH_{arom}). **^{13}C-NMR** (100 MHz, $CDCl_3$): δ 13.9 ($OCH_2\underline{C}H_3$); 23.3 ($\underline{C}H_3C_{arom,quat}$); 28.23 ($\underline{C}H_3C_{quat}CH_3$); 28.33 ($CH_3C_{quat}\underline{C}H_3$); 32.6 ($CH_3\underline{C}_{quat}CH_3$); 47.6 ($\underline{C}H_2C_{arom,quat}$); 53.9 ($\underline{C}H_2C{=}O$); 61.6 ($O\underline{C}H_2CH_3$); 101.2 ($OCH_2O$); 108.0, 108.9 and 121.1 (3 x CH_{arom}); 123.3, 130.5, 131.0, 147.3, 147.4, 148.2, 158.4 and 163.2 (8 x $C_{arom,quat}$); 167.7 (OC=O); 197.2 ($CH_2\underline{C}{=}O$). **IR** (ATR, cm^{-1}): $\nu_{C=O}$ = 1724 and 1692 ; ν_{max} = 2955, 1547, 1489, 1445, 1235, 1206, 1036, 729. **MS** (ESI): *m/z* (%) 382 ($[M + 1]^+$, 100). **HRMS** (ESI): calcd. for $C_{22}H_{24}NO_5^+$: 382.1649 $[M + H]^+$, found: 382.1655. Colorless oil, 81%.

Ethyl 2,7,7-trimethyl-5-oxo-5,6,7,8-tetrahydroquinoline-3-carboxylate 3h

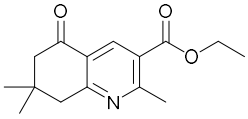

^{1}H-NMR (400 MHz, $CDCl_3$): δ 1.09 (6H, s, $(CH_3)_2C_{quat}$); 1.38 (3H, t, *J* = 7.1 Hz, CH_3CH_2O); 2.53 (2H, s, $CH_2C{=}O$); 2.85 (3H, s, $CH_3C_{arom,quat}$); 3.00 (2H, s, $CH_2C_{arom,quat}$); 4.36 (2H, q, *J* = 7.1 Hz, CH_3CH_2O); 8.69 (1H, s, CH_{arom}). **^{13}C-NMR** (100 MHz, $CDCl_3$): δ 14.4 (OCH_2CH_3); 25.3 ($CH_3C_{arom,quat}$); 28.4 ($(CH_3)_2C_{quat}$); 33.0 ($(CH_3)_2C_{quat}$); 46.6 ($CH_2C_{arom,quat}$); 52.0 ($CH_2C{=}O$); 61.6 (OCH_2CH_3); 124.6 ($C_{arom,quat}$); 125.0 ($C_{arom,quat}$); 137.1 (CH_{arom}); 164.4 ($C_{arom,quat}$); 164.7 ($C_{arom,quat}$); 165.9 (OC=O); 197.3 ($CH_2C{=}O$). **IR** (ATR, cm^{-1}): $\nu_{C=O}$ = 1724 and 1690; ν_{max} = 2957, 1589, 1252, 1217, 1086, 1026, 781, 532. **MS** (ESI): *m/z* (%) 262 ($[M + 1]^+$, 100). Yellow oil, 77-80%. Spectral data matched literature.[675]

Ethyl 2,7,7-trimethyl-5-oxo-4-pentyl-5,6,7,8-tetrahydroquinoline-3-carboxylate 3i

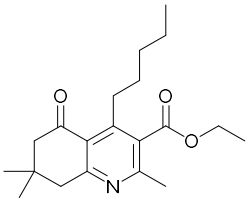

^{1}H-NMR (400 MHz, $CDCl_3$): δ 0.90 (3H, t, *J* = 7.1 Hz, $CH_3CH_2CH_2CH_2CH_2$); 1.08 (6H, s, $(CH_3)_2C_{quat}$); 1.28-1.42 (7H, m, CH_3CH_2O and $CH_3CH_2CH_2CH_2CH_2$); 1.47-1.56 (2H, m, $CH_3CH_2CH_2CH_2CH_2$); 2.51 (3H, s, $CH_3C_{arom,quat}$); 2.52 (2H, s, $CH_2C{=}O$); 2.93-2.97 (2H, m, $CH_3CH_2CH_2CH_2CH_2$); 2.99 (2H, s, $CH_2C_{arom,quat}$); 4.42 (2H, q, *J* = 7.1 Hz, CH_3CH_2O). **^{13}C-NMR** (100 MHz, $CDCl_3$): δ 14.2 ($CH_3CH_2CH_2CH_2CH_2$); 14.3 (OCH_2CH_3); 22.5 ($CH_3CH_2CH_2CH_2CH_2$); 23.3 ($CH_3C_{arom,quat}$); 28.2 ($(CH_3)_2C_{quat}$); 30.6 ($CH_3CH_2CH_2CH_2CH_2$); 31.9 ($CH_3CH_2CH_2CH_2CH_2$); 32.3 ($(CH_3)_2C_{quat}$); 32.6 ($CH_3CH_2CH_2CH_2CH_2$); 48.0 ($CH_2C_{arom,quat}N$); 54.5 ($CH_2C{=}O$); 61.8 (OCH_2CH_3); 123.2, 130.4, 151.7, 158.0 and 163.7 (5 x $C_{arom,quat}$); 168.8 (OC=O); 199.2 ($CH_2C{=}O$). **IR** (ATR, cm^{-1}): $\nu_{C=O}$ = 1717 and 1684; ν_{max} = 2951, 2870, 1557, 1265, 1221, 1188, 1109, 1076. **MS** (ESI): *m/z* (%) 332 ($[M + 1]^+$, 100). **HRMS** (ESI): calcd. for $C_{20}H_{30}NO_3^+$: 332.2221 $[M + H]^+$, found: 332.2223. Colorless oil, 77%.

Ethyl 4-(4-methoxyphenyl)-2,7,7-trimethyl-5-oxo-5,6,7,8-tetrahydroquinoline-3-carboxylate 3j

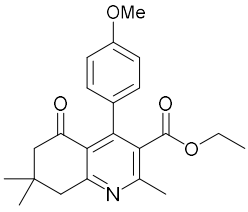

^{1}H-NMR (400 MHz, $CDCl_3$): δ 0.98 (3H, t, *J* = 7.1 Hz, CH_3CH_2O); 1.10 (6H, s, $(CH_3)_2C_{quat}$); 2.46 (2H, s, $CH_2C{=}O$); 2.58 (3H, s, $CH_3C_{arom,quat}$); 3.07 (2H, s, $CH_2C_{arom,quat}$); 3.82 (2H, q, *J* = 7.1 Hz, CH_3CH_2O); 4.00 (3H, s, CH_3O); 6.88-6.90 (2H, m, 2 x CH_{arom}); 7.04-7.06 (2H, m, 2 x CH_{arom}). **^{13}C-NMR** (100 MHz, $CDCl_3$): δ 13.9 (OCH_2CH_3); 23.3 ($CH_3C_{arom,quat}$); 28.3 ($(CH_3)_2C_{quat}$); 32.5 ($(CH_3)_2C_{quat}$); 47.7 ($CH_2C_{arom,quat}$); 53.9 ($CH_2C{=}O$); 55.3 (CH_3O); 61.6 (OCH_2CH_3); 113.4 (2 x CH_{arom}); 123.3 ($C_{arom,quat}$); 129.0 (2 x CH_{arom}); 129.6, 130.7, 148.5, 158.3, 159.4 and 163.2 (6 x $C_{arom,quat}$); 167.9 (OC=O); 197.4 ($CH_2C{=}O$). **IR** (ATR, cm^{-1}): $\nu_{C=O}$ = 1713 and 1697; ν_{max} = 2957, 1545, 1510, 1246, 1233, 1215, 1028, 550. **MS** (ESI): *m/z* (%) 368 ($[M + 1]^+$, 100). Colorless oil, 76%. Spectral data matched literature.[675]

3,3,6,6-Tetramethyl-9-phenyl-3,4,6,7-tetrahydroacridine-1,8(2*H*,5*H*)-dione 3k

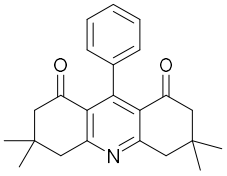

^{1}H-NMR (400 MHz, $CDCl_3$): δ 1.16 (12H, s, 4 x CH_3); 2.46 (4H, s, 2 x CH_2CO); 3.10 (4H, 2 x $CH_2C_{arom,quat}$); 7.00-7.02 (2H, m, 2 x CH_{arom}); 7.37-7.41 (3H, m, 3 x CH_{arom}). **^{13}C-NMR** (100 MHz, $CDCl_3$): δ 28.4 (2 x $(CH_3)_2C_{quat}$); 32.5 (2 x $(CH_3)_2C_{quat}$); 48.1 (2 x $CH_2C_{arom,quat}$); 54.1 (2 x CH_2CO); 125.6 (2 x $C_{arom,quat}$); 126.6 (2 x CH_{arom}); 127.1 (CH_{arom}); 127.8 (2 x CH_{arom}); 138.7 ($C_{arom,quat}$); 152.2 ($C_{arom,quat}$); 166.0 (2 x $C_{arom,quat}$); 197.2 (2 x C=O). **IR** (ATR, cm^{-1}): $\nu_{C=O}$ = 1697 and 1686; ν_{max} = 2957, 1537, 1238, 1109, 1074, 741, 700, 534. **MS** (ESI): *m/z* (%) 348 ($[M + 1]^+$, 100). **HRMS** (ESI): calcd. for $C_{23}H_{26}NO_2^+$: 348.1959 $[M + H]^+$, found: 348.1962. Yellow solid, 70%.

9-(Benzo[*d*][1,3]dioxol-5-yl)-3,3,6,6-tetramethyl-3,4,6,7-tetrahydroacridine-1,8(2*H*,5*H*)-dione 3l

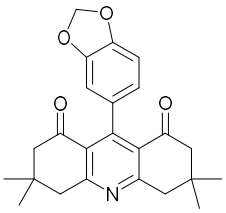

^{1}H-NMR (400 MHz, $CDCl_3$): δ 1.11 (12H, s, 4 x CH_3); 2.47 (4H, s, 2 x CH_2CO); 3.08 (4H, 2 x $CH_2C_{arom,quat}$); 5.99 (2H, s, OCH_2O); 6.40 (1H, d x d, *J* = 7.9 x 1.6 Hz, CH_{arom}); 6.51 (1H, d, *J* = 1.5 Hz, CH_{arom}); 6.80 (1H, d, *J* = 7.9 Hz, CH_{arom}). **^{13}C-NMR** (100 MHz, $CDCl_3$): δ 28.3 (2 x $\underline{C}H_3C_{quat}CH_3$); 28.5 (2 x $CH_3C_{quat}\underline{C}H_3$); 32.5 (2 x $CH_3\underline{C}_{quat}CH_3$); 48.1 (2 x $\underline{C}H_2C_{arom,quat}$); 54.2 (2 x $\underline{C}H_2CO$); 101.1 (OCH_2O); 108.12 (CH_{arom}); 108.16 (CH_{arom}); 119.8 (CH_{arom}); 125.9 (2 x $C_{arom,quat}$); 132.1 ($C_{arom,quat}$); 146.9 ($C_{arom,quat}$); 147.4 ($C_{arom,quat}$); 151.7 ($C_{arom,quat}$); 165.9 (2 x $C_{arom,quat}$); 197.3 (2 x C=O). **IR** (ATR, cm^{-1}): $\nu_{C=O}$ = 1705; ν_{max} = 2695, 2891, 1531, 1234, 1198, 1038, 928, 818, 575. **MS** (ESI): *m/z* (%) 392 ($[M + 1]^+$, 100). **HRMS** (ESI): calcd. for $C_{24}H_{26}NO_4^+$: 392.1857 $[M + H]^+$, found: 395.1860. Yellow solid, 80%.

9-(4-Chlorophenyl)-3,3,6,6-tetramethyl-3,4,6,7-tetrahydroacridine-1,8(2*H*,5*H*)-dione 3m

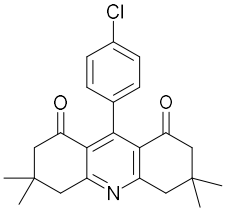

^{1}H-NMR (400 MHz, $CDCl_3$): δ 1.11 (12H, s, 4 x CH_3); 2.46 (4H, s, 2 x CH_2CO); 3.10 (4H, 2 x $CH_2C_{arom,quat}$); 6.91-6.94 (2H, m, 2 x CH_{arom}); 7.32-7.36 (2H, m, 2 x CH_{arom}). **^{13}C-NMR** (100 MHz, $CDCl_3$): δ 28.2 (2 x $\underline{C}H_3C_{quat}\underline{C}H_3$); 32.4 (2 x $CH_3\underline{C}_{quat}CH_3$); 47.9 (2 x $\underline{C}H_2C_{arom,quat}$); 53.9 (2 x $\underline{C}H_2CO$); 125.4 (2 x $C_{arom,quat}$); 127.9 (2 x CH_{arom}); 128.0 (2 x CH_{arom}); 132.9 ($C_{arom,quat}$); 137.0 ($C_{arom,quat}$); 150.9 ($C_{arom,quat}$); 166.1 (2 x $C_{arom,quat}$); 197.1 (2 x C=O). **IR** (ATR, cm^{-1}): $\nu_{C=O}$ = 1697; ν_{max} = 2959, 1535, 1512, 1250, 1234, 1219, 1030, 826, 550. **MS** (ESI): *m/z* (%) 382 ($[M + 1]^+$, 100). **HRMS** (ESI): calcd. for $C_{23}H_{25}ClNO_2^+$: 382.1569 $[M + H]^+$, found: 382.1572. Yellow crystals, 99%.

9-(4-Methoxyphenyl)-3,3,6,6-tetramethyl-3,4,6,7-tetrahydroacridine-1,8(2*H*,5*H*)-dione 3n

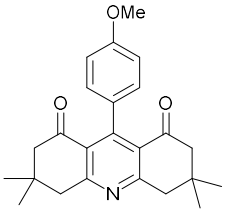

^{1}H-NMR (400 MHz, $CDCl_3$): δ 1.11 (12H, s, 4 x CH_3); 2.46 (4H, s, 2 x CH_2CO); 3.09 (4H, 2 x $CH_2C_{arom,quat}$); 3.83 (3H, s, OCH_3); 6.92 (4H, s, 4 x CH_{arom}). **^{13}C-NMR** (100 MHz, $CDCl_3$): δ 28.4 (2 x $\underline{C}H_3C_{quat}\underline{C}H_3$); 32.5 (2 x $CH_3\underline{C}_{quat}CH_3$); 48.1 (2 x $\underline{C}H_2C_{arom,quat}$); 54.2 (2 x $\underline{C}H_2CO$); 55.2 (CH_3O); 113.4 (2 x CH_{arom}); 125.9 (2 x $C_{arom,quat}$); 128.0 (2 x CH_{arom}); 130.5 ($C_{arom,quat}$); 152.1 ($C_{arom,quat}$); 158.9 ($C_{arom,quat}$); 165.8 (2 x $C_{arom,quat}$); 197.4 (2 x C=O). **IR** (ATR, cm^{-1}): $\nu_{C=O}$ = 1697; ν_{max} = 2955, 1537, 1510, 1234, 1207, 1107, 1030, 827, 546. **MS** (ESI): *m/z* (%) 378 ($[M + 1]^+$, 100). **HRMS** (ESI): calcd. for $C_{24}H_{28}NO_3^+$: 378.2064 $[M + H]^+$, found: 378.2067. Yellow solid, 93%.

3.4.4.3 CTF-Pyr as a photocatalyst for the aromatization of pyrazolines

A small glass test tube was charged with: **CTF-Pyr** (10 mg), the substrate **4** (0.2 mmol, 1 eq.) and EtOAc (5 mL). This was stirred under air and irradiation from a 26 W CFL (~10 cm distance) for 24 hours. The reaction mixture was then filtered and rinsed with acetone to remove the catalyst. The crude mixture was purified by column chromatography (SiO_2, hexane/EtOAc: 1/10) to obtain the product **5**.*

*For compound **5g**: hexane/EtOAc: 2/1. For compound **5f**: gradient $CHCl_3$/EtOAc 10/1 – 3/1.

1,3,5-Triphenyl-1*H*-pyrazole 5a

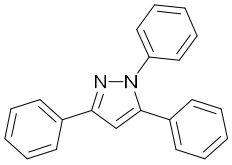

^{1}H-NMR (400 MHz, $CDCl_3$): δ 6.84 (1H, s, $CH_{pyrazole}$); 7.29-7.46 (13H, m, 13 x CH_{arom}); 7.92-7.95 (2H, m, 2 x CH_{arom}). **^{13}C-NMR** (100 MHz, $CDCl_3$): δ 105.3 ($CH_{pyrazole}$); 125.4 (2 x CH_{arom}); 125.9 (2 x CH_{arom}); 127.5 (CH_{arom}); 128.1 (CH_{arom}); 128.4 (CH_{arom}); 128.6 (2 x CH_{arom}); 128.8 (2 x CH_{arom}); 128.9 (2 x CH_{arom}); 129.0 (2 x CH_{arom}); 130.7, 133.2, 140.3, 144.5 and 152.1 (5 x $C_{arom,quat}$). **IR** (ATR, cm^{-1}): ν_{max} = 1597, 1495, 1481, 1454, 1362, 1350, 734, 691, 598, 503. **MS** (ESI): *m/z* (%) 297 ($[M + 1]^+$, 100). Yellow-orange solid, 96%. Spectral data matched literature.[725]

1-Methyl-3,5-diphenyl-1*H*-pyrazole 5b

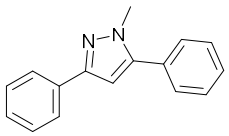

^{1}H-NMR (400 MHz, $CDCl_3$): δ 3.94 (3H, s, CH_3); 6.62 (1H, s, $CH_{pyrazole}$); 7.29-7.33 (1H, m, CH_{arom}); 7.39-7.49 (7H, m, 7 x CH_{arom}); 7.83-7.85 (2H, m, 2 x CH_{arom}). **^{13}C-NMR** (100 MHz, $CDCl_3$): δ 37.7 (CH_3); 103.4 ($CH_{pyrazole}$); 125.7 (2 x CH_{arom}); 127.7 (CH_{arom}); 128.69 (CH_{arom}); 128.76 (2 x CH_{arom}); 128.85 (2 x CH_{arom}); 128.90 (2 x CH_{arom}); 130.8, 133.6, 145.2 and 150.7 (4 x $C_{arom,quat}$). **IR** (ATR, cm^{-1}): ν_{max} = 1483, 1460, 1362, 1275, 762, 746, 691, 669, 567, 476. **MS** (ESI): *m/z* (%) 235 ($[M + 1]^+$, 100). Yellow oil, 71%. Spectral data matched literature.[726]

3-Methyl-1,5-diphenyl-1*H*-pyrazole 5c

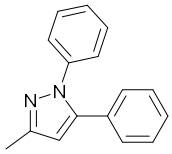

^{1}H-NMR (400 MHz, $CDCl_3$): δ 2.38 (3H, s, CH_3); 6.31 (1H, s, $CH_{pyrazole}$); 7.20-7.30 (10H, m, 10 x CH_{arom}). **^{13}C-NMR** (100 MHz, $CDCl_3$): δ 13.7 (CH_3); 107.8 ($CH_{pyrazole}$); 125.2 (2 x CH_{arom}); 127.2 (CH_{arom}); 128.2 (CH_{arom}); 128.5 (2 x CH_{arom}); 128.7 (2 x CH_{arom}); 128.9 (2 x CH_{arom}); 130.9, 140.3, 143.8 and 149.6 (4 x $C_{arom,quat}$). **IR** (ATR, cm^{-1}): ν_{max} = 1595, 1504, 1454, 1377, 1364, 968, 760, 692, 679, 581. **MS** (ESI): *m/z* (%) 235 ($[M + 1]^+$, 100). Yellow oil, 86%. Spectral data matched literature[727]

3-Methyl-1-phenyl-1*H*-pyrazole 5d

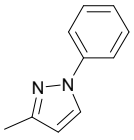

^{1}H-NMR (400 MHz, $CDCl_3$): δ 2.38 (3H, s, CH_3); 6.23 (1H, d, *J* = 2.4 Hz, $CH_{pyrazole}$); 7.21-7.25 (1H, m, CH_{arom}); 7.39-7.43 (2H, m, 2 x CH_{arom}); 7.63-7.65 (2H, m, 2 x CH_{arom}); 7.80 (1H, d, *J* = 2.4 Hz, CH_{arom}).**^{13}C-NMR** (100 MHz, $CDCl_3$): δ 13.8 (CH_3); 107.6 ($CH_{pyrazole}$); 119.0 (2 x CH_{arom}); 126.0 (CH_{arom}); 127.4 ($CH_{pyrazole}$); 129.5 (2 x CH_{arom}); 140.4 ($C_{arom,quat}$); 150.6 ($C_{arom,quat}$). **IR** (ATR, cm^{-1}): ν_{max} = 1595, 1530, 1499, 1362, 1043, 945, 754, 704, 689, 503. **MS** (ESI): *m/z* (%) 159 ($[M + 1]^+$, 100). Brown oil, 76%. Spectral data matches literature.[728]

1-(4-Methoxyphenyl)-3-methyl-5-phenyl-1*H*-pyrazole 5e

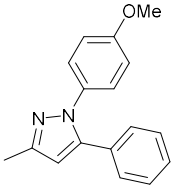

^{1}H-NMR (400 MHz, $CDCl_3$): δ 2.37 (3H, s, $CH_3C_{arom,quat}$); 3.78 (3H, s, CH_3O); 6.29 (1H, s, $CH_{pyrazole}$); 6.81-6.83 (2H, m, 2 x CH_{arom}); 7.17-7.21 (4H, m, 4 x CH_{arom}); 7.26-7.27 (3H, m, 3 x CH_{arom}). **^{13}C-NMR** (100 MHz, $CDCl_3$): δ 13.6 ($CH_3C_{arom,quat}$); 55.5 (CH_3O); 107.2 ($CH_{pyrazole}$); 114.1 (2 x CH_{arom}); 126.7 (2 x CH_{arom}); 128.0 (CH_{arom}); 128.5 (2 x CH_{arom}); 128.7 (2 x CH_{arom}); 130.9, 133.5, 143.8, 149.1 and 158.7 (5 x $C_{arom,quat}$). **IR** (ATR, cm^{-1}): ν_{max} = 1514, 1449, 1246, 1169, 1028, 970, 833, 760, 696, 575. **MS** (ESI): *m/z* (%) 265 ($[M + 1]^+$, 100). Orange oil, 84%. Spectral data matches literature.[729]

4-(3,5-Diphenyl-1*H*-pyrazol-1-yl)benzenesulfonamide 5f

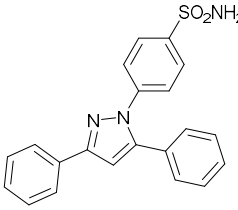

^{1}H-NMR (400 MHz, $CDCl_3$): δ 5.04 (2H, s, NH_2); 6.84 (1H, s, $CH_{pyrazole}$); 7.27-7.30 (2H, m, 2 x CH_{arom}); 7.37-7.39 (4H, m, 4 x CH_{arom}); 7.43-7.47 (2H, m, 2 x CH_{arom}); 7.49-7.51 (2H, m, 2 x CH_{arom}); 7.84-7.87 (2H, m, 2 x CH_{arom}); 7.90-7.92 (2H, m, 2 x CH_{arom}). **^{13}C-NMR** (100 MHz, $CDCl_3$): δ 106.8 ($CH_{pyrazole}$); 125.0 (2 x CH_{arom}); 126.0 (2 x CH_{arom}); 127.5 (CH_{arom}); 128.6 (CH_{arom}); 128.90 (2 x CH_{arom}); 128.95 (2 x CH_{arom}); 129.02 (2 x CH_{arom}); 129.07 (CH_{arom}); 130.2, 132.6, 140.1, 143.5, 144.9 and 153.1 (6 x $C_{arom,quat}$). **IR** (ATR, cm^{-1}): ν_{NH} = 3256; ν_{max} = 3065, 1497, 1341, 1161, 839, 764, 729, 692, 615, 544. **MS** (ESI): *m/z* (%) 376 ([M + 1]$^+$, 100). Yellow solid, 81%. Spectral data matches literature.[730]

4-(5-Methyl-3-phenyl-1*H*-pyrazol-1-yl)benzenesulfonamide 5g

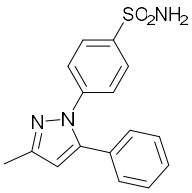

^{1}H-NMR (400 MHz, $CDCl_3$): δ 2.39 (3H, s, $CH_3C_{arom,quat}$); 5.32 (2H, s, NH_2); 6.33 (1H, s, $CH_{pyrazole}$); 7.19-7.20 (2H, m, 2 x CH_{arom}); 7.32-7.34 (5H, m, 5 x CH_{arom}); 7.74-7.76 (2H, m, 2 x CH_{arom}). **^{13}C-NMR** (100 MHz, $CDCl_3$): δ 13.6 ($CH_3C_{arom,quat}$); 109.4 ($CH_{pyrazole}$); 124.8 (2 x CH_{arom}); 127.4 (2 x CH_{arom}); 128.83 (2 x CH_{arom}); 128.87 (CH_{arom}); 128.93 (2 x CH_{arom}); 130.3, 140.0, 143.3, 144.3 and 151.0 (5 x $C_{arom,quat}$). **IR** (ATR, cm^{-1}): ν_{NH} = 3258 and 3159; ν_{max} = 1661, 1506, 1342, 1163, 1098, 839, 610, 540. **MS** (ESI): *m/z* (%) 314 ([M + 1]$^+$, 100). **HRMS** (ESI): calcd. for $C_{16}H_{16}N_3O_2S^+$: 314.0958 [M + H]$^+$, found: 314.0965. Yellow oil, 78%.

3.4.4.4 Larger scale experiment

A large vial was charged with: **CTF-Pyr** (50 mg), 2,7,7-trimethyl-5-oxo-4-phenyl-1,4,5,6,7,8-hexahydroquinoline-3-carboxylate **2d** (339 mg, 1 mmol, 1 eq.) and CH_3CN (25 mL). The reaction mixture was stirred for 40 hours after which it was filtered and rinsed with acetone. The filtrate was evaporated and purified using column chromatography (SiO_2, hexane/EtOAc: 4/1) to give the product as a yellow solid (287 mg, 85%).

3.4.4.5 Recycling experiments

CTF-Pyr (10 mg) and ethyl 2,7,7-trimethyl-5-oxo-4-phenyl-1,4,5,6,7,8-hexahydroquinoline-3-carboxylate **2d** (67.4 mg, 0.2 mmol, 1 eq) were added to a small glass test tube, followed by addition of 5 mL CH_3CN. This was stirred under air and irradiation from a 26 W CFL (~10 cm distance) for 24 hours. The conversion was determined directly from the reaction mixture by taking a small aliquot, evaporating this under a stream of nitrogen and analyzing it using ^{1}H-NMR in DMSO-d_6. The catalyst was filtered off, rinsed with acetone and acetonitrile, dried and reused in the next run.

Chapter 4: Development of NHC-based COFs

Abstract: Catalysis is essential for an efficient and green chemical industry. Existing catalysts often use expensive and toxic metals that are difficult to recycle and separate from the final product. The use of porous organic polymers (POPs) can solve these problems, by either acting as metal-free catalysts or as heterogeneous, recyclable carriers for metal complexes. Whilst imines, bipyridines and phosphines have been extensively explored as ligands in POPs, *N*-heterocyclic carbenes (NHCs) remain underdeveloped. In this chapter the attempted synthesis and possible applications of NHC-containing covalent organic frameworks (COFs), a subclass of POPs, are detailed. Although this project was abandoned, due to difficulty obtaining true COFs, the methods used offer valuable insights into COF synthesis and their potential applications.

Contributions: A major part of the research in this chapter is covered in the master thesis of Isabelle Wijnant[731] and most of the experimental work was performed in collaboration with her.

4.1 Introduction

As stated already many times in this thesis, the use of catalysts to accelerate reactions is essential for an efficient and green chemical industry. However, many problems remain with existing catalysts. The use of transition or noble metals that are expensive, often toxic and difficult to separate and recycle is still prevalent. Moreover, trace amounts of these metals can still be present in the final product, which is not acceptable for all applications (*e.g.* pharmaceuticals). Porous organic polymers (POPs) form a possible solution to this problem. On the one hand, these materials can act as efficient metal-free catalysts for many reactions. On the other hand, they can be used as a heterogeneous carrier material for metal complexes. Many moieties are possible as ligands in these heterogeneous materials, but imines (and the related salen ligands), bipyridines and phosphines have been studied almost exclusively. *N*-heterocyclic carbenes (NHCs) are next to phosphines the most commonly used homogeneous ligands, but they are severely underexplored as heterogeneous ligands, especially on POPs and covalent organic frameworks (COFs).

The synthesis of NHC-containing COFs was envisaged, based on the condensation of amine **1** with aldehydes **Tp** and **2a-b**. The benzimidazolium moieties in the resulting imid-COFs would serve as NHC precursors, as they can be deprotonated to form the NHC-COFs. Next to acting as heterogeneous ligands for metal complexes, the materials themselves could also serve as metal-free organocatalysts. To evaluate the catalytic applications of these NHC-COFs, a test compound **3** was synthesized and complexed with ruthenium to form the novel ruthenium complex **4**. A few reactions were evaluated using the compound **3** and the metal complex **4** as an analogue for the envisaged NHC-COF, of which the oxidation of alcohols using the homogeneous ruthenium complex **4** showed promising results. Unfortunately, while many different conditions for the COF synthesis were evaluated, no crystalline materials could be obtained, and this project was therefore abandoned. Nevertheless, the used methodologies offer insight into the synthesis of new COFs, and the development of applications for them.

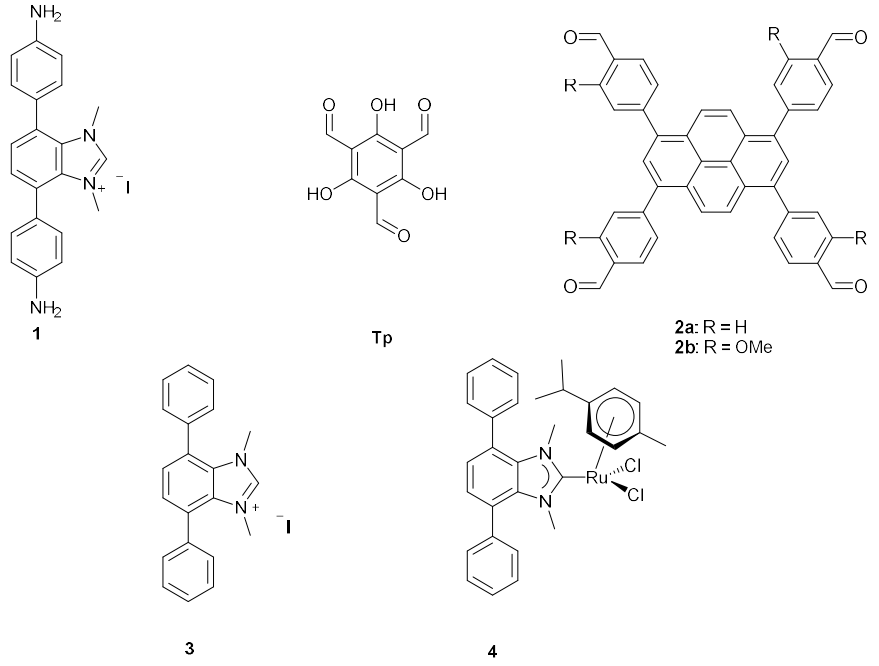

Figure 1: Overview of the synthesized compounds.

4.2 Results and discussion

4.2.1 Synthesis of building blocks

4.2.1.1 Synthesis of amine 1 and test compound 3

First the novel amine building block **1** was synthesized, in conjunction with the unsubstituted analogue **3** which served as a homogeneous test compound. The benzimidazolium compounds **1** and **3** can be viewed as precursors for NHCs, as they can be deprotonated to form the desired NHC. The synthesis route to the amine building block **1** consisted of six steps starting from commercially available 4,7-dibromo-2,1,3-benzothiadiazole **5** (Scheme 1).

The first three steps, towards compound **8**, were already described in the work of Huang *et al.*, and were repeated here.[732] 4,7-Dibromobenzo[*c*]-1,2,5-thiadiazole **5** underwent a reductive ring opening to form the diamine **6** using $NaBH_4$ and $CoCl_2$ as a catalyst. The formed diamine was immediately used for the next step, the benzimidazole synthesis with triethyl orthoformate. This compound could then easily be methylated using methyl iodide to form 4,7-dibromo-1-methyl-1*H*-benzo[*d*]imidazole **8**. The monomethylated benzimidazole **8** was then used as a substrate for the Suzuki coupling reaction to form the arylated products **9a-b**. For the nitrobenzene substituted product **9b** the purification was relatively challenging, as it possessed very low solubility in most common chromatography solvents and the monoarylated side product, while formed in only small quantities, was quite difficult to remove from the main product. Finally, using THF and H_2O as a solvent for reversed phase chromatography, followed by multiple recrystallizations, pure product could be obtained. For the phenyl substituted product **9a**, the purification posed less problems, and it was easily obtained using reversed phase chromatography. The methylation of compounds **9a-b** with a large excess of methyl iodide furnished benzimidazoliums **3** and **10** in excellent yields. Finally, the nitro groups of compound **10** were reduced using hydrazine, HCl and palladium on carbon. The addition of HCl was needed as it suppressed side reactions. Moreover, due to the low solubility of diamine **1**, rinsing with a strong solvent such as DMF when filtering off the catalyst was needed to recover the product completely, otherwise very low yields were obtained.

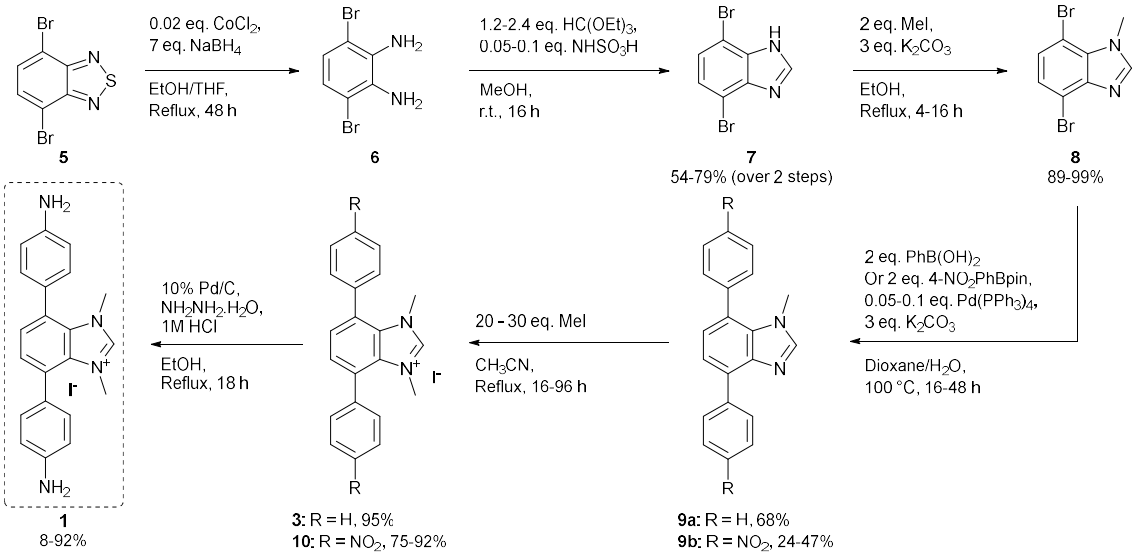

Scheme 1: Synthesis route towards the amine building block **1** and the test compound **3**.

4.2.1.2 Synthesis of aldehydes **2a-b**

The synthesis of 1,3,5-triformylphloroglucinol **Tp** is described in Chapter II. Next to this building block two pyrene-based aldehydes **2a-b** were synthesized using Suzuki couplings. The pyrene core provides tetra-connected building blocks, and is known to provide highly crystalline COFs. The novel methoxy substituted derivative **2b** was also synthesized. Methoxy groups can provide extra stability to imine-linked COFs through steric shielding of the linkage, and strengthening of the interlayer interaction through both hydrogen bonding and reduction of electrostatic repulsion.[202,486] Both aldehydes **2a-b** were obtained in three steps starting from pyrene **11**. First pyrene **11** was regioselective brominated to form 1,3,6,8-tetrabromopyrene **12a**.[733] This was borylated using bis(pinacolato)diboron (B_2pin_2) and [1,1'-bis(diphenylphosphino)ferrocene]dichloropalladium (II) ($PdCl_2$(dppf)) as a catalyst.[733,734] The borylated pyrene **12b** was then coupled with 4-bromobenzaldehyde or 4-bromo-2-methoxybenzaldehyde to give the desired aldehydes **2a-b**.

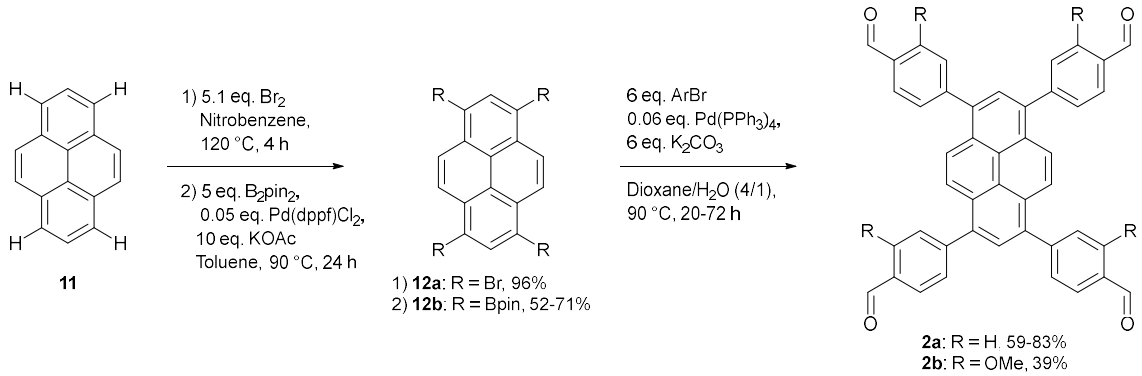

Scheme 2: Synthesis route towards the aldehydes **2a-b**.

4.2.1.3 Synthesis of ruthenium complex **4**

NHC are a class of privileged ligands, as they can complex with a wide variety of metals and catalyze an array of useful reactions. An NHC-COF could therefore serve as a heterogeneous ligand for a wide range of metals. To explore this, the homogeneous analogue of an NHC-COF, compound **3**, was metalated with a ruthenium complex. Ruthenium serves as a catalyst in a very wide range of reactions, such as alkene metathesis reactions, transfer hydrogenations, oxidations…[735–737] Ruthenium can take many different oxidation states (-II to +VIII), explaining its widespread application catalyzing oxidation/reduction reactions. Moreover, ruthenium is rare and therefore precious, and thus heterogenizing it can be very useful.[738] In order to evaluate the potential of a Ru@NHC-COF, the homogeneous complex **4** was synthesized.

To synthetize complex **4**, two procedures were evaluated (Scheme 3). In the first procedure potassium bis(trimethylsilyl)amide (KHMDS) was used to deprotonate the acidic proton of imidazolium **3**. This deprotonated compound was then added dropwise to a solution of the ruthenium(II) dimer, $[RuCl_2(p\text{-cymene})]_2$, followed by refluxing overnight. However, after this reaction only starting material was detected. In the second procedure, benzimidazolium **3** was first converted to the corresponding silver complex by addition of Ag_2O. After addition of the ruthenium(II) dimer transmetalation takes place to produce the NHC ruthenium complex **4**, which could easily be isolated by precipitation and filtration.

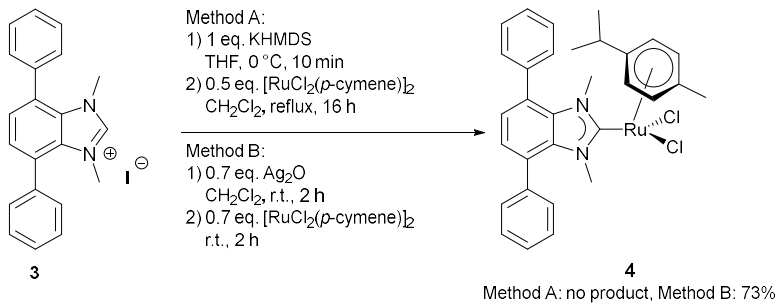

Scheme 3: Synthesis of ruthenium complex **4**.

4.2.2 Applications of the homogeneous catalysts

4.2.2.1 Organocatalysis

To evaluate the potential of the NHC-COFs as potential organocatalysts, the *umpolung* reaction of *trans*-cinnamaldehyde **13** with trifluoroacetophenone **14** to the corresponding γ-butyrolactones **15a-b** was evaluated (Scheme 4). The mechanism of this transformation occurs via nucleophilic addition of the NHC **16**, formed through deprotonation of the homogeneous catalyst **3**, to *trans*-cinnamaldehyde **13**, forming intermediate **17**. *Umpolung* and nucleophilic attack of the β-carbon atom onto trifluoroacetophenone **14** results in the formation of intermediate **19**, which after ring closure liberates the carbene **16** and the product **15**. Initially, in acetonitrile at 70 °C three peaks were observed in the ^{19}F-NMR of the crude reaction mixture, probably corresponding to **14** and **15a-b**. However, these results were not very reproducible, as upon repetition much more complex mixtures were formed. Moreover, even after a thorough screening of the reaction conditions: different solvents (CH_3CN, THF, toluene), temperatures (r.t. to 80°C), time spans, amounts of DBU… no satisfactory results could be obtained. Therefore, it was decided that this reaction does not work well with compound **3** as a catalyst, and we focused on metal catalysis.

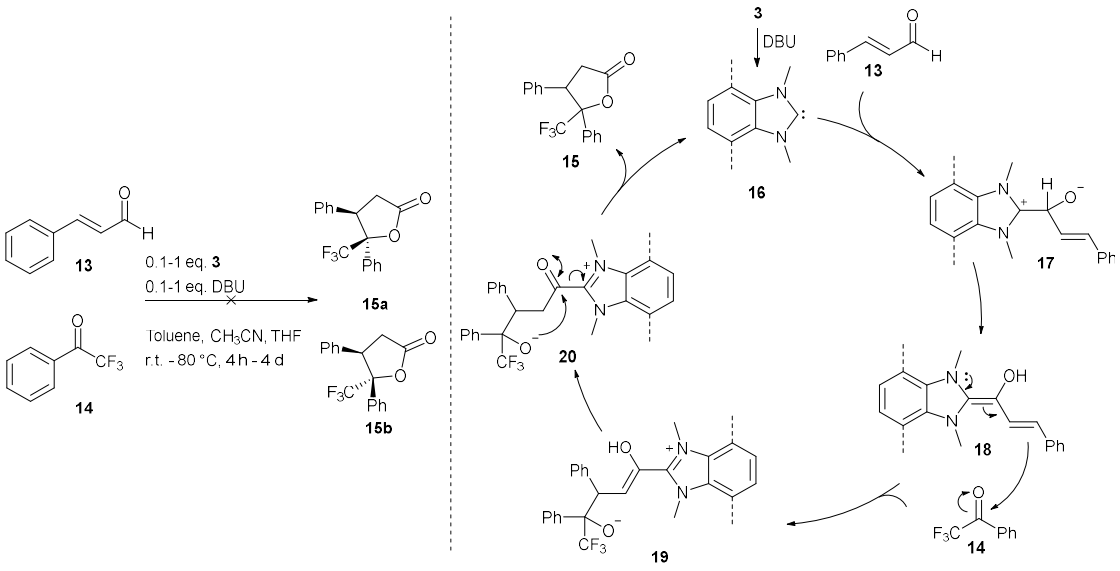

Scheme 4: Attempted *umpolung* reaction of *trans*-cinnamaldehyde **13** with trifluoroacetophenone **14** to the corresponding γ-butyrolactones **15a-b**, using compound **3** as a homogeneous catalyst.

4.2.2.2 Metal catalysis

4.2.2.2.1 C-H arylation of phenylpyridine

As a first test reaction for the metal complex **4**, the direct C-H arylation of 2-phenylpyridine **21** was chosen (Scheme 5). This reaction has the advantage over the commonly used Pd-catalyzed cross-couplings that it does not require the activation of the C-H bond through formation of an organometal species such as an aryl boronic acid or organostannane.[739] An analogous complex with a pyrene core had already been described in the literature as an effective catalyst for C-H arylation/alkylation of arylpyridines.[740] However, when using complex **4** for the arylation of 2-phenylpyridine **21** with chloro- or bromobenzene **22**, no products could be detected, and therefore another reaction was evaluated.

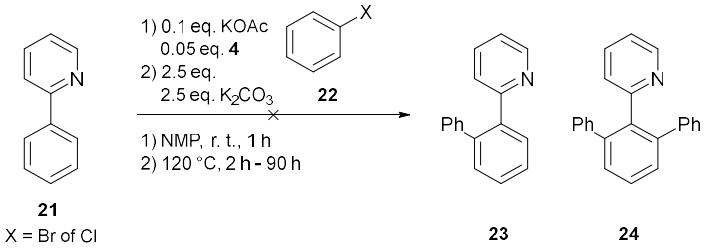

Scheme 5: Attempted arylation of phenylpyridine using ruthenium complex **4** as a catalyst.

4.2.2.2.2 The oxidation of alcohols to carboxylic acids

The oxidations of alcohols to carboxylic acids are important reactions in the chemical industry and academia.[741] In a dehydrogenation reaction the alcohol is oxidized without the use of oxygen or toxic oxidants, by removal of hydrogen. This has important safety and cost advantages, and a good atom economy.[742]

The new, homogeneous ruthenium complex **4** was evaluated for the oxidation of two alcohols: benzyl alcohol **25a** and decan-1-ol **25b**, to their corresponding carboxylic acids **26a-b**. The mechanism of this transformation was based on literature and is shown in Scheme 6.[736] First *p*-cymene and two chloride ligands are lost and replaced with two hydrides, a hydroxide and a phosphine, thus forming the coordinatively unsaturated (16 e^-) complex **27**. The alcohol **25** is added to this complex, forming intermediate **28**, which then liberates H_2 to form complex **29**. This undergoes β-hydride elimination, to form the aldehyde. Internal nucleophilic attack of the hydroxide ligand on this aldehyde forms the hemiacetal. The complex **32** will then again lose hydrogen, followed by β-hydride elimination where the carboxylate is liberated and the coordinatively unsaturated complex **27** is again formed.

The alcohol was reacted in refluxing toluene using KOH and tricyclohexylphosphine tetrafluoroborate. The only formed byproduct, hydrogen gas, escapes during the reaction and the formed carboxylic acid is present as its potassium salt, which precipitates. This was filtered off, acidified and extracted to isolate the carboxylic acid in yields ranging from 12% to 56%. As shown in Table 1, extra equivalents of base did not lead to higher yields. It is also noteworthy that even though full conversions were obtained (^{1}H-NMR), the obtained yields were quite low. Probably some losses occurred during the work up of this reaction, however even after detailed examination of all fractions the source of the relatively low yields could not be tracked down. Nevertheless, this reaction using the novel complex **4** did show great promise, especially if it could be heterogenized on a carrier material.

Table 1: The dehydrogenation of alcohols catalyzed by homogeneous ruthenium complex **4**.[a]

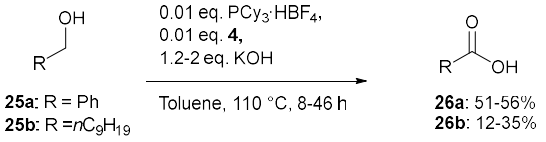

Entry	Substrate	Eq. KOH	Time (h)	Yield (%)[b]
1-3	Benzyl alcohol	1.2	24-46	54-56
4	Benzyl alcohol	2	8	51
6-7	Decan-1-ol	1.2	25	12-34
8	Decan-1-ol	2	17	35

[a] Reaction conditions: Complex **4** (30 mg, 0.05 mmol, 0.01 eq.), alcohol **25** (5 mmol, 1 eq.), PCy_3HBF_4 (18.4 mg, 0.05 mmol, 0.01 eq.), KOH (6-10 mmol, 1.2-1.4 eq.), toluene (10 mL).

[b] Isolated yields

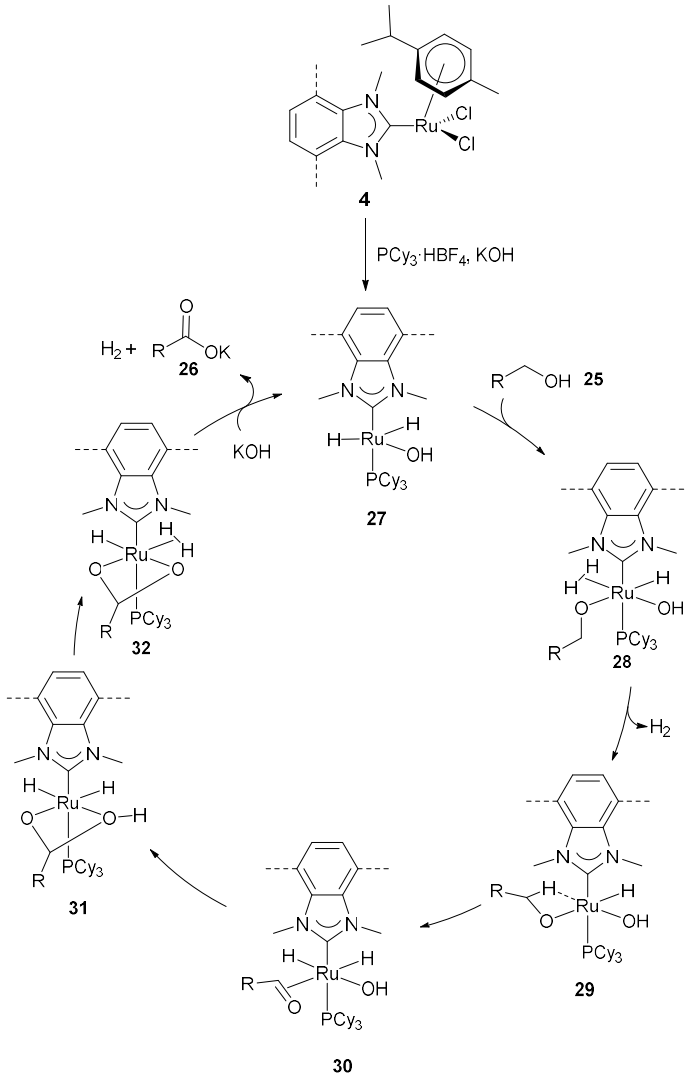

Scheme 6: Mechanism of the alcohol oxidation catalyzed by homogeneous complex **4**.

4.2.3 The attempted synthesis of imidCOFs

The new amine building block **1** was polymerized with tree aldehydes: **Tp**, **2a** and **2b** under solvothermal conditions, to form **imidCOF-1**, **imidCOF-2** and **imidCOF-3**, respectively. These imine- or β-ketoenamine-linked materials were analyzed using PXRD and IR to evaluate the success of the COF synthesis.

The synthesis of the β-ketoenamine-linked **imidCOF-1** from amine **1** and **Tp** was evaluated using different solvent combinations, catalysts, and temperatures (Table 2). All obtained materials possessed similar IR spectra, of which a representative example is given in Figure 2. The sharp signals originating from the free NH_2 groups, at 3343 cm^{-1} and the signals of the aldehydes of **Tp** at 1636 cm^{-1} disappear, confirming the complete reaction of these functional groups. The new bands at 1570 cm^{-1} and 1250-1280 cm^{-1} point to the presence of C=O and C-N functionalities, suggesting the formation of the envisaged β-ketoenamine bonds.[487,743,744] The values for the carbonyl signal in these types of materials are much lower than wat is generally seen for carbonyl groups. Moreover, the C=O and C=C bands fall together in these radialene moieties, and as such the C=O bands are only visible as shoulders on the C=C bands.[487] The broad absorption bands at 3400 cm^{-1} can be attributed to traces of water and the N-H stretching.

Whilst the obtained FTIR data seemed promising, the XRD spectra of the synthesized materials did not show many features pointing to crystallinity. The most promising material, which was synthesized using AcOH in DMAc (Table 2, entry 4), did possess a small shoulder in the region at 4°, pointing to some crystallinity. Moreover, a broad peak could be distinguished around 25°, which points to the presence of π-π stacking between the layers of the polymers (Figure 3).[743,744]

Table 2: Conditions for the synthesis of **imidCOF-1**.[a]

Entry	Catalyst	Solvent	T,t
1	6M AcOH	DMAC/*o*DCB (3/1)	120 °C, 72 h
2		Dioxane/mesitylene (1/1)	
3		*o*DCB/*n*BuOH (1/1)	
4		DMAc	
5		H_2O	
6	$Sc(OTf)_3$	Dioxane/mesitylene (4/1)	r.t., 72 h
7	KOH	H_2O/DMF (3/5)	140 °C, 24 h

[a] Reaction conditions: **Tp** (21 mg, 0.1 mmol, 1 eq.), amine **1** (68 mg, 0.15 mmol, 1.5 eq.).

The initial step in the creation of a β-ketoenamine-linked framework consists of the formation of an imine-linked material, during which error-correction is still possible. Irreversible tautomerization then takes place, locking the structure. The low or non-existing crystallinity of **imidCOF-1** could be caused by the irreversible tautomerization occurring too rapidly. A possible strategy could be the addition of a modulator, a monofunctional molecule similar to the monomers of the COFs, but not able to polymerize (such as aniline or benzaldehyde).[393,745,746] Another possible strategy is the use of reactions that are more reversible, such as the synthesis of imine COFs. The imine COF synthesis was evaluated using amine **1** and aldehydes **2a** and **2b**, again using a wide variety of conditions. Unfortunately, in all these cases no reaction occurred and the pyrene building blocks were recuperated unchanged.

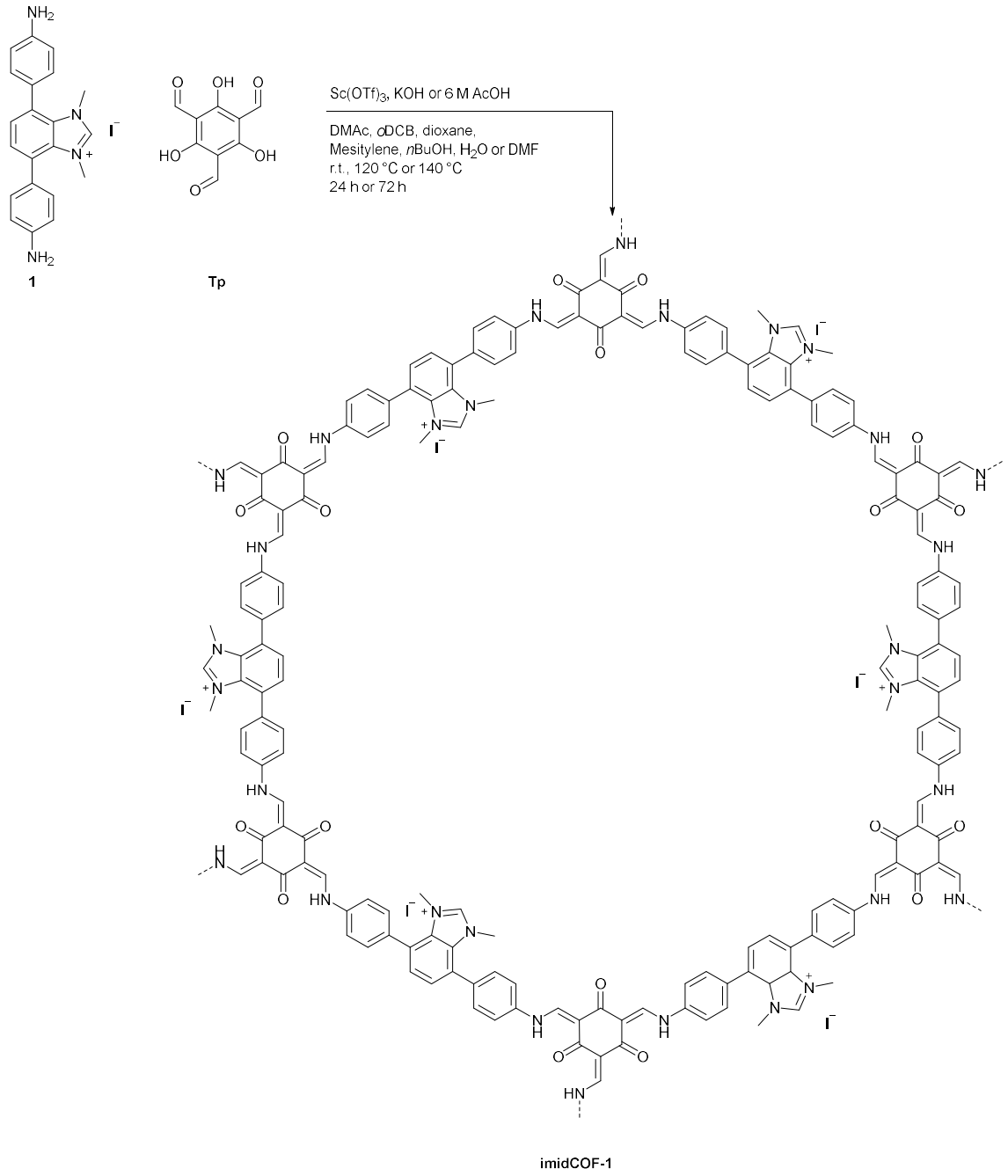

Scheme 7: Attempted synthesis of **imidCOF-1** from amine **1** and **Tp**. The idealized structure of the COF is shown.

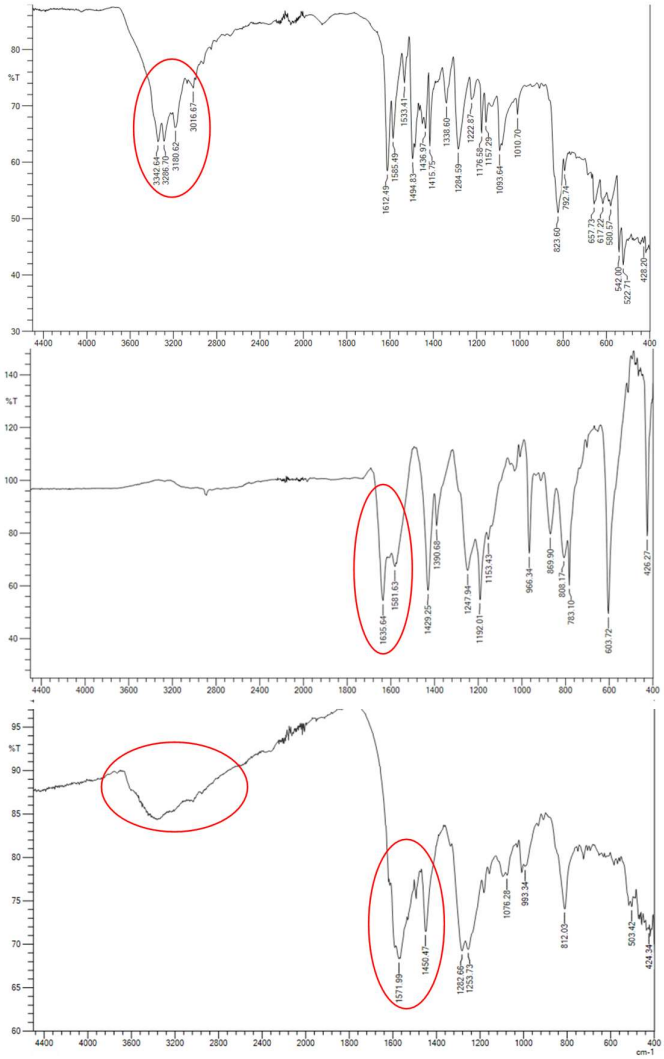

Figure 2: FTIR spectra of amine **1** (top), **Tp** (middle) and **imidCOF-1** (bottom). The red circles indicate characteristic signals.

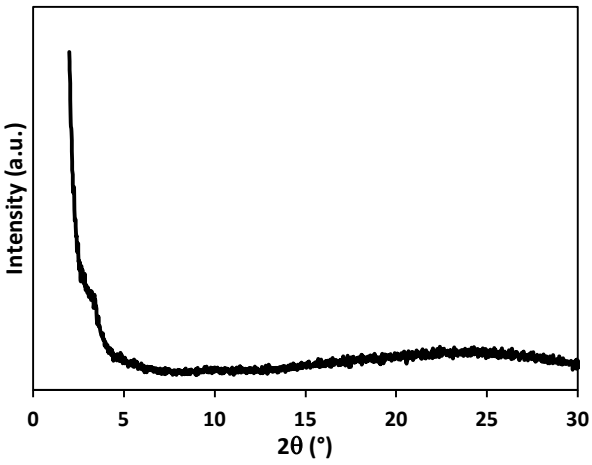

Figure 3: The PXRD spectrum of **imidCOF-1** (Table 2, entry 4). The small shoulder around 2θ = 4° and the broad peak around 2θ = 25° could indicate some (small) measure of crystallinity.

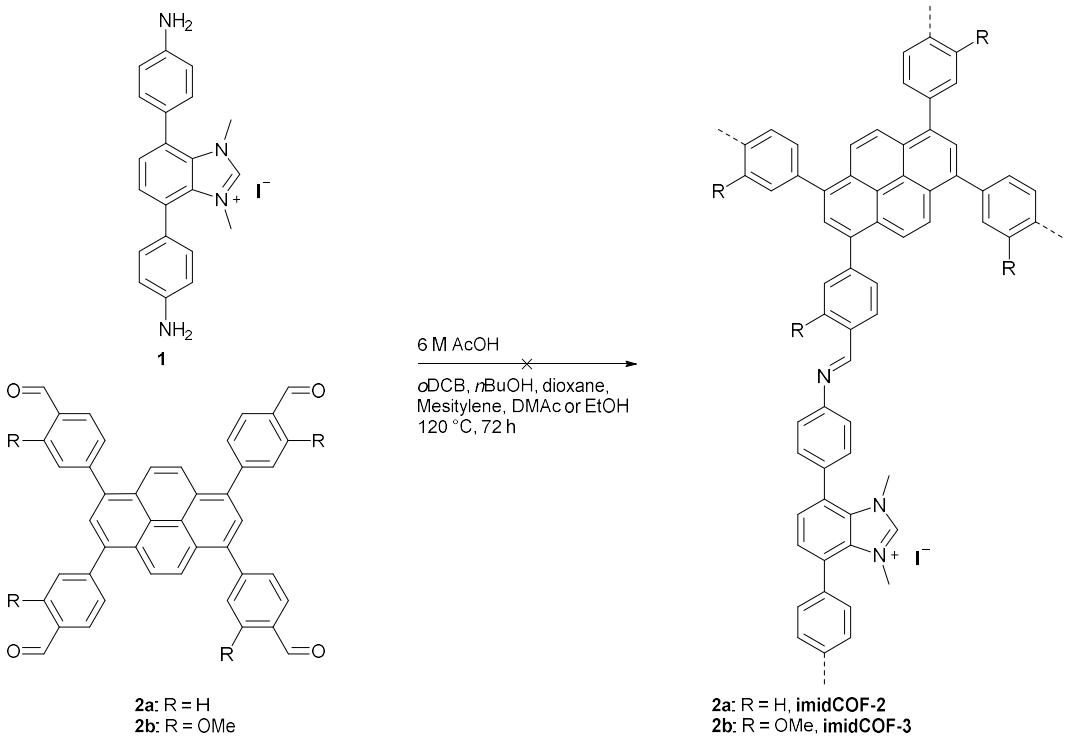

Scheme 8: Attempted synthesis of **COF-2** and **COF-3**.

4.3 Conclusions

NHCs are important ligands and organocatalysts, and the incorporation of these moieties in COFs is an interesting avenue to obtain new, heterogeneous catalysts. However, obtaining optimal conditions, with enough error-correction to obtain truly crystalline materials can seem like looking for a needle in a haystack, and in this example a real COF could unfortunately not be obtained. Nevertheless, some interesting results were discussed in this appendix. Amine **1** and aldehyde **2b** are new compounds, and could still be used as building blocks for novel COFs. Next to this, the new homogeneous ruthenium complex **4**, is a promising catalyst for the oxidation reaction of alcohols. Whilst the isolated yields were still only relatively low, the conversions reached 100% and therefore this application holds some promise. Moreover, this catalyst could easily be developed further as the use of differently substituted aromatics during the Suzuki coupling allows the tuning of the NHC ligand.

4.4 Experimental section

4.4.1 Synthesis of building blocks and catalysts

4.4.1.1 Synthesis of the diamine 1

This synthesis consisted of six steps, of which the first three were already described by Huang *et al*.[19]

Step 1:

A one liter two-necked flask was charged with: 4,7-dibromobenzothiadiazole **5** (10.29 g, 35 mmol, 1 eq.) and $CoCl_2$ (45 mg, 0.35 mmol, 0.01 eq.). This was dissolved in 100 mL THF and 225 mL EtOH. The mixture was refluxed for four hours and $NaBH_4$ (3 x 1.324 g, 3 x 35 mmol, 3 x 1 eq.) was added (three portions, with one hour in between). When the reaction was not finished after four hours of reflux (LC-MS), an extra two equivalents of $NaBH_4$ (2.648 g, 70 mmol, 2 eq.) were added, and the mixture was refluxed for another hour. The mixture was then allowed to cool down to room temperature, water (150 mL) was added, and it was stirred at room temperature for 30 minutes. This was then filtered over Celite®, evaporated under vacuum, redissolved in 100 mL CH_2Cl_2 and washed with 200 mL brine. The water phase was extracted with CH_2Cl_2 (2 x 100 mL). The combined organic phases were dried over $MgSO_4$, filtered and evaporated. The obtained diamine **6** was immediately used for step two.

Step 2:

The diamine **6** (35 mmol, 1 eq.) was dissolved in 175 mL MeOH. Sulfamic acid (166 mg, 1.75 mmol, 0.05 eq.) and 7 mL triethyl orthoformate (6.2 g, 42 mmol, 1.2 eq.) were added. This was stirred at room temperature for sixteen hours after which the full conversion of the reaction was evaluated using LC-MS. If starting material was still present, sulfamic acid (166 mg, 1.75 mmol, 0.05 eq.) and 7 mL triethyl orthoformate (6.2 g, 42 mmol, 1.2 eq.) were again added and the reaction was further stirred for 24 hours. Upon completion (LC-MS) the solvent was evaporated under vacuum and the resulting powder was filtered and washed with 100 mL Et_2O. The benzimidazole **7** was obtained as a brown powder (7.65 g, 79% over two steps).

Step 3:

4,7-Dibromo-1-methyl-1*H*-benzo[*d*]imidazole **7** (7.65 g, 27.72 mmol, 1 eq.), K_2CO_3 (11.49 g, 83.14 mmol, 3 eq.) and 185 mL EtOH were refluxed for one hour, after which 3.45 mL MeI (7.86 g, 55.4 mmol, 2 eq.) was added. The reaction was then stirred under reflux for sixteen hours. The mixture was allowed to cool down to room temperature, 70 mL water was added and the EtOH was evaporated. The obtained precipitate was then filtered off and washed with water (10 mL) and hexane/Et_2O (1/1, 20 mL). After drying under vacuum the title product **8** was obtained as a brown powder (7.95 g, 27.7 mmol, 99%).

4,7-Dibromo-1-methyl-1*H*-benzo[*d*]imidazole 8

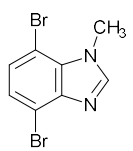

^{1}H-NMR (400 MHz, DMSO-d_6): δ 4.09 (3H, s, CH_3); 7.37 (2H, s, 2 x CH_{arom}); 8.36 (1H, s, CH_{arom}). **^{13}C-NMR** (100.6 MHz, DMSO-d_6): δ 34.1 (CH_3); 102.3 ($C_{arom,quat}$); 112.4 ($C_{arom,quat}$); 125.7 (CH_{arom}); 127.6 (CH_{arom}); 132.0 ($C_{arom,quat}$); 143.4 ($C_{arom,quat}$); 147.5 (CH_{arom}). Brown powder, 99%. The obtained spectral data matched literature.[19732]

Step 4:

To a 500 mL flask were added: 4,7-dibromo-1-methyl-1*H*-benzo[*d*]imidazole **8** (5.24 g, 18.07 mmol, 1 eq.), 4,4,5,5-tetramethyl-2-(4-nitrophenyl)-1,3,2-dioxaborolane (9.00 g, 36.13 mmol, 2 eq.), K_2CO_3 (7.49 g, 54.20 mmol, 3 eq.) and 180 mL dioxane/water (4/1). This was degassed by bubbling the solution with nitrogen for 30 minutes after which $Pd(PPh_3)_4$ (1.25 g, 1.08 mmol, 0.06 eq.) was added. The reaction was stirred at 100 °C until completion (sixteen hours, LC-MS). The reaction mixture was then filtered over Celite® and washed with 70 mL EtOAc. The filtrate was extracted three times with 100 mL EtOAc, after which the combined organic phases were dried over $MgSO_4$, filtered, and evaporated. The product **9b** was further purified via column chromatography (C18, THF/H_2O, 40/60 – 100/0) followed by recrystallization in CH_3CN/THF/H_2O (5/1/1, 105 mL), after which a brown-yellow powder was obtained (3.20 g, 47%).

1-Methyl-4,7-bis(4-nitrophenyl)-1*H*-benzo[*d*]imidazole 9b

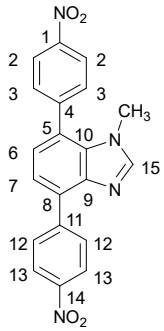

^{1}H-NMR (400 MHz, DMSO-d_6): δ 3.46 (3H, s, CH_3); 7.31 (1H, d, *J* = 7.7 Hz, CH_{arom}^{6}); 7.70 (1H, d, *J* = 7.7 Hz, CH_{arom}^{7}); 7.85 (2H, d, *J* = 8.0 Hz, 2 x CH_{arom}^{12}); 8.35-8.37 (5H, m, 2 x CH_{arom}^{3}, 2 x CH_{arom}^{13} and CH_{arom}^{15}); 8.45-8.47 (2H, m, 2 x CH_{arom}^{2}). **^{13}C-NMR** (100.6 MHz, DMSO-d_6): δ 34.4 (CH_3); 121.3 (CH_{arom}^{7}); 123.1 (2 x CH_{arom}); 123.5 (2 x CH_{arom}); 124.7 (CH_{arom}^{6}); 125.7 ($C_{arom,quat}$); 128.7 ($C_{arom,quat}$); 130.0 (2 x CH_{arom}^{2}); 131.2 (2 x CH_{arom}^{12}); 132.2 ($C_{arom,quat}^{10}$); 142.1 ($C_{arom,quat}$); 144.3 ($C_{arom,quat}$); 144.5 ($C_{arom,quat}$); 146.4 ($C_{arom,quat}^{1}$); 147.0 ($C_{arom,quat}^{14}$); 147.3 (CH_{arom}^{15}). **IR** (ATR, cm^{-1}): $\nu_{N\text{-}O}$ = 1508; $\nu_{C\text{-}N}$ = 1335, ν_{max} = 1589, 1103, 1070, 851, 820, 750, 706, 625. **MS** (ESI): *m/z* (%) 375 ($[M + 1]^+$, 100). Brown to yellow powder, 47%.

Step 5:

1-Methyl-4,7-bis(4-nitrophenyl)-1*H*-benzo[d]imidazole **9b** (1.37 g, 3.66 mmol, 1 eq.), 35 mL CH_3CN and 4.6 mL MeI (10.4 g, 73.20 mmol, 20 eq.) were added to a pressure tube. This was then stirred at 82 °C for 16 hours. After full conversion of the starting material (LC-MS) the reaction mixture was evaporated using a rotavapor in a fume hood. The resulting powder was filtered and washed with 10 mL hexane/EtOAc (2/1), and it was dried under vacuum to give the title compound **10** as a brown-grey powder (1.68 g, 89%).

1,3-Dimethyl-4,7-bis(4-nitrophenyl)-1*H*-benzo[d]imidazol-3-ium iodide 10

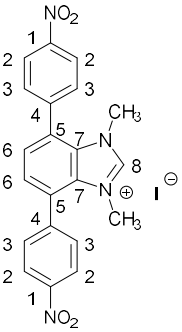

^{1}H-NMR (400 MHz, DMSO-d_6): δ 3.57 (6H, s, 2 x CH_3^{8}); 7.67 (2H, s, 2 x CH_{arom}^{6}); 7.88 (4H, d, *J* = 8.1 Hz, 4 x CH_{arom}^{3}); 8.43 (4H, d, *J* = 8.1 Hz, 4 x CH_{arom}^{2}); 9.72 (1H, s, CH_{arom}^{8}). **^{13}C-NMR** (100.6 MHz, DMSO-d_6): δ 37.1 (2 x CH_3); 123.5 (4 x CH_{arom}^{2}); 127.6 (2 x $C_{arom,quat}^{5}$); 128.2 (2 x CH_{arom}^{6}); 129.7 (2 x $C_{arom,quat}^{7}$); 131.5 (4 x CH_{arom}^{3}); 141.9 (2 x $C_{arom,quat}^{4}$); 146.0 (CH_{arom}^{8}); 147.8 (2 x $C_{arom,quat}^{1}$). **IR** (ATR, cm^{1}): $\nu_{N\text{-}O}$ = 1514; $\nu_{C\text{-}N}$ = 1344; ν_{max} = 1597, 1101, 1013, 854, 750, 694, 613, 494. **MS** (ESI): *m/z* (%) 389 ($[M]^+$, 100). Brown to grey powder, 89%.

Step 6:

A 250 mL two necked flask, under nitrogen atmosphere, was charged with: 1,3-dimethyl-4,7-bis(4-nitrophenyl)-1*H*-benzo[d]imidazol-3-ium iodide **10** (1.36 g, 2.63 mmol, 1 eq.), Pd/C (394 mg) and 80 mL EtOH. To this suspension was then added $NH_2NH_2.H_2O$ (6.2 g, 124 mmol, 47 eq.) and the flask was

heated at 80 °C. After five minutes 25 mL 1M HCl was added and the mixture was further stirred at 80 °C overnight. The completion of the reaction was checked using LC-MS. The mixture was then immediately filtered over a paper filter whilst still hot. The filter cake was then rinsed further with 70 mL of nearly boiling EtOH, thus collecting filtrate I. A second rinse was performed using 50 mL DMF, collecting filtrate II. Both fractions were separately evaporated using a rotavapor in a fume hood. The resulting solids were washed with water (10 mL) and Et_2O (10 mL). Filtrate I gave the product **1** as a white powder and filtrate II as a brown to grey powder. Both had identical purity according to LC-MS and NMR and the combined yield of the product **1** was 1.10 g (92%).

4,7-Bis(4-aminophenyl)-1,3-dimethyl-1*H*-benzo[d]imidazol-3-ium iodide 1

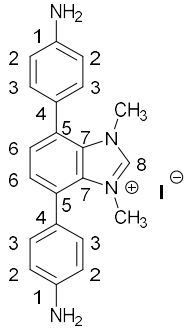

^{1}H-NMR (400 MHz, DMSO-d_6): δ 3.58 (6H, s, 2 x CH_3); 5.43 (4H, s, 2 x NH_2); 6.69 (4H, d, *J* = 8.3 Hz, 4 x CH_{arom}^2); 7.14 (4H, d, *J* = 8.3 Hz, 4 x CH_{arom}^3); 7.37 (2H, s, 2 x CH_{arom}^6); 9.58 (1H, s, CH_{arom}^8). **^{13}C-NMR** (100.6 MHz, DMSO-d_6): δ 36.6 (2 x CH_3); 113.3 (4 x CH_{arom}^2); 122.1 (2 x $C_{arom,quat}^4$); 128.2 (2 x CH_{arom}^6); 128.8 (2 x $C_{arom,quat}^5$); 129.8 (2 x $C_{arom,quat}^7$); 130.5 (4 x CH_{arom}^3); 145.1 (CH_{arom}^8); 149.2 (2 x $C_{arom,quat}^1$). **IR** (ATR, cm^{-1}): ν_{N-H} = 3343 and 1612; ν_{C-N} = 1285; ν_{max} = 1495, 1416, 1339, 1177, 1094, 824, 523. **MS** (ESI): *m/z* (%) 329 ([M]$^+$, 100). White to grey powder, 92%.

4.4.1.2 The synthesis of the homogeneous test compound

The homogeneous test compound **3** was synthesized in two steps starting from previously prepared 4,7-dibromo-1-methyl-1*H*-benzo[*d*]imidazole **8**.

Step 1:

To a 250 mL flask were added: 4,7-dibromo-1-methyl-1*H*-benzo[*d*]imidazole **8** (2.71 g, 9.35 mmol, 1 eq.), phenylboronic acid (2.28 g, 18.7 mmol, 2 eq.), K_2CO_3 (3.88 g, 28.04 mmol, 3 eq.) and 95 mL dioxane/H_2O (4/1). This mixture was degassed by bubbling with nitrogen for 30 minutes after which $Pd(PPh_3)_4$ (648 mg, 0.56 mmol, 0.06 eq.) was added. The mixture was then stirred at 100 °C for 16 hours. After completion (LC-MS), the mixture was filtered over Celite® and washed with 35 mL EtOAc. Water (50 mL) was added to the filtrate and the layers were separated. The water layer was extracted three more times with EtOAc (50 mL). The combined organic phases were then dried over $MgSO_4$, filtered and evaporated. The crude product was purified via column chromatography (C18, THF/H_2O, 23/77 – 100/0) to obtain the title compound **9a** as a brown-yellow powder (1.82 g, 68%).

1-Methyl-4,7-diphenyl-1*H*-benzo[*d*]imidazole 9a

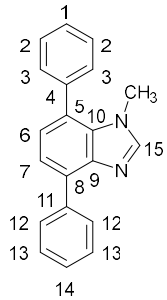

^{1}H-NMR (400 MHz, DMSO-d_6): δ 3.39 (3H, s, CH_3); 7.15 (1H, d, *J* = 7.6 Hz, CH_{arom}^6); 7.36-7.39 (1H, m, CH_{arom}); 7.45-7.52 (8H, m, 8 x CH_{arom}); 8.07 (2H, d, *J* = 7.6 Hz, 2 x CH_{arom}); 8.22 (1H, s, CH_{arom}^{15}). **^{13}C-NMR** (100.6 MHz, DMSO-d_6): δ 34.0 (CH_3); 120.4 (CH_{arom}); 124.6 (CH_{arom}); 126.2 ($C_{arom,quat}$); 127.2 (CH_{arom}); 127.7 ($C_{arom,quat}$); 127.9 (2 x CH_{arom}); 128.2 (2 x CH_{arom}); 129.0 (2 x CH_{arom}); 129.8 (2 x CH_{arom}); 130.5 ($C_{arom,quat}$); 132.2 ($C_{arom,quat}^{10}$); 138.0 ($C_{arom,quat}$); 138.1 ($C_{arom,quat}$); 141.8 ($C_{arom,quat}^9$); 146.3 (CH_{arom}^{15}). **IR** (ATR, cm^{-1}): ν_{max} = 3053, 1470, 1339, 1072, 866, 822, 752, 694, 654, 488. **MS** (ESI): *m/z* (%) 285 ([M + 1]$^+$, 100). Brown-yellow powder, 68%.

Step 2:

1-Methyl-4,7-diphenyl-1*H*-benzo[*d*]imidazole **9a** (1.81 g, 6.36 mmol, 1 eq.), 7.9 mL methyl iodide (18.05 g, 127.2 mmol, 20 eq.) and 65 mL CH_3CN were added to a pressure tube which was heated at 82 °C for sixteen hours. After completion of the reaction (LC-MS) the mixture was evaporated using a rotavapor in a fume hood, filtered and washed with 15 mL hexane/EtOAc (2/1) to obtain the title compound **3** as a grey powder (2.58 g, 95%).

1,3-Dimethyl-4,7-diphenyl-1*H*-benzo[*d*]imidazol-3-ium iodide 3

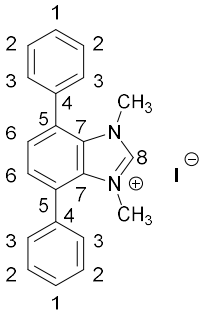

^{1}H-NMR (400 MHz, DMSO-d_6): δ 3.52 (6H, s, 2 x CH_3); 7.54-7.57 (12H, m, 12 x CH_{arom}); 9.66 (1H, s, CH_{arom}^{8}). **^{13}C-NMR** (100.6 MHz, DMSO-d_6): δ 36.7 (2 x CH_3); 128.2 (2 x CH_{arom}); 128.4 (4 x CH_{arom}); 128.8 (2 x $C_{arom,quat}$); 128.9 (2 x CH_{arom}); 129.6 (2 x $C_{arom,quat}^{7}$); 129.9 (4 x CH_{arom}); 135.4 (2 x $C_{arom,quat}$); 145.6 (CH_{arom}^{8}). **IR** (ATR, cm^{-1}): ν_{C-N} = 1341; ν_{max} = 3458, 2982, 1589, 1447, 1088, 849, 762, 706, 490. **MS** (ESI): *m/z* (%) 299 ([M]$^+$, 100). Grey powder, 95%.

4.4.1.3 The synthesis of ruthenium complex **4**

1-Methyl-4,7-diphenyl-1*H*-benzo[*d*]imidazole iodide **3** (50 mg, 0.11 mmol, 1 eq.) and Ag_2O (19 mg, 0.08 mmol, 0.7 eq.) were dissolved in 10 mL CH_2Cl_2 in a 25 mL flask. The flask was protected from light with aluminium foil. After stirring for two hours at room temperature (cymene)ruthenium dichloride dimer ([$RuCl_2$(*p*-cymene)]$_2$) (51 mg, 0.08 mmol, 0.7 eq.) was added, and the reaction was stirred for two more hours at room temperature, after which the reaction mixture was filtered over Celite®. The filtrate was evaporated and redissolved in 10 mL CH_2CH_2, after which 5 mL hexane was added and the mixture was cooled in the freezer for half an hour. The obtained precipitate was filtered off. The precipitate was dissolved in 10 mL $CHCl_3$ and filtered. The filtrate was evaporated, and the title product **4** was obtained as a red powder (50 mg, 0.081 mol, 73%)

(1,3-Dimethyl-4,7-diphenyl-1*H*-benzimidazol-3-ium-2-yl)-(*p*-cymene)ruthenium(IV)-chloride 4

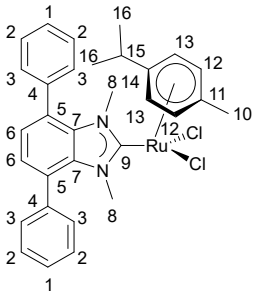

^{1}H-NMR (400 MHz, $CDCl_3$): δ 1.23 (6H, d, *J* = 6.9 Hz, 2 x CH_3^{16}); 2.05 (3H, s, CH_3^{10}); 2.91 (1H, septet, *J* = 6.9 Hz, CH^{15}); 3.73 (6H, s, 2 x CH_3^{8}); 5.11 (2H, d, *J* = 6.0 Hz, 2 x CH^{12}); 5.39 (2H, d, *J* = 6.0 Hz, 2 x CH^{13}); 7.12 (2H, s, 2 x CH^{6}); 7.33-7.50 (10H, m, 10 x CH_{arom}). **^{13}C-NMR** (100.6 MHz, $CDCl_3$): δ 18.9 (CH_3^{10}); 22.7 (2 x CH_3^{16}); 30.9 (CH^{15}); 41.5 (2 x CH_3^{8}); 83.9 (2 x CH^{12}); 85.5 (2 x CH^{13}); 99.3 ($C_{arom,quat}^{11}$); 110.0 ($C_{arom,quat}^{14}$); 125.5 (2 x CH_{arom}^{6}); 126.5 (2 x $C_{arom,quat}$); 128.07-128.10 (m, 6 x CH_{arom}); 129.4 (br s, 2 x CH_{arom}); 130.8 (br s, 2 x CH_{arom}); 133.6 (2 x $C_{arom,quat}^{7}$); 138.5 (2 x $C_{arom,quat}$); 191.7 ($C_{arom,quat}^{9}$). **IR** (ATR, cm^{-1}): ν_{CN} = 1335; ν_{max} = 2963, 2214, 1443, 1362, 1074, 820, 743, 700, 507. **MS** (ESI): *m/z* (%) 569 ([M-Cl^-]$^+$, 100). Red powder, 73%.

4.4.1.4 Syntheses of aldehydes

The synthesis of 1,3,6,8-tetrabromopyrene **12a**

1,3,6,8-Tetrabromopyrene **12a** was synthesized according to a literature procedure.[733] Pyrene **11** (10.00 g, 49.4 mmol, 1 eq.) was dissolved in 150 mL nitrobenzene in a two necked flask. The flask was brought under argon atmosphere and equipped with an addition funnel and a reflux condenser. The addition funnel was charged with 13 mL Br_2 (40.34 g, 252.4 mmol, 5.1 eq.), and this was added dropwise to the reaction mixture. The mixture was heated at 120 °C for four hours, after which the reaction was filtered into an aqueous sodium thiosulfate solution. The solids were washed with MeOH and acetone (100 mL each), to give the product **12a** as a light brown solid (24.49 g, 96%) which was used without further purification.

The synthesis of 1,3,6,8-tetrakis(4,4,5,5-tetramethyl-1,3,2-dioxaborolan-2-yl)pyrene **12b**

A modified literature procedure was used.[734] 1,3,6,8-tetrabromopyrene **12a** (1.00 g, 1.93 mmol, 1 eq.), KOAc (1.90 g, 19.3 mmol, 10 eq), B_2Pin_2 (2.45 g, 9.66 mmol, 5 eq.) and 40 mL toluene were added to a 100 mL flask. This was then degassed by bubbling with nitrogen for 30 minutes, after which $PdCl_2$(dppf) (71 mg, 0.10 mmol, 0.05 eq.) was added. This mixture was stirred under nitrogen at 90 °C for 27 hours. This was then allowed to cool down to room temperature, washed with water and the water layer was further extracted three times with 30 mL CH_2Cl_2. The organic phases were combined, evaporated and the resulting powder was dissolved in 30 mL CH_2Cl_2 and 20 mL hexane, the CH_2Cl_2 was evaporated and the mixture was filtered. The solids were redissolved in Et_2O and cooled in the freezer for 15 minutes. The solids were filtered off, obtaining the title compound **12b** as a grey powder (972 mg, 71%). The obtained spectra matched literature.[733]

The synthesis of 4,4',4'',4'''-(pyrene-1,3,6,8-tetrayl)tetrabenzaldehyde **2a**

1,3,6,8-Tetrakis(4,4,5,5-tetramethyl-1,3,2,-dioxaborolan-2-yl)pyrene **12b** (370 mg, 0.52 mmol, 1 eq.), 4-bromobenzaldehyde (582 mg, 3.14 mmol, 6 eq.) and K_2CO_3 (435 mg, 3.14 mmol, 6 eq.) were dissolved in 5 mL dioxane/water (4/1). Nitrogen was bubbled through this reaction mixture for 30 minutes after which $Pd(PPh_3)_4$ (36 mg, 0.03 mmol, 0.06 eq.) was added. The reaction was then stirred at 90 °C for 31 hours. The mixture was poured out into 15 mL ice water, filtered and washed with 1M HCl (5 mL) and Et_2O (10 mL). The filter cake was dried under vacuum to obtain the product **2a** as an orange powder (269 mg, 83%). The obtained spectra matched literature.[747]

The synthesis of 4,4',4'',4'''-(pyrene-1,3,6,8-tetrayl)tetrakis(2-methoxybenzaldehyde) **2b**

1,3,6,8-Tetrakis(4,4,5,5-tetramethyl-1,3,2,-dioxaborolan-2-yl)pyrene **12b** (636 mg, 0.90 mmol, 1 eq.), 4-bromo-2-methoxybenzaldehyde (1.24 g, 5.40 mmol, 6 eq.) and K_2CO_3 (746 mg, 5.40 mmol, 6 eq.) were dissolved in 25 mL dioxane/water (4/1). Nitrogen was bubbled through this reaction mixture for 30 minutes after which $Pd(PPh_3)_4$ (62 mg, 0.05 mmol, 0.06 eq.) was added and the reaction was stirred at 90 °C for 31 hours. The reaction was poured out into 30 mL ice water, filtered and washed with 1M HCl (10 mL) and Et_2O (20 mL). The product **2b** was thus obtained as a dark yellow powder (501 mg, 68%). A part of this (221 mg) was directly used in COF synthesis, another part (280 mg) was further purified via column chromatography (SiO_2, CH_2Cl_2/EtOAc: 97/3) to give the product **2b** as a yellow powder (146 mg, 39%).

4,4',4'',4'''-(Pyrene-1,3,6,8-tetrayl)tetrakis(2-methoxybenzaldehyde) 2b

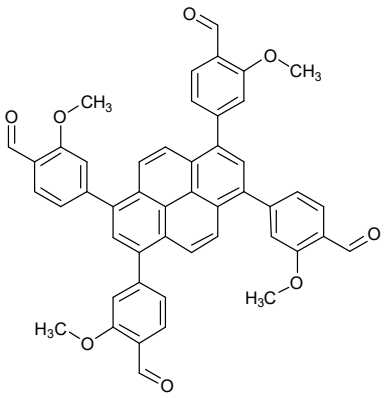

^{1}H-NMR (400 MHz, $CDCl_3$): δ 4.00 (12H, s, 4 x CH_3); 7.27 (4H, d, *J* = 1.0 Hz, 4 x CH_{arom}); 7.34 (4H, d, *J* = 8.0 Hz, 4 x CH_{arom}); 8.02-8.04 (6H, m, 4 x CH_{arom} and 2 x CH_{arom}); 8.20 (4H, s, 4 x CH_{arom}); 10.59 (4 x CHO). **^{13}C-NMR** (100.6 MHz, DMSO-d_6): δ 56.1 (4 x CH_3); 114.0 (4 x CH_{arom}); 123.4 (4 x CH_{arom}); 124.2 (4 x $C_{arom,quat}$); 125.9 (4 x CH_{arom}); 128.5 (2 x CH_{arom}); 128.8 (4 x CH_{arom}); 136.9 (4 x $C_{arom,quat}$); 148.6 (4 x $C_{arom,quat}$); 162.0 (4 x $C_{arom,quat}$); 189.6 (4 x CHO). **IR** (ATR, cm^{-1}): $\nu_{C=O}$ = 1680, ν_{max} = 1599, 1410, 1304, 1196, 1111, 1018, 814, 733, 490. Yellow powder, 39%.*

*MS spectra could not be obtained. Moreover, due to the very low solubility of compound **2b** two aromatic carbon signals were also not found in the ^{13}C-NMR.

4.4.2 Metal catalysis: alcohol oxidation

4.4.2.1 Procedure

A flamedried flask was brough under a nitrogen atmosphere and charged with the catalyst **4** (30 mg, 0.05 mmol, 0.01 eq.), benzyl alcohol **25a** or decan-1-ol **25b** (5 mmol, 1 eq.), PCy_3HBF_4 (18.4 mg, 0.05 mmol, 0.01 eq.), KOH (6-10 mmol, 1.2-1.4 eq.), and 10 mL dry toluene. The reaction mixture was stirred for a set time (8-46 h, Table 1) at 110 °C. The mixture was then cooled down to room temperature, 5 mL EtOAc was added and it was filtered over a paper filter. The filter was further washed with 10 mL EtOAc and 5 mL hexane. The solid was then dissolved in 10 mL H_2O and acidified with 1M HCl. This was then extracted three times with 10 mL EtOAc and the combined organic phases were evaporated under vacuum. When benzyl alcohol **25a** was used benzoic acid **26a** was obtained in yields ranging from 51% to 56%. When decan-1-ol **25b** was used yields of 12% to 35% of decanoic acid **26b** were obtained.

4.4.3 Attempted COF synthesis

4.4.3.1 Procedure

The procedure for the synthesis of **imidCOF-1** is given as a representative example. An Agilent GC vial (size: 22.75 x 75 mm; 20 mm cap) was charged with 1,3,5-triformylphloroglucinol **Tp** (21 mg, 0.1 mmol, 1 eq.) and amine **1** (68 mg, 0.15 mmol, 1.5 eq.). The solvents were added via the sides of the vial, to flush the remaining solids from the walls, and the catalyst was added. This mixture was then sonicated for ten minutes, flash frozen at 77 K in liquid N_2 and degassed by three freeze-pump-thaw cycles, after which the vial was put under argon. The vial was warmed to room temperature and then placed in an oven pre-heated at a 120 °C for 72 hours.* The resulting products were collected via filtration and washed sequentially with copious DMAc-DMF-H_2O-acetone-ethanol-THF. Further purification was done by Soxhlet extraction with methanol for 72 hours. Finally, the material was dried under vacuum overnight.

*The reaction with KOH as catalyst in DMF was performed in a flask equipped with a reflux condenser, at 140 °C, for 24 hours. The reaction with $Sc(OTf)_3$ was performed at room temperature for 72 hours.

Chapter 5: Conclusions and Perspectives

Porous organic polymers (POPs) are an emerging class of materials and attract widespread attention, proven by the greatly expanding number of publications every year (Figure 1). As demonstrated by the extensive literature review (metal-free) POPs can be effective catalysts for a wide variety of transformations, forming an alternative for homogeneous catalysts and other types of heterogeneous materials. The advantages that POPs offer as heterogeneous (photo)catalysts are numerous. These materials possess good mass transfer on account of their high porosity. The insolubility of POPs makes recycling convenient, and by choice of building blocks and linkages the properties of these catalysts can be tailored. The utility of POPs as heterogeneous photocatalysts was further proven in this work, as POPs were used to catalyze photocatalytic oxidation reactions, resulting in the formation of a wide range of imines, quinolines, α-dicarbonyl compounds, pyridines, dihydroquinoline-5-ones, tetrahydroacridine-1,8-diones and pyrazoles.

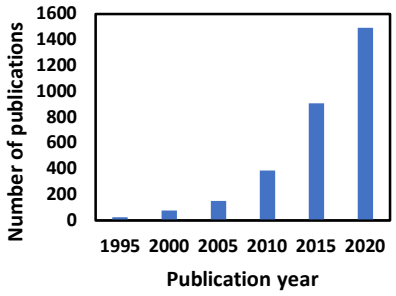

Figure 1: Number of publications based on the key words ''Porous organic polymers'' in Web of Science.

In the first experimental chapter isostructural COFs were synthesized (Scheme 1). The effects of the structural differences were studied by the determination of the bandgaps and the comparison of the photocatalytic activity. Phenylpyridine linkers led to a wider band gap compared to bipyridine, while substitution of the hydroxyl groups of **Tp** with methoxy groups in **TpOMe** resulted in an imine-linked framework with a narrower band gap. To gain even more insight in these materials the use of advanced time-resolved spectroscopic techniques could be considered in future research, allowing the exact determination of the lifetime of the excited state in the materials.

TpBpyCOF, consisting of bipyridine units and β-ketoenamine linkages, possessed the highest photocatalytic activity. This material was used as a photocatalyst for the oxidation of benzylamines **1** to imines **2**, and the transformation of *N*-arylglycine derivatives **3**/**5** to quinolines **4** and α-dicarbonyl compounds **6** (Scheme 1). **TpBpyCOF** was the first reported heterogeneous catalyst for both the oxidation/Povarov cyclization and the α-oxidation. In future research a few avenues could be explored to further enhance this catalyst. On the one hand, the immobilization of the used Lewis acid co-catalyst, $Sc(OTf)_3$, on the COF would confer significant advantages, as this would make the entire catalytic system recyclable. On the other hand, the exploration of other linkages, mainly the C=C linkage, could grant significant advantages. This linkage allows better charge separation, improving the photocatalytic activity, and provides greater stability. The incorporation of other *N*-heterocycles, such as bipyrimidines and bipyrazines could further tailor the photocatalytic activity, however, the

synthesis of these linkers is far from trivial. **Ru@TpBpyCOF**, consisting of ruthenium complexes anchored on **TpBpyCOF**, already possessed an enhanced photocatalytic activity, and is a promising system to explore further. This system could be improved by complexing a Lewis acid onto the material. Moreover, the ruthenium loadings were relatively low. The use of a larger, extended linker could lessen the steric hindrance, and therefore allow for a greater loading.

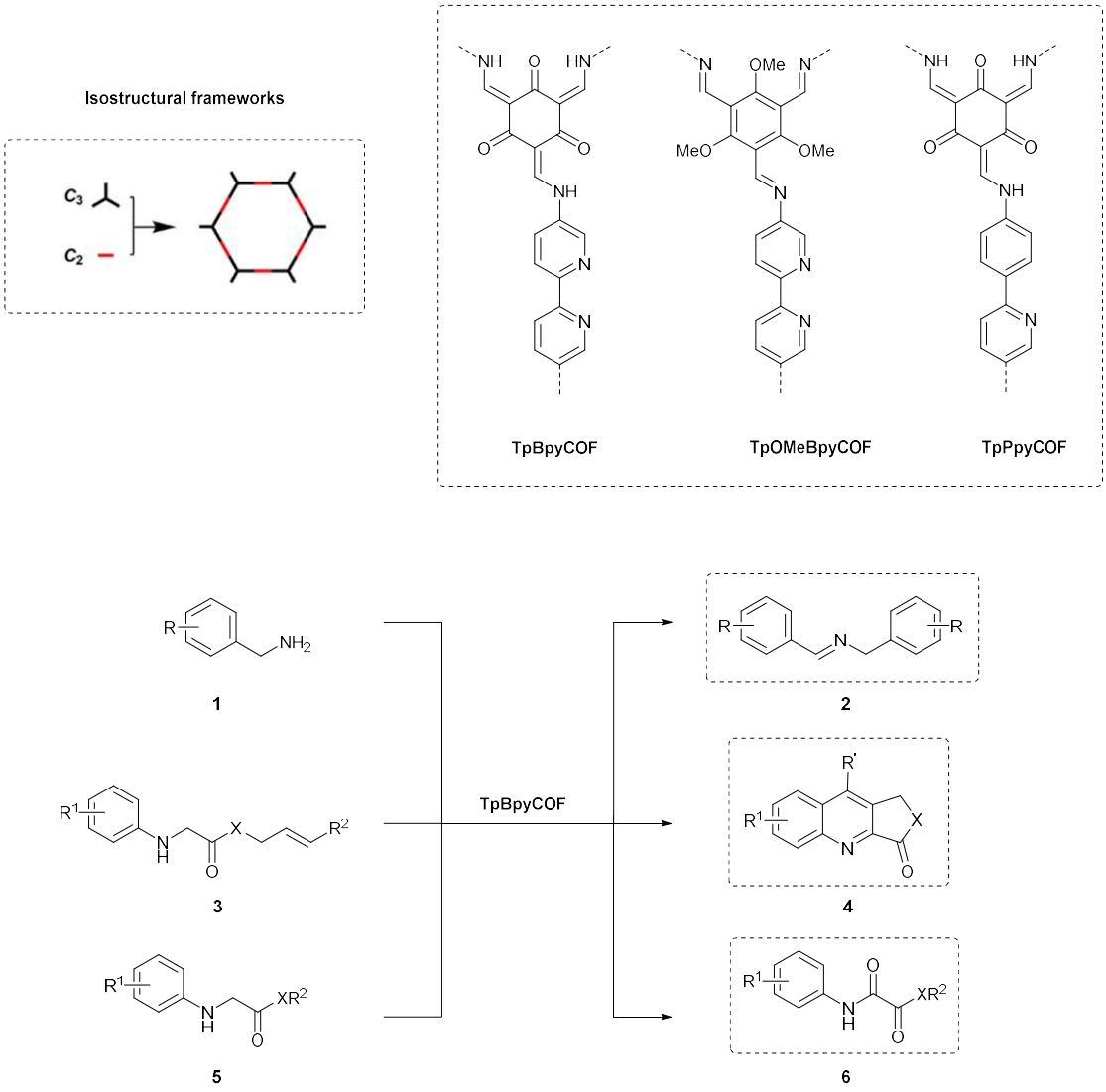

Scheme 1: Overview of the synthesized isostructural frameworks and the application of **TpBpyCOF** as a photocatalyst.

Using similar chemistry as in the described oxidation/Povarov cyclizations a whole range of POP catalyzed reactions could be envisaged, which are still unexplored. An example is given in Scheme 2, of the oxidation-dipolar cycloaddition of heterocycle **7**. Initial experiments indicated that the iminium ion **8/9** was formed (LC-MS) using **TpBpyCOF** as a photocatalyst. Deprotonation and the subsequent 1,3-dipolar cycloaddition, however, were not detected. This was not investigated further, due to time constraints, but could be a promising future application.

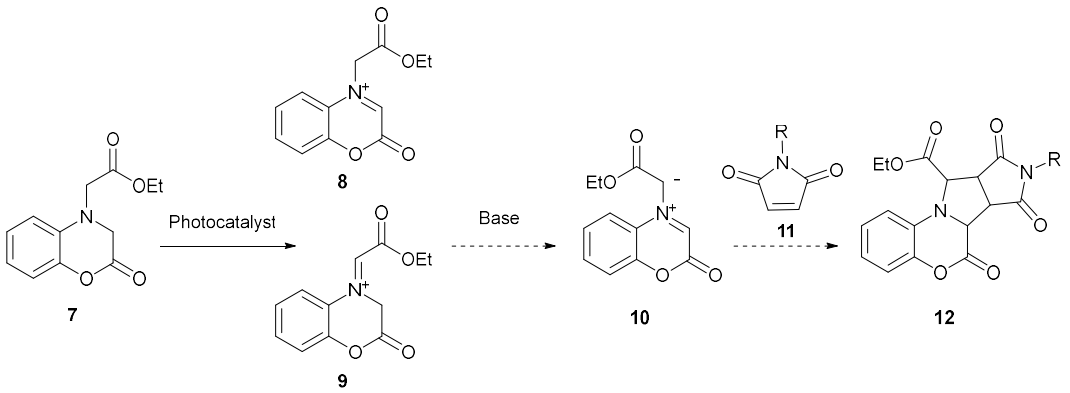

Scheme 2: Envisaged oxidation-deprotonation-1,3-dipolar cycloaddition.

Concerning the application of the bipyridine and phenylpyridine based COFs for the benzylamine oxidation, intriguing findings were made, as these reactions also worked in the dark. The COF-mediated activation of molecular oxygen in the dark, at room temperature was something unprecedented. This is still very poorly understood, and definitely warrants further investigation.

The POP synthesis by Lewis acid catalyzed Friedel-Crafts alkylation was effective, however, it did have limitations. Whilst this method is often applied to produce porous materials, the resulting structures are not well-defined. In addition, the use of solvents that are also reactive (such as CH_2Cl_2, $CHCl_3$, 1,2-DCE) and the competing Scholl reaction complicate the unambiguous definition of the chemical structure of these materials. Using cyanuric chloride CTFs were obtained, and this CTF synthesis does offer significant advantages, compared with the traditional, ionothermal methods. The materials obtained in this work were very easy to make and possessed significant photocatalytic activity. **CTF-Pyr**, which contained the highly photoactive triazine and pyrene moieties possessed the greatest activity. Using this material a very wide range of pyridine derivatives **15** and pyrazolines **16** were produced, in high yields and under exceptionally mild conditions.

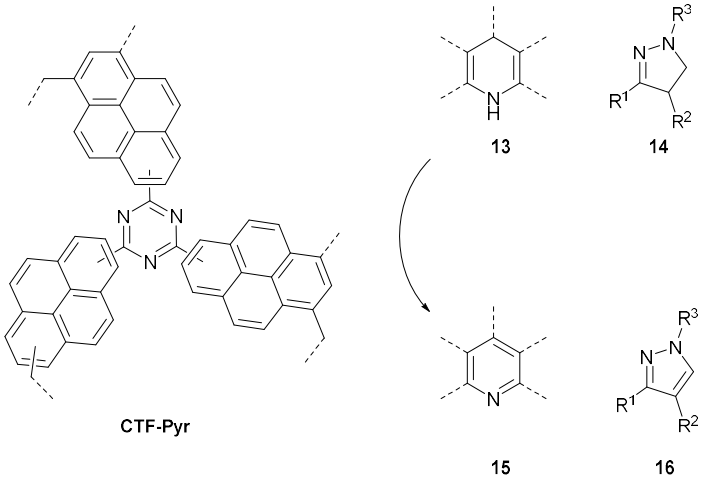

Scheme 3: Overview of the application of CTF-Pyr as photocatalyst for the aromatization of dihydropyridines and pyrazolines.

Future research could focus on two avenues. The use of solvents such as dichloromethane should be avoided, not only for their environmental impact and hazards, but also because they react under the reaction conditions, hereby complicating the structure of the material. Mechanochemical synthesis has been described for this reaction, and would remove this factor from the equation. Next to this,

replacing aluminium chloride with a more mild acid such as *p*TsOH, which has been used in similar transformations, would also greatly enhance the attractiveness of this method.

The reactivity of these POPs in regards to the functionalization of Hantzsch esters could be further explored. As proven by electrochemical measurements, the POPs do not have the required oxidation potential to directly oxidize the substrates. This necessitated the presence of oxygen, to act as a base in the form of the superoxide anion. For this reason we were not able to use the Hantzsch esters as radical precursors, given that these radical reactions have to take place under inert atmosphere. The use of an external base could lower the oxidation potential, to bring it in line with that of the POPs and thus enable these transformations.[748]

Chapter 4 investigated the synthesis of NHC-containing COFs. However, no crystalline materials were successfully produced. Further research could explore alternative reaction conditions and linkages to create these potentially valuable materials. In addition, a homogeneous COF analogue was complexed with ruthenium and evaluated as a catalyst for the oxidative dehydrogenation of alcohols to carboxylic acids, which has significant industrial applications and also warrants further research.

Next to these perspectives pertaining specifically to this work, some more general prospects for future research into these materials are described in the following paragraphs. As stated in the literature review, the large-scale synthesis of most POPs remains problematic. Many of the commonly used building blocks are unavailable on large scales, and do not have scalable synthesis routes. The synthesis routes described in literature often require multiple (protection/deprotection) steps and undesirable reagents, such as chromium based oxidants. Even after expending significant efforts, no better route to the building blocks **Bpy**, **Tp** and **TpOMe** was found. Some challenges for organic synthesis still remain here, as the synthesis of substituted bipyridines or polyaldehydes is far from trivial. Moreover, many heterocycles could be envisaged as promising building blocks for the synthesis of COFs/POPs such as phenanthrolines, (bi)pyrimidines, (bi)pyrazines, (bi)(1,2,4-triazines)… but the synthetic methodology to obtain these linkers is not readily available.

Generally COFs are made on small scales in sealed ampoules, without possibility for scale-up. Large-scale synthesis is one of the essential challenges for future research on these materials, and attracts a lot of attention. However, to the best of my knowledge not a single COF has been produced on a truly large scale. In contrast with this, MOFs have been produced by BASF on a ton-scale, using water as a solvent.[397] Large-scale production is of course an essential prerequisite to more widespread adaptation. When the materials will be cheap and easily available, they can be utilized by researchers and companies that may want to study their applications, but do not have the means to produce and characterize these materials themselves. However, even if large-scale production is feasible, challenges remain towards industrial catalytic applications. MOFs have been available on larger scales for quite some time, and to the best of my knowledge they still have not found application as heterogeneous catalysts in industry.

An interesting paper is this regard is a review titled ‘‘Why does industry not use immobilized transition metal complexes as catalysts’’, as some of the ideas from this paper also translate to MOFs and POPs.[749] The two main problems with advanced materials as heterogeneous catalysts are the absolute requirement that the recycled catalyst is completely identical from run to run, and that the system has to be economically viable. In the pharmaceutical industry, to comply with good manufacturing practice (GMP) requirements, every single batch has to be produced in exactly the same way. A recycled catalyst has almost always, even in a very small way, undergone some sort of change, which makes meeting the demands posed by GMP difficult. In the fine chemical industry only the purity of the batch has to be within specifications, so this poses less of a problem, but even there possible

changes in catalytic activity after each run makes recycling unattractive. In this light, it is of paramount importance that a recycled heterogeneous catalyst is completely identical from batch to batch.

The long term stability of many POPs under reaction conditions is, at times, questionable. Materials are often reported as being perfectly recyclable and stable, whilst the actual data clearly show a negative trend in the obtained yields. Many imine- and β-ketoenamine-linked COFs have been described as recyclable catalysts for the oxidation of benzylic amines. This work and previous literature proves that these COFs are not stable to strong nucleophiles such as benzylic amines, and thus cannot possibly be considered as recyclable catalysts for this transformation. The deactivation of photoactive POPs has been observed both in this work, as in other works, but is still poorly understood. During the photocatalysis many reactive species can be formed, that may interact with the catalysts. Greater understanding of this phenomenon would allow the design of more stable materials.

Moreover, a general shortcoming, of which this work is also guilty, is that only the full conversions (*e.g.* after 24 hours) are measured in recycling experiments. Measuring the conversion at a certain time before full conversion is reached, and comparing these conversions between different runs, gives a better picture. It would be even better to focus on reaction rates, and not on yields. Yield measurements can hide deactivation, whilst rates cannot. Importantly, whilst TONs and TOFs are well defined for homogeneous catalysts, or heterogeneous catalysts with known amounts of active units such as metal complexes, for other heterogeneous catalysts no such definitions have been made. For COFs the weight of one unit cell is sometimes taken, but given the size and weight of such structures (for **TpBpyCOF** this would be 2240 g/mol) this is quite misleading as 10 mol% of COF will be more material then the substrate itself for most transformations. This makes the comparison of reactions rates difficult and is something that should be addressed. Using the mass of catalyst per mol of substrate gives the clearest picture towards the actual catalyst loading of the system.

For POPs to truly take of as heterogeneous catalysts, they need to be more active than their homogeneous counterparts, and offer unique benefits to offset their typically more difficult and expensive synthesis. This is not an easy challenge at all, but very worthwhile as POPs provide a large degree of control of the chemical environment, allowing the construction of highly complex and effective catalysts. In this light the development of multifunctional POPs is laudable, as combining several catalytic moieties in a single material can provide real, tangible benefits compared to the homogeneous counterparts.

To develop more effective POPs, more information is needed on their structure-activity relationship. We know that these materials confer an unprecedented degree of structural control, however, we still rely on the synthesis and measurement of all properties to gain information on the SAR. In an ideal world it would be possible to go with a certain transformation to a computational modeler, who could then simulate which type of material would be an ideal catalyst. Another computational model could then predict which conditions would be suitable for the synthesis of this material, greatly speeding up material development. Next to the benefits computational modeling could give in predicting suitable conditions, another factor that could speed up the discovery process is automation, decreasing the amount of manual labor that is needed to screen all the possible reaction conditions. This still sounds very futuristic and is of course far from trivial. Even a comparatively much simpler calculation, such as simulating bandgaps can give large differences between the calculated and experimental values, as was the case for **TpOMeBpyCOF** in this work. This points to the existence of certain parameters that are not modelled and poorly understood. An example is the stacking behavior of COFs, which is important but typically not well characterized. COFs are often drawn as neat arrays of perfectly stacked layers, while in reality a whole range of stacking modes are possible and very hard to distinguish on the basis of experimental PXRD data. The orbital overlap in the z-axis has a significant

effect on the energy levels of the materials, and therefore the photocatalytic activity, but this is still uncharted territory. In the same vein the influence of defects and non-crystalline regions on the photocatalytic properties has not been thoroughly investigated.

Not all linkages have been developed equally. The imine linkage has been predominantly used due to its relative ease of construction, but given its limited stability and conjugation there are others that are much more suitable to produce photo-active COFs such as the vinylene linkage. The higher degree of electron delocalization in this linkage lowers the recombination of the electron-hole pairs, and therefore increases the photocatalytic efficiency. However, the synthesis of C=C linked COFs is far from trivial, given the low degree of reversibility in the bond forming reactions, and further research in this field is definitely necessary.

On a practical note, more communication between research groups, not only sharing successes, but also failures (*e.g.* failed conditions to make COFs, reaction that do not work, etc.) could also speed up research. Another factor that would make research on these materials more convenient is easier access to advanced analytical techniques such as ssNMR, XPS, TEM, EPR… A centralized national (university) service could help with this, and make the analysis of advanced materials more accessible to other research groups. The communication between different fields, such as materials chemistry, solid state (photo)physics and computational chemistry is at times difficult, with everybody seemingly living in their own worlds. Improving the understanding of each other's work is a challenging prospect, but very worthwhile given the insights that this could bring, not only in the use of POPs as catalysts, but for a wide range of applications.

Summary

Catalysis is essential for modern society, as without it most chemical reactions driving industry would come to a halt. Given the current environmental crisis this importance will only increase, as better catalysts are crucial to make chemical processes more green and to reduce pollution. Catalysis allows us to perform chemical synthesis more selectively, producing less waste and using less energy, thus lowering the environmental impact. Many catalysts however are 'single use', meaning they do not get recycled after the process. The design of new, heterogeneous catalysts that can be easily recovered and recycled is therefore key for a greener chemical industry.

Porous organic polymers (POPs) are a new class of materials, completely constructed from organic building blocks and linked through (strong) covalent bonds. A special subclass of POPs are the covalent organic frameworks (COFs), which are crystalline on account of their highly ordered extended structures. POPs and COFs are porous, lightweight, metal-free, designable and can easily be recycled after every use. These materials could be alternatives for a lot of the catalysts that are currently used, and with more development they could find widespread industrial application.

In this work the focus was on the development of POPs and COFs as heterogeneous photocatalysts. These materials act as photocatalysts by absorption of light with an energy equal to, or greater than the band gap. By this absorption electrons are promoted from the valence to the conduction band. The electrons in the conduction band, and the accompanying holes in the valence band can then participate in redox reactions. Next to this, direct energy transfer from the material to a suited acceptor is also possible. As POPs can be tailor made towards specific applications, by selection of their building blocks and linkages, this class of materials could eventually be fine-tuned as photocatalysts for specific reactions. However, to do this rationally more information is needed on this structure-activity relationship. The synthesis of a range of isostructural COFs was therefore undertaken, to gain information on the effects of small structural changes on the photochemical properties of these materials.

A range of linkers were synthesized and using these building blocks a series of five COFs could be obtained (Scheme 1). The main structure-activity relationships were drawn between **TpBpyCOF**, **TpPpyCOF** and **TpOMeBpyCOF**. The substitution of a nitrogen atom in bipyridine to a carbon in phenylpyridine led to a larger band gap, whilst replacing the hydroxyl groups with methoxy groups led to an imine-linked framework with a smaller band gap compared to its β-ketoenamine-linked analogue. These materials were applied as metal-free photocatalysts for the tandem aerobic oxidation/Povarov cyclization, the α-oxidation of *N*-aryl glycine derivatives and the oxidation of benzylic amines (Scheme 2). **TpBpyCOF**, possessing both bipyridine units and β-ketoenamine linkages possessed the highest activity.

Using **TpBpyCOF** as a catalyst thirteen quinoline fused lactones/lactams **v** were obtained in moderate yields (27-62%). Moreover, when the Lewis acid was omitted the same type of substrates were converted to their α-oxidized analogues **vi** (eleven examples, 15-47%). Photogenerated singlet oxygen was the main driver for these transformations. **TpBpyCOF** could be recycled up to five times, however, the yields did decrease and the material lost its crystallinity. The design of more stable COFs is therefore clearly an important avenue for further research. Next to this, the benzylamine oxidation was also studied and excellent conversions (73-99%) were obtained for a range of seven substrates **ii**, again using **TpBpyCOF** as the most active material. The main active species in this transformation was the superoxide radical anion. Intriguingly, this reaction also showed conversion in the dark, albeit

slower, but the mechanism for this light-independent organocatalytic activation of oxygen is still not clear.

Next to this, **Ru@TpBpyCOF** was synthesized by a bottom up approach using **Ru@Bpy** together with **Bpy** and **Tp** (Scheme 1). This material was structurally identical to **TpBpyCOF**, but contained 1% ruthenium. Preliminary experiments were performed using this material as a photocatalyst for the intermolecular tandem oxidation/Povarov cyclization with very encouraging results (Scheme 3). An especially interesting approach for further research would be to also immobilize the used Lewis acid, $Cu(OTf)_2$, on this material, thus producing a bifunctional heterogeneous photocatalyst/Lewis acid.

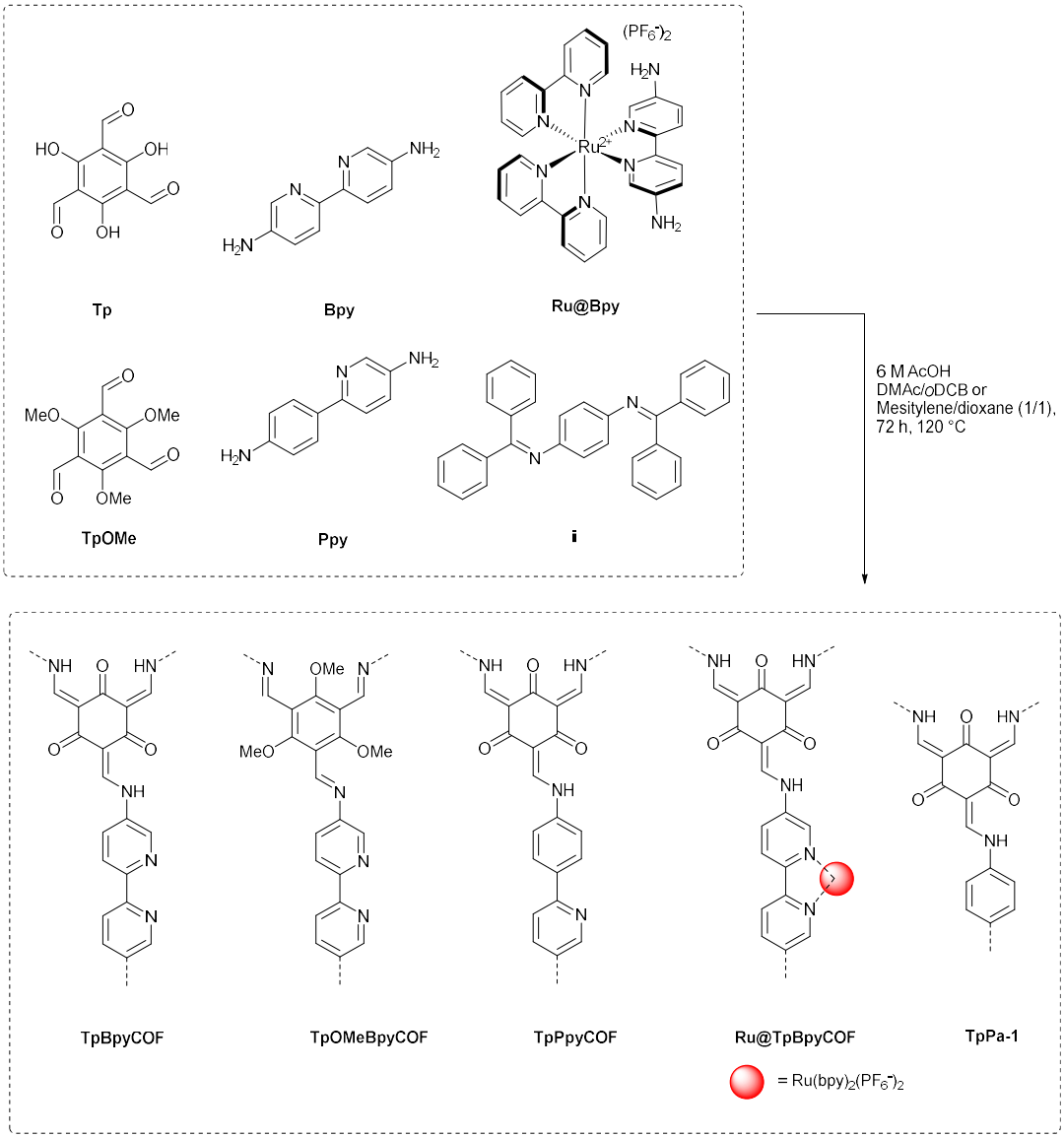

Scheme 1: Overview of the COFs that were synthesized in this work.

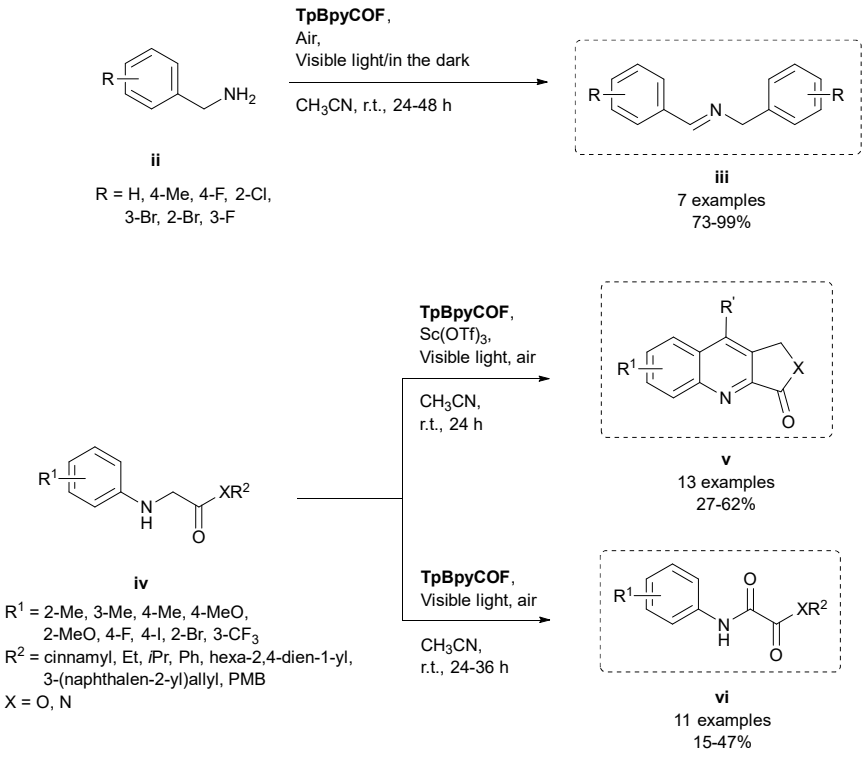

Scheme 2: Overview of the reactions catalyzed by **TpBpyCOF**: benzylamine oxidation (top), tandem oxidation/Povarov cyclization (middle) and α-oxidation of *N*-aryl glycine derivatives (bottom).

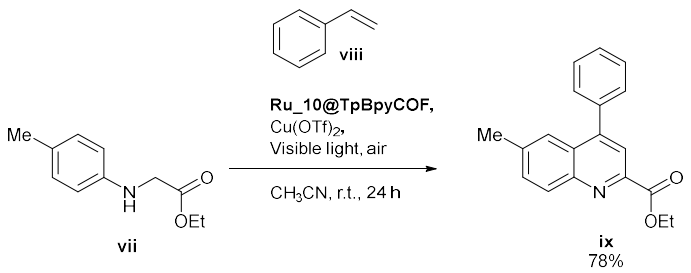

Scheme 3: **Ru_10@TpBpyCOF** catalyzed photocatalytic tandem oxidation/intermolecular Povarov cyclization.

In the second part of this thesis the focus was on the development of amorphous POPs as photocatalysts. These POP photocatalysts are typically synthesized through precious metal catalyzed cross-couplings of highly functionalized, inaccessible building blocks. Covalent triazine frameworks (CTFs), a subclass of POPs, have an especially problematic synthesis. CTFs are generally made through trimerization of aromatic nitriles in $ZnCl_2$ at extremely high temperatures (>400°C) in sealed glass ampoules, a synthesis that is hardly scalable and also causes degradation of the material. The synthesis of POPs through Lewis acid catalyzed alkylation/Scholl coupling of aromatic building blocks allowed for the generation of porous materials, from unfunctionalized building blocks under relatively mild conditions. Moreover, when cyanuric chloride is used as a coupling partner this led to the formation of CTFs.

The synthesis of a range of CTFs was envisaged, using this method, by the coupling of aromatic building blocks (**Trux**, **HMTrux**, **Fl** and **Pyr**) with cyanuric chloride **CC** (Scheme 4). CTFs were obtained using pyrene and fluorene (**CTF-Fl** and **CTF-Pyr**), whilst for truxene and hexamethyltruxene porous materials were formed (**aza-pTrux** and **aza-pHMTrux**), but these were not truly CTFs. These materials were formed by crosslinking with the solvent (dichloromethane) and Scholl coupling, and very little reaction with cyanuric chloride had taken place. The four aromatic building blocks were also polymerized using $AlCl_3$, in dichloromethane, without cyanuric chloride, hereby forming four porous polymers: **pTrux**, **pHMTrux, pFl** and **pPyr** (Scheme 5).

After a thorough characterization of these eight materials they were applied as photocatalysts for the aromatization of *N*-heterocycles, a new application for POPs (Scheme 6). **CTF-Pyr**, containing the photoactive pyrene and triazine moieties was by far the most effective material. Using this photocatalyst a wide range of 21 aromatic *N*-heterocycles including pyridines **xi**, dihydroquinoline-5-ones **xii**, tetrahydroacridine-1,8-diones **xiii** and pyrazoles **xv** were prepared in good to excellent yields (70-99%). These oxidation reactions were carried out under extremely mild conditions: under air and at room temperature. The photocatalyst could be recycled three times without a drop in yield, however, after the fourth time the yield dropped and a longer reaction time was needed to reach full conversion. Moreover, structural analysis pointed out that oxidation of the material itself had taken place, which is again a point of attention for further research.

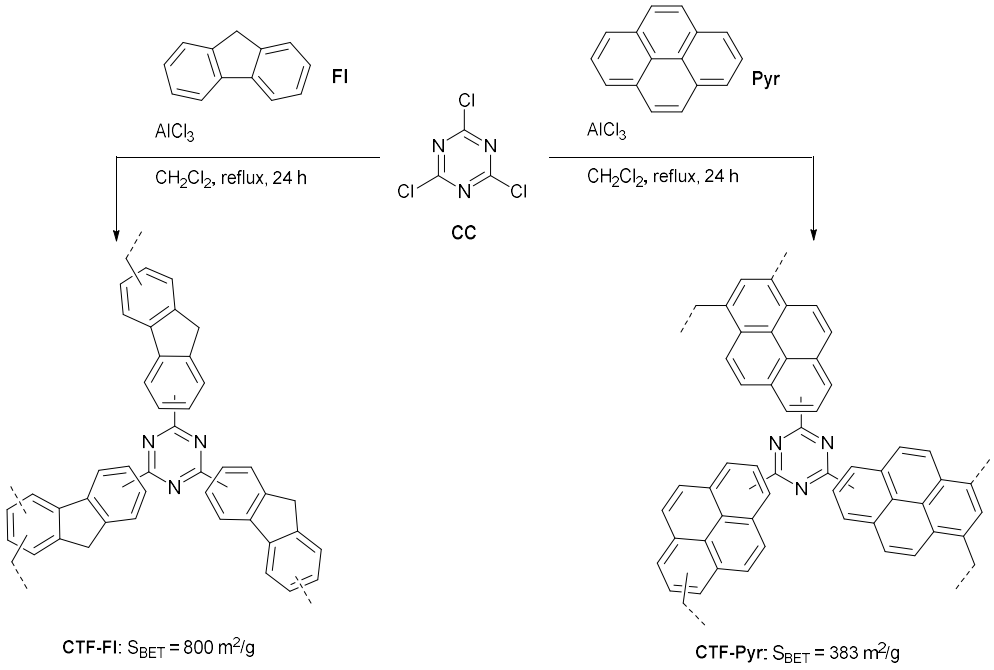

Scheme 4: Synthesis of CTFs: **CTF-Fl** and **CTF-Pyr**. For truxene and hexamethyltruxene, no real CTFs were obtained, these materials were therefore denoted as **aza-pTrux/pHMTRux** and their chemical structures largely correspond with that of **pTrux/HMTRux** (Scheme 5).

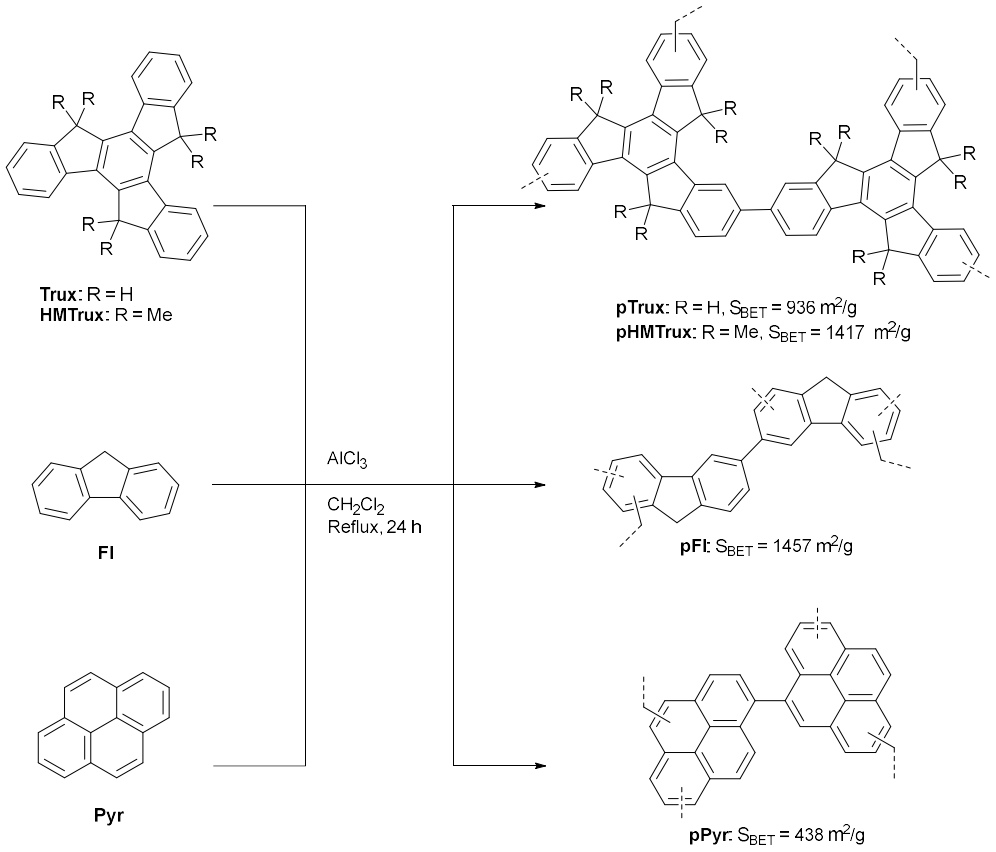

Scheme 5: Synthesis of **pTrux**, **pHMTRux**, **pFl** and **pPyr** by Scholl coupling and crosslinking with dichloromethane.

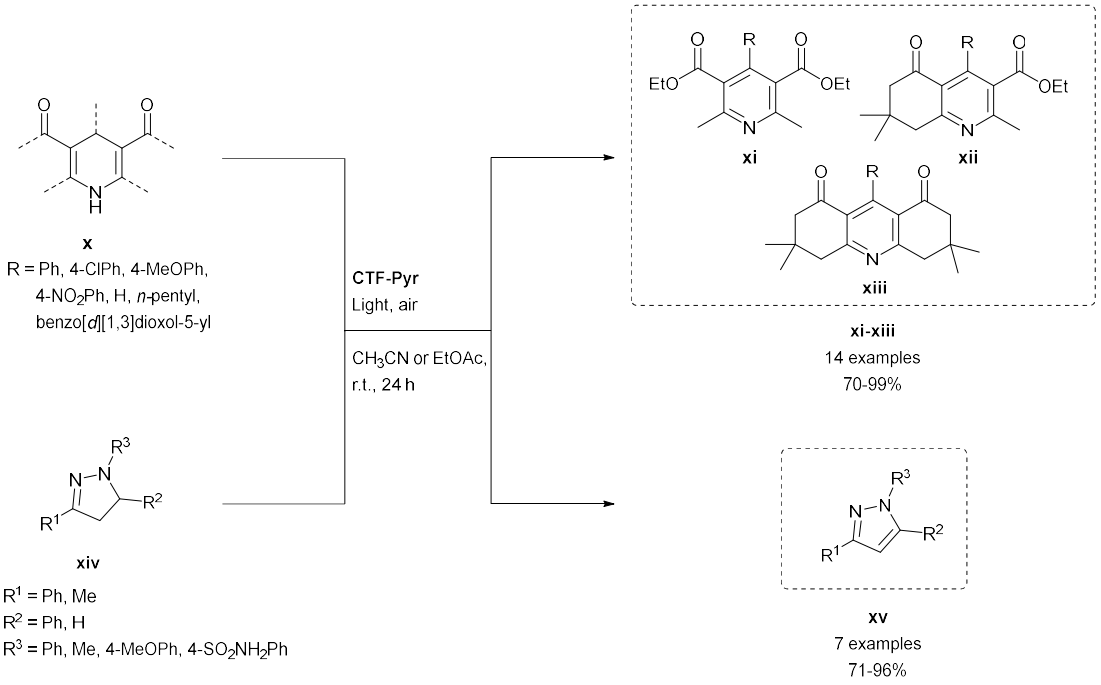

Scheme 6: **CTF-Trux** catalyzed photocatalytic aromatization producing pyridines, dihydroquinoline-5-ones, tetrahydroacridine-1,8-diones and pyrazoles.

In the final section of this thesis, the focus was on the development of NCH-containing COFs. The new diamine linker **xvi** was made through a six step synthesis. The synthesis of β-ketoenamine- and imine-linked COFs was then attempted through condensation of this building block with aldehydes **Tp** and **xvii**. Unfortunately, crystalline materials could not be obtained. Next this, a homogeneous analogue of the envisaged COFs was complexed with ruthenium to form the novel complex **xviii**. Using this complex alcohols **xix** were converted into carboxylic acids **xx** by oxidative dehydrogenation, with promising results.

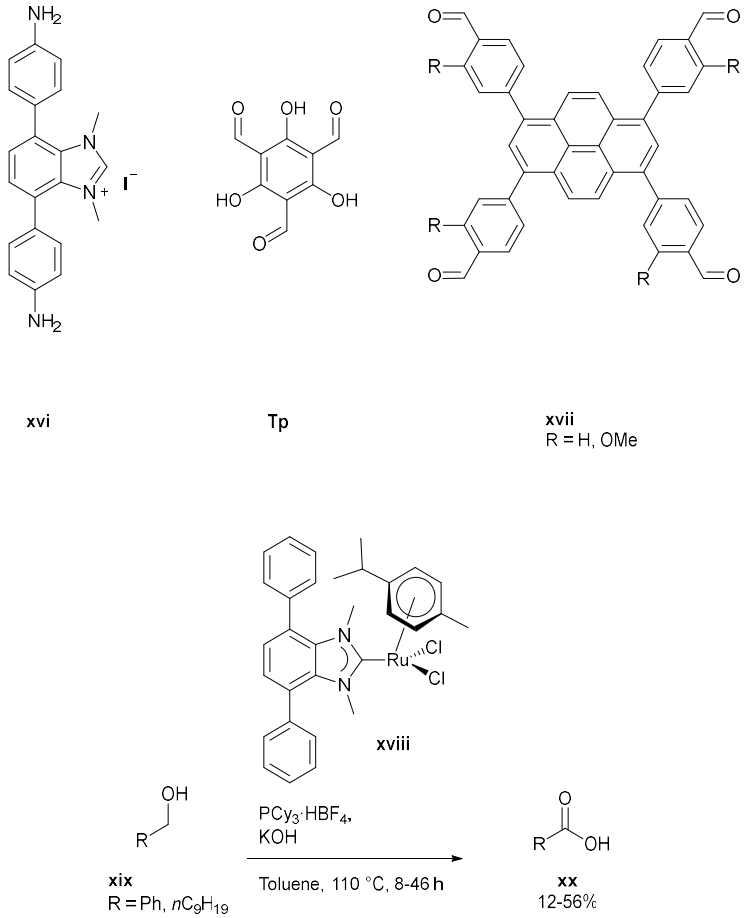

Scheme 7: The building blocks synthesized in Chapter 4 (top) and the application of a homogeneous analogue of the COF, as catalyst for the oxidative dehydrogenation of alcohols (bottom).

POPs were further established in this thesis as emerging heterogeneous photocatalysts for organic synthesis. Using the catalysts synthesized in this study 52 compounds were prepared, including imines, quinolines, α-dicarbonyls derivatives, pyridines, tetrahydroquinoline-5-ones, hexahydroacridine-1,8-diones and pyrazoles, proving the wide applicability of these new photocatalysts. This work gives more insight into the design and application of photoactive POPs and helps their development as sustainable photocatalysts, thus paving the way for a greener chemical industry.

Samenvatting

Katalyse is essentieel voor onze moderne samenleving, aangezien veel chemische processen in de industrie afhankelijk zijn van katalysatoren. De huidige klimaatcrisis zal dit belang enkel nog vergroten, want betere katalysatoren zijn cruciaal om chemische processen groener te maken. Katalyse laat selectievere chemische synthese toe en verlaagt zo de energiebehoefte, afvalproductie en milieu-impact. Veel katalysatoren worden echter slechts één keer gebruikt, en niet gerecycleerd na het proces. De ontwikkeling van nieuwe, heterogene katalysatoren die eenvoudig gerecycleerd kunnen worden, is daarom ook belangrijk voor het genereren van een groenere chemische industrie.

Poreuze organische polymeren (POP's) zijn een nieuwe klasse van materialen. POPs zijn volledig opgebouwd uit organische bouwstenen, die met elkaar verbonden worden door middel van (sterke) covalente bindingen. Een speciale subklasse van POP's zijn de covalente organische roosters (COF's), die zeer geordende structuren aannemen en daardoor kristallijn zijn. POP's en COF's zijn poreus, metaalvrij, *designable* en kunnen eenvoudig gerecycleerd worden na elk gebruik. Deze materialen kunnen groenere alternatieven zijn voor veel van de katalysatoren die momenteel gebruikt worden, en met meer onderzoek zouden ze wijdverspreide industriële toepassingen kunnen vinden.

In dit werk werd de focus gelegd op de ontwikkeling van POP's en COF's als heterogene fotokatalysatoren. Door absorptie van licht met een energie gelijk aan, of groter dan de bandkloof gaan elektronen van de valentieband naar de geleidingsband. De elektronen in de geleidingsband, en het 'elektronengat' in de valentieband kunnen dan redoxreacties initiëren. Daarnaast kan er ook een directe energietransfer plaatsvinden van het materiaal naar een geschikte acceptor. POPs kunnen op maat gemaakt worden voor een specifieke toepassing, door middel van de selectie van hun bouwstenen en bindingen. Ze zouden daarom gefinetuned kunnen worden als fotokatalysatoren voor specifieke reacties. Er is echter meer informatie nodig over hun structuur-activiteitsrelatie om specifieke katalysatoren te kunnen ontwerpen. In deze thesis werd daarom de synthese van een reeks isostructurele COF's ondernomen, om informatie te krijgen over het effect van kleine structurele veranderingen op de fotochemische eigenschappen van deze materialen.

Een reeks bouwstenen werd gesynthetiseerd en aangewend om een serie van vijf COF's te maken (Schema 1). De voornaamste structuur-activiteitsrelaties konden getrokken worden tussen **TpBpyCOF**, **TpPpyCOF** en **TpOMeBpyCOF**. Het vervangen van een stikstofatoom in bipyridine met een koolstof in fenylpyridine leidde tot een grotere bandkloof, terwijl het vervangen van de hydroxylgroepen door methoxygroepen leidde tot een imine-gebonden materiaal met een kleinere bandkloof dan het β-ketoenamine-gebonden analoog. Deze materialen werden aangewend als metaalvrije fotokatalysatoren voor de tandem aerobe oxidatie/Povarov-cyclisatie, de α-oxidatie van *N*-aryl glycinederivaten en de oxidatie van benzylaminen (Schema 2). **TpBpyCOF**, opgebouwd uit bipyridines verbonden met β-ketoenaminebindingen beschikte over de grootste activiteit.

Met **TpBpyCOF** als katalysator werden dertien chinoline-gefuseerde lactonen/lactamen **v** bekomen met matige rendementen (27-62%). In de afwezigheid van het Lewiszuur werd hetzelfde type substraten omgezet tot hun α-geoxideerde analogen **vi** (elf voorbeelden, 15-47%). Fotogegenereerde singlet zuurstof was de voornaamste drijfveer in deze reacties. **TpBpyCOF** kon vijf keer gerecycleerd worden, maar de opbrengsten daalden wel enigszins, en het materiaal verloor ook haar geordende structuur. Het ontwerp van stabielere COF's is daarom ook een belangrijke doelstelling voor toekomstig onderzoek.

Naast deze reacties werd ook de oxidatie van benzylamine verder onderzocht, en uitstekende omzettingen (73-99%) werden bekomen. Het superoxide radicalair anion was het voornaamste actieve species. Deze reactie ging ook door in het donker, maar trager, echter kon het mechanisme voor deze licht-onafhankelijk activatie van zuurstof nog niet achterhaald worden.

Ru@TpBpyCOF werd gesynthetiseerd door middel van een *bottom-up* strategie met **Ru@Bpy**, **Bpy** en **Tp** (Schema 1). Dit materiaal had dezelfde structuur als **TpBpyCOF**, en bevatte 1% ruthenium. Preliminaire experimenten werden uitgevoerd met dit materiaal als katalysator voor de intermoleculaire tandem oxidatie/Povarov-cyclisatie met veelbelovende resultaten (Schema 3). Een interessante verdere uitdieping zou zijn om ook het gebruikte Lewiszuur, $Cu(OTf)_2$, te immobiliseren op dit materiaal om zo een bifunctionele katalysator te bekomen.

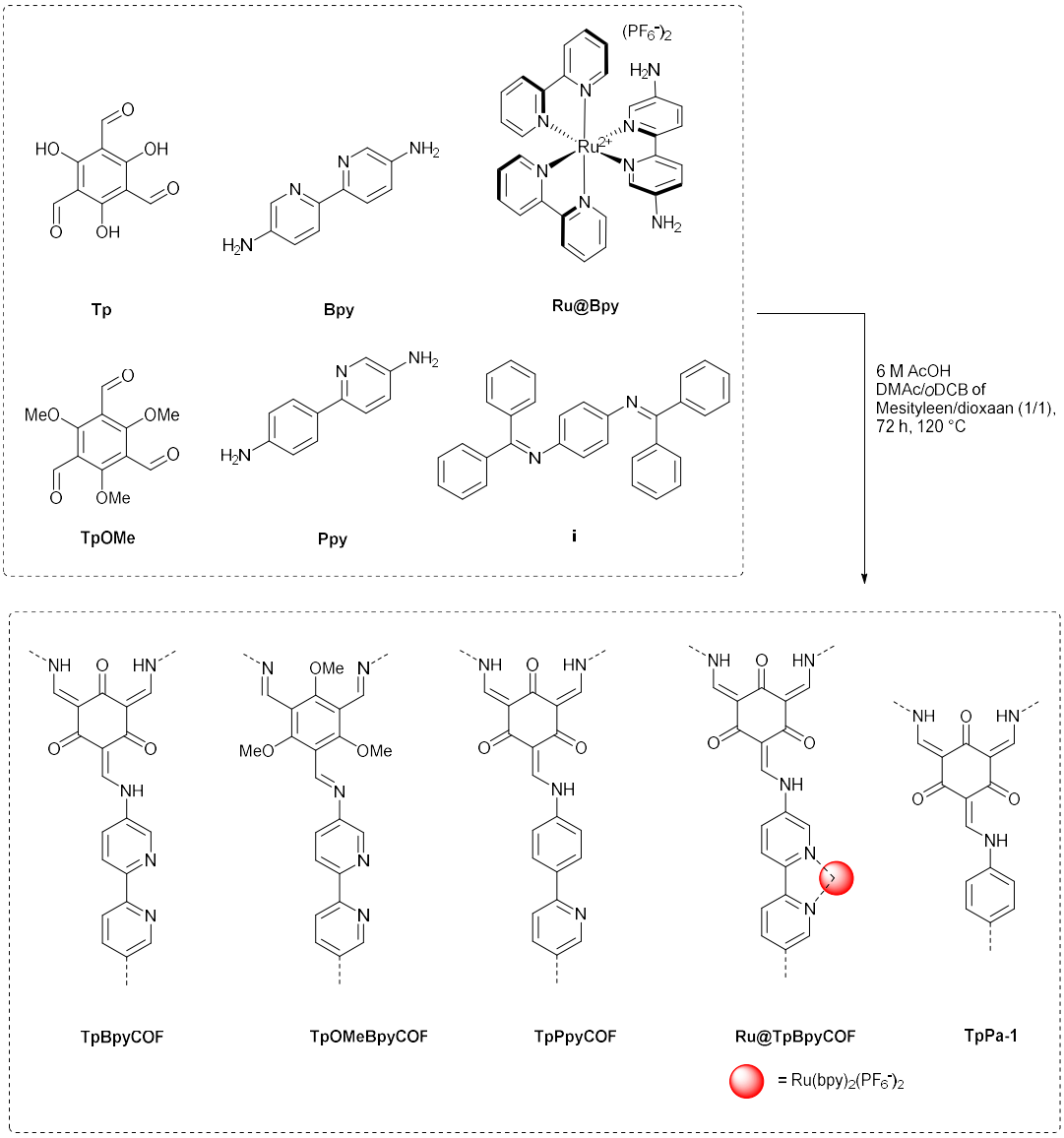

Schema 1: Overzicht van de gesynthetiseerde COF's.

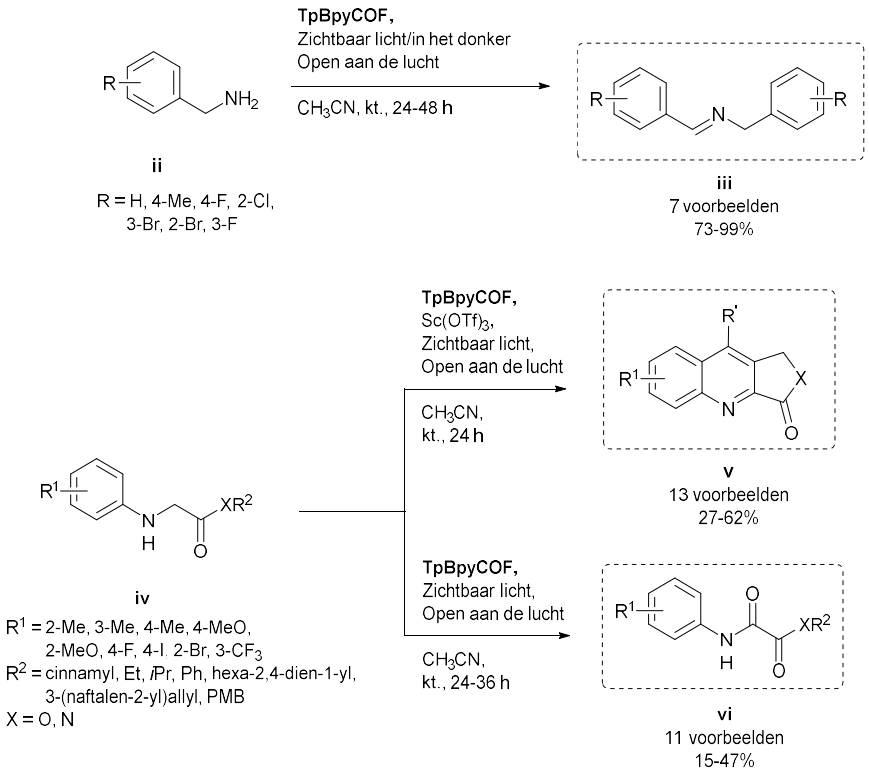

Schema 2: Overzicht van de reacties die door **TpBpyCOF** gekatalyseerd worden: de oxidatie van benzylaminen **ii** (boven), de tandem oxidatie/Povarov cyclisatie (midden) en de α-oxidatie van *N*-aryl glycine derivaten (onderaan).

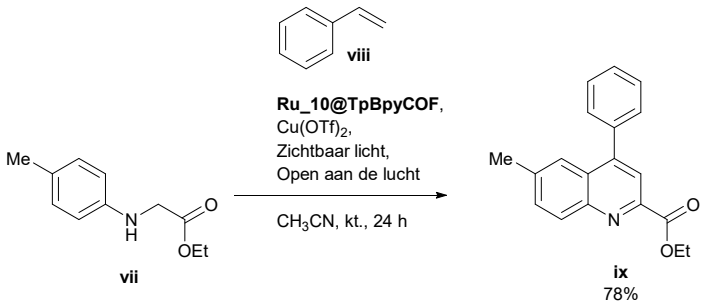

Schema 3: **Ru_10@TpBpyCOF** gekatalyseerde fotokatalytische tandem oxidatie/intermoleculaire Povarov cyclisatie.

In het tweede deel van deze thesis lag de focus op de ontwikkeling van amorfe POP's als fotokatalysator. Deze POP's worden over het algemeen gemaakt door middel van metaal-gekatalyseerde koppelingsreacties van zeer gefunctionaliseerde bouwstenen. Zeker de covalente triazine roosters (CTF's), een subklasse van POP's, hebben een problematische synthese. CTF's worden gemaakt door middel van de trimerisatie van aromatische nitrillen in $ZnCl_2$, bij extreme temperaturen (>400°C) in vacuüm-gesloten glazen ampullen, een synthese die nauwelijks schaalbaar is en de afbraak van de materialen veroorzaakt. De synthese van POP's door middel van Lewiszuur-gekatalyseerde alkylering/Scholl-koppeling van aromatische bouwstenen laat de synthese van poreuze materialen toe uit niet-gefunctionaliseerde bouwstenen en onder vrij milde omstandigheden. Wanneer cyanuurchloride gebruikt wordt als koppelingspartner kunnen op deze manier ook CTF's gevormd worden.

Een reeks CTF's werd gesynthetiseerd door middel van $AlCl_3$-gekatalyseerd Friedel-Craftsalkylering tussen aromatische bouwstenen (**Trux**, **HMTrux**, **Fl** en **Pyr**) en cyanuurchloride **CC**. Met pyreen en

fluoreen werden zo CTF's bekomen (**CTF-Fl** en **CTF-Pyr**). Voor truxeen en hexamethyltruxeen werden wel poreuze materialen gevormd (**aza-pTrux** en **aza-pHMTrux)**, echter bevatten deze nauwelijks stikstof en konden we dus niet van echte CTF's spreken. Deze materialen werden gevormd door middel van crosslinking met het solvent, dichloormethaan, en Scholl-koppeling, zonder veel reactie met cyanuurchloride. De vier aromatische bouwstenen werden ook gepolymeriseerd met $AlCl_3$, in dichloormethaan, maar zonder cyanuurchloride, en hierbij werden vier poreuze polymeren gevormd: **pTrux**, **pHMTrux, pFl** en **pPyr** (Schema 5).

Na een grondige karakterisatie van deze acht materialen werden ze aangewend als fotokatalysatoren voor de aromatisering van *N*-heterocyclische verbindingen, een nieuwe toepassing voor POP's (Schema 6). **CTF-Pyr**, die zowel foto-actieve pyreen- als triazinegroepen bezit, was veruit het meest performante materiaal. Met deze fotokatalysator werd een reeks van 21 aromatische *N*-heterocyclische verbindingen gemaakt, waaronder pyridinen **xi**, dihydrochinoline-5-onen **xii**, tetrahydroacridine-1,8-dionen **xiii** and pyrazolen **xv** in goede tot uitstekende rendementen (70-99%). Deze oxidatiereacties gingen door onder uitzonderlijk milde condities: aan de lucht en bij kamertemperatuur. De fotokatalysator kon drie keer gerecycleerd worden zonder een significante daling van het rendement, bij de vierde keer was er echter een langere reactietijd nodig om eenzelfde omzetting te bekomen. Daarnaast wees de analyse van het materiaal uit dat de katalysator zelf deels geoxideerd werd, hetgeen ook een belangrijk aandachtspunt is in toekomstig onderzoek.

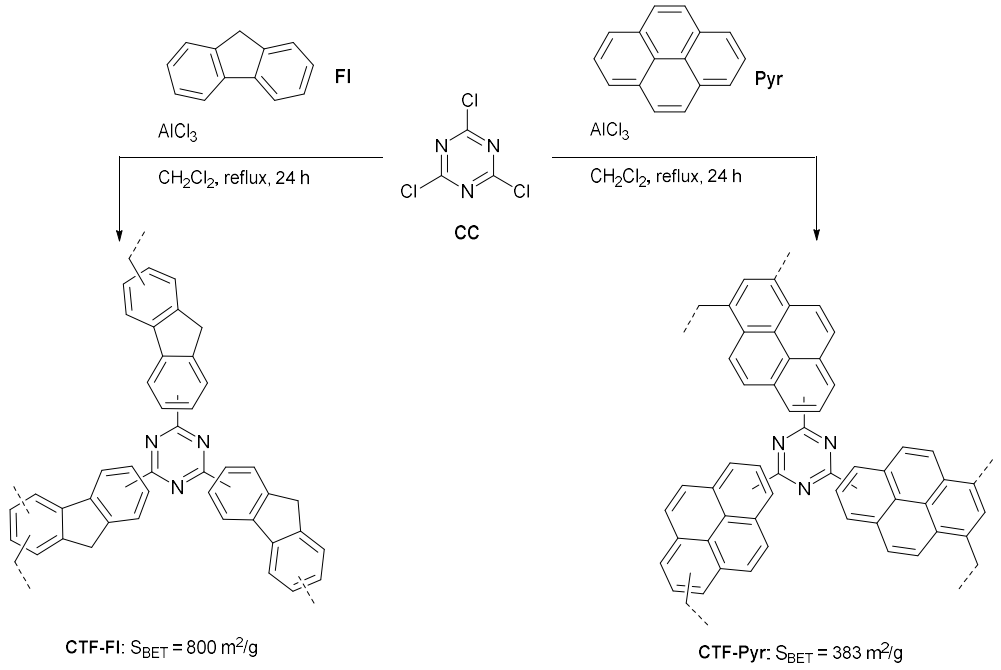

Schema 4: De synthese van CTF's: **CTF-Fl** en **CTF-Pyr**. Voor truxeen en hexamethyltruxeen werden geen echte CTF's bekomen, deze materialen werden benoemd als **aza-pTrux/pHMTRux** en hun chemische structuur komt grotendeeels overeen met die van **pTrux/HMTRux** (Schema 5).

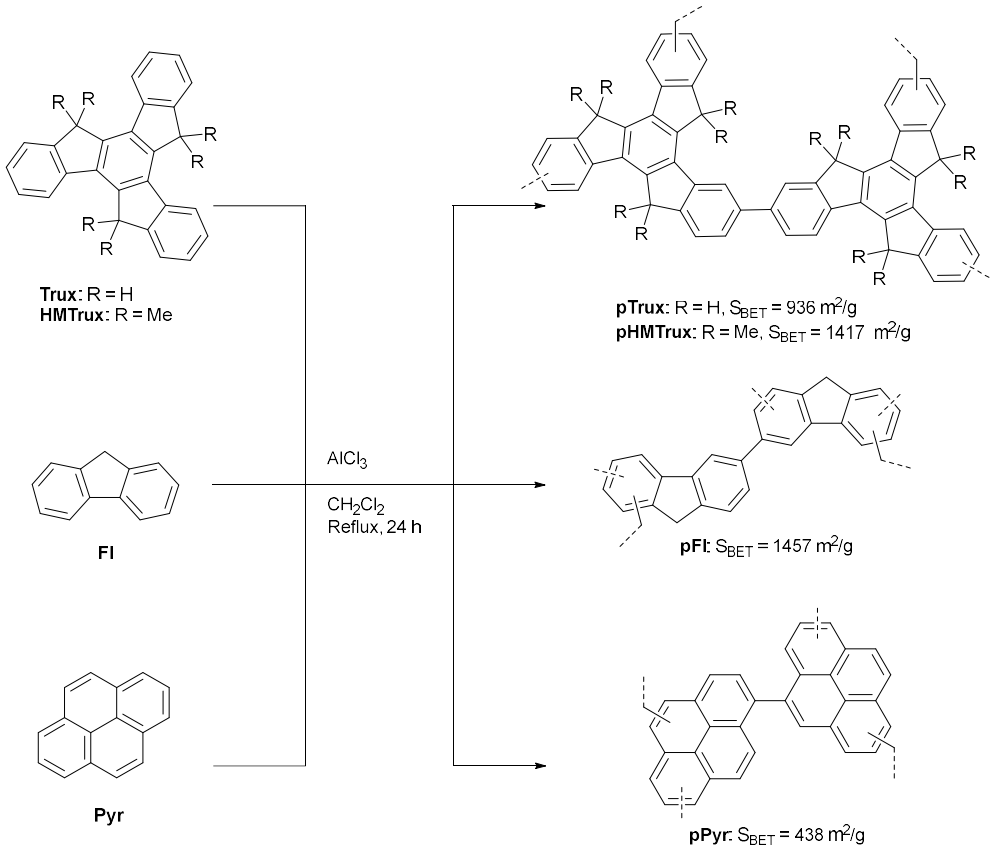

Schema 5: Synthese van **pTrux**, **pHMTRux**, **pFl** en **pPyr** door Scholl-koppeling en crosslinking met dichloormethaan.

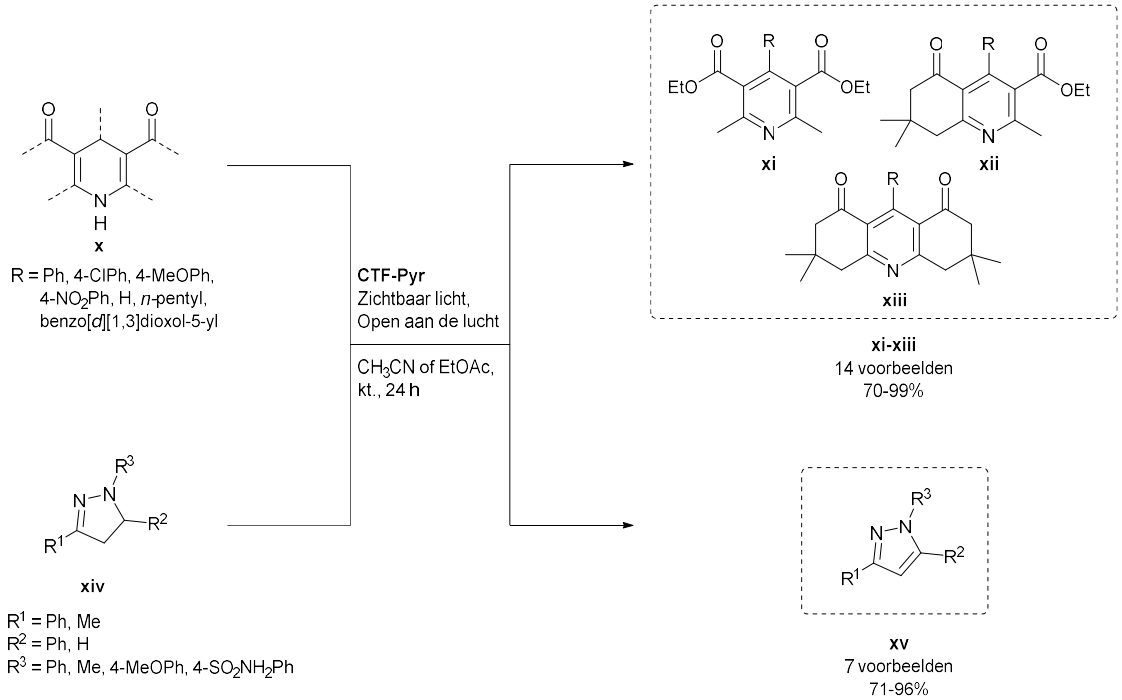

Schema 6: **CTF-Trux**-gekatalyseerde fotokatalytische oxidaties resulterende in pyridinen, dihydrochinoline-5-onen, tetrahydroacridine-1,8-dionen en pyrazolen.

Tenslotte werd er in het laatste deel van deze thesis de synthese van NHC-bevattende COFs onderzocht. Door middel van een zesstaps synthese werd de nieuwe diamine bouwsteen **xvi** bekomen. Dit amine werd vervolgens gecondenseerd met de aldehyden **Tp** en **xvii** om zo β-ketoenamine en imine-gebonden materialen te bekomen. Helaas konden er geen kristallijne COFs gemaakt worden. Daarnaast werd er ook een homogeen analoog van de beoogde COF gesynthetiseerd, en deze werd gecomplexeerd met ruthenium, om zo het complex **xviii** te vormen. Deze katalysator werd met veelbelovende resultaten toegepast in de oxidatieve dehydrogenatie van alcoholen naar carbonzuren.

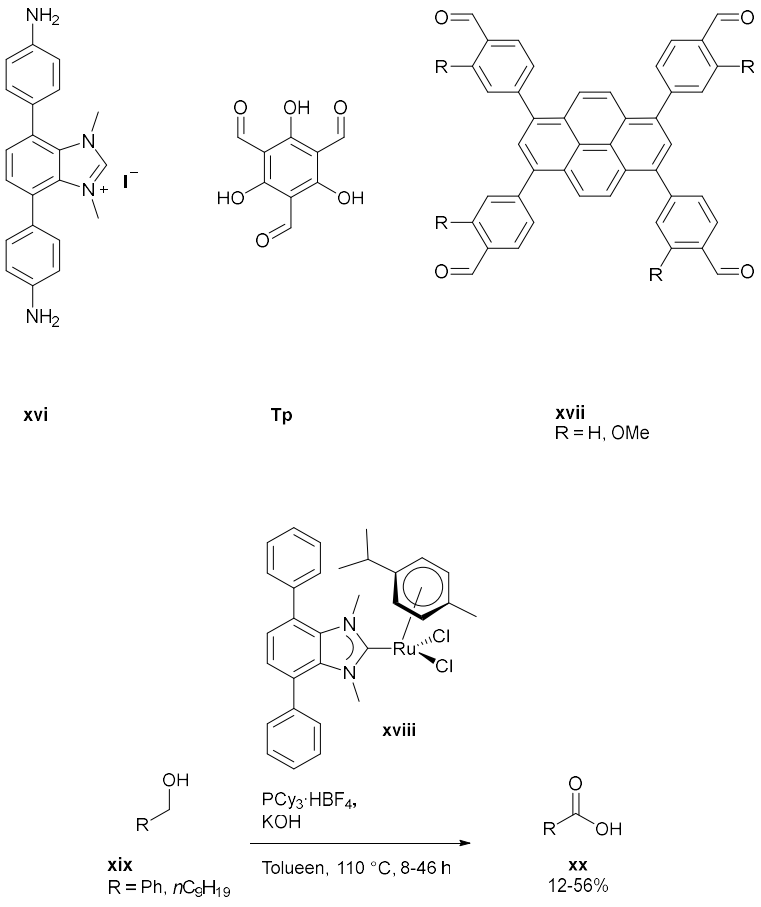

Schema 7: De bouwstenen die werden gesynthetiseerd in Hoofdstuk 4 (boven) en de toepassing van een homogeen analoog van de COF as katalysator voor de oxidatieve dehydrogenatie van alcoholen naar carbonzuren (onder).

In deze thesis werden POP's verder uitgebouwd als veelbelovende heterogene fotokatalysatoren voor organische synthese. Met de gesynthetiseerde materialen werden 52 verbindingen bereid, waaronder iminen, chinolinen, α-dicarbonylverbindingen, pyridinen, dihydrochinoline-5-onen, tetrahydrochinoline-1,8-dionen en pyrazolen, wat de brede inzetbaarheid van deze nieuwe fotokatalysatoren bewijst. Dit werk geeft meer inzicht in het ontwerp en toepassing van foto-actieve POP's en hun ontwikkeling als duurzame fotokatalysatoren, hetgeen de weg vrijmaakt voor een groenere chemische industrie.

References

(1) Hutchings, G. J.; Catlow, C. R. A.; Hardacre, C.; Davidson, M. G. *Phil. Trans. R. Soc. A* **2016**, *374*.

(2) Anastas, P.; Eghbali, N. *Chem. Soc. Rev.* **2010**, *39*, 301–312.

(3) Wacławek, S.; Padil, V. V. T.; Černík, M. *Ecol. Chem. Eng. S* **2018**, *25* (1), 9–34.

(4) De Jong, K. P. In *Synthesis of Solid Catalysts*; de Jong, K. P., Ed.; WILEY-VCH Verlag GmbH & Co. KGaA, **2009**; pp 1–11.

(5) Sheldon, R. A.; Downing, R. S. *Appl. Catal. A: Gen.* **1999**, *189*, 163–183.

(6) Murahashi, S. I.; Zhang, D. *Chem. Soc. Rev.* **2008**, *37* (8), 1490–1501.

(7) Ragaini, F. *J. Chem. Soc. Dalton Trans.* **2009**, No. 32, 6251–6266.

(8) Heitbaum, M.; Glorius, F.; Escher, I. *Angew. Chem. Int. Ed.* **2006**, *45* (29), 4732–4762.

(9) Lin, Y. C.; Huber, G. W. *Energy Environ. Sci.* **2009**, *2*, 68–80.

(10) Thommes, M.; Kaneko, K.; Neimark, A. V.; Olivier, J. P.; Rodriguez-Reinoso, F.; Rouquerol, J.; Sing, K. S. W. *Pure Appl. Chem.* **2015**, *87* (9–10), 1051–1069.

(11) Brunauer, S.; Emmett, P. H.; Teller, E. *J. Am. Chem. Soc.* **1938**, *60* (2), 309–319.

(12) Broekhoff, J. C. P. *Mesopore Determination from Nitrogen Sorption Isotherms: Fundamentals, Scope, Limitations*; B. Delmon, P. Grange, P. Jacobs, G. P., Ed.; Elsevier Scientific Publishing Company, **1979**; Vol. 3.

(13) Roth, W. J.; Nachtigall, P.; Morris, R. E.; Wheatley, P. S.; Seymour, V. R.; Ashbrook, S. E.; Chlubná, P.; Grajciar, L.; Položij, M.; Zukal, A.; Shvets, O.; Čejka, J. *Nat. Chem.* **2013**, *5* (7), 628–633.

(14) Long, J. R.; Yaghi, O. M. *Chem. Soc. Rev.* **2009**, *38* (5), 1213–1214.

(15) Tranchemontagne, D. J.; Mendoza-Cortés, J. L.; O'Keeffe, M.; Yaghi, O. M. *Chem. Soc. Rev.* **2009**, *38* (5), 1257–1283.

(16) Hendon, C. H.; Rieth, A. J.; Korzyński, M. D.; Dincă, M. *ACS Cent. Sci.* **2017**, *3* (6), 554–563.

(17) Tu, W.; Xu, Y.; Yin, S.; Xu, R. *Adv. Mater.* **2018**, *30* (33), 1707582.

(18) Lee, J. S. M.; Cooper, A. I. *Chem. Rev.* **2020**, *120* (4), 2171–2214.

(19) Staudinger, H.; Heuer, W. *Ber. Dtsch. Chem. Ges. (A and B series)* **1934**, *67* (7), 1159–1164.

(20) Davankov, V. A.; Rogoshin, S. V.; Tsyurupa, M. P. *J. Polym. Sci. Polym. Symp.* **1974**, *47*, 95–101.

(21) Joseph, R.; Ford, W. T.; Zhang, S.; Tsyurupa, M. P.; Pastukhov, A. V; Davankov, V. A. *J. Polym. Sci. Part A: Polym. Chem.* **1997**, *35*, 695–701.

(22) Huang, J.; Turner, S. R. *Polym. Rev.* **2018**, *58* (1), 1–41.

(23) Budd, P. M.; Ghanem, B. S.; Makhseed, S.; McKeown, N. B.; Msayib, K. J.; Tattershall, C. E. *Chem. Commun.* **2004**, No. 2, 230–231.

(24) McKeown, N. B.; Budd, P. M. *Chem. Soc. Rev.* **2006**, *35* (8), 675–683.

(25) Côte, A. P.; Benin, A. I.; Ockwig, N. W.; O'Keeffe, M.; Matzger, A. J.; Yaghi, O. M. *Science* **2005**, *310*, 1166–1171.

(26) El-Kaderi, H. M.; Hunt, J. R.; Mendoza-Cortés, J. L.; Côte, A. P.; Taylor, R. E.; O'Keeffe, M.; Yaghi, O. M. *Science* **2007**, *316* (5822), 268–272.

(27) Liu, M.; Guo, L.; Jin, S.; Tan, B. *J. Mater. Chem. A* **2019**, *7* (10), 5153–5172.

(28) Katekomol, P.; Roeser, J.; Bojdys, M.; Weber, J.; Thomas, A. *Chem. Mater.* **2013**, *25* (9), 1542–1548.

(29) Kuhn, P.; Antonietti, M.; Thomas, A. *Angew. Chem. Int. Ed.* **2008**, *47* (18), 3450–3453.

(30) Xu, Y.; Jin, S.; Xu, H.; Nagai, A.; Jiang, D. *Chem. Soc. Rev.* **2013**, *42* (20), 8012–8031.

(31) Jiang, J. X.; Su, F.; Trewin, A.; Wood, C. D.; Campbell, N. L.; Niu, H.; Dickinson, C.; Ganin, A. Y.; Rosseinsky, M. J.; Khimyak, Y. Z.; Cooper, A. I. *Angew. Chem. Int. Ed.* **2007**, *46* (45), 8574–8578.
(32) Tian, Y.; Zhu, G. *Chem. Rev.* **2020**, *120* (16), 8934–8986.
(33) Ben, T.; Ren, H.; Shengqian, M.; Cao, D.; Lan, J.; Jing, X.; Wang, W.; Xu, J.; Deng, F.; Simmons, J. M.; Qiu, S.; Zhu, G. *Angew. Chem. Int. Ed.* **2009**, *48* (50), 9457–9460.
(34) Fritsch, J.; Rose, M.; Wollmann, P.; Böhlmann, W.; Kaskel, S. *Materials* **2010**, *3* (4), 2447–2462.
(35) Rose, M.; Böhlmann, W.; Sabo, M.; Kaskel, S. *Chem. Commun.* **2008**, *1* (21), 2462–2464.
(36) Slater, A. G.; Cooper, A. I. *Science* **2015**, *348* (6238), aaa8075.
(37) Kramer, S.; Bennedsen, N. R.; Kegnæs, S. *ACS Catal.* **2018**, *8* (8), 6961–6982.
(38) Harmer, M. A.; Sun, Q. *Appl. Catal. A: Gen.* **2001**, *221*, 45–62.
(39) Shimizu, K. I.; Satsuma, A. *Energy Environ. Sci.* **2011**, *4* (9), 3140–3153.
(40) Stein, A.; Melde, B. J.; Schroden, R. C. *Adv. Mater.* **2000**, *12* (19), 1403–1419.
(41) Lim, M. H.; Blanford, C. F.; Stein, A. *Chem. Mater.* **1998**, *10* (2), 467–470.
(42) Margolese, D.; Melero, J. A.; Christiansen, S. C.; Chmelka, B. F.; Stucky, G. D. *Chem. Mater.* **2000**, *12* (8), 2448–2459.
(43) Xing, R.; Liu, N.; Liu, Y.; Wu, H.; Jiang, Y.; Chen, L.; He, M.; Wu, P. *Adv. Funct. Mater.* **2007**, *17* (14), 2455–2461.
(44) Morales, G.; Athens, G.; Chmelka, B. F.; Van Grieken, R.; Melero, J. A. *J. Catal.* **2008**, *254* (2), 205–217.
(45) Corma, A. *Chem. Rev.* **1997**, *97* (6), 2373–2419.
(46) DuPont, AMBERLYST™ 15DRY Polymeric Catalyst, 177-03086, June 2019
(47) Kunin, R.; Meitzner, E. F.; Oline, J. A.; Fisher, S. A.; Frisch, N. *Ind. Eng. Chem. Prod. Res. Dev.* **1962**, *1* (2), 140–144.
(48) Meng, Y.; Gu, D.; Zhang, F.; Shi, Y.; Yang, H.; Li, Z.; Yu, C.; Tu, B.; Zhao, D. *Angew. Chem. Int. Ed.* **2005**, *44* (43), 7053–7059.
(49) Liu, F.; Meng, X.; Zhang, Y.; Ren, L.; Nawaz, F.; Xiao, F. S. *J. Catal.* **2010**, *271*, 52–58.
(50) Liu, F.; Kong, W.; Qi, C.; Zhu, L.; Xiao, F. S. *ACS Catal.* **2012**, *2* (4), 565–572.
(51) Román-Leshkov, Y.; Chheda, J. N.; Dumesic, J. A. *Science* **2006**, *312* (4), 1933–1937.
(52) Alamillo, R.; Crisci, A. J.; Gallo, J. M. R.; Scott, S. L.; Dumesic, J. A. *Angew. Chem. Int. Ed.* **2013**, *52* (39), 10349–10351.
(53) Zakrzewska, M. E.; Bogel-Łukasik, E.; Bogel-Łukasik, R. *Chem. Rev.* **2011**, *111* (2), 397–417.
(54) Wang, L.; Wang, H.; Liu, F.; Zheng, A.; Zhang, J.; Sun, Q.; Lewis, J. P.; Zhu, L.; Meng, X.; Xiao, F. S. *ChemSusChem* **2014**, *7* (2), 402–406.
(55) Neel, A. J.; Hilton, M. J.; Sigman, M. S.; Toste, F. D. *Nature* **2017**, *543* (7647), 637–646.
(56) Ren, L. K.; Zhu, L. F.; Qi, T.; Tang, J. Q.; Yang, H. Q.; Hu, C. W. *ACS Catal.* **2017**, *7* (3), 2199–2212.
(57) Corma Canos, A.; Iborra, S.; Velty, A. *Chem. Rev.* **2007**, *107* (6), 2411–2502.
(58) Sun, Q.; Tang, Y.; Aguila, B.; Wang, S.; Xiao, F. S.; Thallapally, P. K.; Al-Enizi, A. M.; Nafady, A.; Ma, S. *Angew. Chem. Int. Ed.* **2019**, *58* (26), 8670–8675.
(59) Kundu, S. K.; Bhaumik, A. *ACS Sustain. Chem. Eng.* **2015**, *3* (8), 1715–1723.
(60) Gomes, R.; Bhanja, P.; Bhaumik, A. *J. Mol. Catal. A: Chem.* **2016**, *411*, 110–116.
(61) Maiti, S.; Chowdhury, A. R.; Das, A. K. *Microporous Mesoporous Mater.* **2019**, *283*, 39–47.
(62) Tanaka, K.; Aoki, H.; Hosomi, H.; Ohba, S. *Org. Lett.* **2000**, *2* (14), 2133–2134.
(63) Yadav, C.; Maka, V. K.; Payra, S.; Moorthy, J. N. *ACS Appl. Mater. Interfaces* **2020**, *2*, 3084–3093.
(64) Modak, A.; Mondal, J.; Bhaumik, A. *ChemCatChem* **2013**, *5* (7), 1749–1753.
(65) Sekerová, L.; Lhotka, M.; Vyskočilová, E.; Faukner, T.; Slováková, E.; Brus, J.; Červený, L.; Sedláček, J. *Chem. Eur. J.* **2018**, *24* (55), 14742–14749.
(66) Schreiner, P. R. *Chem. Soc. Rev.* **2003**, *32* (5), 289–296.

(67) Tan, M. X.; Gu, L.; Li, N.; Ying, J. Y.; Zhang, Y. *Green Chem.* **2013**, *15* (5), 1127–1132.
(68) Kim, J. J.; Lim, C. R.; Reddy, B. M.; Park, S. E. *Mol. Catal.* **2018**, *451*, 43–50.
(69) Ansari, M. B.; Parvin, M. N.; Park, S. E. *Res. Chem. Intermed.* **2014**, *40*, 67–75.
(70) Ansari, M. B.; Jeong, E.-Y.; Park, S.-E. *Green Sustain. Chem.* **2012**, *2*, 1–7.
(71) Malerich, J. P.; Hagihara, K.; Rawal, V. H. *J. Am. Chem. Soc.* **2008**, *130* (44), 14416–14417.
(72) Busschaert, N.; Kirby, I. L.; Young, S.; Coles, S. J.; Horton, P. N.; Light, M. E.; Gale, P. A. *Angew. Chem. Int. Ed.* **2012**, *51* (18), 4426–4430.
(73) Cohen, S. M.; Zhang, Z.; Boissonnault, J. A. *Inorg. Chem.* **2016**, *55* (15), 7281–7290.
(74) Li, X.; Wang, Z.; Sun, J.; Gao, J.; Zhao, Y.; Cheng, P.; Aguila, B.; Ma, S.; Chen, Y.; Zhang, Z. *Chem. Commun.* **2019**, *55* (38), 5423–5426.
(75) Wu, Q.; Gong, W.; Li, G. *ACS Appl. Mater. Interfaces* **2020**, *12*, 17861–17869.
(76) Kuchukulla, R. R.; Li, F.; He, Z.; Zhou, L.; Zeng, Q. *Green Chem.* **2019**, *21* (21), 5808–5812.
(77) Pal, R.; Sarkar, T.; Khasnobis, S. *Arkivoc* **2012**, *2012*, 570–609.
(78) Rezayat, M.; Ghaziaskar, H. S. *Green Chem.* **2009**, *11* (5), 710–715.
(79) Yu, I. K. M.; Tsang, D. C. W. *Bioresour. Technol.* **2017**, *238*, 716–732.
(80) Agarwal, B.; Kailasam, K.; Sangwan, R. S.; Elumalai, S. *Renew. Sust. Energ. Rev.* **2018**, *82*, 2408–2425.
(81) Shimizu, K. ichi; Uozumi, R.; Satsuma, A. *Catal. Commun.* **2009**, *10* (14), 1849–1853.
(82) Thangaraj, B.; Solomon, P. R.; Muniyandi, B.; Ranganathan, S.; Lin, L. *Clean Energy* **2019**, *3* (1), 2–23.
(83) Ma, F.; Hanna, M. A. *Bioresour. Technol.* **1999**, *70* (1), 1–15.
(84) Melero, J. A.; Iglesias, J.; Morales, G. *Green Chem.* **2009**, *11* (9), 1285–1308.
(85) Busca, G. *Chem. Rev.* **2010**, *110* (4), 2217–2249.
(86) Hattori, H. *Chem. Rev.* **1995**, *95*, 537–558.
(87) Cabral, N. M.; Lorenti, J. P.; Plass, W.; Gallo, J. M. R. *Front. Chem.* **2020**, *8* (April), 1–10.
(88) Prat, D.; Wells, A.; Hayler, J.; Sneddon, H.; McElroy, C. R.; Abou-Shehada, S.; Dunn, P. J. *Green Chem.* **2016**, *18* (1), 288–296.
(89) Eglington, M. *New studies in aromatic chloromethylation*, Master thesis, Durham University **1992**, pp 1–43.
(90) Mancheño, M. J.; Royuela, S.; de La Peña, A.; Ramos, M.; Zamora, F.; Segura, J. L. *J. Chem. Educ.* **2019**, *96* (8), 1745–1751.
(91) List, B. *Angew. Chem. Int. Ed.* **2010**, *49* (10), 1730–1734.
(92) Jones, G. In *Organic Reactions*; **1967**; pp 204–273.
(93) Han, J.; Xu, Y.; Su, Y.; She, X.; Pan, X. *Catal. Commun.* **2008**, *9* (10), 2077–2079.
(94) Green, B.; Crane, R. I.; Khaidem, I. S.; Leighton, R. S.; Newaz, S. S.; Smyser, T. E. *J. Org. Chem.* **1985**, *50* (5), 640–644.
(95) Rao, P, S.; Venkataratnam, R. V. *Tetrahedron Lett.* **1991**, *32* (41), 5821–5822.
(96) Su, C.; Chen, Z. C.; Zheng, Q. G. *Synthesis (Stuttg)* **2003**, *4*, 555–559.
(97) Ugale, B.; Nagaraja, C. M. *RSC Adv.* **2016**, *6* (34), 28854–28864.
(98) Dhakshinamoorthy, A.; Heidenreich, N.; Lenzen, D.; Stock, N. *CrystEngComm* **2017**, *19* (29), 4187–4193.
(99) Elhamifar, D.; Kazempoor, S.; Karimi, B. *Catal. Sci. Technol.* **2016**, *6* (12), 4318–4326.
(100) Saravanamurugan, S.; Palanichamy, M.; Hartmann, M.; Murugesan, V. *Appl. Catal. A: Gen.* **2006**, *298*, 8–15.
(101) Islam, S. M.; Roy, A. S.; Dey, R. C.; Paul, S. *J. Mol. Catal. A: Chem.* **2014**, *394*, 66–73.
(102) Xue, B.; Zhu, J.; Liu, N.; Li, Y. *Catal. Commun.* **2015**, *64*, 105–109.
(103) Weber, J.; Antonietti, M.; Thomas, A. *Macromolecules* **2007**, *40* (4), 1299–1304.
(104) Makowski, P.; Weber, J.; Thomas, A.; Goettmann, F. *Catal. Commun.* **2008**, *10* (2), 243–247.

(105) Liu, B.; Ben, T.; Xu, J.; Deng, F.; Qiu, S. *New J. Chem.* **2014**, *38* (6), 2292–2299.
(106) Wang, Y.; Wang, L.; Liu, C.; Wang, R. *ChemCatChem* **2015**, *7* (10), 1559–1565.
(107) Dang, Q. Q.; Zhan, Y. F.; Wang, X. M.; Zhang, X. M. *ACS Appl. Mater. Interfaces* **2015**, *7* (51), 28452–28458.
(108) Marquis, E.; Graton, J.; Berthelot, M.; Planchat, A.; Laurence, C. *Can. J. Chem.* **2004**, *82* (9), 1413–1422.
(109) Carta, M.; Croad, M.; Bugler, K.; Msayib, K. J.; McKeown, N. B. *Polym. Chem.* **2014**, *5* (18), 5262–5266.
(110) Fang, Q.; Gu, S.; Zheng, J.; Zhuang, Z.; Qiu, S.; Yan, Y. *Angew. Chem. Int. Ed.* **2014**, *53* (11), 2878–2882.
(111) Zhang, Y.; Sigen, A.; Zou, Y.; Luo, X.; Li, Z.; Xia, H.; Liu, X.; Mu, Y. *J. Mater. Chem. A* **2014**, *2* (33), 13422–13430.
(112) Feng, L. J.; Wang, M.; Sun, Z. Y.; Hu, Y.; Deng, Z. T. *Des. Monomers Polym.* **2017**, *20* (1), 344–350.
(113) Liu, X.; A, S.; Zhang, Y.; Luo, X.; Xia, H.; Li, H.; Mu, Y. *RSC Adv.* **2014**, *4*, 6447–6453.
(114) Modak, A.; Nandi, M.; Mondal, J.; Bhaumik, A. *Chem. Commun.* **2012**, *48* (2), 248–250.
(115) Modak, A.; Mondal, J.; Bhaumik, A. *Appl. Catal. A: Gen.* **2013**, *459*, 41–51.
(116) Verduzco, R.; Li, X.; Pesek, S. L.; Stein, G. E. *Chem. Soc. Rev.* **2015**, *44* (8), 2405–2420.
(117) Zhang, H.; Xiong, L.; He, Z.; Zhong, A.; Wang, T.; Xu, Y.; Zhou, M.; Huang, K. *Polym. Chem.* **2016**, *7* (30), 4975–4982.
(118) Zhu, R.; Shen, J.; Wei, Y.; Zhang, F. *New J. Chem.* **2011**, *35* (9), 1861–1866.
(119) Dey, S. K.; de Sousa Amadeu, N.; Janiak, C. *Chem. Commun.* **2016**, *52* (50), 7834–7837.
(120) Suresh, V. M.; Bonakala, S.; Atreya, H. S.; Balasubramanian, S.; Maji, T. K. *ACS Appl. Mater. Interfaces* **2014**, *6* (7), 4630–4637.
(121) MacFarlane, D. R.; Pringle, J. M.; Johansson, K. M.; Forsyth, S. A.; Forsyth, M. *Chem. Commun.* **2006**, No. 18, 1905–1917.
(122) Wang, X.; Li, J.; Chen, G.; Guo, Z.; Zhou, Y.; Wang, J. *ChemCatChem* **2015**, *7* (6), 993–1003.
(123) Zhu, L.; Liu, X. Q.; Jiang, H. L.; Sun, L. B. *Chem. Rev.* **2017**, *117* (12), 8129–8176.
(124) Appaturi, J. N.; Ratti, R.; Phoon, B. L.; Batagarawa, S. M.; Din, I. U.; Selvaraj, M.; Ramalingam, R. J. *Dalton Trans.* **2021**, *50* (13), 4445–4469.
(125) Menegatti, R. Green Chemistry – Aspects for the Knoevenagel Reaction. In *Green Chemistry - Environmentally Benign Approaches*; Kidwai, M, Mishra N. K., Eds.; IntechOpen, **2012**; pp 13–32. (126) Beutler, U.; Fuenfschilling, P. C.; Steinkemper, A. *Org. Process Res. Dev.* **2007**, *11* (3), 341–345.
(127) Liu, F.; Li, W.; Sun, Q.; Zhu, L.; Meng, X.; Guo, Y. H.; Xiao, F. S. *ChemSusChem* **2011**, *4* (8), 1059–1062.
(128) Liu, F.; Wang, L.; Sun, Q.; Zhu, L.; Meng, X.; Xiao, F. S. *J. Am. Chem. Soc.* **2012**, *134* (41), 16948–16950.
(129) Hassner, A. 4-Dimethylaminopyridine. In *Encyclopedia of Reagents for Organic Synthesis*; John Wiley & Sons, Ltd, **2001**; Vol. 2, pp 3–4.
(130) Pulko, I.; Wall, J.; Krajnc, P.; Cameron, N. R. *Chem. Eur. J.* **2010**, *16* (8), 2350–2354.
(131) Zhang, Y.; Zhang, Y.; Sun, Y. L.; Du, X.; Shi, J. Y.; Wang, W.; Wang, W. D. *Chem. Eur. J.* **2012**, *18* (20), 6328–6334.
(132) Xu, W.; Xia, W.; Guan, Y.; Wang, Y.; Lu, C.; Yang, G.; Nie, J.; Chen, Z. *React. Funct. Polym.* **2016**, *104*, 15–21.
(133) Masao Tomoi, Yuzo Akada, H. K. *Makromol. Chem. Rapid Commun.* **1982**, *3*, 537–542.
(134) Benaglia, M.; Puglisi, A.; Cozzi, F. *Chem. Rev.* **2003**, *103* (9), 3401–3429.
(135) D'Elia, V.; Liu, Y.; Zipse, H. *Eur. J. Org. Chem.* **2011**, *2011* (8), 1527–1533.

(136) Blaser, H.-U.; Pugin, B.; Studer, M. *Chiral Catalyst Immobilization and Recycling*; de Vos, D. E., Vankelecom, I. F. J., Jacobs, P. A., Eds.; WILEY-VCH, **2000**.
(137) Okay, O. *Prog. Polym. Sci.* **2000**, *25* (6), 711–779.
(138) Ramón, D. J.; Yus, M. *Angew. Chem. Int. Ed.* **2005**, *44* (11), 1602–1634.
(139) Climent, M. J.; Corma, A.; Iborra, S. *RSC Adv.* **2012**, *2* (1), 16–58.
(140) Quintela, J. M.; Peinador, C.; Moreira, M. J. *Tetrahedron* **1995**, *51* (20), 5901–5912.
(141) Kundu, S. K.; Bhaumik, A. *RSC Adv.* **2015**, *5* (41), 32730–32739.
(142) Bhanja, P.; Chatterjee, S.; Bhaumik, A. *ChemCatChem* **2016**, *8* (19), 3089–3098.
(143) Yuan, S.; Feng, L.; He, A.; Liu, L.; Liu, B. *Colloids Surf. A* **2020**, *607*, 125475.
(144) Das, S. K.; Mondal, S.; Chatterjee, S.; Bhaumik, A. *ChemCatChem* **2018**, *10* (11), 2488–2495.
(145) Das, S. K.; Chowdhury, A.; Chakraborty, D.; Kayal, U.; Bhaumik, A. *Mol. Catal.* **2020**, *497*, 111198.
(146) Zaharani, L.; Khaligh, N. G.; Mihankhah, T.; Johan, M. R. *Mol. Divers.* **2021**, *25*, 323–332.
(147) Raj, V.; Lee, J. *Front. Chem.* **2020**, *8*, 623.
(148) Abrouki, Y.; Anouzla, A.; Loukili, H.; Chakir, A.; Idrissi, M.; Abrouki, A.; Rayadh, A.; Zahouily, M.; Kacemi, K. el; Bessiere, J.; Marouf, B.; Sebti, S. D. *Am. J. Biol. Chem. Pharm. Sci.* **2013**, *1* (6), 28–34.
(149) Sharma, V. K.; Singh, S. K. *RSC Adv.* **2017**, *7* (5), 2682–2732.
(150) Tamaddon, F.; Razmi, Z.; Jafari, A. A. *Tetrahedron Lett.* **2010**, *51* (8), 1187–1189.
(151) S. Panda, S.; Khanna, P.; Khanna, L. *Curr. Org. Chem.* **2012**, *16* (4), 507–520.
(152) Chopda, L. V.; Dave, P. N. *ChemistrySelect* **2020**, *5* (19), 5552–5572.
(153) Bugaut, X.; Glorius, F. *Chem. Soc. Rev.* **2012**, *41* (9), 3511–3522.
(154) Peris, E. *Chem. Rev.* **2018**, *118* (19), 9988–10031.
(155) Herrmann, W. A. *Angew. Chem. Int. Ed.* **2002**, *41* (8), 1290.
(156) Rose, M.; Notzon, A.; Heitbaum, M.; Nickerl, G.; Paasch, S.; Brunner, E.; Glorius, F.; Kaskel, S. *Chem. Commun.* **2011**, *47* (16), 4814–4816.
(157) Liu, T. T.; Xu, R.; Yi, J. D.; Liang, J.; Wang, X. S.; Shi, P. C.; Huang, Y. B.; Cao, R. *ChemCatChem* **2018**, *10* (9), 2036–2040.
(158) Gunasekar, G. H.; Park, K.; Ganesan, V.; Lee, K.; Kim, N. K.; Jung, K. D.; Yoon, S. *Chem. Mater.* **2017**, *29* (16), 6740–6748.
(159) Park, K.; Lee, K.; Kim, H.; Ganesan, V.; Cho, K.; Jeong, S. K.; Yoon, S. *J. Mater. Chem. A* **2017**, *5* (18), 8576–8582.
(160) Xu, G.; Zhu, Y.; Xie, W.; Zhang, S.; Yao, C.; Xu, Y. *Chem. Asian J.* **2019**, *14* (19), 3259–3263.
(161) Troschke, E.; Nguyen, K. D.; Paasch, S.; Schmidt, J.; Nickerl, G.; Senkovska, I.; Brunner, E.; Kaskel, S. *Chem. Eur. J.* **2018**, *24* (70), 18629–18633.
(162) Lohr, T. L.; Marks, T. J. *Nat. Chem.* **2015**, *7* (6), 477–482.
(163) Wasilke, J.; Obrey, S. J.; Baker, R. T.; Bazan, G. C. *Chem. Rev.* **2005**, *105*, 1001–1020.
(164) Polgár, L. *Cell. Mol. Life Sci.* **2005**, *62* (19–20), 2161–2172.
(165) Jia, Z.; Wang, K.; Tan, B.; Gu, Y. *ACS Catal.* **2017**, *7* (5), 3693–3702.
(166) Sun, Z.; Liu, F.; Yang, X.; Huang, X.; Zhang, M.; Bian, G.; Qi, Y.; Yang, X.; Zhang, W. *New J. Chem.* **2020**, *4*, 9546–9556.
(167) Merino, E.; Verde-Sesto, E.; Maya, E. M.; Iglesias, M.; Sánchez, F.; Corma, A. *Chem. Mater.* **2013**, *25* (6), 981–988.
(168) Zhang, Y.; Li, B.; Ma, S. *Chem. Commun.* **2014**, *50* (62), 8507–8510.
(169) Guadalupe, J.; Ray, A. M.; Maya, E. M.; Gómez-Lor, B.; Iglesias, M. *Polym. Chem.* **2018**, *9* (36), 4585–4595.
(170) Modak, A.; Bhaumik, A. *ChemistrySelect* **2016**, *6*, 1192–1200.

(171) Wang, T.; Xu, Y.; He, Z.; Zhang, H.; Xiong, L.; Zhou, M.; Yu, W.; Shi, B.; Huang, K. *Macromol. Chem. Phys.* **2017**, *218*, 1600431.
(172) Zhang, H.; Xiong, L.; He, Z.; Zhong, A.; Wang, T.; Xu, Y.; Huang, K. *New J. Chem.* **2016**, *40* (9), 7282–7285.
(173) Meng, G.; Gao, S.; Liu, Y.; Zhang, L.; Song, C.; Huang, K. *New J. Chem.* **2019**, *43* (5), 2269–2273.
(174) Xiong, L.; Zhang, H.; He, Z.; Wang, T.; Xu, Y.; Zhou, M.; Huang, K. *New J. Chem.* **2018**, *42* (2), 1368–1372.
(175) Shinde, D. B.; Kandambeth, S.; Pachfule, P.; Kumar, R. R.; Banerjee, R. *Chem. Commun.* **2015**, *51* (2), 310–313.
(176) Wang, K.; Jia, Z.; Yang, X.; Wang, L.; Gu, Y.; Tan, B. *J. Catal.* **2017**, *348*, 168–176.
(177) Verde-Sesto, E.; Merino, E.; Rangel-Rangel, E.; Corma, A.; Iglesias, M.; Sánchez, F. *ACS Sustain. Chem. Eng.* **2016**, *4* (3), 1078–1084.
(178) Sun, Q.; Aguila, B.; Ma, S. *Mater. Chem. Front.* **2017**, *1*, 1310–1316.
(179) Poli, E.; Merino, E.; Díaz, U.; Brunel, D.; Corma, A. *J. Phys. Chem. C* **2011**, *115* (15), 7573–7585.
(180) Zeidan, R. K.; Davis, M. E. *J. Catal.* **2007**, *247* (2), 379–382.
(181) Hu, Y.; Zhang, J.; Huo, H.; Wang, Z.; Xu, X.; Yang, Y.; Lin, K.; Fan, R. *Catal. Sci. Technol.* **2020**, *10* (2), 315–322.
(182) Hu, X. J.; Li, Z. X.; Xue, H.; Huang, X.; Cao, R.; Liu, T. F. *CCS Chem.* **2019**, *1*, 616–622.
(183) Xiong, L.; Yang, K.; Zhang, H.; Liao, X.; Huang, K. *Nanotechnology* **2016**, *27* (11), 115603.
(184) Rouhi, A. M. *Chem. Eng. News* **2004**, *82* (24), 45–56.
(185) Altava, B.; Burguete, M. I.; García-Verdugo, E.; Luis, S. V. *Chem. Soc. Rev.* **2018**, *47* (8), 2722–2771.
(186) Zhao, X. S.; Bao, X. Y.; Guo, W.; Lee, F. Y. *Mater. Today* **2006**, *9* (3), 32–39.
(187) Sherrington, D. C. *Chem. Commun.* **1998**, 2275–2286.
(188) Merad, J.; Lalli, C.; Bernadat, G.; Maury, J.; Masson, G. *Chem. Eur. J.* **2018**, *24* (16), 3925–3943.
(189) Rueping, M.; Sugiono, E.; Azap, C.; Theissmann, T.; Bolte, M. *Org. Lett.* **2005**, *7* (17), 3781–3783.
(190) Rueping, M.; Antonchick, A. P. *Org. Lett.* **2008**, *10* (9), 1731–1734.
(191) Uraguchi, D.; Sorimachi, K.; Terada, M. *J. Am. Chem. Soc.* **2004**, *126* (38), 11804–11805.
(192) Mutyala, A. K.; Patil, Ni. T. *Org. Chem. Front.* **2014**, *1*, 582–586.
(193) Rueping, M.; Sugiono, E.; Steck, A.; Theissmann, T. *Adv. Synth. Catal.* **2010**, *352*, 281–287.
(194) Bleschke, C.; Schmidt, J.; Kundu, D. S.; Blechert, S.; Thomas, A. *Adv. Synth. Catal.* **2011**, *353* (17), 3101–3106.
(195) Kundu, D. S.; Schmidt, J.; Bleschke, C.; Thomas, A.; Blechert, S. *Angew. Chem. Int. Ed.* **2012**, *51* (22), 5456–5459.
(196) Schmidt, J.; Kundu, D. S.; Blechert, S.; Thomas, A. *Chem. Commun.* **2014**, *50* (25), 3347–3349.
(197) Huangfu, Y.; Sun, Q.; Pan, S.; Meng, X.; Xiao, F. S. *ACS Catal.* **2015**, *5* (3), 1556–1559.
(198) Xu, L. W.; Luo, J.; Lu, Y. *Chem. Commun.* **2009**, 1807–1821.
(199) List, B.; Lerner, R. A.; Barbas, C. F. *J. Am. Chem. Soc.* **2000**, *122* (10), 2395–2396.
(200) Ahrendt, K. A.; Borths, C. J.; MacMillan, D. W. C. *J. Am. Chem. Soc.* **2000**, *122* (17), 4243–4244.
(201) Xu, H.; Chen, X.; Gao, J.; Lin, J.; Addicoat, M.; Irle, S.; Jiang, D. *Chem. Commun.* **2014**, *50* (11), 1292–1294.
(202) Chen, X.; Addicoat, M.; Irle, S.; Nagai, A.; Jiang, D. *J. Am. Chem. Soc.* **2013**, *135* (2), 546–549.
(203) Xu, H.; Gao, J.; Jiang, D. *Nat. Chem.* **2015**, *7* (11), 905–912.
(204) Xu, H. sen; Ding, S. Y.; An, W. K.; Wu, H.; Wang, W. *J. Am. Chem. Soc.* **2016**, *138* (36), 11489–11492.
(205) Wang, L. K.; Zhou, J. J.; Lan, Y. B.; Ding, S. Y.; Yu, W.; Wang, W. *Angew. Chem. Int. Ed.* **2019**, *58* (28), 9443–9447.

(206) Huang, N.; Ding, X.; Kim, J.; Ihee, H.; Jiang, D. *Angew. Chem. Int. Ed.* **2015**, *54* (30), 8704–8707.
(207) Zhang, J.; Han, X.; Wu, X.; Liu, Y.; Cui, Y. *J. Am. Chem. Soc.* **2017**, *139* (24), 8277–8285.
(208) Zhang, Z.; Xie, F.; Jia, J.; Zhang, W. *J. Am. Chem. Soc.* **2010**, *132* (45), 15939–15941.
(209) Zhang, J.; Han, X.; Wu, X.; Liu, Y.; Cui, Y. *ACS Sustain. Chem. Eng.* **2019**, *7* (5), 5065–5071.
(210) Franzén, J.; Marigo, M.; Fielenbach, D.; Wabnitz, T. C.; Kjærsgaard, A.; Jørgensen, K. A. *J. Am. Chem. Soc.* **2005**, *127* (51), 18296–18304.
(211) Hayashi, Y.; Gotoh, H.; Hayashi, T.; Shoji, M. *Angew. Chem. Int. Ed.* **2005**, *44* (27), 4212–4215.
(212) Burés, J.; Armstrong, A.; Blackmond, D. G. *J. Am. Chem. Soc.* **2011**, *133* (23), 8822–8825.
(213) Wang, C. A.; Zhang, Z. K.; Yue, T.; Sun, Y. L.; Wang, L.; Wang, W. D.; Zhang, Y.; Liu, C.; Wang, W. *Chem. Eur. J.* **2012**, *18* (22), 6718–6723.
(214) Wang, C. A.; Li, Y. W.; Han, Y. F.; Zhang, J. P.; Wu, R. T.; He, G. F. *Polym. Chem.* **2017**, *8* (36), 5561–5569.
(215) Yan, Z. Y.; Niu, Y. N.; Wei, H. L.; Wu, L. Y.; Zhao, Y. Bin; Liang, Y. M. *Tetrahedron Asymmetry* **2006**, *17* (23), 3288–3293.
(216) Lan, Y.; Yang, C.; Zhang, Y.; An, W.; Xue, H.; Ding, S.; Zhou, P.; Wang, W. *Polym. Chem.* **2019**, *10* (24), 3298–3305.
(217) Lin, Z. J.; Lü, J.; Li, L.; Li, H. F.; Cao, R. *J. Catal.* **2017**, *355*, 131–138.
(218) Han, X.; Zhang, J.; Huang, J.; Wu, X.; Yuan, D.; Liu, Y.; Cui, Y. *Nat. Commun.* **2018**, *9*, 1294.
(219) Wang, J.; Kan, X.; Shang, J.; Qiao, H.; Dong, Y. *J. Am. Chem. Soc.* **2020**, *142* (40), 16915–16920.
(220) Du, X.; Sun, Y.; Tan, B.; Teng, Q.; Yao, X.; Su, C.; Wang, W. *Chem. Commun.* **2010**, *46* (6), 970–972.
(221) Ma, L.; Wanderley, M. M.; Lin, W. *ACS Catal.* **2011**, *1* (7), 691–697.
(222) An, W. K.; Han, M. Y.; Wang, C. A.; Yu, S. M.; Zhang, Y.; Bai, S.; Wang, W. *Chem. Eur. J.* **2014**, *20* (35), 11019–11028.
(223) Wang, X.; Han, X.; Zhang, J.; Wu, X.; Liu, Y.; Cui, Y. *J. Am. Chem. Soc.* **2016**, *138* (38), 12332–12335.
(224) Ma, H. C.; Chen, G. J.; Huang, F.; Dong, Y. Bin. *J. Am. Chem. Soc.* **2020**, *142* (29), 12574–12578.
(225) Yu, S.-C.; Cheng, L.; Liu, L. *Org. Mater.* **2021**, *03* (02), 245–253.
(226) Kumar, A.; Madden, D. G.; Lusi, M.; Chen, K. J.; Daniels, E. A.; Curtin, T.; Perry, J. J.; Zaworotko, M. J. *Angew. Chem. Int. Ed.* **2015**, *54* (48), 14372–14377.
(227) Schäffner, B.; Schäffner, F.; Verevkin, S. P.; Börner, A. *Chem. Rev.* **2010**, *110* (8), 4554–4581.
(228) Yadav, N.; Seidi, F.; Crespy, D.; D'Elia, V. *ChemSusChem* **2019**, *12* (4), 724–754.
(229) Grignard, B.; Gennen, S.; Jérôme, C.; Kleij, A. W.; Detrembleur, C. *Chem. Soc. Rev.* **2019**, *48* (16), 4466–4514.
(230) Aomchad, V.; Cristòfol, À.; Della Monica, F.; Limburg, B.; D'Elia, V.; Kleij, A. W. *Green Chem.* **2021**, *23* (3), 1077–1113.
(231) Sonnati, M. O.; Amigoni, S.; Taffin De Givenchy, E. P.; Darmanin, T.; Choulet, O.; Guittard, F. *Green Chem.* **2013**, *15* (2), 283–306.
(232) Zhang, S.; Sun, J.; Zhang, X.; Xin, J.; Miao, Q.; Wang, J. *Chem. Soc. Rev.* **2014**, *43* (22), 7838–7869.
(233) Cokoja, M.; Bruckmeier, C.; Rieger, B.; Herrmann, W. A.; Kühn, F. E. *Angew. Chem. Int. Ed.* **2011**, *50* (37), 8510–8537.
(234) Fiorani, G.; Guo, W.; Kleij, A. W. *Green Chem.* **2015**, *17* (3), 1375–1389.
(235) Xie, Y.; Zhang, Z.; Jiang, T.; He, J.; Han, B.; Wu, T.; Ding, K. *Angew. Chem. Int. Ed.* **2007**, *46* (38), 7255–7258.
(236) Wu, Z.; Chen, C.; Guo, Q.; Li, B.; Que, Y.; Wang, L.; Wan, H.; Guan, G. *Fuel* **2016**, *184*, 128–135.
(237) Wilke, A.; Yuan, J.; Antonietti, M.; Weber, J. *ACS Macro Lett.* **2012**, *1* (8), 1028–1031.

(238) Huang, J.; Tao, C. A.; An, Q.; Zhang, W.; Wu, Y.; Li, X.; Shen, D.; Li, G. *Chem. Commun.* **2010**, *46* (6), 967–969.
(239) Gao, C.; Chen, G.; Wang, X.; Li, J.; Zhou, Y.; Wang, J. *Chem. Commun.* **2015**, *51* (24), 4969–4972.
(240) Zhao, Q.; Soll, S.; Antonietti, M.; Yuan, J. *Polym. Chem.* **2013**, *4* (8), 2432–2435.
(241) Zhao, Q.; Yin, M.; Zhang, A. P.; Prescher, S.; Antonietti, M.; Yuan, J. *J. Am. Chem. Soc.* **2013**, *135* (15), 5549–5552.
(242) Soll, S.; Zhang, P.; Zhao, Q.; Wang, Y.; Yuan, J. *Polym. Chem.* **2013**, *4* (19), 5048–5051.
(243) Zhao, Q.; Zhang, P.; Antonietti, M.; Yuan, J. *J. Am. Chem. Soc.* **2012**, *134* (29), 11852–11855.
(244) Wang, X.; Zhou, Y.; Guo, Z.; Chen, G.; Li, J.; Shi, Y.; Liu, Y.; Wang, J. *Chem. Sci.* **2015**, *6* (12), 6916–6924.
(245) Qin, L.; Wang, B.; Zhang, Y.; Chen, L.; Gao, G. *Chem. Commun.* **2017**, *53* (26), 3785–3788.
(246) Li, J.; Jia, D.; Guo, Z.; Liu, Y.; Lyu, Y.; Zhou, Y.; Wang, J. *Green Chem.* **2017**, *19* (11), 2675–2686.
(247) Zhang, W.; Ma, F.; Ma, L.; Zhou, Y.; Wang, J. *ChemSusChem* **2020**, *13* (2), 341–350.
(248) Wang, J.; Sng, W.; Yi, G.; Zhang, Y. *Chem. Commun.* **2015**, *51* (60), 12076–12079.
(249) Cho, H. C.; Lee, H. S.; Chun, J.; Lee, S. M.; Kim, H. J.; Son, S. U. *Chem. Commun.* **2011**, *47* (3), 917–919.
(250) Zhong, H.; Su, Y.; Chen, X.; Li, X.; Wang, R. *ChemSusChem* **2017**, *10* (24), 4855–4863.
(251) Thiel, K.; Zehbe, R.; Roeser, J.; Strauch, P.; Enthaler, S.; Thomas, A. *Polym. Chem.* **2013**, *4* (6), 1848–1856.
(252) Talapaneni, S. N.; Buyukcakir, O.; Je, S. H.; Srinivasan, S.; Seo, Y.; Polychronopoulou, K.; Coskun, A. *Chem. Mater.* **2015**, *27* (19), 6818–6826.
(253) Wang, X.; Dong, Q.; Xu, Z.; Wu, Y.; Gao, D.; Xu, Y.; Ye, C.; Wen, Y.; Liu, A.; Long, Z.; Chen, G. *Chem. Eng. J.* **2021**, *403*, 126460.
(254) Wang, W.; Li, C.; Yan, L.; Wang, Y.; Jiang, M.; Ding, Y. *ACS Catal.* **2016**, *6* (9), 6091–6100.
(255) Kawabe, K. *Catal. Surv. Asia* **2010**, *14* (3), 111–115.
(256) Zhang, Q.; Zhang, S.; Li, S. *Macromolecules* **2012**, *45* (7), 2981–2988.
(257) Wang, J.; Wei Yang, J. G.; Yi, G.; Zhang, Y. *Chem. Commun.* **2015**, *51* (86), 15708–15711.
(258) Sun, Q.; Jin, Y.; Aguila, B.; Meng, X.; Ma, S.; Xiao, F. S. *ChemSusChem* **2017**, *10* (6), 1160–1165.
(259) Saptal, V.; Shinde, D. B.; Banerjee, R.; Bhanage, B. M. *Catal. Sci. Technol.* **2016**, *6* (15), 6152–6158.
(260) Sun, Q.; Aguila, B.; Perman, J.; Nguyen, N.; Ma, S. *J. Am. Chem. Soc.* **2016**, *138* (48), 15790–15796.
(261) Zhong, H.; Goa, J.; Sa, R.; Yang, S.; Wu, Z.; Wang, R. *ChemSusChem* **2020**, *13*, 6323–6329.
(262) Zhi, Y.; Shao, P.; Feng, X.; Xia, H.; Zhang, Y.; Shi, Z.; Mu, Y.; Liu, X. *J. Mater. Chem. A* **2018**, *6* (2), 374–382.
(263) Yang, F.; Li, Y.; Zhang, T.; Zhao, Z.; Xing, G.; Chen, L. *Chem. Eur. J.* **2020**, *26*, 4510–4514.
(264) Liu, X. F.; Li, X. Y.; Qiao, C.; Fu, H. C.; He, L. N. *Angew. Chem. Int. Ed.* **2017**, *56* (26), 7425–7429.
(265) Mu, Z. J.; Ding, X.; Chen, Z. Y.; Han, B. H. *ACS Appl. Mater. Interfaces* **2018**, *10* (48), 41350–41358.
(266) Kuhn, P.; Thomas, A.; Antonietti, M. *Macromolecules* **2009**, *42* (1), 319–326.
(267) Wang, K.; Yang, L. M.; Wang, X.; Guo, L.; Cheng, G.; Zhang, C.; Jin, S.; Tan, B.; Cooper, A. *Angew. Chem. Int. Ed.* **2017**, *56* (45), 14149–14153.
(268) Dey, S.; Bhunia, A.; Esquivel, D.; Janiak, C. *J. Mater. Chem. A* **2016**, *4* (17), 6259–6263.
(269) Zhao, H.; Jin, Z.; Su, H.; Jing, X.; Sun, F.; Zhu, G. *Chem. Commun.* **2011**, *47* (22), 6389–6391.
(270) Roeser, J.; Kailasam, K.; Thomas, A. *ChemSusChem* **2012**, *5* (9), 1793–1799.
(271) Katekomol, P.; Roeser, J.; Bojdys, M.; Weber, J.; Thomas, A. *Chem. Mater.* **2013**, *25* (9), 1542–1548.

(272) Li, Y. M.; Yang, L.; Sun, L.; Ma, L.; Deng, W. Q.; Li, Z. *J. Mater. Chem. A* **2019**, *7* (45), 26071–26076.
(273) Buyukcakir, O.; Je, S. H.; Talapaneni, S. N.; Kim, D.; Coskun, A. *ACS Appl. Mater. Interfaces* **2017**, *9* (8), 7209–7216.
(274) Yu, X.; Sun, J.; Yuan, J.; Zhang, W.; Pan, C.; Liu, Y.; Yu, G. *Chem. Eng. J.* **2018**, *350*, 867–871.
(275) Liu, A.; Zhang, J.; Lv, X. *Chinese J. Catal.* **2018**, *39* (8), 1320–1328.
(276) Biswas, T.; Halder, A.; Paliwal, K. S.; Mitra, A.; Tudu, G.; Banerjee, R.; Mahalingam, V. *Chem. Asian J.* **2020**, *15*, 1683–1687.
(277) Ma, D.; Liu, K.; Li, J.; Shi, Z. *ACS Sustain. Chem. Eng.* **2018**, *6* (11), 15050–15055.
(278) Buyukcakir, O.; Je, S. H.; Choi, D. S.; Talapaneni, S. N.; Seo, Y.; Jung, Y.; Polychronopoulou, K.; Coskun, A. *Chem. Commun.* **2016**, *52* (5), 934–937.
(279) Kim, D.; Subramanian, S.; Thirion, D.; Song, Y.; Jamal, A.; Otaibi, M. S.; Yavuz, C. T. *Catal. Today* **2020**, *356*, 527–534.
(280) Maya, E. M.; Rangel-Rangel, E.; Díaz, U.; Iglesias, M. *J. CO2 Util.* **2018**, *25*, 170–179.
(281) Ravi, S.; Puthiaraj, P.; Ahn, W. S. *J. CO2 Util.* **2017**, *21*, 450–458.
(282) Zhang, N.; Zou, B.; Yang, G. P.; Yu, B.; Hu, C. W. *J. CO2 Util.* **2017**, *22*, 9–14.
(283) Shiels, R. A.; Jones, C. W. *J. Mol. Catal. A: Chem.* **2007**, *261* (2), 160–166.
(284) North, M.; Pasquale, R.; Young, C. *Green Chem.* **2010**, *12* (9), 1514–1539.
(285) Pescarmona, P. P.; Taherimehr, M. *Catal. Sci. Technol.* **2012**, *2* (11), 2169–2187.
(286) Lu, X. B.; He, R.; Bai, C. X. *J. Mol. Catal. A: Chem.* **2002**, *186*, 1–11.
(287) Whiteoak, C. J.; Kielland, N.; Laserna, V.; Escudero-Adán, E. C.; Martin, E.; Kleij, A. W. *J. Am. Chem. Soc.* **2013**, *135* (4), 1228–1231.
(288) Kamphuis, A. J.; Picchioni, F.; Pescarmona, P. P. *Green Chem.* **2019**, *21* (3), 406–448.
(289) Sun, J.; Han, L.; Cheng, W.; Wang, J.; Zhang, X.; Zhang, S. *ChemSusChem* **2011**, *4* (4), 502–507.
(290) Wang, J. Q.; Kong, D. L.; Chen, J. Y.; Cai, F.; He, L. N. *J. Mol. Catal. A: Chem.* **2006**, *249* (1–2), 143–148.
(291) Aprile, C.; Giacalone, F.; Agrigento, P.; Liotta, L. F.; Martens, J. A.; Pescarmona, P. P.; Gruttadauria, M. *ChemSusChem* **2011**, *4* (12), 1830–1837.
(292) Agrigento, P.; Al-Amsyar, S. M.; Sorée, B.; Taherimehr, M.; Gruttadauria, M.; Aprile, C.; Pescarmona, P. P. *Catal. Sci. Technol.* **2014**, *4* (6), 1598–1607.
(293) Wang, J. Q.; Yue, X. D.; Cai, F.; He, L. N. *Catal. Commun.* **2007**, *8* (2), 167–172.
(294) Han, L.; Park, S. W.; Park, D. W. *Energy Environ. Sci.* **2009**, *2* (12), 1286–1292.
(295) Udayakumar, S.; Lee, M. K.; Shim, H. L.; Park, S. W.; Park, D. W. *Catal. Commun.* **2009**, *10* (5), 659–664.
(296) Jose, T.; Cañellas, S.; Pericàs, M. A.; Kleij, A. W. *Green Chem.* **2017**, *19* (22), 5488–5493.
(297) Liu, M.; Liu, B.; Liang, L.; Wang, F.; Shi, L.; Sun, J. *J. Mol. Catal. A: Chem.* **2016**, *418–419*, 78–85.
(298) Meléndez, J.; North, M.; Villuendas, P. *Chem. Commun.* **2009**, No. 18, 2577–2579.
(299) North, M.; Villuendas, P.; Young, C. *Chem. Eur. J.* **2009**, *15* (43), 11454–11457.
(300) Beyzavi, M. H.; Stephenson, C. J.; Liu, Y.; Karagiaridi, O.; Hupp, J. T.; Farha, O. K. *Front. Energy Res.* **2015**, *2* (January), 1–10.
(301) Beyzavi, M. H.; Klet, R. C.; Tussupbayev, S.; Borycz, J.; Vermeulen, N. A.; Cramer, C. J.; Stoddart, J. F.; Hupp, J. T.; Farha, O. K. *J. Am. Chem. Soc.* **2014**, *136* (45), 15861–15864.
(302) Yuan, S.; Zou, L.; Li, H.; Chen, Y.; Qin, J.; Zhang, Q.; Lu, W.; Hall, M. B.; Zhou, H. *Angew. Chem. Int. Ed.* **2016**, *128* (36), 10934–10938.
(303) Zalomaeva, O. V.; Chibiryaev, A. M.; Kovalenko, K. A.; Kholdeeva, O. A.; Balzhinimaev, B. S.; Fedin, V. P. *J. Catal.* **2013**, *298* (February), 179–185.
(304) Zhu, M.; Carreon, M. A. *J. Appl. Polym. Sci.* **2014**, *131* (5), 39738.

(305) Taherimehr, M.; Van de Voorde, B.; Wee, L. H.; Martens, J. A.; De Vos, D. E.; Pescarmona, P. P. *ChemSusChem* **2017**, *10* (6), 1283–1291.
(306) Aguila, B.; Sun, Q.; Wang, X.; O'Rourke, E.; Al-Enizi, A. M.; Nafady, A.; Ma, S. *Angew. Chem. Int. Ed.* **2018**, *57* (32), 10107–10111.
(307) Takahashi, T.; Watahiki, T.; Kitazume, S.; Yasuda, H.; Sakakura, T. *Chem. Commun.* **2006**, No. 15, 1664–1666.
(308) Cheng, W.; Chen, X.; Sun, J.; Wang, J.; Zhang, S. *Catal. Today* **2013**, *200*, 117–124.
(309) Han, L.; Choi, H. J.; Choi, S. J.; Liu, B.; Park, D. W. *Green Chem.* **2011**, *13* (4), 1023–1028.
(310) Sainz Martinez, A.; Hauzenberger, C.; Sahoo, A. R.; Csendes, Z.; Hoffmann, H.; Bica, K. *ACS Sustain. Chem. Eng.* **2018**, *6* (10), 13131–13139.
(311) Sun, J.; Cheng, W.; Fan, W.; Wang, Y.; Meng, Z.; Zhang, S. *Catal. Today* **2009**, *148* (3–4), 361–367.
(312) Watile, R. A.; Deshmukh, K. M.; Dhake, K. P.; Bhanage, B. M. *Catal. Sci. Technol.* **2012**, *2* (5), 1051–1055.
(313) Whiteoak, C. J.; Henseler, A. H.; Ayats, C.; Kleij, A. W.; Pericàs, M. A. *Green Chem.* **2014**, *16* (3), 1552–1559.
(314) Roshan, K. R.; Jose, T.; Kathalikkattil, A. C.; Kim, D. W.; Kim, B.; Park, D. W. *Appl. Catal. A: Gen.* **2013**, *467*, 17–25.
(315) Zhao, Y.; Tian, J. S.; Qi, X. H.; Han, Z. N.; Zhuang, Y. Y.; He, L. N. *J. Mol. Catal. A: Chem.* **2007**, *271*, 284–289.
(316) Sun, J.; Wang, J.; Cheng, W.; Zhang, J.; Li, X.; Zhang, S.; She, Y. *Green Chem.* **2012**, *14* (3), 654–660.
(317) Liu, M.; Zhou, B.; Zhou, L.; Xie, Z.; Li, S.; Chen, L. *J. Mater. Chem. A* **2018**, *6* (21), 9860–9865.
(318) Abednatanzi, S.; Gohari Derakhshandeh, P.; Tack, P.; Muniz-Miranda, F.; Liu, Y. Y.; Everaert, J.; Meledina, M.; Vanden Bussche, F.; Vincze, L.; Stevens, C. V.; Van Speybroeck, V.; Vrielinck, H.; Callens, F.; Leus, K.; Van Der Voort, P. *Appl. Catal. B* **2020**, *269* (May 2019), 118769.
(319) Abednatanzi, S.; Derakhshandeh, P. G.; Leus, K.; Vrielinck, H.; Callens, F.; Schmidt, J.; Savateev, A.; Van Der Voort, P. *Sci. Adv.* **2020**, *6* (14), eaaz2310.
(320) Watanabe, H.; Asano, S.; Fujita, S. I.; Yoshida, H.; Arai, M. *ACS Catal.* **2015**, *5* (5), 2886–2894.
(321) Huang, W.; Ma, B. C.; Lu, H.; Li, R.; Wang, L.; Landfester, K.; Zhang, K. A. I. *ACS Catal.* **2017**, *7* (8), 5438–5442.
(322) Zhao, L.; Shi, S.; Liu, M.; Zhu, G.; Wang, M.; Du, W.; Gao, J.; Xu, J. *Green Chem.* **2018**, *20* (6), 1270–1279.
(323) Wu, Y.; Xu, H.; Chen, X.; Gao, J.; Jiang, D. *Chem. Commun.* **2015**, *51* (50), 10096–10098.
(324) Peng, Y. K.; Tsang, S. C. E. *Nano Today* **2018**, *18*, 15–34.
(325) Xiao, M.; Luo, B.; Wang, S.; Wang, L. *J. Energy Chem.* **2018**, *27* (4), 1111–1123.
(326) Chen, H.; Jena, H. S.; Feng, X.; Leus, K.; Van Der Voort, P. *Angew. Chem. Int. Ed.* **2022**.
(327) Zhang, T.; Xing, G.; Chen, W.; Chen, L. *Mater. Chem. Front.* **2020**, *4* (2), 332–353.
(328) Li, G.; Xie, Z.; Wang, Q.; Chen, X.; Zhang, Y.; Wang, X. *Chem. Eur. J.* **2021**, *27* (3), 939–943.
(329) Zhao, J.; Ren, J.; Zhang, G.; Zhao, Z.; Liu, S.; Zhang, W.; Chen, L. *Chem. Eur. J.* **2021**, *27* (42), 10781–10797.
(330) Xu, S.; Richter, M.; Feng, X. *Acc. Mater. Res.* **2021**, *2* (4), 252–265.
(331) Wang, Y.; Liu, H.; Pan, Q.; Wu, C.; Hao, W.; Xu, J.; Chen, R.; Liu, J.; Li, Z.; Zhao, Y. *J. Am. Chem. Soc.* **2020**, *142* (13), 5958–5963.
(332) Zhao, X.; Pang, H.; Huang, D.; Liu, G.; Hu, J.; Xiang, Y. *Angew. Chem. Int. Ed.* **2022**.
(333) Huang, J.; Golomb, M. J.; Kavanagh, S. R.; Tolborg, K.; Ganose, A. M.; Walsh, A. *J. Mater. Chem. A* **2022**.
(334) Zhang, F.; Hao, H.; Dong, X.; Li, X.; Lang, X. *Appl. Catal. B* **2022**, *305*.

(335) Wei, P. F.; Qi, M. Z.; Wang, Z. P.; Ding, S. Y.; Yu, W.; Liu, Q.; Wang, L. K.; Wang, H. Z.; An, W. K.; Wang, W. *J. Am. Chem. Soc.* **2018**, *140* (13), 4623–4631.
(336) Sun, N.; Jin, Y.; Wang, H.; Yu, B.; Wang, R.; Wu, H.; Zhou, W.; Jiang, J. *Chem. Mater.* **2022**, *34* (4), 1956–1964.
(337) Wu, Z.; Huang, X.; Li, X.; Hai, G.; Li, B.; Wang, G. *Sci. China Chem.* **2021**, *64* (12), 2169–2179.
(338) Chen, R.; Shi, J.; Ma, Y.; Lin, G.; Lang, X.; Wang, C. *Angew. Chem. Int. Ed.* **2019**, *58*, 6430–6434.
(339) Liu, Z.; Su, Q.; Ju, P.; Li, X.; Li, G.; Wu, Q.; Yang, B. *Chem. Commun.* **2020**, *56* (5), 766–769.
(340) Wu, S.; Zhang, Y. F.; Ding, H.; Li, X.; Lang, X. *J. Colloid Interface Sci.* **2022**, *610*, 446–454.
(341) Shi, J. L.; Chen, R.; Hao, H.; Wang, C.; Lang, X. *Angew. Chem. Int. Ed.* **2020**, *59* (23), 9088–9093.
(342) Bartling, H.; Eisenhofer, A.; Konig, B.; Gschwind, R. M. *J. Am. Chem. Soc.* **2016**, *138* (36), 11860–11871.
(343) Kang, X.; Wu, X.; Han, X.; Yuan, C.; Liu, Y.; Cui, Y. *Chem. Sci.* **2020**, *11* (6), 1494–1502.
(344) An, W. K.; Zheng, S. J.; Du, Y. N.; Ding, S. Y.; Li, Z. J.; Jiang, S.; Qin, Y.; Liu, X.; Wei, P. F.; Cao, Z. Q.; Song, M.; Pan, Z. *Catal. Sci. Technol.* **2020**, *10* (15), 5171–5180.
(345) Li, S.; Li, L.; Li, Y.; Dai, L.; Liu, C.; Liu, Y.; Li, J.; Lv, J.; Li, P.; Wang, B. *ACS Catal.* **2020**, *10* (15), 8717–8726.
(346) Li, Z. J.; Ding, S. Y.; Xue, H. D.; Cao, W.; Wang, W. *Chem. Commun.* **2016**, *52* (45), 7217–7220.
(347) Liu, Z.; Yang, X.; Yang, Z.; Su, X.; Xie, Z.; Chen, W.; Zhang, W.; Chen, L. *Appl. Catal. B* **2022**, *312*.
(348) Zhang, W.; Li, S.; Tang, X.; Tang, J.; Pan, C.; Yu, G. *Appl. Catal. B* **2020**, *272*.
(349) Zhang, Q. B.; Ban, Y. L.; Yuan, P. F.; Peng, S. J.; Fang, J. G.; Wu, L. Z.; Liu, Q. *Green Chem.* **2017**, *19* (23), 5559–5563.
(350) Zhang, P.; Yin, Y.; Wang, Z.; Yu, C.; Zhu, Y.; Yan, D.; Liu, W.; Mai, Y. *Macromolecules* **2021**, *54* (7), 3543–3553.
(351) Rajagopalan, A.; Lara, M.; Kroutil, W. *Adv. Synth. Catal.* **2013**, *355*, 3321–3335.
(352) Zhu, R.; Zhou, G.; Teng, J. nan; Li, X.; Fu, Y. *ChemSusChem* **2020**, *13* (19), 5248–5255.
(353) Ayed, C.; Caire Da Silva, L.; Wang, D.; Zhang, K. A. I. *J. Mater. Chem. A* **2018**, *6* (44), 22145–22151.
(354) Zhang, K.; Kopetzki, D.; Seeberger, P. H.; Antonietti, M.; Vilela, F. *Angew. Chem. Int. Ed.* **2013**, *52* (5), 1432–1436.
(355) Li, R.; Ma, B. C.; Huang, W.; Wang, L.; Wang, D.; Lu, H.; Landfester, K.; Zhang, K. A. I. *ACS Catal.* **2017**, *7* (5), 3097–3101.
(356) Ischay, M. A.; Ament, M. S.; Yoon, T. P. *Chem. Sci.* **2012**, *3* (9), 2807–2811.
(357) Crellin, R. A.; Lambert, M. C.; Ledwith, A. *J. Chem. Soc. D* **1970**, 682–683.
(358) Song, C.; Nie, J.; Ma, C.; Lu, C.; Wang, F.; Yang, G. *Appl. Catal. B* **2021**, *287*.
(359) Chen, D.; Chen, W.; Zhang, G.; Li, S.; Chen, W.; Xing, G.; Chen, L. *ACS Catal.* **2022**, *12* (1), 616–623.
(360) Li, R.; Wang, Z. J.; Wang, L.; Ma, B. C.; Ghasimi, S.; Lu, H.; Landfester, K.; Zhang, K. A. I. *ACS Catal.* **2016**, *6* (2), 1113–1121.
(361) Sun, N.; Wang, C.; Wang, H.; Gao, X.; Jiang, J. *ACS Appl. Mater. Interfaces* **2020**, *12* (50), 56491–56498.
(362) Liu, H.; Yan, X.; Chen, W.; Xie, Z.; Li, S.; Chen, W.; Zhang, T.; Xing, G.; Chen, L. *Sci. China Chem.* **2021**, *64* (5), 827–833.
(363) Huang, W.; Ma, B. C.; Lu, H.; Li, R.; Wang, L.; Landfester, K.; Zhang, K. A. I. *ACS Catal.* **2017**, *7* (8), 5438–5442.
(364) Ghasimi, S.; Bretschneider, S. A.; Huang, W.; Landfester, K.; Zhang, K. A. I. *Adv. Sci.* **2017**, *4* (8).
(365) Zhao, Y.; Liu, H.; Wu, C.; Zhang, Z.; Pan, Q.; Hu, F.; Wang, R.; Li, P.; Huang, X.; Li, Z. *Angew. Chem. Int. Ed.* **2019**, *58* (16), 5376–5381.
(366) Shang, P.; Yan, X.; Li, Y.; Liu, J.; Zhang, G.; Chen, L. *Chin. Chem. Lett.* **2022**.

(367) Huang, W.; Wang, Z. J.; Ma, B. C.; Ghasimi, S.; Gehrig, D.; Laquai, F.; Landfester, K.; Zhang, K. A. I. *J. Mater. Chem. A* **2016**, *4* (20), 7555–7559.
(368) Chen, B.; Chen, L.; Yan, Z.; Kang, J.; Chen, S.; Jin, Y.; Ma, L.; Yan, H.; Xia, C. *Green Chem.* **2021**, *23* (10), 3607–3611.
(369) Yang, Y.; Niu, H.; Xu, L.; Zhang, H.; Cai, Y. *Appl. Catal. B* **2020**, *269*.
(370) Liu, S.; Pan, W.; Wu, S.; Bu, X.; Xin, S.; Yu, J.; Xu, H.; Yang, X. *Green Chem.* **2019**, *21* (11), 2905–2910.
(371) Bhadra, M.; Kandambeth, S.; Sahoo, M. K.; Addicoat, M.; Balaraman, E.; Banerjee, R. *J. Am. Chem. Soc.* **2019**, *141* (15), 6152–6156.
(372) Huang, W.; Byun, J.; Rörich, I.; Ramanan, C.; Blom, P. W. M.; Lu, H.; Wang, D.; Caire da Silva, L.; Li, R.; Wang, L.; Landfester, K.; Zhang, K. A. I. *Angew. Chem. Int. Ed.* **2018**, *57*, 8316–8320.
(373) Chen, H.; Liu, W.; Laemont, A.; Krishnaraj, C.; Feng, X.; Rohman, F.; Meledina, M.; Zhang, Q.; Van Deun, R.; Leus, K.; Van Der Voort, P. *Angew. Chem. Int. Ed.* **2021**, *60* (19), 10820–10827.
(374) An, W.-K.; Zheng, S.-J.; Xu, X.; Liu, L.-J.; Ren, J.-S.; Fan, L.; Yang, Z.-K.; Ren, Y.; Xu, C. *Appl. Catal. B* **2022**, 121630.
(375) Chao, J.; Wang, Z.-K.; Liu, H.; Wu, G.; Lei, Z.; Xu, H.; Su, T.; Zhang, L.; Li, Q.; Wang, H.; Zhang, D.-W.; Li, Z.-T.; Yusran, Y. *J. Catal.* **2022**, *413*, 692–702.
(376) Gisbertz, S.; Pieber, B. *ChemPhotoChem* **2020**, *4* (7), 456–475.
(377) Corrigan, N.; Shanmugam, S.; Xu, J.; Boyer, C. *Chem. Soc. Rev.* **2016**, *45* (22), 6165–6212.
(378) Guerra, J.; Cantillo, D.; Kappe, C. O. *Catal. Sci. Technol.* **2016**, *6* (13), 4695–4699.
(379) Nicewicz, D. A.; Nguyen, T. M. *ACS Catal.* **2014**, *4* (1), 355–360.
(380) Chaudhuri, A.; Zondag, S. D. A.; Schuurmans, J. H. A.; Van Der Schaaf, J.; Noël, T. *Org. Process Res. Dev.* **2022**, *26* (4), 1279–1288.
(381) Debruyne, M.; Van Speybroeck, V.; Van Der Voort, P.; Stevens, C. V. *Green Chem.* **2021**, *23* (19), 7361–7434.
(382) Yakushev, A. A.; Abel, A. S.; Averin, A. D.; Beletskaya, I. P.; Cheprakov, A. V.; Ziankou, I. S.; Bonneviot, L.; Bessmertnykh-Lemeune, A. *Coord. Chem. Rev.* **2022**, *458*.
(383) Riente, P.; Noël, T. *Catal. Sci. Technol.* **2019**, *9* (19), 5186–5232.
(384) Rajeshwar, K.; Thomas, A.; Janaky, C. *J. Phys. Chem. Lett.* **2015**, *6* (1), 139–147.
(385) Markushyna, Y.; Smith, C. A.; Savateev, A. *Eur. J. Org. Chem.* **2020**, *2020* (10), 1294–1309.
(386) Savateev, A.; Ghosh, I.; König, B.; Antonietti, M. *Angew. Chem. Int. Ed.* **2018**, *57*, 15936–15947.
(387) Qian, Y.; Zhang, F.; Pang, H. *Adv. Funct. Mater.* **2021**, *31* (37).
(388) Xiao, J. D.; Jiang, H. L. *Acc. Chem. Res.* **2019**, *52* (2), 356–366.
(389) Jiang, Z. W.; Zou, Y. C.; Zhao, T. T.; Zhen, S. J.; Li, Y. F.; Huang, C. Z. *Angew. Chem. Int. Ed.* **2020**, *59*, 3300–3306.
(390) Ren, S.; Bojdys, M. J.; Dawson, R.; Laybourn, A.; Khimyak, Y. Z.; Adams, D. J.; Cooper, A. I. *Adv. Mater.* **2012**, *24* (17), 2357–2361.
(391) Wang, K.; Yang, L. M.; Wang, X.; Guo, L.; Cheng, G.; Zhang, C.; Jin, S.; Tan, B.; Cooper, A. *Angew. Chem. Int. Ed.* **2017**, *56* (45), 14149–14153.
(392) Liu, M.; Huang, Q.; Wang, S.; Li, Z.; Li, B.; Jin, S.; Tan, B. *Angew. Chem. Int. Ed.* **2018**, *57* (37), 11968–11972.
(393) Bourda, L.; Krishnaraj, C.; Van Der Voort, P.; Van Hecke, K. *Mater. Adv.* **2021**, *2*, 2811–2845.
(394) Hu, H.; Yan, Q.; Ge, R.; Gao, Y. *Chinese J. Catal.* **2018**, *39* (7), 1167–1179.
(395) Li, Y.; Chen, W.; Xing, G.; Jiang, D.; Chen, L. *Chem. Soc. Rev.* **2020**, *49* (10), 2852–2868.
(396) Julien, P. A.; Mottillo, C.; Friščić, T. *Green Chem.* **2017**, *19* (12), 2729–2747.
(397) Gaab, M.; Trukhan, N.; Maurer, S.; Gummaraju, R.; Müller, U. *Microporous Mesoporous Mater.* **2012**, *157*, 131–136.
(398) Yilmaz, B.; Trukhan, N.; Müller, U. *Chinese J. Catal.* **2012**, *33* (1), 3–10.

(399) Silva, P.; Vilela, S. M. F.; Tomé, J. P. C.; Almeida Paz, F. A. *Chem. Soc. Rev.* **2015**, *44* (19), 6774–6803.
(400) Porta, R.; Benaglia, M.; Puglisi, A. *Org. Process Res. Dev.* **2016**, *20* (1), 2–25.
(401) Richard Stock, L.; Bisschops, M.; Ransohoff, T. C. The Potential Impact of Continuous Processing on the Practice and Economics of Biopharmaceutical Manufacturing. In *Continuous Processing in Pharmaceutical Manufacturing*; Ganapathy Subramanian, Ed.; WILEY-VCH Verlag GmbH & Co. KGaA, **2015**; pp 479–494.
(402) Kaur, P.; Hupp, J. T.; Nguyen, S. T. *ACS Catal.* **2011**, *1* (7), 819–835.
(403) Dong, W.; Hu, B.; Gao, X.; Li, Y.; Xie, X.; Zhang, Z. *J. Org. Chem.* **2016**, *81* (19), 8770–8776.
(404) Dey, S.; Bhunia, A.; Esquivel, D.; Janiak, C. *J. Mater. Chem. A* **2016**, *4* (17), 6259–6263.
(405) Comins, D. L.; Higuchi, K.; Young, D. W. In Advances in Heterocyclic Chemistry; Academic Press: Cambridge, MA, USA, 2013; Volume 110, pp. 175–235.
(406) Wang, G.-B.; Li, S.; Yan, C.-X.; Zhu, F.-C.; Lin, Q.-Q.; Xie, K.-H.; Geng, Y.; Dong, Y.-B. *J. Mater. Chem. A* **2020**, *8*, 6975–6983.
(407) Zhang, T.; Xing, G.; Chen, W.; Chen, L. *Mater. Chem. Front.* **2020**, *4* (2), 332–353.
(408) Romero, N. A.; Nicewicz, D. A. *Chem. Rev.* **2016**, *116* (17), 10075–10166.
(409) Schultz, D. M.; Yoon, T. P. *Science*. **2014**, p 1239176.
(410) Koike, T.; Atika, M. *Inorg. Chem. Front.* **2014**, *1*, 562.
(411) Teegardin, K.; Day, J. I.; Chan, J.; Weaver, J. *Org. Process. Res. Dev.* **2016**, *20* (7), 1156–1163.
(412) Schilling, W.; Riemer, D.; Zhang, Y.; Hatami, N.; Das, S. *ACS Catal.* **2018**, *8* (6), 5425–5430.
(413) Xia, J. B.; Zhu, C.; Chen, C. *J. Am. Chem. Soc.* **2013**, *135* (46), 17494–17500.
(414) Joshi-Pangu, A.; Lévesque, F.; Roth, H. G.; Oliver, S. F.; Campeau, L. C.; Nicewicz, D.; DiRocco, D. A. *J. Org. Chem.* **2016**, *81* (16), 7244–7249.
(415) Lee, S. H.; Nam, D. H.; Park, C. B. *Adv. Synth. Catal.* **2009**, *351* (16), 2589–2594.
(416) Ni, M.; Leung, M. K. H.; Leung, D. Y. C.; Sumathy, K. *Renew. Sust. Energ. Rev.* **2007**, *11* (3), 401–425.
(417) Andrew Frame, F.; Carroll, E. C.; Larsen, D. S.; Sarahan, M.; Browning, N. D.; Osterloh, F. E. *Chem. Commun.* **2008**, No. 19, 2206–2208.
(418) Tahir, M. B.; Nabi, G.; Rafique, M.; Khalid, N. R. *Int. J. Environ. Sci. Technol.* **2017**, *14* (11), 2519–2542.
(419) Lee, G. J.; Wu, J. J. *Powder Technol.* **2017**, *318*, 8–22.
(420) Ong, C. B.; Ng, L. Y.; Mohammad, A. W. *Renew. Sustain. Energy Rev.* **2018**, *81* (July 2016), 536–551.
(421) Cao, S.; Low, J.; Yu, J.; Jaroniec, M. *Adv. Mater.* **2015**, *27* (13), 2150–2176.
(422) Wang, Y.; Wang, X.; Antonietti, M. *Angew. Chem. Int. Ed.* **2012**, 68–89.
(423) Xiao, J. D.; Jiang, H. L. *Acc. Chem. Res.* **2019**, *52*, 356–366.
(424) Dhakshinamoorthy, A.; Asiri, A. M.; García, H. *Angew. Chem. Int. Ed.* **2016**, *55* (18), 5414–5445.
(425) Fan, H.; Mundstock, A.; Feldhoff, A.; Knebel, A.; Gu, J.; Meng, H.; Caro, J. *J. Am. Chem. Soc.* **2018**, *140* (32), 10094–10098.
(426) Doonan, C. J.; Tranchemontagne, D. J.; Glover, T. G.; Hunt, J. R.; Yaghi, O. M. *Nat. Chem.* **2010**, *2* (3), 235–238.
(427) Mulzer, C. R.; Shen, L.; Bisbey, R. P.; McKone, J. R.; Zhang, N.; Abruña, H. D.; Dichtel, W. R. *ACS Cent. Sci.* **2016**, *2* (9), 667–673.
(428) Halder, A.; Ghosh, M.; Khayum, A. M.; Bera, S.; Addicoat, M.; Sasmal, H. S.; Karak, S.; Kurungot, S.; Banerjee, R. *J. Am. Chem. Soc.* **2018**, *140* (35), 10941–10945.
(429) Kaczmarek, A. M.; Liu, Y. Y.; Kaczmarek, M. K.; Liu, H.; Artizzu, F.; Carlos, L. D.; Van Der Voort, P. *Angew. Chem. Int. Ed.* **2020**, *59* (5), 1932–1940.

(430) Wu, X.; Han, X.; Xu, Q.; Liu, Y.; Yuan, C.; Yang, S.; Liu, Y.; Jiang, J.; Cui, Y. *J. Am. Chem. Soc.* **2019**, *141* (17), 7081–7089.
(431) Das, G.; Biswal, B. P.; Kandambeth, S.; Venkatesh, V.; Kaur, G.; Addicoat, M.; Heine, T.; Verma, S.; Banerjee, R. *Chem. Sci.* **2015**, *6* (7), 3931–3939.
(432) Hu, H.; Yan, Q.; Ge, R.; Gao, Y. *Chinese J. Catal.* **2018**, *39* (7), 1167–1179.
(433) Liu, G.; Sheng, J.; Zhao, Y. *Sci. China. Chem.* **2017**, *60* (8), 1015–1022.
(434) Gonçalves, R. S. B.; Deoliveira, A. B. V.; Sindra, H. C.; Archanjo, B. S.; Mendoza, M. E.; Carneiro, L. S. A.; Buarque, C. D.; Esteves, P. M. *ChemCatChem* **2016**, *8* (4), 743–750.
(435) Wei, P.; Qi, M.; Wang, Z.; Ding, S.; Yu, W.; Liu, Q.; Wang, L.; Wang, H.; An, W.; Wang, W. *J. Am. Chem. Soc.* **2018**, *140*, 4623–4631.
(436) Yan, X.; Liu, H.; Li, Y.; Chen, W.; Zhang, T.; Zhao, Z.; Xing, G.; Chen, L. *Macromolecules* **2019**, *52*, 7977–7983.
(437) Liu, W.; Su, Q.; Ju, P.; Guo, B.; Zhou, H.; Li, G.; Wu, Q. *ChemSusChem* **2017**, *10* (4), 664–669.
(438) Liu, H.; Li, C.; Li, H.; Ren, Y.; Chen, J.; Tang, J.; Yang, Q. *ACS Appl. Mater. Interfaces.* **2020**, *12* (18), 20354–20365.
(439) He, S.; Yin, B.; Niu, H.; Cai, Y. *Appl. Catal. B* **2018**, *239*, 147–153.
(440) Sheng, J. L.; Dong, H.; Meng, X. bin; Tang, H. L.; Yao, Y. H.; Liu, D. Q.; Bai, L. L.; Zhang, F. M.; Wei, J. Z.; Sun, X. J. *ChemCatChem* **2019**, *11* (9), 2313–2319.
(441) Lewis, G. N. *J. Am. Chem. Soc.* **1916**, *38* (4), 762–785.
(442) Woodward, R. B. *Pure Appl. Chem.* **1973**, *33* (1), 145–177.
(443) Staudinger, H. *Ber. Dtsch. Chem. Ges. (A and B series)* **1920**, *53*, 1073–1085.
(444) Hoffman, R. *Sci. Am.* **1993**, *268*, 66–73.
(445) Pedersen, C. J. *J. Am. Chem. Soc.* **1967**, *89* (10), 2495–2496.
(446) Dietrich, B.; Lehn, J. M.; Sauvage, J. P.; Blanzat, J. *Tetrahedron* **1973**, *29*, 1629–1645.
(447) Kiggen, W.; Vögtle, F. *Angew. Chem. Int. Ed.* **1984**, *23* (9), 714–715.
(448) Rowan, S. J.; Cantrill, S. J.; Cousins, G. R. L.; Sanders, J. K. M.; Stoddart, J. F. *Angew. Chem. Int. Ed.* **2002**, *41* (6), 898–952.
(449) Dietrich-Buchecker, C.; Sauvage, J.-P. *Tetrahedron* **1990**, *46* (2), 503–512.
(450) Chichak, K. S.; Cantrill, S. J.; Pease, A. R.; Chiu, S.-H.; Cave, G. W. V.; Atwood, J. L.; Stoddart, J. F. *Science* **2004**, *304*, 1308–1312.
(451) Yaghi, O. M. *J. Am. Chem. Soc.* **2016**, *138* (48), 15507–15509.
(452) Yaghi, O. M.; Guangming, L.; Haillan, L. *Nature* **1995**, *378*, 703–706.
(453) Diercks, C. S.; Yaghi, O. M. *Science* **2017**, *355* (6328), aal1585.
(454) Zhang, Y. B.; Su, J.; Furukawa, H.; Yun, Y.; Gándara, F.; Duong, A.; Zou, X.; Yaghi, O. M. *J. Am. Chem. Soc.* **2013**, *135* (44), 16336–16339.
(455) Beaudoin, D.; Maris, T.; Wuest, J. D. *Nat. Chem.* **2013**, *5* (10), 830–834.
(456) Du, Y.; Yang, H.; Whiteley, J. M.; Wan, S.; Jin, Y.; Lee, S.; Zhang, W. *Angew. Chem. Int. Ed.* **2016**, *128* (5), 1769–1773.
(457) Hunt, J. R.; Doonan, C. J.; LeVangie, J. D.; Côté, A. P.; Yaghi, O. M. *J. Am. Chem. Soc.* **2008**, *130* (36), 11872–11873.
(458) Uribe-Romo, F. J.; Hunt, J. R.; Furukawa, H.; Klöck, C.; O'Keeffe, M.; Yaghi, O. M. *J. Am. Chem. Soc.* **2009**, *131* (13), 4570–4571.
(459) Zhao, C.; Diercks, C. S.; Zhu, C.; Hanikel, N.; Pei, X.; Yaghi, O. M. *J. Am. Chem. Soc.* **2018**, *140* (48), 16438–16441.
(460) Uribe-Romo, F. J.; Doonan, C. J.; Furukawa, H.; Oisaki, K.; Yaghi, O. M. *J. Am. Chem. Soc.* **2011**, *133* (30), 11478–11481.
(461) Nagai, A.; Chen, X.; Feng, X.; Ding, X.; Guo, Z.; Jiang, D. *Angew. Chem. Int. Ed.* **2013**, *52* (13), 3770–3774.

(462) Dalapati, S.; Jin, S.; Gao, J.; Xu, Y.; Nagai, A.; Jiang, D. *J. Am. Chem. Soc.* **2013**, *135* (46), 17310–17313.
(463) Guo, J.; Xu, Y.; Jin, S.; Chen, L.; Kaji, T.; Honsho, Y.; Addicoat, M. A.; Kim, J.; Saeki, A.; Ihee, H.; Seki, S.; Irle, S.; Hiramoto, M.; Gao, J.; Jiang, D. *Nat. Commun.* **2013**, *4*.
(464) Seo, J. M.; Noh, H. J.; Jeong, H. Y.; Baek, J. B. *J. Am. Chem. Soc.* **2019**, *141* (30), 11786–11790.
(465) Wei, P. F.; Qi, M. Z.; Wang, Z. P.; Ding, S. Y.; Yu, W.; Liu, Q.; Wang, L. K.; Wang, H. Z.; An, W. K.; Wang, W. *J. Am. Chem. Soc.* **2018**, *140* (13), 4623–4631.
(466) Nandi, S.; Singh, S. K.; Mullangi, D.; Illathvalappil, R.; George, L.; Vinod, C. P.; Kurungot, S.; Vaidhyanathan, R. *Adv. Energy Mater.* **2016**, *6* (24).
(467) Wang, K.; Jia, Z.; Bai, Y.; Wang, X.; Hodgkiss, S. E.; Chen, L.; Chong, S. Y.; Wang, X.; Yang, H.; Xu, Y.; Feng, F.; Ward, J. W.; Cooper, A. I. *J. Am. Chem. Soc.* **2020**, *142* (25), 11131–11138.
(468) Kandambeth, S.; Mallick, A.; Lukose, B.; Mane, M. V.; Heine, T.; Banerjee, R. *J. Am. Chem. Soc.* **2012**, *134* (48), 19524–19527.
(469) Zhuang, X.; Zhao, W.; Zhang, F.; Cao, Y.; Liu, F.; Bi, S.; Feng, X. *Polym. Chem.* **2016**, *7* (25), 4176–4181.
(470) Jin, E.; Asada, M.; Xu, Q.; Dalapati, S.; Addicoat, M. A.; Brady, M. A.; Xu, H.; Nakamura, T.; Heine, T.; Chen, Q.; Jiang, D. *Science* **2017**, *357*, 673–676.
(471) Pastoetter, D. L.; Xu, S.; Borrelli, M.; Addicoat, M.; Biswal, B. P.; Paasch, S.; Dianat, A.; Thomas, H.; Berger, R.; Reineke, S.; Brunner, E.; Cuniberti, G.; Richter, M.; Feng, X. *Angew. Chem. Int. Ed.* **2020**, *59* (52), 23620–23625.
(472) Liu, Y.; Fu, S.; Pastoetter, D. L.; Khan, A. H.; Zhang, Y.; Dianat, A.; Xu, S.; Liao, Z.; Richter, M.; Yu, M.; Položij, M.; Brunner, E.; Cuniberti, G.; Heine, T.; Bonn, M.; Wang, H. I.; Feng, X. *Angew. Chem. Int. Ed.* **2022**, e202209762.
(473) Lyu, H.; Diercks, C. S.; Zhu, C.; Yaghi, O. M. *J. Am. Chem. Soc.* **2019**, *141* (17), 6848–6852.
(474) Jadhav, T.; Fang, Y.; Patterson, W.; Liu, C.; Hamzehpoor, E.; Perepichka, D. F. *Angew. Chem. Int. Ed.* **2019**, *131* (39), 13891–13895.
(475) Xu, J.; He, Y.; Bi, S.; Wang, M.; Yang, P.; Wu, D.; Wang, J.; Zhang, F. *Angew. Chem. Int. Ed.* **2019**, *131* (35), 12193–12197.
(476) Bi, S.; Yang, C.; Zhang, W.; Xu, J.; Liu, L.; Wu, D.; Wang, X.; Han, Y.; Liang, Q.; Zhang, F. *Nat. Commun.* **2019**, *10* (1), 2467.
(477) Xu, J.; Yang, C.; Bi, S.; Wang, W.; He, Y.; Wu, D.; Liang, Q.; Wang, X.; Zhang, F. *Angew. Chem. Int. Ed.* **2020**, *59* (52), 23845–23853.
(478) Segura, J. L.; Royuela, S.; Mar Ramos, M. *Chem. Soc. Rev.* **2019**, *48* (14), 3903–3945.
(479) Geng, K.; He, T.; Liu, R.; Dalapati, S.; Tan, K. T.; Li, Z.; Tao, S.; Gong, Y.; Jiang, Q.; Jiang, D. *Chem. Rev.* **2020**, *120* (16), 8814–8933.
(480) Nguyen, H. L. *Chem. Sci.* **2021**, *12* (25), 8632–8647.
(481) Tauc, J. *Mat. Res. Bull* **1968**, *3*, 37–46.
(482) Xu, J.; Yang, C.; Bi, S.; Wang, W.; He, Y.; Wu, D.; Liang, Q.; Wang, X.; Zhang, F. *Angew. Chem. Int. Ed.* **2020**, *59* (52), 23845–23853.
(483) Yin, L.; Zhao, Y.; Xing, Y.; Tan, H.; Lang, Z.; Ho, W.; Wang, Y.; Li, Y. *Chem. Eng. J.* **2021**, *419*, 129984.
(484) Wan, S.; Gándara, F.; Asano, A.; Furukawa, H.; Saeki, A.; Dey, S. K.; Liao, L.; Ambrogio, M. W.; Botros, Y. Y.; Duan, X.; Seki, S.; Stoddart, J. F.; Yaghi, O. M. *Chem. Mater.* **2011**, *23* (18), 4094–4097.
(485) Mo, C.; Yang, M.; Sun, F.; Jian, J.; Zhong, L.; Fang, Z.; Feng, J.; Yu, D. *Adv. Sci.* **2020**, *7* (12).
(486) Halder, A.; Karak, S.; Addicoat, M.; Bera, S.; Chakraborty, A.; Kunjattu, S. H.; Pachfule, P.; Heine, T.; Banerjee, R. *Angew. Chem. Int. Ed.* **2018**, *130* (20), 5899–5904.

(487) Kandambeth, S.; Mallick, A.; Lukose, B.; Mane, M. V.; Heine, T.; Banerjee, R. *J. Am. Chem. Soc.* **2012**, *134* (48), 19524–19527.
(488) Uribe-Romo, F. J.; Doonan, C. J.; Furukawa, H.; Oisaki, K.; Yaghi, O. M. *J. Am. Chem. Soc.* **2011**, *133* (30), 11478–11481.
(489) Vitaku, E.; Dichtel, W. R. *J. Am. Chem. Soc.* **2017**, *139* (37), 12911–12914.
(490) Calogero, F.; Freeman, H. S.; Esancy, J. F.; Whaley, W. M.; Dabney, B. J. *Dyes Pigm.* **1987**, *8*, 431–447.
(491) Gofman, I. V.; Goikhman, M. Y.; Podeshvo, I. V.; Eliseeva, E. E.; Bol'Bat, E. E.; Abalov, I. V.; Yakimanskii, A. V. *Russ. J. Appl. Chem.* **2010**, *83* (10), 1862–1867.
(492) Xia, A.; Guo, H.; Qiu, X.; Ding, M.; Gao, L. *J. Appl. Polym. Sci.* **2006**, *102* (2), 1844–1851.
(493) Albrecht, M.; Janser, I.; Lützen, A.; Hapke, M.; Fröhlich, R.; Weis, P. *Chem. Eur. J.* **2005**, *11* (19), 5742–5748.
(494) Zhang, B.; Breslow, R. *J. Am. Chem. Soc.* **1997**, *119*, 1676–1681.
(495) Everaert, J.; Debruyne, M.; Vanden Bussche, F.; Van Hecke, K.; Heugebaert, T. S. A.; Van Der Voort, P.; Van Speybroeck, V.; Stevens, C. V. *Synthesis (Germany)* **2021**, *53*, A-H.
(496) Wang, L.; Zhang, Y.; Liu, L.; Wang, Y. *J. Am. Chem. Soc.* **2006**, *71* (3), 1284–1287.
(497) Choi, H.; Go, M.; Cha, Y.; Choi, Y.; Kwon, K. Y.; Jung, J. H. *New J. Chem.* **2017**, *41* (12), 4793–4796.
(498) Venema, F.; M Nelissen, H. F.; Berthault, P.; Birlirakis, N.; Rowan, A. E.; Feiters, M. C.; M Nolte, R. J. *Chem. Eur. J.* **1998**, *4* (11), 2237–2250.
(499) Bu, R.; Zhang, L.; Liu, X. Y.; Yang, S. L.; Li, G.; Gao, E. Q. *ACS App. Mat. Interfaces* **2021**, *13* (22), 26431–26440.
(500) Divya, K. P.; Sreejith, S.; Ashokkumar, P.; Yuzhan, K.; Peng, Q.; Maji, S. K.; Tong, Y.; Yu, H.; Zhao, Y.; Ramamurthy, P.; Ajayaghosh, A. *Chem. Sci.* **2014**, *5* (9), 3469–3474.
(501) Mehr, S. H. M.; Depmeier, H.; Fukuyama, K.; Maghami, M.; MacLachlan, M. J. *Org. Biomol. Chem.* **2017**, *15* (3), 581–583.
(502) Chaudhry, M. T.; Soto, M. A.; Lelj, F.; MacLachlan, M. J. *Org. Chem. Front.* **2021**, *8* (7), 1437–1446.
(503) Mehr, S. H. M.; Patrick, B. O.; MacLachlan, M. J. *Org. Lett.* **2016**, *18* (8), 1840–1843.
(504) Faisal, M.; Ahmed, M.; Hussain, S.; Larik, F. A.; Saeed, A. *Green Process. Synth.* **2019**, *8* (1), 635–648.
(505) Liu, Y.; Wang, Y.; Li, H.; Guan, X.; Zhu, L.; Xue, M.; Yan, Y.; Valtchev, V.; Qiu, S.; Fang, Q. *Chem. Sci.* **2019**, *10* (46), 10815–10820.
(506) Shinde, D. B.; Aiyappa, H. B.; Bhadra, M.; Biswal, B. P.; Wadge, P.; Kandambeth, S.; Garai, B.; Kundu, T.; Kurungot, S.; Banerjee, R. *J. Mater. Chem. A* **2016**, *4* (7), 2682–2690.
(507) Cui, W. R.; Zhang, C. R.; Jiang, W.; Liang, R. P.; Qiu, J. D. *ACS Appl. Nano Mater.* **2019**, *2* (8), 5342–5349.
(508) Li, Z.; Zhi, Y.; Shao, P.; Xia, H.; Li, G.; Feng, X.; Chen, X.; Shi, Z.; Liu, X. *Appl. Catal. B* **2019**, *245*, 334–342.
(509) Bhadra, M.; Sasmal, H. S.; Basu, A.; Midya, S. P.; Kandambeth, S.; Pachfule, P.; Balaraman, E.; Banerjee, R. *ACS Appl. Mater. Interfaces* **2017**, *9* (15), 13785–13792.
(510) Aiyappa, H. B.; Thote, J.; Shinde, D. B.; Banerjee, R.; Kurungot, S. *Chem. Mater.* **2016**, *28* (12), 4375–4379.
(511) Halder, A.; Karak, S.; Addicoat, M.; Bera, S.; Chakraborty, A.; Kunjattu, S. H.; Pachfule, P.; Heine, T.; Banerjee, R. *Angew. Chem. Int. Ed.* **2018**, *57* (20), 5797–5802.
(512) Cui, W.-R.; Zhang, C.-R.; Jiang, W.; Liang, R.-P.; Qiu, J.-D. *ACS Appl. Nano Mater.* **2019**, *2* (8), 5342–5349.

(513) Borgmans, S.; Rogge, S. M. J.; de Vos, J. S.; Stevens, C. V.; Van Der Voort, P.; Van Speybroeck, V. *Angew. Chem. Int. Ed.* **2021**, *60* (16), 8913–8922.
(514) Traxler, M.; Gisbertz, S.; Pachfule, P.; Schmidt, J.; Roeser, J.; Reischauer, S.; Rabeah, J.; Pieber, B.; Thomas, A. *Angew. Chem. Int. Ed.* **2022**.
(515) Gibson, G. L.; McCormick, T. M.; Seferos, D. S. *J. Am. Chem. Soc.* **2012**, *134* (1), 539–547.
(516) Rawat, K. S.; Borgmans, S.; Braeckevelt, T.; Stevens, C. V.; Van Der Voort, P.; Van Speybroeck, V. *ACS Appl. Nano Mater.* **2022**.
(517) Stegbauer, L.; Zech, S.; Savasci, G.; Banerjee, T.; Podjaski, F.; Schwinghammer, K.; Ochsenfeld, C.; Lotsch, B. V. *Adv. Ener. Mater.* **2018**, *8* (24).
(518) Hankin, A.; Bedoya-Lora, F. E.; Alexander, J. C.; Regoutz, A.; Kelsall, G. H. *J. Mater. Chem. A* **2019**, *7* (45), 26162–26176.
(519) Cai, K.; Wang, W.; Zhang, J.; Chen, L.; Wang, L.; Zhu, X.; Yu, Z.; Wu, Z.; Zhou, H. *J. Mater. Chem. A* **2022**.
(520) Liu, Z.; Su, Q.; Ju, P.; Li, X.; Li, G.; Wu, Q.; Yang, B. *Chem. Commun.* **2020**, *56* (5), 766–769.
(521) Kabatc, J.; Kucybaia, Z.; Pietrzak, M.; Sigalski, F.; Paczkowski, J. *Polymer (Guildf)* **1999**, *40*, 735–745.
(522) Pitre, S. P.; McTiernan, C. D.; Ismaili, H.; Scaiano, J. C. *J. Am. Chem. Soc* **2013**, *135* (36), 13286–13289.
(523) Zou, Y. Q.; Chen, J. R.; Liu, X. P.; Lu, L. Q.; Davis, R. L.; Jørgensen, K. A.; Xiao, W. J. *Angew. Chem. Int. Ed.* **2012**, *51* (3), 784–788.
(524) Yu, X.; Cohen, S. M. *Chem. Commun.* **2015**, *51* (48), 9880–9883.
(525) Chen, Y.; Hu, J.; Ding, A. *RSC Adv.* **2020**, *10* (13), 7927–7932.
(526) Nicolaou, K. C.; Mathison, C. J. N.; Montagnon, T. *J. Am. Chem. Soc.* **2004**, *126* (16), 5192–5201.
(527) Chen, H.; Liu, C.; Wang, M.; Zhang, C.; Luo, N.; Wang, Y.; Abroshan, H.; Li, G.; Wang, F. *ACS Catal.* **2017**, *7* (5), 3632–3638.
(528) Hammond, C.; Schümperli, M. T.; Hermans, I. *Chem. Eur. J.* **2013**, *19* (39), 13193–13198.
(529) Éll, A. H.; Samec, J. S. M.; Brasse, C.; Bäckvall, J. E. *Chem. Commun.* **2002**, *10*, 1144–1145.
(530) Sun, C. L.; Li, H.; Yu, D. G.; Yu, M.; Zhou, X.; Lu, X. Y.; Huang, K.; Zheng, S. F.; Li, B. J.; Shi, Z. J. *Nat. Chem.* **2010**, *2* (12), 1044–1049.
(531) Xiong, K.; Wang, Y.; Zhang, F.; Li, X.; Lang, X. *Appl. Catal. B.* **2023**, *322*, 122135.
(532) Hartman, P. E.; Hartman, Z.; Ault, K. T. *Photochem. Photobiol.* **1990**, *51* (1), 59–66.
(533) Watts, R. J.; Teel, A. L. *Water Res.* **2019**, *159*, 46–54.
(534) Fónagy, O.; Szabó-Bárdos, E.; Horváth, O. *J. Photochem. Photobiol. A* **2021**, *407*, 113057.
(535) Hyung, S. C.; Jun, W. K.; Cha, Y. N.; Kim, C. *J. Immunoassay. Immunochem.* **2006**, *27* (1), 31–44.
(536) Rodríguez, E. M.; Márquez, G.; Tena, M.; Álvarez, P. M.; Beltrán, F. J. *Appl. Catal. B* **2015**, *178*, 44–53.
(537) Wang, Y.; Li, X.; Dong, X.; Zhang, F.; Lang, X. *J. Colloid Interface Sci.* **2022**, *616*, 846–857.
(538) Su, F.; Mathew, S. C.; Möhlmann, L.; Antonietti, M.; Wang, X.; Blechert, S. *Angew. Chem. Int. Ed.* **2011**, *50* (3), 657–660.
(539) Qiu, X.; Len, C.; Luque, R.; Li, Y. *ChemSusChem* **2014**, *7* (6), 1684–1688.
(540) Wendlandt, A. E.; Stahl, S. S. *Org. Lett.* **2012**, *14* (11), 2850–2853.
(541) Dong, C. P.; Higashiura, Y.; Marui, K.; Kumazawa, S.; Nomoto, A.; Ueshima, M.; Ogawa, A. *ACS Omega* **2016**, *1* (5), 799–807.
(542) Long, J.; Wang, L.; Gao, X.; Bai, C.; Jiang, H.; Li, Y. *Chem. Commun.* **2012**, *48* (99), 12109–12111.
(543) Sun, N.; Jin, Y.; Wang, H.; Yu, B.; Wang, R.; Wu, H.; Zhou, W.; Jiang, J. *Chem. Mater.* **2022**, *34* (4), 1956–1964.
(544) Shi, J. L.; Chen, R.; Hao, H.; Wang, C.; Lang, X. *Angew. Chem. Int. Ed.* **2020**, *59* (23), 9088–9093.

(545) Jiménez-Almarza, A.; López-Magano, A.; Mas-Ballesté, R.; Alemán, J. *ACS Appl. Mater. Interfaces* **2022**, *14* (14), 16258–16268.
(546) Chen, R.; Shi, J.; Ma, Y.; Lin, G.; Lang, X.; Wang, C. *Angew. Chem. Int. Ed.* **2019**, *58*, 6430–6434.
(547) Desrat, S.; Van De Weghe, P. *J. Org. Chem.* **2009**, *74* (17), 6728–6734.
(548) Nicolaou, K. C.; Chen, J. S.; Zhang, H.; Montero, A. *Angew. Chem. Int. Ed.* **2008**, *120* (1), 191–195.
(549) Nicolaou, K. C.; Zhang, H.; Chen, J. S.; Crawford, J. J.; Pasunoori, L. *Angew. Chem. Int. Ed.* **2007**, *119* (25), 4788–4791.
(550) Wang, H.; Ganesan, A. *Tetrahedron Lett.* **1998**, *39* (49), 9097–9098.
(551) Wall, M. E.; Wani, M. C.; Cook, C. E.; Palmer, K. H.; McPhail, A. T.; Sim, G. A. *J. Am. Chem. Soc.* **1966**, *88* (16), 3888–3890.
(552) Anzini, M.; Cappelli, A.; Vomero, S.; Seeber, M.; Menziani, M. C.; Langer, T.; Hagen, B.; Manzoni, C.; Bourguignon, J. J. *J. Med. Chem.* **2001**, *44* (8), 1134–1150.
(553) Blair, A.; Zmuda, F.; Malviya, G.; Tavares, A. A. S.; Tamagnan, G. D.; Chalmers, A. J.; Dewar, D.; Pimlott, S. L.; Sutherland, A. *Chem. Sci.* **2015**, *6* (8), 4772–4777.
(554) More, D. A.; Shinde, G. H.; Shaikh, A. C.; Muthukrishnan, M. *RSC Adv.* **2019**, *9* (52), 30277–30291.
(555) Jia, X.; Peng, F.; Qing, C.; Huo, C.; Wang, X. *Org. Lett.* **2012**, *14* (15), 4030–4033.
(556) Earle, M. J.; Vibert, A.; Jahn, U. Tris(4-bromophenyl)aminium Hexachloroantimonate. In *Encyclopedia of Reagents for Organic Synthesis*; John Wiley & Sons, Ltd, **2011**; Vol. 1, pp 1–6.
(557) Wang, J.; Li, L.; Guo, Y.; Li, S.; Wang, S.; Li, Y.; Zhang, Y. *Org. Biomol. Chem.* **2020**, *18* (40), 8179–8185.
(558) Cornel, V.; Lovely, C. J. Boron Trifluoride Etherate. In *Encyclopedia of Reagents for Organic Synthesis*; John Wiley & Sons, Ltd, **2007**; Vol. 2.
(559) Li, X. M.; Tang, L.; Qian, Z. M.; He, Y. H.; Guan, Z. *Tetrahedron Lett* **2020**, *61* (47), 152346.
(560) Specklin, S.; Decuypere, E.; Plougastel, L.; Aliani, S.; Taran, F. *J. Org. Chem.* **2014**, *79* (16), 7772–7777.
(561) Jerezano, A. V.; Labarrios, E. M.; Jiménez, F. E.; Del Cruz, M. C.; Pazos, D. C.; Gutiérrez, R. U.; Delgado, F.; Tamariz, J. *Arkivoc* **2013**, *2014* (3), 18–53.
(562) Jordan, A.; Sneddon, H. F. *Green Chem.* **2019**, *21* (8), 1900–1906.
(563) Arcelli, A.; Bongini, A.; Porzi, G.; Rinaldi, S. *J. Phys. Org. Chem.* **2012**, *25* (2), 132–141.
(564) Ouannes, C.; Wilson, T. *J. Am. Chem. Soc.* **1968**, *90* (23), 6527–6528.
(565) Saito, I.; Inoue, K.; Matsuura, T. *Photochem. Photobiol.* **1975**, *21*, 27–30.
(566) Bhadra, M.; Kandambeth, S.; Sahoo, M. K.; Addicoat, M.; Balaraman, E.; Banerjee, R. *J. Am. Chem. Soc.* **2019**, *141* (15), 6152–6156.
(567) Zhu, S.; Rueping, M. *Chem. Commun.* **2012**, *48* (98), 11960–11962.
(568) Sun, N.; Jin, Y.; Wang, H.; Yu, B.; Wang, R.; Wu, H.; Zhou, W.; Jiang, J. *Chem. Mater.* **2022**, *34* (4), 1956–1964.
(569) Mojarrad, A. G.; Zakavi, S. *Catal. Sci. Technol.* **2018**, *8* (3), 768–781.
(570) Hao, W.; Chen, D.; Li, Y.; Yang, Z.; Xing, G.; Li, J.; Chen, L. *Chem. Mater.* **2019**, 8100–8105.
(571) Yang, F.; Chu, X.; Sun, J.; Zhang, Y.; Li, Z.; Liu, H.; Bai, L.; Qu, Y.; Jing, L. *Chin. Chem. Lett.* **2020**, *31* (10), 2784–2788.
(572) Zhi, Y.; Li, K.; Xia, H.; Xue, M.; Mu, Y.; Liu, X. *J. Mater. Chem. A* **2017**, *5* (18), 8697–8704.
(573) Saito, H.; Nosaka, Y. *J. Phys. Chem. C* **2014**, *118* (29), 15656–15663.
(574) Yamaguchi, T.; Sugiura, Y.; Yamaguchi, E.; Tada, N.; Itoh, A. *Asian J. Org. Chem.* **2017**, *6* (4), 432–435.
(575) Ushakov, D. B.; Plutschack, M. B.; Gilmore, K.; Seeberger, P. H. *Chem. Eur. J.* **2015**, *21* (17), 6528–6534.

(576) Jiang, G.; Chen, J.; Huang, J. S.; Che, C. M. *Org. Lett.* **2009**, *11* (20), 4568–4571.
(577) Hermitage, S.; Jay, D. A.; Whiting, A. *Tetrahedron Lett.* **2002**, *43* (52), 9633–9636.
(578) Zhang, F.; Li, X.; Dong, X.; Hao, H.; Lang, X. *Chinese J. Catal.* **2022**, *43* (9), 2395–2404.
(579) Zhang, K.; Kopetzki, D.; Seeberger, P. H.; Antonietti, M.; Vilela, F. *Angew. Chem. Int. Ed.* **2013**, *125* (5), 1472–1476.
(580) Jati, A.; Dey, K.; Nurhuda, M.; Addicoat, M. A.; Banerjee, R.; Maji, B. *J. Am. Chem. Soc.* **2022**, *144* (17), 7822–7833.
(581) Yang, X.-J.; Janiak, C.; Rgen Heinze, J.; Drepper, F.; Mayer, P.; Piotrowski, H.; Klü, P. *Inorganica Chim. Acta* **2001**, *318*, 103–116.
(582) Yang, X.; Li, L.; Li, Y.; Zhang, Y. *J. Org. Chem.* **2016**, *81* (24), 12433–12442.
(583) Gupta, G.; Iqbal, P.; Yin, F.; Liu, J.; Palmer, R. E.; Sharma, S.; Leung, K. C. F.; Mendes, P. M. *Langmuir* **2015**, *31* (24), 6917–6923.
(584) Albrecht, M.; Janser, I.; Lützen, A.; Hapke, M. *Chem. Eur. J.* **2005**, *11*, 5742–5748.
(585) Sun, Q.; Aguila, B.; Perman, J.; Nguyen, N.; Ma, S. *J. Am. Chem. Soc.* **2016**, *138* (48), 15790–15796.
(586) Lützen, A.; Hapke, M.; Staats, H.; Bunzen, J. *Eur. J. Org. Chem.* **2003**, No. 20, 3948–3957.
(587) Jih, R. H.; Das, A. R.; Chia, W. Y.; Huang, J. J.; Hsu, M. H. *Org. Lett.* **2005**, *7* (15), 3211–3214.
(588) Spaleniak, G. P.; Daszkiewicz, Z.; Kyzioł, J. B. *Chem. Pap.* **2009**, *63* (3), 313–322.
(589) Hager, D.; Macmillan, D. W. C. *J. Am. Chem. Soc.* **2014**, *136* (49), 16986–16989.
(590) Shen, H. C.; Ding, F. X.; Luell, S.; Forrest, M. J.; Carballo-Jane, E.; Wu, K. K.; Wu, T. J.; Cheng, K.; Wilsie, L. C.; Krsmanovic, M. L.; Taggart, A. K.; Ren, N.; Cai, T. Q.; Deng, Q.; Chen, Q.; Wang, J.; Wolff, M. S.; Tong, X.; Holt, T. G.; Waters, M. G.; Hammond, M. L.; Tata, J. R.; Colletti, S. L. *J. Med. Chem.* **2007**, *50* (25), 6303–6306.
(591) Vitaku, E.; Dichtel, W. R. *J. Am. Chem. Soc.* **2017**, *139* (37), 12911–12914.
(592) Foster, J. S.; Prentice, A. W.; Forgan, R. S.; Paterson, M. J.; Lloyd, G. O. *ChemNanoMat* **2018**, *4* (8), 853–859.
(593) Li, H.; Homan, E. A.; Lampkins, A. J.; Ghiviriga, I.; Castellano, R. K. *Org. Lett.* **2005**, *7* (3), 443–446.
(594) Nielsen, B. E.; Gotfredsen, H.; Rasmussen, B.; Tortzen, C. G.; Pittelkow, M. *Synlett* **2013**, *24* (18), 2437–2442.
(595) Wang, H.; Qian, C.; Liu, J.; Zeng, Y.; Wang, D.; Zhou, W.; Gu, L.; Wu, H.; Liu, G.; Zhao, Y. *J. Am. Chem. Soc.* **2020**, *142* (10), 4862–4871.
(596) Wu, F.; Wang, L.; Ji, Y.; Zou, G.; Shen, H.; Nicewicz, D. A.; Chen, J.; Huang, Y. *iScience* **2020**, *23* (8), 101395.
(597) Bouziane, A.; Hélou, M.; Carboni, B.; Carreaux, F.; Demerseman, B.; Bruneau, C.; Renaud, J. L. *Chem. Eur. J.* **2008**, *14* (18), 5630–5637.
(598) Wang, Y.; Peng, F.; Liu, J.; Huo, C.; Wang, X.; Jia, X. *J. Org. Chem.* **2015**, *80* (1), 609–614.
(599) Ohshima, T.; Miyamoto, Y.; Ipposhi, J.; Nakahara, Y.; Utsunomiya, M.; Mashima, K. *J. Am. Chem. Soc.* **2009**, *131* (40), 14317–14328.
(600) Peilleron, L.; Retailleau, P.; Cariou, K. *Adv. Synth. Catal.* **2019**, *361* (22), 5160–5169.
(601) Blackburn, L.; Taylor, R. J. K. *Org. Lett.* **2001**, *3* (11), 1637–1639.
(602) Li, X. M.; Tang, L.; Qian, Z. M.; He, Y. H.; Guan, Z. *Tetrahedron Lett.* **2020**, *61* (47).
(603) Tafipolsky, M.; Amirjalayer, S.; Schmid, R. *J. Comput. Chem.* **2007**, *28* (7), 1169–1176.
(604) Schmid, R.; Tafipolsky, M. *J. Am. Chem. Soc.* **2008**, *130* (38), 12600–12601.
(605) Tafipolsky, M.; Schmid, R. *J. Phys. Chem. B* **2009**, *113* (5), 1341–1352.
(606) Vanduyfhuys, L.; Verstraelen, T.; Vandichel, M.; Waroquier, M.; Van Speybroeck, V. *J. Chem. Theory Comput.* **2012**, *8* (9), 3217–3231.

(607) Bureekaew, S.; Amirjalayer, S.; Tafipolsky, M.; Spickermann, C.; Roy, T. K.; Schmid, R. *Phys. Status Solidi B* **2013**, *250* (6), 1128–1141.
(608) Tafipolsky, M.; Amirjalayer, S.; Schmid, R. *J. Phys. Chem. C* **2010**, *114* (34), 14402–14409.
(609) Amirjalayer, S.; Snurr, R. Q.; Schmid, R. *J. Phys. Chem. C* **2012**, *116* (7), 4921–4929.
(610) Wieme, J.; Vanduyfhuys, L.; Rogge, S. M. J.; Waroquier, M.; Van Speybroeck, V. *J. Phys. Chem. C* **2016**, *120* (27), 14934–14947.
(611) Rogge, S. M. J.; Wieme, J.; Vanduyfhuys, L.; Vandenbrande, S.; Maurin, G.; Verstraelen, T.; Waroquier, M.; Van Speybroeck, V. *Chem. Mater.* **2016**, *28* (16), 5721–5732.
(612) Frisch M. J.; Trucks G. W.; Schlegel H. B.; Scuseria G. E.; Robb M. A.; Cheeseman J. R.; Scalmani G.; Barone V.; Petersson G. A.; Nakatsuji H.; Li X.; Caricato M.; Marenich A. V.; Bloino J.; Janesko B. G.; Gomperts R.; Mennucci B.; Hratchian H. P.; Ortiz J. V.; Izmaylov A. F.; Sonnenberg J. L.; Williams-Young D.; Ding F.; Lipparini F.; Egidi F.; Goings J.; Peng B.; Petrone A.; Henderson T.; Ranasinghe D.; Zakrzewski V. G.; Gao J.; Rega N.; Zheng G.; Liang W.; Hada M.; Ehara M.; Toyota K.; Fukuda R.; Hasegawa J.; Ishida M.; Nakajima T.; Honda Y.; Kitao O.; Nakai H.; Vreven T.; Throssell K.; Montgomery Jr. J. A. ; Peralta J. E.; Ogliaro F.; Bearpark M. J.; Heyd J. J.; Brothers E. N.; Kudin K. N.; Staroverov V. N.; Keith T. A.; Kobayashi R.; Normand J.; Raghavachari K.; Rendell A. P.; Burant J. C.; Iyengar S. S.; Tomasi J.; Cossi M.; Millam J. M.; Klene M.; Adamo C.; Cammi R.; Ochterski J. W.; Martin R. L.; Morokuma K.; Farkas O.; Foresman J. B.; Fox D. J. Gaussian 16 Revision C.01, **2016**. Gaussian Inc. Wallingford CT.
(613) Lee, C.; Yang, W.; Parr, R. G. *Phys. Rev. B* **1988**, *37* (2), 785.
(614) Becke, A. D. *J. Chem. Phys* **1993**, *98* (492), 5648–5652.
(615) Stephens, P. J.; Devlin, F. J.; Chabalowski, C. F.; Frisch, M. J. *J. Phys. Chem.* **1994**, *98* (45).
(616) Grimme, S.; Antony, J.; Ehrlich, S.; Krieg, H. *J. Chem. Phys.* **2010**, *132* (15), 154104.
(617) Frisch, M. J.; Pople, J. A.; Binkley, J. S. *J. Chem. Phys.* **1984**, *80* (7), 3265–3269.
(618) Verstraelen, T.; Vandenbrande, S.; Heidar-Zadeh, F.; Vanduyfhuys, L.; Van Speybroeck, V.; Waroquier, M.; Ayers, P. W. *J. Chem. Theory Comput.* **2016**, *12* (8), 3894–3912.
(619) Verstraelen, T.; Tecmer, P.; Heidar-Zadeh, F.; González-Espinoza, C. E.; Chan, M.; Kim, T. D.; Boguslawski, K.; Fias, S.; Vandenbrande, S.; Berrocal, D.; Ayers, P. W. **2017**. http://theochem.github.com/horton/.
(620) Vanduyfhuys, L.; Vandenbrande, S.; Verstraelen, T.; Schmid, R.; Waroquier, M.; Van Speybroeck, V. *J. Comput. Chem.* **2015**, *36* (13), 1015–1027.
(621) Vanduyfhuys, L.; Vandenbrande, S.; Wieme, J.; Waroquier, M.; Verstraelen, T.; Van Speybroeck, V. *J. Comput. Chem.* **2018**, *39* (16), 999–1011.
(622) Chen, J.; Martínez, T. J. *Chem. Phys. Lett.* **2007**, *438* (4–6), 315–320.
(623) Bush, B. L.; Bayly, C. I.; Halgren, T. A. *J. Comput. Chem.* **1999**, *20* (14), 1495–1516.
(624) Allinger, N. L.; Yuh, Y. H.; Lii, J. H. *J. Am. Chem. Soc.* **1989**, *111* (23), 8551–8566.
(625) Verstraelen, T.; Vanduyfhuys, L.; Vandenbrande, S.; Rogge, S. M. J. Yaff, yet another force field. http://molmod.ugent.be/software/.
(626) Cui, Q.; Bahar, I. *Normal Mode Analysis: Theory and Applications to Biological and Chemical Systems*; CRC press, **2005**.
(627) Ghysels, A.; Verstraelen, T.; Hemelsoet, K.; Waroquier, M.; Van Speybroeck, V. *J. Chem. Inf. Model.* **2010**, *50* (9), 1736–1750.
(628) Colón, Y. J.; Snurr, R. Q. *Chem. Soc. Rev.* **2014**, *43* (16), 5735–5749.
(629) Favre-Nicolin, V.; Černý, R. *J. Appl. Crystallogr.* **2002**, *35* (6), 734–743.
(630) Plimpton, S. *J. Comput. Phys.* **1995**, *117* (1), 1–19.
(631) Rogge, S. M. J.; Vanduyfhuys, L.; Ghysels, A.; Waroquier, M.; Verstraelen, T.; Maurin, G.; Van Speybroeck, V. *J. Chem. Theory Comput.* **2015**, *11* (12), 5583–5597.
(632) Nosé, S. *Mol. Phys.* **1984**, *52* (2), 255–268.

(633) Hoover, W. G. *Phys. Rev. A* **1985**, *31* (3), 1695–1697.
(634) Martyna, G. J.; Klein, M. L.; Tuckerman, M. *J. Chem. Phys.* **1992**, *97* (4), 2635–2643.
(635) Martyna, G. J.; Tobias, D. J.; Klein, M. L. *J. Chem. Phys.* **1994**, *101* (5), 4177–4189.
(636) Martyna, G. J.; Tuckerman, M. E.; Tobias, D. J.; Klein, M. L. *Mol. Phys.* **1996**, *87* (5), 1117–1157.
(637) Blöchl, P. E. *Phys. Rev. B* **1994**, *50* (24), 17953–17979.
(638) Kresse, G.; Hafner, J. *Phys. Rev. B* **1993**, *47* (1), 558–561.
(639) Kresse, G.; Furthmiiller B ', J. *Comput. Mater. Sci.* **1996**, *6*, 15–50.
(640) Kresse, G.; Furthmü, J. *Phys. Rev. B* **1996**, *54* (16), 11169–11186.
(641) Perdew, J. P.; Burke, K.; Ernzerhof, M. *Phys. Rev. Lett.* **1996**, *77* (18), 3865–3868.
(642) Grimme, S.; Antony, J.; Ehrlich, S.; Krieg, H. *J. Chem. Phys.* **2010**, *132* (15), 154104.
(643) Grimme, S.; Ehrlich, S.; Goerigk, L. *J. Comput. Chem.* **2011**, *32* (7), 1456–1465.
(644) Heyd, J.; Scuseria, G. E.; Ernzerhof, M. *J. Chem. Phys.* **2003**, *118* (18), 8207–8215.
(645) Huo, C.; Yuan, Y.; Wu, M.; Jia, X.; Wang, X.; Chen, F.; Tang, J. *Angew. Chem. Int. Ed.* **2014**, *53* (49), 13544–13547.
(646) Zhan, Z.; Cheng, X.; Ma, X.; Li, J.; Hai, L.; Wu, Y. *Tetrahedron* **2015**, *71* (38), 6928–6934.
(647) Wang, D.; Li, L.; Feng, H.; Sun, H.; Almeida-Veloso, F.; Charavin, M.; Yu, P.; Désaubry, L. *Green Chem.* **2018**, *20* (12), 2775–2780.
(648) Raeymackers, N. *Synthesis of ferroptosis inhibitors in plants*, Master Thesis, Ghent University, **2021**, pp 1-80.
(649) Reischauer, S.; Pieber, B. *iScience* **2021**, *24*, 102209.
(650) Kärkäs, M. D.; Porco, J. A.; Stephenson, C. R. J. *Chem. Rev.* **2016**, *116* (17), 9683–9747.
(651) Hoffmann, N. *Chem. Rev.* **2008**, *108* (3), 1052–1103.
(652) McAtee, R. C.; McClain, E. J.; Stephenson, C. R. J. *Trends Chem.* **2019**, *1* (1), 111–125.
(653) Crisenza, G. E. M.; Melchiorre, P. *Nat. Commun.* **2020**, *11* (1).
(654) Alahmed, A. H.; Briggs, M. E.; Cooper, A. I.; Adams, D. J. *J. Mat. Chem. A* **2019**, *7* (2), 549–557.
(655) Geng, T.; Liu, M.; Zhang, C.; Hu, C.; Xia, H. Y. *Polym. Adv. Technol.* **2020**, *31* (6), 1388–1394.
(656) Yan, J.; Sun, H.; Wang, Q.; Lu, L.; Zhang, B.; Wang, Z.; Guo, S.; Han, F. *New J. Chem.* **2022**, *46*, 7580.
(657) Puthiaraj, P.; Cho, S. M.; Lee, Y. R.; Ahn, W. S. *J. Mater. Chem. A* **2015**, *3* (13), 6792–6797.
(658) Goubard, F.; Dumur, F. *RSC Adv.* **2015**, *5* (5), 3521–3551.
(659) Mohamed, M. G.; Elsayed, M. H.; Elewa, A. M.; EL-Mahdy, A. F. M.; Yang, C. H.; Mohammed, A. A. K.; Chou, H. H.; Kuo, S. W. *Catal. Sci. Technol.* **2021**, *11* (6), 2229–2241.
(660) Orofino, C.; Kanibolotsky, A. L.; Skabara, P. J. *Arkivoc* **2021**, *2021* (6).
(661) Liu, L.; Telfer, S. G. *J. Am. Chem. Soc.* **2015**, *137* (11), 3901–3909.
(662) Grzybowski, M.; Skonieczny, K.; Butenschön, H.; Gryko, D. T. *Angew. Chem. Int. Ed.* **2013**, *52* (38), 9900–9930.
(663) Guadalupe, J.; Ray, A. M.; Maya, E. M.; Gómez-Lor, B.; Iglesias, M. *Polym. Chem.* **2018**, *9* (36), 4585–4595.
(664) Guo, L.; Niu, Y.; Xu, H.; Li, Q.; Razzaque, S.; Huang, Q.; Jin, S.; Tan, B. *J. Mater. Chem. A* **2018**, *6* (40), 19775–19781.
(665) Das, S. K.; Bhanja, P.; Kundu, S. K.; Mondal, S.; Bhaumik, A. *ACS Appl. Mater. Interfaces* **2018**, *10* (28), 23813–23824.
(666) Song, W. C.; Xu, X. K.; Chen, Q.; Zhuang, Z. Z.; Bu, X. H. *Polym. Chem.* **2013**, *4* (17), 4690–4696.
(667) Wisser, F. M.; Berruyer, P.; Cardenas, L.; Mohr, Y.; Quadrelli, E. A.; Lesage, A.; Farrusseng, D.; Canivet, J. *ACS Catal.* **2018**, *8* (3), 1653–1661.
(668) Chaoui, N.; Trunk, M.; Dawson, R.; Schmidt, J.; Thomas, A. *Chem. Soc. Rev.* **2017**, *46* (11), 3302–3321.

(669) Troschke, E.; Grätz, S.; Lübken, T.; Borchardt, L. *Angew. Chem. Int. Ed.* **2017**, *129* (24), 6963–6967.
(670) Liras, M.; Pintado-Sierra, M.; Iglesias, M.; Sánchez, F. *J. Mater. Chem. A* **2016**, *4* (44), 17274–17278.
(671) Osadchii, D. Y.; Olivos-Suarez, A. I.; Bavykina, A. V.; Gascon, J. *Langmuir* **2017**, *33* (50), 14278–14285.
(672) Kwong, H. L.; Yeung, H. L.; Yeung, C. T.; Lee, W. S.; Lee, C. S.; Wong, W. L. *Coord. Chem. Rev.* **2007**, *251* (17–20), 2188–2222.
(673) Henry, G. D. *Tetrahedron* **2004**, *60* (29), 6043–6061.
(674) Evdokimov, N. M.; Kireev, A. S.; Yakovenko, A. A.; Antipin, M. Y.; Magedov, I. V.; Kornienko, A. *J. Org. Chem.* **2007**, *72* (9), 3443–3453.
(675) Bai, C. B.; Wang, N. X.; Wang, Y. J.; Lan, X. W.; Xing, Y.; Wen, J. L. *RSC Adv.* **2015**, *5* (122), 100531–100534.
(676) Vanden Eynde, J.-J.; D'Oraxio, R.; Van Haverbeke, Y. *Tetrahedron* **1994**, *50* (8), 2479–2484.
(677) Böcker, R. H.; Guengerich, F. P. *J. Med. Chem.* **1986**, *29* (9), 1596–1603.
(678) Memari, H. R.; Altork, M.-B.; Sadeghi, M. M.; Samani, Z. S. *Indian J. Chem.* **2001**, *40B*, 727–728.
(679) Chavan, S. P.; Dantale, S. W.; Kalkote, U. R.; Jyothirmai, V. S.; Kharul, R. K. *Synth. Commun.* **1998**, *28* (15), 2789–2792.
(680) Ko, K.-Y.; Kim, J.-Y. *Tetrahedron Lett.* **1999**, *40*, 3207–3208.
(681) Bagley, M. C.; Lubinu, M. C. *Synthesis (Stuttg)* **2006**, No. 8, 1283–1288.
(682) Lu, J.; Bai, Y.; Wang, Z.; Yang, B. Q.; Li, W. *Synth. Commun.* **2001**, *31* (17), 2625–2630.
(683) Heravi, M. M.; Behbahani, F. K.; Oskooie, H. A.; Shoar, R. H. *Tetrahedron Lett.* **2005**, *46* (16), 2775–2777.
(684) Han, B.; Liu, Z.; Liu, Q.; Yang, L.; Liu, Z. L.; Yu, W. *Tetrahedron* **2006**, *62* (11), 2492–2496.
(685) Wei, X.; Wang, L.; Jia, W.; Du, S.; Wu, L.; Liu, Q. *Chin. J. Chem.* **2014**, *32* (12), 1245–1250.
(686) Chhetri, K.; Bhuyan, S.; Mandal, S.; Chhetri, S.; Lepcha, P. T.; Lepcha, S. W.; Basumatary, J.; Roy, B. G. *Curr. Res. Green Sust. Chem.* **2021**, *4*.
(687) Küçükgüzel, G.; ŞenkardeŞ, S. *Eur. J. Org. Chem.* **2015**, *97* (1), 786–815.
(688) Kumar, K. A. *Int. J. Pharmtech Res.* **2013**, *5* (4), 1473–1486.
(689) Makino, K.; Ho Sik, K.; Kurasawa, Y. *J. Heterocycl. Chem.* **1999**, *36*, 321.
(690) Vidau, C.; Brunet, J. L.; Badiou, A.; Belzunces, L. P. *Toxicol. In Vitro* **2009**, *23* (4), 589–597.
(691) Fu, Q.; Cai, P. P.; Cheng, L.; Zhong, L. K.; Tan, C. X.; Shen, Z. H.; Han, L.; Xu, T. M.; Liu, X. H. *Pest Manag. Sci.* **2020**, *76* (3), 868–879.
(692) Casadia, I.; de Albuquerque, D. Y.; Carmo Capiotto, A. Do; Pereira de Pereira, C. M.; Pizzuti, L. *Curr. Org. Synth.* **2017**, *14* (5).
(693) Van Leeuwen, T.; Buzzetti, L.; Perego, L. A.; Melchiorre, P. *Angew. Chem. Int. Ed.* **2019**, *131* (15), 5007–5011.
(694) Wang, C.; Lu, Z. *Org. Lett.* **2017**, *19* (21), 5888–5891.
(695) Mao, S.; Li, F.; Lv, Y.; Lv, C.; Yu, S. *Heterocycles* **2017**, *94* (10), 1895–1902.
(696) Yü, S. J.; Wu, S.; Zhao, X. M.; Lü, C. W. *Res. Chem. Intermed.* **2017**, *43* (5), 3121–3130.
(697) Ananthnag, G. S.; Adhikari, A.; Balakrishna, M. S. *Catal. Commun.* **2014**, *43*, 240–243.
(698) Kolla, S. T.; Rayala, N. R.; Sridhar, B.; Bhimapaka, C. R. *Org. Biomol. Chem.* **2022**, *20* (2), 334–338.
(699) Montazerozohori, M.; Karami, B.; Nasr-Esfahani, M.; Musavi, S. A. *Heterocycl. Commun.* **2007**, *13* (5), 289–294.
(700) Bodor, N.; Farag, H. H.; Barros, M. D. C.; Wu, W. M.; Buchwald, P. *J. Drug Target.* **2002**, *10* (1), 63–71.
(701) Singh, R. K.; Prasad, D. N.; Bhardwaj, T. R. *Med. Chem. Res.* **2013**, *22* (11), 5324–5336.

(702) Monakhova, Y. B.; Diehl, B. W. K. *Anal. Methods* **2016**, *8* (23), 4632–4639.
(703) Fulmer, G. R.; Miller, A. J. M.; Sherden, N. H.; Gottlieb, H. E.; Nudelman, A.; Stoltz, B. M.; Bercaw, J. E.; Goldberg, K. I. *Organometallics* **2010**, *29* (9), 2176–2179.
(704) Ortiz, M. E.; Nú N ˜ Ez-Vergara, L. J.; Camargo, C.; Squella, J. A. *Pharm. Res.* **2004**, *21*, 428–435.
(705) Pizarro-Urzúa, N. A.; Núñez-Vergara, L. J. *J. Photochem. Photobiol. A* **2005**, *175* (2–3), 129–137.
(706) Memarian, H. R.; Abdoli-Senejani, M.; Tangestaninejad, S. *J. Iran. Chem. Soc.* **2006**, *3* (3), 285–292.
(707) Ozawa, T.; Akira, H. *Chem. Pharm. Bull.* **1978**, *26* (8), 2572–2575.
(708) Lismont, M.; Dreesen, L.; Heinrichs, B.; Páez, C. A. *Photochem. Photobiol.* **2016**, *92* (2), 247–256.
(709) Mendoza, C.; Désert, A.; Khrouz, L.; Páez, C. A.; Parola, S.; Heinrichs, B. *Environ. Sci. Pollut. Res..* **2021**, *28*, 25124–25129.
(710) Pavlishchuk, V. V; Addison, A. W. *Inorganica Chim. Acta* **2000**, *298*, 97–102.
(711) Su, F.; Mathew, S. C.; Möhlmann, L.; Antonietti, M.; Wang, X.; Blechert, S. *Angew. Chem. Int. Ed.* **2011**, *50* (3), 657–660.
(712) Qiu, X.; Len, C.; Luque, R.; Li, Y. *ChemSusChem* **2014**, *7* (6), 1684–1688.
(713) Chen, Z. Y.; Zhang, W. *Chin. Chem. Lett.* **2007**, *18* (12), 1443–1446.
(714) Sardar, B.; Jamatia, R.; Pal, D.; Srimani, D. *Asian J. Org. Chem.* **2021**, *10* (8), 2195–2204.
(715) Pavithra, D.; Ethiraj, K. R. *Polycycl. Aromat. Compd.* **2022**, *42* (4), 1078–1090.
(716) Dey, S.; Basak, P.; Ghosh, P. *ChemistrySelect* **2020**, *5* (48), 15209–15217.
(717) Antonyraj, C. A.; Kannan, S. *Appl. Catal. A: Gen.* **2008**, *338* (1–2), 121–129.
(718) Kumar, A.; Maurya, R. A. *Tetrahedron Lett.* **2007**, *48* (22), 3887–3890.
(719) Safaei-Ghomi, J.; Bamoniri, A. H.; Soltanina-Telkabadi, M. *Chem. heterocycl. compounds* **2006**, *42*, 892–896.
(720) Wu, X. F.; Neumann, H.; Beller, M. *Eur. J. Org. Chem.* **2011**, No. 25, 4919–4924.
(721) Patil, N. T.; Singh, V. *Chem. Commun.* **2011**, *47* (39), 11116–11118.
(722) Zhao, G. L.; Shi, M. *Tetrahedron* **2005**, *61* (30), 7277–7288.
(723) Bercovici, D. A.; Brewer, M. *J. Am. Chem. Soc.* **2012**, *134* (24), 9890–9893.
(724) Gul, H. I.; Mete, E.; Taslimi, P.; Gulcin, I.; Supuran, C. T. *J. Enzyme Inhib. Med. Chem.* **2017**, *32* (1), 189–192.
(725) Mallouk, S.; Bougrin, K.; Doua, H.; Benhida, R.; Soufiaoui, M. *Tetrahedron Lett.* **2004**, *45* (21), 4143–4148.
(726) Baddar, F. G.; Al-Hajjar, F. H.; El-Rayyes, N. R. *J. Heterocyclic. Chem.* **1978**, *15*, 385–393.
(727) Texier-Boullet, F.; Klein, B.; Hamelin, J. *Synthesis (Germany)* **1986**, *1986* (5), 409–411.
(728) Cristau, H. J.; Cellier, P. P.; Spindler, J. F.; Taillefer, M. *Eur. J. Org. Chem.* **2004**, No. 4, 695–709.
(729) Butler, R. N.; Hanniffy, J. M.; Stephens, J. C.; Burke, L. A. *J. Org. Chem.* **2008**, *73* (4), 1354–1364.
(730) Hu, J.; Chen, S.; Sun, Y.; Yang, J.; Rao, Y. *Org. Lett.* **2012**, *14* (19), 5030–5033.
(731) Wijnant, I. *Ontwikkeling van NHC-gebaseerde heterogene katalysatoren*, Master Thesis, Ghent University, **2021**, pp 1-75.
(732) Huang, N.; Wang, P.; Addicoat, M. A.; Heine, T.; Jiang, D. *Angew. Chem. Int. Ed.* **2017**, *56* (18), 4982–4986.
(733) Zych, D.; Kurpanik, A.; Slodek, A.; Maroń, A.; Pająk, M.; Szafraniec-Gorol, G.; Matussek, M.; Krompiec, S.; Schab-Balcerzak, E.; Kotowicz, S.; Siwy, M.; Smolarek, K.; Maćkowski, S.; Danikiewicz, W. *Chem. Eur. J.* **2017**, *23* (62), 15746–15758.
(734) Hammer, B. A. G.; Baumgarten, M.; Müllen, K. *Chem. Commun.* **2014**, *50* (16), 2034–2036.
(735) Yaşar, S.; Karaca, E. Ö.; Şahin, Ç.; Özdemir, I.; Şahin, O.; Büyükgüngör, O. *J. Organomet. Chem.* **2015**, *789–790*, 1–7.
(736) Santilli, C.; Makarov, I. S.; Fristrup, P.; Madsen, R. *J. Org. Chem.* **2016**, *81* (20), 9931–9938.

(737) Ablialimov, O.; Kedziorek, M.; Malinska, M.; Wozniak, K.; Grela, K. *Organometallics* **2014**, *33* (9), 2160–2171.
(738) (715) Schmidbaur, H.; Cihonski, J. L. Noble metals (Chemistry). *Encyclopedia of Physical Science and Technology*; Elsevier, **2003**; pp 463–492.
(739) Popowycz, F.; Métay, E.; Lemaire, M. *C. R. Chimie* **2011**, *14* (7–8), 621–628.
(740) Gonell, S.; Peris, E. *ACS Catal.* **2014**, *4* (8), 2811–2817.
(741) Balaraman, E.; Khaskin, E.; Leitus, G.; Milstein, D. *Nat. Chem.* **2013**, *5* (2), 122–125.
(742) Wang, W. Q.; Cheng, H.; Yuan, Y.; He, Y. Q.; Wang, H. J.; Wang, Z. Q.; Sang, W.; Chen, C.; Verpoort, F. *Catalysts* **2020**, *10* (1).
(743) Deblase, C. R.; Silberstein, K. E.; Truong, T. T.; Abruña, H. D.; Dichtel, W. R. *J. Am. Chem. Soc.* **2013**, *135* (45), 16821–16824.
(744) EL-Mahdy, A. F. M.; Hung, Y. H.; Mansoure, T. H.; Yu, H. H.; Hsu, Y. S.; Wu, K. C. W.; Kuo, S. W. *J. Taiwan Inst. Chem. Eng.* **2019**, *103*, 199–208.
(745) Zhu, L.; Zhang, Y. B. *Molecules* **2017**, *22* (7), 1149.
(746) Daugherty, M. C.; Vitaku, E.; Li, R. L.; Evans, A. M.; Chavez, A. D.; Dichtel, W. R. *Chem. Commun.* **2019**, *55* (18), 2680–2683.
(747) Bhunia, S.; Das, S. K.; Jana, R.; Peter, S. C.; Bhattacharya, S.; Addicoat, M.; Bhaumik, A.; Pradhan, A. *ACS Appl. Mater. Interfaces* **2017**, *9* (28), 23843–23851.
(748) Bissonnette, N. B.; Ellis, J. M.; Hamann, L. G.; Romanov-Michailidis, F. *Chem. Sci.* **2019**, *10* (41), 9591–9596.
(749) Hübner, S.; de Vries, J. G.; Farina, V. *Adv. Synth. Catal.* **2016**, *358* (1), 3–25.

Curriculum Vitae

Personalia

Maarten Debruyne

°31/10/1995, 2300 Turnhout


Madeliefjesstraat 13, 9000 Gent


mgadbruy@ugent.be
maarten_debruyne@hotmail.com


https://www.linkedin.com/in/maarten-debruyne/


0494062162

Education

2018 - present: PhD student at the SynBioC Research Group, Department of Green Chemistry and Technology, Faculty of Bioscience Engineering, Ghent University

- *PhD thesis*: Development of porous organic polymers as heterogeneous photocatalysts
- *Promotor*: Prof. dr. ir. Christian Stevens
- *Co-promotor*: Prof. dr. ir. Veronique Van Speybroeck,
- *Funding*: BOF GOA Ghent University

2016 - 2018: Master of Science in Bioscience Engineering: Chemistry and Bioprocess Technology, Faculty of Bioscience Engineering, Ghent University

- *Master thesis*: Synthesis end enzymatic glycosylation of mono and bicyclic 3-hydroxy-β-lactams
- *Promoters*: Prof. dr. ir. Matthias D'hooghe
  Prof. dr. Tom Desmet

2013 - 2016: Bachelor in Bioscience Engineering: Chemistry and Food Technology, Faculty of Bioscience Engineering, Ghent University

Publications related to this PhD thesis

M. Debruyne, V. Van Speybroeck, P. Van Der Voort, C. V. Stevens. Porous organic polymers as metal free heterogeneous organocatalysts. *Green Chem.*, **2021**, *23*(19), 7361–7434.

M. Debruyne, S. Borgmans, J. De Vos, K. Sing Rawat, A. Laemont, H. Salemi, J. Everaert, F. Vanden Bussche, H. Vrielinck, K. Leus, R. Morent, N. De Geyter, D. Poelman, P. Van Der Voort, V. Van Speybroeck, C. V. Stevens. Engineering of phenylpyridine- and bipyridine-based covalent organic frameworks for the photocatalytic tandem aerobic oxidation/Povarov cyclization. *Manuscript in preparation.*

M. Debruyne, N. Raeymackers, A. Laemont, H. Vrielinck, K. Leus, D. Poelman, R. Morent, N. De Geyter, P. Van Der Voort, V. Van Speybroeck, C. V. Stevens, T. Heugebaert. Development of porous organic polymers as metal-free photocatalysts for the aromatization of *N*-heterocycles. *Manuscript in preparation.*

Publications resulting from active participation in other projects

L. Decuyper, J. Franceus, S. Dhaene, **M. Debruyne**, K. Vandoorne, N. Piens, G. Dewitte, T. Desmet, M. D'hooghe. Chemoenzymatic approach toward the synthesis of 3-O-(α/β)-glucosylated 3-hydroxy-β-lactams. *ACS Omega* **2018**, *3*, 15235–15245.

F. Vanden Bussche, A. M. Kaczmarek, S. Veerapandian, J. Everaert, **M. Debruyne**, S. Abednatanzi, P. Van Der Voort, C. V. Stevens. *N*-rich porous polymer with isolated Tb^{3+}-ions displays unique temperature dependent behavior through the absence of thermal quenching. *Chem. Eur. J.*, **2020**, 26, 15596.

J. Everaert, **M. Debruyne**, F. Vanden Bussche, K. Van Hecke, T. Heugebaert, P. Van Der Voort, P., V. Van Speybroeck, C. V. Stevens. Synthesis of Nitrile-Functionalized Polydentate *N*-Heterocycles as Building Blocks for Covalent Triazine Frameworks. *Synthesis*, **2021**, 53, A-H.

H. Salemi, **M. Debruyne**, V. Van Speybroeck, P. Van Der Voort, M. D'hooghe, C. V. Stevens. Covalent organic framework supported palladium catalysts. *J. Mater. Chem. A*., **2022**, 10, 20707-20729.

Active participation at conferences

L. Decuyper, J. Franceus, S. Dhaene, **M. Debruyne**, K. Vandoorne, N. Piens, G. Dewitte, T. Desmet, M. D'hooghe. Chemoenzymatic approach toward the synthesis of 3-O-(α/β)-glucosylated 3-hydroxy-β-lactams. Poster presentation, *22nd Merck Organic Chemistry Symposium* (December 6-7, **2018**, Blankenberge, Belgium).

M. Debruyne, P. Van Der Voort, V. Van Speybroeck, C. V. Stevens. Phenylpyridine and bipyridine based covalent organic frameworks as metal free photocatalysts for the visible light aerobic oxidation/Povarov cyclization. Poster presentation, *17th Belgian Organic Synthesis Symposium* (July 3-8, **2022**, Namur, Belgium).

M. Debruyne, P. Van Der Voort, V. Van Speybroeck, C. V. Stevens. Phenylpyridine and bipyridine based covalent organic frameworks as metal free photocatalysts for the visible light aerobic oxidation/Povarov cyclization. Oral presentation, CRF-ChemCYS 2022 (October 12-14, **2022**, Blankenberge, Belgium).